USF UNIVERSITY OF SOUTH FLORIDA
Department of Civil and Environmental Engineering

# DESIGN AND EVALUATION OF STEEL BRIDGES WITH DOUBLE COMPOSITE ACTION

**FINAL REPORT**

*funded by:*

Florida and US Department of Transportation
Contract No. # BD544-18

*Principal Investigators:*

*Rajan Sen, Ph.D, P.E. USF*
*Steven Stroh, P.E. URS*

**February 2010**

# DESIGN AND EVALUATION OF STEEL BRIDGES WITH DOUBLE COMPOSITE ACTION

**Contract No. # BD544-18**

**Final Report on a Research Project**
**Sponsored by**

**Florida and US Department of Transportation**

**Principal Investigators:**

**Rajan Sen, Ph.D., P.E. (USF)**
**Steven Stroh, P.E. (URS)**

Dennis Golabek, P.E., URS
Post-Doctoral Fellow: Niranjan Pai, Ph.D., P.E.
Graduate Student: Purvik Patel
Department of Civil and Environmental Engineering
University of South Florida, Tampa, FL

**February 2010**

**Technical Report Documentation Page**

| 1. Report No. | 2. Government Accession No. | 3. Recipient's Catalog No. |
|---|---|---|
| | | |

| 4. Title and Subtitle | 5. Report Date |
|---|---|
| Design and Evaluation of Steel Bridges with Double Composite Action | February 2010 |
| | 6. Performing Organization Code |

| 7. Author(s) | 8. Performing Organization Report No. |
|---|---|
| N. Pai., P. Patel and, R. Sen, (USF); S. Stroh, D. Golabek (URS) | USF/2010/ST/1 |

| 9. Performing Organization Name and Address | 10. Work Unit No. (TRAIS) |
|---|---|
| Department of Civil and Environmental Engineering<br>University of South Florida<br>Tampa, FL 33620-5350 | 11. Contract or Grant No.<br>Contract BD544, RPWO # 18 |

| 12. Sponsoring Agency Name and Address | 13. Type of Report and Period Covered |
|---|---|
| Florida Department of Transportation<br>Structures Research Center<br>2007 East Paul Dirac Drive<br>Tallahassee, FL 32310 | Final Report<br>October 2004-September 2009 |
| | 14. Sponsoring Agency Code<br>FDOT |

15. Supplementary Notes

16. Abstract

This report presents findings from a cooperative USF/URS/FDOT research study undertaken to develop design rules for double composite steel bridges. In the study, a 48 ft long, 16 ft wide, 4 ft. 10⅛ in. deep trapezoidal HPS 70W box section designed to AASHTO's LRFD 2004 specifications was fabricated and tested. The section has an 8 in. thick top slab and a 7 in. thick bottom slab and represented the entire negative moment region of a full-size, continuous bridge.

The specimen was tested to evaluate fatigue, service and ultimate provisions of the AASHTO code. Instrumentation was provided to monitor load, strain, slip deflection and crack widths at critical locations. Results showed that after 5.6 million cycles of fatigue loading there was a 17% loss in stiffness but no slip. The service tests showed that 1% reinforcement for the top slab is adequate. The specimen failed due to crushing of the bottom slab caused by buckling of the thin (3/8 in.) bottom flange in the final service test. Finite element analysis was used to simulate the failure and showed that the bottom flange buckles at relatively low loads, but due to composite action with concrete at shear stud locations, it can still effectively carry additional compressive load until the bottom flange yields due to plastic buckling. Subsequently the concrete bottom slab carries all additional load until it crushes.

Supplementary provisions are proposed for designing double composite members. These limit the maximum compressive stress in the bottom slab to $0.6f'_c$ and set a requirement for the location of the neutral axis to ensure ductility. Due to the strain limit on the concrete bottom slab, it may not be possible to achieve net section plastic capacity. An illustrative numerical application of these rules is included as a MATHCAD file.

| 17. Key Word | 18. Distribution Statement |
|---|---|
| Double composite, steel bridges, innovative design of superstructure | |

| 19. Security Classif. (of this report) | 20. Security Classif. (of this page) | 21. No. of Pages | 22. Price |
|---|---|---|---|
| Unclassified | Unclassified | 497 | |

**Form DOT F 1700.7** (8-72) Reproduction of completed page authorized

# DISCLAIMER

The opinions, findings and conclusions expressed in this publication are those of the authors and not necessarily those of the US and Florida Department of Transportation.

# ACKNOWLEDGEMENTS

The investigation reported in this study was a joint USF/URS/FDOT research project funded by a contract awarded to the University of South Florida, Tampa by the Florida Department of Transportation (FDOT) with Mr. Marc Ansley as the Program Manager. We are deeply indebted to Mr. Ansley for his contribution to this study. We thank Mr. William Potter and Mr. Steven Eudy (FDOT) for their exceptional assistance.

We thank Prof. Julio Martinez Calzon, Madrid, Spain for providing the research team with valuable resources including an English version copy of the Spanish Code for Road Composite Bridges that is unavailable for sale.

This project could not have been completed without the help of several undergraduate and graduate USF students many of whom volunteered their time. Special thanks to Lori Elkins, Vladimir Simonovsky, Julio Aguilar and Javier Fuentes.

# CONVERSION FACTORS, US CUSTOMARY TO METRIC UNITS

| ***Multiply*** | ***by*** | ***to obtain*** |
|---|---|---|
| Inch | 25.4 | Mm |
| Foot | 0.3048 | Meter |
| square inches | 645 | square mm |
| cubic yard | 0.765 | cubic meter |
| pound (lb) | 4.448 | Newton |
| kip (1000) | 4.448 | kilo newton (kN) |
| Newton | 0.2248 | Pound |
| kip/ft | 14.59 | kN/meter |
| Pound/$in^2$ | 0.0069 | MPa |
| kip/$in^2$ | 6.895 | MPa |
| MPa | 0.145 | Ksi |
| ft-kip | 1.356 | kN-m |
| in-kip | 0.113 | kN-m |
| kN-m | 0.7375 | ft-kip |

# EXECUTIVE SUMMARY

Conventional continuous steel bridges primarily benefit from composite action with concrete deck in the positive moment region. Similar composite action may also be achieved in the negative moment region by casting a bottom concrete slab between the points of inflection. Such a section is referred to as double composite since it utilizes composite action in both the positive and negative moment regions (top flange and bottom flange respectively).

Savings in double composite bridges arise because expensive steel is replaced by inexpensive concrete to carry compressive loads. Although double composite bridges have been designed and constructed since at least 1978 there has been limited research. Thus, current designs rely on existing provisions for designing conventional composite bridges. This fails to fully exploit advantages or recognize the weaknesses, if any, of double composite action.

This report presents findings from a cooperative research project involving the University of South Florida (USF), URS Corporation (URS) and the Florida Department of Transportation (FDOT) in which full-scale tests and theoretical analyses were carried out to develop appropriate limit state rules for designing double composite bridges. The intent was to fully develop the concept so that it is ready for implementation on a prototype structure. The principal objectives may be summarized as follows:

1. To design and fabricate a double composite box girder section using existing rules and to evaluate its performance under service, fatigue and strength limit states.
2. To conduct appropriate parametric design/analysis to optimize the performance of doubly composite box girders and establish new design criteria if required.
3. To develop a model example to illustrate the design of double composite box structures.

A 4 ft. 10⅛ in. deep, 53 ft. long, 16 ft. wide box girder bridge representing the entire negative moment section at a support of a continuous full-size box girder bridge was designed to the 2004 American Association of State Highway and Transportation Officials (AASHTO) Load and Resistance Factor Design (LRFD) specifications 3rd Edition 2004 and the Florida Structures Design Guidelines, January 2005. The High Performance Steel (HPS) 70 trapezoidal box had a 1 ¾ in. thick top flange, ¾ in. webs and a ⅜ in. thick bottom flange. It was fabricated by Tampa Steel, Inc. and shipped to FDOT's Structural Research Center, Tallahassee where the 7 in. thick bottom slab and the 8 in., thick top slab were cast.

Three series of tests – fatigue, service and strength were conducted and the specimen instrumented using 162 channels to allow measurement of load, strain, deflection and slip. The intent of the instrumentation was to determine the extent to which prevailing specifications were valid for the design of double composite sections. The fatigue test preceded the service tests. In the testing, the specimen was asymmetrically supported so that the span was divided into two unequal spans of 23 ft. and 25 ft. Loads were applied at the free end of the 25 ft span with the other end restrained to ensure equilibrium.

In the fatigue test, a total of 5.6 million cycles were applied at a frequency of 1.16 Hz. The number of cycles corresponded to the fatigue life of the shear connectors in the double composite section. These were welded to the ⅜ in. thick bottom flange spaced at 23 in. lengthwise and 8 in. apart in the transverse direction. The magnitude of the fatigue load was dictated by the capacity of the actuators and varied from 5 to 105 kips. In the testing, the top slab cracked at loads well below predicted values and there was a 17% reduction in stiffness at the end of the test. There was no slip but based on strain data in the concrete and steel there was evidence of localized distress.

Three series of service loads were conducted that corresponded to stress limits specified in the AASHTO code for Grade 50 and Grade 70 steels. These were designated as Service I (maximum load 421 kips corresponding to rebar stress of $0.6f_y$), Service II (maximum load 638 kips corresponding to stress in the steel flange of $0.95F_y - F_y = 50$ ksi) and Service III (maximum load 894 kips corresponding to stress in the steel flange of $0.95F_y - F_y = 70$ ksi). In each case the load was applied and removed five times. A further ultimate test was planned (load = 1200 kips) but not conducted because of failure of the specimen under the first cycle of the service III loading.

The results from the service tests showed that the 1% reinforcement provided in the top slab was adequate. Measured crack widths ranged from 0.015 in. and 0.022 in. for Service I test and between 0.018 in. and 0.024 in. for Service II test. There was a significant reduction in stiffness in the $2^{nd}$ to $5^{th}$ load application compared to the first cycle. Moreover, strain data from the first load application was not replicated in subsequent applications. This variation in strain in the bottom slab concrete indicated localized distress from bottom flange buckling.

The bottom slab failed by crushing in the shorter hold down span under the first application of 894 kip service load along the line of shear connectors in the high moment zone close to the support. Bottom steel flange in this area was found to have buckled plastically.

Finite element analysis of the specimen was conducted using ANSYS. The three-dimensional model incorporated material and geometric non-linearity. Individual shear studs used in the bottom flange were modeled and construction sequence taken into consideration in the loading history. Non-linearity from separable contact elements between the bottom slab and the bottom flange and non-linear buckling of the bottom flange were also incorporated in the model. The model showed that at the failure region, the bottom steel flange buckled at moderate loads (about 320 kip) due to combined transverse and longitudinal load effects. Numerical results indicate that despite buckling, the bottom steel flange still carried loading until the net section yielded at loads exceeding 600 kip. This suggests that analyses based on simple handbook buckling solutions grossly under predict the compressive load capacity of the bottom flange. Once the net section of the bottom steel flange yields plastically, compression is primarily carried by the bottom concrete slab until it crushes at its ultimate failure strain.

Based on the experimental results, new provisions are proposed which limited the maximum stress in the bottom slab and also included ductility criterion. Due to the limitation in

the concrete stress, a double composite section will not achieve net plastic section capacity. The application of these rules is shown by an illustrative example that is included in Appendix G as a MATHCAD file.

# TABLE OF CONTENTS

# LIST OF TABLES

# LIST OF FIGURES

# 1. INTRODUCTION

## 1.1 Introduction

Steel girder bridges are commonly designed to take advantage of composite action with the concrete deck slab to improve the load carrying capacity and performance of the girder. This idea can be extended to double composite behavior by including a concrete slab in the plane of the bottom flange in the negative moment region of the girder. In addition to the obvious savings in replacing steel flange material with less costly concrete, this concept offers the potential for further savings due to increased stiffness over the piers with a corresponding favorable redistribution of moments, reduced deflections and improved fatigue performance. Provision of a composite bottom flange in the negative moment region of a continuous span also offers the potential for meeting compactness criteria for a thinner web due to the lowering of the neutral axis, thus allowing a plastic design methodology and further improved girder performance.

The concept of double composite girder bridges was identified as a potential new design that would improve the economy of steel bridges and foster new levels of competition with concrete bridge structures in a study completed by the University of South Florida several years ago [1.1-1.2]. In particular, the double composite concept was developed for plate girder bridges in the 200-400 ft. span range, where spliced, post-tensioned concrete I-girders and segmental concrete box girders typically represent the most economical structure type [1.3].

The primary focus of the earlier study [1.1-1.2] was on the identification of a new and innovative concept. As a result, limited analytical evaluation of the double composite concept was carried out. Nor was any systematic study conducted to evaluate the use of high performance steels (HPS). This study builds on the previous work [1.1-1.2], extending the analytical work to include HPS and conducting full-scale testing to verify the performance of this new bridge design concept. The intent is to fully develop the concept so that it is ready for implementation on a prototype structure.

**Figure 1.1** First Double Composite Bridge, Ciervana Bridge (*Courtesy J.M. Calzon*)

## 1.2 Literature Review

Double-composite design is not new [1.4-1.16] but has seen limited application worldwide. The first such bridge constructed is reportedly the Ciervana bridge (Fig. 1.1) built in Spain in 1978 [1.6]. Other bridges were constructed in Germany and South America [1.4, 1.8, 1.10-1.12, 1.14]. More recently, this concept was included in the Kap Shui Mun Cable Stayed Bridge, Hong Kong [1.5, 1.7]. A double composite bridge was completed in Canada on the Fredericton-Moncton Highway in 2001 [1.13, 1.16]. No examples of such design were found in the U.S, although the concept of a double-composite design was recognized in a report on innovative short and medium span bridge concepts prepared for the American Iron and Steel Institute [1.9].

Double composite construction has been used predominantly in conjunction with rectangular or trapezoidal box sections but the literature provides limited information on their design. In Spanish practice, bottom corner cells (Fig. 1.2) are provided in the negative moment region [1.6]. This is to "*(1) stabilize the bottom and web plates; (2) better shear connection of the torsional and bending actions in the bottom concrete slab; (3) increase the compact conditions of the cross-section and allowing the use of plastic analysis in ultimate design."* It is also stated that "*this (bottom) concrete slab is reinforced only for resisting torsion and its own weight in transversal direction, but it is not considered in the positive bending, unless including some special bars in the lateral edges close to the supporting bottom plates of the slab in order to increase the total positive resistance when it could be necessary"*.

Martinez-Calzon 1995 [1.6] refers to the Spanish design specifications [1.17]. Section 5.6.4 of this code specifies "*in the area of negative bending, the combined effect of shear stress in the slab caused by external loading and tensile stress due to general bending*" needs to be analyzed. It adds "*in thin slabs… this effect may be decisive… and it will be necessary to guarantee the slab strength by testing as the present standards do not include realistic values of resistance to shear stress for high quantities of reinforcement*". For crack control, a minimum 1% steel is specified with the crack width limited to 0.2 mm.

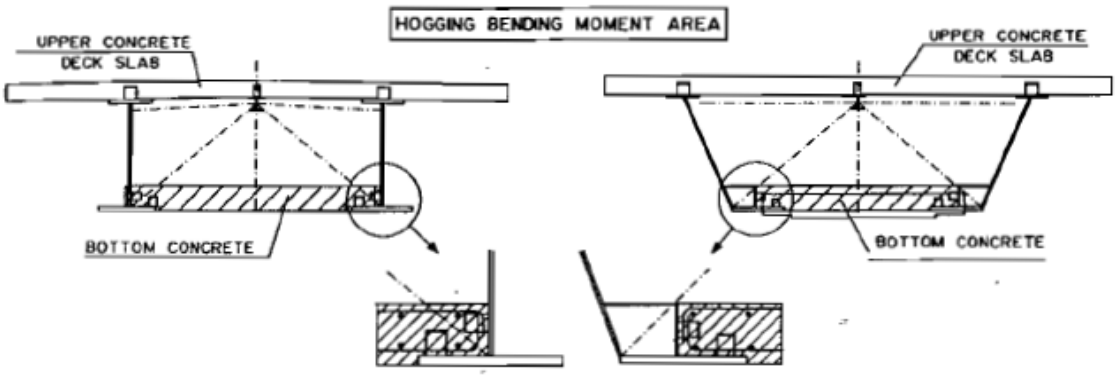


**Figure 1.2** Details in Spanish Double Composite Design [1.6]

The research team contacted Prof. Calzon regarding the steel limits in the negative moment zone. His response was the following [1.18]:

"The reinforcement ratio on the slabs over intermediate supports depends mainly on the local behaviour (sic) of the slab:

> If the support of the slab is only longitudinal (the slab is supported on the webs, without contact with any diaphragms), the longitudinal tensile forces in the slab are originated only by the global bending. In these cases, a minimum value for the reinforcement ratio about 1% is correct and the Spanish code indicates the reinforcement ratio is required as a function of the diameter of the bars in order to guarantee that the tensile stresses, calculated with the hypothesis of cracker section, are under a defined limit that is equivalent to a crack width limit.
>
> If the slab has also a transversal support, then the global bending moment is combined with the local bending moment and what is more important, with significant local shear forces mainly originated by concentrated loads. In this case, it is required that concrete cracking is not significant in order to guarantee an appropriate interlock at the concrete interface that enable to consider the contribution of the concrete to the shear resistance of the slab. In this case, the Spanish Code does not fix any limit value but a minimum value for the reinforcement ratio should be 2% and preferably 2.5%. Besides, the crack width must always be less than 0.1mm."

Double composite bridges replaced steel composite bridges with fully prestressed slabs in German designs where creep and shrinkage resulted in "involuntary prestress of the steel top chord". The reinforcement in the top slab is substantial; mention is made that in the Caroni River (with a 24 cm thick top slab supported by steel cross girders spaced 3.75 m intervals) the reinforcement was 4.8% [1.8]. Such dense reinforcement resulted in higher shear strength.

To evaluate fatigue in high speed railway bridges, tests were carried out in Germany on two 6.8 m long 1.1 m deep girders under negative moments (Fig. 1.3). The 120 cm x 30 cm slab was reinforced longitudinally in three layers by twelve 18 mm diameter bars. This corresponds to 2.5% of the concrete section. After 2 million cycles, cracking in the slab was evenly distributed at 15 cm and did not exceed 0.2 mm.

The measured tensile stresses in the reinforcement and the girder were smaller than the calculated value for cracked concrete provided there were no shear connector failures. Following the fatigue test, the full plasticity of the girder was realized in ultimate load tests though further increases were not possible because of local instability of the bottom chord [1.8]. It should be noted that in Germany "Perfobond" shear connectors are used. These are plates with holes for rebars that can be welded directly to the flanges (Fig. 1.4).

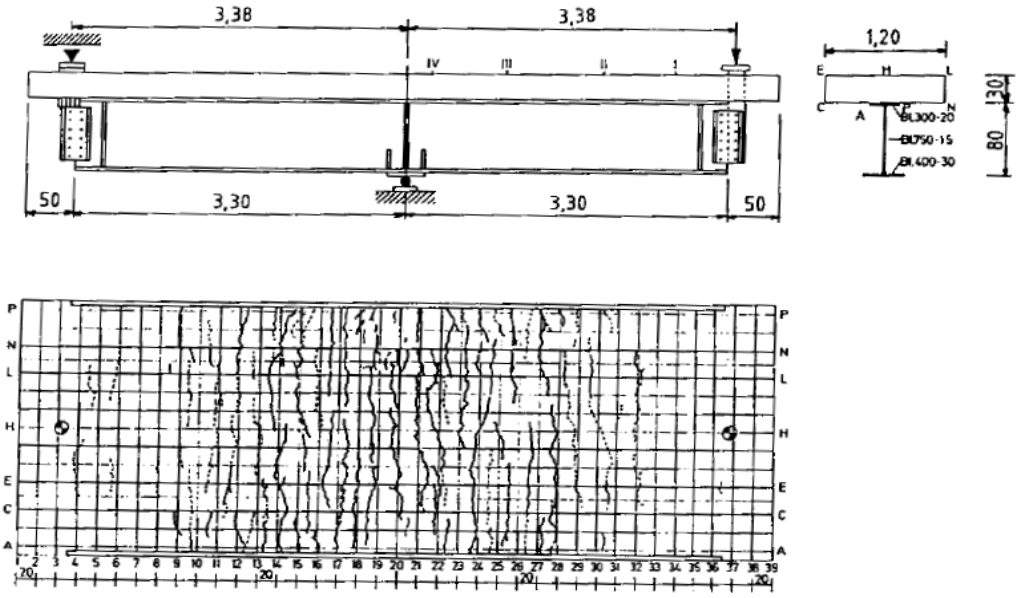


**Figure 1.3** Test Setup and Slab Cracking in Double Composite Girder Test [1.8]

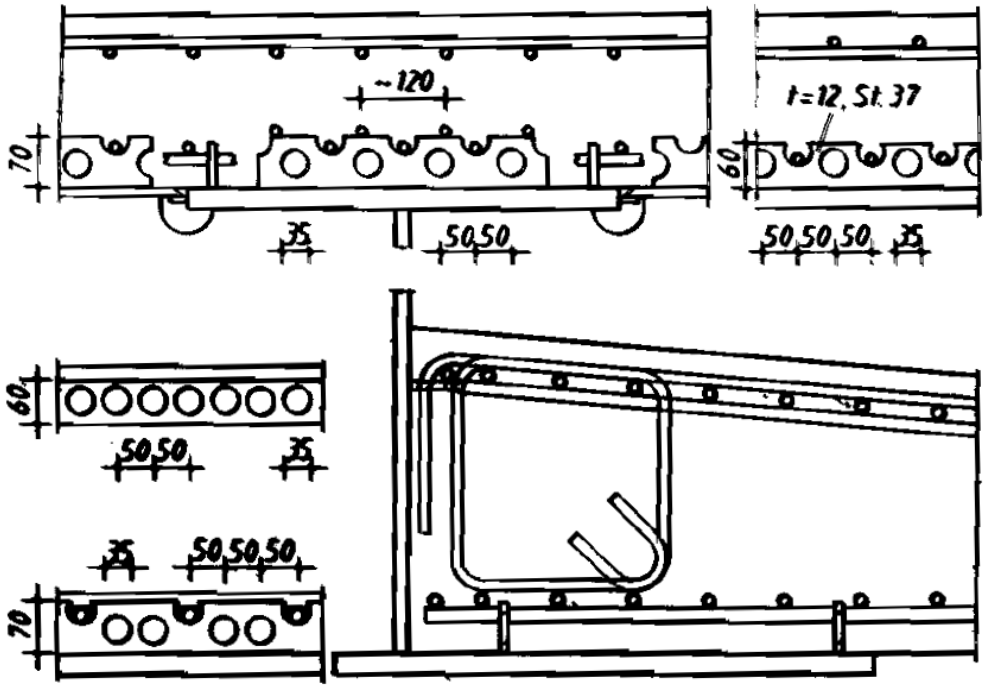


**Figure 1.4** Perfobond Shear Connectors [1.4]

In designing double composite cable stayed bridges [1.4] it was assumed that the *"dead weight of the steel structure and the concrete bottom chord act onto to the corresponding composite section; and that the weight of the concrete top chord acts onto the section of steel structure, concrete bottom chord and reinforcement of the top slab"*.

Two double composite box bridges were built over the St. John and Jemseg Bridges, on the Fredericton-Moncton Highway, Canada that was opened in 2001 (1.13, 1.16). The overall depth of the box is 3 m (see Fig. 1.5). The concrete bottom slab was poured and the combined system of bottom concrete slab and steel box girder launched (1.13).

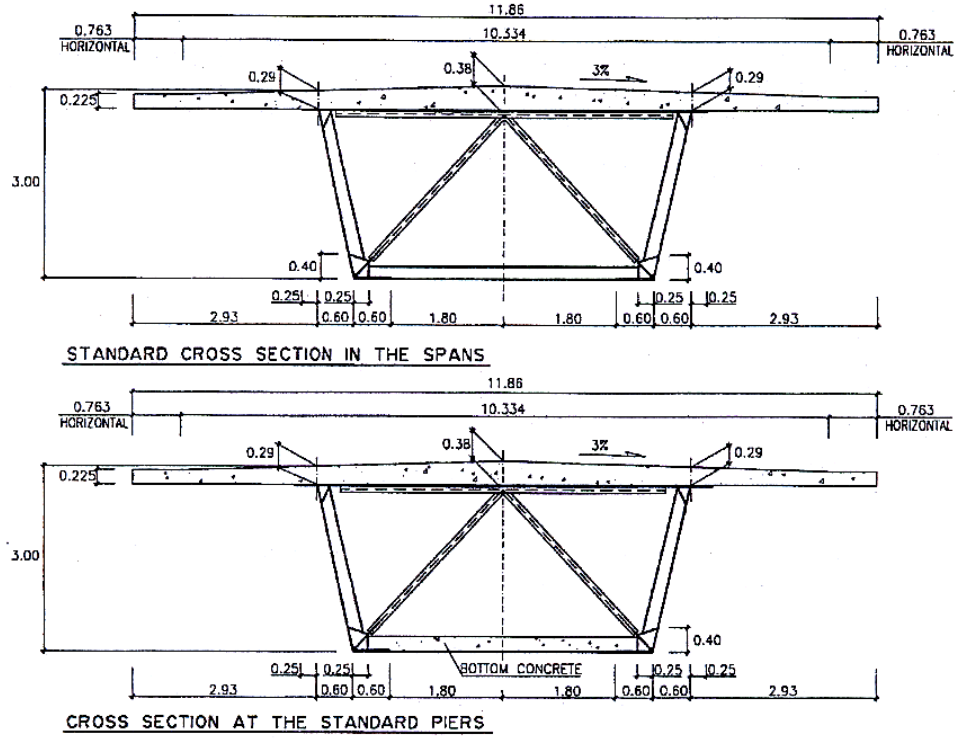


**Figure 1.5** Cross-Section of St John River Bridge, New Brunswick, Canada [1.13]

## 1.3 Objectives

The literature review indicates that though double composite construction has been successfully used for at least 25 years, details on design are sparse or conflicting. For example, the reinforcing steel provided in the top slab varied from 1% to 4.8%. In the only testing carried out, the reinforcement provided was 2.5%.

The proposed study is a cooperative effort between the University of South Florida, URS Corporation and Florida Department of Transport's Structural Research Center. The goal of the proposed project is to provide FDOT with the necessary evaluations, testing and verification to

allow implementation of the double composite concept in a future prototype project using high performance steel.

In order to meet the overall goal of this project, it was necessary to design and fabricate a prototype structure that could be tested under service, fatigue and ultimate load that would enable its structural response to be evaluated. Numerical analysis could then be used to extend the results of this study.

The principal objectives may be summarized as follows:

1. To design and fabricate a double composite box girder section using existing rules and to evaluate its performance under service, fatigue and strength limit states.
2. To conduct appropriate parametric design/analysis to optimize the performance of doubly composite box girders and establish new design criteria if required.
3. To develop a model example to illustrate the design of double composite box structures.

## 1.4 Organization of Report

This report has ten chapters and eight appendices. Chapters 2 to 4 provide information on the design, fabrication and instrumentation of the full-scale box specimen. The results from the fatigue, service and ultimate tests are summarized in Chapter 5-7 respectively. Finite element modeling and parametric studies to extend the experimental results are contained in Chapters 8. Rules for designing and construction of double composite bridges are presented in Chapter 9. An example design is contained in Chapter 10.

Nine appendices cover design calculations for the full-scale test specimen, material properties, instrumentation information, results from the fatigue, service, ultimate load tests, detailed information relating to the finite element analysis, and an alternative simplified failure analysis proposed by FDOT.

## References


1.1 Sen, R., Stroh, S., Olbinska, J., Hassiotis, S. and Mullins, G. (1999). "Development of a New Concept for Florida's Bridges, Vol. I & II." Final Report submitted to Florida Department of Transportation, January, pp. 350 (combined).

1.2 Stroh, S. and Sen, R. (2000). "Steel Bridges with Double-Composite Action: Innovative Design." Transportation Research Record, *Journal of the Transportation Research Board*, No 1696, Vol. 1, pp. 299-309.

1.3 Steel Bridge News (2003). "Development of a New Concept for Florida's Bridges." National Steel Bridge Alliance, Chicago, IL, Vol. 4, No. 4, p. 1, October.

1.4 Saul, Reiner (1992). "Longspan Bridges with Double Composite Action, Composite Construction in Steel and Concrete II." *Proceedings of an Engineering Foundation Conference*, June 14-19, Potosi, MO, Pub. ASCE New York, pp. 608-622.

1.5 Stroh, Steven (1994). "Design of a Double Deck Cable Stayed Bridge for Combined Highway and Railway Traffic." *Proceedings of the 10th Joint US-Japan Workshop on Performance on Strengthening of Bridge Structures and Research Needs*, Lake Tahoe, Nevada, May.

1.6 Martinez-Calzon, Julio (1995). "Strict Box Composite Bridges A New Design of the Optimum Use of Composite Topology." *Proceedings of the 12th Annual International Bridge Conference and Exhibition*, June 19-21, Pittsburgh, PA, Engineers' Society of Western Pennsylvania, pp. 258-264.

1.7 Stroh, Steven, and Lovett, Thomas (1995). "Kap Shui Mun Cable Stayed Bridge." *Proceedings of the Fourth International Bridge Engineering Conference*, Vol. I, Transportation Research Board, San Francisco, August, pp. 259-265.

1.8 Saul, Reiner (1996). "Bridges with Double Composite Action." *Structural Engineering International*, International Association for Bridge and Structural Engineering, Vol. 6, No 1, pp. 32-36.

1.9 AIAI (1996). "High Performance Steel Bridge Concepts." A Report Prepared for the American Iron and Steel Institute (AISI) by J. Muller International Bridge Engineering Consultants. Published by AISI, Washington, D.C., November.

1.10 Saul, Reiner (1997). "Design and Construction of Long Span Steel Composite Bridges in Composite Construction in Steel and Concrete III." *Proceedings of an Engineering Foundation Conference*, Irsee, Germany, pp. 700-712.

1.11 Saul, R. (1998). “Cost and Time Efficient Design and Construction of Steel and Steel Composite Bridges.” *Journal of Constructional Steel Research*, Vol. 46, No. 1-3, CD ROM.

1.12 Saul, Reiner (1998). “Steel and Steel Composite Bridges.” *New Steel Construction*, June/July, pp. 30-33.

1.13 Calzon, J.M. (1998). “Strict Box Composite Bridges: A Proposal for the Optimization of Materials.” *Developments in Short and Medium Span Bridges ’98*, Calgary, Canada, 1-16.

1.14 Thewalt, A., Troger, A., Rusch, A. and Wanzek, T. (2005). “Hermann-Liebmann Bridge in Leipzig - Construction Method with Spannverbund-Girder.” *Stahlbau* Vol. 74 No.9 September p 664-672 (in German).

1.15 Calzon, J.M. (2006). “The Miraflores Bridge Over the River Guadalquivir in Cordoba. Composite Construction in Steel and Concrete V.” July 18-23, Kruger National Park, Berg-en-Dal, Mpumalanga, South Africa, p. 467-476.

1.16 Calzon, J.M. (2006). “Puentes Estructuras Actitudes.” Turner, p. 164-165.

1.17 RPX-95 (1995). “Recommendations for the Design of Composite Road Bridges.” Ministerio de Fomento, Department of Roads, Madrid.

1.18 Private Communication (2006). Sen/Calzon, July 7.

# 2. TEST SPECIMEN DESIGN

## 2.1 Introduction

The primary focus of this study was to test the performance of a double composite steel box girder using a full-scale test specimen for three limit states; fatigue, service and strength. A full-scale specimen does not require scaling factors and is reasonably sized to simulate actual field conditions. The double composite steel box girder is envisioned as an economical alternate to conventional steel bridges or post-tensioned concrete I-girders for multi-span bridges having main spans ranging from 200 to 400 feet (e.g., water crossings). The preliminary size of the test specimen was based on an assumed bridge span arrangement of 170-212.5-170 feet. In order to test double composite action, the test configuration consisted of a simply supported beam with an overhang whereby a concentrated load applied downward at the free end would produce a "negative" moment at the center support. Sections 2.2 through 2.9 summarize the steps involved in the design of the test specimen.

## 2.2 Test Specimen Gross Dimensions

The gross dimensions and design capacity of the test specimen were primarily controlled by the space constraints and load generating capacity of the testing facility. Laboratory testing was performed at the Florida Department of Transportation Structures Research Center located in Tallahassee, Florida. Prior to the preliminary design phase, representatives of URS and USF met with FDOT personnel to discuss the facility and test equipment capacities. The facility consists of a large enclosed space that contained a reaction frame assembly as depicted in Fig. 2.1. The team initially anticipated using the reaction frame for testing and thereby established the size of the specimen accordingly.

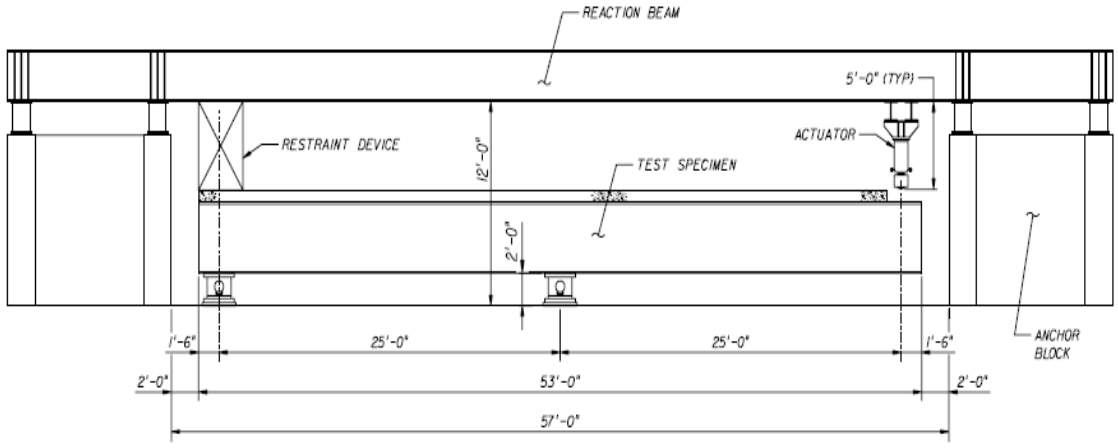


**Figure 2.1** Initial Testing Layout Using the Reaction Frame Assembly

The reaction frame assembly is supported by two anchor blocks (see Fig. 2.2a) separated by a clear space of 57 feet. In order to provide adequate clearance for setup and testing between the anchor blocks and the ends of the girder, the overall length of the test specimen was set at 53 feet. The beams of the reaction frame assembly were located twelve feet above the facility floor. The heights of the hydraulic actuators and the girder bearing assemblies are approximately five feet and two feet, respectively. Therefore, the maximum overall depth of the specimen was limited to five feet.

(a) (b) (c)

**Figure 2.2** Reaction Frame Anchor Block and Actuators

## 2.3 Testing Layout

The initial testing layout involved placing the test specimen symmetrically about a center support within the confines of the reaction frame assembly. An uplift restraint device and one or more load actuators attached to the reaction frame would then be applied 1ft. 6 in. from opposite ends of the girder, resulting in a 25 foot simply supported span and a 25 foot overhang (see Fig. 2.1). However, the final testing setup geometry was slightly different, whereby the reaction frame beams were removed and uplift was restrained by a floor-mounted hold-down assembly located 23 feet from the center support as shown in Fig. 2.3.

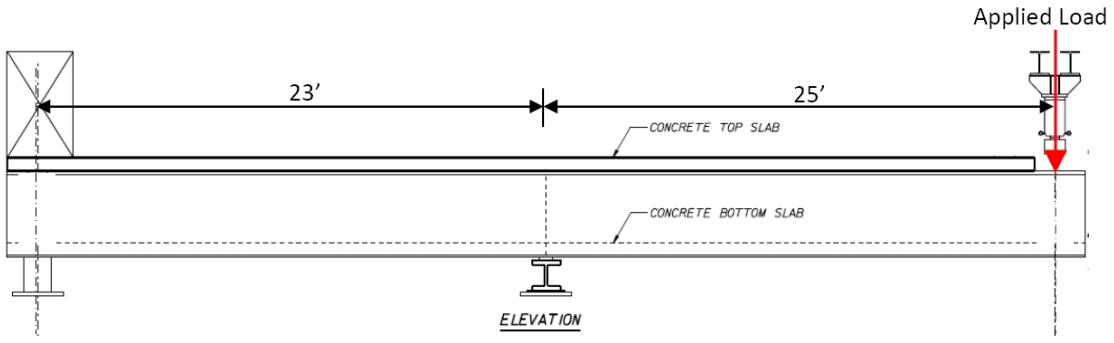


**Figure 2.3** Final Layout Testing

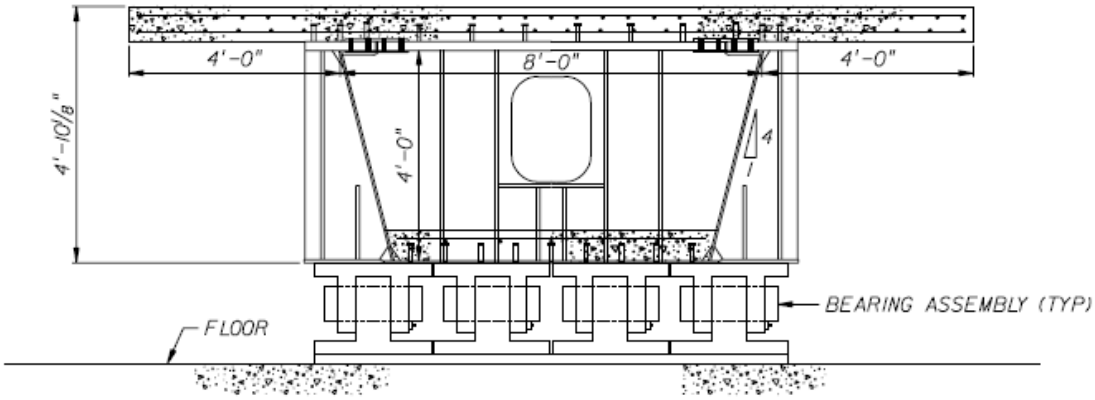


**Figure 2.4** Section View at Center Support

## 2.4 Capacity of Test Equipment

The loads for testing the performance of the specimen at service and strength limit states were applied by two 800 kip capacity hydraulic actuators (see Fig. 2.2b) outfitted with 600 kip load cells. A separate actuator having a capacity of 110 kips was used for fatigue testing (see Fig. 2.2c). However, the fatigue actuator loading was limited to between 5 kips and 105 kips in order to sustain a downward force on the specimen throughout all of the fatigue cycles.

The maximum girder uplift reaction was limited to 1200 kips based on the capacity of the hold down assembly installed in the floor of the testing facility. Therefore, based on the testing setup originally envisioned, the maximum bending moment that could be safely generated in the test specimen was 30,000 kip-ft. This would also produce a potential maximum center support reaction of 2400 kips. However, due to the strength limitations of the pin type bearing assemblies then available at the test facility, additional steel plates with bearing stiffeners were welded to the exterior of the test specimen box girder at the center support location, as shown in Fig. 2.4, to distribute the reaction force across multiple bearings. Note, however, that a different bearing assembly was ultimately used in place of the pin type bearings for the final testing setup.

## 2.5 Design Specifications

In order to provide a comparative analysis to traditional box girder designs, and to represent actual Florida bridges, the test specimen was designed using the Load and Resistance Factor Design (LRFD) method in accordance with the *AASHTO LRFD Bridge Design Specifications, 3rd Edition, 2004* [2.1] and *FDOT Structures Design Guidelines for LRFD, January 2005* [2.2]. A complete set of design calculations for the test specimen are presented in Appendix A.

## 2.6 Design of Box Girder

One goal of the project is to evaluate cracking of the top deck under service loads, therefore, the depth of the test specimen deck was set to the FDOT minimum bridge deck thickness of eight inches [2.1]. Using the AASHTO LRFD criteria for determining effective flange widths [2.2], a slab width of eight feet per web may thus be considered fully effective in composite action, resulting in a total slab width for the specimen of sixteen feet. Thereby, the center to center distance at the top of webs was set at eight feet (see Fig. 2.4). Considering the previously determined maximum section height of five feet, the interior height of the box was set at four feet, allowing for the 8 in. thick deck and the thicknesses of the top and bottom flange plates. Finally, the webs of the box girder were inclined at a typical 1:4 horizontal-to-vertical inclination resulting in a bottom flange width of six feet.

Once the general cross-section dimensions were established for the test specimen, attention turned to the selection of materials. High performance structural steel (HPS) of grade 70 ksi (ASTM A709) and reinforcing steel of grade 60 ksi (ASTM A615) were chosen for the design. HPS 70 steel was selected for the box since it was considered at the time to be more cost effective than HPS 50 for the anticipated span lengths. Furthermore, AASHTO LRFD permits members constructed with grade 70 steel and lower to be designed using plastic analysis[2.2], thereby providing additional economy.

The bottom steel flange and concrete slab thicknesses were based on several issues: economy, thru-thickness bending and deflection of the steel bottom flange. The primary advantage of the double composite system lies in reducing the thickness of the steel bottom flange and eliminating the bottom flange longitudinal stiffeners steel material by replacing it with a lower cost concrete material. Therefore, the bottom steel flange thickness was reduced as much as possible. The first consideration was the concrete strength. Potential field applications include water crossings, which the FDOT classifies as moderately aggressive or extremely aggressive environments[2.1]. For this type of environment, an FDOT Class IV concrete having a compressive strength of 5500 psi is applicable. Since concrete strength is based on minimum criteria, a 3400 psi compressive strength was specified anticipating that the average 28 day strength would be 5500 psi. The modular ratio (i.e., $E_s/E_c$) for 5500 psi concrete and HPS 70 steel is approximately seven; thus, a slab thickness of seven inches equates to a steel thickness of one inch when performing section property calculations. Realizing that actual concrete cylinder test results typically show 28 days strengths far greater than specified, calculations were performed using a “predicted” concrete strength of 7500 psi when computing the composite strength of the test specimen and testing equipment support reactions.

The steel bottom flange was initially sized using the deflection criteria presented in AASHTO LRFD [2.2]. It quickly became apparent that in order to utilize a thin steel bottom flange, temporary supports would be needed to minimize deflection and bending during placement of the bottom slab concrete. Temporary supports, consisting of WT’s, were installed transversely underneath the steel bottom flange at 3 ft.-0 in. spacing. This required extending the steel bottom flange two inches past the web/flange juncture to allow sufficient clearance for

bolting the WT's directly to the flange as shown in Fig. 2.5. The temporary bracing was subsequently removed after the bottom slab had cured.

**Figure 2.5** Temporary Support for Bottom Flange with Bolted Connections

As with concrete, literature regarding HPS 70 steel indicated that actual yield strengths were typically higher than specified, averaging around 80 ksi. In order to determine the final cross-section dimensions for the test specimen, several trial sections were analyzed using "predicted" material strengths of 7,500 psi and 80 ksi for the concrete and structural steel, respectively. The size of the top steel flanges was ultimately set at 16 in. x 1¾ in., and the thickness of the box girder webs was set at ¾ in. in order to meet AASHTO LRFD criteria related to web slenderness and member compactness [2.2].

Plastic moments for the test specimen, as determined using AASHTO LRFD equations [2.2] for the "design" and "predicted" material strengths, were 24,252 kip-ft. and 27,963 kip-ft., respectively. This resulted in approximately 7% reserve capacity in regards to the testing facility equipment, which was deemed to be sufficient when considering all the variables. A finite element model analysis also predicted comparable results.

## 2.7 Design of Shear Connectors

To ensure that the bottom concrete slab fully participated in composite action for negative bending, shear connectors were welded to the steel bottom flange as shown in Fig. 2.6. The shear connectors were designed to meet AASHTO LRFD strength and fatigue requirements [2.2]. Based on the thickness of the steel bottom flange, ¾ in. diameter studs were chosen in order to meet AISC specifications [2.3]. The first step of the design process was to determine the minimum number of shear connectors needed to satisfy strength requirements using the AASHTO LRFD equations. The transverse spacing of the connectors was established using the AASHTO LRFD equations for box girder top flanges [2.2].

In regards to fatigue, the primary testing constraint was the capacity of the fatigue actuator. Using the S-N curve equations from AASHTO LRFD [2.2], in conjunction with the actuator shear force range of 100 kips, the spacing and number of cycles were varied until a

reasonable solution was found (see Appendix D). These calculations were performed using section properties based on the “design” concrete strength. The number of cycles required to meet the fatigue resistance was initially calculated as approximately 8.3 million cycles. However, this was later reduced to 5.6 million cycles to account for the actual concrete strength (as determined through testing) and the increase in shear force range due to the change in the test span arrangement.

Similarly, the shear connectors affixed to the top flange of the test specimen box girder were designed to ensure that the top slab longitudinal reinforcement fully participated in composite action for negative bending.

**Figure 2.6** Shear Connectors and Interior Cross Frames

## 2.8 Design of Test Specimen Components

In general, test specimen components, including the cross frames and diaphragms, were designed for the failure load based on the predicted material properties. Furthermore, component loads were increased by 15% to ensure that the main member failed first.

Interior cross frames, as shown in Fig. 2.6, were located midway between the center support and the girder ends and were designed to brace the top flanges against the horizontal forces induced by the inclination of the webs, to permit fillet welds for the flange to web connections, and to maintain the shape of the box during loading. Additionally, full depth diaphragms were placed at the center and hold down support locations and were detailed with bearing stiffeners and access holes.

The loading cross frame at the actuator location was designed to resist fatigue as well as the service and ultimate limit state test loads. The concrete top deck slab was not poured at this

location in order for the actuator loads to be applied directly to the steel cross frame and top flanges. For fatigue loading, only one actuator was used which was applied to the midpoint of the top chord as shown in Fig. 2.7. The cross frame was completely detailed with bolted connections to eliminate any potential fatigue failure at the connections due to the high number of loading cycles required. In addition, the use of double angles allowed the connections to be concentrically loaded. The top and bottom chords of the loading cross frame were designed to withstand the horizontal forces created by the inclination of the box girder webs.

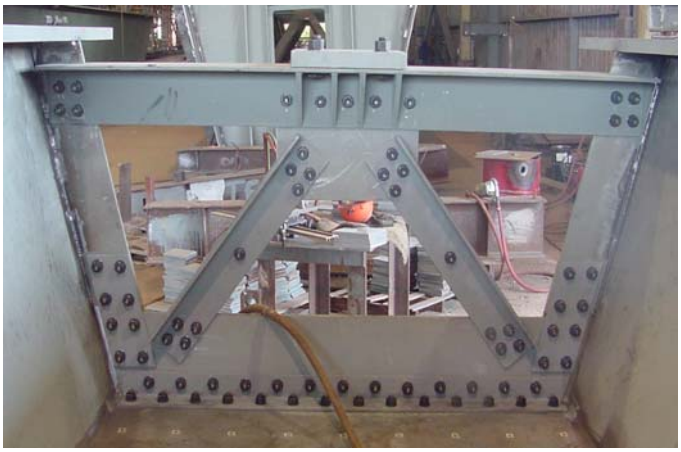

**Figure 2.7** Loading Cross Frame

The concrete top slab of the girder included steel reinforcing bars in both the longitudinal and transverse directions. In the longitudinal direction, the amount of reinforcement was determined based upon AASHTO LRFD minimum requirements [2.2], whereby, the total cross-sectional area of the longitudinal reinforcement shall not be less than one percent of the total cross-sectional area of the concrete deck. Additionally, the reinforcing steel is placed in two layers, with approximately two-thirds of the steel placed in the top layer. Applying these rules to a slab cross-sectional area of 1,536 in.$^2$ resulted in having thirty-three #5 bars and twenty-six #4 bars placed in the top and bottom layers, respectively. Transverse reinforcement was also used in the construction of the top slab based on AASHTO LRFD temperature and shrinkage criteria [2.2], and consisted of layers of #4 bars evenly spaced one foot apart. In regards to the bottom slab, the initial design called for welded wire fabric (WWF) reinforcement, but was later changed to #4 bars arranged both longitudinally and transversely using 18 inch spacing. The actual spacing is believed to be between 18in. to 22 in. longitudinally and 18 in. transversely.

## 2.9 Resonance

Lastly, a comparison between the natural frequency of the test specimen and the operating frequency of the fatigue actuator was made. For the test specimen, acting as a cantilever beam, the natural frequency was determined to be 128 Hz (see Appendix A), which is significantly greater than the operating frequency of 3 Hz for the fatigue actuator. Therefore, resonance was not an issue.

## References

2.1 FDOT Structures Design Guidelines (2005).Tallahassee, FL 2005.

2.2 AASHTO LRFD Bridge Design Specifications (2004). 3rd Edition, Washington, DC.

2.3 AISC (2006). Manual of Steel Construction, LRFD, 3rd Edition, Chicago, IL.

# 3. FABRICATION

## 3.1 Introduction

This chapter describes the fabrication of the double composite box girder section whose design was presented in the previous chapter. The 53 feet long steel box section was fabricated by Tampa Steel, Tampa, Florida and transported to the Structures Research Center in Tallahassee where the top and bottom concrete slabs were cast later. Section 3.2 provides an outline of the steps involved in fabricating the box specimen. Information on the casting of the top and bottom slabs is based on details provided by the Structures Research Center [3.1]. Section 3.3-3.4 summarizes the steps involved in the fabrication of the bottom and top slabs respectively.

## 3.2 Fabrication of Steel Box

High performance ASTM A709 grade 70 ksi steel (HPS 70W) was used in the fabrication of the box section. Material properties for this steel may be found in Appendix B. The dimensions of the steel plates (in inches) purchased from Burn Harbor Plate Inc. Cleveland, OH are 1.75 ×50×642 (top flange), 0.375×80×642 (bottom flange) and 0.75×102×642 (web). Fig. 3.1 shows the plates as-received.

The steel was cut to match the sizes of the flanges and webs. These were (1) Two top flanges 16 in. wide and 1.75 in. thick; (2) Two web plates 49.47 in. wide and 0.75 in. thick; and (3) a bottom flange of width 76 in. and 0.375 in. thick.


**Figure 3.1** HPS Steel Plates from Mill

The steps used in the fabrication of the box are summarized below and shown in Fig. 3.2-3.13 as follows:

1. Flange and web sections were cut out from the respective steel plates (Fig. 3.2).
2. Assembly of individual web/flange plates and their subsequent welding (Fig. 3.3-3.4).
3. Drilling of holes in the bottom flange for installation of temporary bracing to support the dead load of the bottom slab. WT 5×9.5 sections were bolted to the bottom flange at intervals of 3 feet (Fig. 3.5).
4. Assembly of complete box section (Fig. 3.6).
5. Fabrication and painting of diaphragms (Fig. 3.7-3.8) and their welded attachment to the box section (Fig. 3.9).
6. Fabrication and painting of bolted loading and intermediate cross-frame and their attachment to the box section (Fig. 3.10).
7. Attachment of ¾ in. diameter stud shear connectors to the top (Fig. 3.11) and bottom flanges (Fig. 3.12). The spacing and design criteria of shear connectors are included in Appendix A on pg-A.30. Fig. 3.13 is a view of the completed box shipped to Tallahassee in August 2006.

KTA-Tator Inc were contracted to provide quality assurance shop inspection services during the fabrication of the box section [3.2].


**Figure 3.2** Cut Pieces from Plates


**Figure 3.3** Assembly of Top Flange / Web

**Figure 3.4** SAC Welding of Top Flange/Web and View of Assembly Prior to Shot Blasting

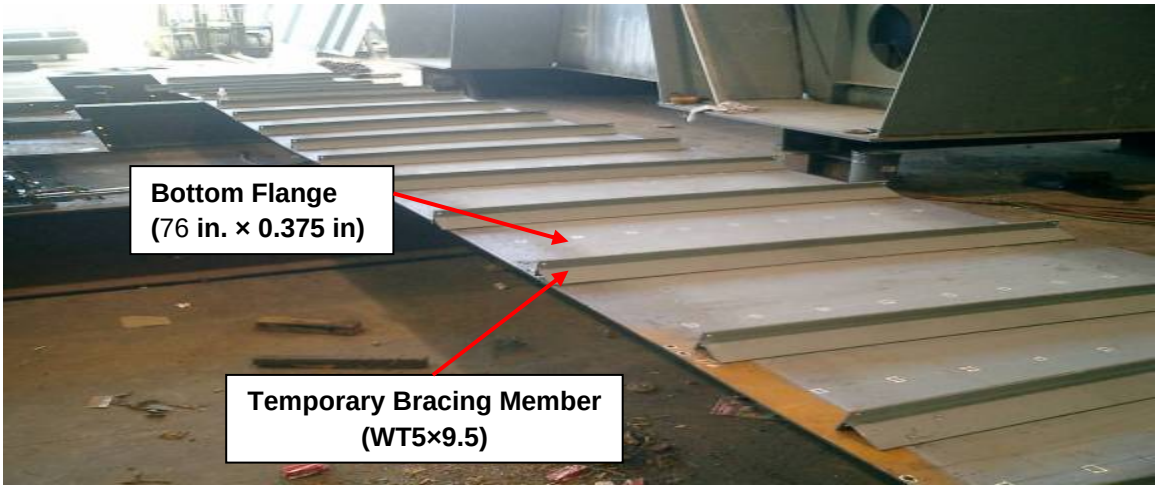


**Figure 3.5** Temporary Bracing of Bottom Flange

**Figure 3.6** Assembly of Steel Box Section

**Figure 3.7** Fabrication of Diaphragm

**Figure 3.8** Fabricated Painted Diaphragms

**Figure 3.9** Diaphragm Welded to Steel Box

**Figure 3.10** Loading and Intermediate Cross-Frame in Box Girder


**Figure 3.11** Close-up of Stud Shear Connector and Welding of Studs to the Top Flange

**Figure 3.12** View of Shear Connectors Welded to the Bottom Flange

**Figure 3.13** Steel Box Girder Ready for Shipment to Tallahassee

## 3.3 Placement of Bottom Concrete Slab

The bottom slab has to be cast prior to the top slab for two reasons; access and stability of the bottom flange. Placing the top slab prior to the bottom slab would severely restrict access to inside the box for concrete placement operations for the bottom slab. Furthermore, it would be unlikely that the steel bottom flange alone could resist the added stress due to the top slab weight and therefore the bottom concrete slab needs to be placed to stiffen and act compositely with the steel bottom flange. Consideration was given to using self-consolidating concrete but this was considered unsuitable for actual field conditions. Since self-consolidating concrete (SCC) has a high "flowability," it may be difficult to control the thickness of the pour due to the transverse and longitudinal grades that is inherent in an actual bridge. A total of 6.9 cubic yards of concrete was needed to achieve the 7 in. thick bottom slab.

The steps involved in the fabrication were as follows:

1. Support the soffit of the steel box at the center support and at the hold down end.
2. Place reinforcement in the bottom of the steel box (Fig. 3.14) on concrete blocks spaced 4 ft. on centers (Fig. 3.14).
3. Position two 2 in. × ⅜ in. flat plates on top of the bolsters to mark location of the top of the 7 in. and to provide a means for screeding (Fig. 3.14).
4. Place concrete using a vibrator and wooden screed board (Fig. 3.15).
5. Remove steel plate once the concrete hardened. Grout was placed to fill in the grove created by the flat plate.

It was very difficult to place the bottom slab concrete due to the confined space and because there was nothing solid to screed against. These constructability issues could potentially create problems and hinder the quality work needed. This is addressed in Chapter 9.

## 3.4 Placement of Top Concrete Slab

The steps involved in the fabrication were as follows

1. Support the soffit of steel box at the center support, hold down end and the actuator end.
2. Install stay-in-place forms in accordance with manufacturer's drawings (Fig. 3.16).
3. Construct and install overhang hang brackets to support cantilevered portion of the slab at 2 ft. on centers (Fig. 3.16).
4. Complete formwork for 8 in. slab.
5. Place reinforcement on the top of the stay in place forms as per the design (Fig. 3.17).
6. Place concrete using a vibratory screed board (Fig. 3.18).

Two concrete trucks were needed to place all the concrete. Cylinder tests (Table B.1 on pg-B.2 in Appendix B) showed that the strength of the concrete in the actuator span (see Fig. 3.19) was higher than that of the hold-down span. The top slab was cast on Dec 12, 2007, which was about 5 months after casting the bottom slab (cast on July 17, 2007). This information was used for estimation of shrinkage strains in the top and bottom slab in subsequent analysis.

**Figure 3.14** Reinforcement for Bottom Concrete Slab

**Figure 3.15** Pouring of Bottom Concrete Slab

**Figure 3.16** Stay in Place Forms and Overhang Brackets for Top Slab

**Figure 3.17** Reinforcement for Top Concrete Slab


**Figure 3.18** Pouring of Top Concrete Slab


**Figure 3.19** Top Concrete Slab

## References

3.1 Potter, W. (2008). “Double Composite Slab Placement.” WORD file, Structures Research Lab, FDOT, Tallahassee.

3.2 KTA-Tator, Inc. (2008). “Final Report: Field Inspection Report.” Austin, Texas.

# 4. INSTRUMENTATION

## 4.1 Introduction

The full-scale double composite box girder beam described in the previous chapter was subject to two series of tests. In the first series, a fatigue test was conducted while in the second series three sets of service load tests were carried out. A planned ultimate load test could not be undertaken because the specimen failed during the final service load test.

The load set-up was identical for both series and consequently, the instrumentation was also similar. However, because of the much larger loads required in the service and ultimate load tests, the configuration of the center support differed.

This chapter provides an overview of the test program and provides details of the test program and instrumentation scheme that is referenced in subsequent chapters. Section 4.2 describes the test program and Section 4.3 presents the basis and details of the instrumentation that was used in the testing. Location of gages are based on information provided by FDOT [4.1-4.2].

## 4.2 Test Program

As noted in the literature review, a number of double composite bridges were built primarily in Europe on the basis of prevailing codes. However, it was not known whether their provisions were valid and whether problems would arise under service conditions. Therefore fatigue and service tests were carried out on the full-scale test specimen to address these concerns.

### 4.2.1 Fatigue Test

The fatigue test was conducted as there was no prior experimental data available on the performance of double composite bridges under fatigue loading. This was important because of the very thin (⅜ in.) bottom steel flange used. The welding of shear studs to such a thin bottom plate (to ensure composite action) can induce deformation and localized stresses that may be unfavorable under fatigue loading.

The intent of the test was to verify the applicability of AASHTO [4.3] provisions for the design of shear connectors and to document the performance of stud shear connectors in the negative flexure region. The load range used in the testing was dictated by the capacity of the actuator and varied from 5-105 kips. The corresponding number of cycles (5.65 million) was calculated in accordance with AASHTO LRFD Bridge Design Specifications.

### 4.2.2 Service Test

The top concrete slab was designed to current AASHTO specifications with the longitudinal reinforcement ratio set at 1%. It was not known whether a higher limit was necessary since compact double composite sections can support higher loads. Tests were therefore conducted to evaluate three AASHTO specified service loads, referred to as Service I, Service II and Service III. Critical parameters in these tests were the stresses in the rebar, stresses in the concrete and steel, and the maximum crack width.

Under Service I, the stresses in the rebar were targeted to $0.6f_y$. Service II loads were targeted to $0.95F_y$ in the top steel flange, with $F_y$ taken as 50 ksi. This was intended to represent performance of normal grade structural steel. The final service load test, Service III targeted the stress in the top steel flange at $0.95F_y$, with $F_y$ taken as 70 ksi to represent the high performance steel (HPS) used for the specimen. The loads corresponding to these three service conditions were respectively 421 kips, 638 kips and 894 kips. In each series, the loads were planned to be applied five times. A final ultimate load test corresponding to a 1200 kip load was planned following the conclusion of the service tests. Details of the test program are summarized in Table 4.1

**Table 4.1** Test Program

| Description | Load (kips) | Criteria | Critical |
|---|---|---|---|
| Fatigue | 5-105 | 5.65 million cycles | Slip, changes in stiffness |
| Service I | 421 | 0.6 $f_y$ stress in rebar | Crack width, stresses in rebar, steel and concrete, and deflections |
| Service II | 638 | 0.95 $F_y$ in top steel flange based on Grade 50 steel | Crack width, stresses in rebar, steel and concrete, and deflections |
| Service III | 894 | $0.95F_y$ in top steel flange based on HPS ($F_y$= 70 ksi) | Crack width, stresses in rebar steel and concrete and deflections |
| Ultimate | 1200 | AASHTO | Failure mode, ductility |

*Test Set Up*

Fig. 4.1a shows the load set-up envisaged originally in which the section is centrally supported with a load applied at one end and the section held down at the other end. However, because of space constraints, this arrangement was found to be unworkable and an alternative scheme was adopted in which the specimen was loaded asymmetrically with a simple span of 23 ft. and a cantilever span of 25 ft. as shown in Fig. 4.1b.

*Center Support*

Because of the significantly higher loads encountered in the service load tests, the center support differed for the two test series. For the fatigue test, the box section was supported across its entire width by a 7 in. wide, 1½ in. thick neoprene pad that rested on a W14 x 370 section as shown in Fig. 4.2 (left) below. This was replaced by a semi-circular 4 in. diameter cylinder support that also extended over the entire width of the section in the service tests and rested on

several longitudinally oriented deep structural steel members that distributed the reaction loads over the floor of the test facility (Fig. 4.2 right).

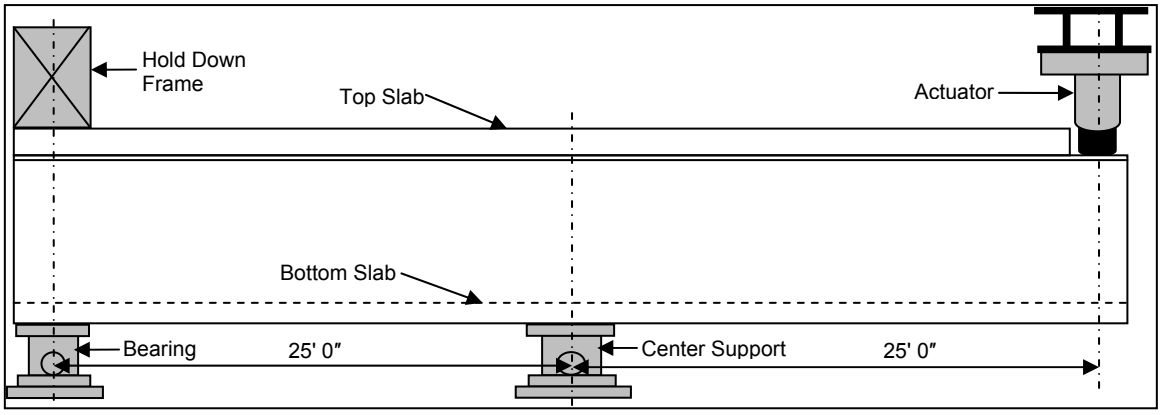


**Figure 4.1a** Test Set Up As Designed

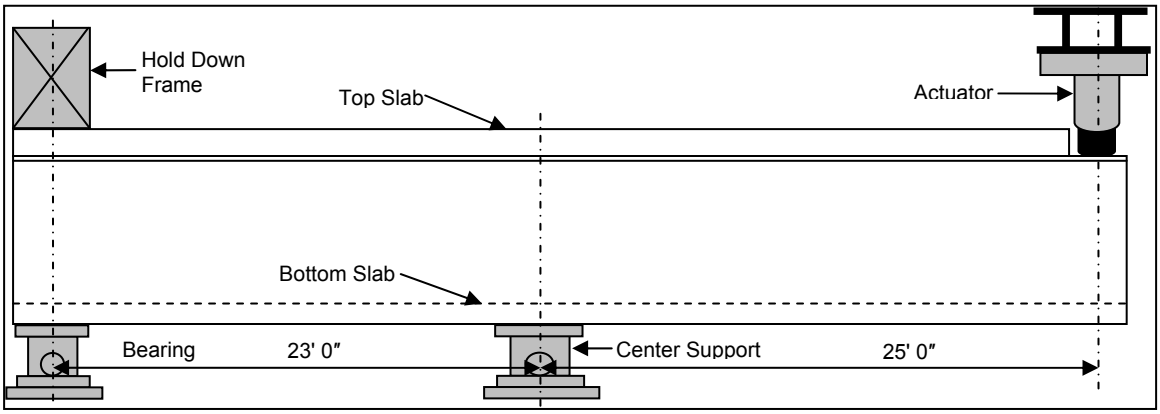


**Figure 4.1b** Actual Test Set-Up

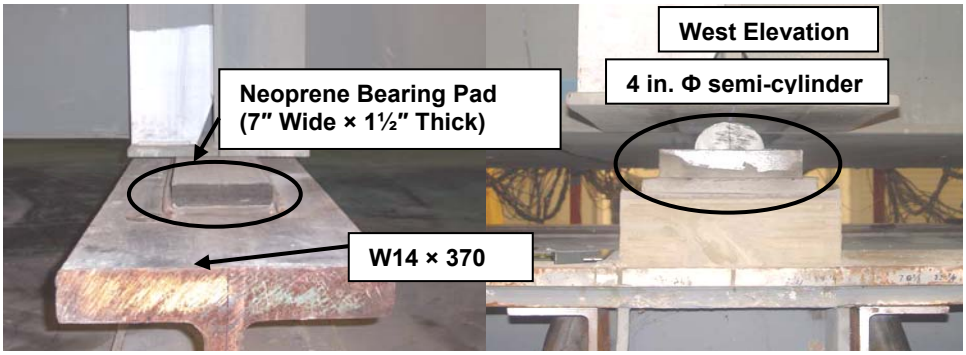


**Figure 4.2** Center Support for Fatigue and Service Load Test

## 4.3 Instrumentation

The instrumentation was designed to address the critical needs from the testing summarized in Table 4.1. A total of 140 sensors were used in the fatigue testing and 162 sensors in the remaining tests. Details are summarized in Table 4.2.

**Table 4.2** Instrumentation Summary

| Type | Location | Fatigue | Service | Comment |
|---|---|---|---|---|
| Load Cells | Hold Down End | 2 | 2 | No load cell at the center support |
| | Load End (Cantilevered End) | | 2 | |
| Slip | Hold Down End | 4 | 4 | Fig. 4.7 |
| | Load End (Cantilevered End) | 5 | 5 | Fig. 4.6 |
| Deflection | 2 @ Load End 4 @ center<br>2 @ Hold Down End | 8 | 8 | Fig. 4.12 |
| | 2 each @ 2 ft. ¼ in. from center symmetrically under bottom flange | None | 4 | These sensors were not provided in the fatigue tests to prevent fatigue damage and also because the top slab was not expected to crack for the applied load range<br>Fig. 4.12<br><br>Fig. 4.15 and Fig. 4.16 |
| | 1 each @ 6 ft. 3 in. from center symmetrically | | 2 | |
| | 1 each @ 12 ft. 6 in. from center symmetrically | | 2 | |
| | 1 each @ 18ft. 9 in. from center symmetrically | | 2 | |
| | 1 each at center support under top flange symmetrically | | 2 | |
| | 2 each under top flange 12 ft. 6 in. from the center support symmetrically | | 4 | |
| Crack Gages | Two locations where maximum crack developed under fatigue loading on either side of the center support | | 4 | |
| Rebar Strain | 16 longitudinal bars located 1 ft. away on either side of the center support | 32 | 32 | Includes "8 spare" but all channels worked Fig. 4.17– 4.18 |
| Top Concrete Slab | 5 @ center line of intermediate support symmetrically. 5 @ 4 ft. 10⅛ in. from center sym. 1 each @ 11 ft. 6 in. from center symmetrically. | 17 | 17 | Invalid data due to cracking |
| Bottom Concrete Slab | 3 @ 4 ft. 10⅛ in. from center support symmetrically<br>1 each @ 11 ft. 6 in. from center symmetrically<br>2 each 1 ft. from the hold down end and the loaded end | 12 | 12 | Fig. 4.19 and Fig.4.20 |
| Steel Box | | | | |
| Top Flange | 2 over center support<br>2 each distance 4 ft. 10⅛ in. from center support sym.<br>2 each @ 11 ft. 6 in. from center symmetrically | 10 | 10 | Fig. 4.19 and Fig. 4.20 |
| Web | 6 exterior, 3 interior at 4 ft. 10⅛ in. sym from center support | 36 | 36 | Fig. 4.19 and Fig. 4.20 |
| Bottom Flange | 1 @ 2 ft. ¼ in. from center support sym.<br>3@ 4ft. 10⅛ in. sym w.r.t. center support<br>1 each at 11 ft. 6 in. from center support<br>2 each 1 ft. from holding/loading end | 14 | 14 | Fig 4.19 and Fig 4.20 |

Since all 17 strain gages bonded to the top surface of the concrete slab were damaged, these were not monitored. As a result, 123 channels were actually monitored for the fatigue test and 145 channels monitored for the three service load tests.

### 4.3.1 Loading Rate

The fatigue load was cycled at 1.16Hz so that 100,000 cycles could be completed each day. The service load was incremented at a constant rate of 1 kip per second.

### 4.3.2 Description of Loading Frame

Fig. 4.3 is a view of the centrally supported test specimen; the hold down and actuator ends are in the north-south direction. The east and west orientations are also marked in this photo since they are referred to later on.

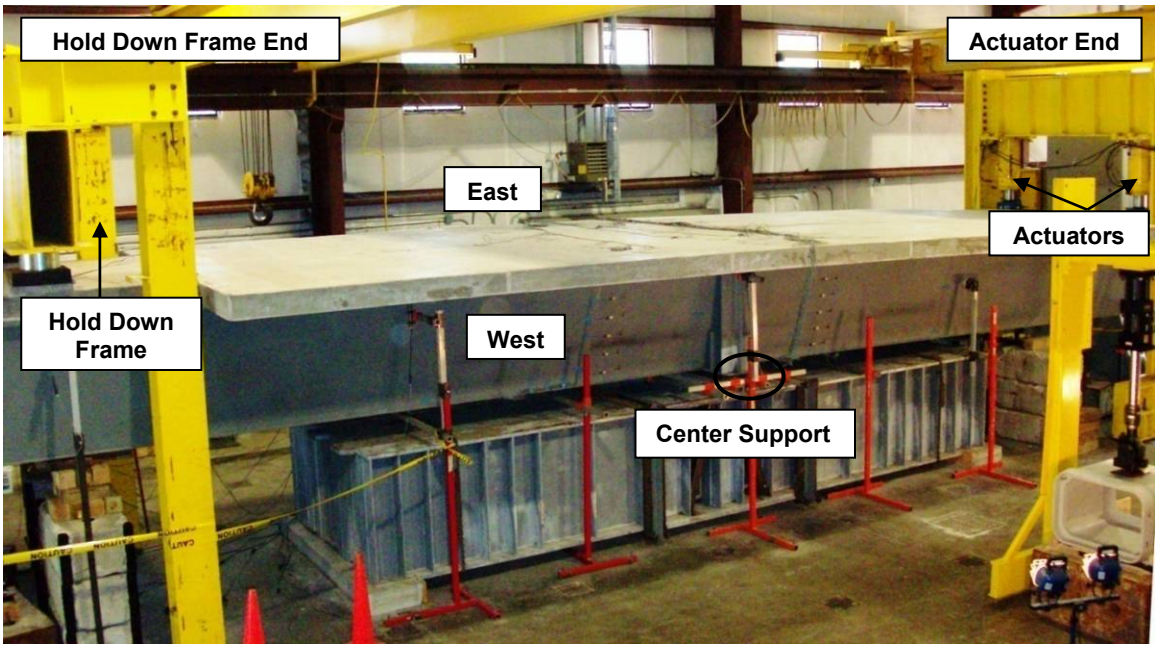


**Figure 4.3** Service Test Set–Up

### 4.3.3 Load Cells

The two load cells used to monitor reactions at the hold down end are shown in Fig. 4.4. The MTS System has a built-in load cell that was also monitored and recorded to the files. However, they were used in the service load tests and are shown in Fig. 4.5.

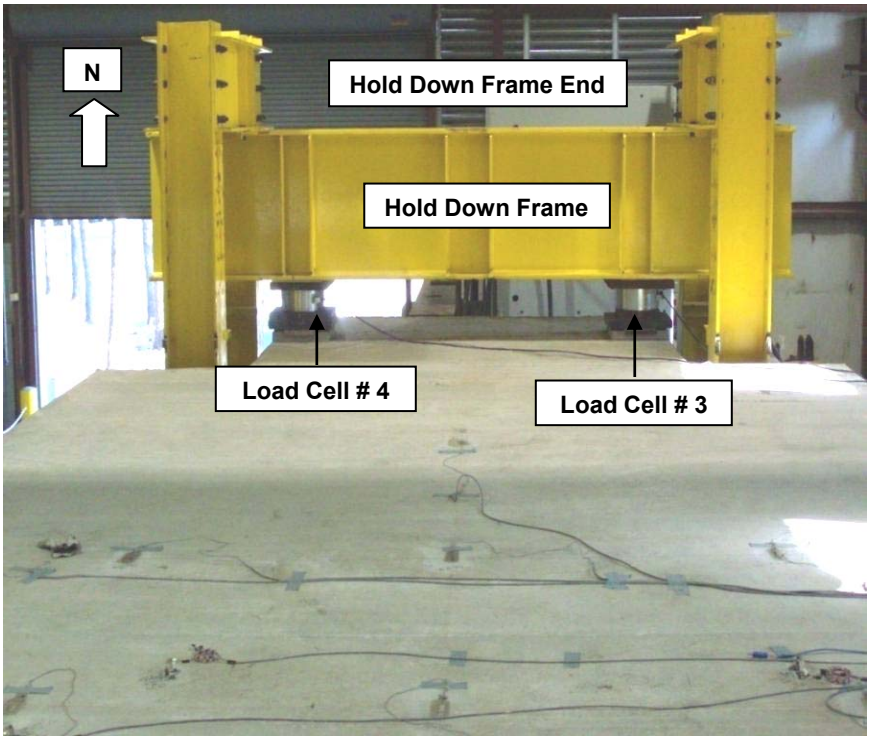


**Figure 4.4** Load Cells at Hold Down Frame End

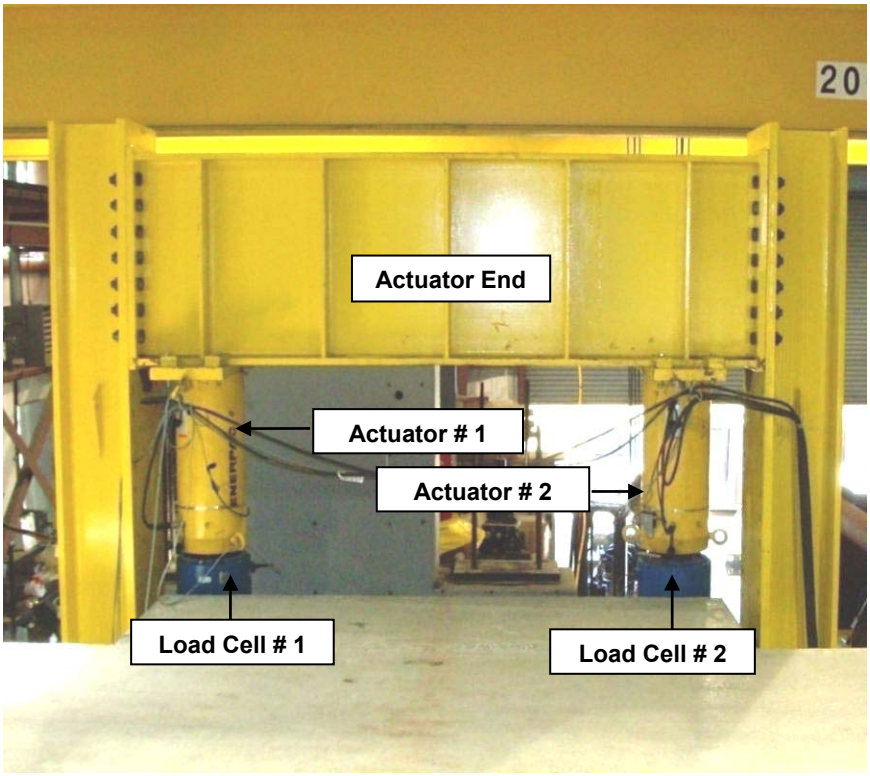


**Figure 4.5** Load Cells at Actuator End

### 4.3.4 Slip

The extent of the composite action in both the top and bottom sections was monitored at the actuator end (Fig. 4.6) and the hold down end (Fig. 4.7) for both fatigue and service load tests. As shown in these figures, slip was monitored at five locations (LVDTs 30, 31, 34, 35, 36) at the actuator end (Fig. 4.6) and four locations (LVDTs 32, 33, 37, 38) at the hold down end (Fig. 4.7).

In each case, the relative movement of the top or bottom concrete slab was recorded with respect to steel locations that were available, e.g. Fig. 4.8, Fig. 4.9 or by using appropriately attached rigid steel members Fig. 4.10 or Fig. 4.11.

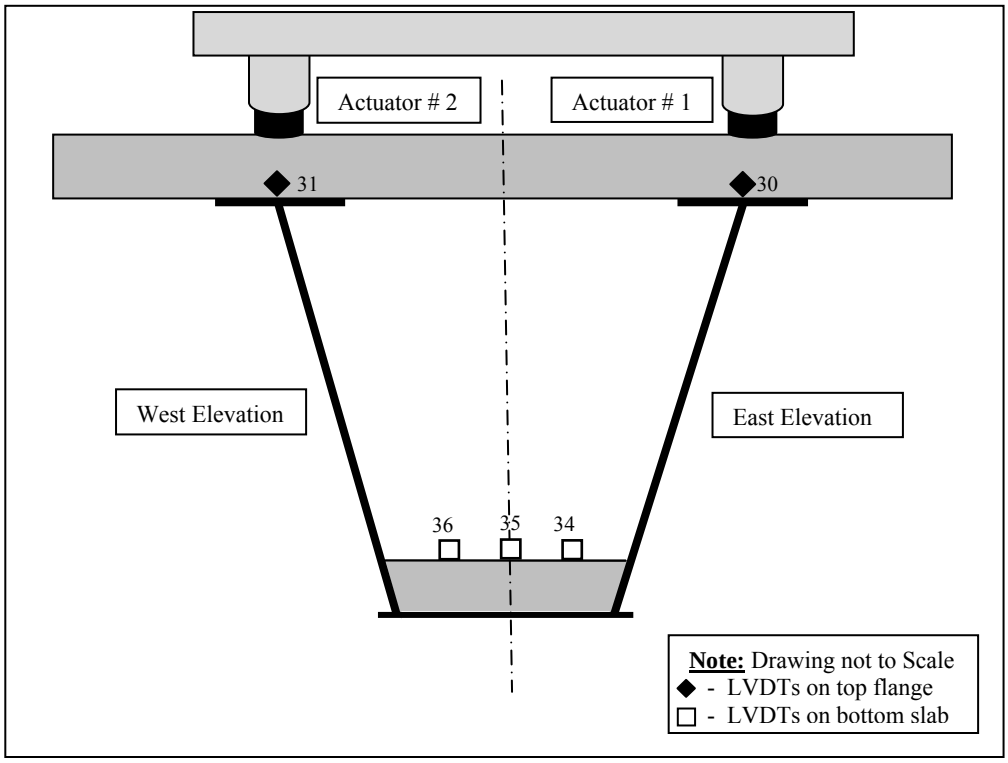


**Figure 4.6** Slip at Actuator End

### 4.3.5 Deflection

Deflections were monitored at critical locations in both the fatigue and service tests. Deflections were measured at 8 locations in the fatigue test and at 24 locations in the service tests. The role of the measurements was not only to asses the deflection caused by the loads along the span but also to monitor movement of the compression flange close to the support, movement of the center support and any twisting effects induced by the loading.

Fig. 4.12 and Fig. 4.13, show the plan and elevation layout of LVDTs measuring deflection for service load test. Sixteen of the 24 LVDTs monitored movement of the bottom flange while the remaining 8 monitored movement of the top flange.

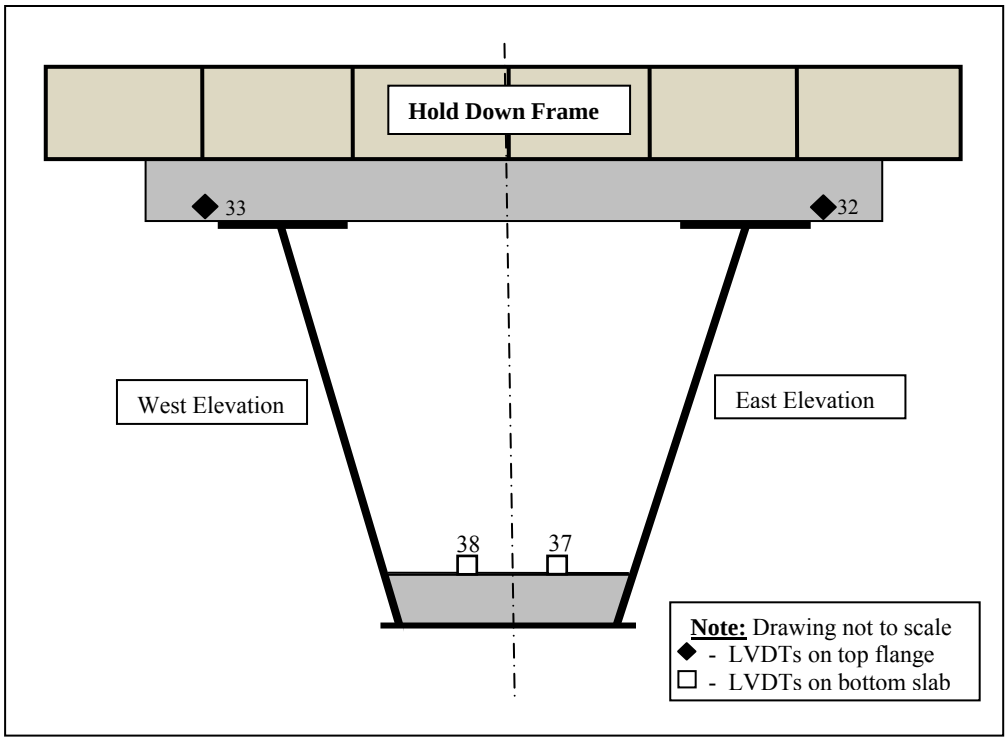


**Figure 4.7** Slip at Hold Down End

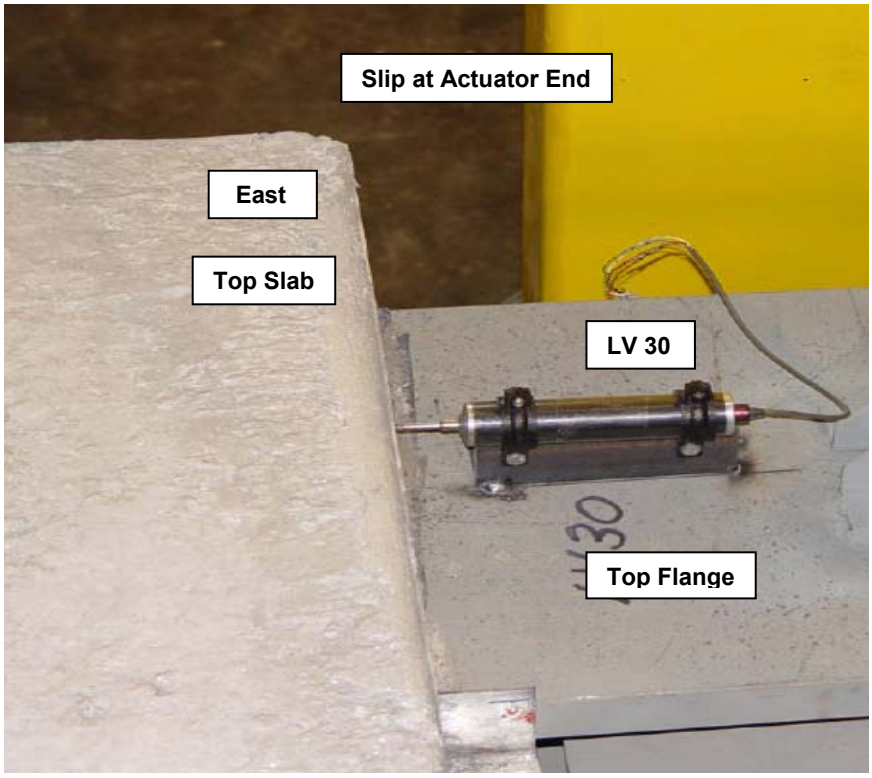


**Figure 4.8** Slip at Top Slab at Actuator End

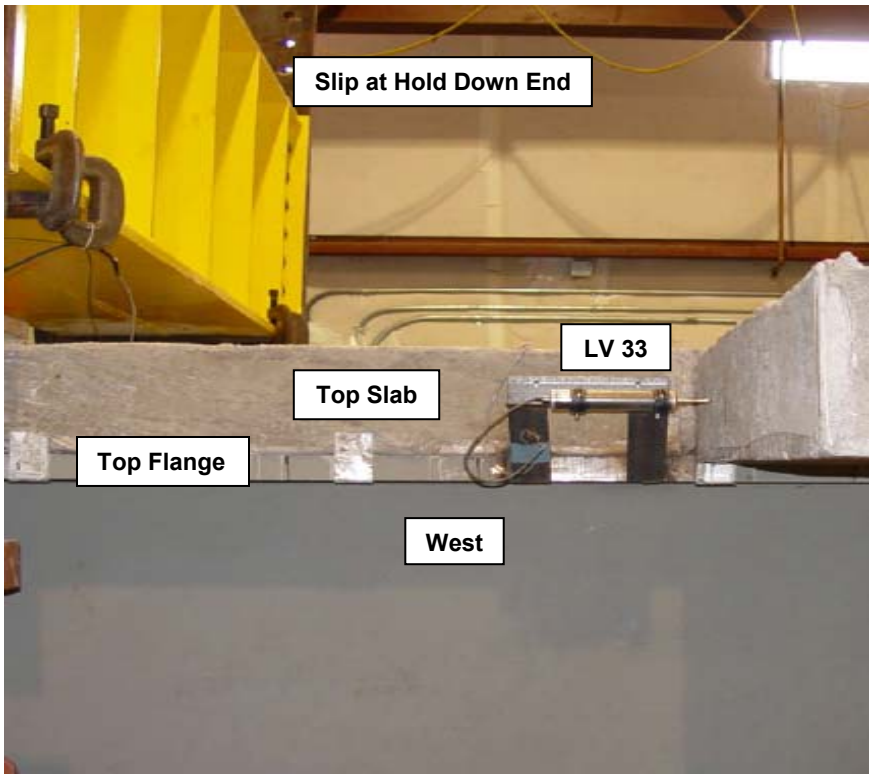


**Figure 4.9** Slip at Top Slab at Hold Down End

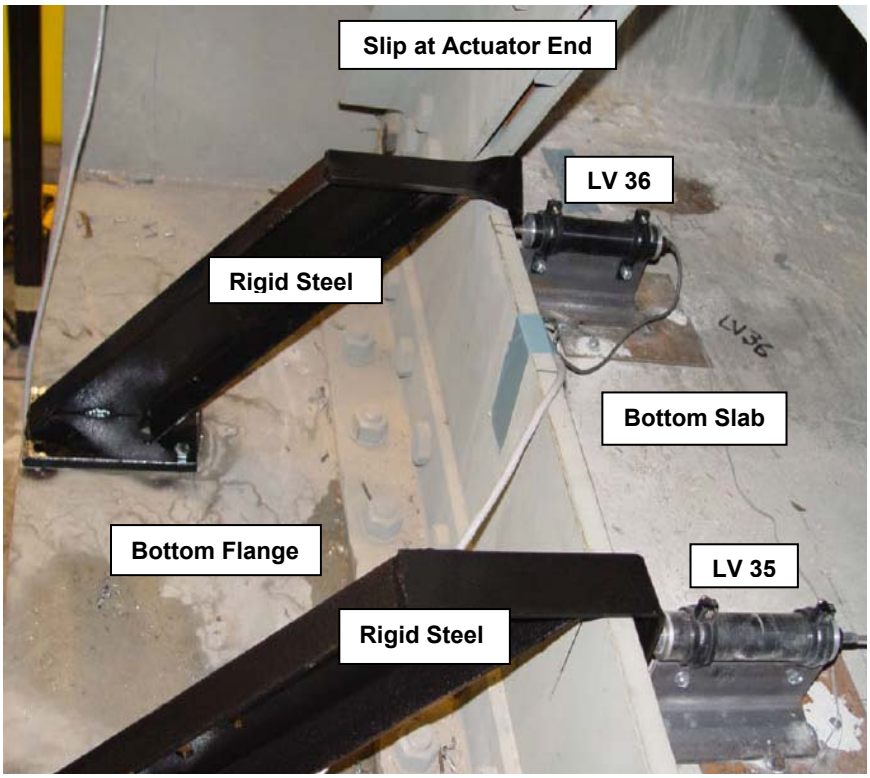


**Figure 4.10** Slip at Bottom Slab at Actuator End

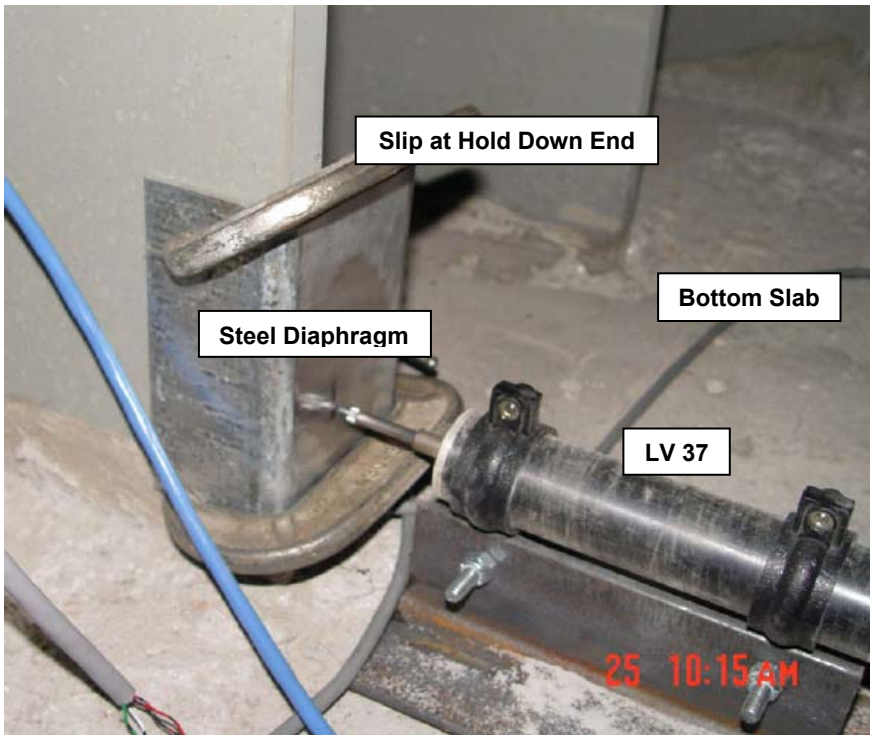


**Figure 4.11** Slip at Bottom Slab at Hold Down End

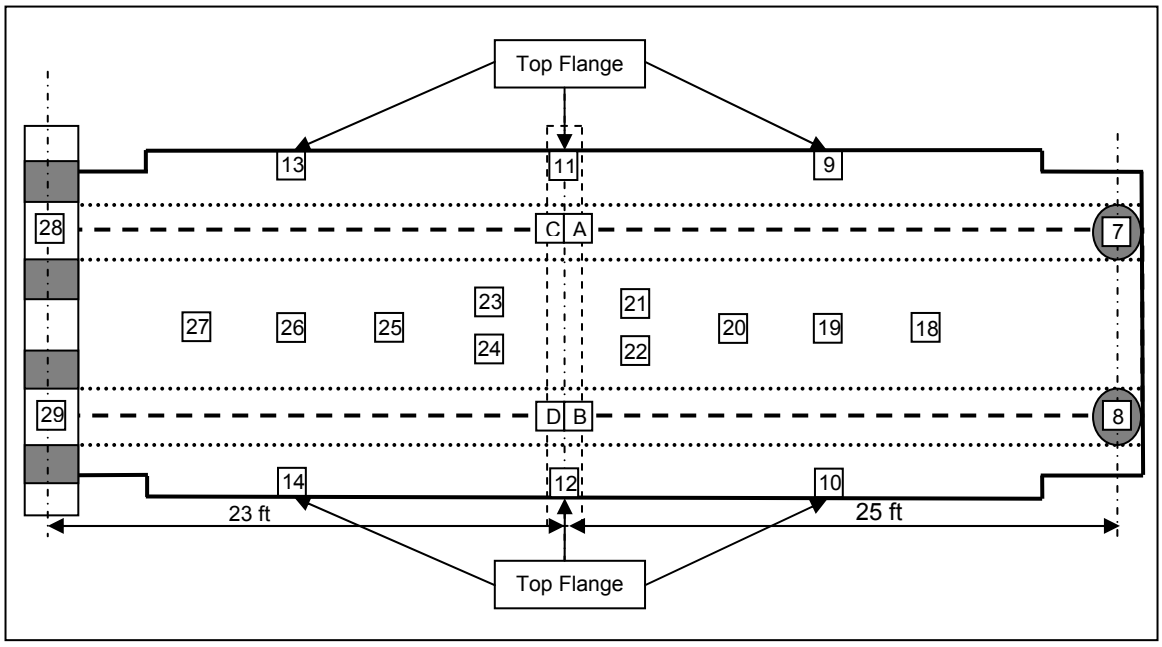


**Figure 4.12** Plan View of LVDTs Recording Deflection

The most critical deflection measurements were by LVDTs numbered 21, 22, 23 and 24, which were located 2 ft. ¼ in. on either side of the center support (shown in Fig. 4.12 and Fig.

4.14). LVDTs 23 and 24 became important because the bottom flange buckled in that region. The maximum deflection was recorded by LVDTs 7 and 8 located at the cantilevered free end.

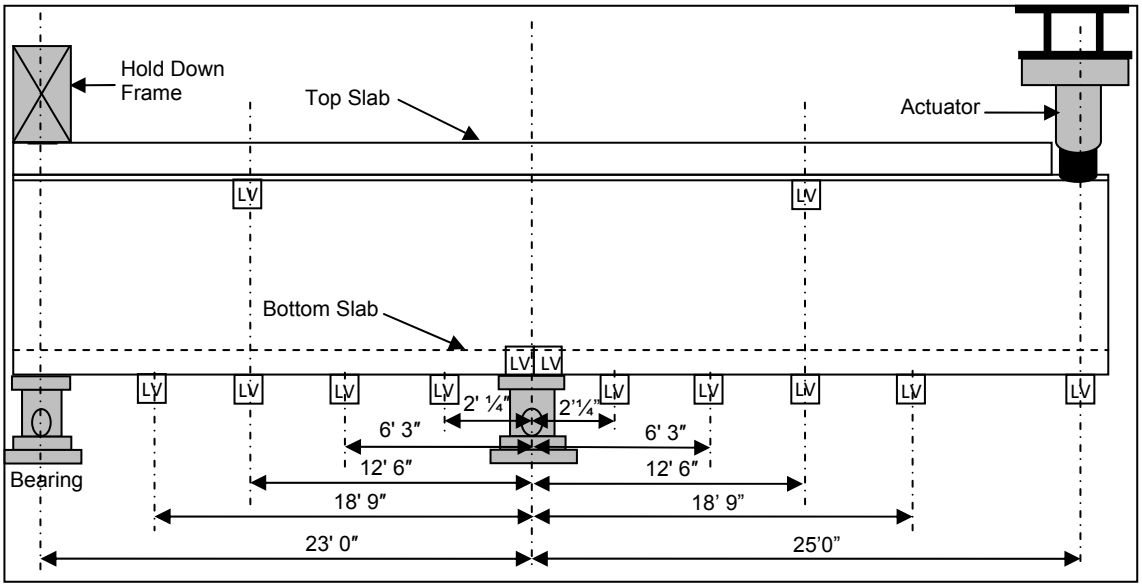


**Figure 4.13** Elevation Layout of LVDTs Recording Deflection

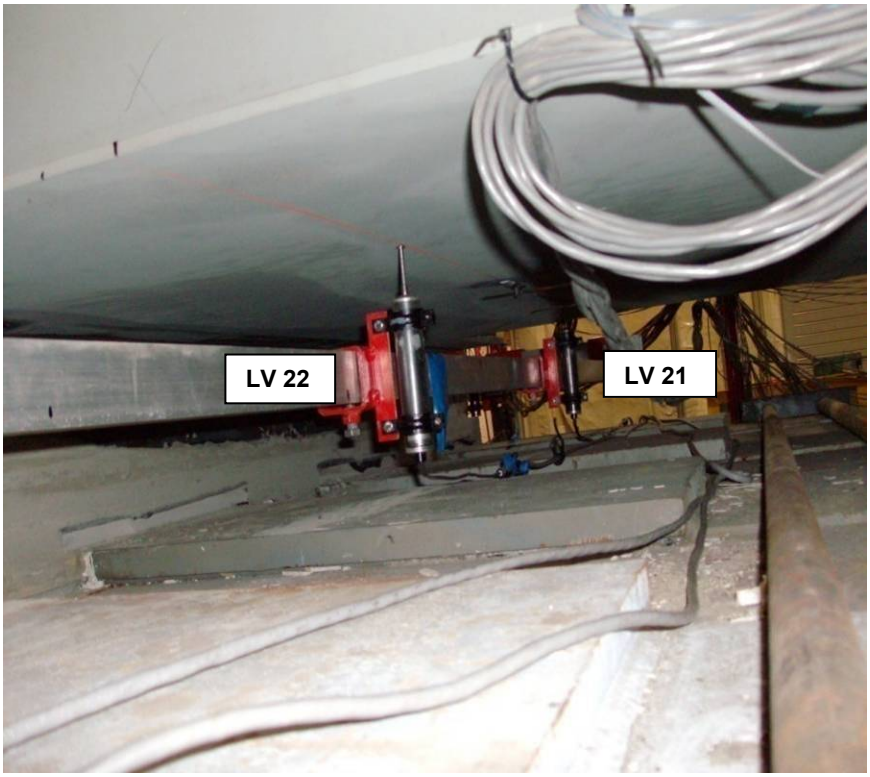


**Figure 4.14** Deflection at 2 ft. ¼ in. from Center Support on Actuator Side

### 4.3.6 Crack Width

Crack gages were installed following the completion of the fatigue test when the locations for the maximum crack width were known. These were installed at four locations, two each at 1ft. either side of the center support. The final crack width was determined by adding the initial crack width to the electronically measured crack width. Fig. 4.15 and Fig. 4.16 show the position of these gages relative to the cross-section for both the hold down and actuator spans.

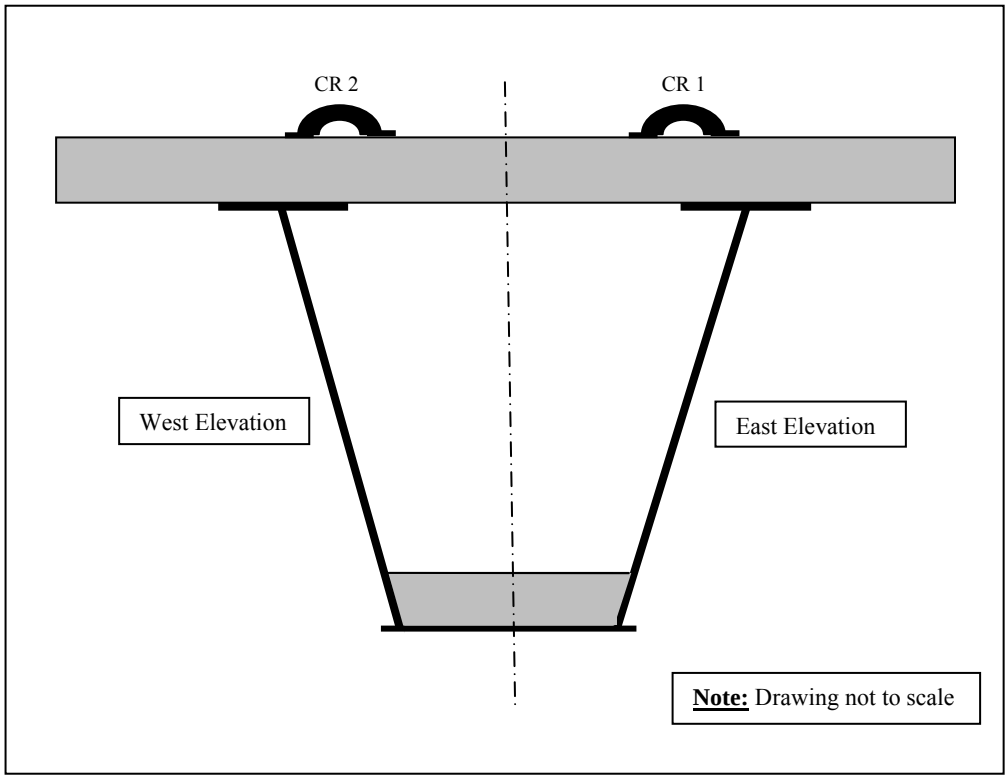


**Figure 4.15** Crack Width Gages on Actuator Side

### 4.3.7 Rebar Strain

Rebar strain is a critical parameter since it dictates crack-width under service loads. In the original instrumentation plan, 12 longitudinal bars were instrumented 1 ft. from the center support in both the hold down and actuator spans. It was thought that the likelihood of malfunction was high since these gages are subjected to wet concrete during the slab casting, and consequently four additional bars were instrumented as a safeguard. However, all 24 gages and the eight spares worked so rebar strain was monitored at 32 locations in all.

Fig. 4.17 and 4.18 show the layout of the gages. For clarity, they have been re-numbered as 1-16A and 1-16 in these drawings instead of 57A or B – 68 A or B, where A represented the actuator side and B represented the hold down side. This numbering is retained in the results presented in Chapter 6.

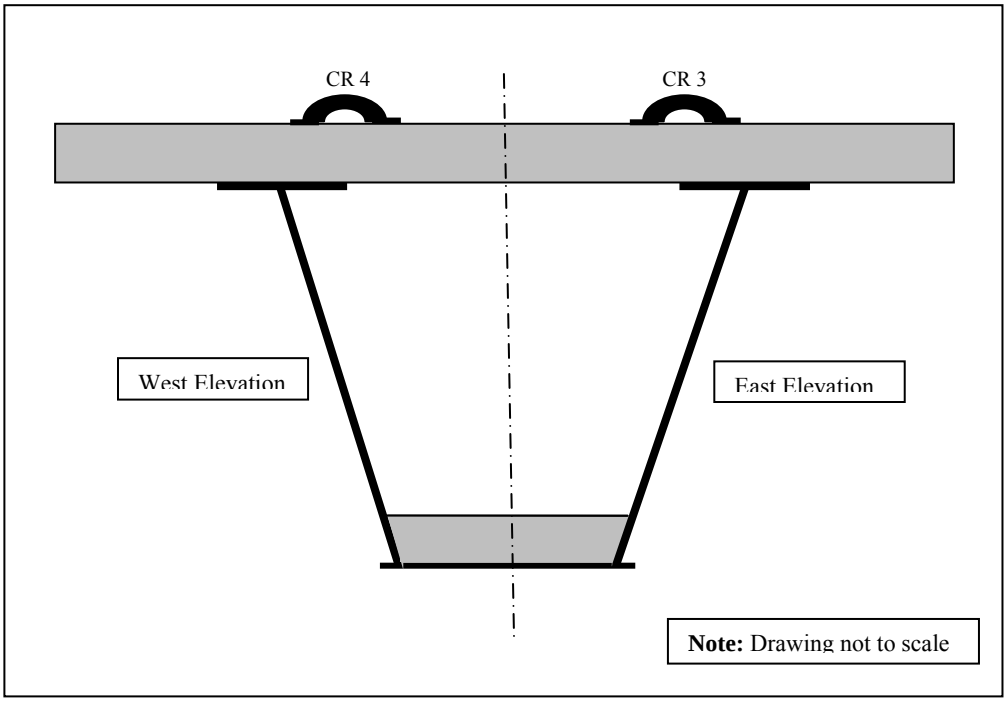


**Figure 4.16** Crack Width Gages on Hold Down Side

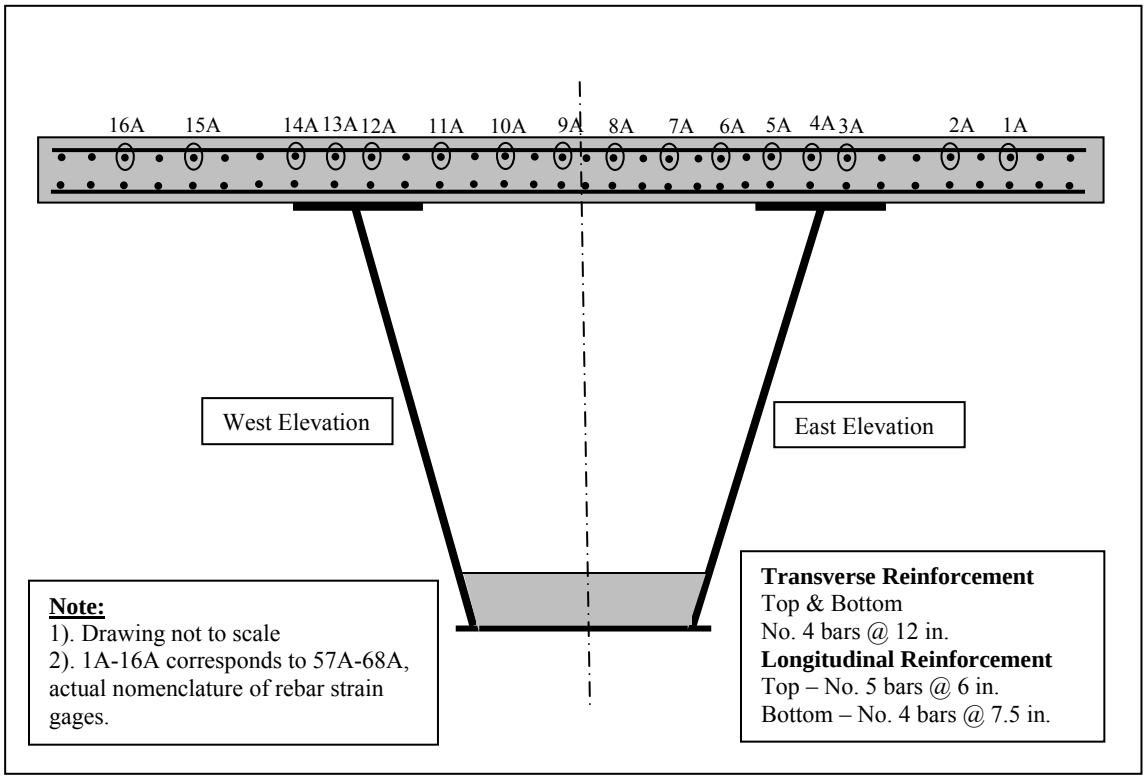


**Figure 4.17** Rebar Gages on Actuator Side

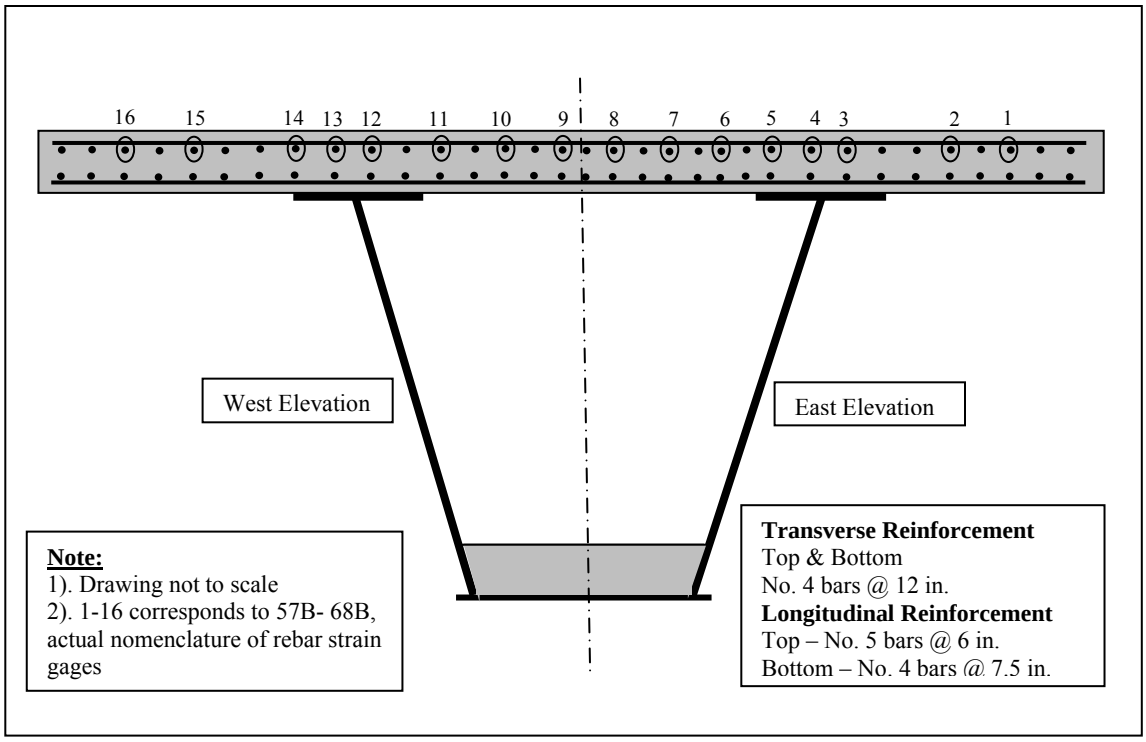


**Figure 4.18** Rebar Gages on Hold Down Side

### 4.3.8 Strain in Steel and Concrete

Strain in the concrete and steel were monitored using 89 gages. Of these, 17 gages attached to the top slab were damaged when the slab cracked and were therefore not monitored subsequently. Details on their placement are summarized in Table 4.2.

The position and movement of the neutral axis is a critical parameter in design since it is a measure of composite action. This was determined from strain measurements at two sections located distant 4 ft. 10⅛ in. (the depth of the box section) from the center support where the stress field would not be severely impacted by the diaphragm located at the support. The layout of these gages is shown in Fig. 4.19 and Fig. 4.20 for the actuator and the hold-down sections respectively. It may be seen from Fig.4.19-20, that six strain gages were attached to the exterior surface and three others to the interior surface at coincident locations on each web.

Three gages were also attached to the steel bottom flange at these sections to monitor strains in the bottom flange. These strain gages were placed symmetrically on either side of the center support. The spacing between these gages was 18 in. Similarly, 3 strain gages were installed on the top surface of the bottom slab to monitor strains in concrete.

A total of 4 strain gages (71, 72, 75, 76) were attached to the top flange with 2 strain gages placed symmetrically on either side of the intermediate support. These strain gages were used to monitor strain in the steel top flange. One strain gage was placed on each side of the bottom flange at 2 ft. ¼ in. from center support. The bottom flange buckled at approximately 2 ft.

¼ in. from the center support on hold down side under Service III load. This critical section had only one strain gage attached to the bottom flange as shown in Fig. 4.21.

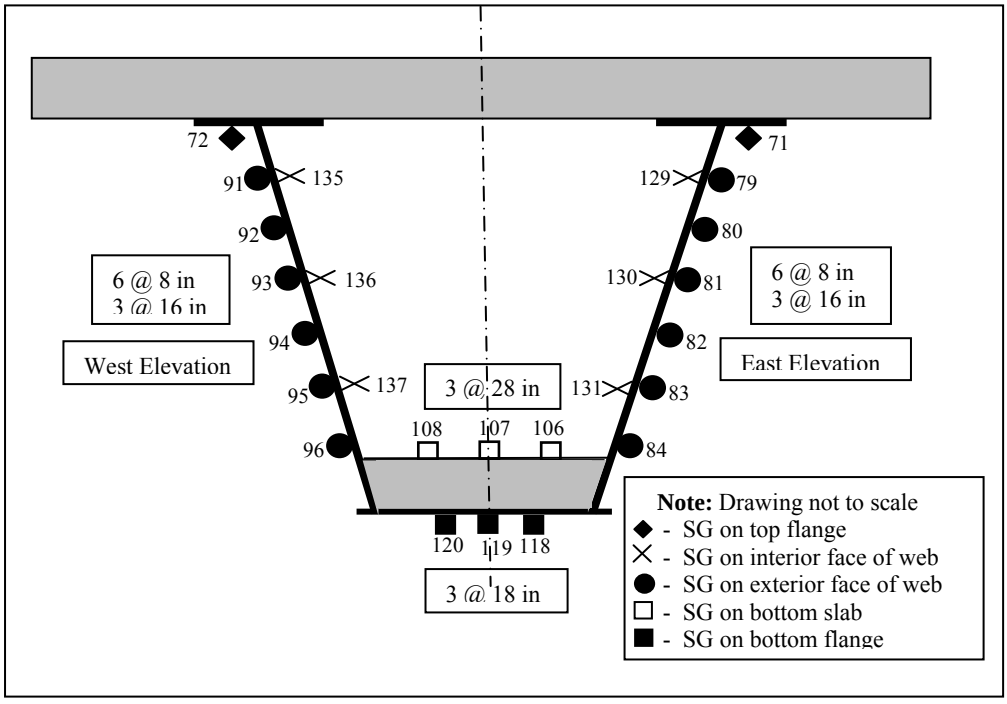


**Figure 4.19** Critical Section at 4 ft. 10⅛ in. from Center Support on Actuator Side

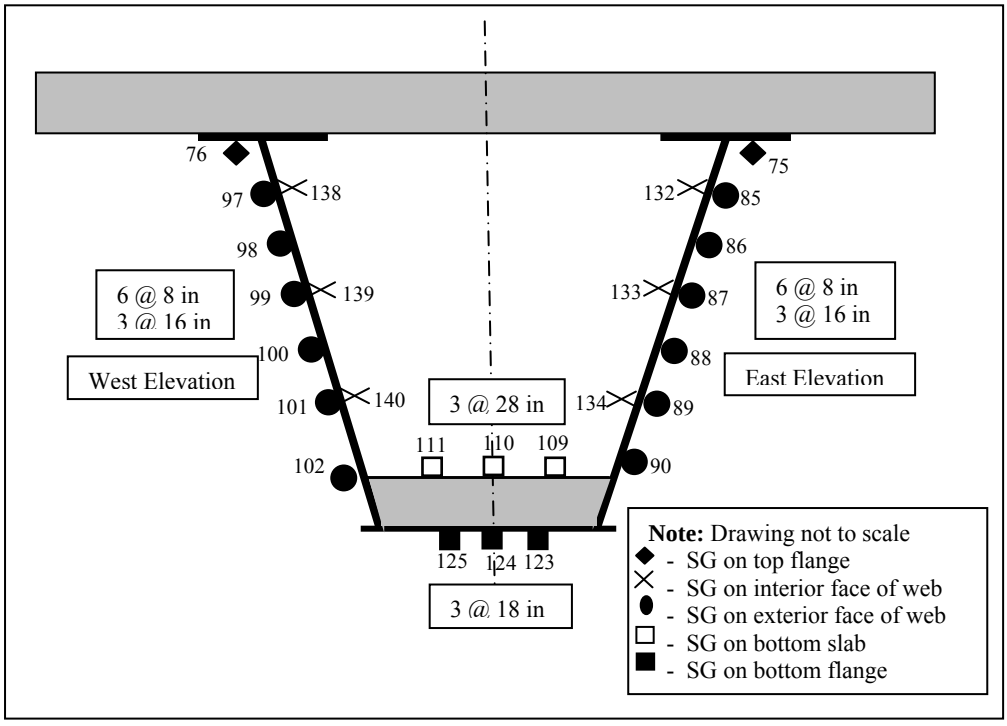


**Figure 4.20** Critical Section at 4 ft. 10⅛ in. from Center Support on Hold Down Side

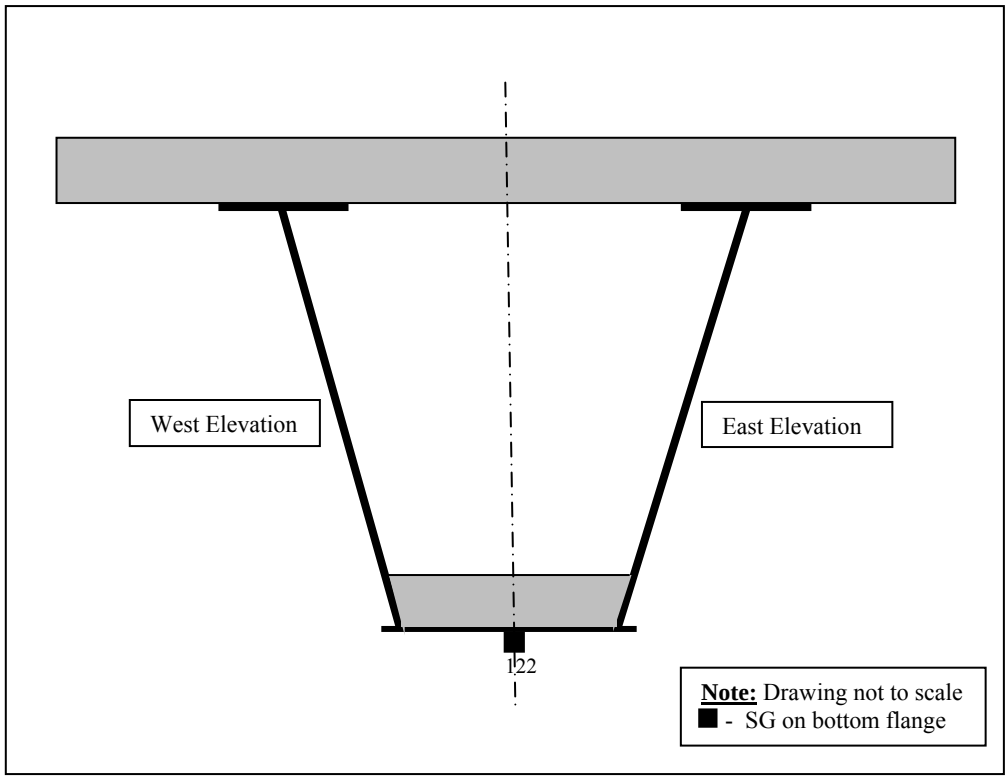


**Figure 4.21** Critical Section at 2 ft. ¼ in. from Center Support on Hold Down side

## References

4.1 Potter, W. (2008). "FatigueS." PDF file, Structures Research Lab, FDOT, Tallahassee.

4.2 Potter, W. (2008). "Servicea." PDF file, Structures Research Lab, FDOT, Tallahassee.

4.3 AASHTO LRFD Bridge Design Specifications (2004). 3rd Edition, Washington, DC.

# 5. FATIGUE TEST RESULTS

## 5.1 Introduction

The fatigue characteristics of shear connectors used in composite bridges have been the subject of numerous investigations extending over the past 50 years. While fatigue characteristics of shear connectors used in the bottom slab in the negative moment region were expected to be similar to that for the top slab, tests were conducted primarily for verification purposes because of the much reduced thickness of the bottom plate in double composite construction. The thickness of the bottom plate (0.375 in.) was less than 1/4th that of the top plate (1.75 in.). Welding of the 0.75 in. shear connectors to such a thin plate could result in minor distortions to the steel surface that could introduce additional tensile stresses in the shear connectors that had hitherto not been considered.

The test program is described in Section 5.2. An overview of the test procedure is summarized in Section 5.3. The results are summarized in Section 5.4 with a discussion and conclusions in Section 5.5 and 5.6 respectively.

## 5.2 Test Program

The key parameters in the fatigue testing were the load range, the frequency and the number of fatigue cycles. The load range was dictated by the capacity of the fatigue testing system (110 kips). For this reason, the load range was limited to 100 kips and varied from 5 kips to 105 kips. The load was applied at the free end of the bridge specimen as shown in Fig. 4.1b.

Based on this load range, the predicted fatigue cycles were calculated in accordance with the AASHTO LRFD specifications (6.10.10.2-2) as 5.65 million cycles. The calculations (see Appendix D) took into account the actual strength of the concrete measured just prior to the testing (Table 5.1).

The frequency was dictated by the capacity of the pump and was selected to be 1.16Hz. This corresponded to 100,000 fatigue cycles over 24 hours of continuous testing. Thus, it would take at least 56.5 days for the testing to be completed.

## 5.3 Test Procedure

The fatigue test was started after completion of two static tests that provided baseline measurements. In these tests, the specimen was loaded to 105 kip at the rate of 1 kip/sec and all measurements recorded. Although the predicted cracking load was 154 kips, the top slab cracked under the application of the first static cycle and all gages monitoring strain in the top concrete

slab were determined to be invalid. This is thought to have been a result of shrinkage of the concrete against the top flange, which induces significant tensile stress in the concrete (see Section 8.3.1 Chapter 8). The location of the cracking was noted and their maximum value recorded at the end of the testing.

**Table 5.1** Fatigue Test Parameters

| Parameter | Fatigue Test |
|---|---|
| Load Range | 5-105 kips |
| Frequency | 1.16 Hz |
| Number of Cycles | 5.65 million |
| Concrete strength<br>Top slab<br>Actuator side<br>Hold down side | <br><br>9905 psi<br>7590 psi |
| Bottom slab | 8178 psi |

Following completion of the static tests, the instrumentation was zeroed out and the load range set at 5 to 105 kips. The fatigue test was then initiated at a frequency of 1.16 Hz under a load control mode. Testing was interrupted periodically and a static cycle applied for the same load range to monitor the response. Ten such measurements were taken at approximate 0.5 million intervals with the last one at the end of the test.

The fatigue test commenced on May 15$^{th}$ 2008 and was temporarily stopped on July 8$^{th}$ 2008 after approximately 4.9 million cycles had been completed because fatigue cracks were discovered in the reaction frame. Following replacement of the reaction frame, testing was resumed after 2 weeks on July 23$^{rd}$ 2008 and concluded on July 30$^{th}$ 2008. Because damage under fatigue is cumulative, this interruption was not expected to affect the outcome.

## 5.4 Test Results

The fatigue testing was intended to evaluate the performance of shear connectors primarily at the bottom slab where the flange was very thin. Loss of composite action could be detected from slip measurements of both the top and bottom slabs. The instrumentation at these locations is shown in Fig. 4.6 and 4.7 in Chapter 4.

Despite the relatively small fatigue load, previous tests have indicated that concrete can deteriorate under these conditions. Such effects can be detected from deflection, strain data and the location of the neutral axis.

### 5.4.1 Deflection

Deflection was monitored at the cantilevered end, at the hold down frame end and at the center support. Deflection recorded at the cantilevered end is the most relevant for evaluating the effect of fatigue loading.

Fig. 5.1 and 5.2 shows the deflection at the cantilevered end measured by LVDTs # 7 and 8 respectively. This shows the deflection at these locations for the static cycle, after 0.5 million, 1.5 million, 3.0 million, 4.9 million and 5.65 million cycles. The results for 0.5 million and 3 million cycles in Fig. 5.1 are anomalous since they are not reproduced in Fig. 5.2 and are believed to be due to lateral sway and torsional issues due to center point loading.

The deflection profile in Fig. 5.1 indicates that the maximum deflection was 0.65 in. after 1st static test (the theoretical deflection from simple cracked beam analysis was 0.56 in.) and progressively increased to 0.76 in. after completion of 5.65 million cycles. The progressive increase in deflection suggests an overall stiffness reduction possibly caused by additional cracking of the top and bottom slabs (indicated by the strain data shown in Fig. 5.4).

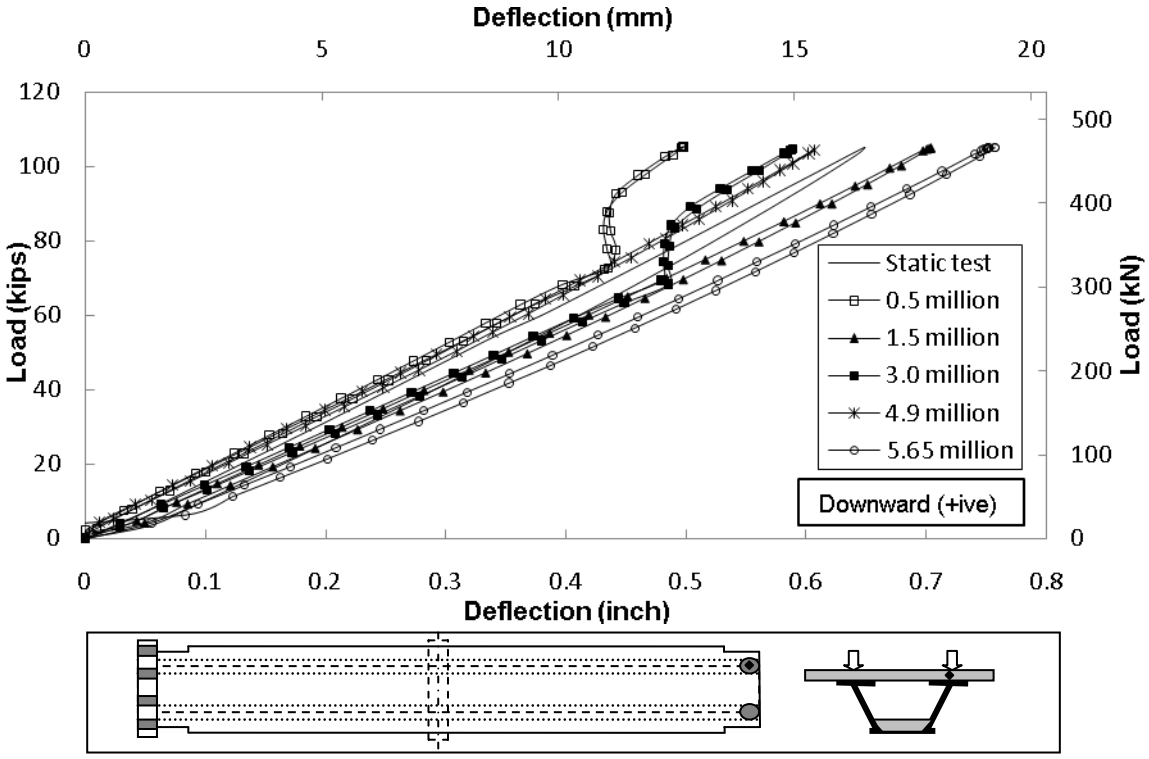


**Figure 5.1** Deflection at Actuator End LVDT # 7

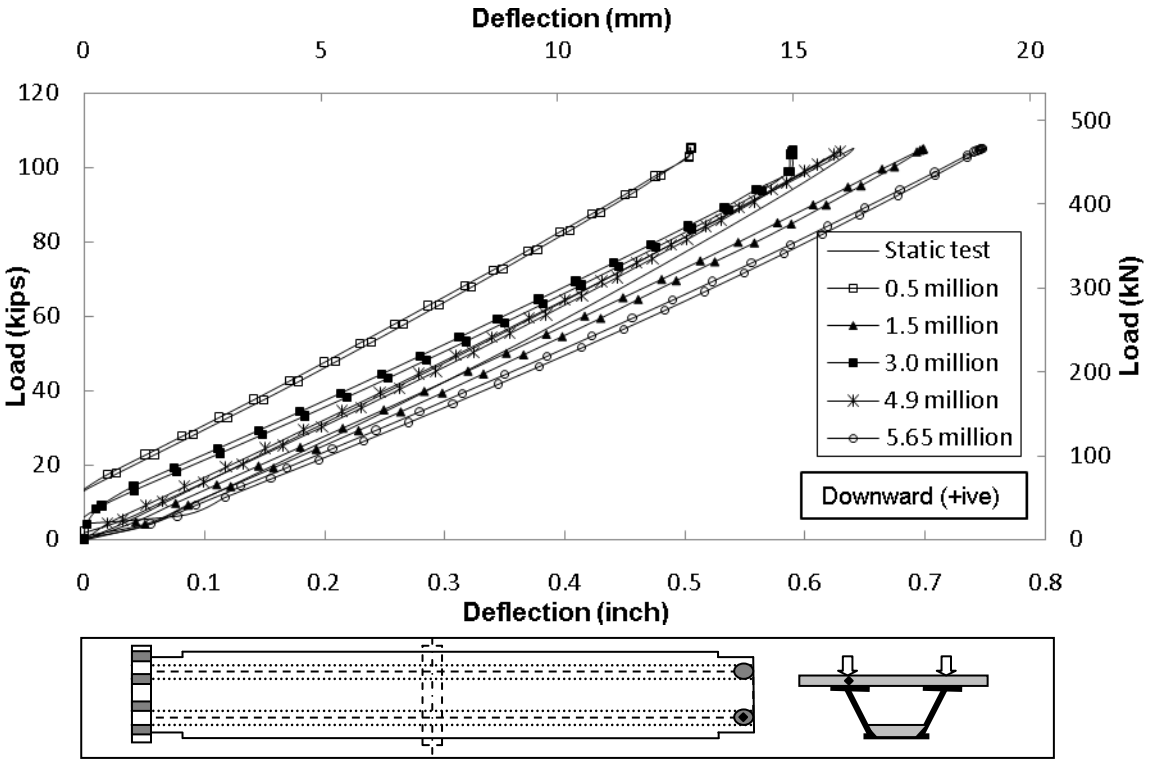


**Figure 5.2** Deflection at Actuator End LVDT # 8

### 5.4.2 Slip

The relative movement between the top and bottom slabs and the respective steel surfaces at both the loaded and the hold down ends were monitored throughout the testing (see details in Fig 4.6 and 4.7). No slip was recorded at either ends for both the top and bottom slabs (see Figs. D.9–D.17 on pg-D.11-D.15 in Appendix D). Only displacements exceeding 0.002 in. were taken as slip since this was the smallest value that could be measured by the LVDT.

### 5.4.3 Strain in Concrete

The concrete strain in the bottom slab at the section located 4 ft. 10⅛ in. from center support on either side was monitored throughout the fatigue loading. Although loading was in the elastic range, the observed strains were in general non-linear.

Figs. 5.3 and 5.4 plot the variation in the concrete strain at symmetric flange locations. The strains shown in Fig. 5.3 are very small but reverse from tensile to compressive strain. Analysis presented in Chapter 8 suggests that this type of behavior results when the bottom surface of the bottom slab has significant open cracks resulting in upward shift in the neutral axis of the bottom slab. The compressive response is attained as the crack closes sufficiently to shift the neutral axis closer to that of an uncracked slab. The cracks are caused by shrinkage and likely to have been affected by the presence of blocks used to set the thickness of the bottom slab (Fig. 5.5) since these would restrain the shrinkage and induce tension in the concrete. Additionally

these cracks could have resulted from the restraint provided by the webs and due to the presence of intermediate diaphragms. Shrinkage steel specified was determined in accordance with AASHTO LRFD Specification (5.10.8) and was only placed in one layer since the bottom slab is protected or confined by the steel bottom flange.

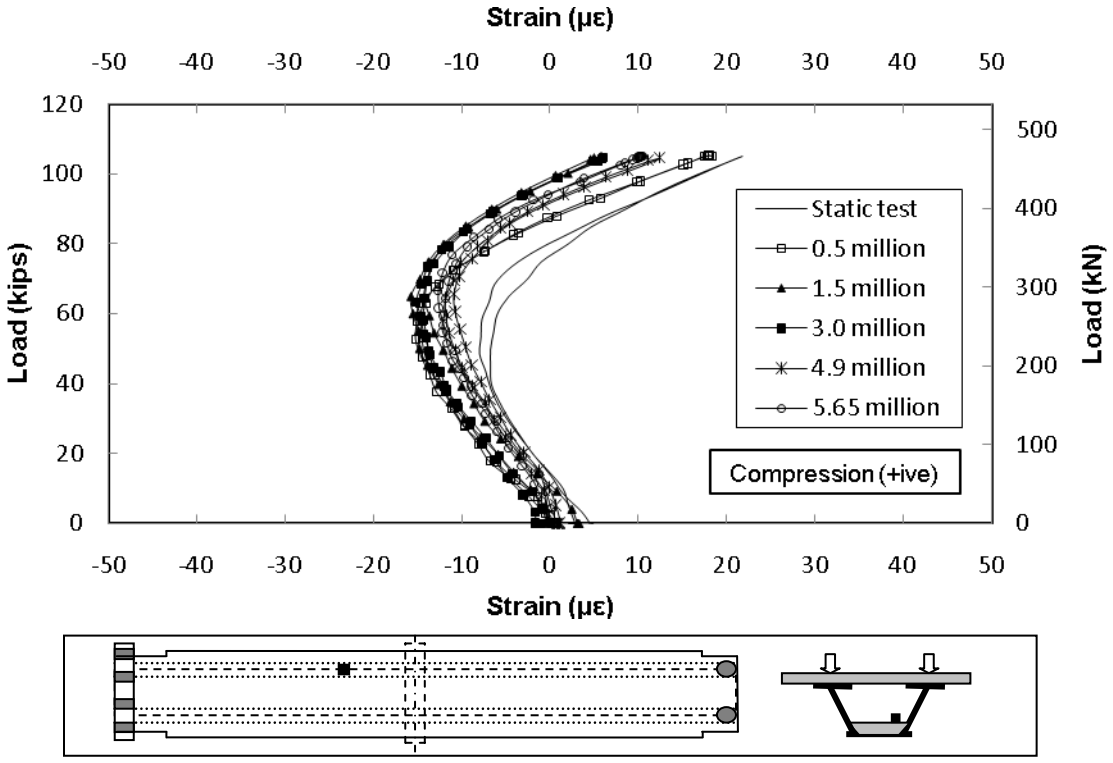


**Figure 5.3** Strain in Bottom Concrete Slab on Hold Down Side SG 109

The concrete strain variation in Fig. 5.4 indicates a change in the response after 1.5 million cycles. The response is characterized by low stiffness at low loads (up to 30 kips), followed by increased stiffness in the range from 30-50 kips after which the stiffness remains constant. The slab in this region most likely had moderate cracking causing the stiffness to reduce initially. The apparent increase in stiffness is thought to be a result of crack closure which shifts the neutral axis, after which the slope of the response is consistent for all the different measurements shown in Fig. 5.4.

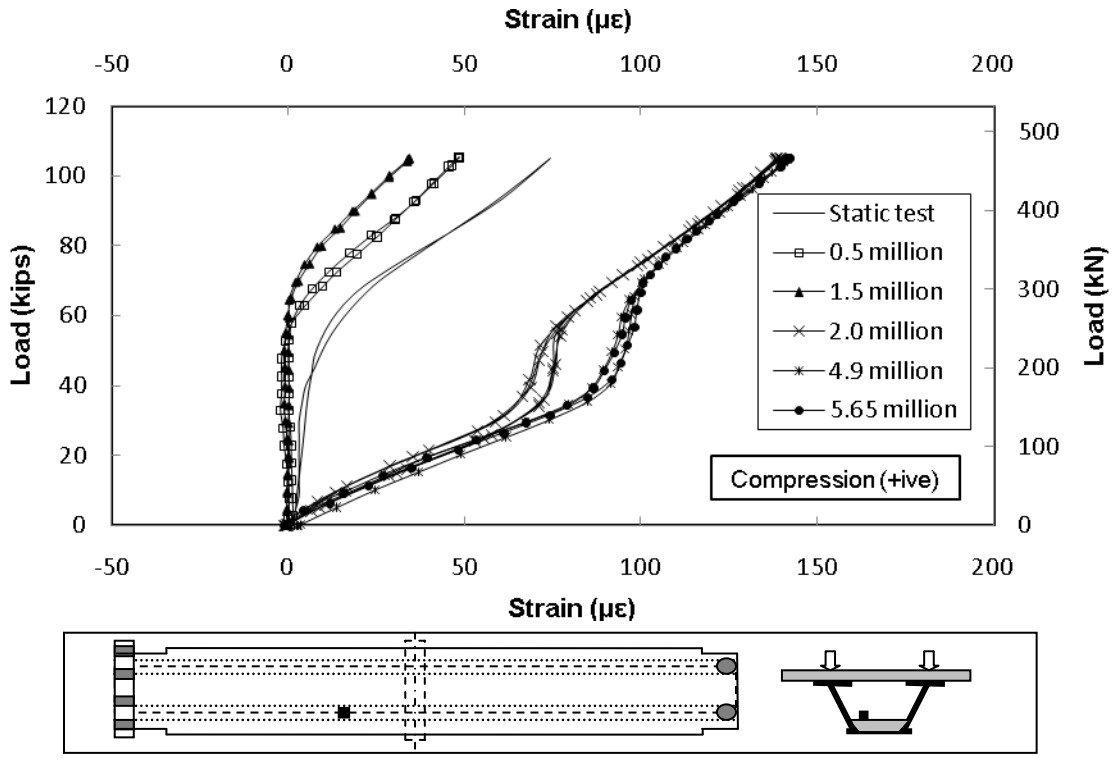


**Figure 5.4** Strain in Bottom Concrete Slab on Hold Down Side SG 111

**Figure 5.5** Placement of Bottom Concrete Slab

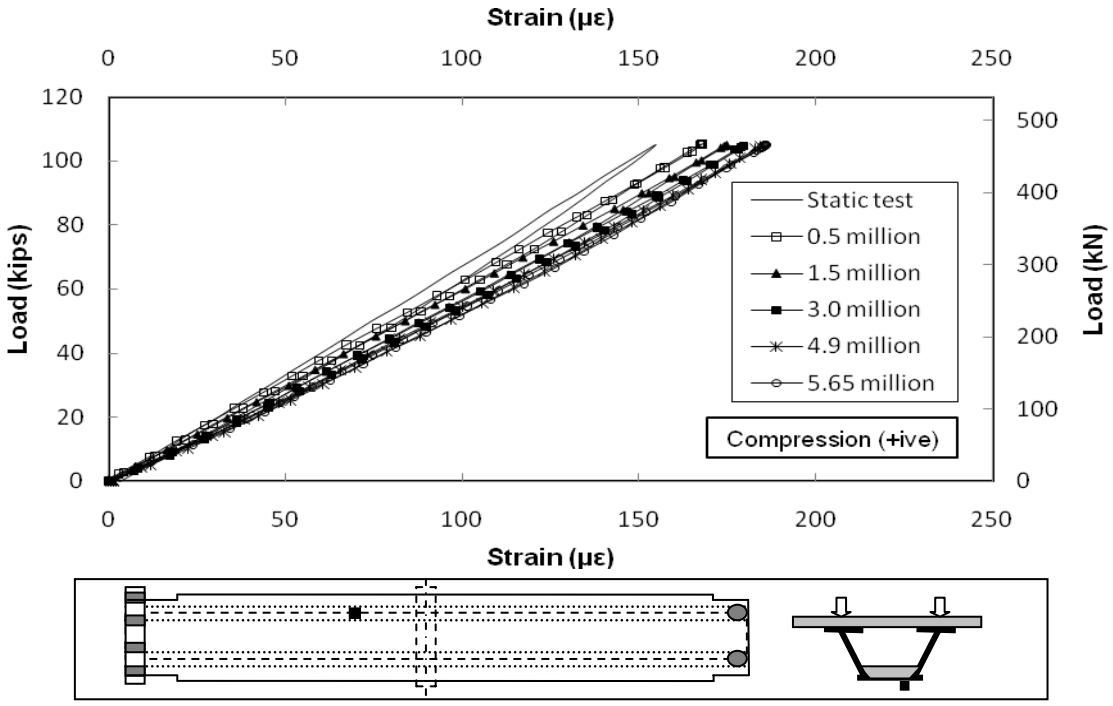


**Figure 5.6** Strain in Bottom Flange on Hold Down Side SG 123

### 5.4.4 Strain in Steel

Strain was monitored in the steel box 4 ft 10⅛ in. away from the support (see Figs. 4.19 and 4.20). The variation in strain with the number of cycles at symmetrical locations on the hold-down span is shown in Figs. 5.6 and 5.7. The results for the actuator side were similar and may be found in Appendix D.

The strain variation in the bottom flange is almost linear in Fig. 5.6 though its magnitude increases with the number of cycles by over 30% (140 με to 185 με). The increase may be the result of shrinkage cracks forming in the bottom slab (see Fig 5.3) over the duration of the test, which would result in the bottom flange having to carry more load. There is no similar increase in the corresponding gage located along the other web (Fig. 5.7) though in this case there is non-linearity in the lower load range, e.g. from 30-50 kips. This is probably because of change in load distribution as the cracks formed in the bottom slab close. The profile in Fig. 5.7 is similar to that for the concrete strain measured at the same location (Fig. 5.4).

### 5.4.5 Top Rebar Strain

The strain in the reinforcement located 1 ft away symmetrically from the supports was also monitored. Results summarized in Table 5.2 show the strains recorded for the first and last cycles. The identifiers for the bars listed in this table may be found in Fig. 4.17 and 4.18.

Inspection of Table 5.2 shows that in general strains increased (about 25%) with loading indicating that cracking had increased. The strains in the hold down end were larger (relative to the actuator end) despite the applied moments being lower, due to center support diaphragm rotation, which pulls on the top deck on the hold down side (see Section 8.3 in Chapter 8). Higher strains were observed over the rebars on the web compared to rebars placed in center and cantilevered portion of the box girder section because of shear lag.

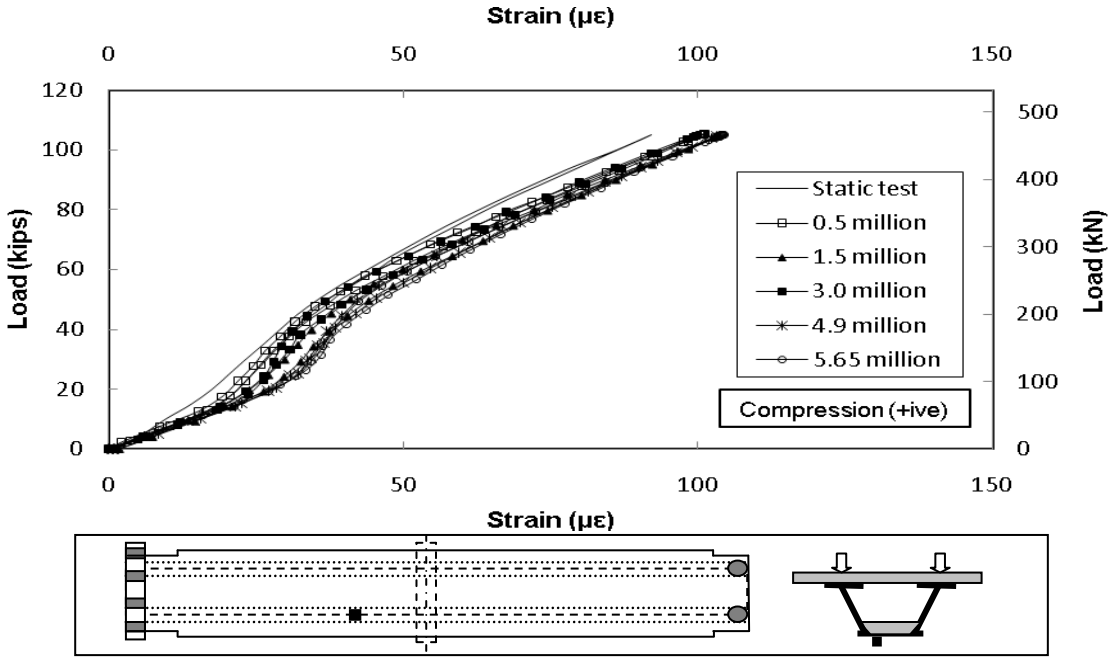


**Figure 5.7** Strain in Bottom Flange on Hold Down Side SG 125

### 5.4.6 Variation of Neutral Axis

The strains recorded in the web at the critical section 4 ft 10⅛ in. from the support were used to plot the variation in the neutral axis. The neutral axis was plotted by averaging the strains measured at three coincident locations inside and outside the web (sees Fig. 4.19 and 4.20).

The variation in the neutral axis for the two webs on the actuator end at the end of the 5.65 million cycles is shown in Figs. 5.8 and 5.9. The corresponding plots for the hold down end are shown in Figs. 5.10 and 5.11. The neutral axis varied from 24 in. at 10 kips to 28 in. (relative to the top slab) at 100 kips indicating the increased cracking of the top slab after 5.65 million cycles. Table 5.3 compares the change in the neutral axis location from the initial and final static cycles for the two web locations at the actuator and holding down ends.

Inspection of Table 5.3 shows that the location of the neutral axis increases with increasing number of cycles indicating that there was degradation in the top concrete stiffness because of increased cracking.

**Table 5.2** Strain in Top Slab Reinforcement After 5.65 Million Cycles

| Rebar gages (Actuator Side) | Maximum Strain (με) | | Percent Increase (%) | Rebar gages (Hold Down side) | Maximum Strain (με) | | Percent Increase (%) |
|---|---|---|---|---|---|---|---|
| | First Cycle | Last Cycle | | | First Cycle | Last Cycle | |
| 1A | 167 | 198 | 16 | 1 | 116 | 163 | 29 |
| 2A | 154 | 201 | 24 | 2 | 212 | 226 | 6 |
| 3A | 200 | 269 | 26 | 3 | 454 | 435 | -5 |
| 4A | 341 | 416 | 18 | 4 | 565 | 556 | -2 |
| 5A | 306 | 408 | 25 | 5 | 680 | 642 | -6 |
| 6A | 455 | 474 | 4 | 6 | 445 | 381 | -17 |
| 7A | 73 | 77 | 6 | 7 | 108 | 102 | -6 |
| 8A | 84 | 87 | 3 | 8 | 377 | 456 | 17 |
| 9A | 233 | 285 | 18 | 9 | 592 | 785 | 25 |
| 10A | 121 | 145 | 17 | 10 | 187 | 180 | -4 |
| 11A | 242 | 282 | 14 | 11 | 579 | 569 | -2 |
| 12A | 114 | 372 | 69 | 12 | 264 | 272 | 3 |
| 13A | 80 | 335 | 76 | 13 | 158 | 182 | 13 |
| 14A | 74 | 178 | 59 | 14 | 245 | 272 | 10 |
| 15A | 65 | 66 | 2 | 15 | 94 | 96 | 2 |
| 16A | 95 | 99 | 4 | 16 | 145 | 159 | 9 |

**Table 5.3** Location on Neutral Axis after 5.65 Million Cycles

| Load (kips) | Actuator Side (inch) | | | | Hold Down Side (inch) | | | |
|---|---|---|---|---|---|---|---|---|
| | East Elevation | | West Elevation | | East Elevation | | West Elevation | |
| | First | Last | First | Last | First | Last | First | Last |
| 10 | 22 | 24 | 21 | 24.5 | 22 | 24 | 20.5 | 23 |
| 20 | 23.5 | 24.5 | 23 | 25.5 | 24 | 24.5 | 23 | 24.5 |
| 30 | 24 | 25 | 24 | 26 | 24.5 | 25 | 24 | 25 |
| 40 | 24.5 | 25 | 24.5 | 26.5 | 25 | 25 | 24.5 | 25.5 |
| 50 | 25 | 26 | 25 | 27 | 25 | 26 | 25 | 26 |
| 60 | 25.5 | 26 | 25.5 | 27.25 | 26 | 26 | 25.5 | 26.5 |
| 70 | 26 | 27.5 | 25.5 | 27.5 | 26 | 27 | 26 | 27 |
| 80 | 26.5 | 27.5 | 26 | 27.5 | 16.5 | 27.5 | 26.5 | 28 |
| 90 | 26.5 | 28 | 26 | 28 | 26.5 | 28.5 | 26.5 | 28.5 |
| 100 | 27 | 28 | 26.5 | 28 | 27 | 28.5 | 27 | 28.5 |

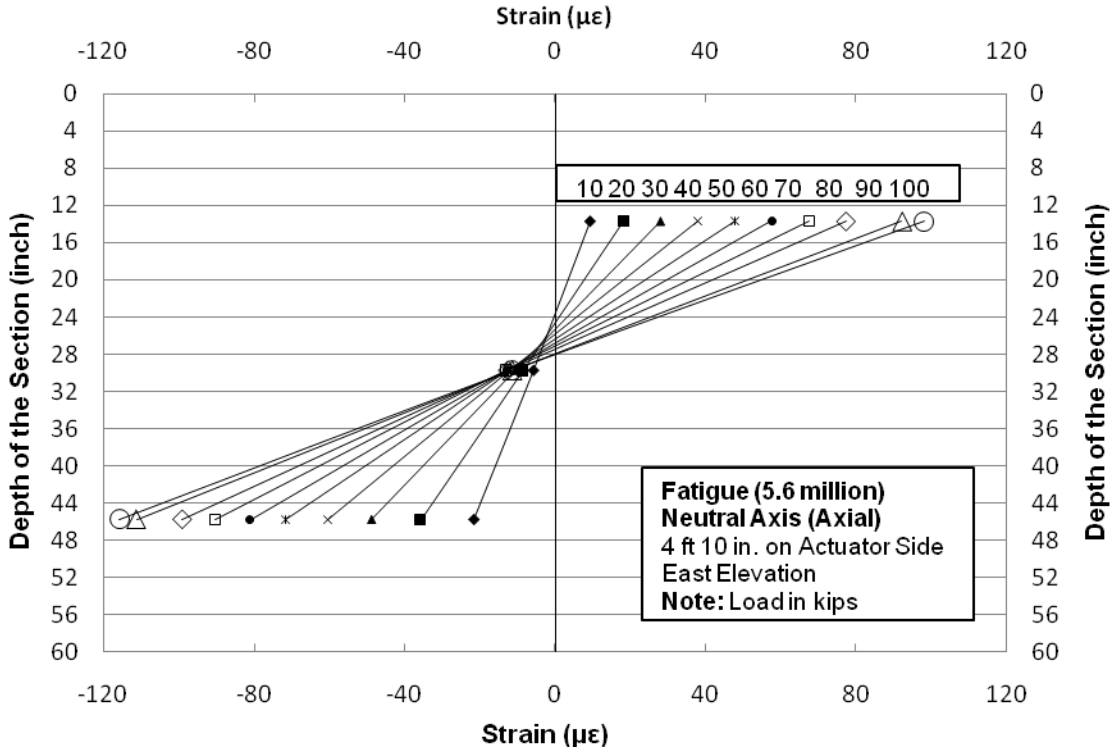


**Figure 5.8** Neutral Axis on Actuator Side (East Elevation)

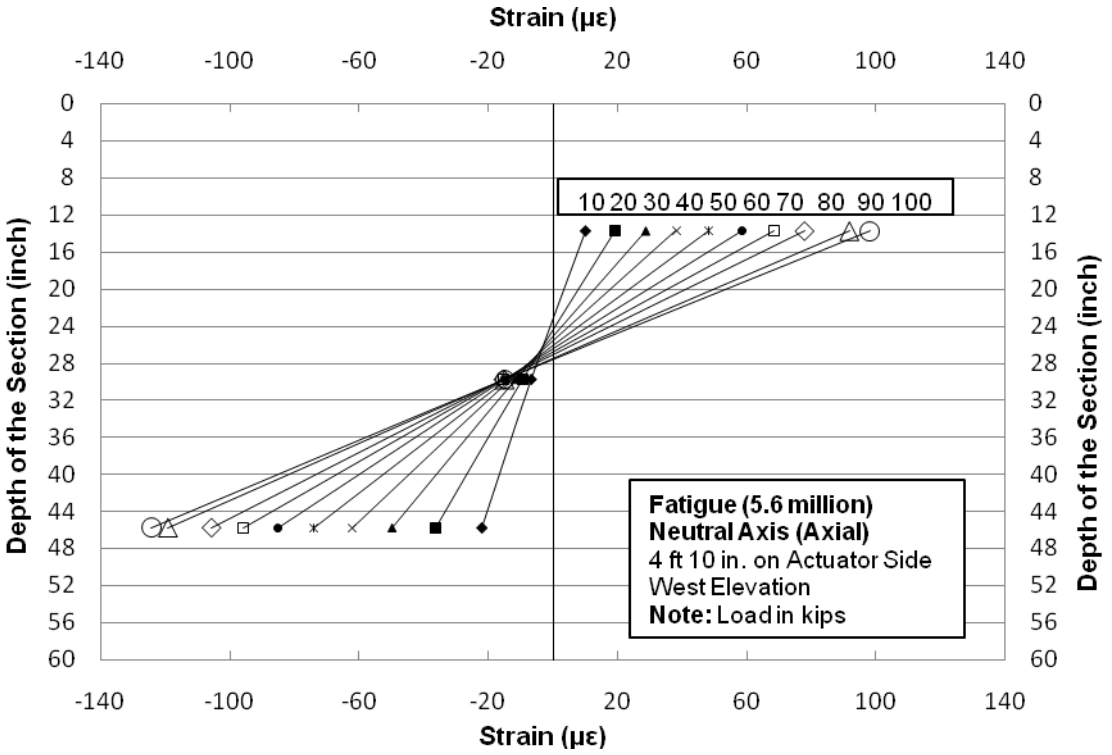


**Figure 5.9** Neutral Axis on Actuator Side (West Elevation)

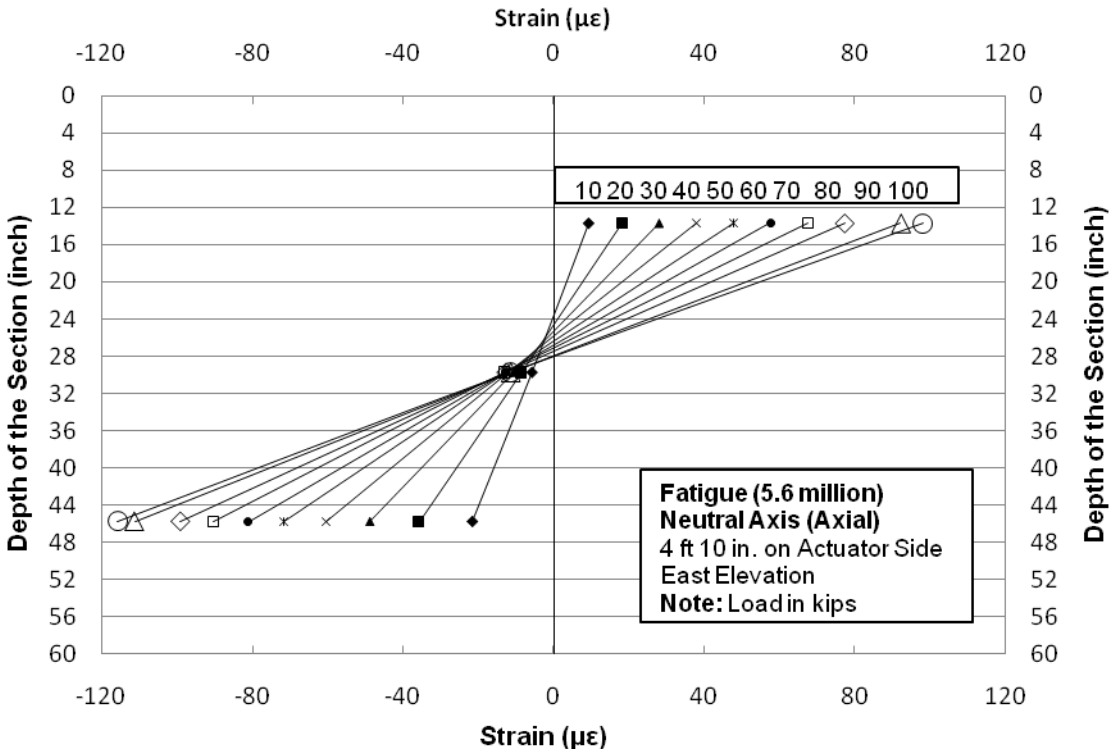


**Figure 5.10** Neutral Axis on Hold Down Side (East Elevation)

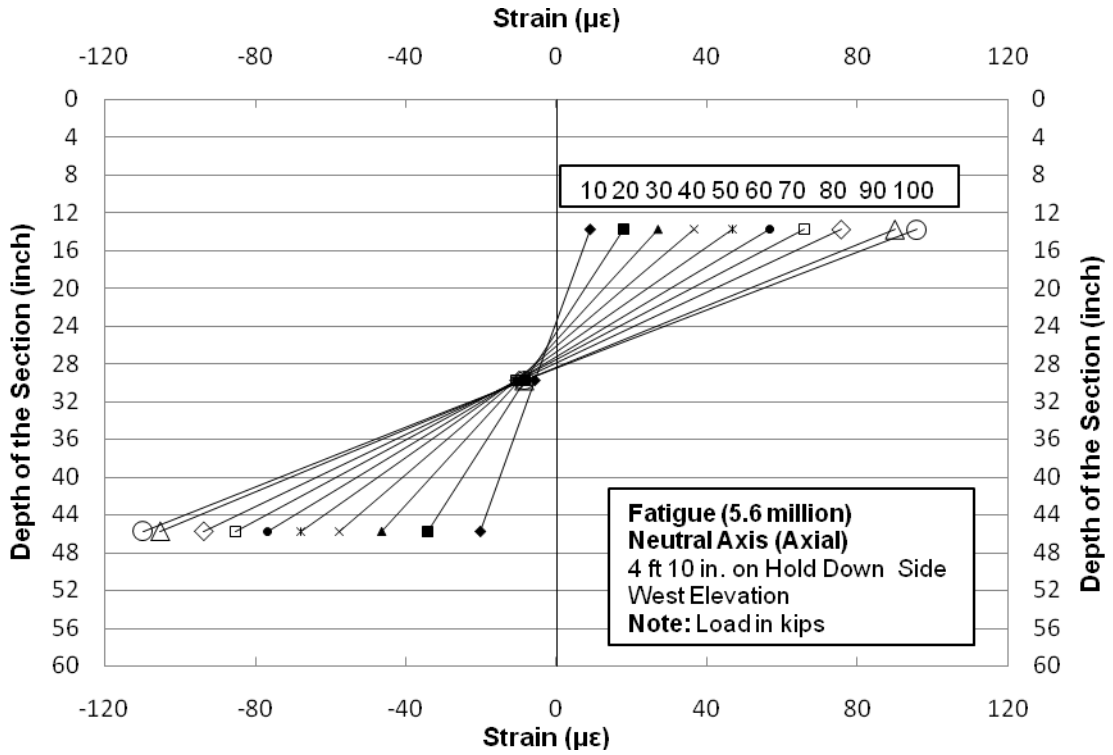


**Figure 5.11** Neutral Axis on Hold Down Side (West Elevation)

### 5.4.7 Crack Width on Top Slab

Although the modulus of rupture was higher than the calculated stresses from the applied fatigue load, the top slab cracked during initial static cycle. As stated earlier, this is believed to be due to concrete shrinkage. Cracks developed close to the intermediate support (Fig. 5.12). Table 5.5 summarizes the measured maximum crack widths at the end of the test at these locations.

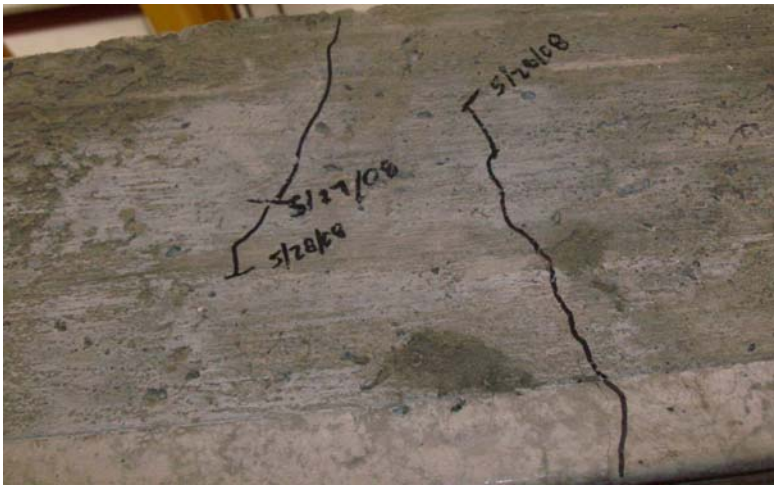

**Figure 5.12** Structural Cracks at Intermediate Support on Hold Down Side

**Table 5.4** Crack Width on Top Slab After 5.65 Million Cycles

| Crack gages | After5.65 Million (inch) | Comments |
|---|---|---|
| 1 | 0.005 | Actuator side |
| 2 | 0.005 | Actuator side |
| 3 | 0.005 | Hold down side |
| 4 | 0.007 | Hold down side |

## 5.5 Discussion

The fatigue test was conducted at relatively low loads compared to the calculated failure load of 1200 kips. While no slip was recorded, there were definite signs of stiffness degradation. Since the applied stress range fell well below the endurance limit for the steel (about half its tensile strength) or the welded connections, it can be attributed wholly to concrete. It was possibly due to a combination of cracking and localized debonding of the concrete bottom slab (see Fig. 5.5). The slab cracked at loads well below its modulus of rupture indicating that factors such as shrinkage, restraint and temperature may have been responsible.

The loss of stiffness was indicated by non-linearity in strains, a downward shift in the position of neutral axis (Table 5.3) and increased deflection. The maximum deflection increased from 0.64 in. at the end of the first static cycle to 0.78 in. at the end of the test.

The cross-section close to where failure occurred later under Service III (Chapter 7) showed signs of a changed response after 1.5 million load cycles. The variation in strain in both the concrete and the steel was significantly different (see Fig. 5.4 and 5.6). This was not observed at the corresponding section on the actuator span (see Figs.D.56-58 and D.64-66 in Appendix D). This suggests that there may have been localized debonding at low loads (less than 30 kips) due to bottom slab cracking.

## 5.6 Observation and Conclusions

- The top concrete slab cracked under the first static cycle even though calculated stresses were well below its modulus of rupture. This is most likely due to top slab shrinkage (see Section 8.3 in Chapter 8).

- Strains in concrete and steel in the bottom slab close to the location where failure eventually occurred were non-linear at very low loads (see Fig. 5.4 and 5.6). The non-linearity is consistent with presence of cracks, which close as the loads increase (see Section 8.3 in Chapter 8).

- There was no significant slip observed at either end with respect to either top slab or bottom slab.

- The stiffness of the bottom concrete slab reduced after 1.5 million cycles possibly because shrinkage cracking and local debonding under multi-axial stresses (see Fig. 5.5)

- There was an 18% reduction in stiffness of the section after completion of the fatigue test in terms of the maximum measured deflection (see Fig. 5.1). This is consistent with continued cracking of concrete over time due to shrinkage and the fatigue load.

- The rebar strains were approximately 25% higher after completion of 5.65 million dynamic cycles (see Table 5.2). Again, this is consistent with continued cracking of concrete over time due to shrinkage and the fatigue load.

# 6. SERVICE TEST RESULTS

## 6.1 Introduction

Three series of service load tests were carried out following completion of the fatigue tests reported in Chapter 5. The primary goal of these tests was to verify the adequacy of using existing design guidelines in designing double composite bridges. In the first test, the applied load was calculated to limit the stress in the reinforcing steel to $0.6f_y$ (421 kips). In the second test, it was limited to a top flange stress of $0.95F_y$ (638 kips) assuming Grade 50 steel, since this grade of steel is commonly used in practice. In the final service test, the stress in the top flange HPS steel was limited to $0.95F_y$ (894 kips) assuming yield strength of 70 ksi.

This chapter summarizes information from the first two service tests. The final service test is described in the next chapter. For the two tests covered in this chapter, the same load was applied and removed a total of five times. In all cases, the structural response from the first load application differed *significantly* from the subsequent four applications. Results for the latter four load applications were consistent and appeared to indicate that the anomalous results from the first application were due to other factors, e.g. seating at the supports or onset of plastic deformation. For this reason, the results presented in this chapter are those for the *final* cycle. The other results may be found in Appendix E.

The instrumentation for all three service load tests was identical and is reported in Chapter 4. In all cases, 145 channels of data were collected at a scan rate 10 Hz that is every $1/10^{th}$ of a second. Section 6.2 summarizes the results from the first service test while Section 6.3 reports those for the second test. Concluding remarks are summarized in Section 6.4

## 6.2 Service I Test Results

Compared to the fatigue test, the service tests recorded data from an additional 22 channels that measured deflection along the span and the maximum crack width (see Fig. 4.12 and 4.13). The intent of this test was to determine the service response when the stress in the rebar reached $0.6f_y$. Results are presented for deflection, slip, rebar strain, crack width and concrete/steel strains at critical locations.

### 6.2.1 Deflection

Deflection was measured at the cantilevered end, along the span, at both the hold down frame end and near (2 ft. ¼ in.) the center support (see Fig 4.12 and 4.13 for details). A photo of the deflected shape of the test specimen in the $5^{th}$ cycle is shown in Fig. 6.1. A plot of the deflection at the free end from the two LVDTs (#7 and #8) is shown in Fig. 6.2. The degree of

agreement in the measured deflection by these two LVDTs indicates the absence of any twisting deformation.

**Figure 6.1** Deflected Shaped of Double Composite Box Girder

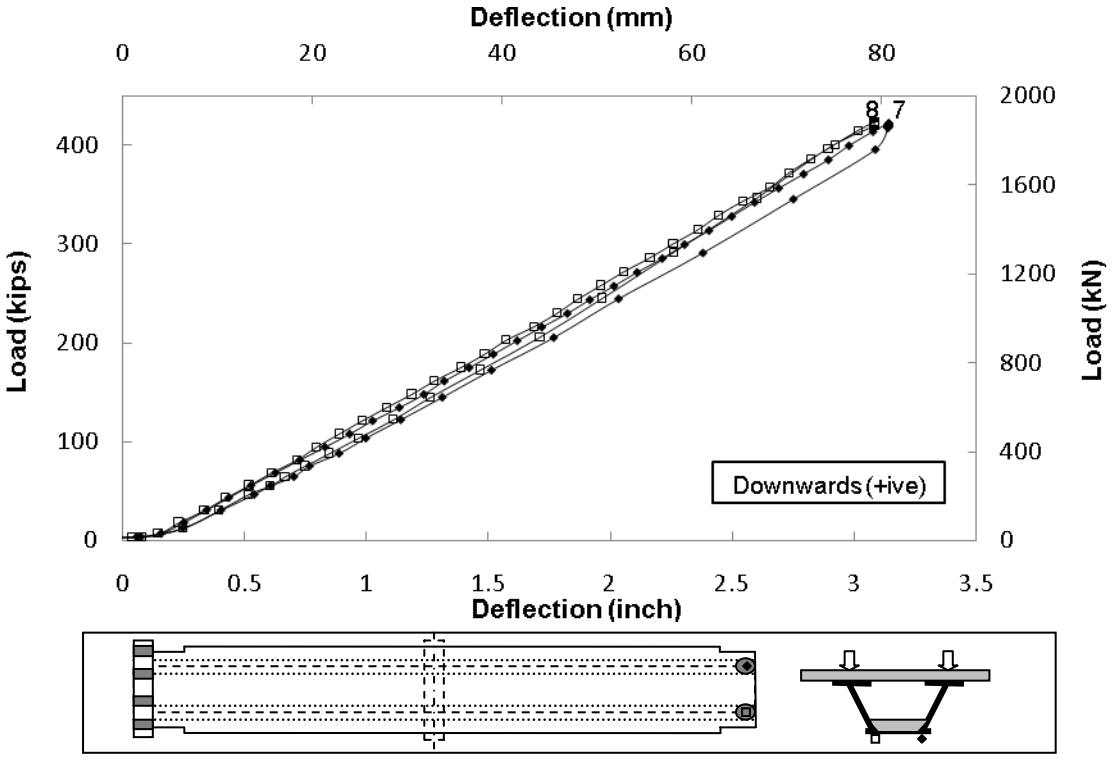


**Figure 6.2** Deflection at Cantilevered End

The average maximum deflection under the 421 kip load was 3.13 in. that was significantly greater than the predicted 2.25 in. value. This is not surprising given the stiffness loss observed under fatigue loading (Fig. 5.2).

Table 6.1 compares the average deflection obtained from the fatigue test after 3 different fatigue cycles (1st, 1.5 million and 5.65 million) with the corresponding values from the service tests for the first, second and fifth cycles.

**Table 6.1** Displacement at Cantilevered End

| Load (kips) | Average Displacement at Cantilevered End (inch) | | | | | |
|---|---|---|---|---|---|---|
| | **Fatigue (Static 1)** | **Fatigue (1.5 million)** | **Fatigue (5.65 million)** | **Service I 1st Cycle** | **Service I 2nd Cycle** | **Service I 5th Cycle** |
| 0 | 0 | 0 | 0 | 0 | 0 | 0 |
| 50 | 0.314 | 0.351 | 0.387 | 0.093 | 0.420 | 0.430 |
| 100 | 0.613 | 0.666 | 0.71 | 0.483 | 0.809 | 0.912 |
| 200 | - | - | - | 1.155 | 1.600 | 1.603 |
| 300 | - | - | - | 2.025 | 2.29 | 2.293 |
| 400 | - | - | - | 2.890 | 2.964 | 2.966 |
| 421 | - | - | - | 3.002 | 3.067 | 3.13 |

Inspection of Table 6.1 shows that the deflection at 100 kips increased from 0.71 in. at the end of the fatigue test to 0.912 in. after the 5th cycle of the service load. The 28% increase indicates additional cracking in the specimen under the application of the load. However, this does not explain why the deflection was lower than that obtained from the fatigue test under the first cycle (0.483 in. vs 0.71 in.). Note that although deflection in the first cycle at 50 kips (0.093 in.) is lower than in subsequent cycles, the incremental deflection between 50 kip and 100 kip is fairly close, indicating similar stiffness response.

Fig. 6.3 shows the deflection profile along the length of the test specimen. The longitudinal profile indicates change in the deflected shape close to center support on the hold down side. In this plot, the deflection data is averaged at locations where multiple LVDTs are present, that is, at the hold-down end, 2 ft. ¼ in. from the support and at the cantilevered end. Since both the hold down support and the center support moved about 0.2 in. (see Figure E8, Appendix E) under load, the measured values incorporate rigid body movement / rigid body rotation. As a result, the reported deflection is higher. This issue is discussed further in the finite element comparisons presented in Chapter 8.

Since strain data from the fatigue test was markedly non-linear close (4 ft. 10⅛ in.) to the center support on the hold down side at loads well below 50 kips (see Fig. 5.4), results of the deflection measurement 2 ft. ¼ in. from the center support from the two LVDTs (#23, #24) are plotted in Fig 6.4 for the 1st cycle and all subsequent cycles for LVDT #23 in Fig. 6.5.

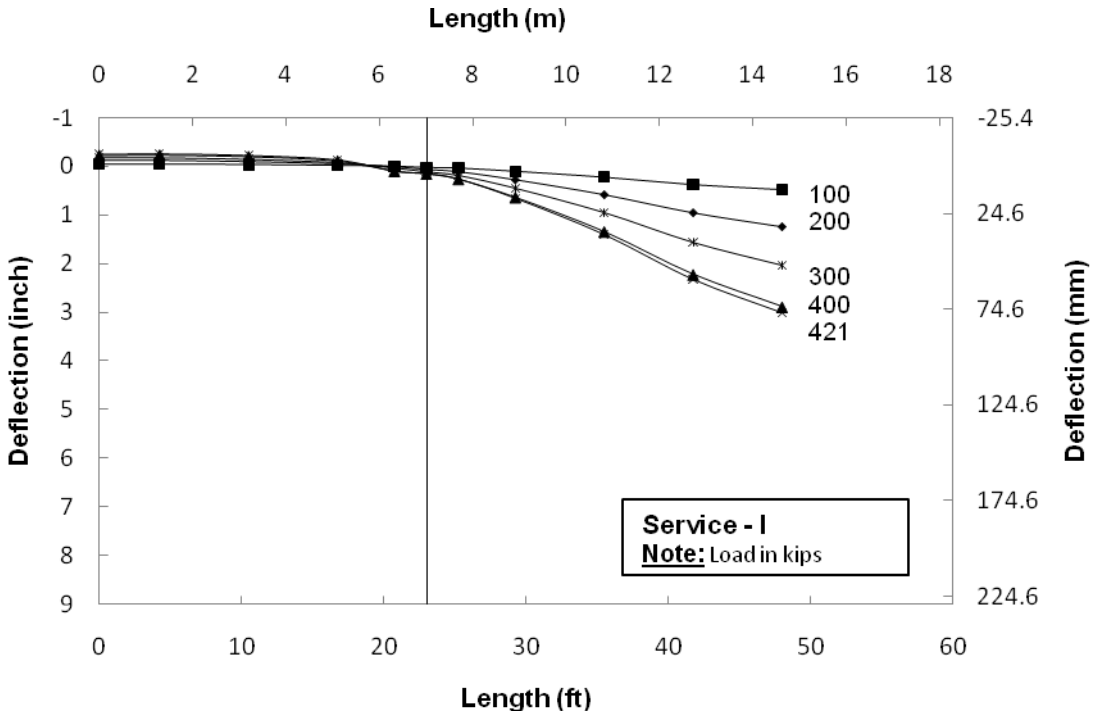


**Figure 6.3** Longitudinal Deflection of Double Composite Box Girder

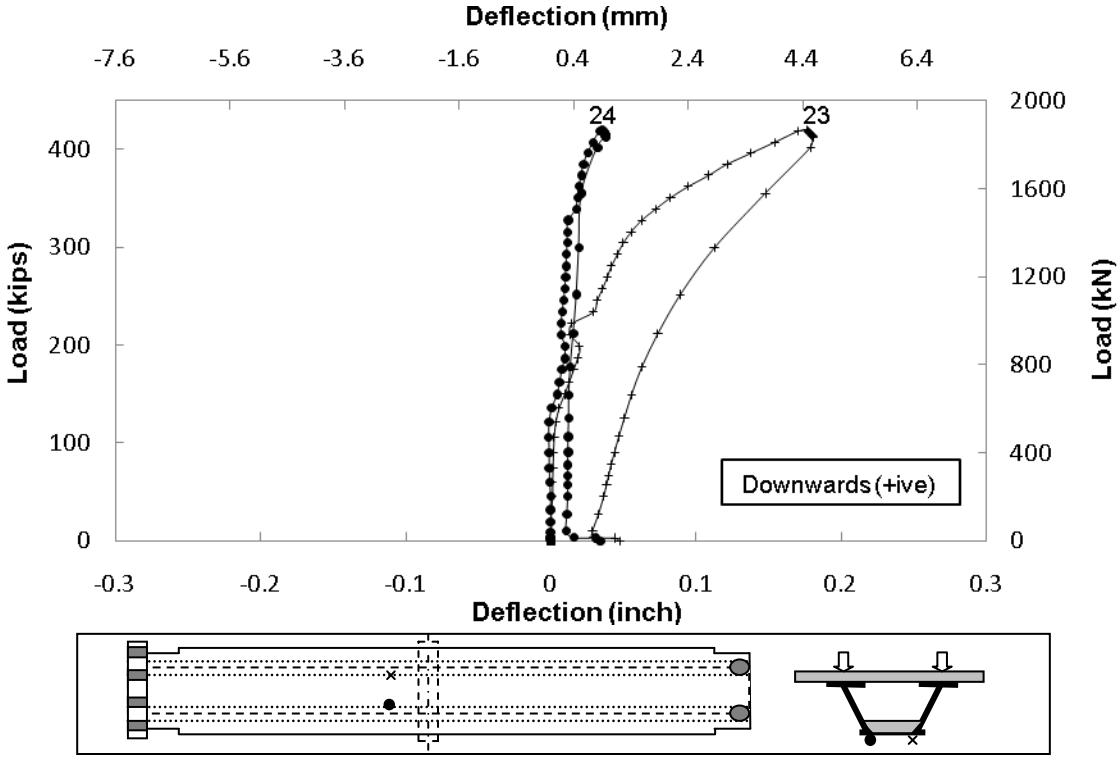


**Figure 6.4** Deflection of Bottom Flange on Hold Down Side (1st Cycle)

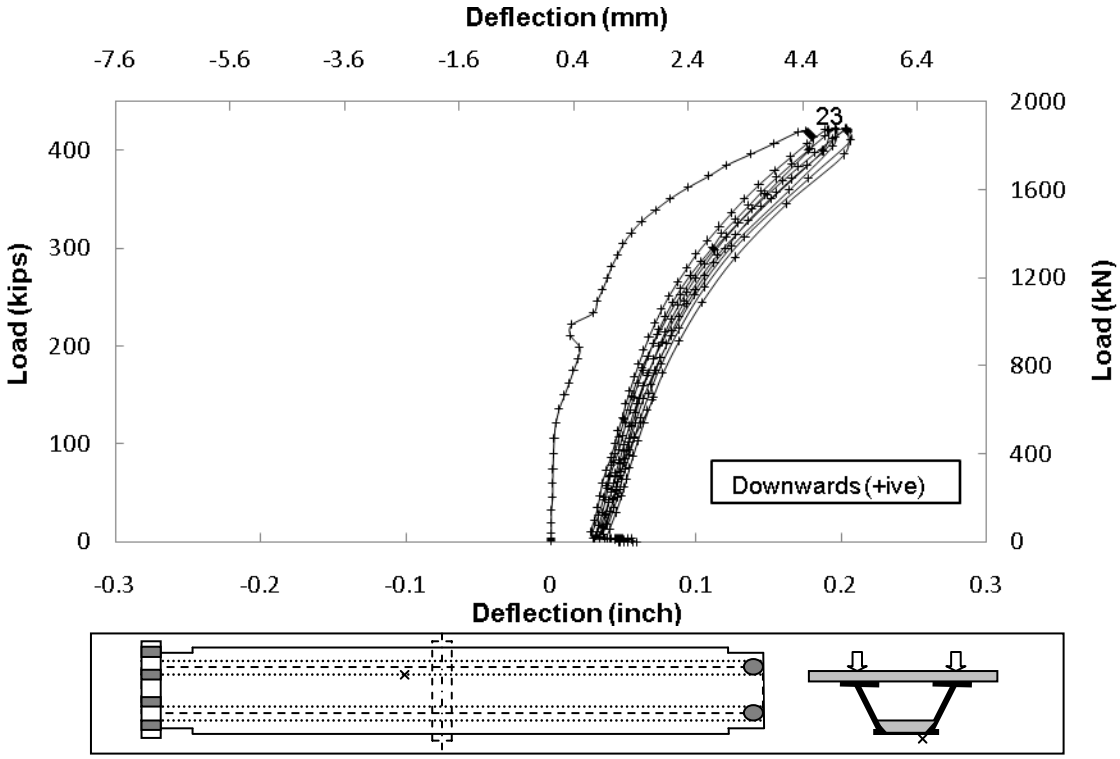


**Figure 6.5** Deflection of Bottom Flange on Hold Down Side (5 cycles)

Since the LVDTs are located on the hold down side, LVDTs #23 and #24 were expected to measure upward (negative) deflection as the span rotates slightly between the hold down end and the center support. However, Fig. 6.4 shows that the bottom flange had downward deflection at both LVDT locations. There is a change in the deflection recorded by LVDT 23 at 130 kips followed by significant non-linearity in the 210-230 kip range. Analysis presented in Chapter 8 revealed that this is a result of significant buckling of the bottom flange near this region.

Fig. 6.5 shows that in subsequent loading cycles (2-5) the displacement path follows the unloading curve for cycle 1. The 'zero shift' suggests some degree of permanent plastic deformation due to the buckling. Deflection values recorded by LVDT 23 for all five load cycles are tabulated in Table 6.2.

### 6.2.2 Slip

Horizontal slip was recorded between concrete and steel interfaces at the actuator and hold down ends (see Fig. 4.6 to Fig. 4.11 for details).

Slip was recorded in the the top slab at the hold down frame end (Fig. 6.6). The maximum recorded slip was 0.012 in. No slip was recorded at the actuator end in both the top and bottom slabs. LVDTs measuring non-zero slip were mounted on plates welded on to the exterior vertical face on sides of the top flange (see Fig. 4.9). This type of mounting may have

inadvertently resulted in measurement of deflection caused by rotation of the top flange instead of in-plane slip. LVDTs for slip measurements at other locations (see Figs. 4.8, 4.9 and 4.11) were mounted on horizontal surfaces and therefore not prone to this type of error.

**Table 6.2** Displacement in Failure Region – LVDT #23

| Load (kips) | Displacement in Failure Region (inch) from LVDT 23 | | | | |
|---|---|---|---|---|---|
| | 1st Cycle | 2nd Cycle | 3rd Cycle | 4th Cycle | 5th Cycle |
| 0 | 0 | 0.047 | 0.050 | 0.056 | 0.056 |
| 50 | 0.001 | 0.033 | 0.037 | 0.041 | 0.043 |
| 100 | 0.002 | 0.044 | 0.049 | 0.054 | 0.057 |
| 130 | 0.005 | 0.049 | 0.054 | 0.058 | 0.066 |
| 150 | 0.009 | 0.054 | 0.057 | 0.061 | 0.70 |
| 190 | 0.018 | 0.064 | 0.067 | 0.071 | 0.75 |
| 200 | 0.020 | 0.067 | 0.070 | 0.074 | 0.080 |
| 210 | 0.013 | 0.067 | 0.070 | 0.078 | 0.083 |
| 222 | 0.014 | 0.071 | 0.074 | 0.083 | 0.088 |
| 234 | 0.029 | 0.076 | 0.078 | 0.088 | 0.093 |
| 300 | 0.050 | 0.108 | 0.111 | 0.113 | 0.120 |
| 400 | 0.154 | 0.176 | 0.177 | 0.182 | 0.188 |
| 421 | 0.176 | 0.191 | 0.191 | 0.204 | 0.203 |

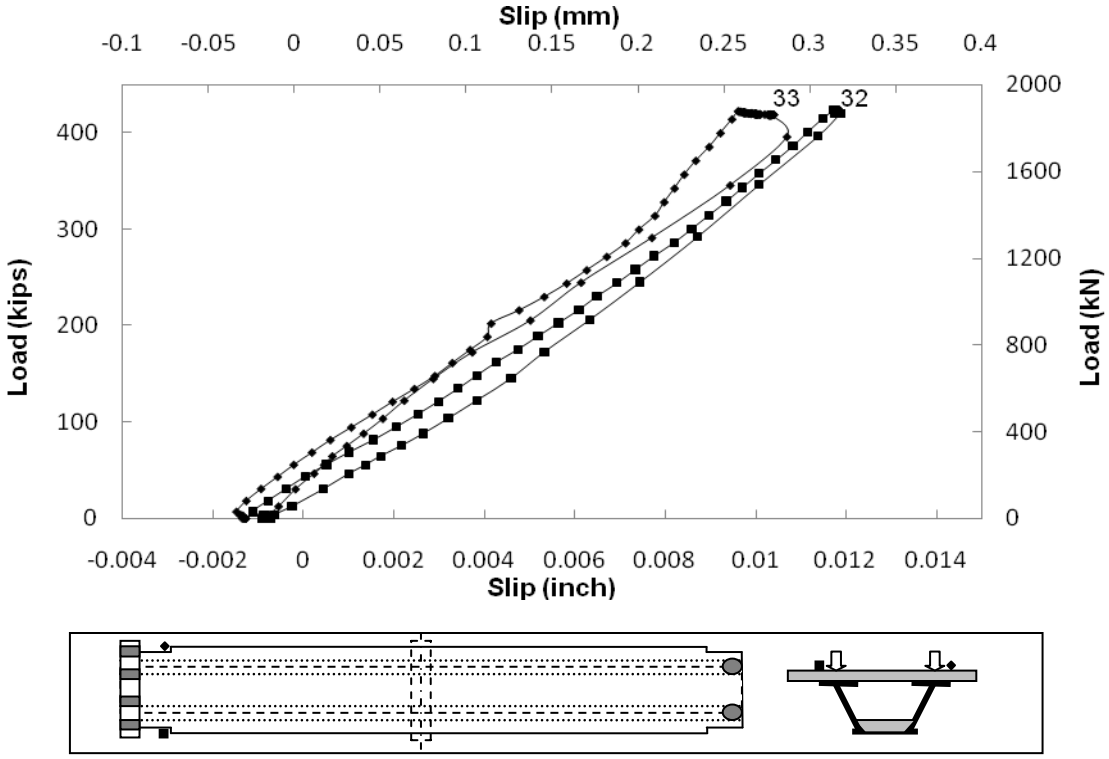


**Figure 6.6** Slip at Hold Down End

### 6.2.3 Top Rebar Strain

A total of 32 strain gages located 1 ft on either side of the center support were used to monitor the rebar strain. Details on their location and nomenclature may be found in Fig. 4.17 and Fig. 4.18. In order to clearly show the strain variation in all 16 gages, results for eight gages are shown in Fig. 6.7 and the remaining eight in Fig. 6.8. Only results for the rebars located in the actuator span are shown since these values were higher. The variation was similar in the gages located in the hold-down span and may be found in Figs E.19-20 on pg-E.15 of Appendix E.

Since the tests were conducted to limit the rebar strain to $0.6f_y$, the strain corresponding to this stress (1241με) appears as a vertical line in Figs. 6.7-6.8. Because of shear lag effects, strains are generally largest over the web.

Values of the maximum measured strain for all rebars from both the actuator and hold down spans are summarized in Table 6.3. The strain recorded in the rebars on the actuator side was higher because the static moment was higher.

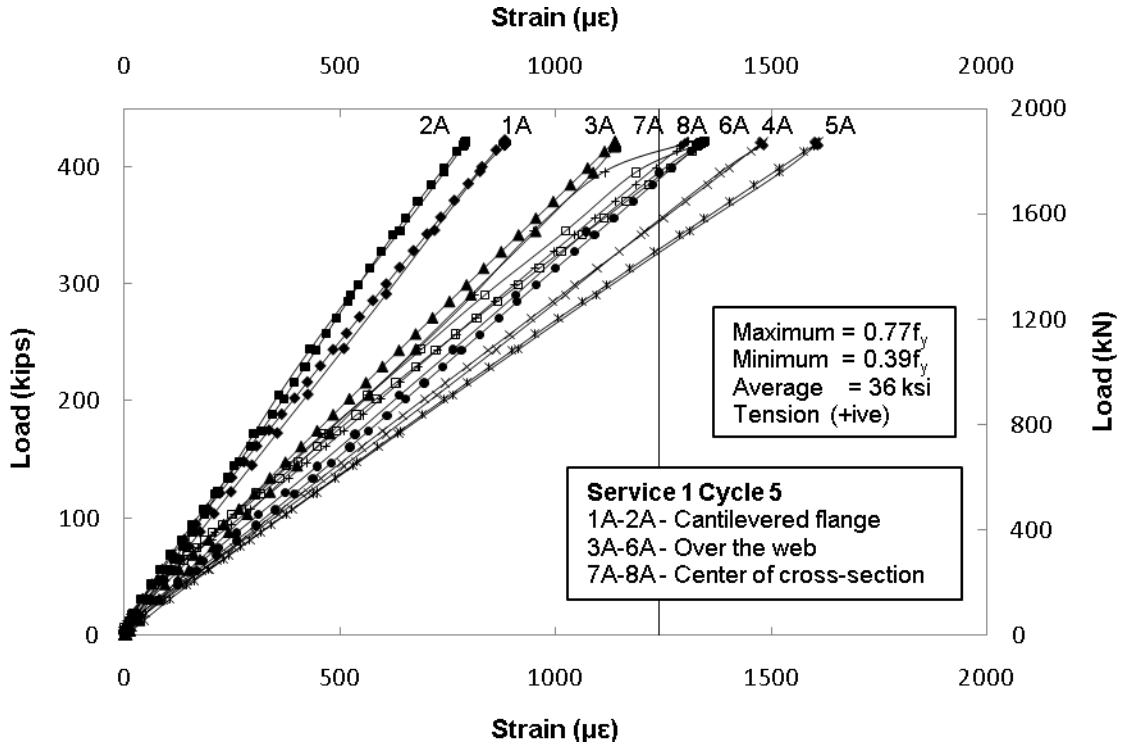


**Figure 6.7** Strain in Top Slab Reinforcement on Actuator side

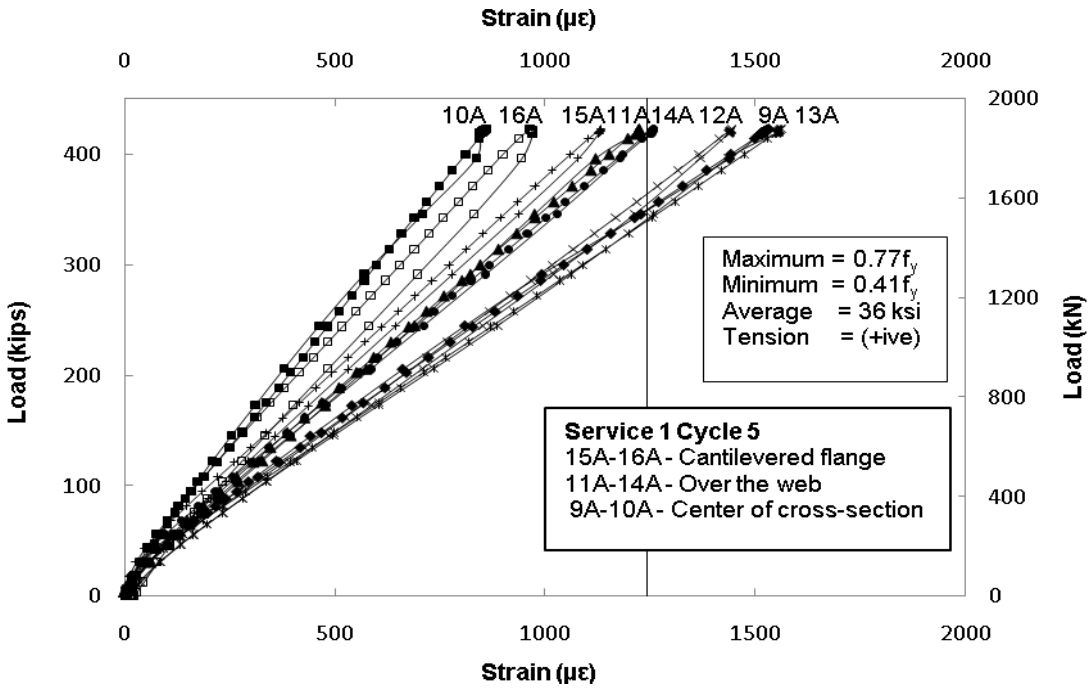


**Figure 6.8** Strain in Top Slab Reinforcement on Actuator side

**Table 6.3** Maximum Strain/Stress in Rebars on Actuator and Hold Down Side

| Rebar gages (Actuator Side) | Maximum Strain (με) | Maximum stress (ksi) | Rebar gages (Hold Down Side) | Maximum strain (με) | Maximum Stress (ksi) |
|---|---|---|---|---|---|
| 1A | 885 | 26 | 1 | 1353 | 39 |
| 2A | 793 | 23 | 2 | 901 | 26 |
| 3A | 1140 | 33 | 3 | 1295 | 38 |
| 4A | 1482 | 43 | 4 | 1589 | 46 |
| 5A | 1613 | 47 | 5 | 1784 | 52 |
| 6A | 1340 | 39 | 6 | 912 | 26 |
| 7A | 1309 | 38 | 7 | 1123 | 33 |
| 8A | 1349 | 39 | 8 | 1285 | 37 |
| 9A | 1530 | 44 | 9 | 1325 | 38 |
| 10A | 861 | 25 | 10 | 725 | 21 |
| 11A | 1223 | 35 | 11 | 1405 | 41 |
| 12A | 1445 | 42 | 12 | 584 | 17 |
| 13A | 1563 | 45 | 13 | 1225 | 36 |
| 14A | 1258 | 36 | 14 | 1167 | 34 |
| 15A | 1133 | 33 | 15 | 714 | 21 |
| 16A | 970 | 28 | 16 | 978 | 28 |

**Note:** Static moment was 10104 kip-ft. on the actuator side and 10067 kip-ft. on the hold down side

### 6.2.4 Crack Width

After the fatigue test was completed, the locations where the crack width was highest were identified (see Fig. 5.12 and Table 5.4). Four crack gages were installed at these locations, two on either side of the center support approximately 1 foot away.

The variation of crack width with load is shown in Fig. 6.9. Surprisingly, the crack width is larger on the hold down span (#3, #4) where moments were lower (Table 6.4) rather than the actuator span (#1, #2). Results presented in Chapter 8 suggests that this occurs primarily due to rotation of the center support diaphragm, which results in it pulling the top slab on the hold down (tension) side. Another contributing factor is thought to be the weaker concrete on the hold down side (see Table 5.1). The largest crack width was 0.0217 inch at sensor 3 on the hold down side. Table 6.4 summarizes the crack width data for the service load test.

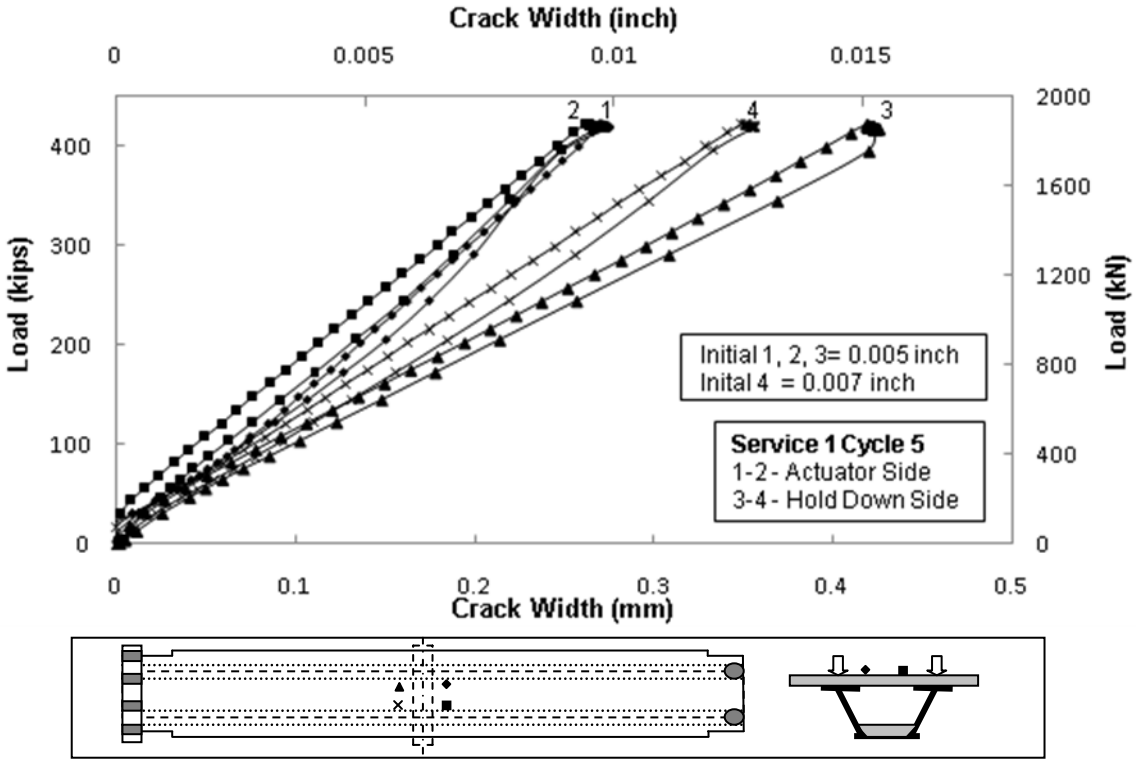


**Figure 6.9** Crack Gages at Center Support on Actuator Side and Hold Down side

**Table 6.4** Crack Width on Top Slab for Service I

| Crack gages | Initial Crack Width (inch) | Measured Crack Width (inch) | Total Crack Width (inch) |
|---|---|---|---|
| Actuator side | | | |
| 1 | 0.005 | 0.0099 | 0.0149 |
| 2 | 0.005 | 0.0106 | 0.0156 |
| Hold Down Side | | | |
| 3 | 0.005 | 0.0167 | 0.0217 |
| 4 | 0.007 | 0.0141 | 0.0211 |

### 6.2.5 Strain in Concrete

The strain in the concrete bottom slab was monitored at symmetric locations 4 ft. 10⅛ in. from the center support by gages 106-111. Of these gages 106-108 are on the actuator span and 109-111 (gage 110 did not work) on the hold-down span (see Fig. 4.19-20).

Fig 6.10 plots the variation in strain with load for the five gages that worked. The variation is highly non-linear even though the loads were in the elastic range. There is stress reversal in gages 106-109. Analysis presented in Chapter 8 reveals that this complex response is caused by different degrees of cracking of the bottom surface of the bottom slab. Due to absence of a bottom mat of reinforcement, the bottom surface of the bottom slab is expected to crack due to shrinkage. Cracking shifts the neutral axis of the bottom slab higher, thereby inducing tension as the load is transferred eccentrically through the shear studs located at the bottom surface (see response of gages 106-109). Eventually, the crack closes, resulting in increased stiffness and development of compressive strains. Moderate amounts of cracking will not shift the neutral axis significantly, but it still results in lower stiffness of the slab until the cracks close (see response of gage 111). The strain profile matches that recorded in the fatigue test (Fig. 5.4).

Fig. 6.11-12 compares the strain data from the fatigue test with those from the service load case for gages 111 and 109 respectively. Fatigue test data after 1.5 million cycles indicates presence of a wide crack since the strain is essentially zero for loads below 70 kips. Note that the slope of the curve beyond 70 kip is similar to those of the measurements taken at 5.65 million cycles and service I test. The response measured after 5.65 million cycles suggest partial crack closure. This may have been caused by redistribution of loads due to continued shrinkage of top and bottom slab concrete. Another potential factor is local buckling of the steel, which would result in sufficient longitudinal strain being developed at a low load to close the crack and start transferring loads to the concrete.

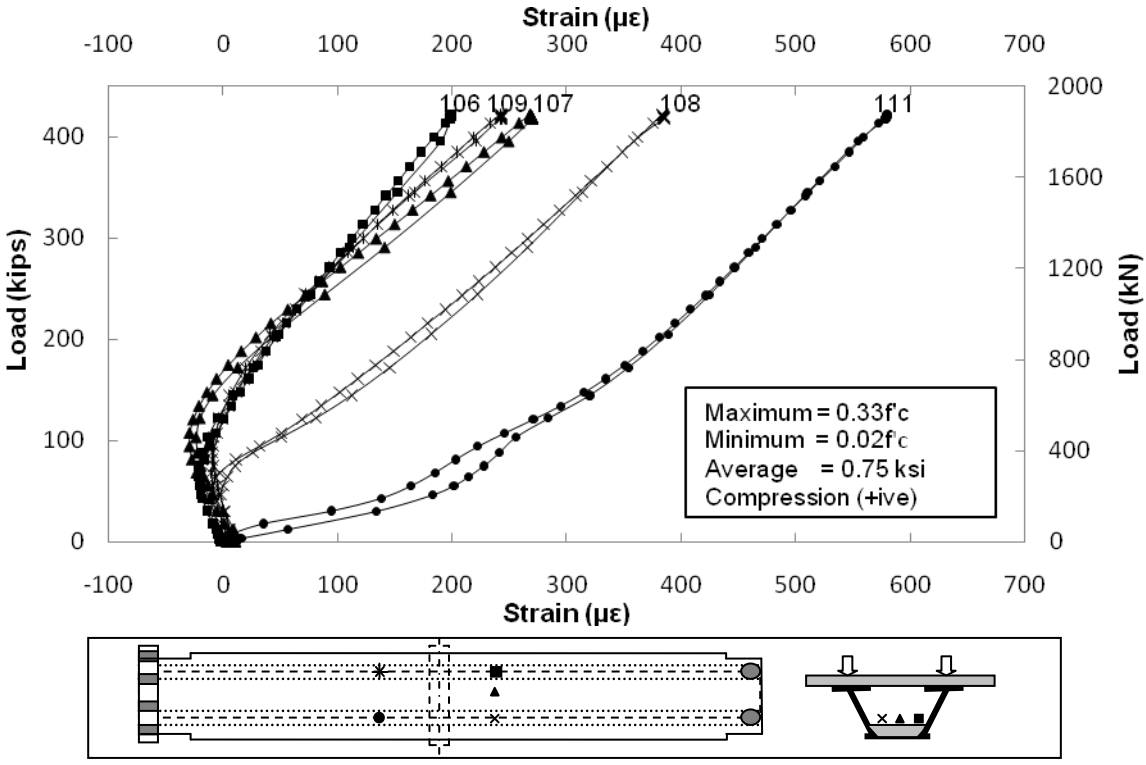


**Figure 6.10** Srain in Bottom Concrete Slab (5th Cycle)

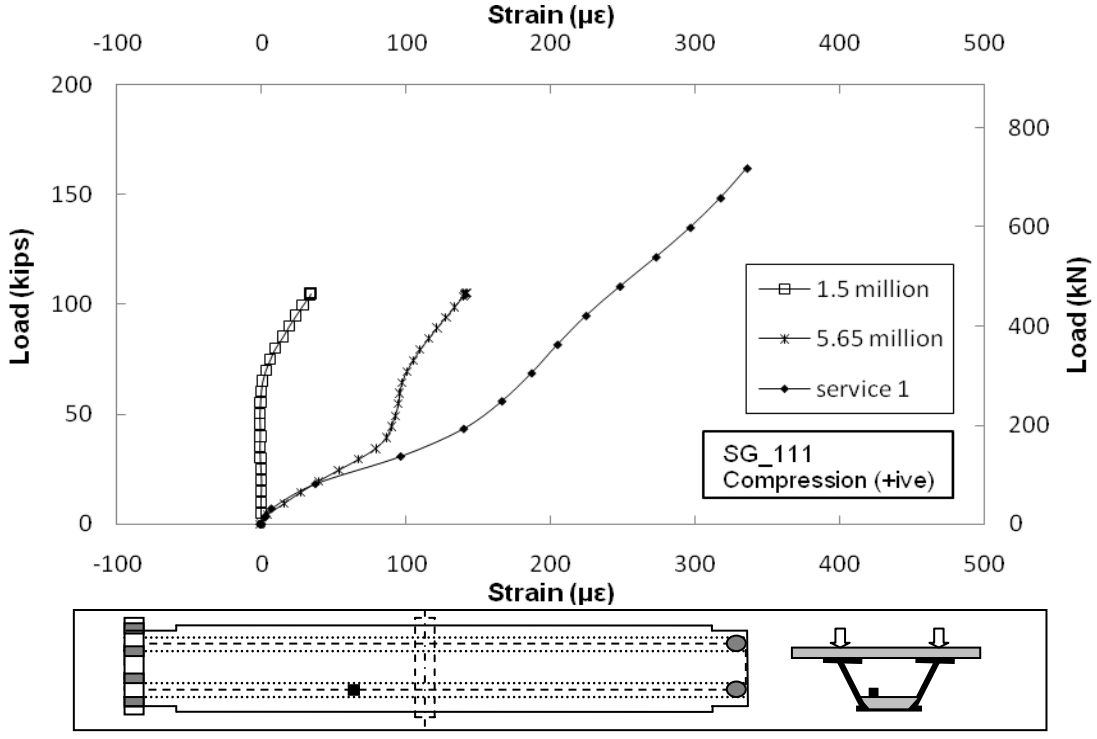


**Figure 6.11** Comparison of Concrete Strain of Fatigue and Service Test for SG 111

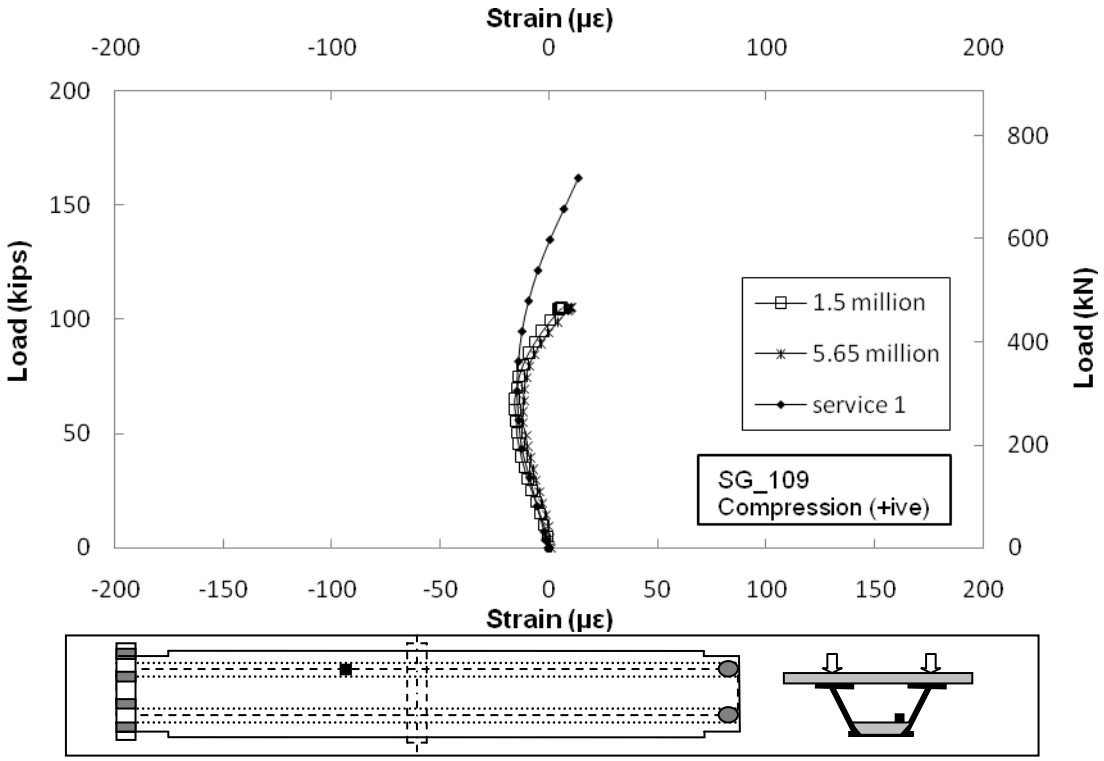


**Figure 6.12** Comparison of Concrete Strain of Fatigue and Service Test for SG 109

### 6.2.6 Strain in Steel

Strains were monitored in the top flange, webs and the bottom flange (see Fig. 4.19 and Fig. 4.20 for details) at the section located 4 ft. 10⅛ in. from the center support. Only results for the strains at the eight locations in the bottom flange are presented. In the actuator span, the gages were numbered 118-120 while corresponding gages in the hold down span were numbered 123-125. Two additional gages (#121, 122) were placed transversely 2 ft. ¼ in from the center support.

Fig. 6.13 and Fig. 6.14 show the variation in strain with load in the actuator and hold down spans respectively. The strain variation is not identical at the two locations and is more non-linear on the hold down side even though the moment is smaller. The maximum recorded strains were 1208 με (35 ksi) and 1145 με (33.2 ksi) in gages 120 and 125 on the actuator and hold down sides respectively.

Fig. 6.15 and Fig. 6.16 compare the strains from fatigue and service load for gages 123 and 125 on the hold down span. The plots only show part of the data for the purposes of comparison. The maximum strain is lower for gage 123 (Fig. 6.15) compared to gage 125 (Fig. 6.16). However, it does not display the same non-linearity as was observed in the concrete gages (Fig. 6.11).

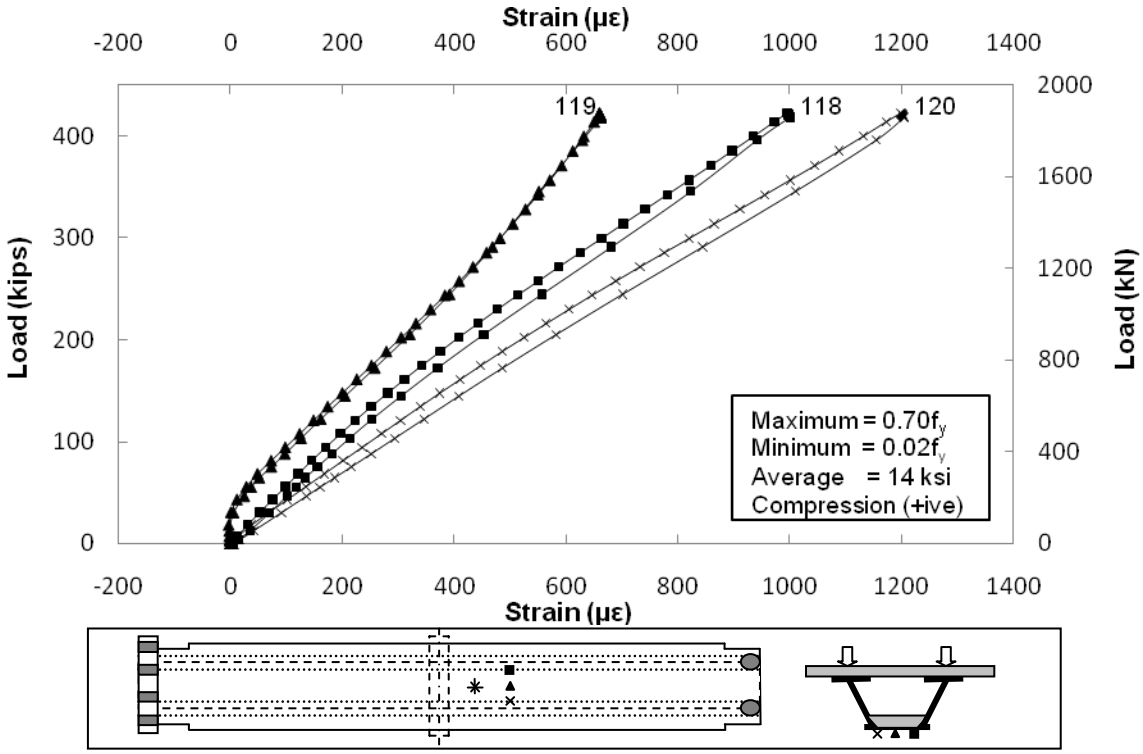


**Figure 6.13** Strain in Bottom Flange on Actuator side

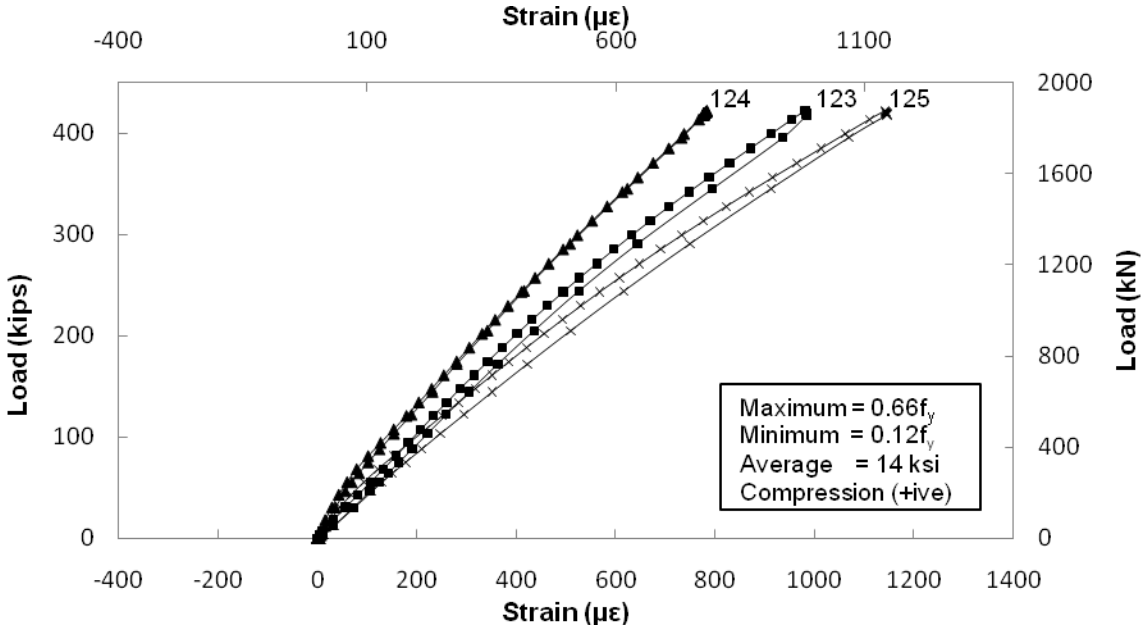


**Figure 6.14** Strain in Bottom Flange on Hold Down Side

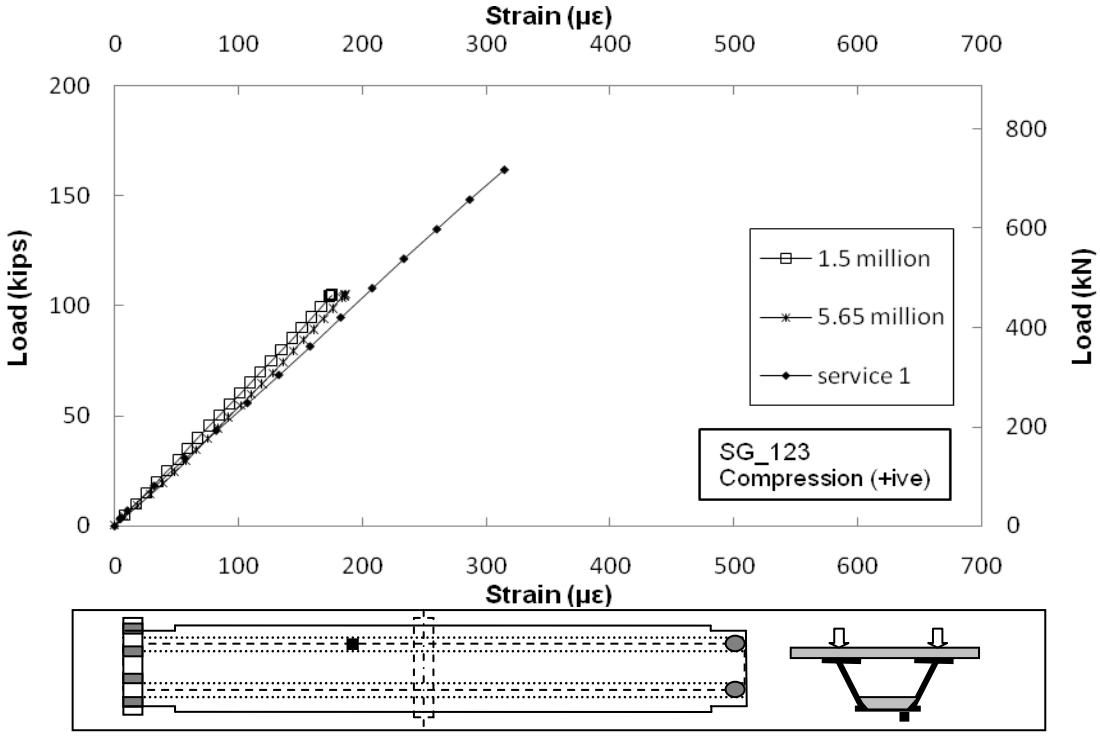


**Figure 6.15** Comparison of Steel Strain of Fatigue and Service Test for SG 123

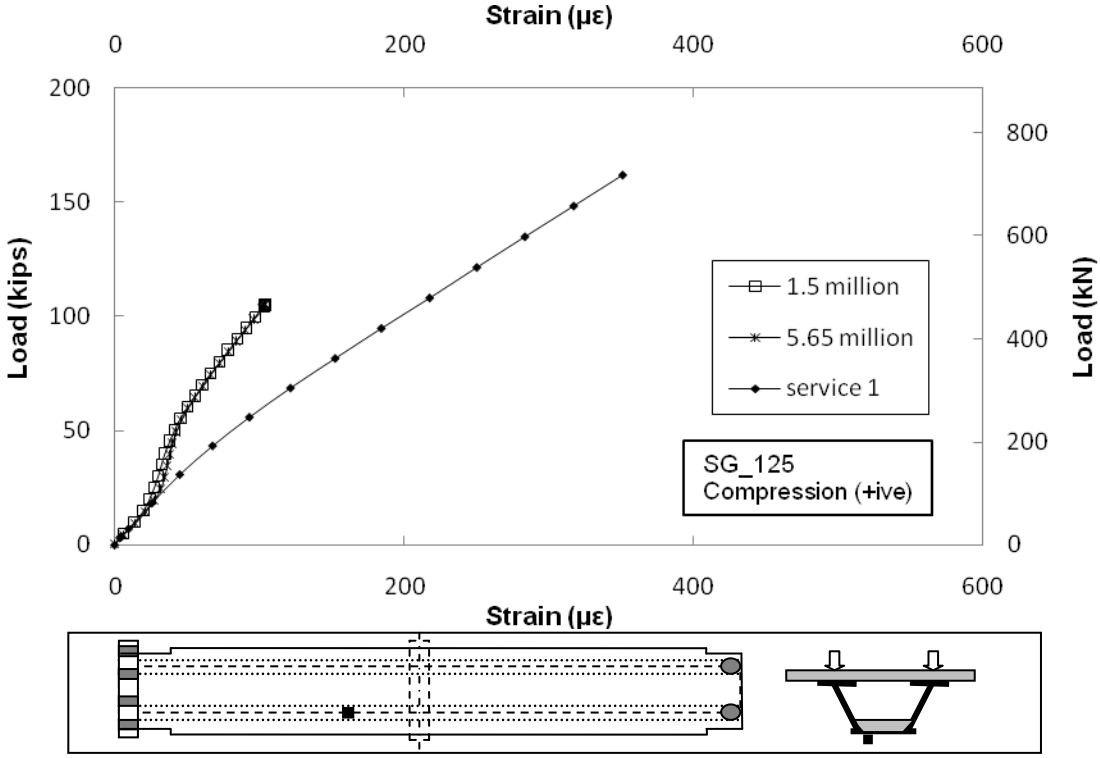


**Figure 6.16** Comparison of Steel Strain of Fatigue and Service Test for SG 125

### 6.2.7 Neutral Axis

Strains measured at three coincident locations on the web were averaged and used to plot the neutral axis (as for the fatigue test).

Figs. 6.17–6.20 plot the neutral axis for each web on the actuator and hold down spans respectively. Table 6.5 summarizes this information. Results show that the neutral axis drops with increasing load from 29 to 32.5 in. for the actuator span and from 28.5 to 33 in. on the hold down side. This is most a likely result of the combined effect of cracking of the top slab and the stiffening observed in the bottom slab (see Fig. 6.10) due to crack closure.

**Table 6.5** Variation of Neutral Axis

| Load | Actuator Side (inch) | | | | Hold Down Side (inch) | | | |
|---|---|---|---|---|---|---|---|---|
| | East Elevation | | West Elevation | | East Elevation | | West Elevation | |
| | Fatigue | Service 1 | Fatigue | Service 1 | Fatigue | Service 1 | Fatigue | Service 1 |
| 100 | 28 | 29 | 28 | 28 | 28 | 29 | 28 | 28.5 |
| 200 | - | 31 | - | 30 | - | 30 | - | 31 |
| 300 | - | 32 | - | 31 | - | 31 | - | 32 |
| 400 | - | 32.5 | - | 32 | - | 32 | - | 33 |
| 421 | - | 32.5 | - | 32 | - | 32 | - | 33 |

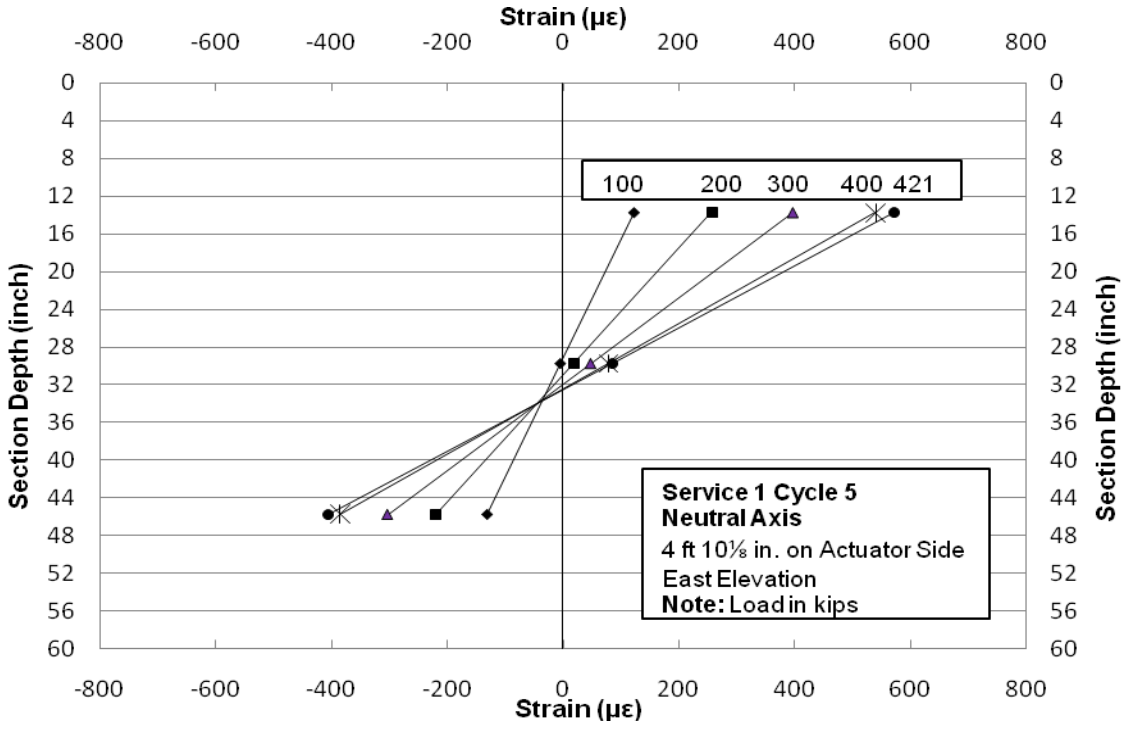


**Figure 6.17** Neutral Axis on Actuator Side (East Elevation)

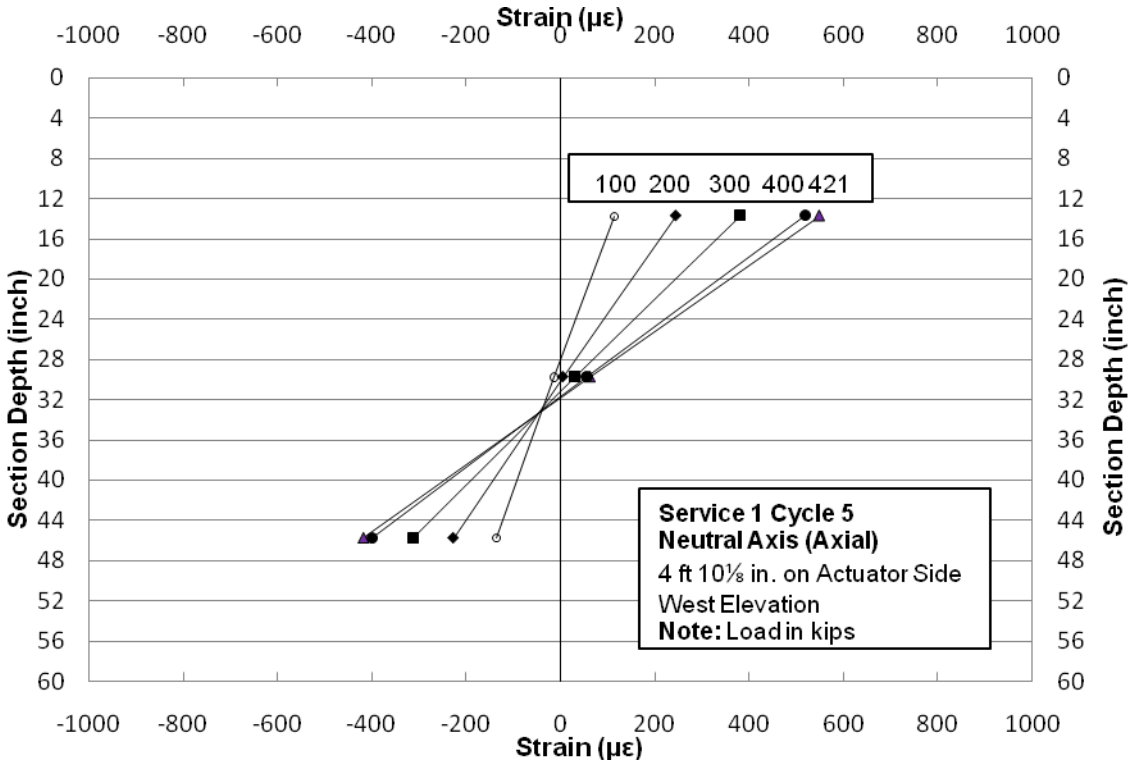


**Figure 6.18** Neutral Axis on Actuator Side (West Elevation)

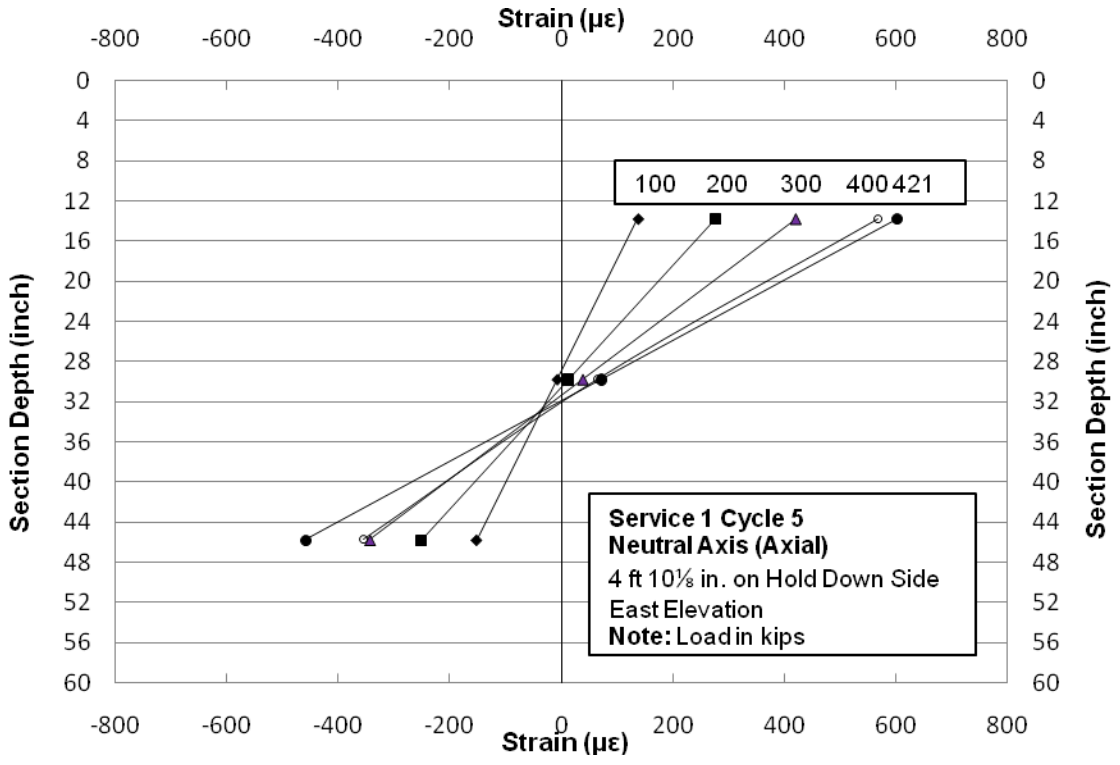


**Figure 6.19** Neutral Axis on Hold Down Side (East Elevation)

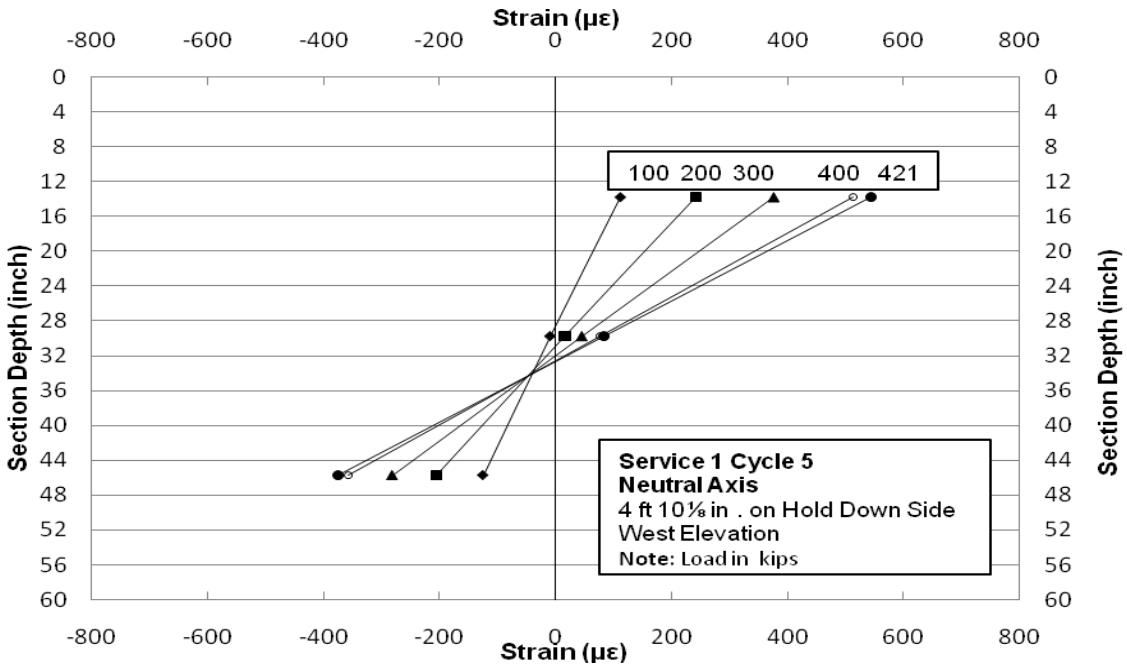


**Figure 6.20** Neutral Axis on Hold Down Side (West Elevation)

## 6.3 Service II Load Test Results

As mentioned earlier, all test parameters and instrumentation used for the Service I test were retained for the Service II test. Thus, the load was applied and removed five times and all data recorded at a scan rate of 10 Hz. The only change made was to the maximum load that was increased from 421 kips to 638 kips. This load corresponded to the condition where the stress in the top flange was limited to $0.95F_y$ with $F_y$ taken as 50 ksi, that is, 47.5 ksi.

The same results reported for Service I, namely deflection, slip, rebar strain, crack width, steel strain and position of the neutral axis are also reported for this loading condition. The same variation in results between different cycles was observed (see Appendix E) and as before the results presented are those from the $5^{th}$ cycle. However, unlike Service I test where initial readings were small and therefore taken to be zero, this was not the case for Service II test especially for strain and deflection data (see Table E.2 in Appendix E). In view this, data presented has *non-zero* initial readings.

### 6.3.1 Deflection

Fig. 6.21 shows the variation in the average deflection of the box specimen along its length for loads ranging 100 to 638 kips. A discontinuity close to the support (2 ft. ¼ in.) may be discerned in the hold-down span for the 638 kip load suggesting localized buckling.

Fig. 6.22 plots the variation of deflection with load for LVDTs 7 and 8 at the free end. The readings overlap indicating the absence of any torsional effect. The maximum deflection recorded was 5 inch.

Table 6.6 compares the measured deflection at the cantilevered free end from the fatigue test (start and end) with those from the first and fifth cycles from service I and II. The comparison shows that for the same 100k load, deflections are greater under the first service II cycle compared to at the end of the fatigue test (1.3907 vs 0.737 in.). Inspection of Table 6.6 also shows that there is some slight stiffening at higher loads, e.g. the deflection under the maximum 639k load reduces from 5.458 in. (1st cycle) to 4.992 in. (5th cycle).

As for the service II load case, the deflection data from the first application of the load is not consistent with those recorded for the remaining four cycles. Fig. 6.23 presents the results for LVDTs 23 and 24 (located 2 ft. ¼ in. from center support on hold down side) for the first cycle. The non-linear response can be readily seen. This is caused by buckling of the bottom flange. However, for subsequent load applications shown in Fig. 6.24 and 6.25 the loading and unloading paths are the same. Note the shift in the zero reading indicating residual deflection due to plastic yielding.

The load deflection plot for LVDTs 23 and 24 shown in Figs. 6.23-6.25 are summarized for selected loads in Tables 6.7 and 6.8 respectively. The results confirm that the deflection response from the first application is stiffer than those from subsequent load applications.

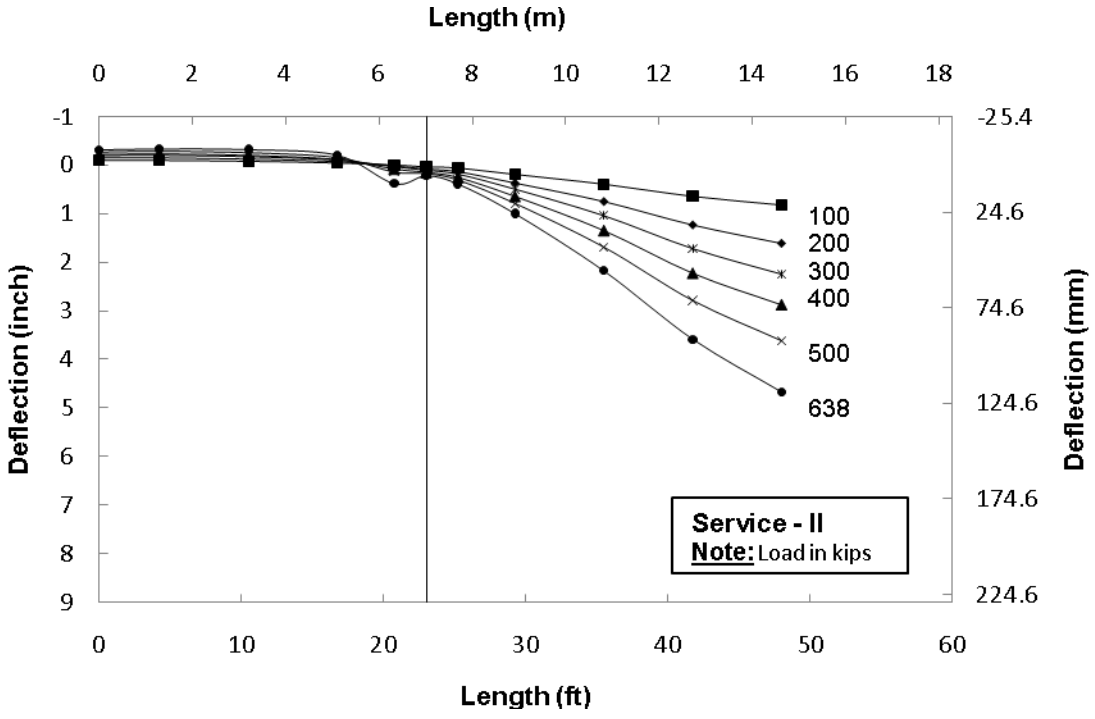


**Figure 6.21** Longitudinal Deflection of Double Composite box girder

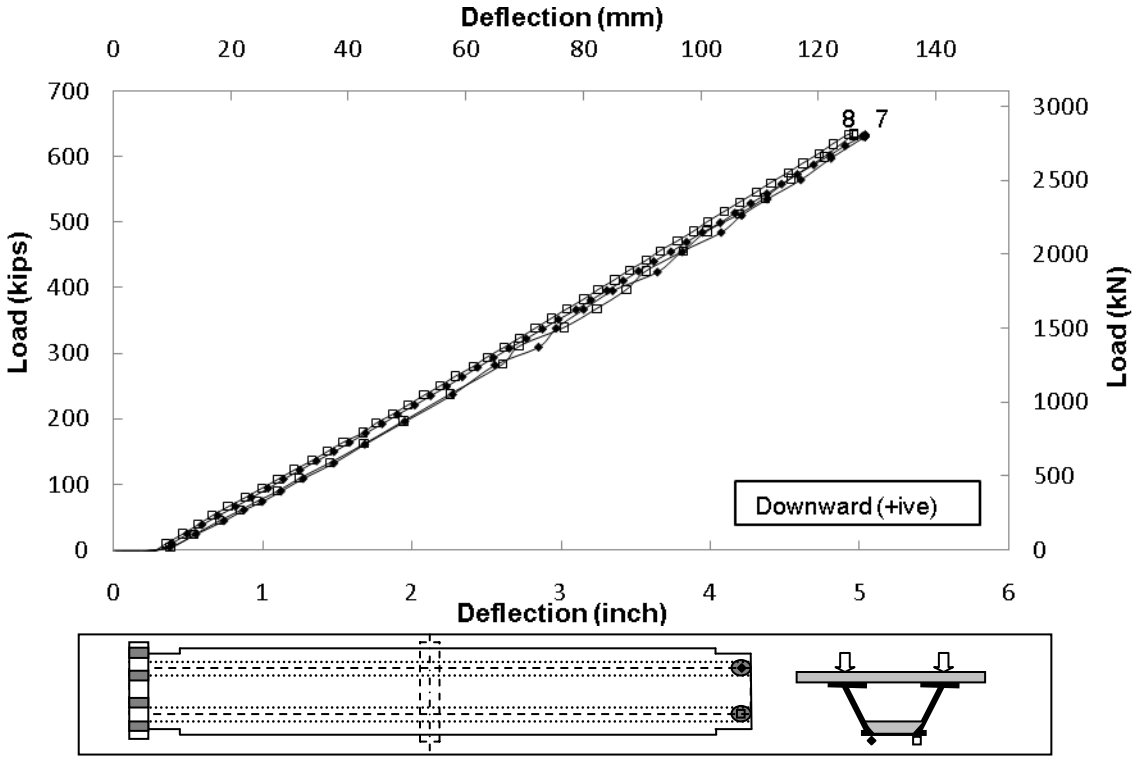


**Figure 6.22** Deflection at Cantilevered End

**Table 6.6** Displacement at Cantilevered End

| Load (kips) | Average Displacement at Cantilevered End (inch) | | | | | |
|---|---|---|---|---|---|---|
| | Fatigue (Static 1) | Fatigue (5.65 million) | Service I 1st Cycle | Service II 1st Cycle | Service I 5th Cycle | Service II 5th Cycle |
| 0 | 0 | 0 | 0 | 0.6654 | 0.228 | 0.2756 |
| 50 | 0.314 | 0.387 | 0.093 | 1.0575 | 0.430 | 0.6797 |
| 100 | 0.614 | 0.737 | 0.483 | 1.3907 | 0.912 | 1.0139 |
| 200 | - | - | 1.155 | 2.1505 | 1.603 | 1.8865 |
| 300 | - | - | 2.025 | 2.9063 | 2.293 | 2.6316 |
| 400 | - | - | 2.890 | 3.5388 | 2.966 | 3.2746 |
| 421 | - | - | - | - | - | - |
| 500 | - | - | - | 4.2742 | - | 4.0206 |
| 600 | - | - | - | 5.1064 | - | 4.7600 |
| 638 | - | - | - | 5.4580 | - | 4.9925 |

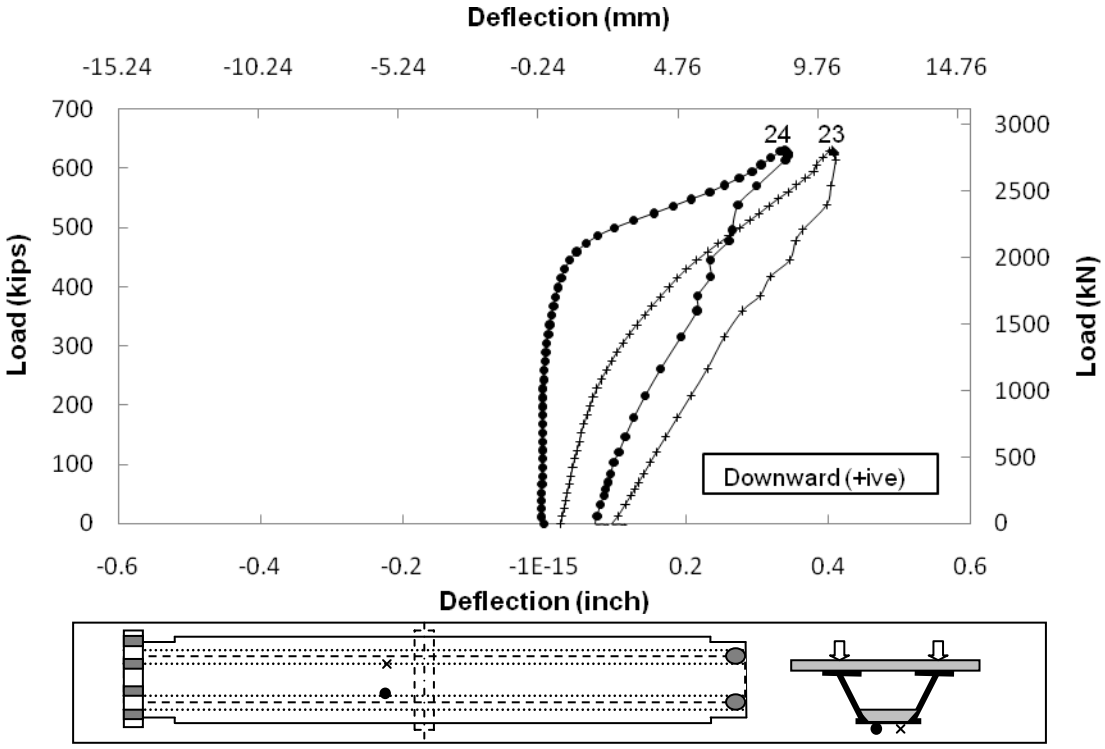


**Figure 6.23** Deflection of Bottom Flange on Hold Down Side (1st Cycle)

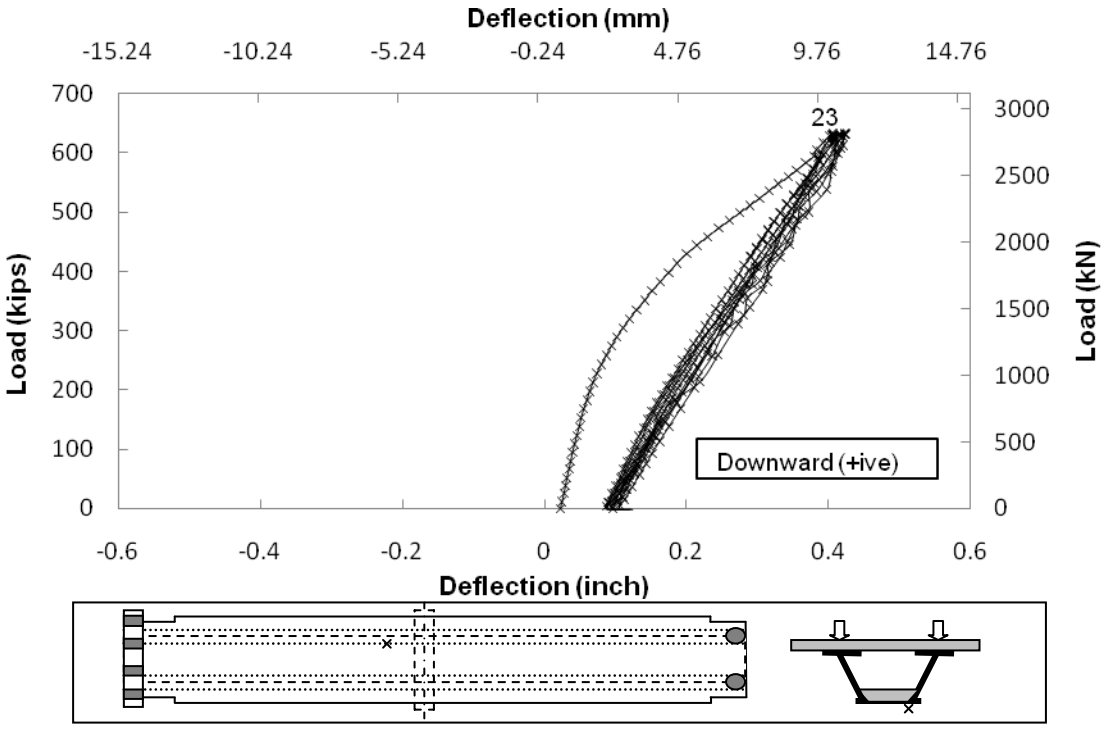


**Figrue 6.24** Deflection in Failure Region for LVDT 23

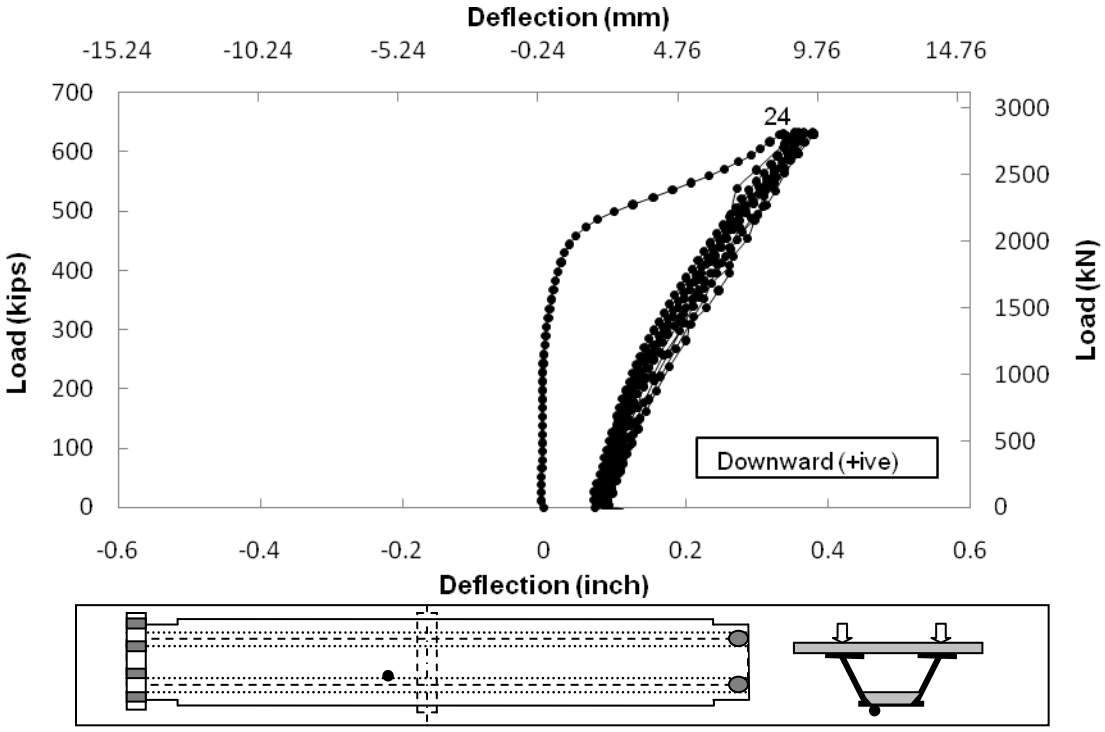


**Figure 6.25** Deflection in Failure Region for LVDT 24

**Table 6.7** Displacement in Failure Region for LVDT 23

| Load (kips) | Displacement in Failure Region for LVDT 23 (inch) | | | | |
|---|---|---|---|---|---|
| | 1st Cycle | 2nd Cycle | 3rd Cycle | 4th Cycle | 5th Cycle |
| 0 | 0.02315 | 0.097239 | 0.107456 | 0.086231 | 0.089324 |
| 50 | 0.0324 | 0.1193 | 0.1213 | 0.1070 | 0.1098 |
| 100 | 0.0400 | 0.1385 | 0.1442 | 0.1232 | 0.1273 |
| 200 | 0.0642 | 0.1787 | 0.1881 | 0.1729 | 0.1771 |
| 300 | 0.1108 | 0.2317 | 0.2438 | 0.2189 | 0.2368 |
| 400 | 0.1754 | 0.2888 | 0.2928 | 0.2742 | 0.2922 |
| 500 | 0.2753 | 0.3485 | 0.3498 | 0.3329 | 0.3322 |
| 600 | 0.3794 | 0.4012 | 0.4144 | 0.3900 | 0.3966 |
| 638 | 0.4059 | 0.4227 | 0.4242 | 0.4067 | 0.4163 |

**Table 6.8** Displacement in Failure Region for LVDT 24

| Load (kips) | Displacement in Failure Region for LVDT 24 (inch) | | | | |
|---|---|---|---|---|---|
| | 1st Cycle | 2nd Cycle | 3rd Cycle | 4th Cycle | 5th Cycle |
| 0 | -0.0013 | 0.0712 | 0.0819 | 0.0858 | 0.0864 |
| 50 | -0.0042 | 0.0782 | 0.0824 | 0.0908 | 0.0943 |
| 100 | -0.0030 | 0.0885 | 0.0947 | 0.1002 | 0.1044 |
| 200 | -0.0027 | 0.1147 | 0.1228 | 0.1314 | 0.1360 |
| 300 | 0.0032 | 0.1545 | 0.1673 | 0.1680 | 0.1833 |
| 400 | 0.0192 | 0.2085 | 0.2138 | 0.2208 | 0.2348 |
| 500 | 0.0981 | 0.2698 | 0.2736 | 0.2828 | 0.2852 |
| 600 | 0.2918 | 0.3287 | 0.3431 | 0.3480 | 0.3573 |
| 638 | 0.3383 | 0.3532 | 0.3586 | 0.3659 | 0.3784 |

### 6.3.2 Slip

Fig. 6.26 and 6.27 plot the slip recorded at the actuator and hold down ends respectively. Slip was observed on the top slab at both ends. The slip data is nonlinear indicating that the mechanism is complex. The maximum slip recorded at top slab interface at the actuator end (given by LVDT 31) was 0.017 inch. The maximum slip recorded at top slab interface at the hold down end (given by LVDT 32) was 0.024 in.

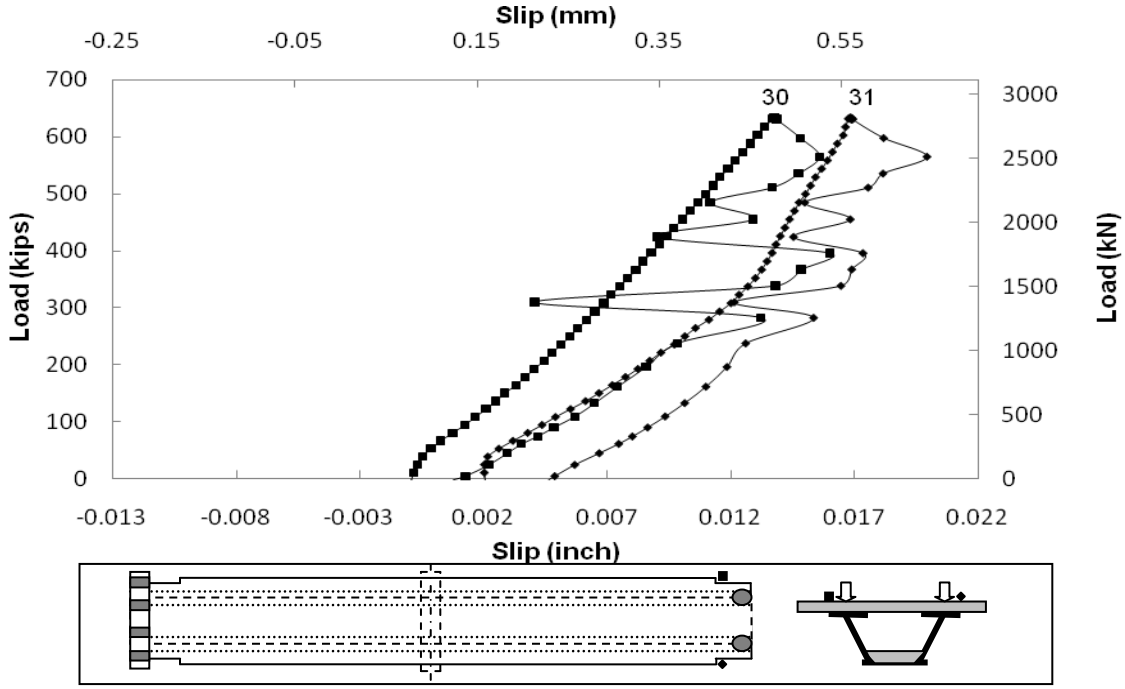


**Figure 6.26** Slip at the Actuator End

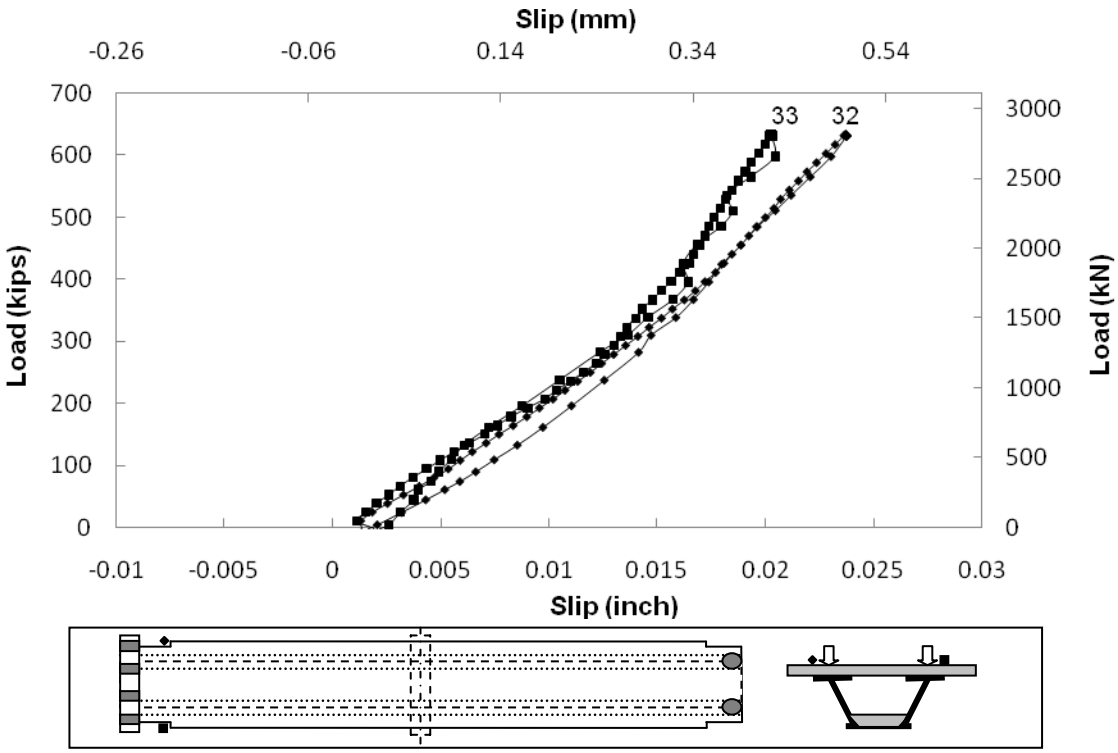


**Figure 6.27** Slip at Hold Down End

### 6.3.3 Top Rebar Strain

The rebar strain was monitored 1 ft. away from the center support by 32 strain gages as before. Fig. 6.28 and Fig. 6.29 plot the variation in strain with load in the rebar in the actuator span for the 16 rebars. Each plot provides data for 8 bars (see Fig. 4.17 and 4.18 for their identification). The strain variation for rebars on the hold down side is presented in Figs. E.55-56 on pg E.33 of Appendix E.

The strain varies linearly with load. As before, higher strains were observed in the rebars located over the webs than in rebars located in the center because of shear lag effects. The average stress in the bars on the actuator side was 55 ksi. In some rebars, the calculated stress exceeded the nominal yield strength value of 60 ksi. Since the yield strength of the bars (73.1 ksi Appendix B) was considerably greater than 60 ksi, stresses higher than 60 ksi were calculated. Complete stress and strain information for all 32 bars is summarized in Table 6.9.

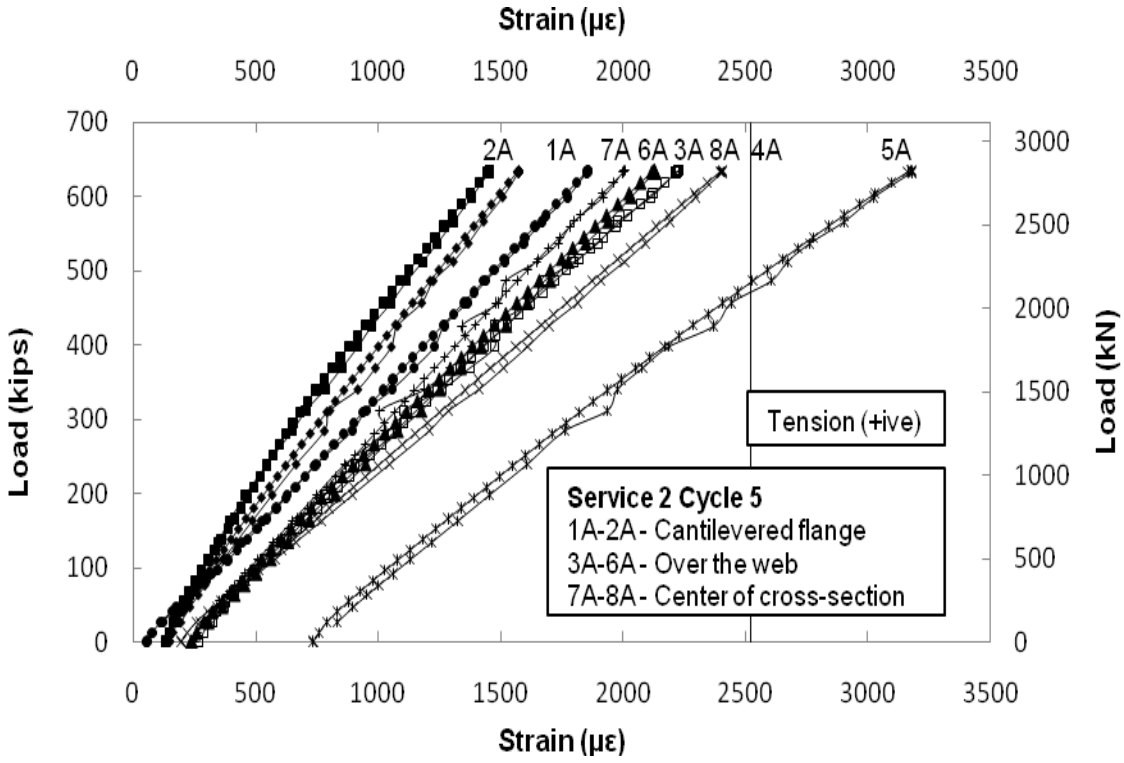


**Figure 6.28** Strain in Top Slab Reinforcement on Actuator Side

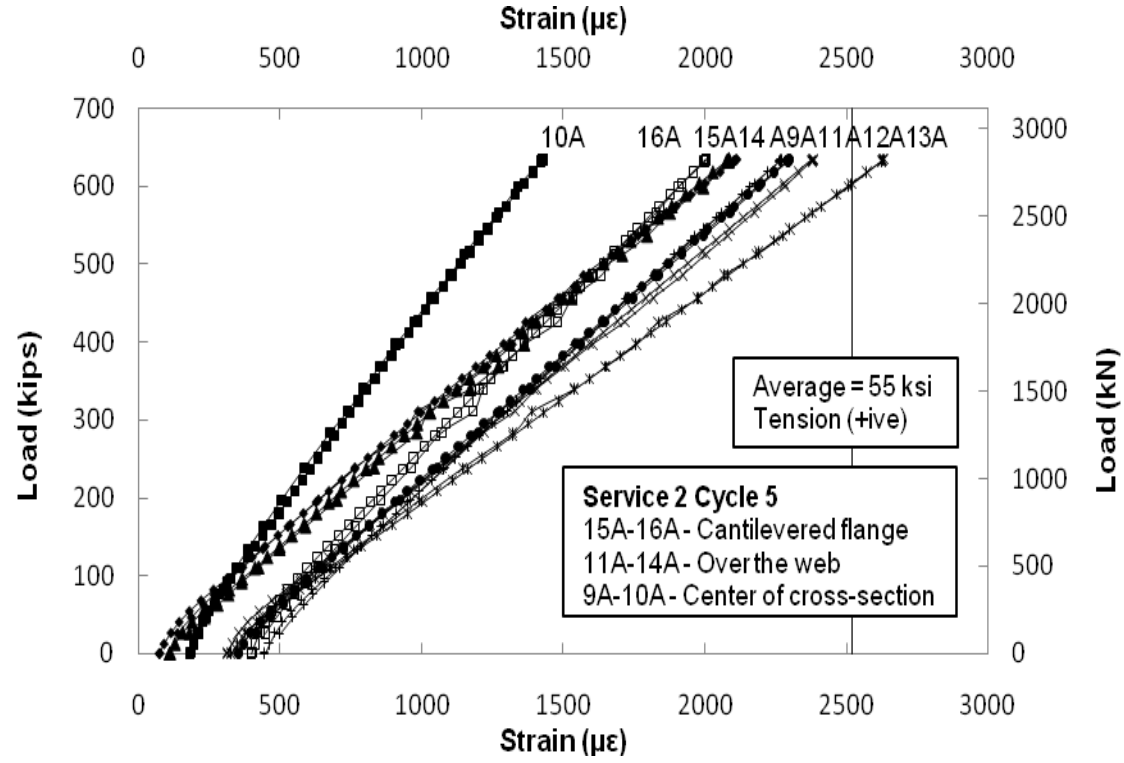


**Figure 6.29** Strain in Top Slab Reinforcement on Actuator Side ($5^{th}$ Cycle)

**Table 6.9** Stress in Rebars on Actuator and Hold Down Sides

| Rebar gages Actuator Side | Maximum Strain (με) | Maximum Stress | Rebar gages Hold Down side | Maximum strain (με) | Maximum Stress |
|---|---|---|---|---|---|
| 1A | 1576 | 46 | 1 | 2159 | 63 |
| 2A | 1456 | 42 | 2 | 1541 | 45 |
| 3A | 2128 | 62 | 3 | 2166 | 63 |
| 4A | 2406 | 70 | 4 | 2365 | 69 |
| 5A | 3182 | - | 5 | 2732 | - |
| 6A | 1857 | 54 | 6 | 1145 | 33 |
| 7A | 2009 | 58 | 7 | 1989 | 58 |
| 8A | 2227 | 65 | 8 | 1719 | 50 |
| 9A | 2112 | 61 | 9 | 1704 | 49 |
| 10A | 1427 | 41 | 10 | 1280 | 37 |
| 11A | 2085 | 60 | 11 | 1978 | 57 |
| 12A | 2382 | 69 | 12 | 1018 | 30 |
| 13A | 2632 | - | 13 | 2462 | 71 |
| 14A | 2297 | 67 | 14 | 2042 | 59 |
| 15A | 2271 | 66 | 15 | 2070 | 60 |
| 16A | 2004 | 58 | 16 | 1874 | 54 |

### 6.3.4 Crack Width

Fig. 6.30 shows the variation in crack width with load. The highest increase in crack width recorded was 0.0188 in. on the hold down span in gage 3. The initial crack width was measured manually using a crack comparator. Table 6.10 summarizes the crack width information.

**Table 6.10** Crack Width on Top Slab for Service II

| Crack gages | Initial Crack Width (inch) | Measured Crack Width (inch) | Total Crack Width (inch) |
|---|---|---|---|
| Actuator side | | | |
| 1 | 0.005 | 0.0146 | 0.0196 |
| 2 | 0.005 | 0.0135 | 0.0184 |
| Hold Down Side | | | |
| 3 | 0.005 | 0.0188 | 0.0237 |
| 4 | 0.007 | 0.0167 | 0.0237 |

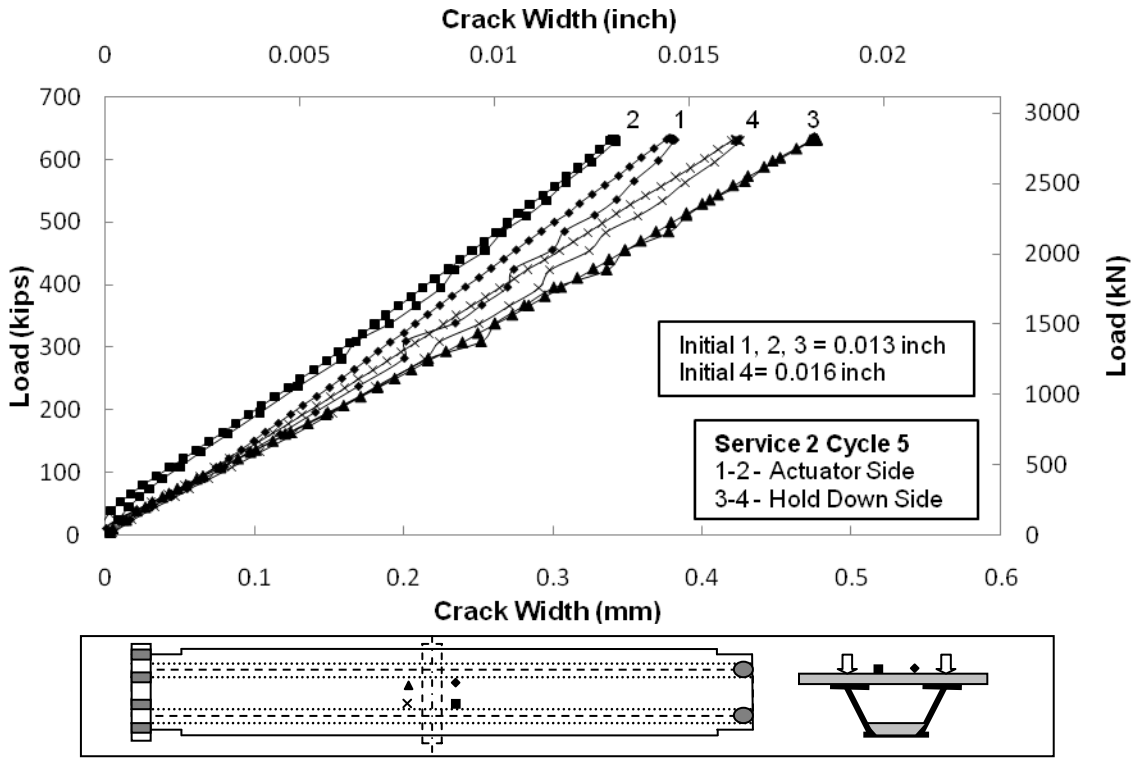


**Figure 6.30** Crack width at center support on Actuator and Hold Down Side

### 6.3.5 Strain in Concrete

Fig. 6.31 shows the variation in strain in the bottom concrete slab with load for the five gages that worked. Information on the location of these gages may be found in Figs. 4.19-20.

The strain variation in these gages is highly non-linear at low loads accompanied by stress reversal. Again, this signifies that the response was complex and the presence of open cracks at the bottom surface of the bottom slab. The maximum measured strain was 815 με by gage 111 located 4 ft. 10⅛ in. from the center support on the hold down span. The corresponding maximum calculated stress assuming the code value for the modulus was 0.43f'c.

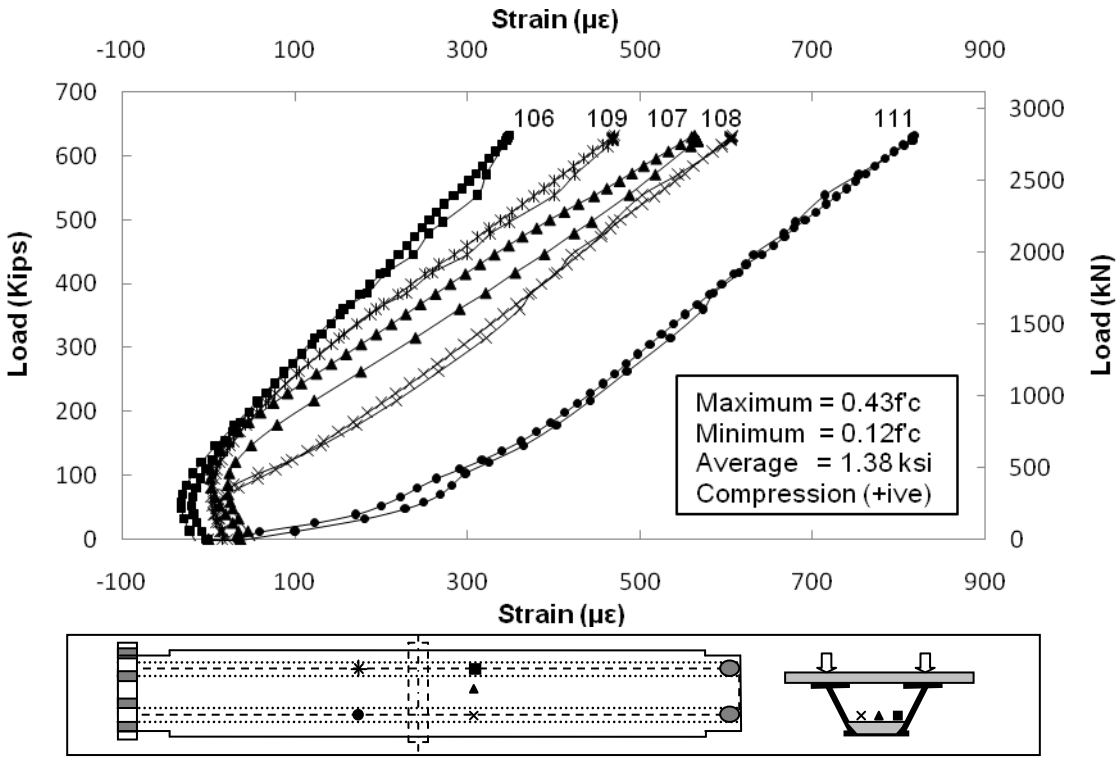


**Figure 6.31** Strain in Bottom Concrete Slab

Fig. 6.32 and Fig. 6.33 compare the variation in strain in gages 109 and 111 located 4 ft. 10⅛ in. from the center support on the hold down span. The plots show only part of the data for comparison purposes. The results for gage 109 show that there was practically no change in behavior of the concrete under fatigue loading. However, this was not the case for strain recorded by gage 111 where the post-fatigue response is more consistent with partial crack closure, perhaps due to load distribution from continued shrinkage and buckling of the bottom flange.

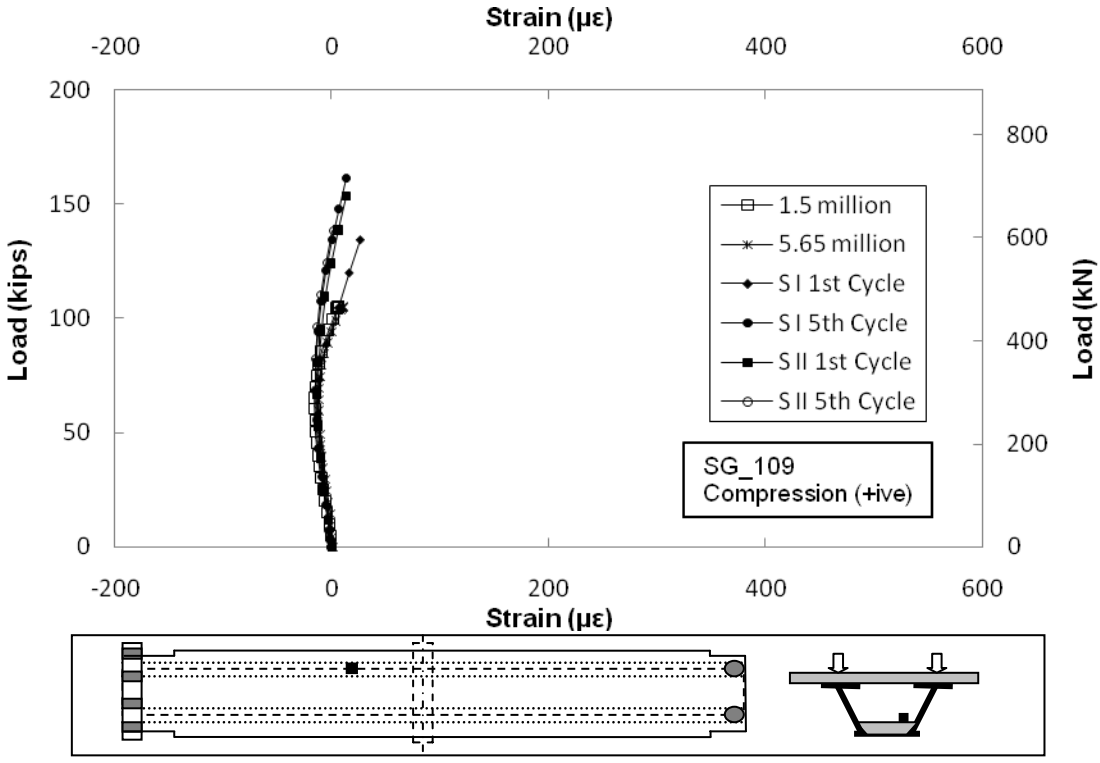


**Figure 6.32** Comparison of Concrete Strain of Fatigue and Service Test for SG 109

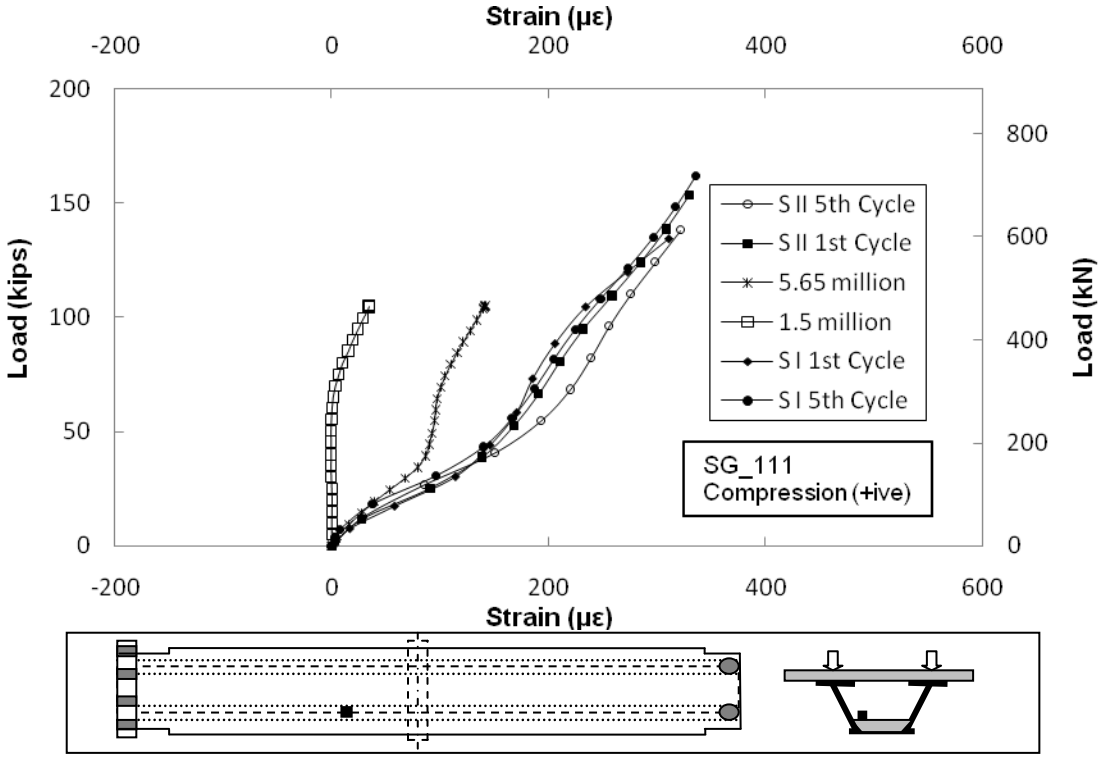


**Figure 6.33** Comparison of Concrete Strain of Fatigue and Service Test for SG 111

### 6.3.6 Strain in Steel

As before, strains were monitored in the top flange, webs and the bottom flange (see Fig. 4.19 and Fig. 4.20 for details) at the section located 4 ft. 10⅛ in. from the center support.

Unlike Service I where the maximum load was controlled by the rebar strain, the maximum load for Service II was controlled by the top flange steel strain. For this reason, the results for the top flange steel strain at the center support are plotted (gages 73, 74) in Fig. 6.34. The strain variation is linear and the maximum recorded value was 1932με. This exceeds the targeted stress of 47.5 ksi.

Results for the steel strain at four locations in the bottom flange on the actuator span are plotted in Fig. 6.35. Of these, gage 121 measured the transverse strain which is negligible. Of the remaining gages, gage 119 positioned at the center shows the strain dropping after approximately 150k to about half its maximum value. This is an indication of buckling, which induces tensile loads on the bottom fiber due to localized flexure. This trend is not repeated in the two gages located over the web (118, 120). For these gages, the response is non linear but similar. The apparent stiffening is again a result of buckling induced flexural tensile strains at the bottom fiber. This trend was not observed in Service I (see Fig. 6.13 and 6.14).

The strains in the corresponding gages on the hold-down span are qualitatively similar (Fig. 6.36). There was no significant strain in the transverse direction (gage 122) but the strain in gage 124 dropped off and reversed from its maximum value at a load below 150 kip. As for the hold down side, the response of gages 123 and 125 located at the webs were comparable. The results from Fig. 6.35 and 6.36 suggest localized buckling near the location of these gages in the middle of the box and 4 ft. 10⅛ in from the center support.

The maximum strain recorded on the actuator side was 2191με for strain gage 120 (Fig. 6.35). On the hold-down side, the corresponding strain in gage 125 was 2379 με. Both exceeded the targeted 47.5 ksi stress (Fig. 6.36).

Fig. 6.37 and 6.38 compare the strain variation in gages 123 and 125 in the hold down span for the fatigue cycle (1.5 million, 5.65 million cycles) and for the first and fifth cycles from service I and II. The plots show only part of the data for comparison purposes. The results show a significant reduction in stiffness for the $5^{th}$ cycle. Again, this suggests that there was some degradation of the specimen under the service II loads due to buckling.

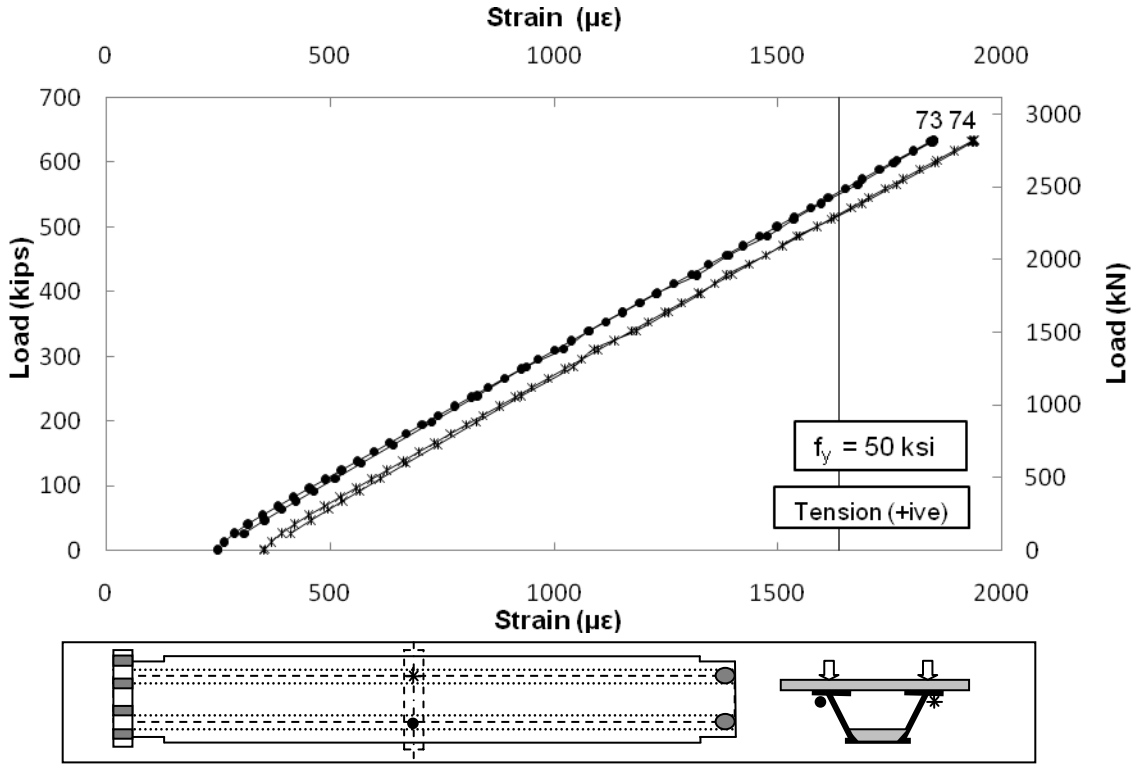


**Figure 6.34** Strain in Top Flange at Center Support

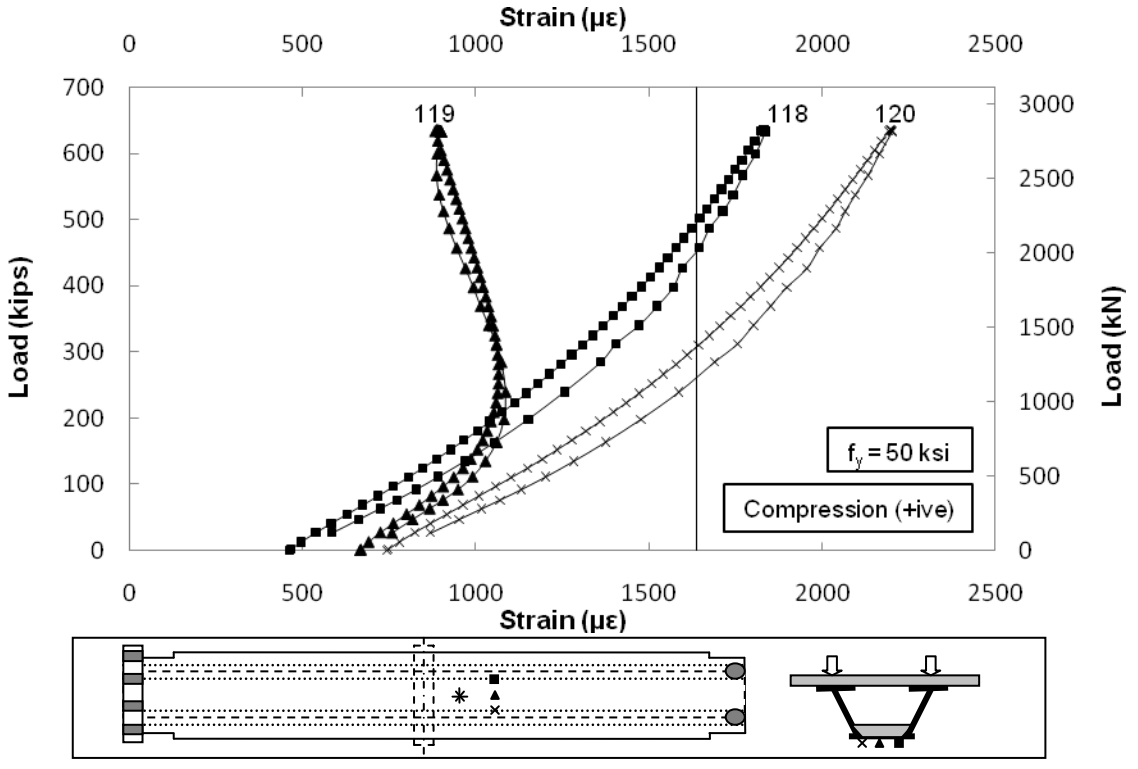


**Figure 6.35** Strain in Bottom Flange on Actuator side

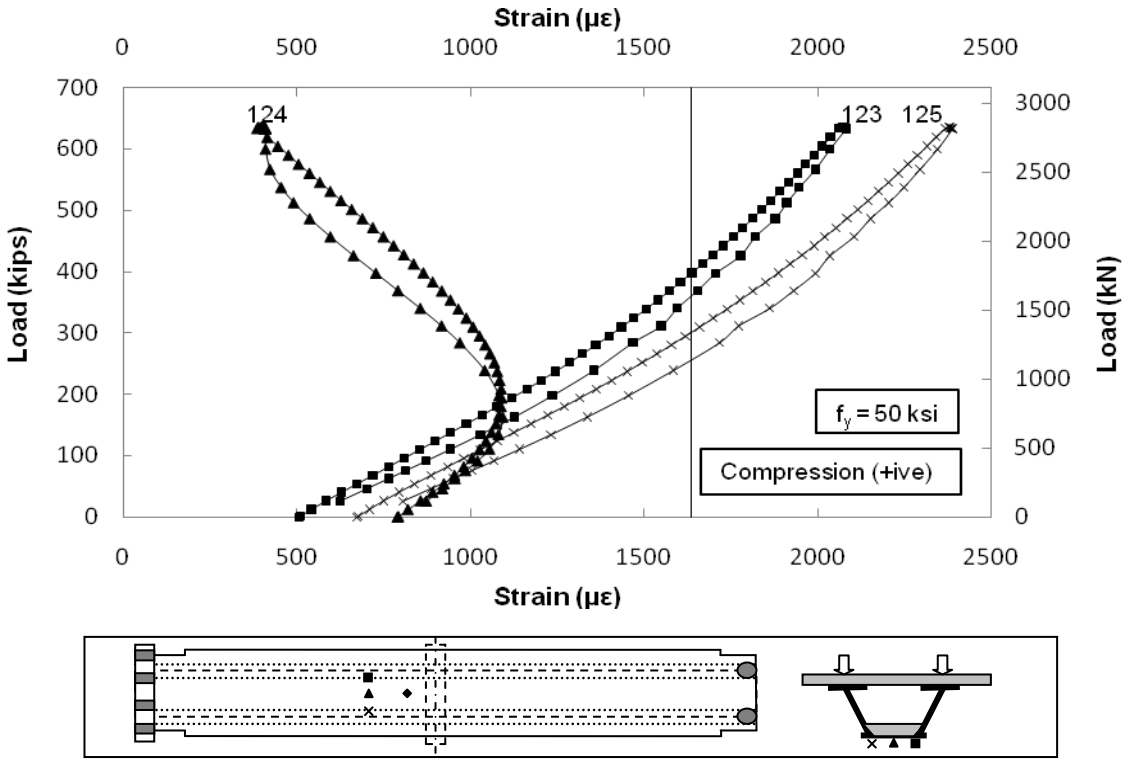


**Figure 6.36** Strain in Bottom Flange on Hold Down side (5th Cycle)

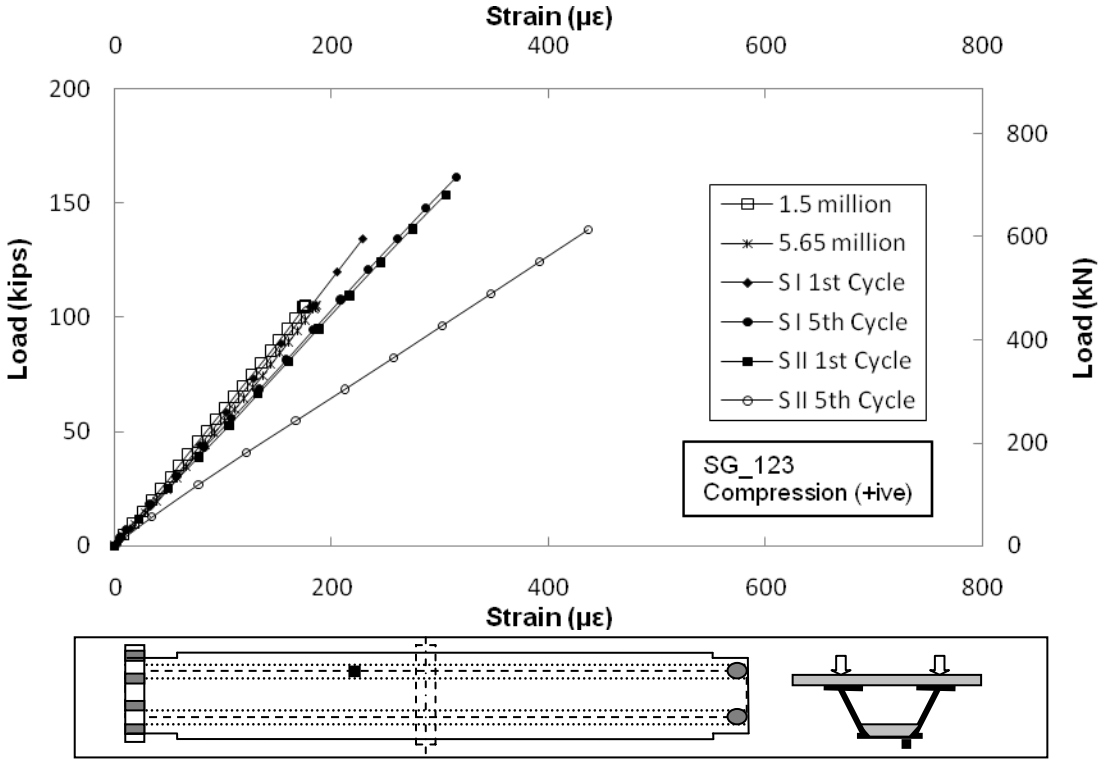


**Figure 6.37** Comparison of Steel Strain of Fatigue and Service Test for SG 123

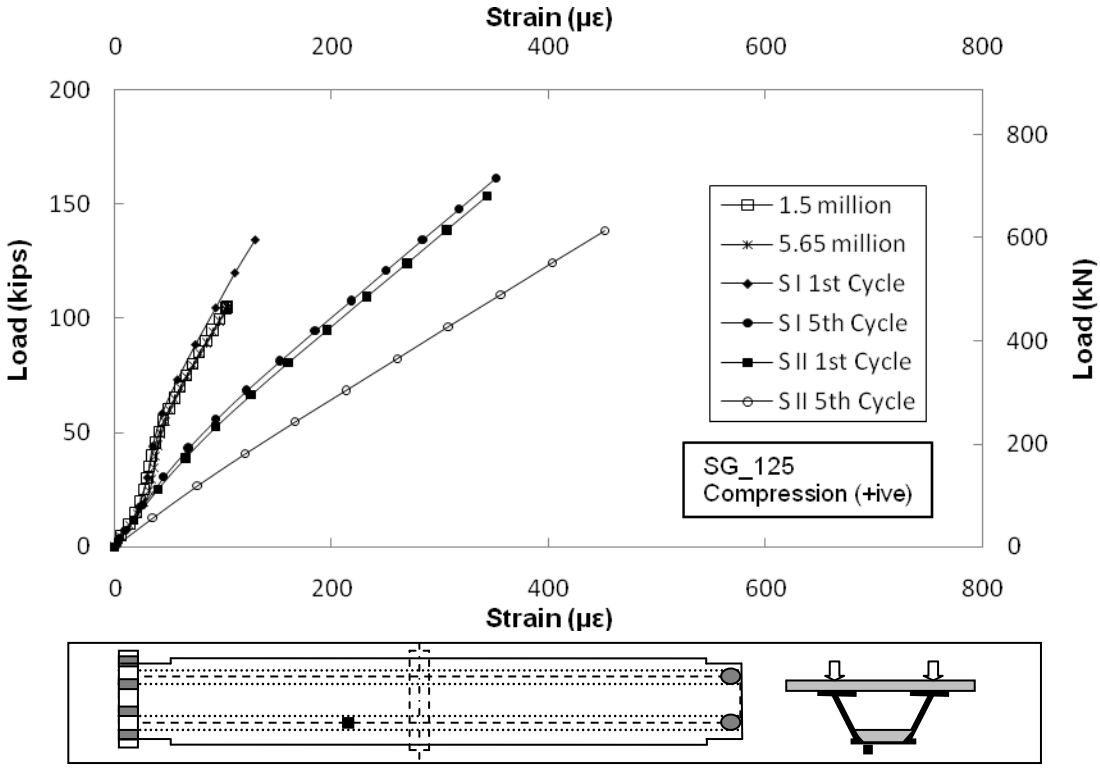


**Figure 6.38** Comparison of Steel Strain of Fatigue and Service Test for SG 125

### 6.3.7 Neutral Axis

As before the neutral axis was computed by averaging web strains at three coincident locations (see Figs. 4.19-4.20). Results for the neutral axis are plotted for each 100 kip interval.

Figs. 6.39-6.42 plot the neutral axis for each web on both the actuator and hold down spans respectively. Variation in strain with load is summarized in Table 6.11.

**Table 6.11** Variation of Neutral Axis

| Load (kips) | Actuator Side (inch) | | | | Hold Down Side (inch) | | | |
|---|---|---|---|---|---|---|---|---|
| | East Elevation | | West Elevation | | East Elevation | | West Elevation | |
| | S-1 | S-II | S-1 | S-II | S-1 | S-II | S-1 | S-II |
| 100 | 29 | 32 | 28 | 30 | 29 | 31 | 28.5 | 31 |
| 200 | 31 | 32 | 30 | 30.5 | 30 | 31 | 31 | 32 |
| 300 | 32 | 32.5 | 31 | 31 | 31 | 32 | 32 | 32 |
| 400 | 32.5 | 32.5 | 32 | 31.5 | 32 | 32 | 33 | 32.5 |
| 500 | | 32.5 | | 32 | | 32 | | 33 |
| 600 | | 33 | | 32.5 | | 32.5 | | 33.5 |
| 638 | | 33 | | 32.5 | | 32.5 | | 33.5 |

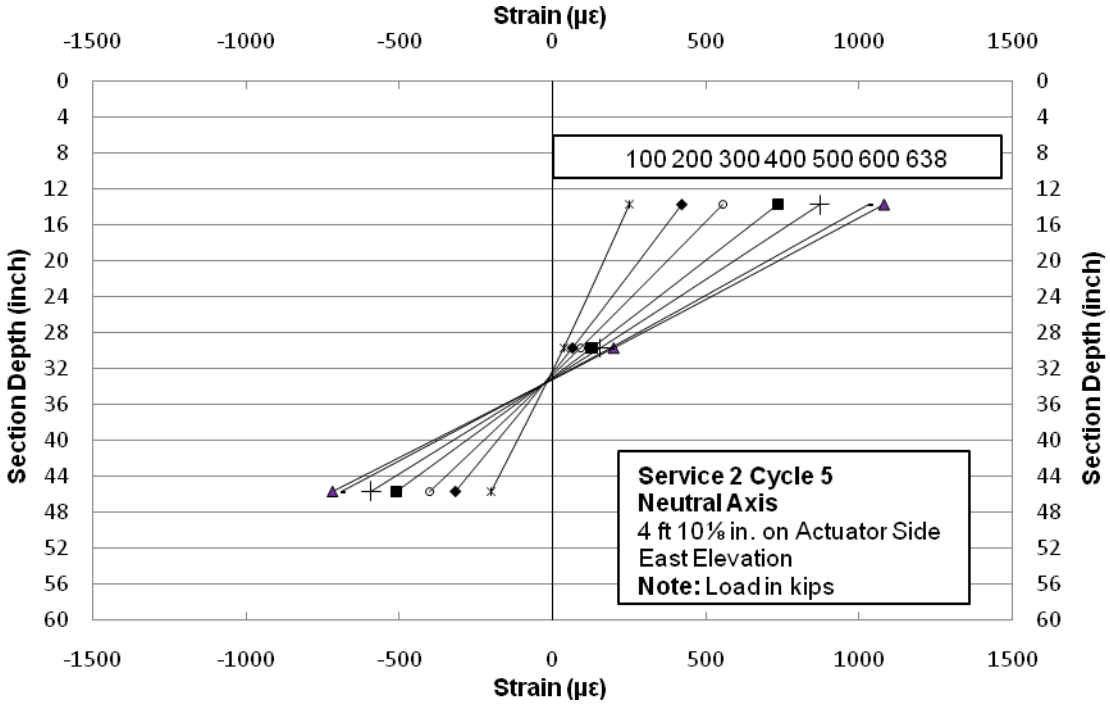


**Figure 6.39** Neutral Axis on Actuator Side (East Elevation)

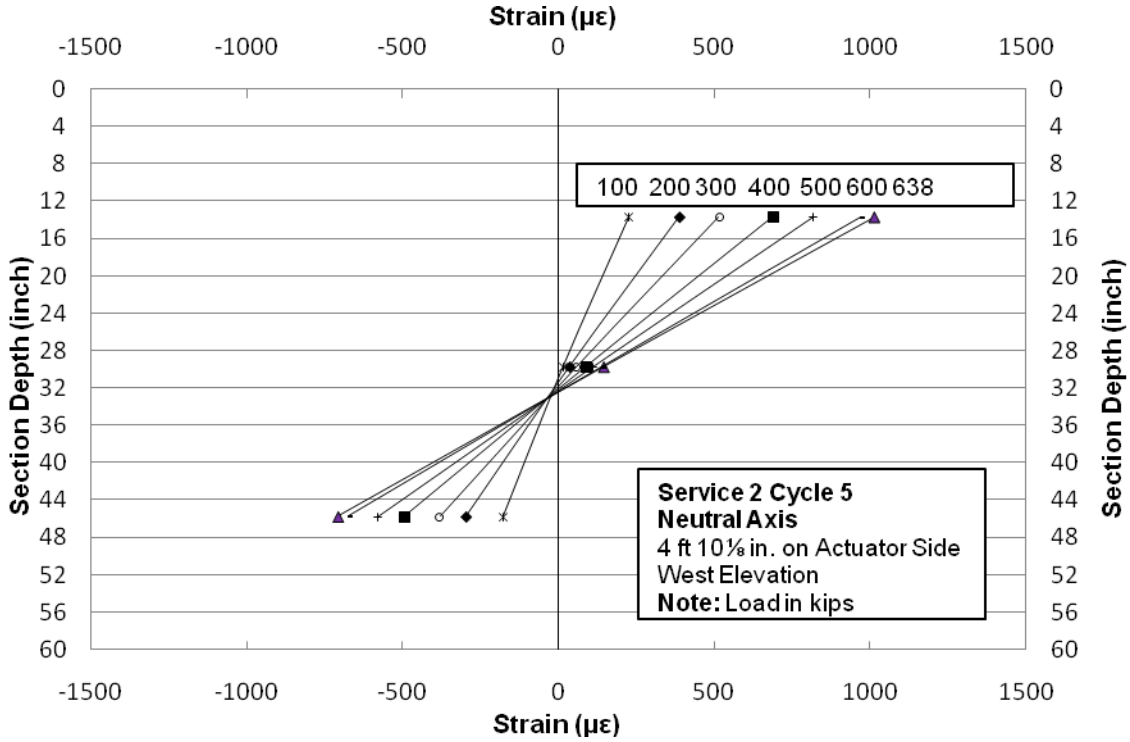


**Figure 6.40** Neutral Axis on Actuator Side (West Elevation)

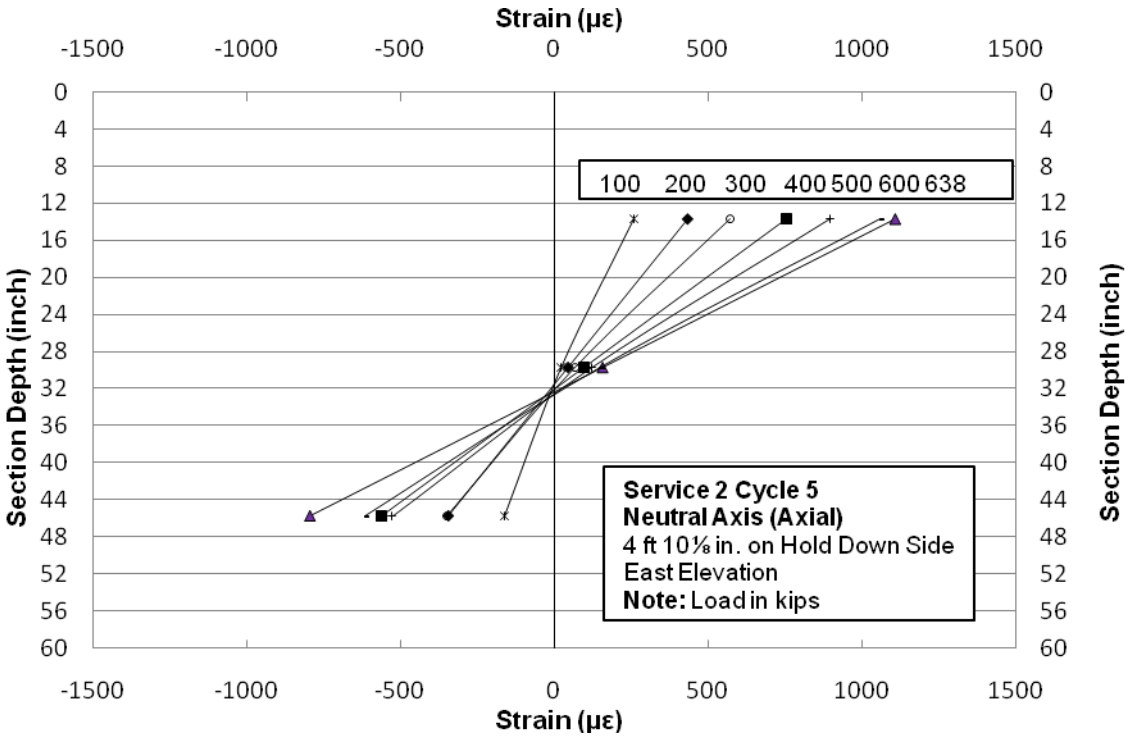


**Figure 6.41** Neutral Axis on Hold Down Side (East Elevation)

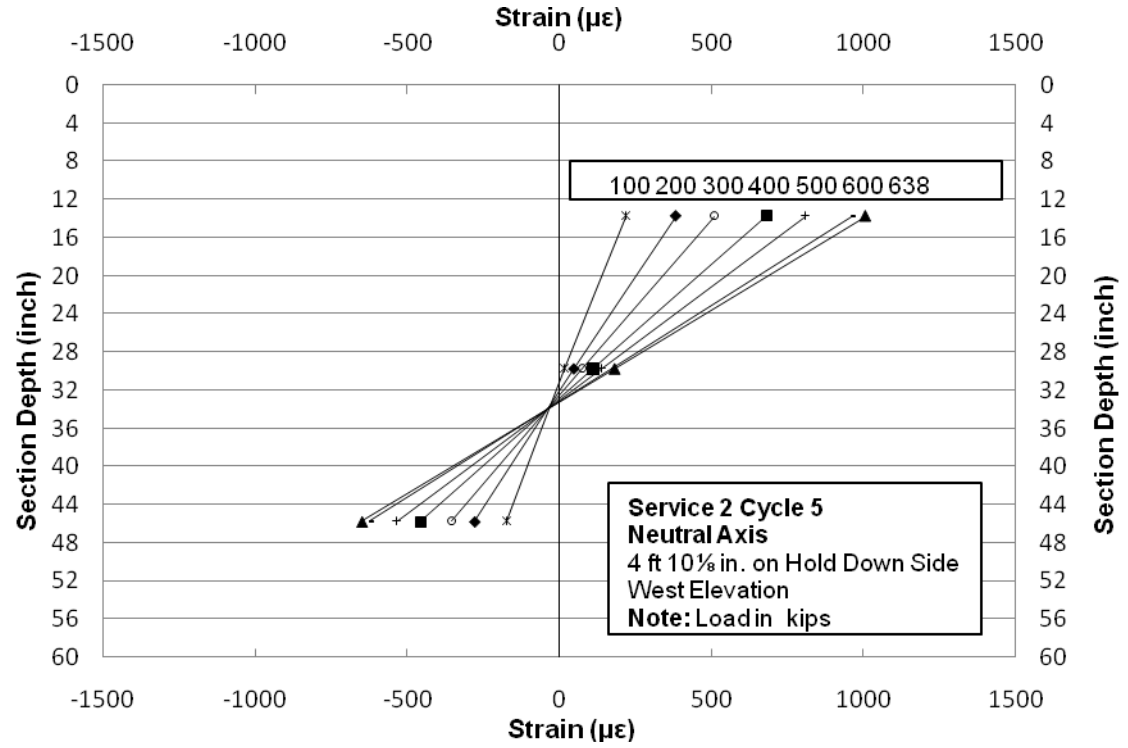


**Figure 6.42** Neutral Axis on Hold Down Side (West Elevation)

## 6.4 Conclusions

**Service I**

- The response from the first load application differed significantly from subsequent applications of the same load (see Fig. 6.5). This is thought to be due to occurrence of local buckling in the first cycle resulting in a permanent change in the stiffness of the structure.

- The deflection in the critical failure region close to center support (Fig. 6.5) was non-linear even though the load was in the elastic range. This is consistent with buckling of the bottom flange.

- The average crack width was 18 mils (0.018 in.) while the maximum was 21 mils (0.021 in.).

- The strain variation in the bottom steel flange and the bottom concrete slab were non-linear (see Fig. 6.16 and 6.11). The strain in the concrete indicated partial crack closure at about 30 kips.

- The concrete bottom slab underwent stress reversal at relatively low loads (Fig. 6.10). Most likely the result of significant open cracks in the bottom surface of the bottom slab.

**Service II**

- The response from the first load application differed significantly from subsequent applications of the same load as for Service I.

- The average crack width was 21 mils (0.021 in.) while the maximum was 24 mils (0.024 in).

- The deflection in the critical failure region close to center support was non-linear and there was evidence of localized distortion in the bottom plate. Buckling of the bottom plate occurred at relatively low loads (below 50 kips - see Fig. 6.23 to 6.25).

- The strain recorded in the top flange exceeded $0.95F_y$ (47.5 ksi) limit (see Fig 6.34). The strain recorded for the bottom flange was non-linear (see Fig. 6.36). Comparison of strain with fatigue and service I load test reveals that there is a reduction in the stiffness of the specimen due to increased strain in the bottom plate on the hold down side (see Fig. 6.38). This increase in strain is observed at very low loads.

- The concrete bottom slab underwent stress reversal at low loads. There is degradation of concrete at higher loads. Concrete showed signs of low stiffness consistent with partially open cracks at loads below 50 kips (see Fig. 6.33).

## References

6.1 Salmon, C.G. and Johnson, J.E. (1996). *"Steel Structures: Design and Behavior"*, Harper Collins, NY, NY, 4th Edition, p.639.

# 7. ULTIMATE LOAD TEST RESULTS

## 7.1 Introduction

Three series of service load tests were planned following completion of the fatigue test reported in chapter 5. The first two of these service tests is reported in the previous chapter.

The final service test was designed to evaluate the response when the applied load (894 kips) corresponded to a stress of $0.95F_y$ (66.5 ksi) in the Grade 70 steel. The test was to be conducted in the same manner, that is, the load would be applied and removed a total of 5 times with the instrumentation remaining unchanged (see chapter 4 for details). The targeted ultimate load was 1200 kips or failure whichever occurred first. However, as the specimen failed in the first cycle of the third service test it is referred to as the 'ultimate' load test.

This chapter summarizes the results of the ultimate load test. A description of the failure mode is first presented in Section 7.2 followed by results in Section 7.3. A summary of results is presented in section 7.4 with the conclusions listed in Section 7.5. As for the Service II results all data presented have initial non-zero (residual) values (see Table E.2, Appendix E) to account for buckling caused at a relatively low load. For completeness, zeroed-out results from all the tests are presented in Appendix E.

## 7.2 Failure Mode

The specimen failed due to crushing of bottom slab caused by premature buckling of the bottom flange close to the center support on the hold-down span while the maximum 894 kip load was being maintained to allow inspection of the extent of cracking of the top slab. Since buckling is not possible if the flange were continuously bonded to the concrete bottom slab, failure was inevitably initiated due to debonding of the concrete. Indirect evidence of such debonding was reported in the previous chapters (see Fig. 5.5, 6.11, 6.16, 6.33 and 6.38).

### 7.2.1 Description

Fig. 7.1 shows the failed bottom flange in the hold down span. The buckled flange extended transversely over almost its entire 6 ft width and between the first and second shear stud lines (11 in. and 34 in. from the center support) in the longitudinal direction. Immediately following failure, the applied load dropped from 894 to 394 kips.

Fig. 7.2 shows the condition of the bottom slab at the failed location. This picture was taken after the top slab had been taken out and debris from the bottom slab removed. While parts of the slab are bonded to the steel flange, there are regions where the concrete crushed and

debonded from the steel. The absence of shear studs suggests that the concrete bond with the shear stud was not compromised.

Additional photos are shown in Figs. 7.3-7.6. Fig. 7.3 provides different views of the buckled flange plate. Unlike Fig. 7.2, these photos were taken immediately after failure and show the damage. In Figs. 7.4-7.5, sections of the concrete separated exposing the reinforcement.


**Figure 7.1** Failed Bottom Flange on Hold Down Side

**Figure 7.2** View of Bottom Slab on Hold Down Side After Clean-up

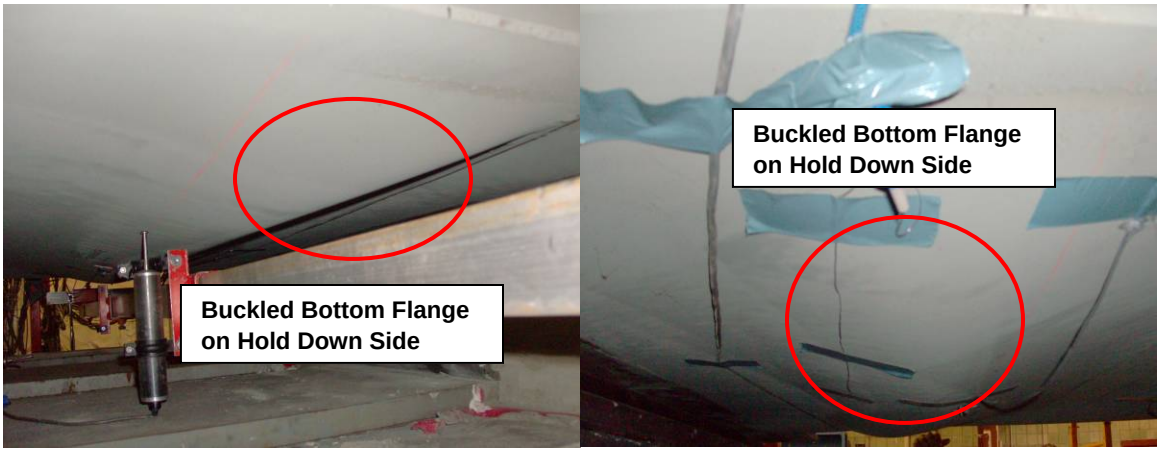


**Figure 7.3** Failed Bottom Flange on Hold Down Side


**Figure 7.4** Failed Bottom Concrete Slab on Hold Down Side

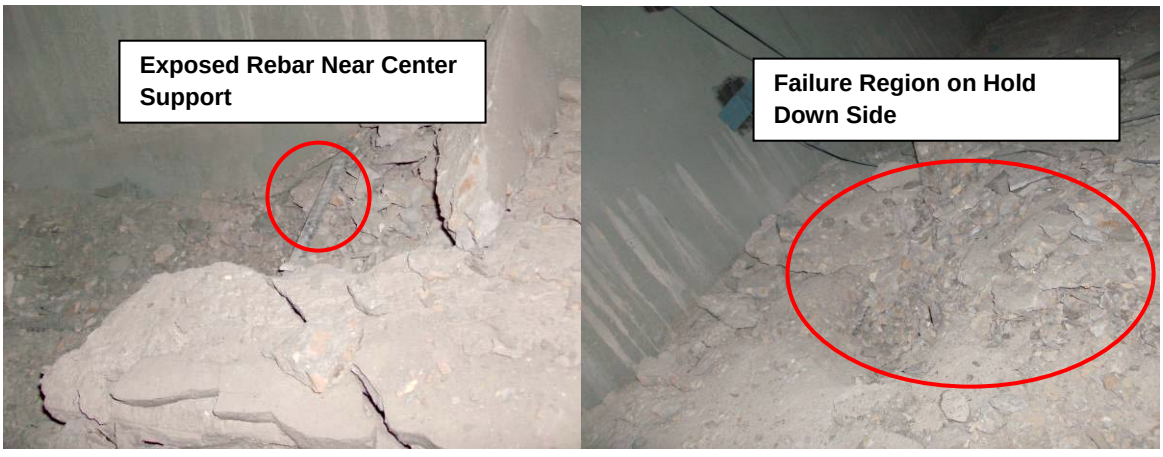


**Figure 7.5** Failed Bottom Concrete Slab on Hold Down Side


**Figure 7.6** Views of Buckled Bottom Flange

## 7.3 Ultimate Load Test Results

The intent of this test was to determine the service response when the stress in the steel flanges reached $0.95F_y$ or 66.5 ksi. Results are presented for deflection, slip, rebar strain, crack width and concrete/steel strains at critical locations.

### 7.3.1 Deflection

The deflection was measured at the cantilevered end, along the span at the hold down frame end and near (2 ft ¼ in.) the center support. Instrumentation details may be found in Figs. 4.12-4.13.

Fig 7.7 is a photo of the deflected shape of the box specimen as it approached failure. Fig. 7.8 shows the variation in the deflection along its length with increasing load. The permanent deformation caused by the last application of the Service II load (Fig. 6.21) at 2 ft ¼ in. from the center support in the hold down span is reproduced in this case. This is shown in Table 7.1 in which the deflection measured by LVDT 23/24 from the 5$^{th}$ cycle (Service II) and the ultimate load case are compared.

Since the structure failed at a load that was 40% higher than 638 kips (894 kips) this response clearly shows that loads were still being transferred despite the serious distress in the thin bottom flange.

The maximum recorded deflection at the cantilevered end of 8.12 in. was 70% greater than the predicted value of 4.78 in. based on a cracked transformed section. This is primarily due to plastic yielding of the top flange, parts of the web and the bottom flange at the center support, which resulted in significant rotation of the cantilever span. Other contributing factors are thought to include reduction in the concrete stiffness arising from fatigue loading (Fig. 5.4) and environmental effects, e.g. shrinkage cracking and localized debonding.

Table 7.2 compares the ultimate deflection at different loads with those from fatigue (static and 5.65 million cycles), and the first and fifth cycles from service I and II. The results show that for the same load, the deflections from the ultimate test were comparable to those from the earlier tests. For example, the deflection at ultimate at 400 kips was 4.015 in., larger than the value recorded for the 5$^{th}$ cycle in Service II and comparable to that for the 5$^{th}$ cycle in Service I (2.966 in.). This trend is followed at 600 kips (4.565 in. vs 4.545 in. from the 1$^{st}$ cycle).

Fig. 7.9 shows the variation in the deflection at the cantilevered end with load. This shows that following failure, the load immediately dropped from its maximum value of 894 kips to 394 kips.

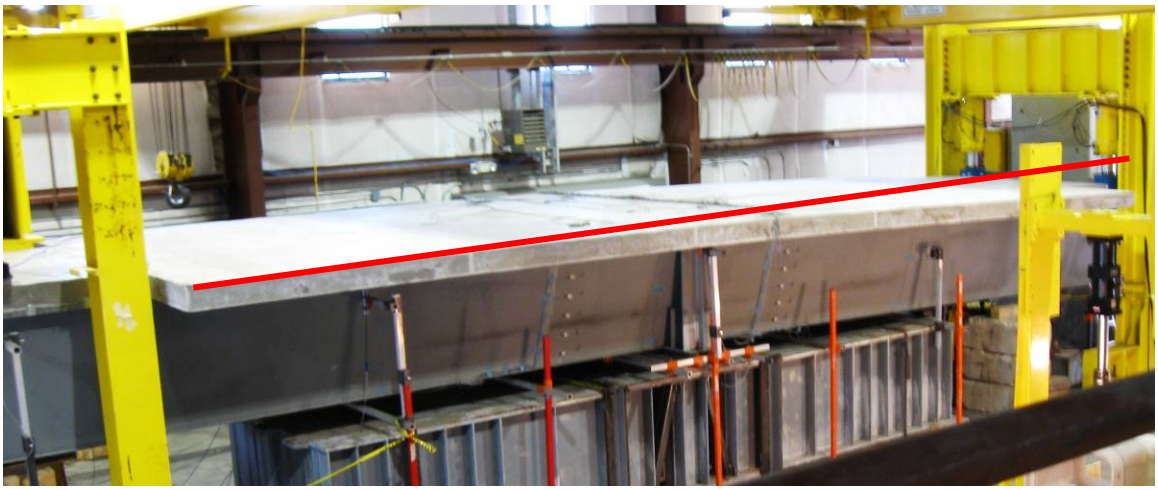

**Figure 7.7** Deflection of Double Composite Box Beam

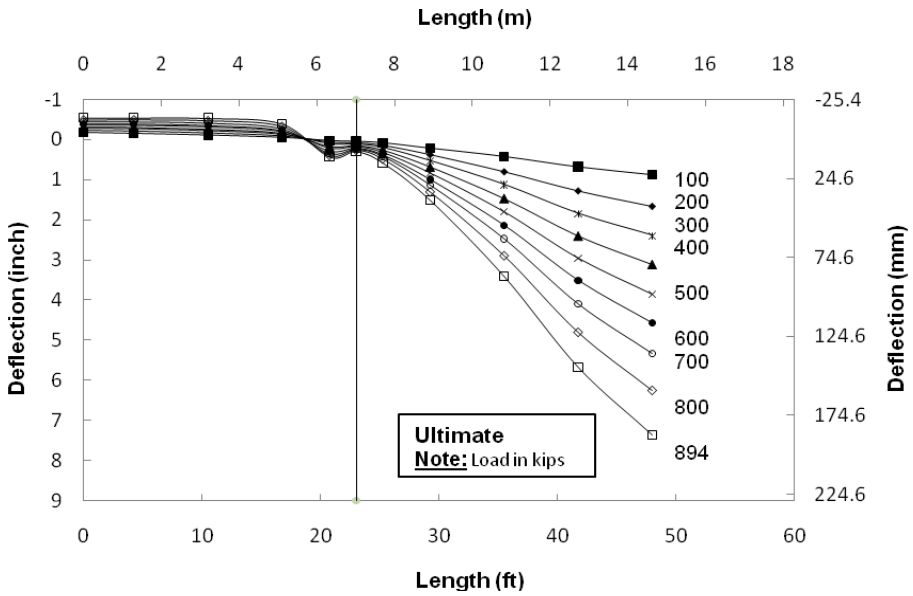


**Figure 7.8** Deflection of Double Composite Box Beam at Load Intervals (downwards = +tive).

**Table 7.1** Deflection in Failure Region (downwards = +tive)

| Load (kips) | Deflection in Failure Region (inch) | | | |
|---|---|---|---|---|
| | LVDT 23 | | LVDT 24 | |
| | Service II 5th Cycle | Ultimate | Service II 5th Cycle | Ultimate |
| 0 | 0.0893 | 0.137* | 0.0864 | 0.110* |
| 50 | 0.1098 | 0.132 | 0.0943 | 0.093 |
| 100 | 0.1273 | 0.152 | 0.1044 | 0.105 |
| 200 | 0.1771 | 0.197 | 0.1360 | 0.134 |
| 300 | 0.2368 | 0.224 | 0.1833 | 0.178 |
| 400 | 0.2922 | 0.253 | 0.2348 | 0.239 |
| 500 | 0.3322 | 0.351 | 0.2852 | 0.279 |
| 600 | 0.3966 | 0.382 | 0.3573 | 0.350 |
| 638 | 0.4163 | 0.413 | 0.3784 | 0.384 |
| 700 | - | 0.444 | - | 0.425 |
| 800 | - | 0.532 | - | 0.482 |
| 894 | - | 0.571 | - | 0.531 |

* Includes permanent deflections introduced by prior tests

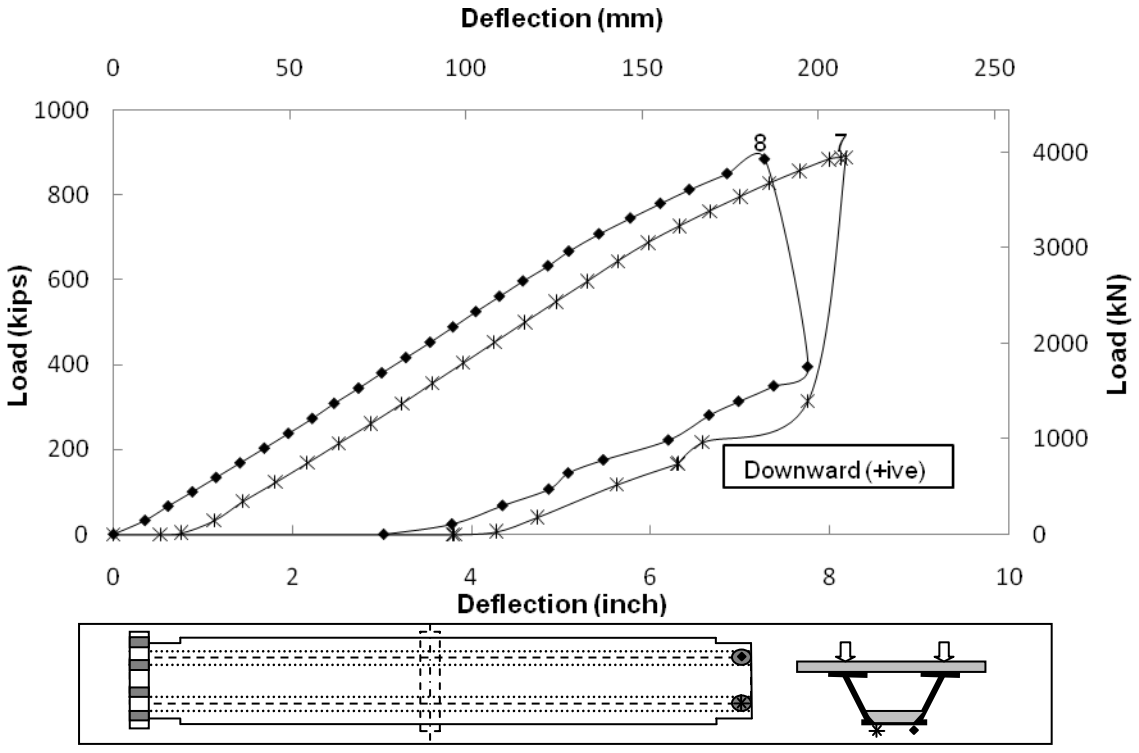


**Figure 7.9** Deflection at Cantilevered End

**Table 7.2** Average Deflection at Actuator End (downwards = +tive)

| Load (kips) | Average Displacement at Cantilevered End (inch) | | | | | | |
|---|---|---|---|---|---|---|---|
| | Fatigue (Cycle 1) | Fatigue (5.65 m Cycle) | Service I 1st Cycle | Service II 1st Cycle | Service I 5th Cycle | Service II 5th Cycle | Ultimate |
| 0 | 0 | 0 | 0 | 0.6654* | -0.228* | 0.034* | 0.56* |
| 50 | 0.314 | 0.387 | 0.093 | 1.0575 | 0.430 | 0.438 | 1.27 |
| 100 | 0.614 | 0.737 | 0.483 | 1.3907 | 0.912 | 0.861 | 1.67 |
| 200 | - | - | 1.155 | 2.1505 | 1.603 | 1.624 | 2.46 |
| 300 | - | - | 2.025 | 2.9063 | 2.293 | 2.375 | 3.23 |
| 400 | - | - | 2.890 | 3.5388 | 2.966 | 3.118 | 4.015 |
| 421 | - | - | - | - | - | - | - |
| 500 | - | - | - | 4.2742 | - | 3.762 | 4.59 |
| 600 | - | - | - | 5.1064 | - | 4.497 | 5.36 |
| 638 | - | - | - | 5.4580 | - | 4.726 | - |
| 700 | - | - | - | - | - | - | 6.12 |
| 800 | - | - | - | - | - | - | 7.064 |
| 894 | - | - | - | - | - | - | 8.179 |

* Includes permanent deflections introduced by prior tests

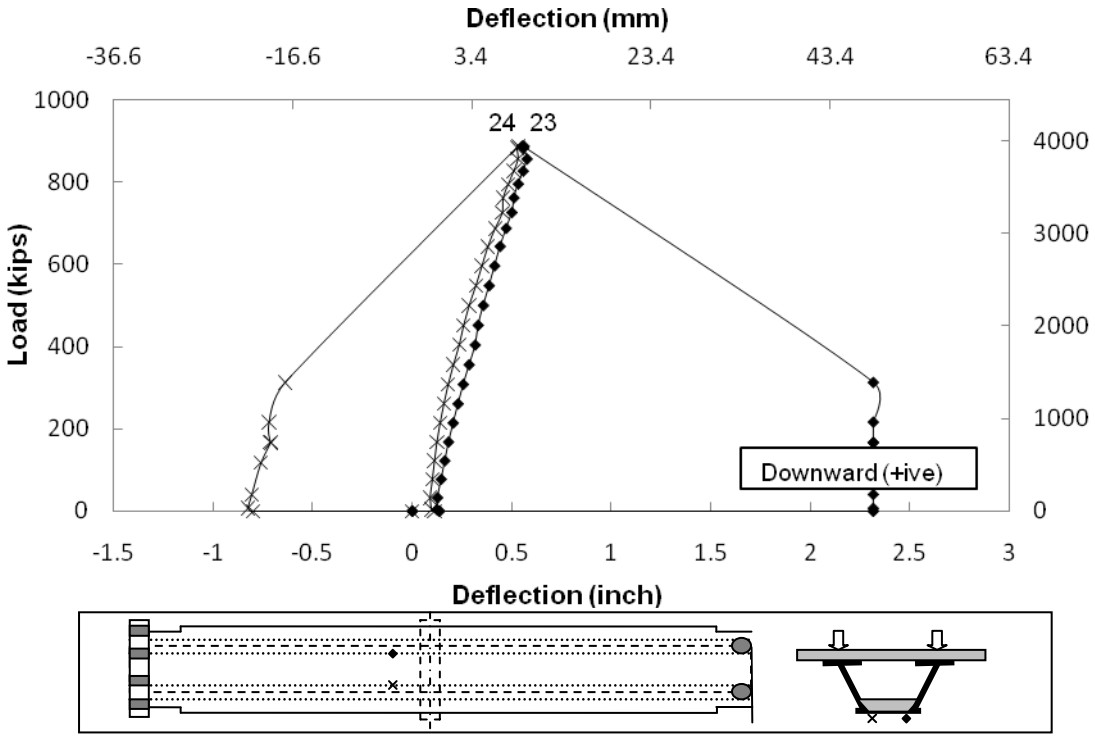


**Figrue 7.10** Deflection at Failure Region on Hold Down Side

Table 7.1 compares the deflection measured by LVDTs 23 and 24 at the critical section 2 ft ¼ in. from the center support on the hold down span from the 5th cycle of service II and the ultimate load case. Inspection of this table shows there is an initial downward deflection measured even at zero load during the ultimate test due to permanent deformation caused by Service II test. The data also indicates that the deflection measured at ultimate was lower than 5th cycle of service II in some cases. This is consistent with earlier tests where the deflection measured in the first cycle was significantly lower compared to later cycles (see Fig. 6.5, 6.24 and 6.25). In the absence of buckling, these locations would be expected to deflect upwards (-tive deflection). The downward deflections measured are a result of the local buckling of the bottom flange. The results for the ultimate load case tabulated in Table 7.1 are also plotted in Fig. 7.10 for completeness.

### 7.3.2 Slip

Slip was recorded in both the top and bottom slabs under ultimate load. The variation of slip in the top slab at the actuator end is plotted in Fig. 7.11 (LVDT # 31). This shows that there was no slip prior to failure when a slip of 0.55 in. was recorded.

Slip was recorded in both the top and bottom slabs at the hold down end. The variation of slip with load at this location is plotted in Fig. 7.12. The slip was significantly greater in the top slab registering a maximum value of 0.038 in (LVDT # 32). In contrast, the slip was less than a third of this value in the bottom slab (0.008 in.) in LVDT # 37 and 38.

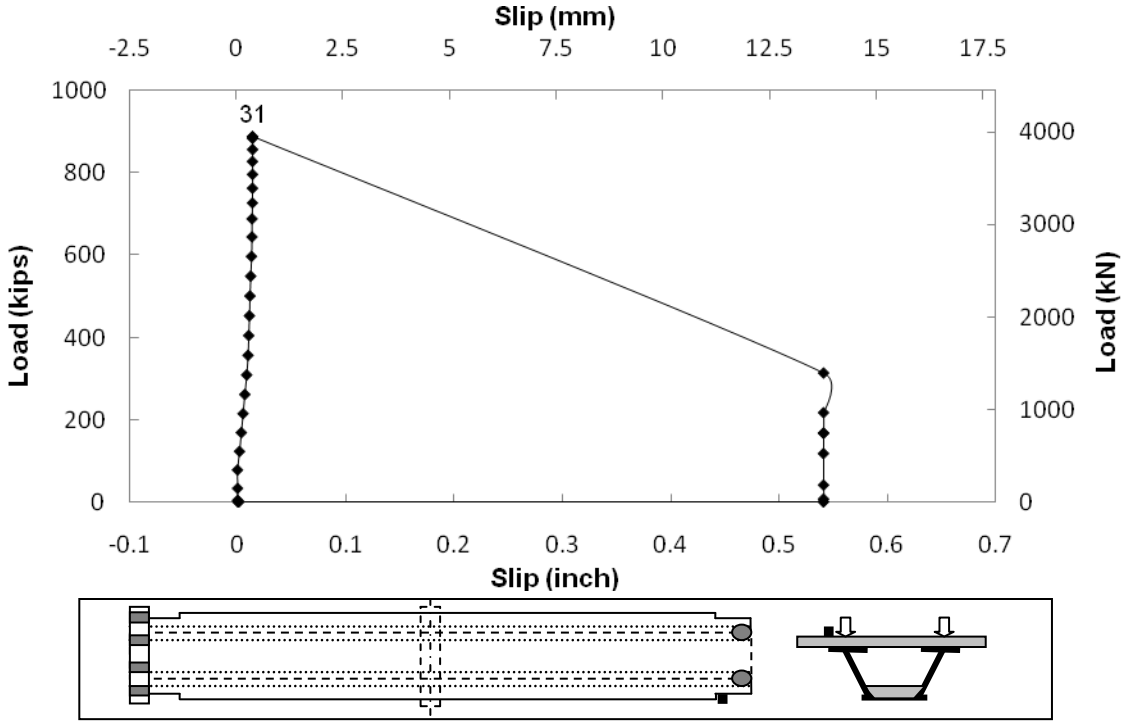


**Figure 7.11** Slip in Top Slab at Actuator End

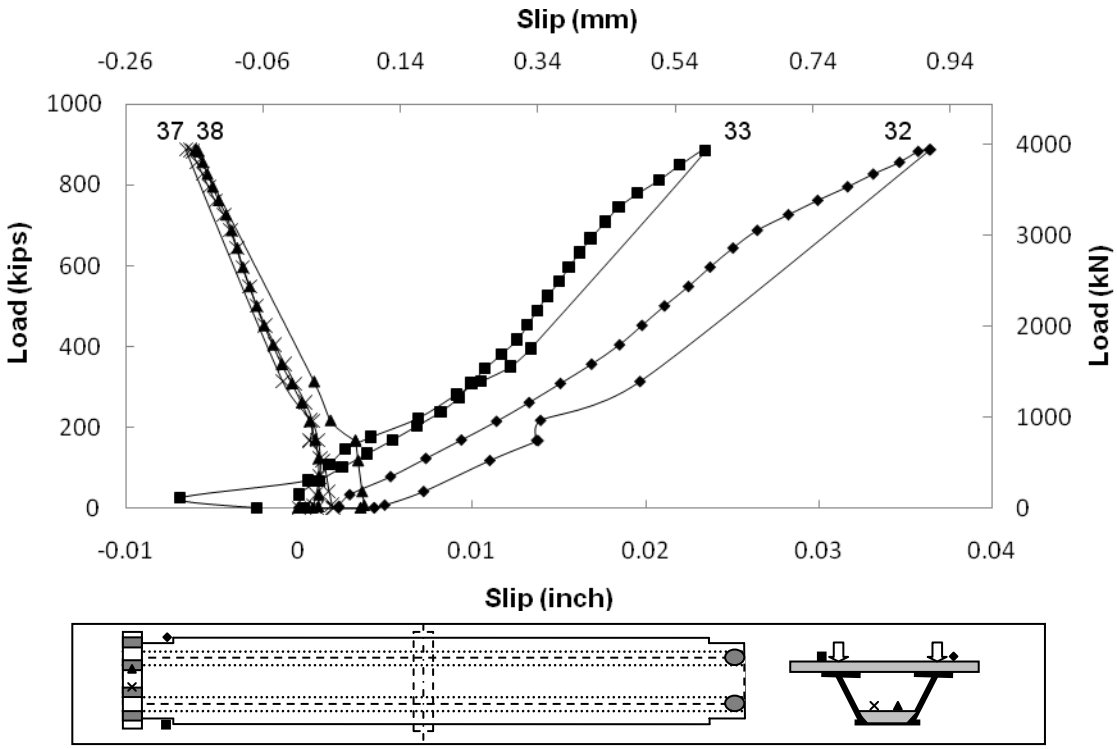


**Figure 7.12** Slip in Top and Bottom Slab at the Hold Down End

**Table 7.3** Strain in Top Slab Reinforcement

| Rebar gages (Actuator Side) | Maximum Strain (με) | Maximum Stress (ksi) | Rebar gages (Hold Down side) | Maximum strain (με) | Maximum Stress (ksi) |
|---|---|---|---|---|---|
| 1A | 2767 | - | 1 | 3299 | - |
| 2A | 2051 | 59 | 2 | 2075 | 60 |
| 3A | 3113 | - | 3 | 7410 | - |
| 4A | 3359 | - | 4 | 6957 | - |
| 5A | 8020 | - | 5 | 6066 | - |
| 6A | 2727 | - | 6 | 1726 | 50 |
| 7A | 2914 | - | 7 | 2810 | - |
| 8A | 4734 | - | 8 | 2552 | - |
| 9A | 3637 | - | 9 | 2715 | - |
| 10A | 2135 | 62 | 10 | 2205 | 64 |
| 11A | 2904 | - | 11 | 2916 | - |
| 12A | 3308 | - | 12 | 1219 | 35 |
| 13A | 15588 | - | 13 | 3540 | - |
| 14A | 5850 | - | 14 | 3689 | - |
| 15A | 3345 | - | 15 | 3245 | - |
| 16A | 2928 | - | 16 | 2714 | - |

### 7.3.3 Top Rebar Strain

The strain in the rebars was monitored as before. Since loads were much higher at ultimate, 26 of the 32 instrumented bars yielded. Table 7.3 summarizes the recorded maximum strain and the corresponding calculated stress in the rebar for both the actuator and hold down spans. Where the rebars yielded, no calculated value of stress is shown. The maximum strain recorded on the actuator side was 15588 με and 7410 με on the hold down side.

The variation in strain with load is plotted in Fig. 7.13 and 7.14 for rebars in the hold down spans. The strain variation of the rebar in the actuator span can be found in Appendix F (Fig. F.7 and F.8 on pg F.5).

The static moment on the actuator and hold down sides were 21456 kip-ft and 21378 kip-ft respectively.

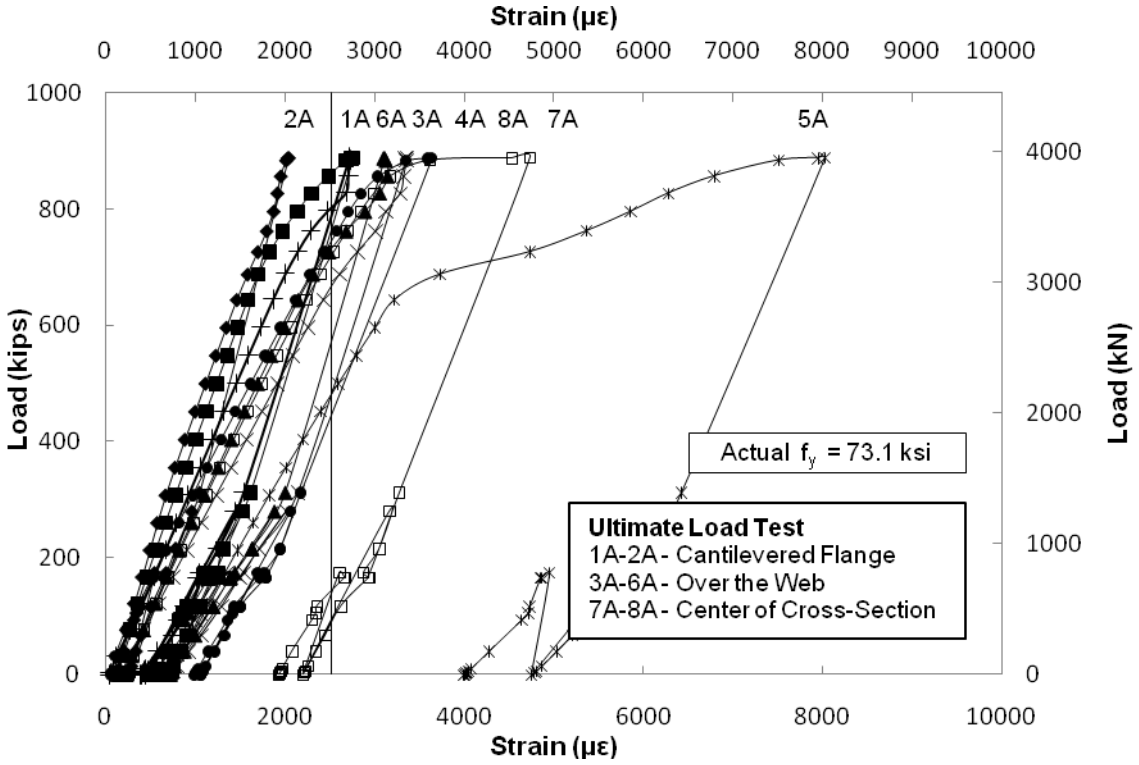


**Figure 7.13** Strain in Rebars on Hold Down Side

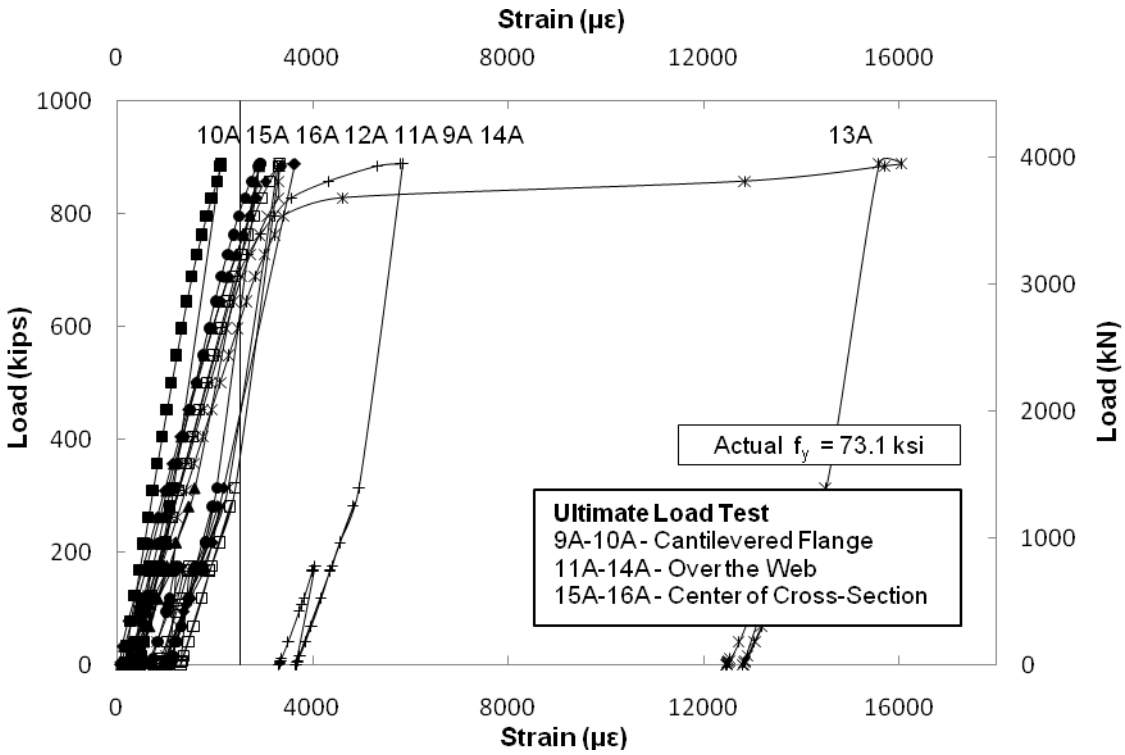


**Figure 7.14** Strain in Rebars on Hold Down Side

### 7.3.4 Crack Width

Crack width was monitored for the top slab as before approximately 1 ft from the center support on the actuator and hold down sides. Fig. 7.15 shows the variation in crack width with load up to the maximum load of 894 kips. The maximum increase in crack width of 0.0624 inch was recorded at the hold down span by crack gage # 4 (see Fig. 4.15 and 4.16). A summary of the recorded crack widths is presented in Table 7.4.

**Table 7.4** Crack Width on Top Slab for Ultimate

| Crack gages | Initial Crack Width (inch) | Final Crack width (inch) | Cumulative Crack width (inch) |
|---|---|---|---|
| Actuator side | | | |
| 1 | 0.013 | 0.0257 | 0.0387 |
| 2 | 0.013 | 0.0356 | 0.0486 |
| Hold Down Side | | | |
| 3 | 0.013 | 0.0325 | 0.0455 |
| 4 | 0.016 | 0.0624 | 0.0784 |

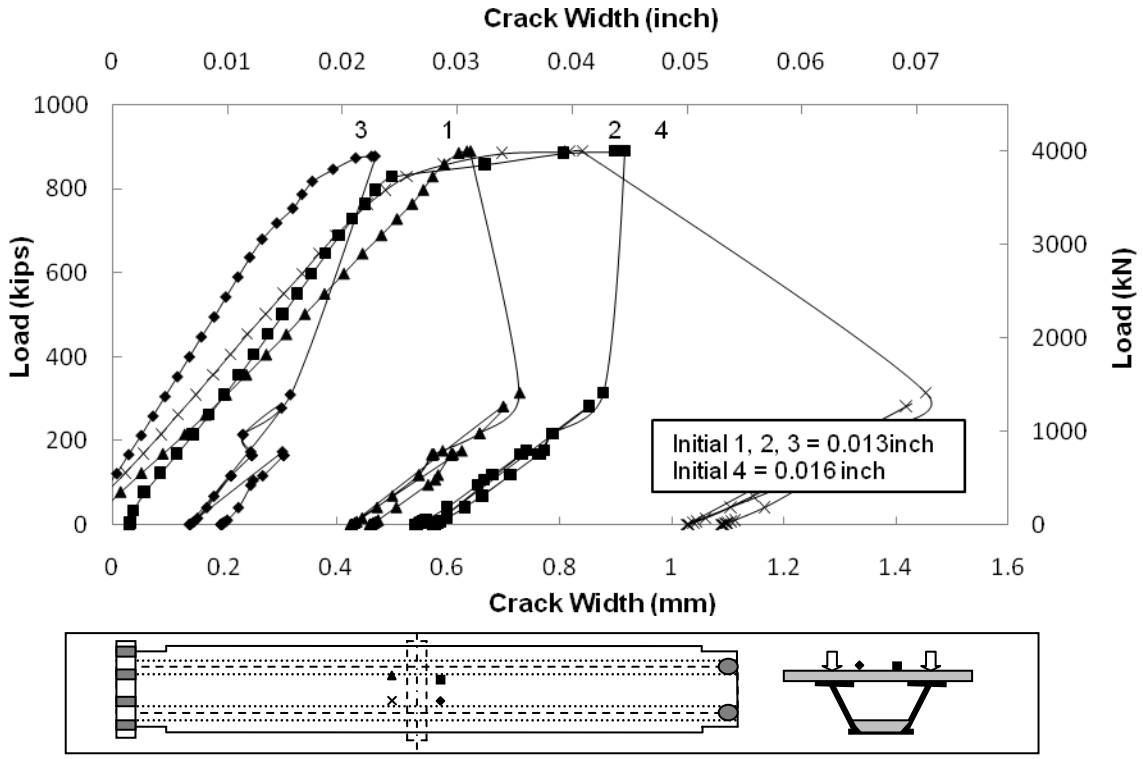


**Figure 7.15** Crack Width on Top Slab

### 7.3.5 Strain in Concrete

Strain in the bottom concrete slab was monitored on either side of center support 4 ft 10⅛ in. (see Figs. 4.19 and 4.20) away. There was no strain gage in the failure region.

Fig. 7.16 shows the variation in strain with load in the two gages (#109, 111) closest to the failure location on the hold down side of the center support. The variation is initially non-linear but is largely linear subsequently. The concrete underwent stress reversal from tension to compression at low loads in gage 109. Analysis presented in Chapter 8 suggests that the initial non-linearity is caused by presence of shrinkage cracks near the bottom fiber of the bottom slab. A wide crack would lead to no load transfer to the concrete until the crack is closed. This type of behavior is seen in SG109, where the strain is extremely low until a load of 200 kips. A moderate crack is expected to reduce the stiffness of the concrete until the crack closes, which is the type of response seen in SG 111, where there is a noticeable change in stiffness between the actuator load of 100 kips and 200 kips.

While the strain in gage 109 reduced to zero at failure, there is a residual strain of approximately 400 με in gage 111. The maximum recorded strain was 1150 με by gage 111.

Fig. 7.17 and 7.18 compare the variation in strain measured by gages 109 and 111 from fatigue (1.5 million, 5.65 million cycles), service I, II (5th cycle) and the ultimate load. Results for gage 109 follows the same path indicating that there was no change in stiffness. In contrast, gage 111 shows significant change after the 5.65 million cycles that is carried over in the service tests. Data measured afer 1.5 million cycle of the fatigue tests shows lack of measurable strain for actuator loads of nearly 70 kip, which is consistent with open cracks. The non-zero strain response measured at 5.65 million cycles at the same loads indicate that the cracks had partially closed. This could be a result of loads redistributing due to shrinkage of top and bottom slab and fatigue loading. This could also result from local buckling of the bottom flange (due to fatigue loading and shrinkage) causing the longitudinal strains to be high enough at low loads to close the cracks.

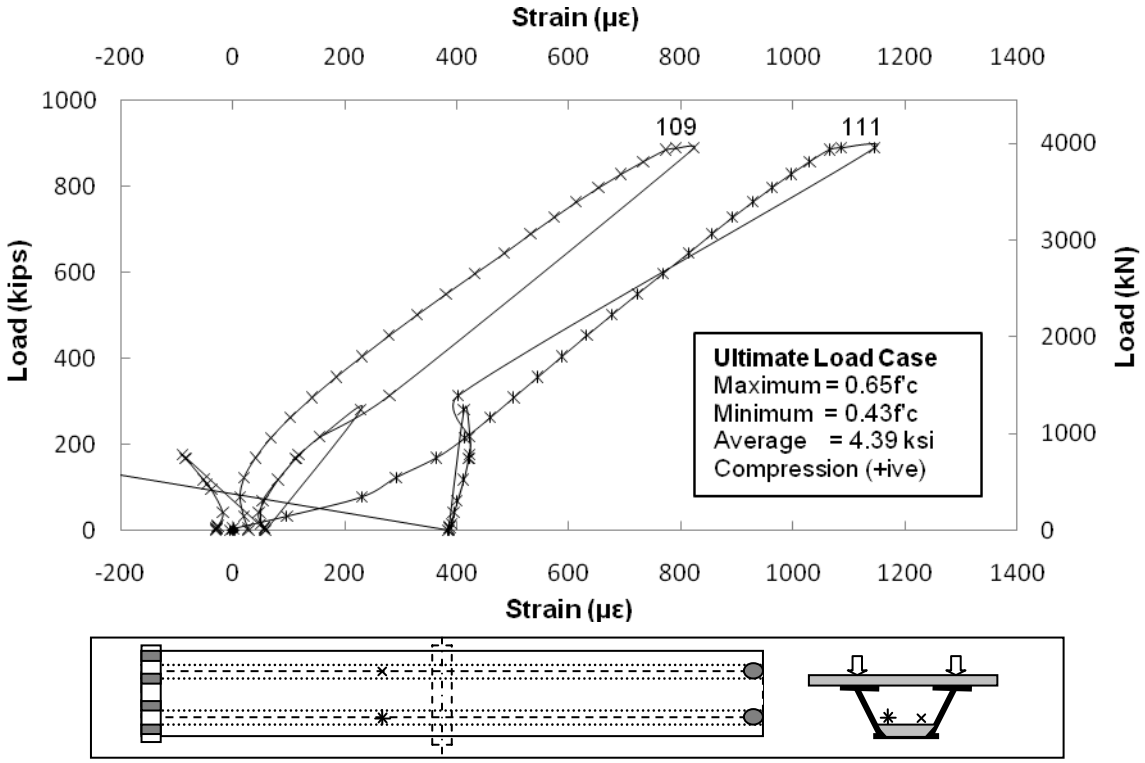


**Figure 7.16** Strain in Concrete on Hold Down Side

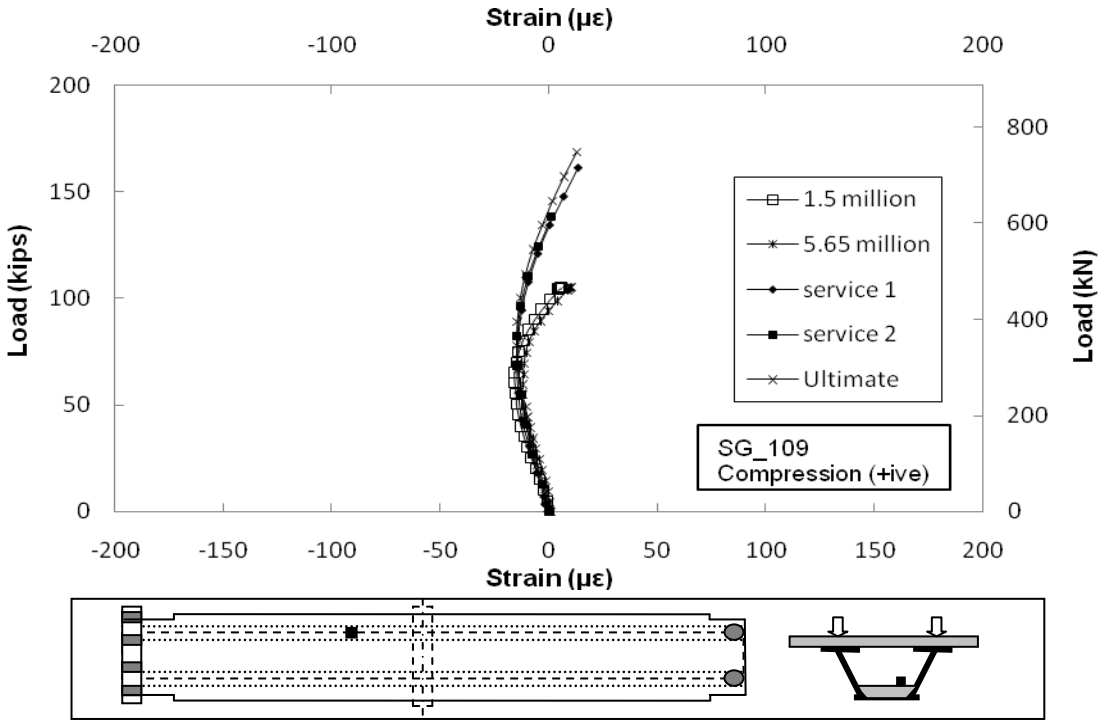


**Figure 7.17** Comparison of Concrete Strain of Fatigue and Service Test for SG 109

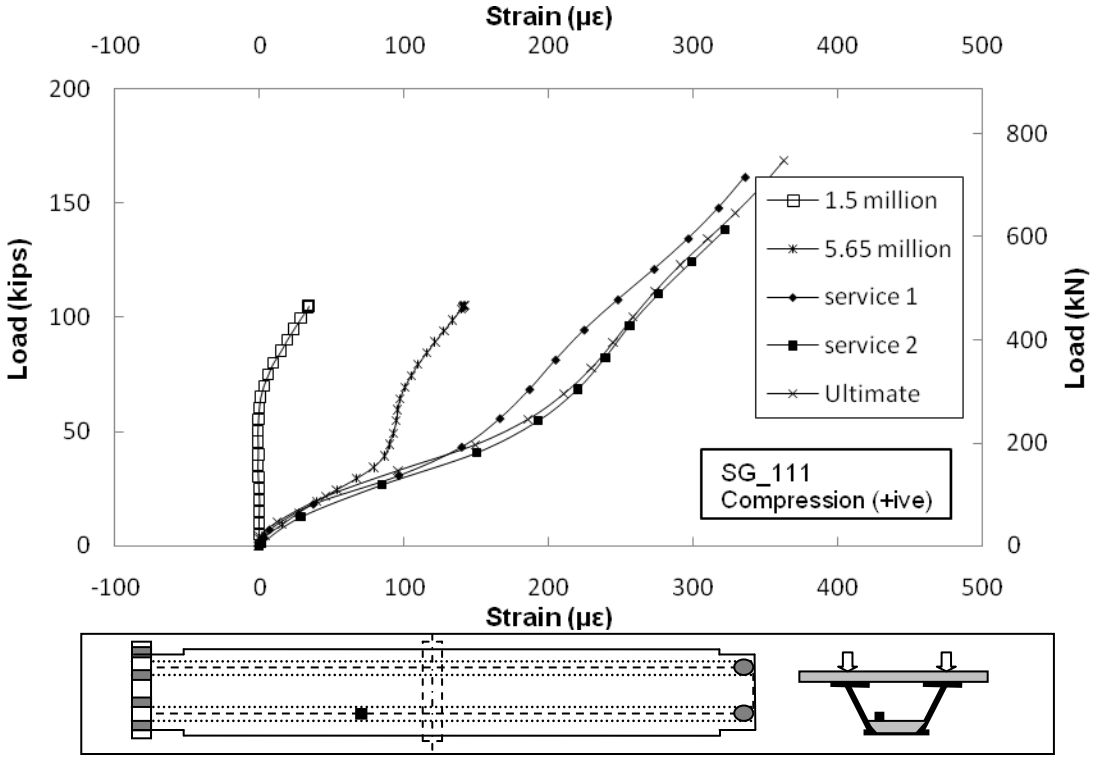


**Figure 7.18** Comparison of Concrete Strain of Fatigue and Service Test for SG 111

### 7.3.6 Strain in Steel

Strain in the steel box was monitored as before. The nearest instrumented section was located 4 ft 10⅛ in. from center support on the hold down side. Unfortunately there was only one transverse strain gage located in the failure region (see Fig. 4.19, 4.20 and 4.21 for details). Strain was also recorded in the top flange, webs and the bottom flange.

Fig. 7.19 plots the variation in strain developed in the top flange at the location of the maximum moment at the center support. The top flange began to yield at 839 kips and the maximum recorded strain was 3850 με.

The behavior of the bottom flange is more complex. Small transverse strains (<300 με) were recorded by gage 122. The variation of strain with load for the three gages (123-125) located at the exterior surface of the bottom flange 4 ft 10⅛ in. from the center support in the hold down span is shown in Fig. 7.20. The maximum compressive strain was 2533 με from gage 123 and 2947 με from gage 125. The response of these gages is slightly non-linear with a discontinuity at a load of 638 kips. Data indicates that bottom fiber of bottom flange near SG125 yields at actuator load of 725 kip. Unlike the top flange, there is no significant increase in strains past yield because the flexural stresses in the buckled flange cause tensile strains in the bottom fiber, which reduces the strains from the net compressive load acting on the section.

A similar discontinuity was recorded by gage 124 but at a lower load. The strain in this gage started as compressive but changed to tensile at around 150 kips. Subsequently, it continued as tensile reaching a maximum value of around 600 με. This reversal signifies localized bending stresses caused by buckling of the bottom flange.

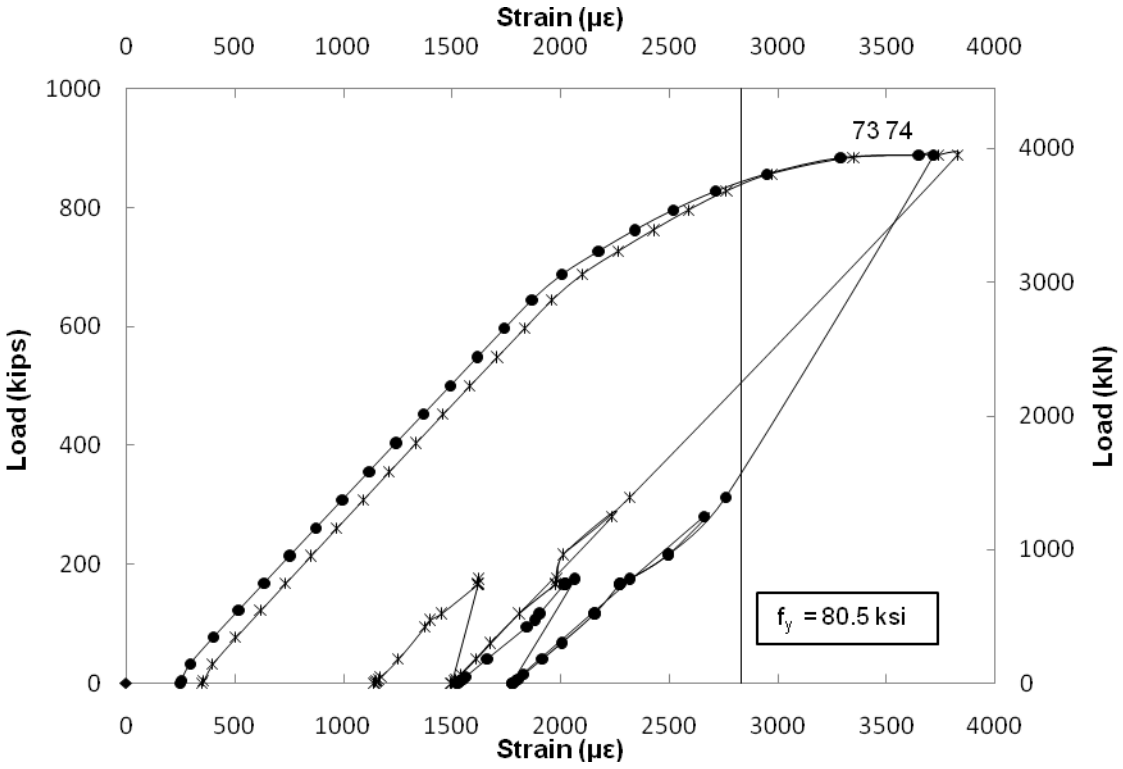


**Figure 7.19** Strain in Top Flange at Center Support

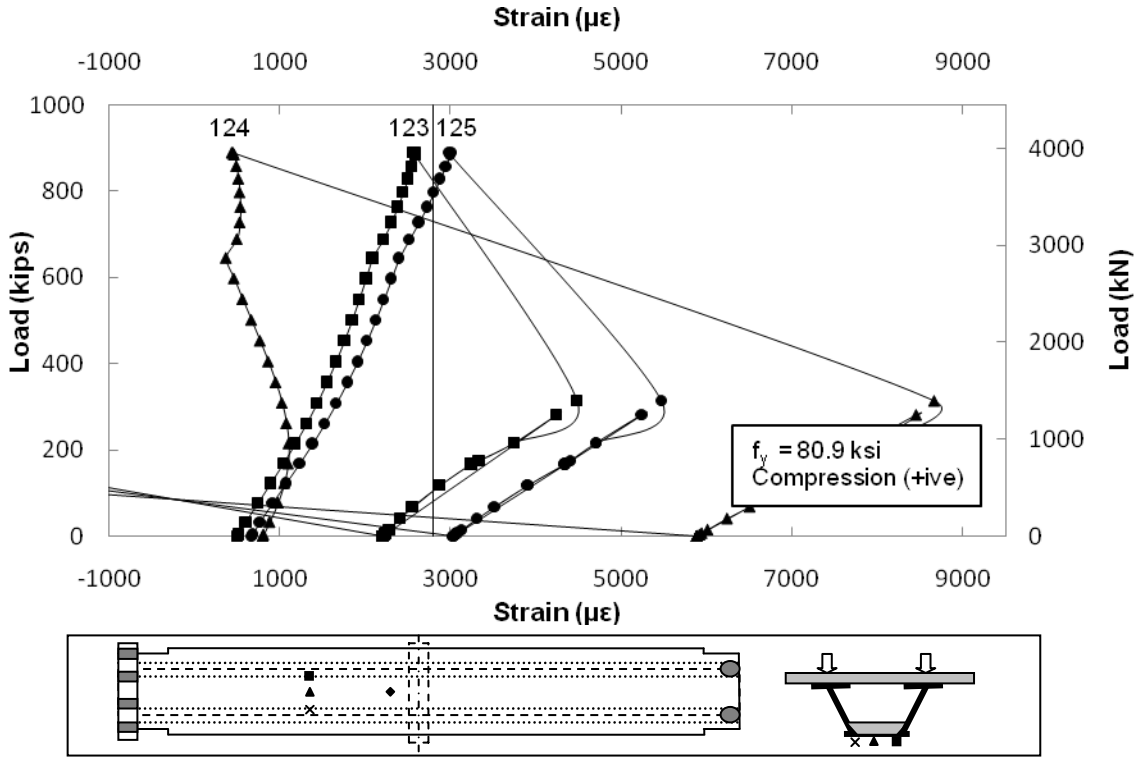


**Figure 7.20** Strain in Bottom Flange on Hold Down Side

### 7.3.7 Neutral Axis

As with earlier tests, strains measured at three coincident locations on the web were averaged and used to plot the neutral axis.

Figs. 7.21–7.24 plot the neutral axis for each web on the actuator and hold down spans respectively. Table 7.5 summarizes this information. Results show that the neutral axis drops with increasing load from 30 to 33 in. for the actuator span and from 31 to 33.5 in. the hold down end.

## 7.4 Summary

In the ultimate load test, the specimen was loaded up to 894 kips and held at the maximum load for inspection. During the first minute that the load was maintained, the specimen failed close to the center support on the hold down side (Fig. 7.1-7.6).

The bottom concrete slab crushed near center support on the hold down span, followed by significant buckling of the steel bottom flange in the region. The failure region was located about 2 ft. from the center support on the hold down side. Deflection data from LVDT 23 suggested localized buckling of bottom flange in the compression region due to prior loading (Service II test). Bottom flange strain gage data at 4 ft.10⅛ in. from the center support towards on the hold down side indicate that the bottom fiber of the bottom flange yielded at a load of 725 kip. Bottom slab top fiber strain measured at the same location was only 1235 με just prior to failure. There was no slip recorded on the actuator side until the specimen failed. The stress in top slab rebars exceeded the yield point in 26 of the 32 rebars.

**Table 7.5** Variation of Neutral Axis

| Load (kips) | Actuator Side (inch) | | | | Hold Down Side (inch) | | | |
|---|---|---|---|---|---|---|---|---|
| | East Elevation | | West Elevation | | East Elevation | | West Elevation | |
| | S-II | Ultimate | S-II | Ultimate | S-II | Ultimate | S-II | Ultimate |
| 100 | 32 | 32 | 30 | 30 | 31 | 31 | 31 | 31 |
| 200 | 32 | 32 | 30.5 | 30 | 31 | 31 | 32 | 31.5 |
| 300 | 32.5 | 32 | 31 | 31 | 32 | 31.5 | 32 | 32 |
| 400 | 32.5 | 32.5 | 31.5 | 31 | 32 | 32 | 32.5 | 32 |
| 500 | 32.5 | 32.5 | 32 | 32 | 32 | 32 | 33 | 32.5 |
| 600 | 33 | 33 | 32.5 | 32 | 32.5 | 32.5 | 33.5 | 32.5 |
| 638 | 33 | - | 32.5 | - | 32.5 | - | 33.5 | - |
| 700 | - | 33 | - | 32 | - | 32.5 | - | 33 |
| 800 | - | 33 | - | 32 | - | 33 | - | 33 |
| 894 | - | 33 | - | 32.5 | - | 33 | - | 33.5 |

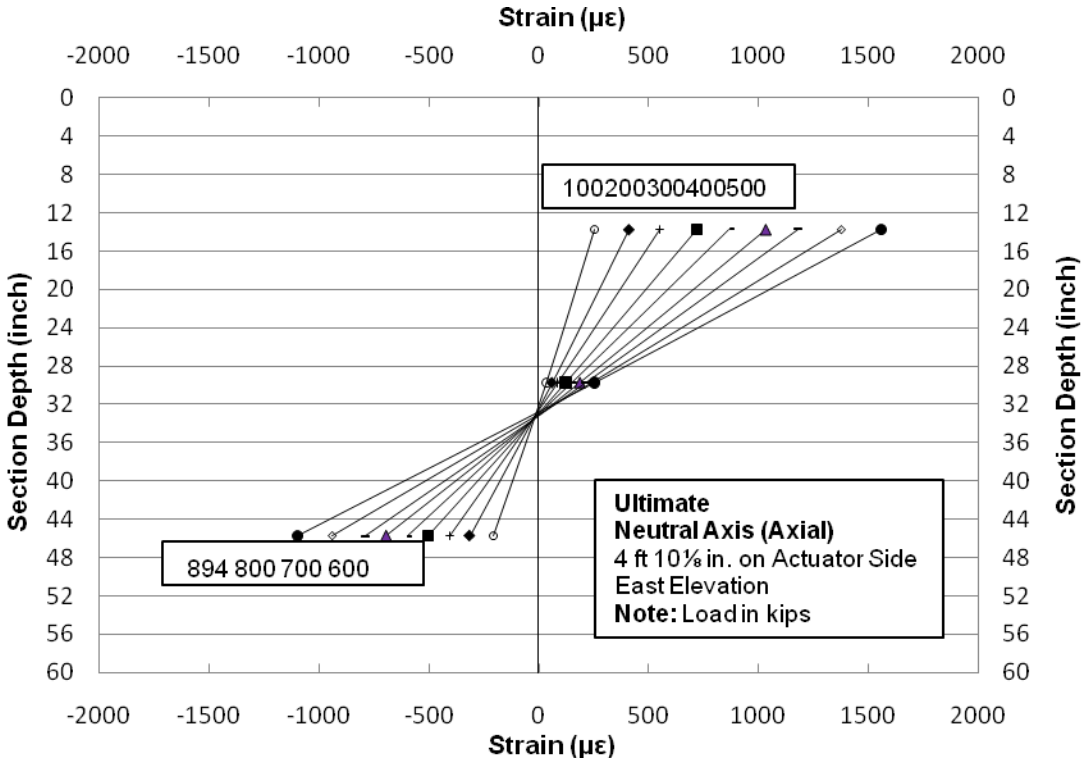


**Figure 7.21** Neutral Axis on Actuator Side (East Elevation)

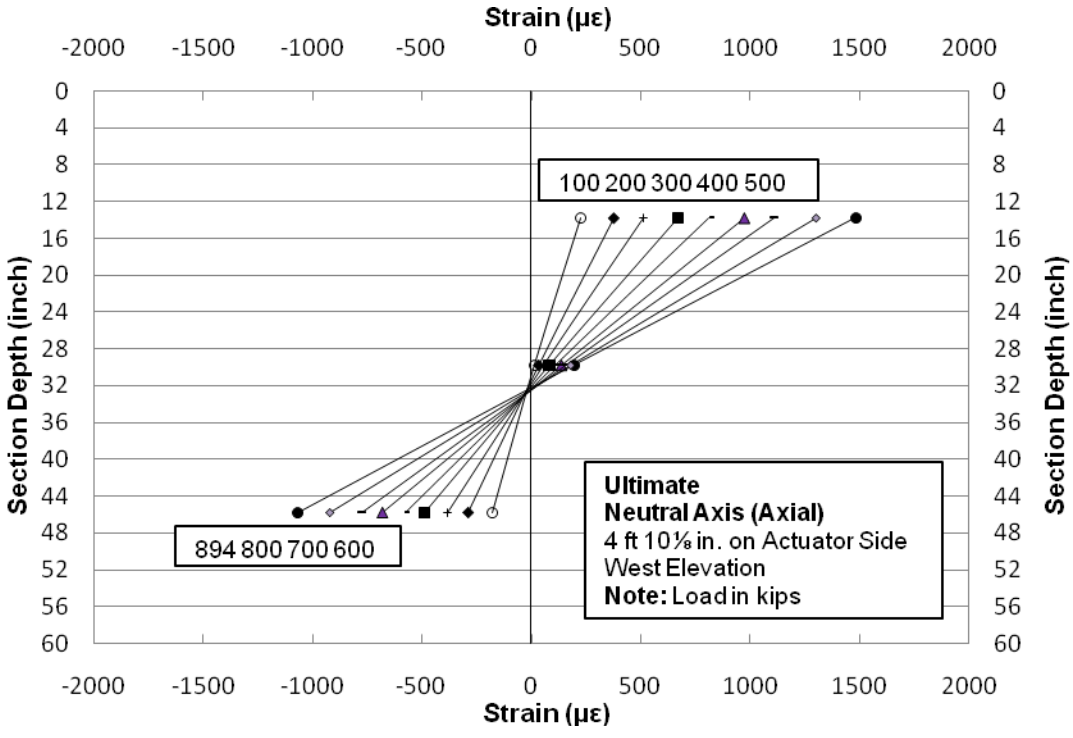


**Figure 7.22** Neutral Axis on Actuator Side (West Elevation)

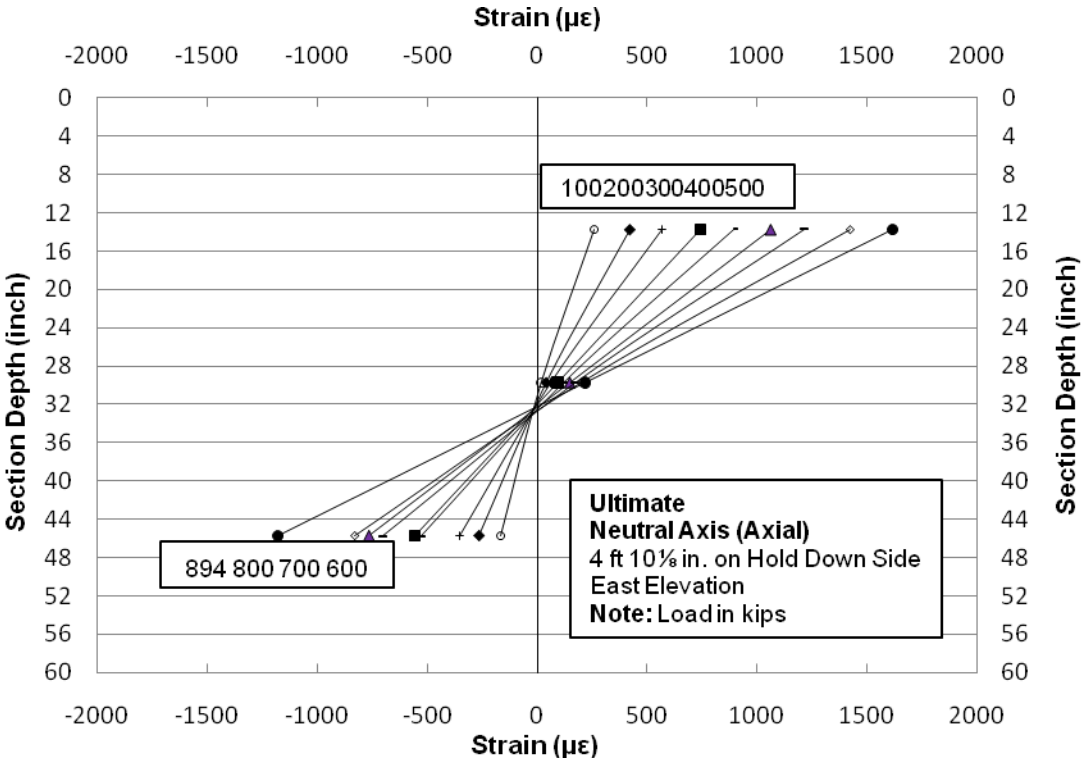


**Figure 7.23** Neutral Axis on Hold Down Side (East Elevation)

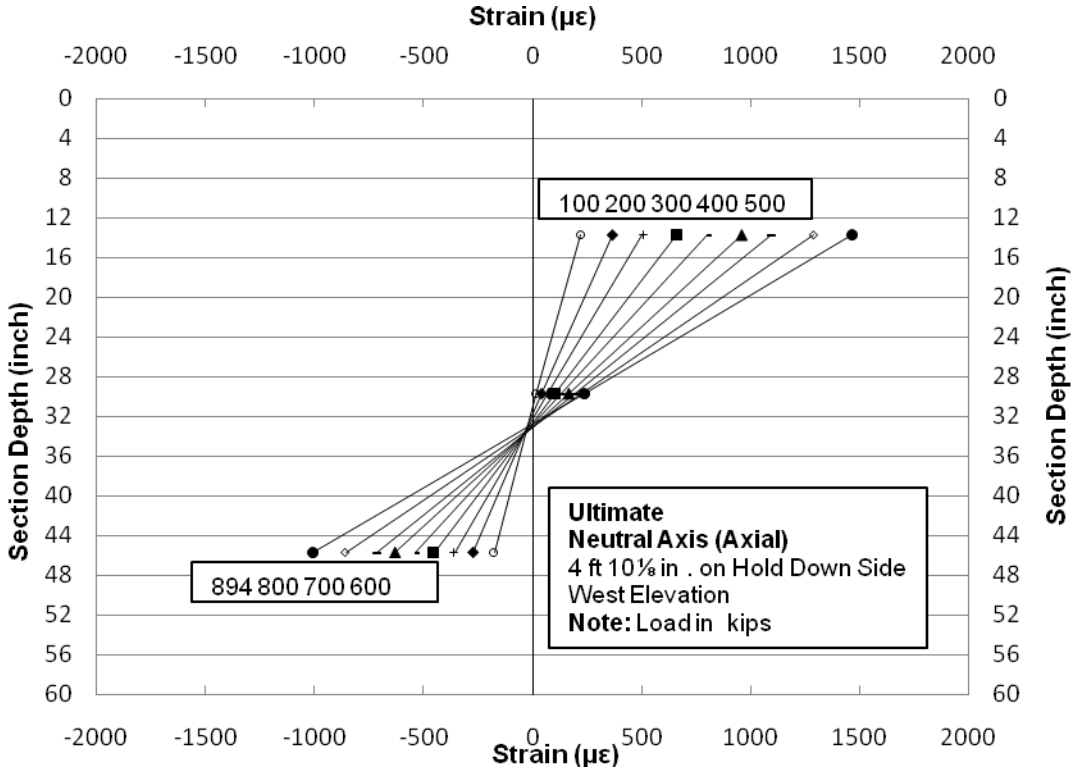


**Figure 7.24** Neutral Axis on Hold Down Side (West Elevation)

Strain data for the concrete and steel indicated that the response was non-linear. The top flange yielded at a load of 839 kips. This exceeded the $0.95F_y$ limit that was used to calculate the applied load. Gages #124 and #119 indicated that buckling had been initiated at relatively low loads (30 kips) in Fig. 7.20.

## 7.5 Conclusions

- Even though the bottom flange had buckled during prior tests, load transfer was not affected.
- The strain in the bottom slab and the bottom flange indicated that the section cannot be designed for full plastic capacity. This is because the concrete failed at a much lower strain and was unable to act compositely with the steel.
- Measured strain in the top flange at the center support was significantly higher than predicted from simple analysis.

## References

7.1 Salmon, C.G. and Johnson, J.E. (1996). *"Steel Structures: Design and Behavior"*, Harper Collins, NY, NY, Fourth Edition, p.639.

# 8. FINITE ELEMENT ANALYSIS

## 8.1 Introduction

As noted in Chapter 2, the double composite test specimen was designed in accordance with the AASHTO LRFD design guidelines and classical beam theory using transformed section properties to account for composite action (see Appendix A). Since this analysis primarily accounts for linear behavior, it is incapable of duplicating the complex non-linear response observed during the test (see Chapter 7).

The primary objective of the numerical analysis presented here is to explain various observations that were un-anticipated based on the design calculations, and several counter-intuitive responses that are difficult to explain from a superficial inspection of the test data. Some key items that needed to be understood include:

- Failure of the test specimen at a significantly lower load than predicted by the original design analysis. As noted in Chapters 6 and 7, many of the measurements obtained during the test suggest that the bottom flange buckled at a low load and this was believed to be responsible for the premature failure of the test specimen. However, this simplified hypothesis does not explain all the observations. Additional questions that needed to be answered, include:
    - What caused the bottom flange to buckle and at what load?
    - Does the bottom flange carry any load once it has buckled? If so, until what load is it effective?
    - How does the bottom slab respond after the bottom flange buckles?
    - What was the stress and strain in concrete at failure?
- The test specimen failed on the hold-down side despite being subjected to a lower moment than the corresponding location on the actuator side.
- During Service I tests, the bottom slab strain gages 106, 107 and 109 developed tensile stresses for actuator load of up to approximately 100 kips (see Fig. 6.10) that subsequently reversed to compression.
- The bottom slab strain gage 111 predicted nearly infinite stiffness for loads up to nearly 70 kips after 1.5 million cycles of fatigue loading (see Fig. 6.11). In subsequent tests, the gage displayed low stiffness for loads up to approximately 30 kips (see Fig. 6.11) and then stiffened significantly at higher loads.
- The bottom flange longitudinal strains measured by gages 123 and 125 (see Fig. 6.36) show a stiffening response at higher loads. The slope of gage 124 changes directions at actuator load of approximately 200 kips.

A three-dimensional non-linear finite element model was developed to numerically simulate the ultimate response of the double composite test specimen and better understand the observed behavior. Section 8.2 describes the finite element model, including mesh, material properties, boundary condition and loading. Section 8.3 compares numerical predictions for deflection and strain to measured values. Section 8.4 provides an outline of the behavior of the test specimen during ultimate test starting from initial loading to eventual failure. The results of parametric studies performed to assist in double composite design based on the findings of this chapter are presented in Section 8.5. Finally, key findings from the chapter are summarized in Section 8.6.

## 8.2 Finite Element Model

As noted in Chapter 7, the failure mechanism involved crushing of the bottom slab and buckling of the bottom flange on the hold-down side near the center support. This meant that the numerical model developed to duplicate the test specimen failure needed to:

- accurately predict stresses resulting from the construction procedure (including changes in the structure by the addition of the bottom and top slabs, the use of temporary bracing on the bottom flange during the bottom slab pour, and the use of different support conditions during the bottom slab and top slab construction (see Section 3.3 and 3.4).
- account for shrinkage strains developed due to elapsed time between pouring of the bottom slab and the top slab, and between pouring of the top slab and final tests.
- consider cracking of concrete including accurately accounting for open and closed cracks.
- incorporate large deformation analysis (p-delta effects) to capture non-linear buckling response.
- model contact between the bottom slab and the bottom flange to accurately capture post-buckling interaction between these two parts
- capture elastic-plastic response of HPS and rebar steel.
- include non-linear stress-strain response of the top and bottom concrete slabs.

A three-dimensional finite element model was developed using the general purpose structural analysis software, ANSYS 11 [8.1]. ANSYS has an extensive library of element types (including linear and quadratic shells, solids and beams) that facilitates the modeling of complex non-linear behavior listed above to duplicate the structural response observed during the test.

### 8.2.1 Finite Element Mesh

Prior to testing, finite element analysis was performed assuming perfect composite action between the bottom flange and the bottom slab based on prevailing practice [8.2] (see Section H.2.1 for details). This approach failed to correctly predict the observed failure load and the failure mode (bottom slab crushing caused by bottom flange buckling). However, once the failure was found to be a result of bottom flange buckling, the finite element model was refined accordingly so that the numerical results captured the experimental observations.

Fig. 8.1 shows the final post-test finite element mesh that was used for the analysis. Due to symmetry about the centerline box, only half the specimen was modeled. The top flange and concrete slabs were modeled using 8 node brick elements and the web and bottom flange were modeled with 4 node shell elements. The model incorporates diaphragms, cross-frames, loading frame, temporary bracing members used prior to curing of the bottom slab and individual shear studs. Interface between the bottom slab and the bottom flange was modeled with contact elements. The use of contact elements ensures that mating surfaces do not penetrate each other while allowing the surfaces to separate (such as when the bottom flange buckles).

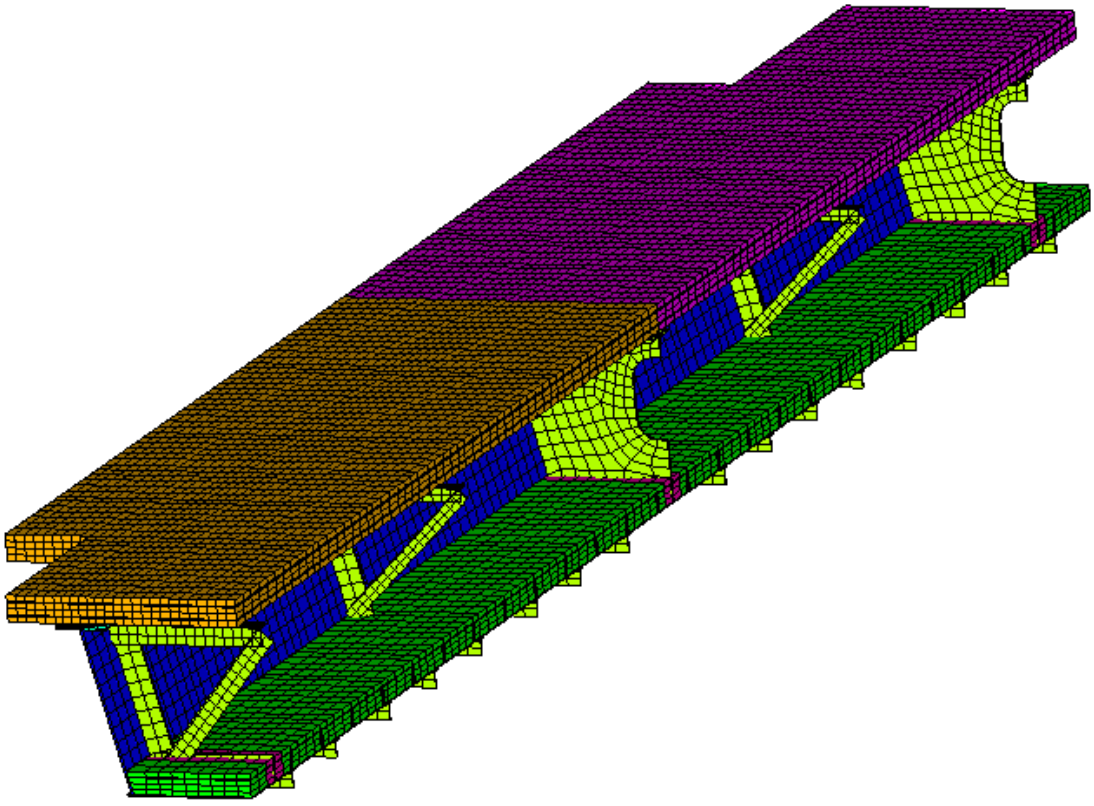

**Figure 8.1** Finite Element Mesh

This mesh is far more complex than typically used in bridges [8.2] due to the need to explicitly model individual shear studs, temporary bracing of the bottom flange, the cross-frames, loading frame and diaphragms. Available computational resources limited the size of the mesh that was considered practical given run-times and data storage requirements. The mesh density was selected based on studies performed on representative simpler models of the bottom flange to ensure it could accurately predict buckling based on closed-form predictions available in the literature such as Roark's Handbook [8.3]. The final model comprised of 31K nodes and 46K elements. The run time for the model varied between 28-36 hrs on a Quad core Q9300 PC with Vista 64 and 6GB of RAM. The size of a typical result file generated from a single analysis ranged from between 30 GB to 120 GB. In combination with the inherent complexity of non-linear analysis, the long run times and computational resources required for the final model made the refinement and debugging process extremely time consuming.

### 8.2.2 Material Properties

To accurately account for the observed behavior of the structure, material models of the structural steel (HPS), reinforcing steel and concrete incorporated the non-linear portion of the stress-strain curves. Steel response was modeled as elastic and nearly perfectly plastic. Concrete model included cracking at tensile stresses exceeding the modulus of rupture and included parabolic stress-strain curve (see section H.3 and H.4 for details). Based on measured material properties (see Appendix B), different concrete strengths were used for the bottom slab, and the two spans of the top slab. Also, different yield strengths and elastic modulus were used for the top flange, web and bottom flange based on material testing data (see Appendix B).

### 8.2.3 Boundary Conditions and Loading

As stated in Section 8.2.1, only half the section was modeled due to symmetry. Symmetry boundary conditions were applied at the vertical plane located at the center line (CL) of the box section. The center support was treated as a hinge (vertical and longitudinal displacements were constrained). Temporary vertical constraints were used at the soffit at the actuator and hold down ends during analysis of the construction of the bottom and top slab. For the test loading, top slab nodes at the hold down location were constrained vertically. Test loading was applied as a vertical displacement in increments of 0.02 inches to the top flange nodes at the actuator locations. The loading was incremented until the structural analysis stopped due to structural instability.

## 8.3 Model Results

Unlike the actual specimen which was subjected to multiple cyclic loads, the finite element model was loaded monotonically to failure. Consequently, numerical results from the finite element model are compared primarily with the results of the ultimate test. However, in some instances, numerical results are also compared to service tests to explain non-linear behaviors observed only during the first cycle of the Service I and Service II tests. In graphs that follow, *numerical results are represented using lines or dashed-lines, while experimental data is shown using symbols*. Also, since only half the specimen was modeled numerically, the

numerical results for east and west sensors are identical. Since the finite element model does not include residual deflections caused by Service I and Service II tests, in most cases, experimental displacements shown are zeroed out at the beginning of the ultimate test. However, since residual strains are required to identify onset of yielding, experimental strains presented are not zeroed. To ensure accurate comparison with experimental data, numerical results do not include strains and deflections caused by dead load. Table 8.1 summarizes the findings from the comparison of strains and displacements that follow.

### 8.3.1 Global Behavior

Fig. 8.2 shows vertical deflections measured near the center support of the specimen and the hold down end. Numerical predictions for these locations are nearly zero since supports are modeled by constraining the vertical displacement, i.e., assuming infinitely stiff supports. However, the structural members used as supports in the experimental setup (see Fig. 4.2) are flexible and result in measurable deflections. At the center support there was a downward displacement of nearly 0.4 in. measured on the actuator side (LVDTs A and B) and about 0.25 in. on the hold down side (LVDTs C and D). This means that there is a rigid body deflection of approximately 0.325 in. (average of all four gages) at the center support. At the hold down end, there is an upward deflection of nearly 0.4 in. (LVDTs 28 and 29 going from about -0.2 in to -0.6 in). This upward movement results in a rigid body rotation of the entire test specimen about the center support. The amount of vertical deflection caused by this rotation can be computed by using simple geometric principle of similar triangles. For example, an upward 0.40 in deflection at the hold down end would result in a downward deflection of 25 ft/23 ft × 0.40 in = 0.43 in at the actuator end. The rigid body displacement caused by flexibility of the center support and hold down has been removed from all measured displacements subsequently shown in this chapter.

Fig. 8.3 shows a graph of the actuator deflections at LVDTs 7 and 8. Numerical results show an excellent match to the experimental measurements. Both numerical and experimental results show a drop of in stiffness towards the end of the test. Numerical results are available for loads exceeding the experimental failure load because the concrete bottom slab in the numerical model does not crush abruptly as observed in the experiments. Allowing the concrete to crush in the model causes numerical instability leading to solutions stopping at moderate load levels. To overcome this problem, crushing is modeled by significantly reducing the stiffness of concrete at high compressive stresses. This leads to the structure being stable for loads slightly higher than the observed failure load. The exact failure point in the numerical results is obtained by determining the load at which the average bottom fiber concrete strains in the bottom slab exceeds the ultimate strain limit of 3000με. This is discussed further in Section 8.4.

**Table 8.1** Summary of Comparisons between Numerical Results and Experimental Data

| Item | Comparison | Comments |
|---|---|---|
| **Overall Stiffness** | Excellent (see Figs. 8.3-8.6) | Numerical model deflections are nearly identical to measured deflection (after experimental results are adjusted for support deflections) at locations except at buckled zone. |
| **Stiffness in buckled zone** | Fair (see Fig. 8.5, 8.7 and 8.8) | Numerical model over predicts exact load where significant buckling occurs, but captures the qualitative behavior well. Variation are thought to be caused due to cracks in the bottom slab (see Section 8.3.3) and finite element mesh density (see Appendix H). |
| **Failure Load** | Excellent (see Fig. 8.12) | Predicts failure load accurately (failure criteria is defined as bottom slab strain reaching 3000 με average strain at the bottom fiber of the bottom slab). |
| **Bottom Flange Strains** | Fair (see Fig. 8.13) | Numerical predictions do not match strains measured in the buckled region during ultimate test, but match qualitatively. They match better with strains measured in during Service I and Service II tests (see Appendix H). The mismatch is a result of accumulated plastic strains in the from prior service tests. |
| **Bottom Slab Strains** | Fair (see Fig. 8.14) | Numerical results match on an average basis. Mismatch results from varying crack sizes on the bottom slab. |
| **Top Flange Strain** | Very good (see Fig. 8.18.) | Numerical predictions are accurate except at center support. Experimental data shows significant non-linearity at lower loads due to residual strains from prior service tests. |
| **Web Strains** | Excellent (see Fig. 8.19) | Numerical predictions capture the response and are close to measured values. |

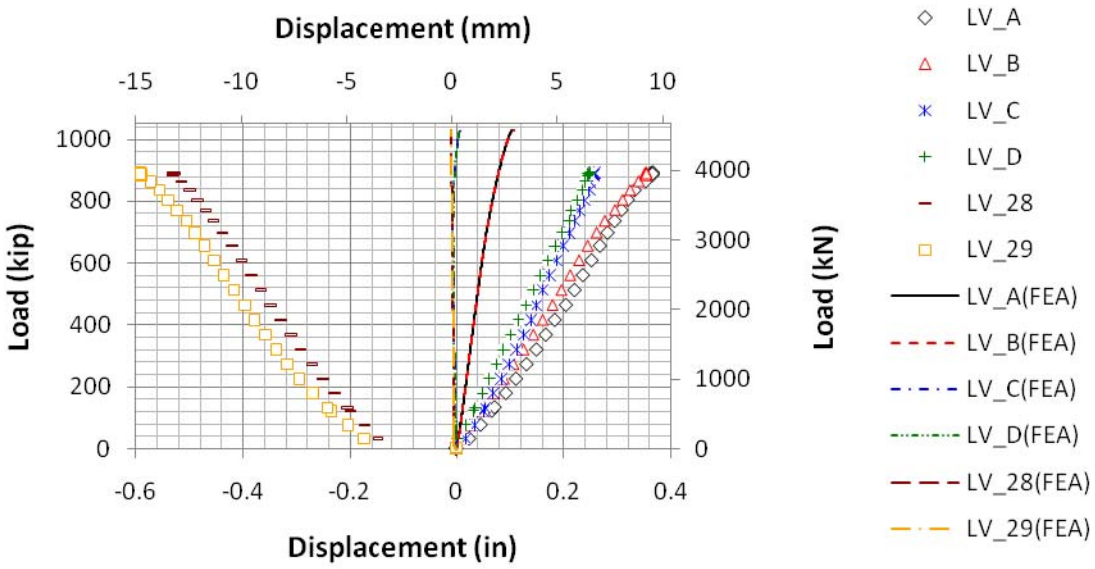


**Figure 8.2** Deflections (+tive Downwards) Near Center Supports (LV A through LV D) and Hold Down End (LV 28 and 29).

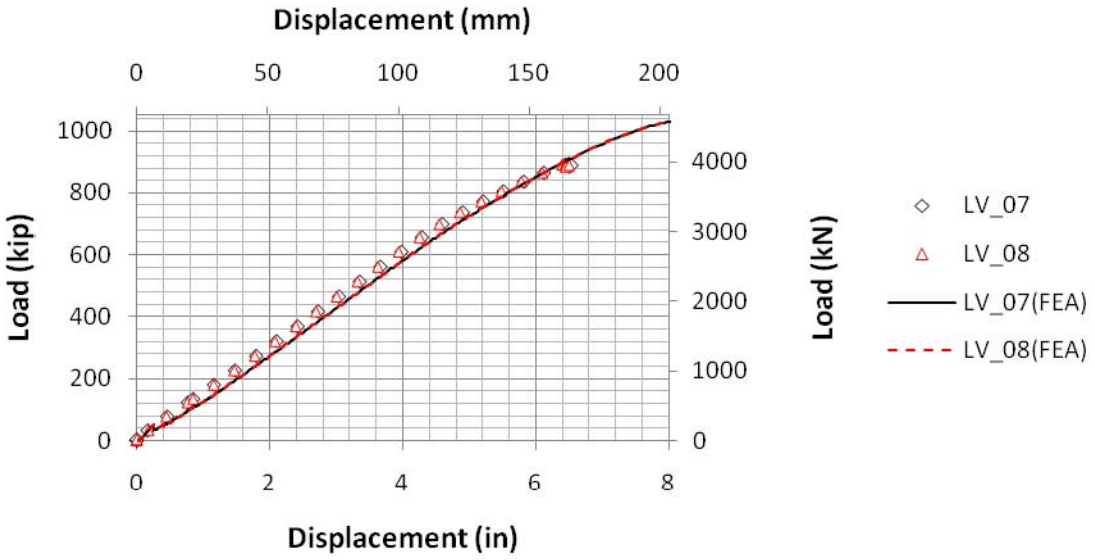


**Figure 8.3** Actuator Deflection (+tive Downwards)

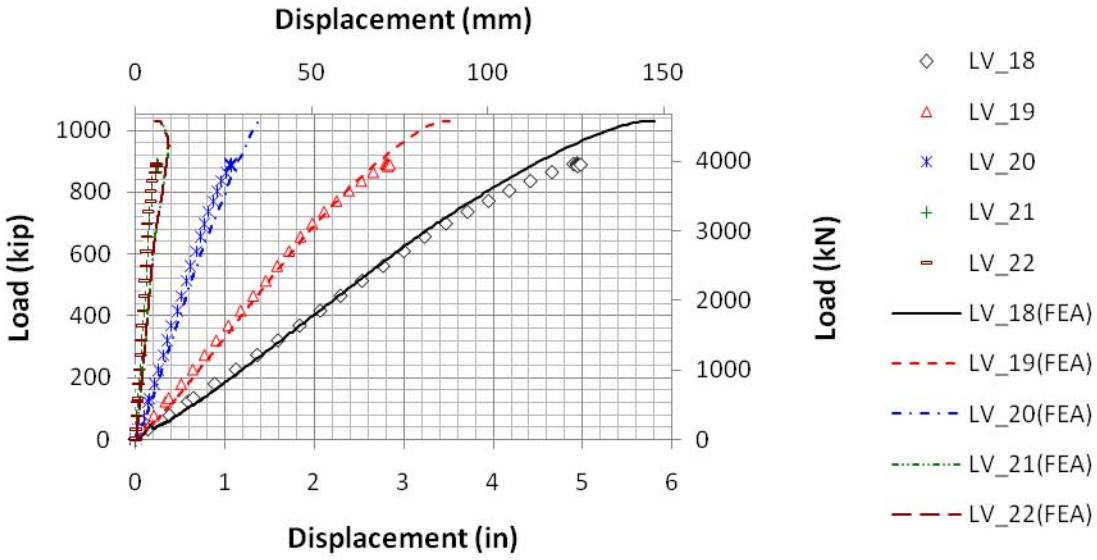


**Figure 8.4** Bottom Flange Deflection (+tive Downwards) on Actuator Side.

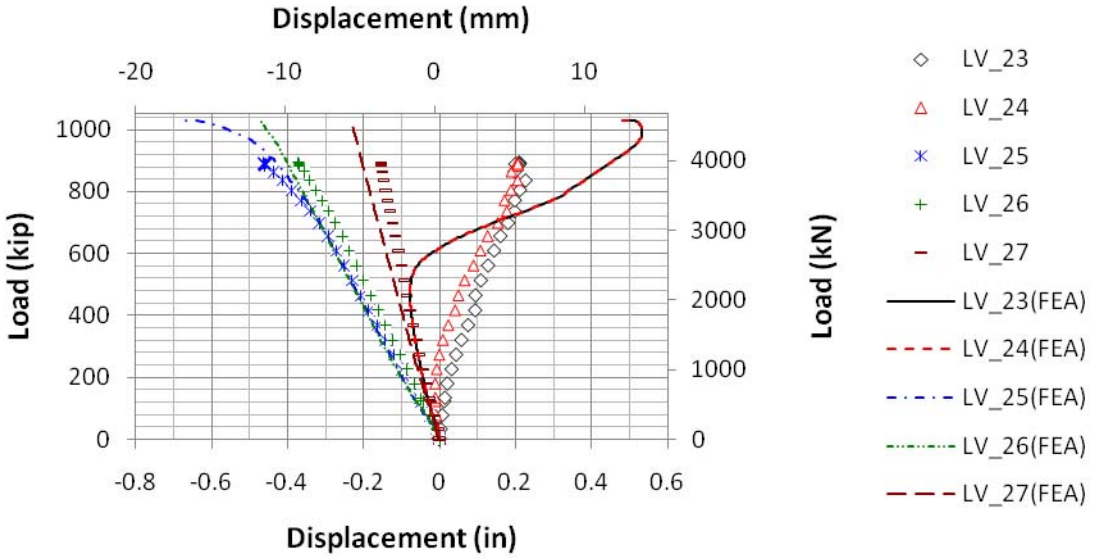


**Figure 8.5** Bottom Flange Deflection (+tive Downwards) on Hold Down Side.

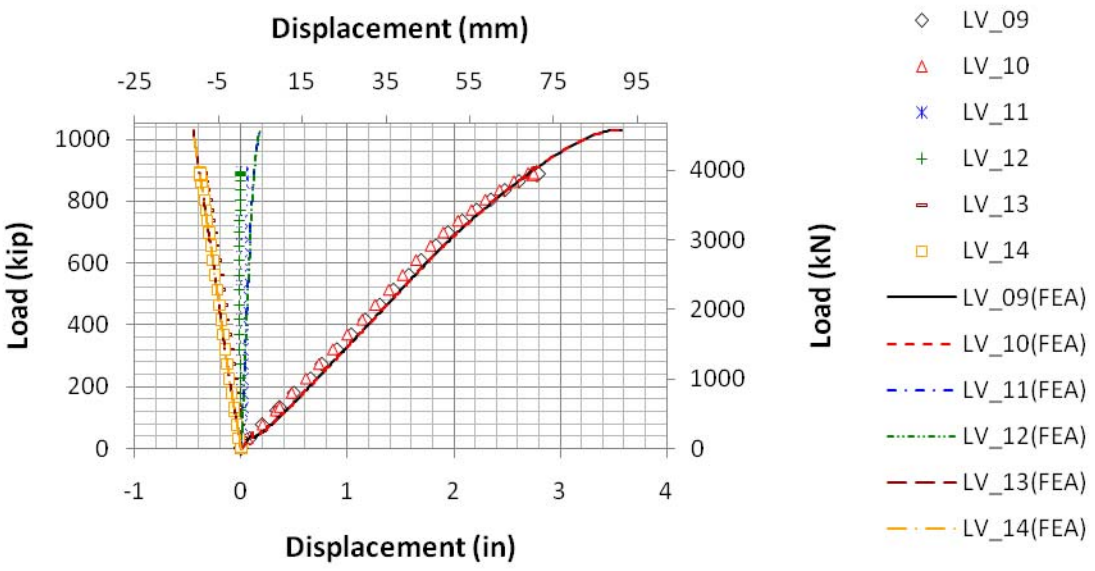


**Figure 8.6** Top Flange Deflection (+tive Downwards).

Figs. 8.4 through 8.6 show deflections at other locations along the span. Again, the numerical results match very well with experimental data at all locations except at LVDT 23 and 24 on the hold-down side, where the specimen failed due to buckling.

LVDTs 23 and 24 are located 2'-0 1/4" from the center support on the hold down side. LVDT 23 is located 1'-6" east of the centerline box, while LVDT 24 is located 1'-6" west of the centerline box. Experimental measurements from LVDTs 23 and 24 for the 1$^{st}$ cycle for Service I and Service II tests are shown respectively in Fig. 8.7 and Fig. 8.8. From Fig. 8.7, it can be seen that LVDT 23 first shows response characterized by significant loss of stiffness at a load of 300 kip. The corresponding point for LVDT 24 from Fig. 8.8 occurs at a load of 420 kip. A similar response is obtained in the numerical predictions at a load of 500 kip. Analysis presented in the next section shows that this level of loss of stiffness is expected to occur about 180 kip after the onset of buckling. This suggests that the bottom flange at LVDT 23 buckled at a load of about 120 kip, while that at LVDT 24 buckled at 240 kip. The numerical prediction of buckling load of the bottom flange is 320 kip (see Section 8.3.2).

These results show that buckling occurred at different loads on the east and west side of the bottom flange despite being located at the same distance from the center support. Since the east side (LVDT 23) buckled at a lower load, the bottom flange stress has to be higher on the east side than on the west side. Also, since experimental buckling loads of 120 kip and 240 kip are both lower than numerical prediction of 320 kip, it is reasonable to conclude that stress in the bottom flange at these locations was higher than estimated by the numerical analysis. Careful review of experimental data suggests that this could have occurred due to different degrees of cracking of bottom slab (see Fig. 8.14 and Section 8.3.3). Clearly, it is difficult to capture

variability of crack sizes in numerical analysis and thus differences between numerical predictions and experimental data in regions affected by cracking is inevitable.

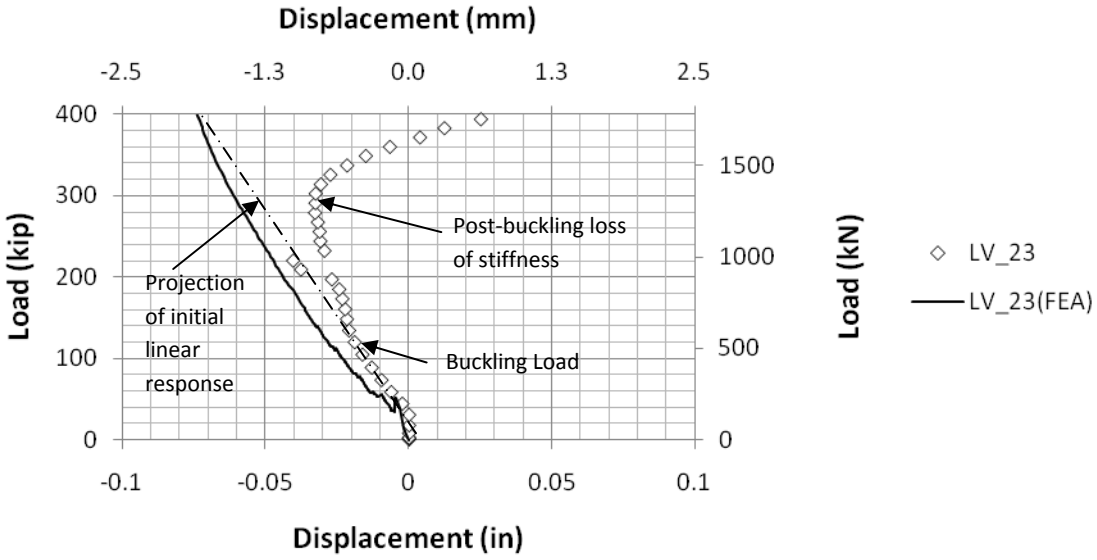


**Figure 8.7** Service I, Cycle I Bottom Flange Deflection (+tive Downwards) Near Failure Region on Hold Down Side. See Figure 4.12 For LVDT Locations.

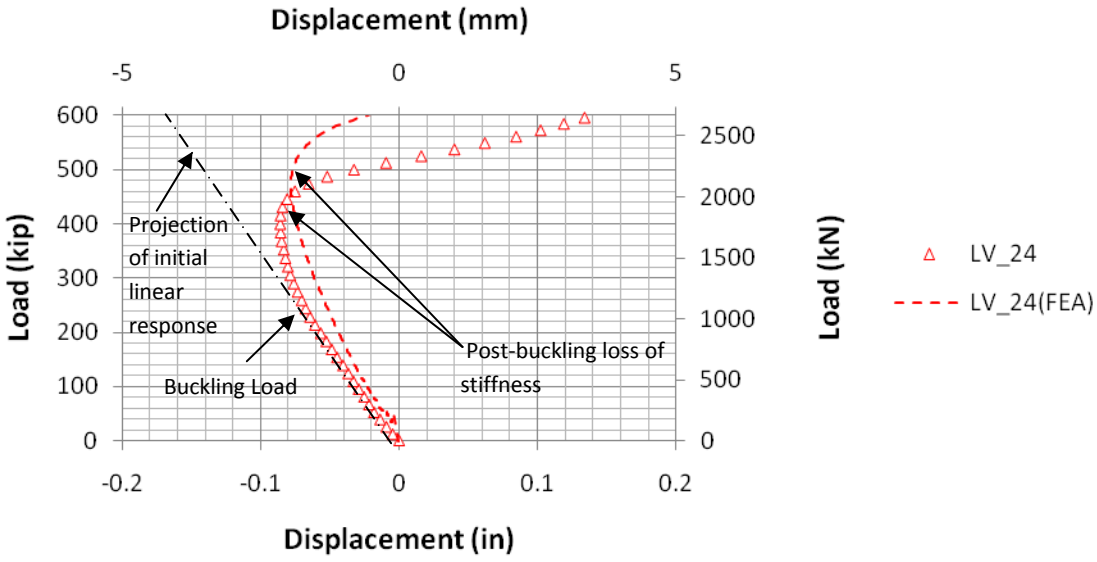


**Figure 8.8** Service II, Cycle I Bottom Flange Deflection (+tive Downwards) Near Failure Region on Hold Down Side. See Figure 4.12 for LVDT Locations.

### 8.3.2 Buckling Response of Bottom Flange

Fig. 8.9 shows bottom flange longitudinal stresses for actuator loads up to 600 kip. At a load of about 320 kip, the top and bottom fiber stress starts to increase rapidly in a non-linear manner, indicating onset of buckling. The mid-plane stress at that load is approximately 25 ksi. As noted in the previous section, the computed 320 kip load is higher than the 120 kip buckling load observed for LVDT 23 (Fig. 8.7) and 240 kip buckling load observed for LVDT 24. This may have resulted from different degrees of cracking of the bottom slab (see section 8.3.3.2 for details).

To verify the buckling load obtained from the full model, a separate ANSYS model was created consisting of three continuous 23 in (long) × 72 in (wide) spans of the composite bottom flange and bottom slab to determine the buckling stress using linear Eigen value analysis (instead of non-linear p-delta analysis). To accurately model rotation constraints, individual shear studs were explicitly modeled. The analysis predicted the longitudinal buckling stress to be 25.3 ksi, which is identical to the 25 ksi mid-plane stress obtained from the full model.

Fig. 8.10 shows that the top fiber of the bottom flange begins to yield at a load of around 620 kip indicated by significant change in slope. Note that the longitudinal stress at yield is higher than the uni-axial yield stress value of 80.9 ksi determined from tests because Von-Mises stress used to determine the yield criteria is affected by the biaxial state of stress (see Fig. 8.11 for computed transverse stress). The onset of yielding results in a drop in mid-plane stresses, which continues until the bottom fiber of the bottom flange yields at a load of about 840 kip. At that point the bottom flange has nearly zero mid-plane stress indicating an inability to carry any load due to net section yielding. Fig. 8.10 also includes mid-plane and top fiber stresses at the same location from a separate model, which assumed full composite action (i.e., design assumption). It can be seen that the response of the mid plane stress for the test specimen model is nearly identical to that for the full composite model up to loads of about 620 kip. This shows that despite having buckled at a load of 320 kip, the bottom flange could effectively carry loads exceeding 600 kip, beyond which plastic buckling causes significant loss of stiffness. In Fig. 8.10, the mid plane stress in the bottom flange where this occurred is nearly 40 ksi.

As shown above, the effective capacity of the bottom flange was reduced by about 50% (from 80.9 ksi to 40 ksi) due to buckling. Fig. 8.12 shows the computed bottom slab bottom fiber strain for the test specimen (composite at shear studs only) and from additional analysis of the design assuming perfect composite action (the design assumption). It can be seen that between actuator loads of 0 and 620 kip, the slopes of the two curves are comparable, indicating similar stiffness. However, beyond a load of 620 kip, the bottom slab in the test specimen model develops significantly higher strains at the same loading. The higher bottom slab load eventually leads to section failure by crushing. This explains the cause of premature failure of the specimen when compared to the predicted ultimate load of nearly 1200 kip (see Fig 8.12, Full Composite curve). A more detailed account of the failure is presented in section 8.4.

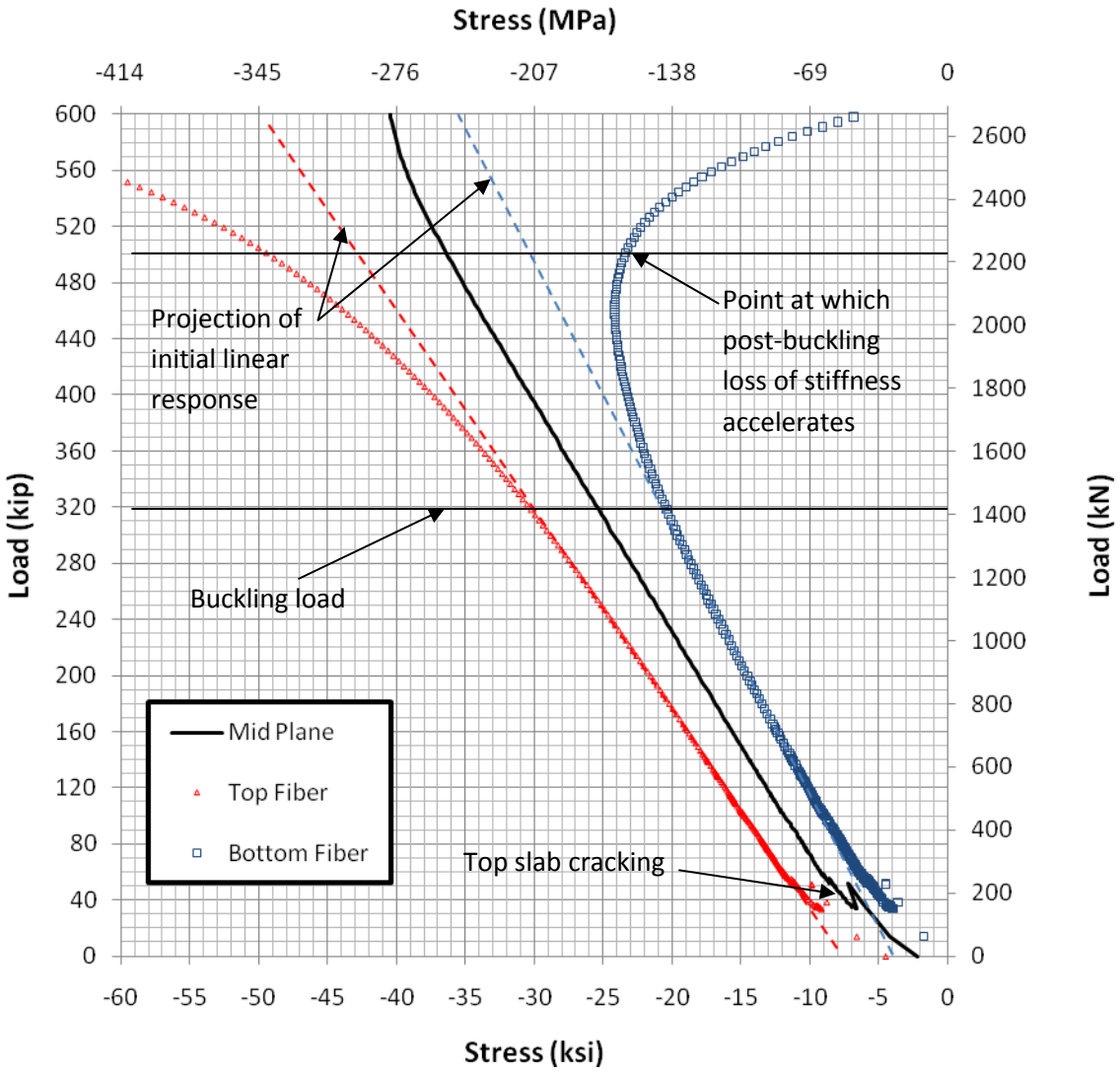


**Figure 8.9** Computed Bottom Flange Longitudinal Stresses (-tive Compression) at Centerline of the Box Section in the Buckled Region

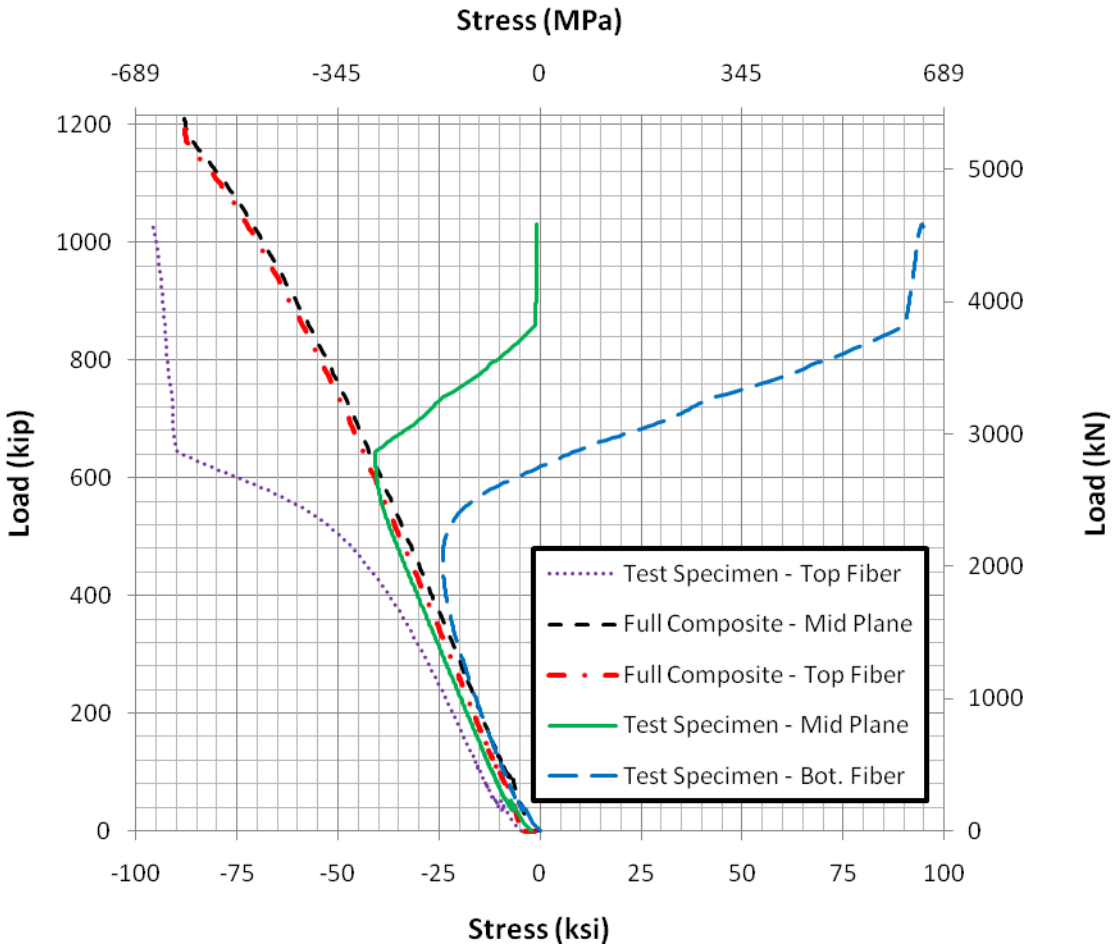


**Figure 8.10** Computed Bottom Flange Longitudinal Stress (-tive Compression) at Center of the Box the Buckled Region

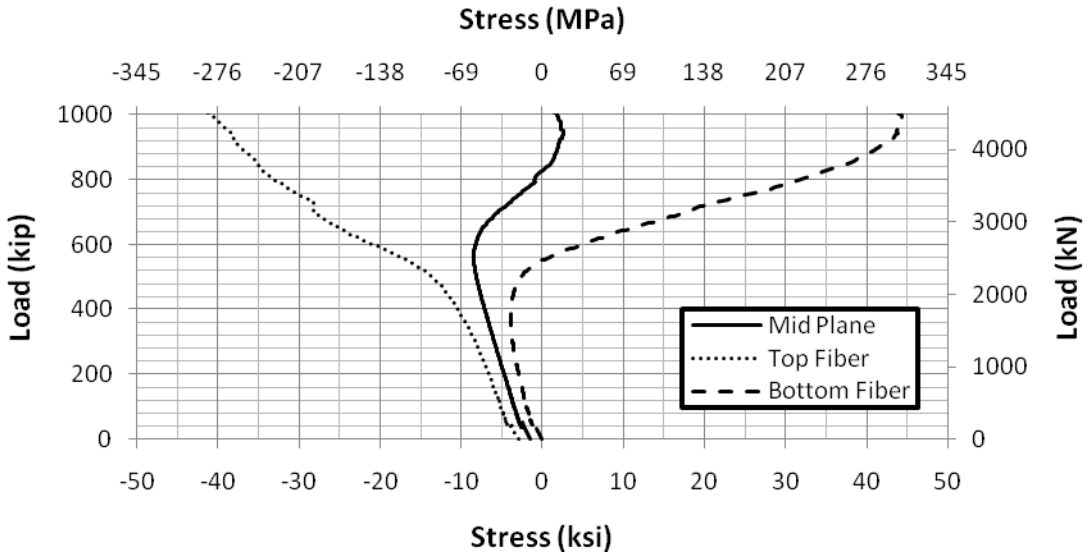


**Figure 8.11** Computed Bottom Flange Transverse Stress (-tive Compression) at Center of the Box the Buckled Region

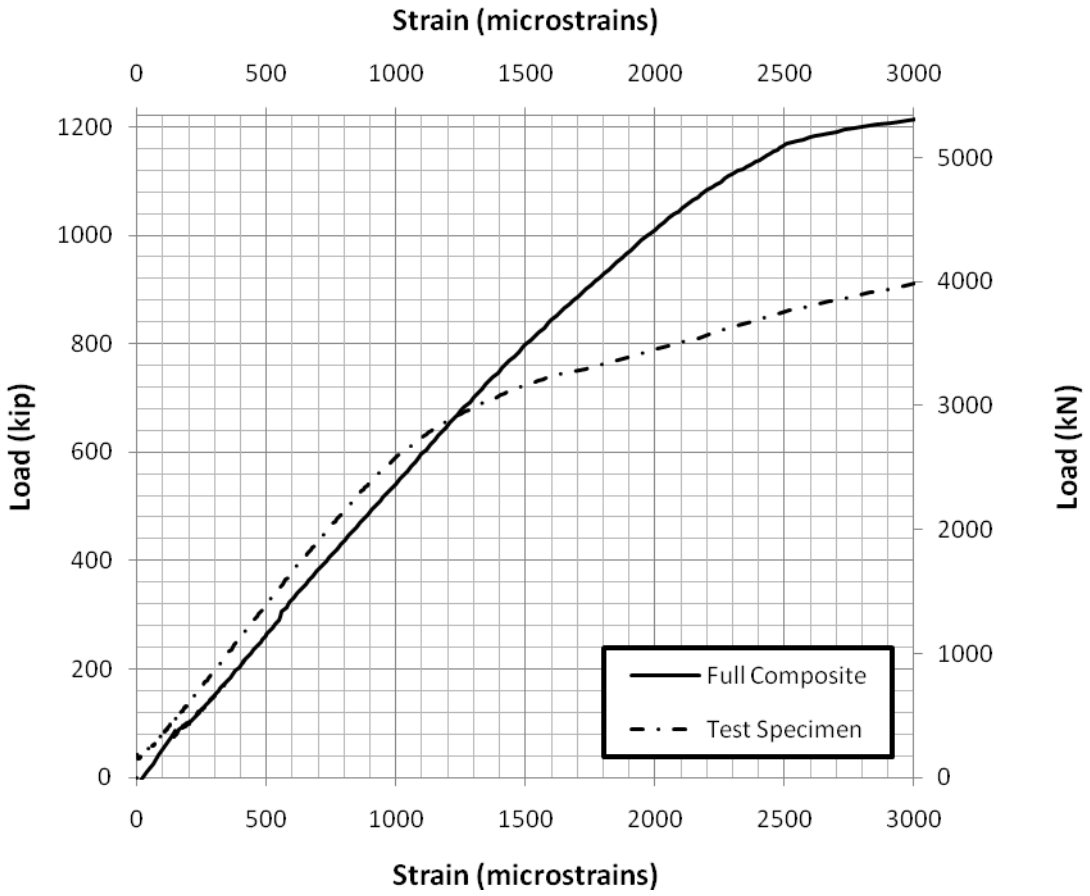


**Figure 8.12** Computed Average Bottom Slab Bottom Fiber Strains (+tive Compression) at Center of the Box in the Buckled Region

### 8.3.3 Critical Strain Comparison

#### 8.3.3.1 Bottom Flange Strain

Results presented so far show that the bottom flange buckles at a load of 320 kip, followed by the onset of loss of bottom flange capacity at a load of 620 kip. At an actuator load of 840 kip, the bottom flange is completely ineffective. Note that due to premature buckling observed in experimental data, the bottom flange will yield at loads significantly below numerically predicted yielding load of 620 kip. Fig. 8.13 shows the bottom flange strain measured on the hold down side at 4'-10 1/8 in. from the center support. There is a zero shift in the experimental data of about 500 με caused by plastic yielding of the region due to multiple applications of the service II loading of 638 kip. Other than that, the curves are qualitatively similar for gages 123 and 125. It can be seen that for all actuator loads, gage 123 located on the east side has lower compressive strain than gage 125 located on the west side. Fig. 8.9 shows that superposition of tensile stresses resulting from local flexural response (due to buckling) with compressive strain from global section bending causes the compressive strain in the bottom fiber

to decrease. This suggests that at a given load, the flexural component of strain is higher for gage 123, which is consistent with the lower buckling load obtained on the east side from the displacement response (see Figs. 8.7 and 8.8).

Note the change in slope at a load of about 620 kip in all three gages, which is consistent with behavior shown in Fig. 8.10. Strain predictions for gage 124 do not match numerical predictions for ultimate load due to prior plastic yielding. Since gage 124 is located at centerline box section, where the flexural stress from buckling are maximum, it reasonable to expect it to accumulate significant plastic strain. Notice that the general behavior obtained is consistent with that predicted by Fig. 8.10 for the bottom fiber at the failure location. Appendix H contains comparison of these gages for the first cycle of Service I, Service II and ultimate load. The comparison between numerical predictions and experimental data for SG 124 is better for Service I and Service II loads due to absence of plastic buckling.

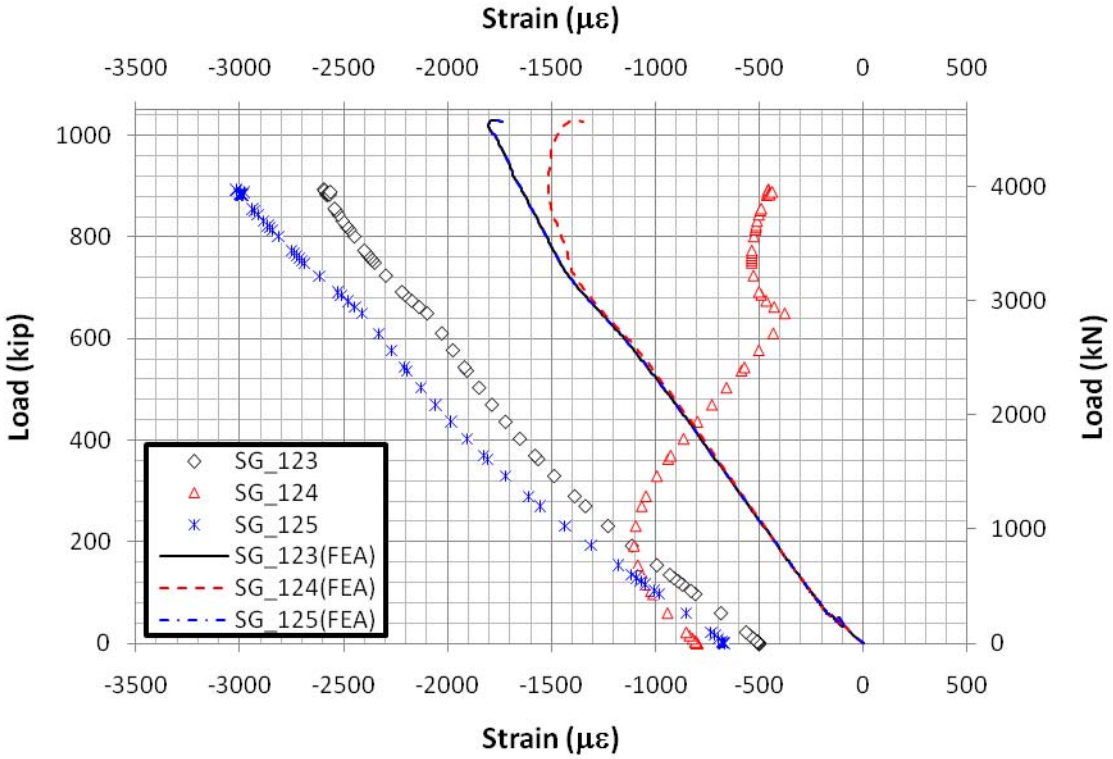


**Figure 8.13** Bottom Flange Strain (-tive compression) on the Hold Down Side. SG 123,124 and 125 located 4'-10 1/8" from Center Support. SG 124 at Center Line Box Section, SG 123 1'-6" East and SG 125 1'-6" West

### 8.3.3.2 Bottom Slab Strain

Fig. 8.14 shows the measured top fiber strain of the bottom slab 4'-10 1/8" from the center support on the hold down side. Experimental data for gage 109 shows increase towards tensile strains for loads up to nearly 100 kip, beyond which the slope is comparable to the numerical predictions. Careful investigation of this response and comparison with numerical data at other locations suggests that this is a result of cracking of the bottom slab starting at the bottom

surface of the bottom slab due to shrinkage (there was no bottom layer of shrinkage steel provided in the bottom slab). The cracking shifts the neutral axis upwards, thereby causing small tensile loads on the top fiber until the crack closes sufficiently to cause compression in the whole section. It can be seen that strain measurements for loads upto 100 kip are nearly zero confirming that the slab is not actually carrying significant loads until the crack closes. This type of behavior is qualitatively seen in Fig. 8.15 which was obtained from numerical results near the actuator. Notice that the curve changes direction when the bottom fiber stress becomes zero, indicating crack closure and a shift in the neutral axis.

Data for SG 111 shows reduced stiffness response for the first 160 kip of actuator loading, where the strains increase rapidly. This again is believed to have been caused by cracking of the bottom slab. The extent of cracking is moderate and does not shift the neutral axis signficantly, however results in reduced stiffness until the crack closes. To confirm this hypothesis, a separate model was run with computed shrinkage strains increased by 50%. Fig. 8.16 shows the comparison of experimental data with high shrinkage run. The numerical data is seen to better match the observations from gage 111.

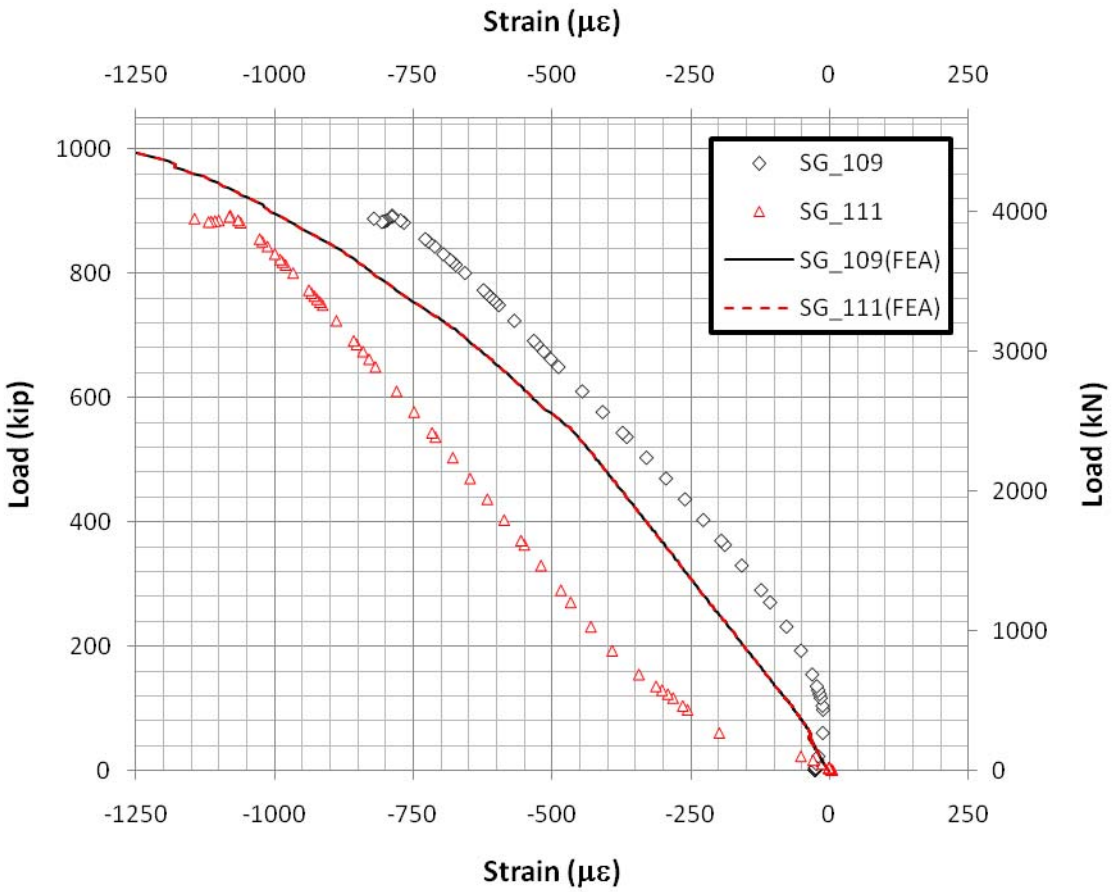


**Figure 8.14** Bottom Slab Strain (-tive compression) on the Hold Down Side. SG 109 and 111 Located 4'-10 1/8" from Center Support. SG 109 1'-6" East and SG 125 1'-6" West of Centerline of Box Section.

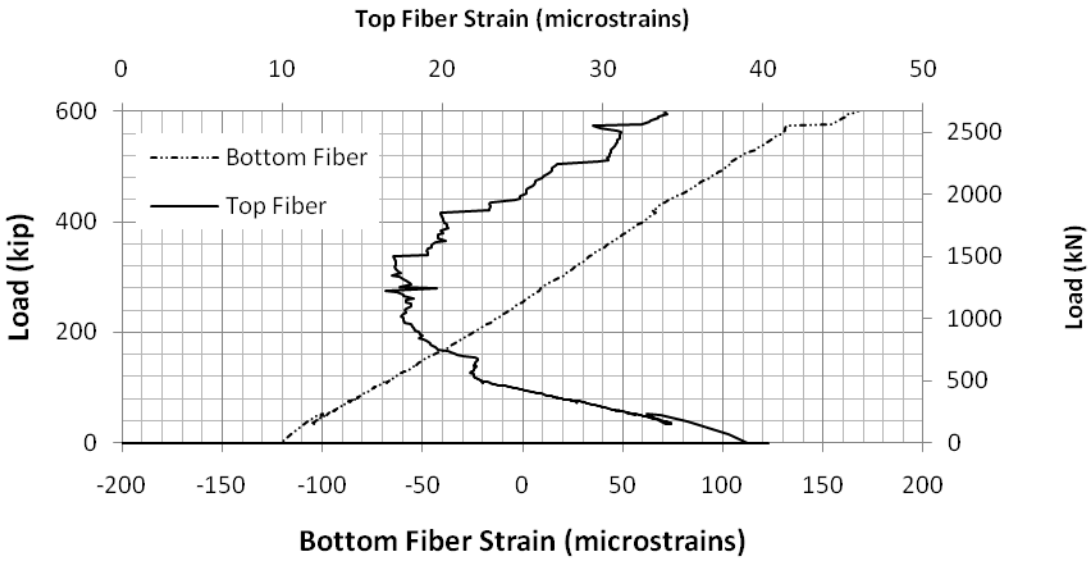


**Figure 8.15** Computed Bottom Slab Top and Bottom Strain (-tive Tension) at Center Line Box, 1.5ft from the Actuator Towards the Center Support.

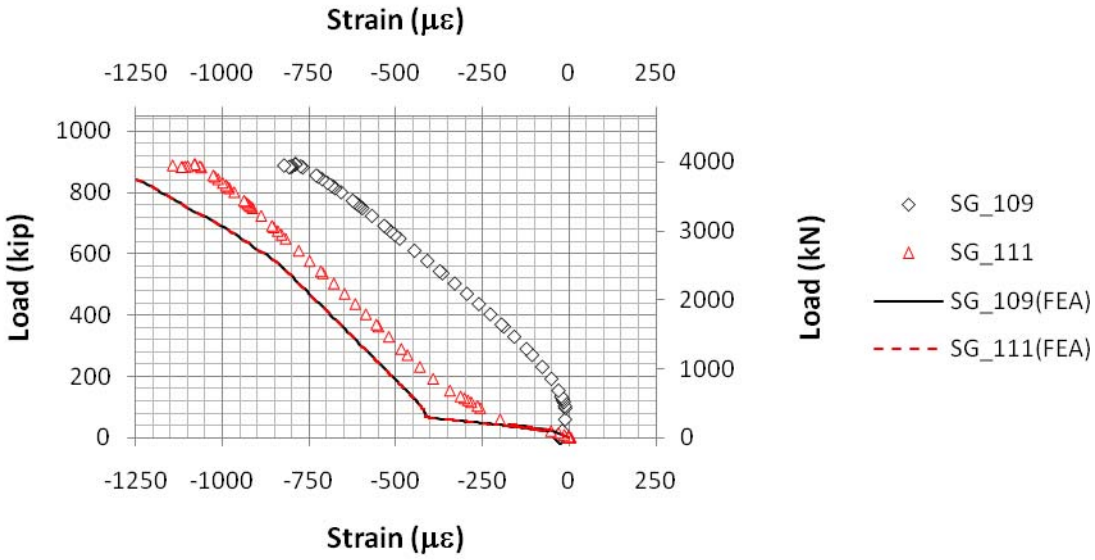


**Figure 8.16** Bottom Slab Strain (-tive Compression) on the Hold Down Side. Shrinkage Strains Increased by 50% Over CEB FIP Predictions. SG 109 and 111 Located 4'-10 1/8" From Center Support. SG 109 1'-6" East and SG 125 1'-6" West of Centerline of Box Section.

The above comparisons show that bottom slab strain measurements are very sensitive to concrete cracks including shrinkage cracks formed at the bottom surface of the slab. Although the data match is not as good as other strain measurements, Fig. 8.14 suggests that the average experimental strain near the failure zone is close to the numerical predictions. For example, at a

load of 800 kip, gage 111 reads close to 1000 με while gage 109 reads about 650 με, the average of the two is close to the numerical prediction of 825 με.

The key finding from the review of bottom slab strains is that the bottom slab had significant cracks including many at the bottom surface of the slab due to shrinkage. An open crack results in the bottom slab not carrying any loads until the crack closes (see Fig. 8.14, gage 109). This means that the steel bottom flange in these regions has to carry excessive loads. This is confirmed by reviewing bottom flange strain data in the same region prior to buckling (Service I, Cycle I) shown in Fig. 8.17. Here gage 123 located on the east side (same side as gage 109 in Fig. 8.14) has higher strain because the cracked concrete slab does not carry significant loads until the crack closes. This variability in response due to different crack size explains the different buckling loads obtained on the east side and west side (see Figs. 8.7 and 8.8). It is also the primary cause of the difference between the numerical predictions of buckling load and those obtained from experimental measurements.

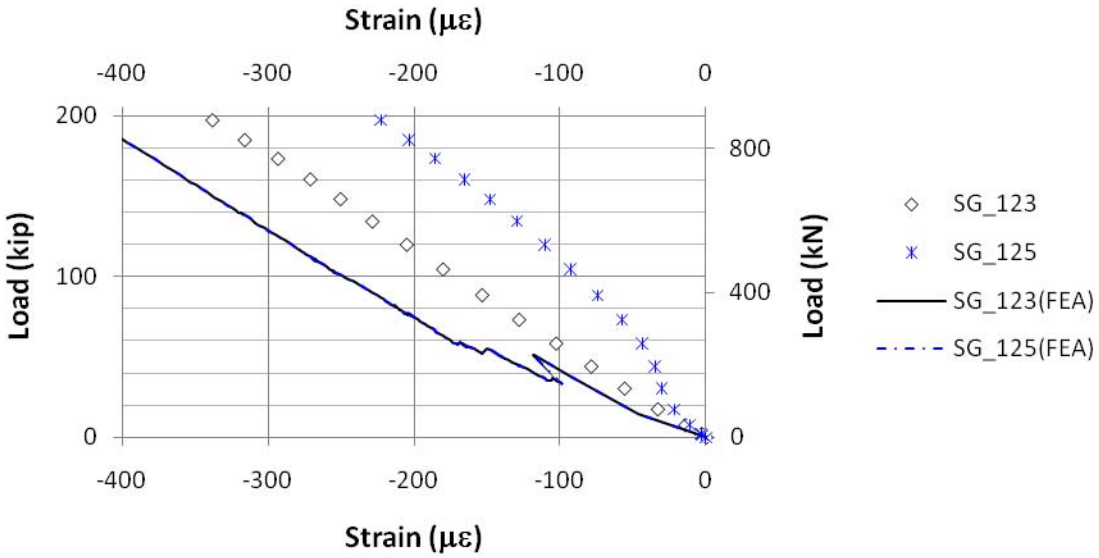


**Figure 8.17** Bottom Flange Strain (-tive Compression) on the Hold Down Side from Service I Test, Cycle I. SG 123 And 125 Located 4'-10 1/8" from Center Support. SG 123 1'-6" East from Centerline Box Section and SG 125 1'-6" West.

### 8.3.3.3 Top Flange Strain

Fig. 8.18 shows the top flange strain at the center support (gages 73 and 74) along with gages on the hold down side (gages 75 and 76 ) located 4'-10 1/8 in. from the center support. The experimental measurements for gages 75 and 76 near the failure zone agree well with the numerical predictions and are essentially linear until 620 kip with a slight change in slope beyond that load.

The top flange strain data at the center support from gages 73 and 74 has essentially the same response as the numerical predictions (except for the zero shift) until a load of 800 kip.

Both numerical and experimental results show a change in slope at an acuator load of 620 kip. Experimental results show significant non-linearity at loads exceeding 820 kip, at strains of about 2600 με and yielding response at strains exceeding 3000 με. The response from the numerical analysis shows yielding at a strain of 2833 με, which is consistent with the input value used in the analysis. This difference between the experimental and numerical results at center support did not impact the final failure load prediction since strain at the failure region (see gages 75 and 76) is still in the linear range and match well.

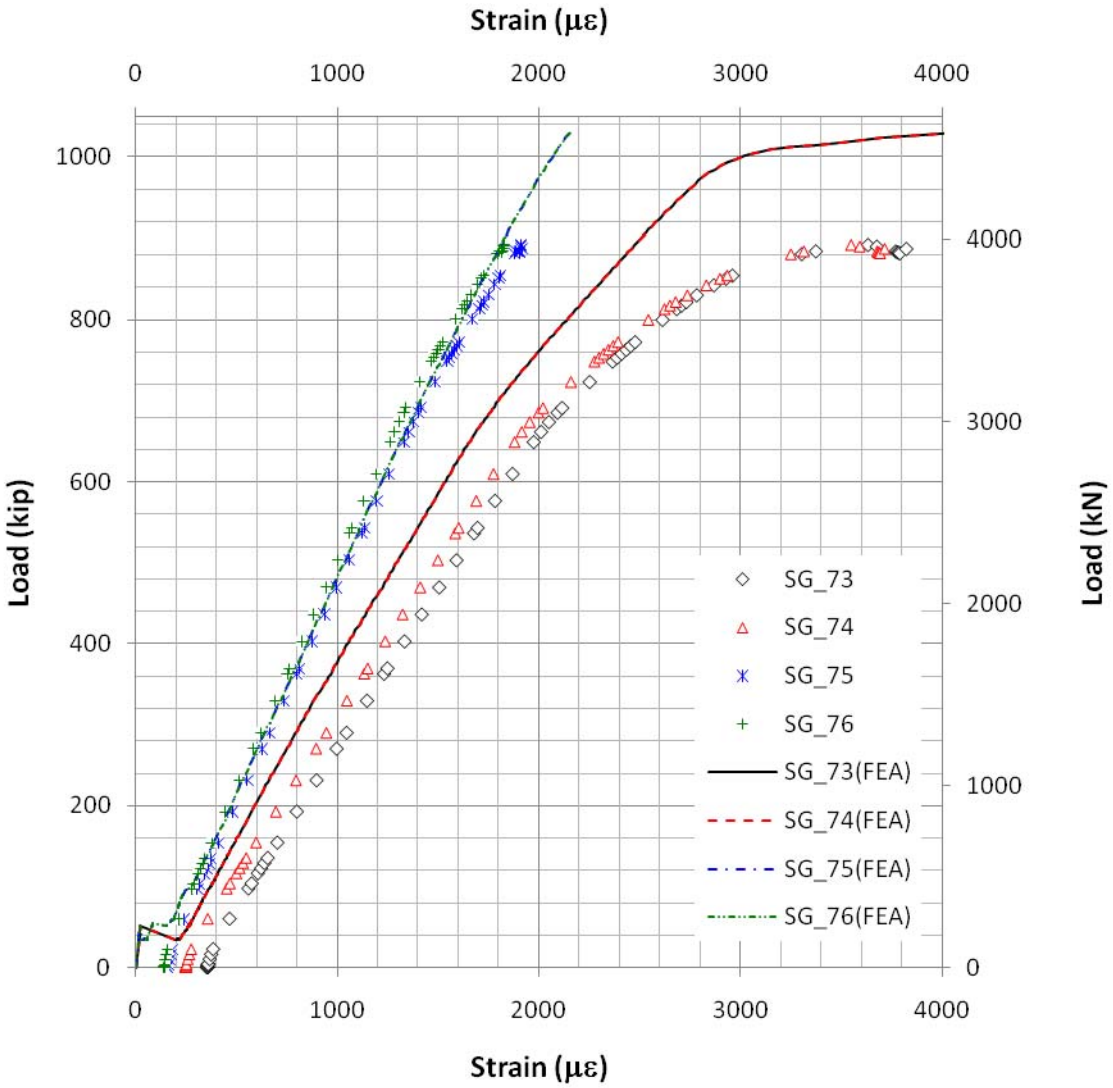


**Figure 8.18** Top Flange Strain (+tive Tension) at Center Support and the Hold Down Side from Ultimate Test. SG 73 and 74 Located at Center Support on East and West Side Respectively. SG 75 and 76 Located 4'-10 1/8" from Center Support on East and West Side Respectively (See Figure 4.20 for Location)

### 8.3.3.4 Web Strains

Web strains measured 4'-10 1/8" from the center support on the exterior face on the west side are shown in Fig. 8.19. The agreement between experimental data and numerical predictions is quite good. The response is practically linear for the entire range. Fig. 8.20 shows the computed web strain obtained at 200 kip load increments 4'-10 1/8" from the center support on the hold down side. This indicates a downward shift in the neutral axis as the load is increased from 200 kip to 600 kip, but then a slight upward shift at 800 kip. This is better illustrated in Fig. 8.21 which shows the variation of neutral axis as a function of the actuator load. This shows that as the top slab cracks and the rebar yields, the neutral axis of the section shifts downwards until a load of 600 kip, beyond which point the bottom flange yields (see Section 8.3.2) and causes the neutral axis to shift upwards.

### 8.3.3.5 Rebar Strain

The east side top slab rebar strain measured 1 ft from the center support on the hold down side are shown in Fig. 8.22. It is not possible to provide an accurate comparison of the rebar strains since the numerical model had more bars but of lesser area each than the actual test specimen. The total area of the rebars matched that provided in the test specimen. The rebar was distributed evenly in the numerical model to avoid numerical instabilites that result from cracking of concrete in localized areas. Numerical data reported is for the bars located closest to the position of the gage. The sudden increase in numerical strain data at a load of about 40 kip results from cracking of the top slab. Fig. 8.22 shows that the numerical prediction is close to the experimental data for gage 59B, which is located over the web. For rebars located on the overhang region (57B and 58B), the strain is overpredicted, however, it is consistent with experimental data in predicting that the strain measurement for gage 57B is larger than that for gage 58B.

Fig. 8.23 shows the cracked regions of the top slab from the numerical analysis (red circles indicate cracks). The hold down side is seen to crack extensively when compared to the actuator side. This is due two reasons (a) first, the concrete strength on the hold side is lower than that on the actuator side (7.6 ksi versus 10.1 ksi) and (b) the diaphragm located at the center support rotates due to actuator loads in such a manner that it pulls the entire top slab more uniformly on the hold down side. This results in a more severe cracking on the hold down side and causes the neutral axis to shift lower at a low load. The resulting lower stiffness lead to higher strains on the bottom flange on the hold down side which eventually lead to the buckling failure. This explains why the bottom flange fails in the hold down side despite having slightly lower moments (<1% lower) than on the actuator side. This hypothesis was further supported from results from models where the diaphragm was not explicitly modeled, but approximated by suitable boundary conditions. These models predicted more severe buckling on the actuator side than on the hold down side.

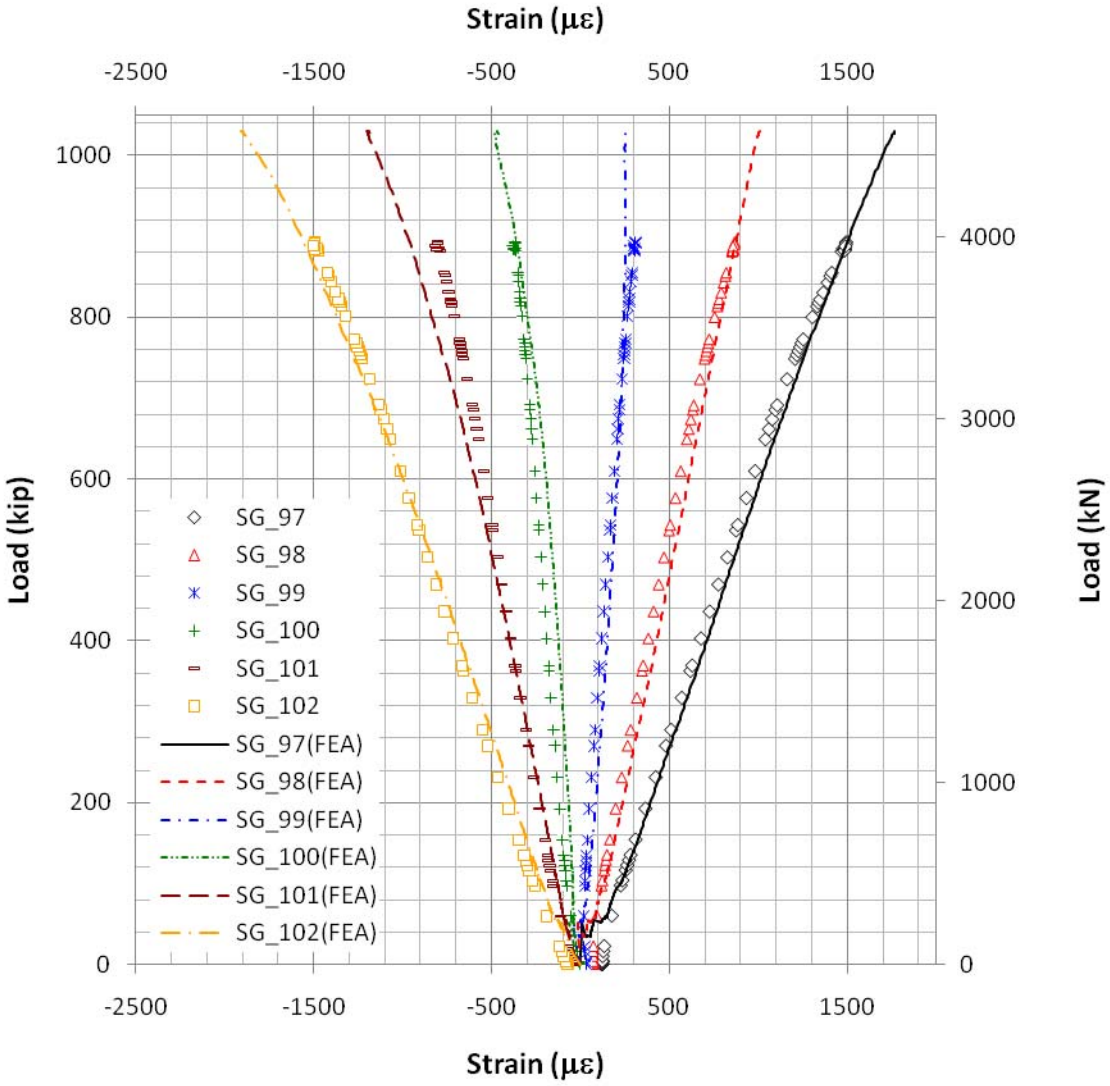


**Figure 8.19** West Web Strain from Ultimate Test (+tive Tension) 4'-10 1/8" from Center Support on Hold Down Side. See Figure 4.20 for Locations.

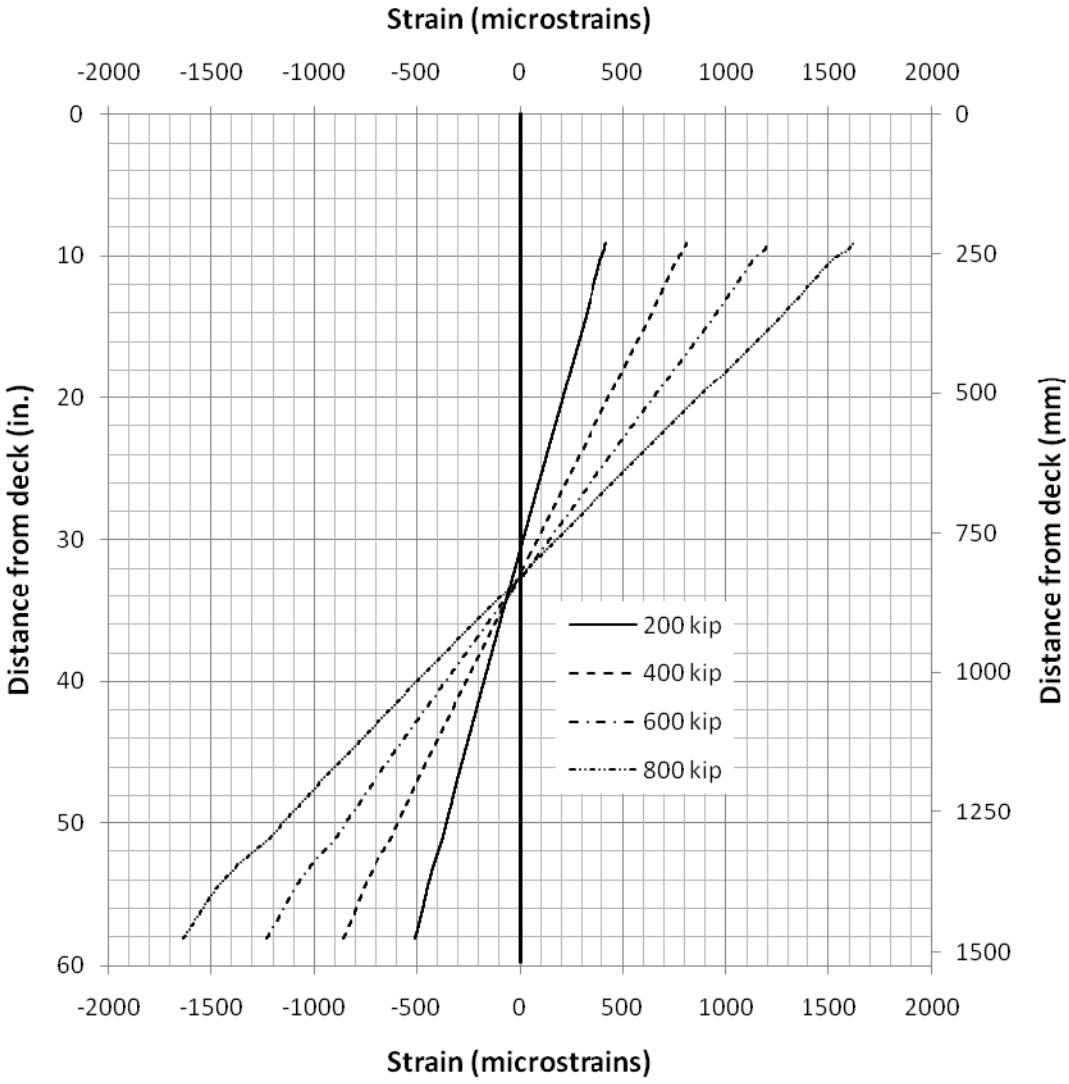


**Figure 8.20** Determination of Neutral Axis 4'1- 1/8" from the Center Support on the Hold Down Side from Numerical Results

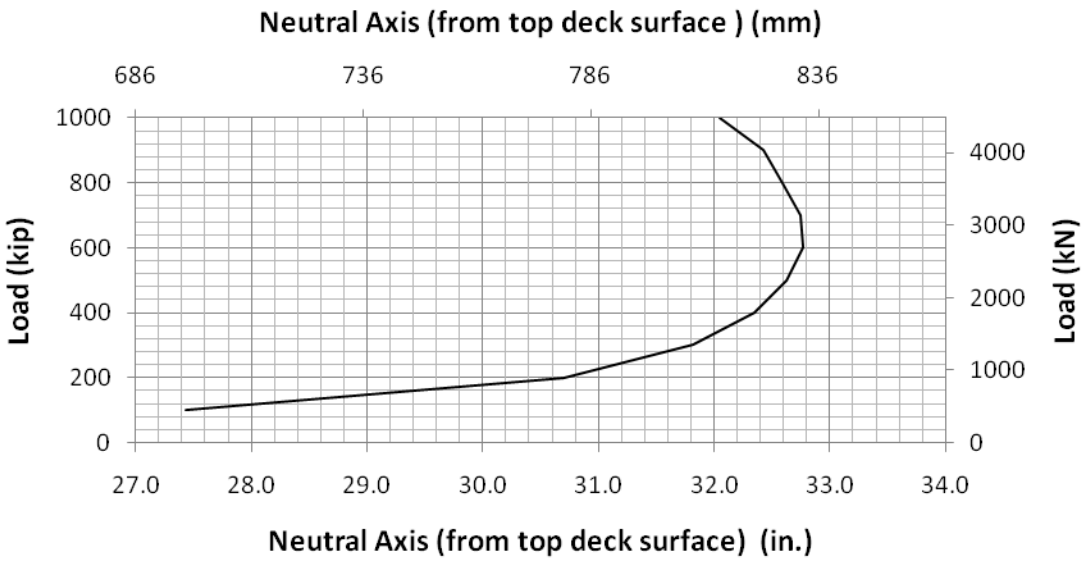


**Figure 8.21** Neutral axis position 4'-10 1/8" from the center support on the hold down side from numerical results

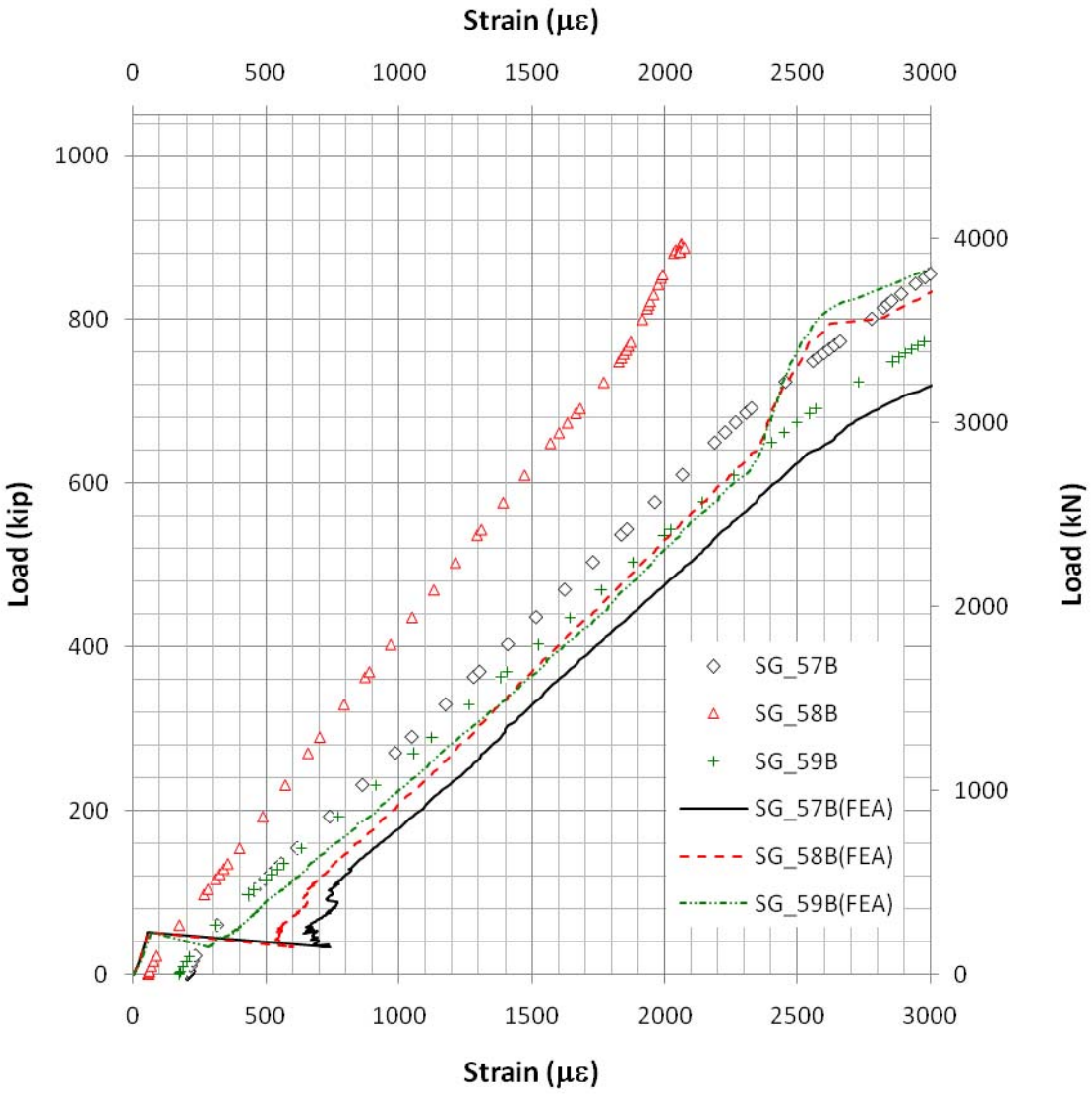


**Figure 8.22** Rebar Strain 1 ft from Center Support on Hold Down Side. See Figure 4.18 For Location.

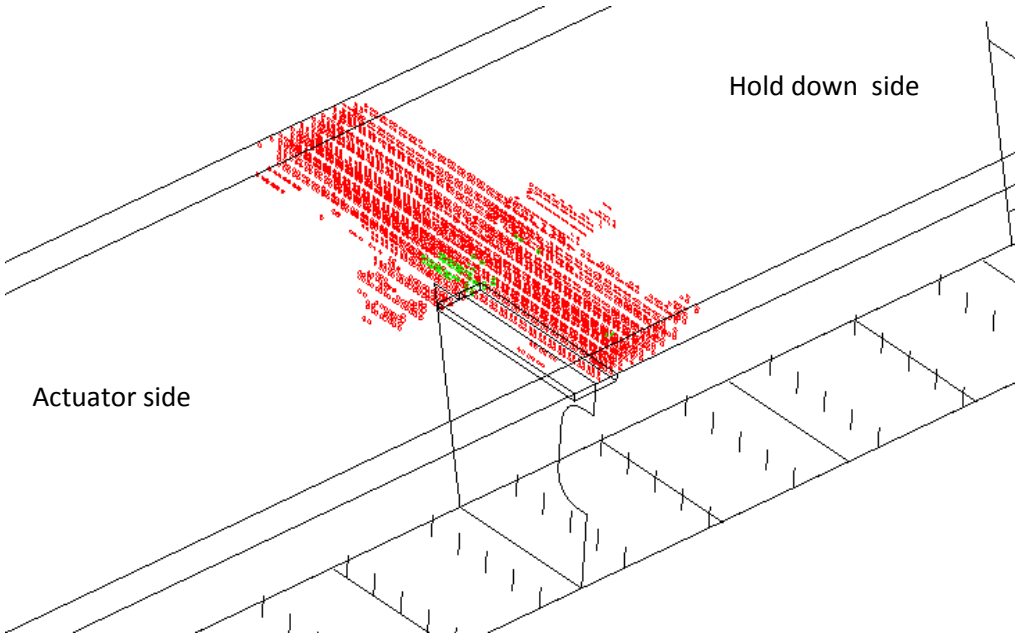


**Figure 8.23** Cracked Regions (in Red) from the Numerical Model at Actuator Load of 34 Kip

## 8.4 Failure Mode

Based on the results presented so far, events leading to failure of the double composite test specimen can be summarized as follows:

- The initial part of the structural response at a load of about 50 kip is marked by slight non-linearity due to top slab cracking. Other than that the initial response is largely linear (see Fig. 8.9). The top slab cracks more severely on the hold down side due to lower concrete strength and nature of diaphragm rotation (see Fig. 8.23) than the actuator side. This results in higher reduction of section properties on the hold down side than on the actuator side.

- Downward deflection of the bottom flange under dead load of the steel and the bottom slab results in eccentricity of the load from full box section loads. This eccentricity results in local flexural stresses. The superposition of local flexural stresses with compressive stress caused by global section bending causes the highest compressive stress to occur on the top fiber of the bottom flange (see Fig. 8.9). The bottom fiber stresses are lower than the mid-plane stress due to superposition with tensile flexural stress. The out of plane deformation leads to nearly linear increase in section stress (see Fig. 8.9) until an actuator load of 320 kip. At that load the non-linearity seen in the top and bottom fiber stresses start to increase rapidly indicating buckling.

- The buckling load observed in experiments was 120 kip for the east side and 240 kip for the west side (see Figs. 8.7 and 8.8). This premature buckling is thought to have been caused by inability of the cracked concrete to carry loads until crack closure (see Figs. 8.14 -8.16).

- The response of the bottom flange is stabilized due to embedment into concrete. The bottom flange continues to resist additional loading until an actuator load of 620 kip at which the top fiber starts to yield in compression (see Fig. 8.10 and Fig. 8.13).

- Fig. 8.12 showing concrete strains suggests that prior to onset of plastic yielding of the bottom flange due to buckling, the response of the structure is similar to fully composite design.

- At an actuator load of 620 kip, the bottom flange mid-plane stress reaches its maximum useful limit. The mid plane stress keeps reducing as further load is applied. Analysis of the results indicates that shear lag effects on the bottom flange are important only after the bottom flange yields significantly. At failure load, the bottom flange region adjacent to the web is still effective in carrying a small fraction of the applied load, while the region close to center-line box carries practically no load (see Appendix H, Fig. H.42).

- All additional load is carried by the concrete slab until it fails when the bottom fiber reaches a strain of 3000 με (see Fig. 8.12). See Appendix H, Section H.4and Appendix I for a discussion on choice of concrete ultimate strain limit.

The above results show that shear studs embedded in concrete provide rotational stiffness at edges increasing the buckling load significantly beyond that predicted by using a simply supported plate assumption found in handbooks (ex. [8.3]). The difference in buckling load in this case is nearly 200% (8.7 ksi versus 25.3 ksi).

Another interesting point to note is that although buckling occurred at a lower load in the experiments, the final analytically predicted failure load agrees well with the test data (see Fig. 8.12). The reason for this is that the failure resistance of the section is determined by the combined resistance of the bottom flange (say, $R_{BF}$) and the bottom slab (say, $R_{BS}$). $R_{BF}$ is determined by buckling behavior of the flange and $R_{BS}$ is determined by the compressive strain in concrete. At ultimate load, $R_{BF}$ is only about 9% of $R_{BS}$. This is because as extreme fibers of the bottom flange start to yield (both in compression and tension) due to buckling, it sheds significant portion of its load to the bottom slab. This load transfer is seen to start at an actuator load of about 620 kip in Fig. 8.10 and Fig. 8.12. This means that the ultimate capacity of the section is primarily a function of the bottom slab strength and thus not very sensitive to the exact bottom flange buckling load.

## 8.5 Parameter Study

As noted in Section 8.4, the ultimate capacity of the double composite section is dictated by the combined capacity of the bottom flange and the bottom slab. The latter is easy to determine based on current design guidelines and an upper strain limit of 3000 με. The effective capacity of the bottom flange is difficult to determine due to the inherent complexity in

computing the buckling and post-buckling load carrying capacity. This section presents findings on studies performed using a simpler model of the bottom flange with 3/8 in. thick 70 ksi yield strength steel of the same dimensions as the test specimen and 7 in. thick bottom slab. The shear stud spacing was varied to understand the options available to a designer to improve the bottom flange capacity.

Table 8.2 shows the results from the study. Since the mesh used was considerably finer than that for the full model and the loads applied are purely axial, the effective stress capacity is lower than that obtained from the full model. Note that the stress reported is at mid span of the buckling region at centerline box. This is the location with the maximum buckling stress. The results shown indicate that the bottom flange capacity can be increased by about 80% by reducing the shear stud spacing by 50%. This doubles the number of shear studs. A zig zag pattern can be used to retain the same number of shear studs as the baseline and still increase the bottom flange capacity by 37%. It must be pointed out that as long as bottom flange buckling is a possibility, a significant increase in bottom flange effective resistance will still only result in a marginal increase in the section ultimate capacity since the bottom flange resistance is a small fraction of the bottom slab resistance (see last paragraph of Section 8.4).

**Table 8.2** Results of Parametric Study

| Case | Transverse Shear Stud Spacing (in) | Longitudinal Shear Stud Spacing (in) | Effective Bottom Flange Resistance Stress (ksi) | Comment |
|---|---|---|---|---|
| 1 | 8 | 23 | 27 | Baseline configuration |
| 2 | 4 | 23 | 31.5 | Marginal improvement |
| 3 | 8 | 11.5 | 49 | 80% improvement |
| 4 | 8 | 11.5 | 37 | Zig zag pattern. 37% improvement |

## 8.6 Summary

This chapter presented results of the numerical study performed using a non-linear finite element model. The model was complex due to multiple sources of non-linearity including buckling, cracking and contact. Comparison of deflection and strain data from the model showed that the model captured the global behavior of the structure quite well. The analysis was able to explain the causes of many of the experimental observations that were difficult to understand (see Section 8.1). Many of the complex behaviors result from open cracks in the bottom slab resulting from concrete shrinkage. Numerical results suggest that the theoretical buckling capacity of the bottom flange is 25 ksi, which occurs at a load of 320 kip. However, due to cracking of the bottom slab it was ineffective until the cracks closed; the bottom flange buckled at a lower load in

the experiment (120 kip and 240 kip at the east and west side). Despite this difference, the ultimate capacity of the structure was predicted well by the models (see Section 8.4). Parametric studies of the composite bottom flange suggest that the effective bottom flange capacity can be increased by varying shear stud spacing.

## References

8.1 SAS IP Inc. (2007). "Release 11.0 Documentation for ANSYS." ANSYS, Inc., Canonsburg, PA.

8.2 Chung, W., and Sotelino, E.D.(2006). "Three-Dimensional Finite Element Modeling of Composite Girder Bridges." *Engineering Structures*, Vol. 28, pp. 63–71.

8.3 Young, W., and Budynas, R. (2001). "Roark's Formulas for Stress and Strain." McGraw-Hill Professional, New York.

# 9. DESIGN RECOMMENDATIONS

## 9.1 Introduction

The test specimen was tested under fatigue, service and ultimate loads that enabled its structural response to be evaluated. For the fatigue and service tests, the double composite box girder behavior was as expected. However, the flexural strength capacity of the double composite box was less than anticipated. In order to establish design recommendations, numerical analyses were undertaken to understand the behavior of the double composite steel box. This chapter summarizes these findings. A description of the failure mode is first presented in Section 9.2, followed by an evaluation of the beam behavior in Section 9.3. A discussion of the results is summarized in Section 9.4 with the design recommendations listed in Section 9.5. Section 9.6 provides construction guidelines.

## 9.2 Failure of Test Specimen

Sudden failure of the specimen occurred at an actuator load of 894 kips which produced a moment of 22,350 ft-kips at the center support. A visual examination of the failed specimen showed that the concrete had crushed between one and three feet from the center support on the hold down side of the specimen (see Fig. 9.1) in conjunction with buckling of the steel bottom flange. The bottom slab on the actuator side did not show any signs of deterioration (see Fig. 9.2). Due to the unsymmetrical support layout, the moment on the hold down side at the pertinent strain gage location is approximately 2% lower than that of the actuator side. The top flange strain gages at the center support, labeled 73 and 74, recorded strains of approximately 3800 $\mu\varepsilon$ which exceeds the theoretical yield strain of approximately 2800 $\mu\varepsilon$. Note that these were the only strain gages located at the center support. Additional gages located 4 ft $10^1/_8$ in. from the center support (see Fig. 4.19, 4.20 and 9.3) recorded strains as shown in the Tables 9.1 and 9.2.

## 9.3 Mathematical Model of Double Composite Behavior

From a design efficiency standpoint, it would be beneficial to be able to evaluate double composite behavior using *classical beam theory*. The customary method is to devise a cross section of a single material whose deformational response to loading is equivalent to that of the actual composite section for which:

- sections that were plane prior to loading are assumed to remain plane after loading, whereby strain varies linearly with respect to distance from the neutral axis

- materials are assumed to behave elastically and to follow Hooke's Law, whereby stress is directly proportional to strain ( i.e., $\sigma = E\varepsilon$ )

**Figure 9.1** Bottom Slab Showing the Extent of Concrete Crushing

**Figure 9.2** Bottom Slab on Actuator Side Showing No Signs of Deterioration


**Figure 9.3** Strain Gages Located Along Depth of Web

**Table 9.1** Strain Gage Measurement on the Hold Down Side at Ultimate Load

| Element | Gage No. | | Strain ($\mu\varepsilon$) | |
|---|---|---|---|---|
| | East Elev. | West Elev. | East Elev. | West Elev. |
| Bottom of TF | 75 | 76 | 1912 | 1827 |
| Web 1 | 85/132 | 97/138 | 1614 | 1481 |
| Web 2 | 87/133 | 99/139 | -217 | -213 |
| Web 3 | 89/134 | 101/140 | -952 | -941 |
| Top of Bottom Slab | 109 | 111 | -789 | -1080 |
| Bot. of Bottom Flange | 123 | 125 | -2586 | -3010 |

"+ive" = Tension, "-ive" = Compression

**Table 9.2** Strain Gage Measurement on the Actuator Side at Ultimate Load

| Element | Gage No. | | Strain ($\mu\varepsilon$) | |
|---|---|---|---|---|
| | East Elev. | West Elev. | East Elev. | West Elev. |
| Bottom of TF | 71 | 72 | 1916 | 1834 |
| Web 1 | 79/129 | 91/135 | 1558 | 1464 |
| Web 2 | 81/130 | 93/136 | 255 | 218 |
| Web 3 | 83/131 | 95/137 | -1098 | -1131 |
| Top of Bottom Slab | 106 | 108 | -517 | -835 |
| Bot. of Bottom Flange | 118 | 120 | -2090 | -2444 |

"+ive" = Tension, "-ive" = Compression

### 9.3.1 Linear Strain Behavior

By plotting the strains associated with top flange and web mounted gages, one can observe that for actuator loads greater than 421 kips, the neutral axis location does not significantly change. The shift of the neutral axis below 421 kips is attributed to the cracking of the top slab. Strains for each loading, Service I, Service II and Ultimate were generated for the four measured locations; Top Flange, Webs 1, 2, and 3 (refer to Tables 9.1 & 9.2 and Fig. 4.19, 4.20 and 9.3). As can be seen from Fig. 9.4, the strain variations are nearly linear.

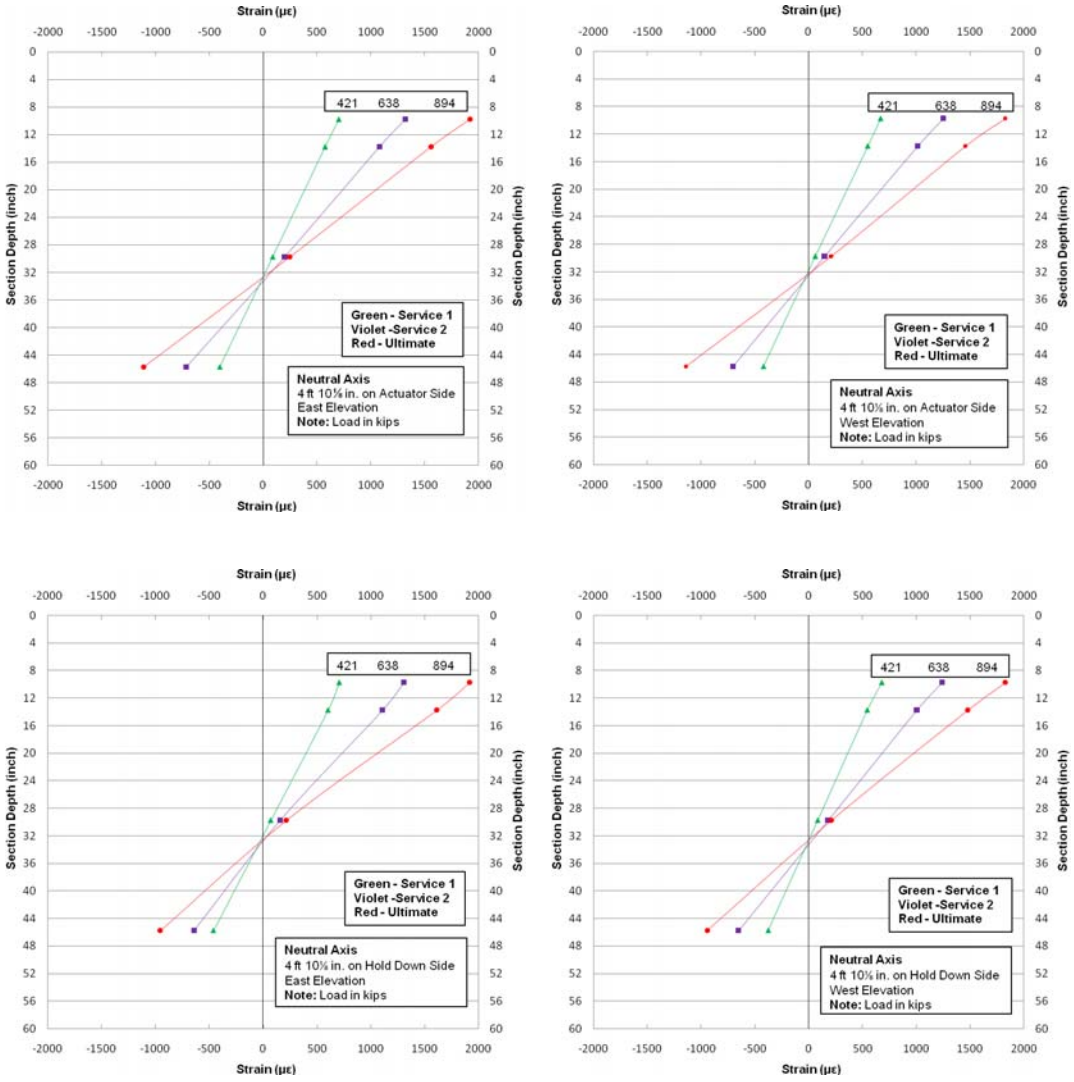


**Figure 9.4** Strain Gage Data Used to Determine Location of Neutral Axis

### 9.3.2 Modular Ratio

In order to compare the laboratory test results to predicted values from classical beam theory, it was first necessary to calculate the transformed section properties for the test specimen. Transformed sections are commonly used to analyze the behavior of composite members comprised of two or more materials with different strength properties (see Fig. 9.5). The modular ratios (i.e. $n = E_s / E_c$) used to perform the mathematical transformations were based on the average elastic modulus for the box girder steel, $E_s = 30{,}300$ ksi, as determined through laboratory tests.

The initial elastic modulus for the concrete, $E_c$ was computed using AASHTO [9.1] Equation 5.4.2.4-1, whereby;

$$E_c = 33{,}000 K_1 w_c^{1.5} \sqrt{f_c^{'}}$$

For this equation, the compressive strength of the bottom slab concrete was taken as $f_c^{'} = 8428$ psi, the average strength determined from cylinder tests. Also, a correction factor of $K_1 = 0.9$ was employed to account for the presence of Florida limerock aggregate [9.2]. Whereby, $E_c = 4761$ ksi.

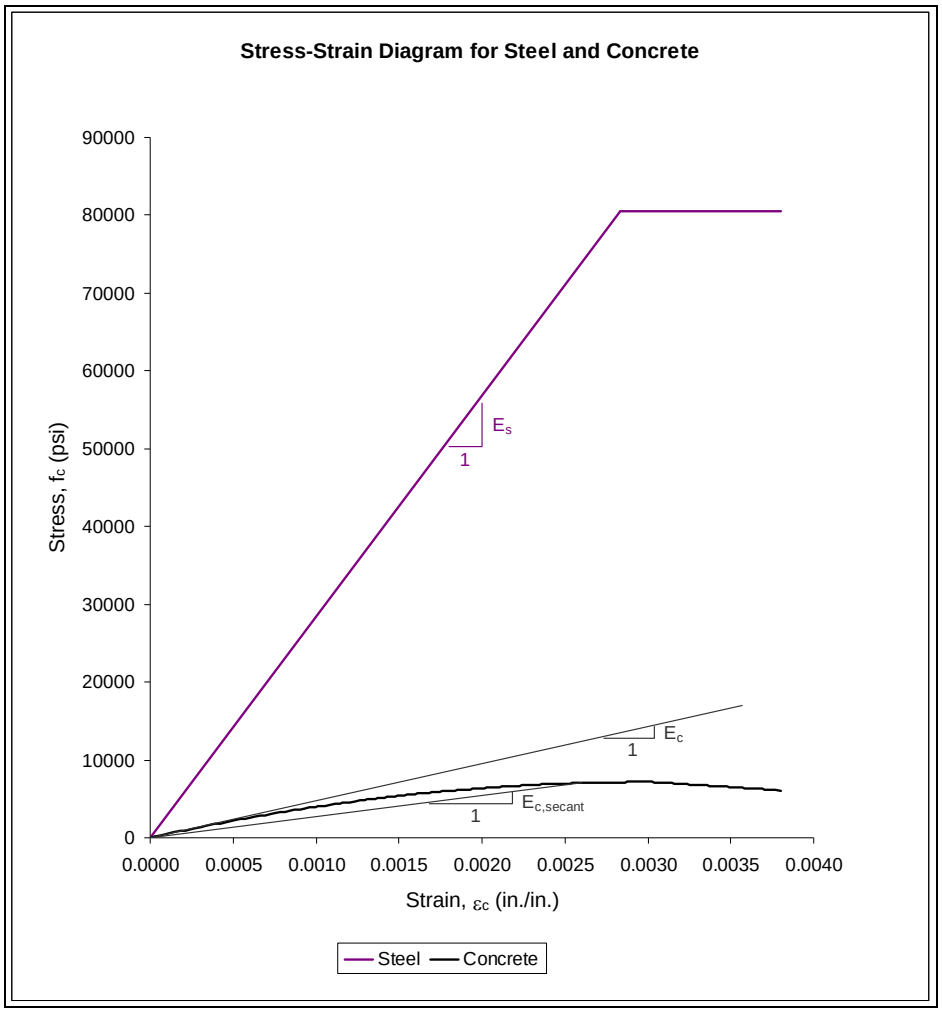


**Figure 9.5** Concrete and Steel Strain Diagram

However, the relationship of stress to strain for concrete, particularly at high stress levels is non-linear (see Fig. 9.6). Therefore, the stress-strain diagram was utilized to determine the elastic modulus at any given level of strain.

The stress-strain diagram was plotted using a Modified Hognestad [9.3] model, whereby the maximum compressive stress, $f_c^{"}$, and corresponding strain, $\varepsilon_0$, are set at $f_c^{"} = 0.85 f_c^{'}$ and $\varepsilon_0 = 2 f_c^{"} / E_c$, respectively. For strains at or below the $\varepsilon_0$ limit, the relationship of stress to strain is defined by the formula;

$$f_c = f_c^{"}\left[\frac{2\varepsilon_c}{\varepsilon_0} - \left(\frac{\varepsilon_c}{\varepsilon_0}\right)^2\right]$$

For strains exceeding $\varepsilon_0$, the stress-strain relationship linearly decreases to $f_c = 0.85 f_c^{"}$ at an ultimate strain value of $\varepsilon_u = 0.0038$.

The stress-strain diagram is then used to determine a *strain-dependent* elastic modulus by first drawing a straight line from the plotted strain value to the origin. The slope of this line, $E_{c,\sec ant}$, is then used to compute the modular ratio as $n = E_s / E_{c,\sec ant}$. As evident from Fig. 9.6, the secant elastic modulus decreases in value at an increasing rate as strain increases to and beyond the point of maximum stress.

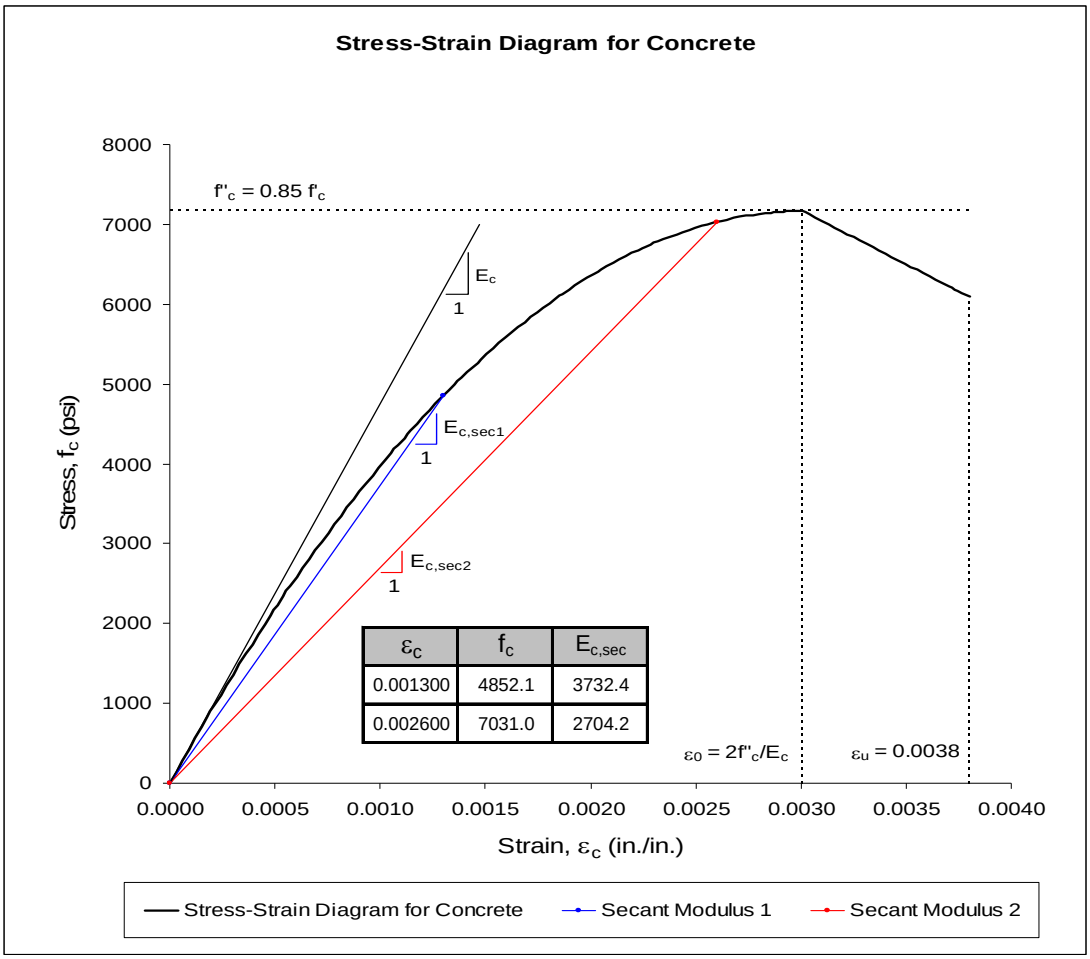


**Figure 9.6** Concrete Stress-Strain Diagram

To fulfill the composite beam assumptions using transformed section properties, the use of the secant elastic modulus, which follows Hooke's Law, can then be used to determine the stress distribution of the composite section.

### 9.3.3 Shear Lag in the Concrete Bottom Slab

The test specimen was designed using AASTHO LRFD Article 4.6.2.6, which specifies effective flange widths for composite members. The test specimen had a seven inch thick

concrete bottom slab, six feet in width. A set of three gages was placed across the top of the concrete bottom slab at locations 4 ft $10^{1}/_{8}$ in. from the center support on both the actuator and hold sides (see Fig. 4.19 and 4.20). Gage readings are summarized in Table 9.3 and the plotted results are shown in Fig 9.7. Gage 110, which was located in the middle of the cross section on the hold down side, did not function. Gage 107 measurements were always greater than the minimum edge gage readings.

Fig. 9.7 below shows that the strain variations remained essentially linear as loads were increased. Considering the above finding and results from the FEA, it appears that the entire width of the concrete bottom slab was effective in resisting bending for negative moments.

**Table 9.3** Strain Gage Readings at Bottom Slab for Service I, Service II and Ultimate

| Gage | | | Service 1 | | | Service 2 | | | Ultimate | | |
|---|---|---|---|---|---|---|---|---|---|---|---|
| 109 | 110 | 111 | -243 | * | -580 | -460 | * | -792 | -789 | * | -1080 |
| 106 | 107 | 108 | -200 | -269 | -385 | -371 | -537 | -591 | -518 | -940 | -835 |

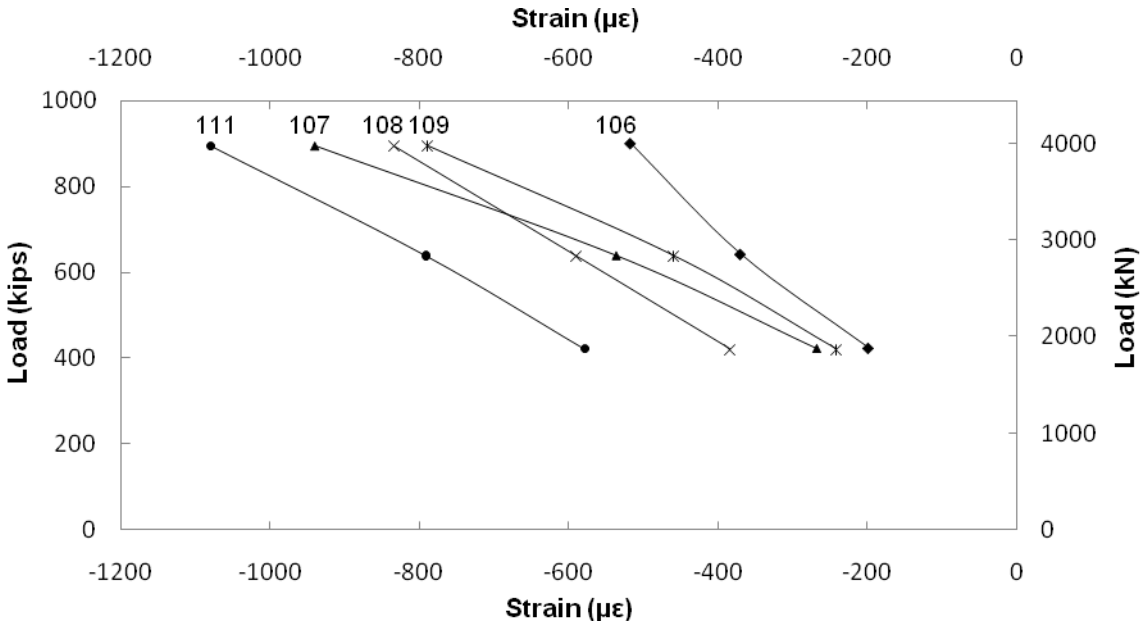


**Figure 9.7** Strain Recorded on Bottom Slab

### 9.3.4 Steel Bottom Flange Capacity

The test specimen was designed with a thin steel bottom flange, studded with shear connectors, which was intended to provide composite action with the concrete bottom slab and aid in the flexural strength of the composite section. However, test data and the FEA indicate that

the steel bottom flange may not have been fully effective due to the longitudinal spacing of the shear connectors. Using classical plate buckling equations and assuming simple supported edges with a span length equal to the shear connector spacing, the buckling strength of the $^{3}/_{8}$ in. thick plate is approximately 9 ksi, which would indicate that the steel bottom flange was ineffective in providing flexural strength to the composite section. However, the results of the FEA showed that the onset of buckling of the bottom flange started at an actuator load of 320 kips, but was effective up to a load of 620 kips corresponding to stresses of approximately 25 and 40 ksi, respectively. Further explanation on the effectiveness of the steel bottom flange is given in Section 8.3.2.

### 9.3.5 Elastic Section Properties

Strain gage readings recorded during the laboratory tests were used to compute stresses at critical locations for the test specimen assuming a) that a member cross section that was plane before loading remained plane under load, and b) strains varied linearly along the length of the member as a function of the length of the moment arms. Based on these assumptions, strain values for the critical locations were extrapolated using the available web and top flange strain gage data as shown in Tables 9.5B and 9.5C. Recorded data from gages directly affixed to the bottom slab and bottom flange were affected by shrinkage cracking (See Chapter 8 for additional information); therefore, for comparison, strains for the bottom slab were computed using linear extrapolation of the web gage readings. Note, however, that the strains reported are cumulative and may reflect plastic deformation caused by a prior load application.

Stresses for the critical locations were then computed using Hooke's law, whereby stress is proportionally related to strain (i.e., $\sigma = E\varepsilon$) when materials are not stressed beyond their elastic limit. The elastic moduli shown in Tables 9.5, 9.6 and 9.7 for the steel top flange and web sections were determined through laboratory testing. The elastic moduli used to calculate stress in the concrete bottom slab were computed using a stress-strain diagram and the secant modulus method as described in Section 9.3.2. Due to the limited effectiveness of the bottom flange as discussed in Section 8.3.2, stresses based on classical beam theory (CBT) were computed using transformed section properties under two different scenarios.

The first scenario, Case 1, assumed buckling of the steel bottom flange whereby the bottom steel flange is not included in the section property calculations. The second scenario, Case 2, assumed that some portion of the bottom flange was effective in resisting bending of the specimen. The effective width of the bottom flange was determined by adjusting the flange width until the calculated neutral axis for the transformed section matched the actual neutral axis location (see Table 9.4) based on experimental data.

**Table 9.4** Summary of Neutral Axis Locations

| Load Case, P (kips) | Neutral Axis |
|---|---|
| 320 | 25.92 |
| 620 | 25.33 |
| 894 | 25.59 |

For both scenarios, the modular ratio used to compute the transformed section properties (see Table 9.5A, 9.6A, and 9.7A) was based upon the elastic modulus at mid-depth of the bottom slab (average) as previously computed using the stress-strain diagram and secant modulus method. The modulus of elasticity for the steel section was based on averaging the values from the top and bottom flanges and web determined by laboratory testing (see Appendix B). In addition, the section properties are based on the assumption that the top slab has significantly cracked whereby only the reinforcing bars are included in the section properties calculations.

Inspection of the results revealed that one could reasonably predict the stresses at the critical locations using classical beam theory for experimental loads at or below 620 kips (see Tables, 9.6B and 9.6C). At a load of 320 kips (see Tables 9.5B and 9.5 C), classical beam theory somewhat under predicts stresses since the top slab in the test specimen has not cracked significantly and is still contributing to the flexural resistance. At 620 kips, the effective width of the bottom flange based on the experimental determined neutral axis is small which compares well with the FEA results that indicated the steel bottom flange did not contribute to the flexural resistance. In addition, Figure 8.12 indicates that the strain in the bottom fiber of the bottom slab is approximately $1200\mu\varepsilon$ compared to $1650\mu\varepsilon$ using classical beam theory. However, for greater loads, up to the maximum applied load of 894 kips (see Tables 9.7B and 9.7C), stress at mid-depth of the top flange could not be accurately predicted using CBT since the top flanges have yielded.

**Table 9.5A** P = 320 kips – Transformed Section Properties

| | Girder Ht. (in) | $b_{BF,eff}$ (in) | $I_{cg}$ ($in^4$) | $S_{TF,mid}$ ($in^3$) | $S_{BS,top}$ ($in^3$) | NA (in) | $E_s$ (ksi) | $E_c$ (ksi) | n |
|---|---|---|---|---|---|---|---|---|---|
| Case 1 | 58.125 | 0.0 | 100350 | 4068.0 | 5831.9 | 24.582 | 30300 | 4106 | 7.38 |
| Case 2 | 58.125 | 0.0 | 100350 | 4068.0 | 5831.9 | 24.582 | 30300 | 4106 | 7.38 |

**Table 9.5B** P = 320 kips – Stresses at 4 ft $10^1/_8$" from Center Support (HD Side)

| | | | | Test Results | | | | | | | | Beam Theory | |
|---|---|---|---|---|---|---|---|---|---|---|---|---|---|
| Location | Elev. | Gage | | Strains | | E | | $\sigma_y$ | Stress | | | Case 1 | Case2 |
| | (in) | East | West | (με) | (με) | (ksi) | (ksi) | (ksi) | (ksi) | (ksi) | Avg (ksi) | σ (ksi) | σ (ksi) |
| Middle of TF | 49.250 | 73 | 74 | 890[2] | 815[2] | 28400 | 28400 | 80.471 | 25.29 | 23.14 | 24.21 | 38.50 | 38.50 |
| Bot of TF | 48.375 | 75 | 76 | 725[1] | 681[1] | 28400 | 28400 | 80.471 | 20.59 | 19.34 | 19.97 | 35.86 | 35.86 |
| Web 1 | 44.375 | 85/132 | 97/138 | 610[1] | 553[1] | 31690 | 31690 | 80.458 | 19.34 | 17.53 | 18.43 | 29.83 | 29.83 |
| Web 2 | 28.375 | 87/133 | 99/139 | 70[1] | 72[1] | 31690 | 31690 | 80.458 | 2.20 | 2.27 | 2.23 | 5.72 | 5.72 |
| Web 3 | 12.375 | 89/134 | 101/140 | -375[1] | -365[1] | 31690 | 31690 | 80.458 | -11.87 | -11.58 | -11.73 | -18.40 | -18.40 |
| Top of Bot Slab | | 109 | 111 | -153[1] | -514[1] | | | | | | | | |
| Top of Bot Slab | 7.375 | | | -545[3] | -516[3] | 4329[4] | 4352[4] | 8.428 | -2.36 | -2.25 | -2.30 | -3.51 | -3.55 |
| Mid-depth of Bot Slab | 3.875 | | | -652[3] | -617[3] | 4244[4] | 4272[4] | 8.428 | -2.77 | -2.64 | -2.70 | -4.23 | -4.24 |
| Bot of Bot Slab | 0.375 | | | -760[3] | -717[3] | 4159[4] | 4193[4] | 8.428 | -3.16 | -3.01 | -3.09 | -4.94 | -4.94 |

[1] recorded data from strain gages
[2] calculated based on length of moment arm
[3] extrapolated using Web strain gage data
[4] from stress-strain graph using secant modulus
"-" Compression
"+" Tension

**Table 9.5C** P = 320 kips – Stresses at Center Support

| | | | | Test Results | | | | | | | | Beam Theory | |
|---|---|---|---|---|---|---|---|---|---|---|---|---|---|
| Location | Elev. | Gage | | Strains | | E | | $\sigma_y$ | Stress | | | Case 1 | Case 2 |
| | (in) | East | West | (με) | (με) | (ksi) | (ksi) | (ksi) | (ksi) | (ksi) | Avg (ksi) | σ (ksi) | σ (ksi) |
| Middle of TF | 49.250 | 73 | 74 | 1128[1] | 1032[1] | 28400 | 28400 | 80.471 | 32.04 | 29.31 | 30.67 | 48.77 | 48.77 |
| Bot of TF | 48.375 | 75 | 76 | 918[2] | 863[2] | 28400 | 28400 | 80.471 | 26.08 | 24.50 | 25.29 | 45.43 | 45.43 |
| Web 1 | 44.375 | 85/132 | 97/138 | 773[2] | 701[2] | 31690 | 31690 | 80.458 | 24.50 | 22.20 | 23.35 | 37.79 | 37.79 |
| Web 2 | 28.375 | 87/133 | 99/139 | 88[2] | 91[2] | 31690 | 31690 | 80.458 | 2.79 | 2.87 | 2.83 | 7.24 | 7.24 |
| Web 3 | 12.375 | 89/134 | 101/140 | -475[2] | -463[2] | 31690 | 31690 | 80.458 | -15.04 | -14.67 | -14.86 | -23.31 | -23.31 |
| Top of Bot Slab | | 109 | 111 | -194[2] | -651[2] | | | | | | | | |
| Top of Bot Slab | 7.375 | | | -690[3] | -654[3] | 4214[4] | 4243[4] | 8.428 | -2.91 | -2.78 | -2.84 | -4.45 | -4.45 |
| Mid-depth of Bot Slab | 3.875 | | | -826[3] | -781[3] | 4107[4] | 4142[4] | 8.428 | -3.39 | -3.24 | -3.32 | -5.36 | -5.36 |
| Bot of Bot Slab | 0.375 | | | -963[3] | -909 | 3999[4] | 4041[4] | 8.428 | -3.85 | -3.67 | -3.76 | -6.26 | -6.26 |

[1] recorded data from strain gages
[2] calculated based on length of moment arm
[3] extrapolated using Web strain gage data
[4] from stress-strain graph using secant modulus
"-" Compression
"+" Tension

**Table 9.6A** P = 620 kips – Transformed Section Properties

| | Girder Ht. (in) | $b_{BF,eff}$ (in) | $I_{cg}$ ($in^4$) | $S_{TF,mid}$ ($in^3$) | $S_{BS,top}$ ($in^3$) | NA (in) | $E_s$ (ksi) | $E_c$ (ksi) | n |
|---|---|---|---|---|---|---|---|---|---|
| Case 1 | 58.125 | 0.0 | 95915 | 4036.7 | 5295.1 | 25.489 | 30300 | 3644 | 8.32 |
| Case 2 | 58.125 | 3.8 | 96822 | 4047.7 | 5392.5 | 25.330 | 30300 | 3644 | 8.32 |

**Table 9.6B** P = 620 kips – Stresses at 4 ft $10^1/_8$ in. from Center Support (HD Side)

| | | | | Test Results | | | | | | | | Beam Theory | |
|---|---|---|---|---|---|---|---|---|---|---|---|---|---|
| Location | Elev. | Gage | | Strains | | E | | $\sigma_y$ | Stress | | | Case 1 | Case2 |
| | (in) | East | West | (με) | (με) | (ksi) | (ksi) | (ksi) | (ksi) | (ksi) | Avg (ksi) | σ (ksi) | σ (ksi) |
| Middle of TF | 49.250 | 73 | 74 | 1502[2] | 1429[2] | 28400 | 28400 | 80.471 | 42.66 | 40.58 | 41.62 | 38.85 | 38.73 |
| Bot of TF | 48.375 | 75 | 76 | 1282[1] | 1214[1] | 28400 | 28400 | 80.471 | 36.41 | 34.48 | 35.44 | 36.09 | 36.00 |
| Web 1 | 44.375 | 85/132 | 97/138 | 1087[1] | 993[1] | 31690 | 31690 | 80.458 | 34.44 | 31.46 | 32.95 | 29.78 | 29.75 |
| Web 2 | 28.375 | 87/133 | 99/139 | 152[1] | 151[1] | 31690 | 31690 | 80.458 | 4.81 | 4.79 | 4.80 | 4.55 | 4.76 |
| Web 3 | 12.375 | 89/134 | 101/140 | -632[1] | -622[1] | 31690 | 31690 | 80.458 | -20.03 | -19.72 | -19.88 | -20.68 | -20.24 |
| Top of Bot Slab | | 109 | 111 | -461[1] | -793[1] | | | | | | | | |
| Top of Bot Slab | 7.375 | | | -926[3] | -886[3] | 4028[4] | 4059[4] | 8.428 | -3.73 | -3.60 | -3.66 | -3.37 | -3.55 |
| Mid-depth of Bot Slab | 3.875 | | | -1114[3] | -1063[3] | 3879[4] | 3920[4] | 8.428 | -4.32 | -4.17 | -4.24 | -4.03 | -4.24 |
| Bot of Bot Slab | 0.375 | | | -1302[3] | -1239[3] | 3731[4] | 3780[4] | 8.428 | -4.86 | -4.69 | -4.77 | -4.69 | -4.94 |

[1] recorded data from strain gages
[2] calculated based on length of moment arm
[3] extrapolated using Web strain gage data
[4] from stress-strain graph using secant modulus
"-" Compression
"+" Tension

**Table 9.6C** P = 620 kips – Stresses at Center Support

| | | | | Test Results | | | | | | | | Beam Theory | |
|---|---|---|---|---|---|---|---|---|---|---|---|---|---|
| Location | Elev. | Gage | | Strains | | E | | $\sigma_y$ | Stress | | | Case 1 | Case 2 |
| | (in) | East | West | (με) | (με) | (ksi) | (ksi) | (ksi) | (ksi) | (ksi) | Avg (ksi) | σ (ksi) | σ (ksi) |
| Middle of TF | 49.250 | 73 | 74 | 1903[1] | 1810[1] | 28400 | 28400 | 80.471 | 54.05 | 51.40 | 52.72 | 49.21 | 49.07 |
| Bot of TF | 48.375 | 75 | 76 | 1624[2] | 1538[2] | 28400 | 28400 | 80.471 | 46.12 | 43.68 | 44.90 | 45.72 | 45.60 |
| Web 1 | 44.375 | 85/132 | 97/138 | 1377[2] | 1258[2] | 31690 | 31690 | 80.458 | 43.63 | 39.85 | 41.74 | 37.73 | 37.69 |
| Web 2 | 28.375 | 87/133 | 99/139 | 192[2] | 191[2] | 31690 | 31690 | 80.458 | 6.10 | 6.07 | 6.08 | 5.77 | 6.03 |
| Web 3 | 12.375 | 89/134 | 101/140 | -801[2] | -788[2] | 31690 | 31690 | 80.458 | -25.37 | -24.99 | -25.18 | -26.20 | -25.64 |
| Top of Bot Slab | | 109 | 111 | -584[2] | -1005[2] | | | | | | | | |
| Top of Bot Slab | 7.375 | | | -1173[3] | -1123[3] | 3833[4] | 3873[4] | 8.428 | -4.50 | -4.35 | -4.42 | -4.35 | -4.27 |
| Mid-depth of Bot Slab | 3.875 | | | -1411[3] | -1346[3] | 3645[4] | 3696[4] | 8.428 | -5.14 | -4.98 | -5.06 | -5.19 | -5.11 |
| Bot of Bot Slab | 0.375 | | | -1649[3] | -1570[3] | 3456[4] | 3519[4] | 8.428 | -5.70 | -5.52 | -5.61 | -6.03 | -5.94 |

[1] recorded data from strain gages
[2] calculated based on length of moment arm
[3] extrapolated using Web strain gage data
[4] from stress-strain graph using secant modulus
"-" Compression
"+" Tension

**Table 9.7A** P = 894 kips – Transformed Section Properties

| | Girder Ht. (in) | $b_{BF,eff}$ (in) | $I_{cg}$ ($in^4$) | $S_{TF,mid}$ ($in^3$) | $S_{BS,top}$ ($in^3$) | NA (in) | $E_s$ (ksi) | $E_c$ (ksi) | n |
|---|---|---|---|---|---|---|---|---|---|
| Case 1 | 58.125 | 0.0 | 89703 | 3988.8 | 4627.2 | 26.761 | 30300 | 3058 | 9.91 |
| Case 2 | 58.125 | 42.2 | 96285 | 4069.5 | 5286.0 | 25.590 | 30300 | 3058 | 9.91 |

**Table 9.7B** P = 894 kips – Stresses at 4 ft 10 $^1/_8$" from Center Support (HD Side)

| | | | | Test Results | | | | | | | | Beam Theory | |
|---|---|---|---|---|---|---|---|---|---|---|---|---|---|
| Location | Elev. | Gage | | Strains | | E | | $\sigma_y$ | Stress | | | Case 1 | Case2 |
| | (in) | East | West | (με) | (με) | (ksi) | (ksi) | (ksi) | (ksi) | (ksi) | Avg (ksi) | σ (ksi) | σ (ksi) |
| Middle of TF | 49.250 | 73 | 74 | 2869[2] | 2802[2] | 28400 | 28400 | 80.471 | 81.47 | 79.57 | (5) | 39.40 | 38.54 |
| Bot of TF | 48.375 | 75 | 76 | 1912[1] | 1827[1] | 28400 | 28400 | 80.471 | 54.30 | 51.89 | 53.09 | 36.44 | 35.79 |
| Web 1 | 44.375 | 85/132 | 97/138 | 1614[1] | 1481[1] | 31690 | 31690 | 80.458 | 51.15 | 46.94 | 49.04 | 29.70 | 29.51 |
| Web 2 | 28.375 | 87/133 | 99/139 | 217[1] | 213[1] | 31690 | 31690 | 80.458 | 6.88 | 6.75 | 6.81 | 2.72 | 4.37 |
| Web 3 | 12.375 | 89/134 | 101/140 | -952[1] | -941[1] | 31690 | 31690 | 80.458 | -30.17 | -29.82 | -30.00 | -24.26 | -20.76 |
| Top of Bot Slab | | 109 | 111 | -789[1] | -1080[1] | | | | | | | | |
| Top of Bot Slab | 7.375 | | | -1391[3] | -1338[3] | 3660[4] | 3702[4] | 8.428 | -5.09 | -4.96 | -5.02 | -3.30 | -2.89 |
| Mid-depth of Bot Slab | 3.875 | | | -1672[3] | -1603[3] | 3438[4] | 3492[4] | 8.428 | -5.75 | -5.60 | -5.67 | -3.89 | -3.44 |
| Bot of Bot Slab | 0.375 | | | -1952[3] | -1868[3] | 3216[4] | 3283[4] | 8.428 | -6.28 | -6.13 | -6.21 | -4.49 | -4.00 |

[1] recorded data from strain gages
[2] calculated based on length of moment arm
[3] extrapolated using Web strain gage data
[4] from stress-strain graph using secant modulus
"-" Compression
"+" Tension

**Table 9.7C** P = 894 kips – Stresses at Center Support

| | | | | Test Results | | | | | | | | Beam Theory | |
|---|---|---|---|---|---|---|---|---|---|---|---|---|---|
| Location | Elev. | Gage | | Strains | | E | | $\sigma_y$ | Stress | | | Case 1 | Case 2 |
| | (in) | East | West | (με) | (με) | (ksi) | (ksi) | (ksi) | (ksi) | (ksi) | Avg (ksi) | σ (ksi) | σ (ksi) |
| Middle of TF | 49.250 | 73 | 74 | 3634[1] | 3549[1] | 28400 | 28400 | 80.471 | (5) | (5) | (5) | 50.10 | 48.82 |
| Bot of TF | 48.375 | 75 | 76 | 2422[2] | 2314[2] | 28400 | 28400 | 80.471 | 68.79 | 65.73 | 67.26 | 46.36 | 45.34 |
| Web 1 | 44.375 | 85/132 | 97/138 | 2045[2] | 1876[2] | 31690 | 31690 | 80.458 | 64.80 | 59.46 | 62.13 | 37.82 | 37.38 |
| Web 2 | 28.375 | 87/133 | 99/139 | 275[2] | 270[2] | 31690 | 31690 | 80.458 | 8.72 | 8.55 | 8.63 | 3.64 | 5.54 |
| Web 3 | 12.375 | 89/134 | 101/140 | -1206[2] | -1192[2] | 31690 | 31690 | 80.458 | -38.22 | -37.78 | -38.00 | -30.54 | -26.30 |
| Top of Bot Slab | | 109 | 111 | -999[2] | -1368[2] | | | | | | | | |
| Top of Bot Slab | 7.375 | | | -1762[3] | -1696[3] | 3367[4] | 3420[4] | 8.428 | -5.93 | -5.80 | -5.87 | -4.16 | -3.66 |
| Mid-depth of Bot Slab | 3.875 | | | -2118[3] | -2031[3] | 3086[4] | 3125[4] | 8.428 | -6.53 | -6.41 | -6.47 | -4.91 | -4.36 |
| Bot of Bot Slab | 0.375 | | | -2473[3] | -2367[3] | 2805[4] | 2889[4] | 8.428 | -6.94 | -6.84 | -6.89 | -5.67 | -5.06 |

[1] recorded data from strain gages
[2] calculated based on length of moment arm
[3] extrapolated using Web strain gage data
[4] from stress-strain graph using secant modulus
"-" Compression
"+" Tension

## 9.4 Discussion

The test specimen was tested under fatigue, service and ultimate loads that enabled its structural response to be evaluated. For the fatigue and service tests, the double composite box girder behavior was as expected. However, the flexural strength capacity of the double composite box was less than anticipated. The above numerical analyses were undertaken in order to understand the behavior of the double composite steel box and are discussed in the following sections.

### 9.4.1 Plastic Moment

Initially, the maximum flexural strength of the test specimen was computed to be 27,963 ft-kips (see Appendix A), which correlated with an applied load of 1118 kips (or 559 kips per actuator). However, the specimen failed during testing at an applied load of only 894 kips (refer to Chapter 7). The predicted failure load assumed that the section would reach plastic moment capacity in which the top and bottom steel flanges would reach yield stress while the stress for the concrete bottom slab would be limited to $0.85f'_c$. The predicted material strengths for the steel and concrete were 80,000 psi and 7500 psi, respectively. The actual material strength for the steel plates ranged between 75,900 and 83,000 psi. The concrete strength for the bottom slab ranged between 7925 to 8884 psi. Using strengths for the steel and concrete of 80,600 psi yield strength and 8428 psi cylinder strength, respectively, the plastic moment for negative bending would be 29,046 ft-kips. Furthermore, as discussed in Section 9.3.4, the steel bottom flange was ineffective below an applied load of 620 kips, thus assuming it failed, the plastic moment would reduce to 23,783 ft-kips. Both of these values are still greater than the actual failure moment of 22,350 ft-kips.

As stated previously, only top flange strains were measured at the center support. At failure, these gages indicated that the steel had yielded, Realizing that the load was being held (and actually decreasing until jack pressure was reapplied) at the time of failure, it appears that both the concrete bottom slab and the steel top flanges were behaving as plastic springs in the vicinity of the center support until the concrete finally crushed. It is evident that the failure load may have been lower if a previous load had been held for a sufficient length of time to allow the ultimate strain of the concrete to be reached resulting in failure.

To understand why the test specimen failed at an applied moment less than that predicted by plastic analysis, one must consider two significant differences between single and double composite box girders that affect structural behavior. One difference is related to how and when dead loads are applied to the concrete slabs. In bridges using single composite action, the steel is erected first and the top slab is then placed in a specified sequence. This sequence is intended to minimize the amount of stress that the slab experiences due to dead loads, while the box girder steel is strained significantly. For a double composite steel box, the construction sequence will most likely require the bottom slab to be placed prior to any portion of the top slab, as was the case for the test specimen. The bottom slab is thereby stressed under dead loads and will have a similar strain history compared to that of the steel box.

The second difference is related to the geometry of a box girder cross section. When a single composite box girder experiences positive bending, the effective flange area available to resist compression is so large that the plastic neutral axis is typically located within, or in close proximity to, the concrete top slab. This leads to relatively small strains in the concrete slab when the steel tension flange reaches yield stress. For a double composite box girder undergoing negative bending, the effective flange area is limited to the width of the bottom steel flange, whereby the plastic neutral axis may lie in the box girder webs some distance from the concrete bottom slab, as was the case for the test specimen. This causes the bottom slab to experience

significant strains in order to maintain geometric compatibility with the top tension flanges when yielding. For the test specimen in positive moment, the concrete effective flange width is 16 feet versus 6 feet for negative moment. As shown in Figure 9.8, the locations of the elastic and plastic neutral axes (ENA and PNA) vary significantly between the positive and negative moment sections due to the relatively large top slab.

Both of these issues, in conjunction with the issues discussed in Sections 9.4.2 and 9.4.3, lead to the recommendation that double composite steel box girders are to be designed as non-compact sections using transformed section properties (see Section 9.3.5) for strength design.

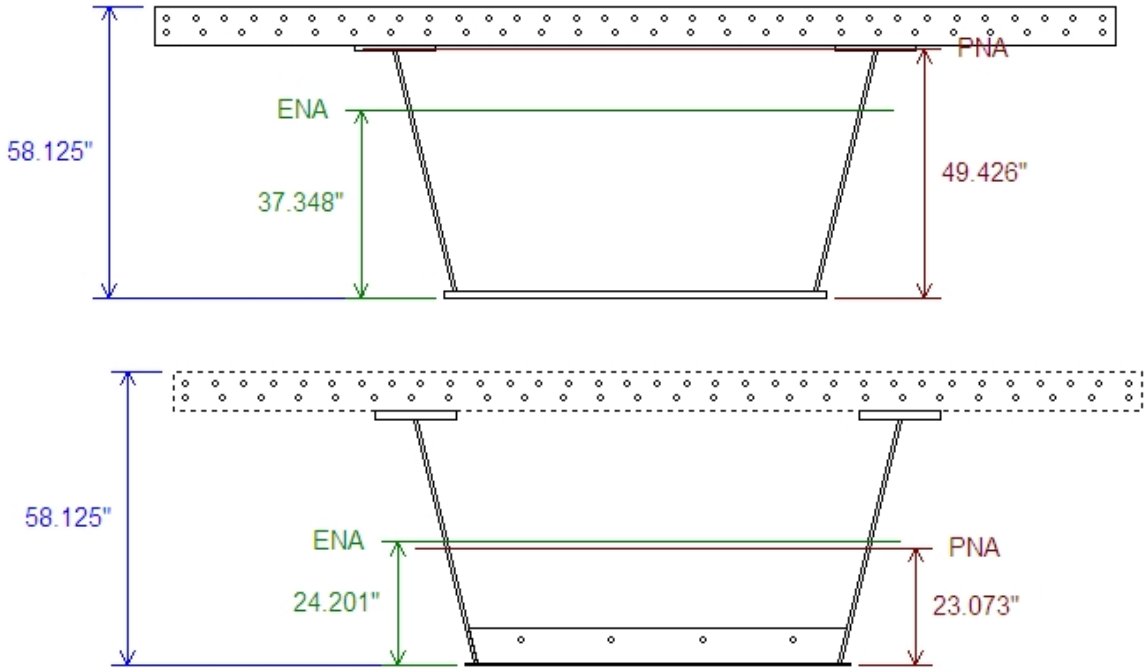


**Figure 9.8** Location of Neutral Axes for Positive Moment (top) and Negative Moment (bottom) Sections

### 9.4.2 Concrete Compressive Strength Limitation

When designing a double composite steel box, of primary importance is the construction sequence. Namely, when load is applied to the steel section alone versus when the concrete bottom slab is in place. For the test specimen, the difference between the strain histories of the steel section alone versus the composite section consisting of the steel box and concrete bottom slab only involved the dead load of the steel box and the bottom slab concrete. This is insignificant when compared to the applied loads and, therefore, one can assume that the steel tub and concrete bottom slab have the same strain history. Thus, at low strains relative to the steel properties, the concrete will "soften" due to the non-linearity of its stress-strain curve as shown in Figures 9.5 and 9.6, and as discussed in Section 9.3.2.

Referring to Fig. 9.9, the value of the secant modulus up to $0.6f'_c$ does not significantly differ from the AASHTO formula computed value when considering the effects on the entire composite beam properties. Furthermore, using the AASHTO formula for $E_c$ to compute the transformed section properties would give a conservative estimate in regards to calculating the concrete stress.

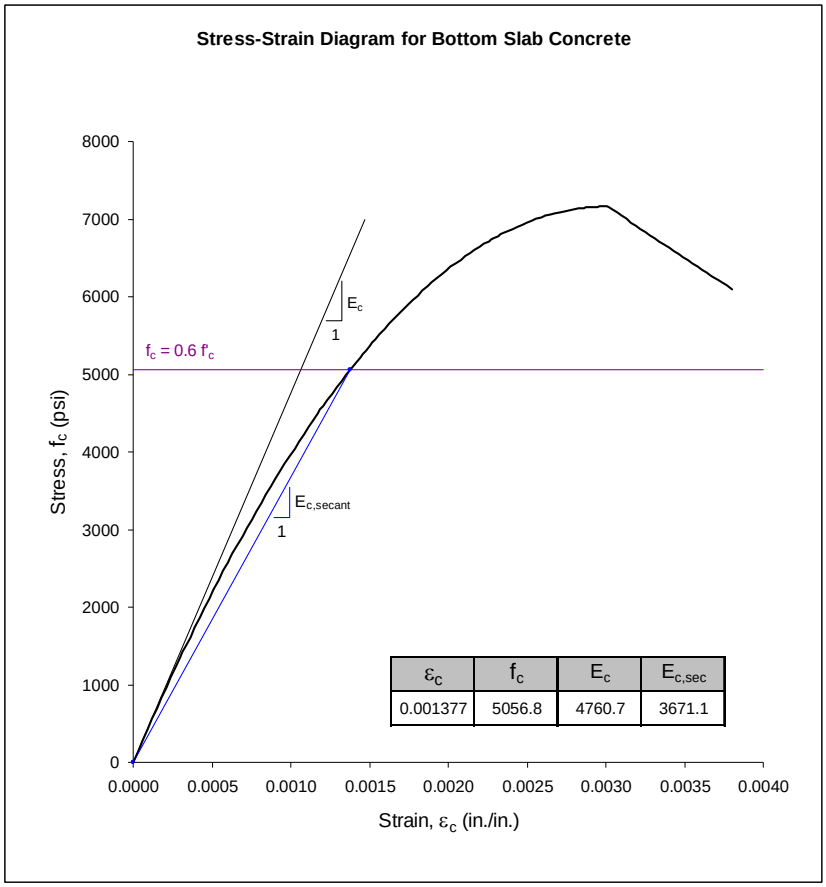


**Figure 9.9** Stress-Strain Diagram for Bottom Slab Concrete

### 9.4.3 Ductility

Another important design principle for providing a safe structure is ductility. The AASHTO LRFD specifications provide an equation to prevent premature crushing of the concrete. The preferred failure mode is excessive yielding of the steel which would show visual distress of the structure prior to collapse. In order to evaluate this concept, Fig. 9.10 was plotted to compare applied moments to the rotation of the cross section, $\phi$. $\phi$ is calculated by taking the top flange strain and dividing it by the distance to the neutral axis, $y_{bar}$. As shown in Fig. 9.10, the test specimen exhibited some ductility by failing approximately 23% past the theoretical yield rotation (i.e. yielding of the top flanges). Realizing that the test specimen did not meet the

ductility limits set forth in AASHTO but still provided ductility, it appears that the AASHTO LRFD criteria could be applied for the design of a double composite section.

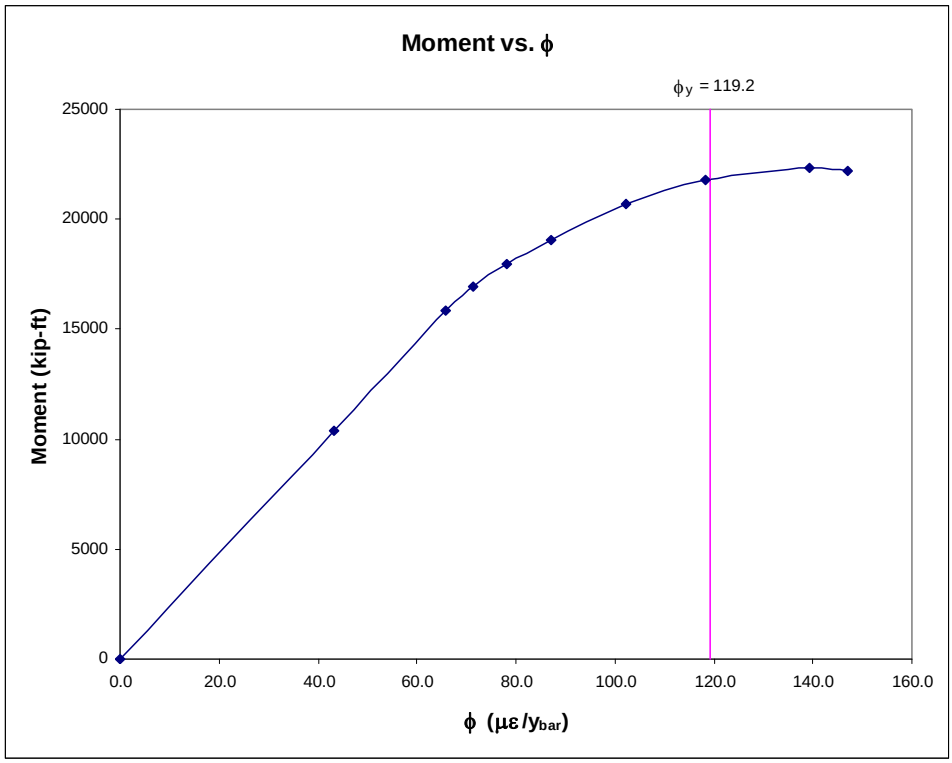


**Figure 9.10** Moment v/s Curvature Diagram for Ductility

### 9.4.4 Double Composite Action

As discussed in Chapter 8, the steel bottom flange was ineffective above an actuator load of 620 kips, yet the bottom slab continued to provide resistance to additional loads. The test data and results of the FEA clearly indicate that the concrete bottom slab was fully effective and composite with the steel tub even though the steel bottom flange was ineffective in regards to flexural strength. This then provides a designer with additional options: a) utilizing the steel bottom flange for flexural strength by using a sufficiently thick flange or using smaller shear connector spacing to adequately brace the flange against buckling; or b) using a thin steel bottom plate primarily acting as formwork for the concrete bottom slab. In either option, the steel bottom flange needs to meet any requirements for constructability.

## 9.5 Design Recommendations

These design recommendations pertain to bridge superstructures comprised of fabricated straight steel tub sections in a continuous bridge of moderate length whose negative moment areas incorporate a composite concrete bottom slab. Based on the findings of this research, it is

recommended that the design of this type of structure be based on the AASHTO LRFD Bridge Design Specifications as modified by the following sections.

### 9.5.1 Fatigue Limit State

The fatigue characteristics of the shear connectors utilized in the bottom slab in the negative moment region were expected to be similar to those for the top slab shear connectors, since they were designed using the same design criteria. The test findings showed no significant deviation in behavior within the limitations as stated in Chapter 5. Therefore, using the current AASHTO LRFD specifications for shear connector design appears to be valid.

### 9.5.2 Service Limit State

The primary objective of the service test was to evaluate the adequacy of the longitudinal reinforcing steel in the concrete deck to limit excessive cracking in order to insure durability of the deck. Based on these findings, the AASHTO LRFD criteria of providing an amount of steel equal to 1% of the total cross sectional area of the deck, with two-thirds located in the top layer, appears to be adequate. However, when utilizing Grade 70 steel, designers may want to check that the stress in the top slab reinforcement is less than nominal yielding at Load Combination Service II.

### 9.5.3 Strength Limit State ~ Flexural Design

For strength design, a double composite box girder shall be evaluated as a non-compact section and must satisfy the following additional requirements:

- The maximum longitudinal compressive stress in the concrete bottom slab at the strength limit state, determined as specified in AASHTO Article 6.10.1.1.1d, shall not exceed $0.6f'_c$. The modular ratio should be taken as $n = E_s / E_c$, where $E_c$ is determined as defined in Article 5.4.2.4.

- In order to prevent premature crushing of the concrete, the section shall satisfy the ductility requirement (see Figure 9.11):
  $D_p < 0.42\ D_t$
  where:
  $D_p$ = distance from the bottom of the concrete bottom slab to the neutral axis of the composite section at the plastic moment (in.)
  $D_t$ = depth of the composite section measured from the top layer of reinforcing to the bottom of the concrete bottom slab (in.)

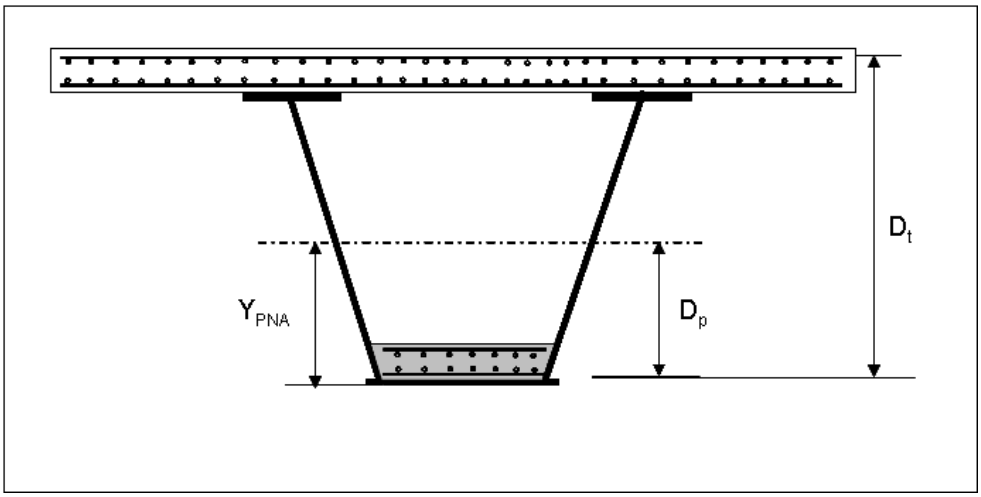


**Figure 9.11** Ductility Requirement for Double Composite Box

- The steel bottom flange must meet AASHTO LRFD criteria for box flanges for all stages of construction. This also includes the following:
  - limiting the deflection to L/360 when considering, but not limited to, self-weight, dead load of the concrete bottom slab, and construction live loads.
  - limiting the through-thickness bending to 20 ksi.

  The designer may want to consider using temporary bracing to satisfy the above criteria.

- This study did not evaluate creep effects and therefore makes no design recommendations on this matter. Designers are referred to AASHTO LRFD C6.10.1.1.1a for additional information.

- It is recommended that a bottom layer of reinforcing steel be provided in the bottom slab to reduce cracking due to shrinkage.

### 9.5.4 Recommendations for Using an Refined Analysis (FEA)

Considerable effort was needed to get the analysis results presented in Chapter 8 to accurately predict the observed behavior. To accurately predict ultimate load of a double composite section, any refined analysis needs to include several sources of non-linearity noted in Chapter 8, including those from buckling, contact between bottom flange and bottom slab, cracking and plasticity. It also needs to include all geometric details, such as individual shear studs and diaphragms. This type of analysis is not considered practical for everyday design tasks due to need for expensive software and hardware, and the amount of manpower needed to achieve good results. Consequently, a slightly conservative design based on classical beam theory and guidelines provided in this chapter is recommended.

## 9.6 Construction Guidelines

When a double composite steel box is utilized under actual field conditions, several additional steps are necessary compared to traditional bridge construction procedures. These include the following:

- During fabrication of the steel box:
  - Shear connectors attached to the bottom steel flange can be installed during fabrication.
  - Install any temporary bracing for the bottom steel flange.
  - Install guide rails for screeding the concrete bottom slab using a bolted and/or approved welded connection (these can be left in place if needed).

- After delivery of the structural steel to the job site, erection of the structural steel is dependent on the installation of the concrete bottom slab (see note below). In general, the erection of the framing system follows normal procedures but must identify the sequence in which the concrete bottom slab is placed. This sequence also needs to include:
  - Installing the reinforcing bars for the bottom concrete slab,
  - Placing and screeding the bottom slab concrete to the designated thickness.

- After the bottom slab concrete has cured, remove the temporary bracing of the steel bottom flange (if applicable).

- Continue with steel erection and/or normal bridge construction (i.e., complete top deck construction).

One of the primary decisions the designer needs to make is to determine when to place the bottom slab concrete. One needs to consider whether to have the concrete placed in the fabrication shop, at the job site prior to erection of the steel girders, or during or after erection of the steel framing system. The primary concern is stability of the unstiffened steel bottom flange.

To meet the stress demands from handling the box during fabrication and loads induced by shipping, the bottom steel flange should be of sufficient thickness to resist buckling during these operations. The designer can then decide whether to place the bottom concrete slab prior to, during or subsequent to the steel erection. In all cases, the unstiffened bottom flange needs to be of sufficient strength to resist all applied loads in addition to the dead load of the wet concrete bottom slab.

## References

9.1 AASHTO LRFD Bridge Design Specifications (2007). 4th Edition, Washington, D.C.

9.2 FDOT Structures Design Guidelines (2005).Tallahassee, FL.

9.3 Hognestad, E. (1951). "A Study of Combined Bending and Axial Loads in Reinforced Concrete Members." *University of Illinois Bulletin,* Vol. 49, No. 22, 128 pp.

# 10. MODEL DESIGN OF A DOUBLE COMPOSITE BRIDGE

## 10.1 Introduction

A model design of a double composite box girder bridge is presented in this chapter. Normal grade 50 steel is used. The design is based on the AASHTO LRFD Bridge Design Specifications, 3rd Edition, 2004 [10.1], the FDOT Structures Design Guidelines (FSDG), January 2005 [10.2] and design recommendations presented in the previous chapter based on the results of the testing.

A three span continuous twin box girder bridge consisting of two 190 ft. end spans and a 236 ft. main span is designed. This configuration was selected because it is identical to an AISI design example for a composite box girder bridge [10.3]. The design illustrates the application of the design provisions for flexure and shear at an interior pier section where the moments are negative. In the design it was assumed that the bottom slab was cast first, with the top slab cast after the bottom slab had hardened. As a result, the weight of the top slab is resisted by the composite bottom flange.

Design moments were determined using **QConBridge** [10.4], a software program developed by the Washington State Department of Transportation (WSDOT). All detailed calculations were carried out using **MathCAD v14.0** as shown in Appendix G.

## 10.2 Design Overview

The design of double composite bridges involves designing two composite sections corresponding to both the positive and negative moment regions in the continuous element. The basis of design for both sections is similar; differences arise because the load for which the section acts compositely is not identical and depends on the sequence in which the slabs are cast. Since efficient design requires the bottom steel flange to be as thin as possible, limits are set on its minimum thickness based on buckling considerations. Additional requirements have been proposed in this study that limit the maximum stress in the bottom concrete slab as outlined in the previous chapter.

### 10.2.1 Design Steps

The steps involved in the design example are summarized in this section. Only a design for the negative moment section is presented here. The steps listed below are consistent with those in the design example included in the AISI [10.3] as follows:

1) General information and bridge geometry (Section 10.3).

2) Material properties in accordance with AASHTO and ASTM specifications (Section 10.4).

3) Calculation of loads in accordance with AASHTO LRFD provisions (Section 10.5)

4) Calculation of load factors and load combinations for Strength I and Fatigue limit states in accordance with *Article 3.4* of LRFD guidelines (Section 10.6 and Section 10.8).

5) Structural analysis for the load distribution in accordance with *Article 4.6.2.2* of LRFD provisions (Section 10.7).

6) Calculation of section properties for non-composite, short-term composite and long-term composite sections (Section 10.9)

7) Determination of the plastic neutral axis location in accordance with *Article D6.1.*

8) Checking section for Strength I limit state and flexural requirements. Specifically the section should be checked for web slenderness, nominal flexural capacity and flexural resistance of box flanges, stresses in the concrete bottom slab, and shear (Section 10.11 and 10.13).

9) Check that bottom slab satisfies slab ductility requirement to avoid premature crushing of concrete slab (Section 10.11).

10) Detail shear connectors in bottom flange per prevailing LRFD provisions for fatigue and strength limit states (Section 10.14).

11) Consider provisions for temporary bracing of bottom flange to support the bottom concrete slab until it hardens (Section 10.15).

## 10.3 General Information and Geometry

This section presents general information on the bridge and its geometry. General information is summarized in Table 10.1. Information on the bridge geometry including its cross sectional dimensions are summarized in Table 10.2. Figure 10.1 shows the entire cross-section of the double composite bridge with two box girders. Figure 10.2 shows the typical cross-section of the box girder section considered for the design of negative flexure section.

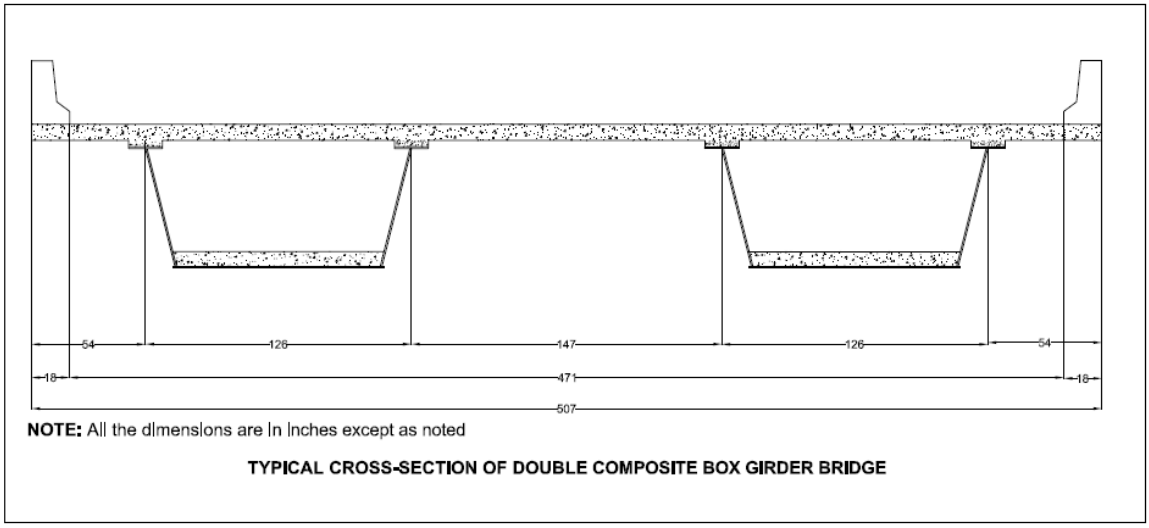


**Figure 10.1** Typical Cross-Section of Double Composite Bridge

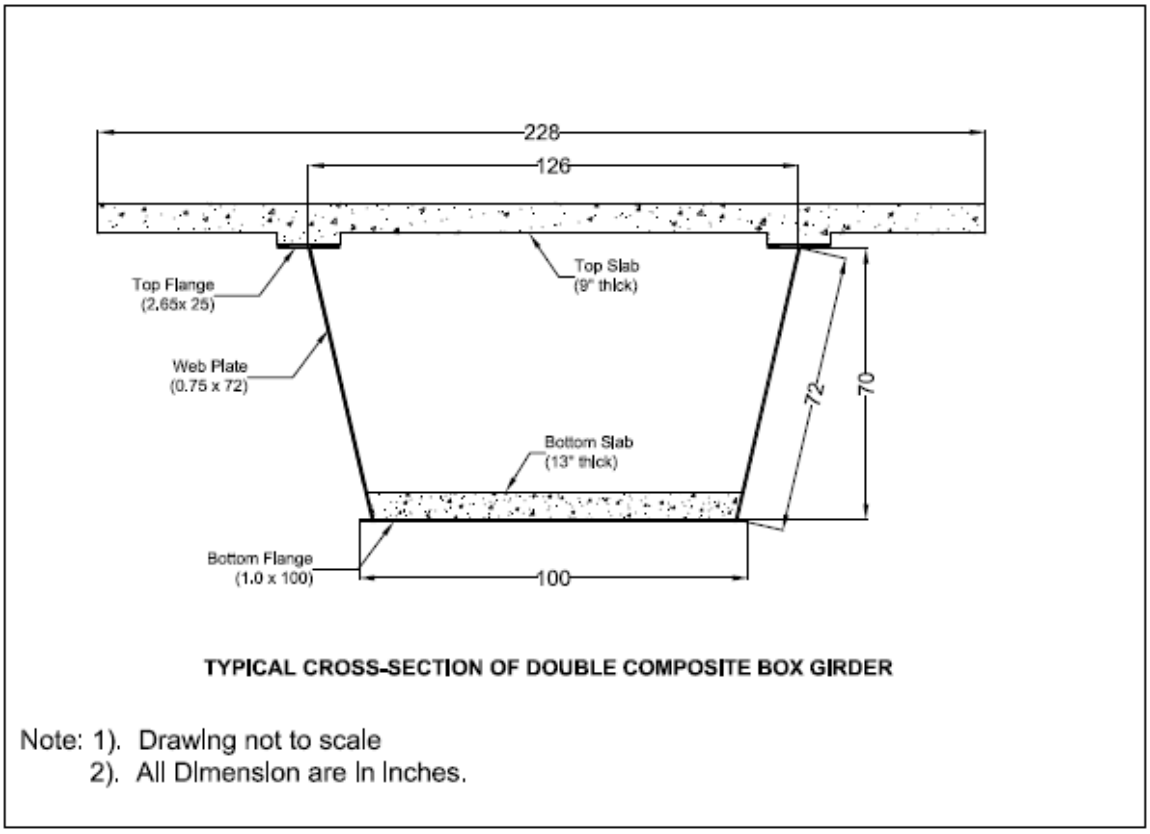


**Figure 10.2** Typical Cross-Section of Double Composite Box Girder

**Table 10.1** General Information

| General Information | Notation | Parameter |
|---|---|---|
| Number of box girders | $N_g$ | 2 |
| Number of spans | $N_{sp}$ | 3 |
| Number of design lanes | $N_L$ | 3 |
| Length of middle span | $L_2$ | 236 ft. |
| Length of side span (equal length) | $L_1$ | 190 ft. |
| Girder spacing | GS | 11.375 ft. |
| Roadway width | $R_w$ | 40 ft. |
| Concrete deck thickness (structural) | $t_{ts}$ | 9 in |
| Concrete bottom slab thickness | $t_{bs}$ | 13 in. |
| Concrete deck overhang (width) | $OH_c$ | 4.5 ft. |
| Side walks | | None |
| Haunch thickness | $t_h$ | 3 in. |
| Reinforcement ratio | $R_r$ | 0.01 |

**Table 10.2** Geometry of Box Girder Section

| Girder Dimensions | Notation | Parameter |
|---|---|---|
| Web Depth (plumb) | $D_w$ | 70 in. |
| Inclination to vertical is 14.03 deg | $\Theta$ | 14.036° |
| Web Depth (inclined) | D | 72.15 in. |
| Web plate thickness | $t_w$ | 0.75 in. |
| Top flange thickness | $t_{tf}$ | 2.65 in. |
| Top flange width | $b_{tf}$ | 25 in. |
| Bottom flange thickness | $t_{bf}$ | 1.00 in. |
| Bottom flange width | $b_{bf}$ | 100 in. |
| Height of girder | HG | 73.65 in. |
| Top slab width | $b_{ts}$ | 507 in. |
| Top slab thickness | $t_{ts}$ | 9 in. |
| Bottom slab width | $b_{bs}$ | 99.25 in. |
| Bottom slab thickness | $t_{bs}$ | 13 in. |
| Area of web plate | $A_w = 2Dt_w$ | 108.23 in.$^2$ |
| Area of top flanges | $A_{tf} = 2b_{tf}t_{tf}$ | 132.5 in.$^2$ |
| Area of bottom flange | $A_{bf} = b_{bf}tb_f$ | 100 in.$^2$ |
| Area of Steel Section | $A_s = A_w + A_{tf} + A_{bf}$ | 340.73 in.$^2$ |
| Area of top slab | $A_{ts} = b_{ts}t_{ts}$ | 4563 in.$^2$ |
| Area of bottom slab | $A_{bs} = b_{bs}t_{bs}$ | 1290.25 in.$^2$ |

## 10.4 Materials

Table 10.3 summarizes information on the compressive strength of the concrete, the yield strength of the steel and the unit weight of the stay-in-place form and future wearing surface assumed in the design.

**Table 10.3** Material Properties

| Material | Notation | Unit Weight | Notation | Design Value (ksi) |
|---|---|---|---|---|
| Concrete | $\gamma_c$ | 145 pcf | $f'_c$ | 6.5 |
| Structural steel | $\gamma_s$ | 490 pcf | $F_y$ | 50 |
| Reinforcing steel | - | - | $f_{yr}$ | 60 |
| Shear connectors | - | - | $f_{ys}$ | 60 |
| Stay in place form | $\gamma_{sip}$ | 20 psf | - | - |
| Future wearing surface | $\gamma_{ws}$ | 21 psf | - | - |

### 10.4.1 Concrete

The compressive strength of the concrete is assumed to be 6500 psi. The concrete used in the bridge must conform to AASHTO Specifications. Normal weight concrete is used with a unit weight of 145 pcf. Table 10.4 summarizes design parameters assumed in the design.

**Table 10.4** Design Parameters

| Design Parameters | Notations | Design Value (ksi) |
|---|---|---|
| Design concrete strength | $f_c$ | 6.5 |
| Modulus of concrete | $E_c$ | 4181 |
| Yield strength of steel | $F_y$ | 50 |
| Modulus of steel | $E_s$ | 29000 |
| Shear modulus of steel | $G_s$ | 12000 |

The modulus of concrete in Table 10.4 was calculated in accordance with FSDG for limestone aggregates as:

$$E_c = 0.9 \times 33000 \times w_c^{1.5} \times \sqrt{f'_c} = 0.9 \times 33000 \times \left(0.145\right)^{1.5} \times \sqrt{6.5} = 4181\text{ksi}$$

### 10.4.2 Structural Steel

Grade 50 structural steel conforming to ASTM A709 specifications was used for the box girder plates. Nominal yield strength is 50 ksi and unit weight is 490 pcf.

### 10.4.3 Steel Reinforcement

Grade 60 steel bars conforming to ASTM 615 specifications are used for reinforcing both the top and bottom slabs. Nominal yield strength is 60 ksi.

### 10.4.4 Shear Connectors

Shear connectors used are in accordance with AASHTO M 169 and ASTM A108 specifications. The ¾ in. diameter shear connectors used in the top and bottom concrete slab have a nominal yield strength of 60 ksi.

### 10.4.5 Miscellaneous

Stay-in-place forms are used for the placement of the top concrete slab. Unit weight is 20 psf. The unit weight of the future wearing surface is taken as 21 psf. The unit weight of the 1.5 ft. wide concrete barrier is taken as 581 plf.

## 10.5 Design Loads

This section provides information for the design dead, live and fatigue loads which were calculated in accordance with AASHTO LRFD provisions. The loads presented here were calculated for the negative moment section at an interior pier. Since the model bridge is straight and has uniform deck and overhang widths, the design loads are equally shared between the two box girders.

### 10.5.1 Dead Load

Dead loads used in the design were grouped into four separate load cases to account for the various stages of construction and differing load factors specified in AASHTO LRFD. Permanent loads which generated moments resisted by the steel girder only (i.e., non-composite section) were grouped into load case DC1 as shown in Table 10.5. This included the self-weight of the steel girder, an additional 10% allowance for steel detailing elements (e.g., shear studs, stiffeners, etc.) and the reinforced concrete bottom slab prior to curing.

**Table 10.5** Non-composite Dead Loads Per Box Girder

| Dead Loads | Load Case | Unit Weight | Cross-sectional Area ($in^2$) | Load (klf) |
|---|---|---|---|---|
| Steel Section | DC1 | 490 pcf | 340.73 | 1.16 |
| Steel Details | DC1 | 490 pcf | 31.82 | 0.116 |
| Bottom Slab | DC1 | 150 pcf | 1287 | 1.34 |
| Total | | | | 2.62 |

Permanent loads which resulted in negative moments carried by the composite section, comprised of the structural steel and the bottom slab, were grouped into load case DC2 as shown in Table 10.6. This included the weight of the stay-in-place forms and the reinforced concrete top slab, including haunches.

**Table 10.6** Composite Dead Loads Per Box Girder

| Dead Loads | Load Case | Unit Weight | Cross-sectional Area ($in^2$) | Load (klf) |
|---|---|---|---|---|
| SIPs | DC2 | 20 psf | n/a | 0.27 |
| Haunches | DC2 | 150 pcf | 132 | 0.156 |
| Top Slab | DC2 | 150 pcf | 2281.5 | 2.377 |
| Total | | | | 2.803 |

The superimposed loads resulting from the placement of the concrete traffic barriers and future wearing surface were classified as separate load cases (i.e., DC3 and DW) in order to account for the differing load factors specified in AASHTO LRFD. The weight of the barrier and the weight allowance for the wearing surface, as shown in Table 10.7, were selected to match the values used in the AISI example in order to maintain a consistent loading condition.

Moments generated by the superimposed dead loads are resisted by the fully composite box girder, including the structural steel webs and flanges, the bottom slab concrete and the longitudinal reinforcing steel located in the top slab.

**Table 10.7** Superimposed Dead Loads Per Box Girder

| Dead Loads | Load Case | Unit Weight | Length (ft.) | Load (klf) |
|---|---|---|---|---|
| Concrete barrier | DC3 | n/a | n/a | 0.581 |
| Wearing Surface | DW | 21 psf | 20 | 0.420 |

### 10.5.2 Live Load

Vehicular live load considered for the design was based on the AASHTO HL-93 model, whereby live load is a combination of a design truck or a design tandem and design lane loads (see *AASHTO 3.6.1.2*). The design truck used was the HS 20 truck.

Since the calculation of live load moments for multi-span continuous bridges is tedious, *QConBridge*, a free software program from the Washington State Department of Transportation [10.2], was used to calculate the design live load moments, as well as the dead load moments. The calculated live load moments are resisted in full by the short-term composite section, D, as defined in section 10.9.

### 10.5.3 Fatigue Load

The fatigue loading used in the design of the bottom slab shear connectors was calculated in accordance with AASHTO *Article 3.6.1.4*. An HS 20 design truck was used to calculate the maximum fatigue related moments using the *QConBridge* software.

## 10.6 Load Factors and Load Modification Factors

This section provides information on the load factors for the Strength I and Fatigue limit states and the load modification factors used in the design.

### 10.6.1 Load Factors

The load factors for dead load, live load and fatigue load for the Strength I and Fatigue limit states are specified in Table 10.8. These factors are in accordance with *Article 3.4* of LRFD guidelines.

**Table 10.8** Load Factors for Strength I and Fatigue

| Limit State | Dead Load $\gamma_{DC}$ | Wearing Surface $\gamma_{DW}$ | Live Load $\gamma_{LL}$ |
|---|---|---|---|
| Strength I | 1.25 | 1.50 | 1.75 |
| Fatigue | - | - | 0.75 |

### 10.6.2 Load Modification Factors

Load modification factors are multipliers associated with ductility, redundancy and operational importance as described in *Articles 1.3.2, 1.3.3 and 1.3.4* of the AASHTO LRFD specifications. Once determined, the individual modification factors are multiplied together to obtain a single number. They can also vary in relation to the limit state under consideration. However, in this design example, the load modifier for each of the limit states considered, Strength I and Fatigue, is simply one. Therefore, the final design moments are unaffected by the load modification factors.

## 10.7 Distribution Factors

Distribution factors are used to distribute the live load moments and shears in the lateral direction. The distribution factors used in this design were determined using the approximate method for beam-slab bridges in accordance with *Article 4.6.2.2* of the LRFD guidelines. The following conditions must be satisfied to use the approximate method:

a) Width of the deck is constant.

b) Number of beams is not less than four unless otherwise specified.

c) Beams are parallel and have approximately the same stiffness.

d) The roadway portion of the overhang does not exceed 36 inches, unless otherwise specified.

e) The cross-section is consistent with one of the cross-sections shown in *Table 4.6.2.2.1-1* in the LRFD specifications.

Since the conditions specified above are met, live loads may be uniformly distributed among all of the beams. The following equation is used for determining the distribution factors for live load moment and shear. The live load distribution factor, $DF_{LL}$, for moment and shear works out to be 1.467.

$$DF_{LL} = 0.05 + \left( 0.85 \times \frac{N_L}{N_g} \right) + \frac{0.425}{N_L} \qquad \text{(AASHTO Table 4.6.2.2.2b-1)}$$

$N_L$ = Number of lane, $N_g$ = Number of girders

$$\therefore DF_{LL} = 0.05 + \left( 0.85 \times \frac{3}{2} \right) + \frac{0.425}{3} = 1.467$$

In this example there are 3 design lanes ($N_L$) and two box girders ($N_g$), so the ratio $N_L/N_g$ is 1.5. If this ratio exceeds 1.5, a more refined analysis is required to take into consideration torsional effects.

Since fatigue load is placed only on one lane, its distribution factor must accordingly be adjusted using the above equation. This distribution factor turns out to be 0.9 as follows:

$$DF_{LL} = 0.05 + \left( 0.85 \times \frac{1}{2} \right) + \frac{0.425}{1} = 0.9$$

In addition to lateral distribution, live load has to account for dynamic effects in accordance with *Article 3.6.2*. The dynamic load allowance factor for the strength and fatigue limit states are 1.33 and 1.15, respectively.

## 10.8 Load Combinations

The AASHTO LRFD load combinations considered for the model design were Strength I and Fatigue. The box girder section was designed for Strength I, and the shear connectors were designed for strength and fatigue. The maximum negative moment occurs at the interior pier supports. The maximum unfactored and factored moments for the Strength I load combination are summarized in Table 10.9. Table 10.10 summarizes the maximum unfactored and factored shear forces at the interior pier section.

In these tables, the DC1 load case represents dead load forces resisted by the non-composite steel girder section only, DC2 forces are resisted by the composite steel girder and bottom slab section, the DC3 forces were generated by the placement of the concrete traffic barriers, DW represents loads from a future wearing surface, and LL+IM are live load plus impact forces.

**Table 10.9** Maximum Unfactored and Factored Moments at Interior Pier Section

| DC1 | DC2 | DC3 | DW | LL+IM | 1.25 DC1 | 1.25 DC2 | 1.25 DC3 | 1.5 DW | 1.75 LL+IM | Max. Neg. Moment $M_u$ |
|---|---|---|---|---|---|---|---|---|---|---|
| 6536 | 12410 | 2670 | 1930 | 10580 | 8170 | 15513 | 3338 | 2895 | 18515 | 48430 |

**Note:** All moments are expressed in ft-kips

**Table 10.10** Maximum Unfactored and Factored Shear at Interior Pier Section

| DC1 | DC2 | DC3 | DW | LL+IM | 1.25 DC1 | 1.25 DC2 | 1.25 DC3 | 1.5 DW | 1.75 LL+IM | Max. Shear $V_u$ |
|---|---|---|---|---|---|---|---|---|---|---|
| 206 | 321 | 70 | 49 | 302 | 258 | 401 | 88 | 74 | 529 | 1348 |

**Note:** All shear forces are expressed in kips

### 10.8.1 Location of Inflection Points

The negative moment section extends from the points of inflection in the end span ($L_1$) and the main span ($L_2$). The location of these inflection points is affected by several factors such as the type of loading (uniform or concentrated), position of load (placement of truck load for maximum effect), span geometry (interior to exterior span ratio).

In this example, the ratio of the main to the end span is 1.24 (236/190). For this case, the inflection point is $0.27L_1$ [10.5] from the interior support. This works out to be 0.27 x 190 = 51 ft. from the interior support in the end span.

The inflection point in the main span ($L_2$) for different span ratios ranging from 1.0 to 1.7 was found to vary from $0.2L_2$ to $0.25L_2$. For this case where the ratio is 1.24, the inflection point

is at a distance of $0.22L_2$ (52 ft.) from interior support in the main span. The total length of the section under negative moment is therefore 51 ft. + 52 ft. = 103 ft.

On a conservative note, the inflection points can be generalized to be taken as 0.3L, where L is the span length for span ratio varying from 1.2-1.4.

## 10.9 Section Properties

The section properties of the steel box girder cross-section must be calculated for both non-composite and composite action. Composite action additionally takes into consideration the effects of concrete creep for transient (i.e., short-term) and sustained (i.e., long-term) loading by using different values of the modular ratio, *n*, in accordance with *Article 6.10.1.1*. The modular ratio is given by:

$$n = \frac{E_s}{E_c} = \frac{29000}{4181} = 6.9 \quad \text{whereby} \quad 3n = 20.7$$

Section properties for five different sections must be calculated. These are non-composite (Section A), short-term composite section with bottom slab (Section B), long-term composite section with bottom slab (Section C), short-term composite section considering top slab rebars, bottom slab and structural steel (Section D), and long-term composite section considering top slab rebars, bottom slab and structural steel (Section E). These properties are summarized in Table 10.11. The section property calculations can be found in Appendix G.

**Table 10.11** Section Properties for Non-composite and Composite Sections

| Section | Section Properties | | | | | | |
|---|---|---|---|---|---|---|---|
| | Cross-sectional Area ($in.^2$) | Moment of Inertia ($in.^4$) | Neutral Axis (in.) | | Section Modulus ($in.^3$) | | |
| | | | Bottom | Top | Bottom Flange | Bottom Slab | Top Flange |
| A | 341 | 340456 | 39.707 | 33.943 | 8574 | - | 10030 |
| B | 528 | 449569 | 28.295 | 45.355 | 16551 | 118390 | 10325 |
| C | 403 | 395991 | 34.726 | 38.924 | 11403 | 243044 | 10173 |
| D | 549 | 525077 | 30.329 | 55.321 | 17312 | 123529 | 12120 |
| E | 424 | 439256 | 37.039 | 48.611 | 11859 | 252302 | 11997 |

## 10.10 Plastic Neutral Axis

The location of the plastic neutral axis must be determined in order to ensure that the section meets the ductility requirement described in *Article 6.10.7.3* of AASHTO LRFD. The location of the plastic neutral axis can be determined using the formulas presented in *Article D6.1* of the LRFD guidelines. The following steps are used to calculate the plastic moment:

1). *Determine general location of the plastic neutral axis by comparing forces in the flanges and webs*

Calculate forces due to structural steel, bottom concrete slab and reinforcement in top concrete slab. Table 10.12 shows the calculation of forces in the cross-section.

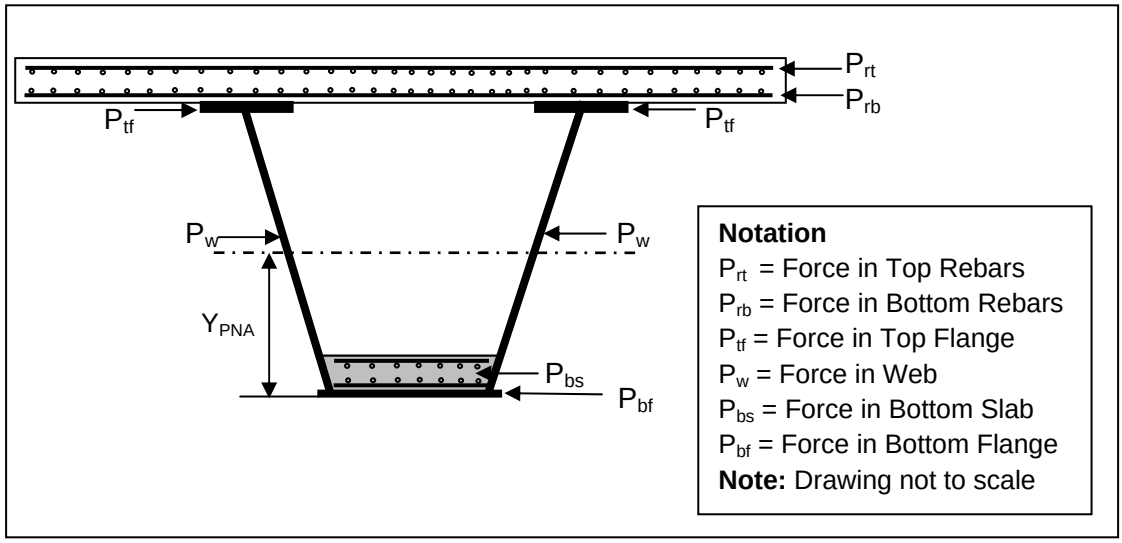


**Figure 10.3** Forces in the Cross Section

**Table 10.12** Forces in the Cross Section

| Force | Expression | Input Values | Force (kips) |
|---|---|---|---|
| Force in top rebars | $P_{rt} = 0.0067 \times b_{eff} \times t_{ts} \times f_{yr}$ | $= 0.0067 \times 232\ in. \times 9\ in. \times 60\ ksi$ | 841.2 |
| Force in bottom rebars | $P_{rb} = 0.0033 \times b_{eff} \times t_{ts} \times f_{yr}$ | $= 0.0033 \times 232$ in. $\times 9$ in. $\times 60$ksi | 414.3 |
| Force in top flange | $P_{tf} = 2 \times b_{tf} \times t_{tf} \times F_y$ | $= 2 \times 25\ in. \times 2.5\ in. \times 50ksi$ | 6625 |
| Force in web | $P_w = 2 \times D \times t_w \times F_y$ | $= 2 \times 72.15\ in. \times 0.75\ in. \times 50ksi$ | 5411.4 |
| Force in bottom flange | $P_{bf} = b_{bf} \times t_{bf} \times F_y$ | $= 100$ in. $\times 1.0$ in. $\times 50$ksi | 5000 |
| Force in bottom slab | $P_{bs} = 0.85 \times f_c \times b_{bs} \times t_{bs}$ | $= 0.85 \times 6.5ksi \times 99$ in. $\times 12$ in. | 7128 |

The total tension force in the top slab rebar, flanges and webs is greater than the compression force in the bottom flange and bottom concrete slab. Therefore, the plastic neutral axis lies somewhere in the web.

$$P_{re} + P_{tf} + P_w > P_{bf} + P_{bs}$$

2). *Calculate the location of the plastic neutral axis from the bottom of the bottom flange.*

The plastic neutral axis ($Y_{PNA}$) is taken from the bottom of the bottom flange. Its location is determined by summing forces as follows:

$$P_{re} + P_{tf} + \left(\frac{P_w}{D}\right) \times \left[\frac{(D_w + t_{bf}) - Y_{PNA}}{\cos\theta}\right] - P_{bf} - P_{bs} - \left(\frac{P_w}{D}\right) \times \left[\frac{Y_{PNA} - t_{bf}}{\cos\theta}\right] = 0$$

Substituting values obtained in the previous step in the above equation, $Y_{PNA}$ is found.

$$\therefore 1255.5 + 6625 + \left(\frac{5411.43}{72.15in.}\right) \times \left[\frac{(70in. + 1in.) - Y_{PNA}}{\cos(14.036)}\right] - 5000 - 7128$$
$$- \left(\frac{5411.43}{72.15in.}\right) \times \left[\frac{Y_{PNA} - 1in.}{\cos(14.036)}\right] = 0$$

$$\therefore Y_{PNA} = \frac{1325\ kip}{154\ .5\left(kip/in.\right)} = 8.603\ in.$$

Thus, $Y_{PNA}$ is located 8.603 in. from the extreme bottom fiber of the box girder section, which places it within the concrete bottom slab.

**Note:** The equilibrium equation used here does not account for the loss of compressive force for the bottom slab concrete above the plastic neutral axis. However the result is adequate for the design.

## 10.11 Strength I Limit State

Design checks related to the Strength I limit state are presented in this section. The model design section must satisfy the AASHTO LRFD requirements for composite members and the design recommendations presented in Chapter 9 of this document, including limits for web slenderness, concrete compressive stress, steel top flange stress and concrete slab ductility.

### 10.11.1 Web Slenderness

Web slenderness criterion is checked as per *Article 6.10.6.2.3* of the AASHTO specifications. The following equation defines the slenderness limit of the web in composite and non-composite sections in the negative flexure region.

$$2\frac{D_c}{t_w} \le 5.7\sqrt{\frac{E_s}{F_y}}$$

Where $D_c$ = depth of the web in compression in the elastic range determined as specified in *Article D6.3.1.*

$$D_c = \left(\frac{-f_c}{|f_c| + f_t}\right)d - t_{tf} = \left(\frac{-(-46.90)}{|-46.90| + 52.64}\right) - 2.5 \ge 0$$

$$\therefore D_c = 30.32in.$$

Substituting the value of $D_c$ in the above equation.

$$L.H.S = 2\times\frac{30.32in.}{0.75in.} = 80.89 \qquad R.H.S = 5.7\times\sqrt{\frac{29000ksi}{50ksi}} = 137.27$$

$$\therefore L.H.S \le R.H.S$$

Therefore, the section satisfies the AASHTO web slenderness criteria.

### 10.11.2 Slab Ductility Requirement for Bottom Slab

In order to prevent premature crushing of the concrete in the bottom slab, the ductility requirement for the bottom concrete slab must be satisfied. The following equation gives the ductility criteria to avoid premature crushing of concrete.

$D_p < 0.42D_t$

where: $D_p$ = distance from the bottom of the concrete bottom slab to the neutral axis of the composite section at the plastic moment (in.)

$D_t$ = depth of the composite section measured from the top layer of reinforcing to the bottom of the concrete bottom slab (in.)

$$D_p = Y_{PNA} - t_{bf} = 8.603\,in - 1.0in = 7.603\,in$$

$$D_t = D_w + t_{tf} + t_h + t_{ts} - 2in = 70in + 2.65in + 3in + 9in - 2in = 82.65in$$

$$\frac{D_p}{D_t} = \frac{7.603\,in.}{82.5in.} = 0.092$$

Therefore, the bottom slab satisfies the slab ductility requirement to avoid the premature crushing of concrete.

### 10.11.3 Compressive Stress in Concrete Slab

As explained in Chapter 9 of this document, stress in the composite concrete bottom slab shall be limited to 0.6f'c.

The maximum stress developed in the bottom slab due to factored loads is given by:

$$f_{bsu} = \frac{M_{DC2}}{S_{bsB}} + \frac{M_{D3} + M_{DW}}{S_{bsD}} + \frac{M_{LL}}{S_{bsD}} \geq \frac{M_{DC2}}{S_{bsC}} + \frac{M_{D3} + M_{DW}}{S_{bsE}} + \frac{M_{LL}}{S_{bD}}$$

$$\therefore\ f_{bsu} = \frac{15513\ \ ft - kip}{118391\ \ in^3} + \frac{3338\ + 2895\ \ ft - kip}{123529\ \ in^3} + \frac{18515\ \ ft - kip}{123529\ \ in^3} = 3.97\,ksi$$

$$\therefore\ f_{bsu} \geq 0.6 \times 6.5ksi = 3.9\,ksi$$

Eventhough, the stress in bottom concrete slab exceeds 0.6f'c by 2 %, for the purpose of this example the bottom slab is acceptable.

$\therefore f_{bsu} \le 0.6 f'_c$ is satisfied for the bottom slab

### 10.11.4 Flexural Resistance of Steel Flanges

The flexural resistance of the bottom steel flange in compression and the top steel flanges in tension to resist negative moments are checked in this section. The flexural resistance of the box flanges in negative flexure shall be determined in accordance with *Article 6.11.8* of the LRFD guidelines.

Assuming that torsional shear stresses in the flange are negligible, the nominal flexural resistance of the compression flange is determined in accordance with *Article 6.11.8.2*.

$$F_{nc} = R_b \times R_h \times F_y \times \Delta$$

Where, $R_b$ = 1.0, web load-shedding factor determined as specified in *Article 6.10.1.10.2.*
$R_h$ =1.0, hybrid factor determined as specified in *Article 6.10.1.10.1.*
$\Delta$ = 1.0 (assumed)

$$\therefore F_{nc} = 1.0 \times 1.0 \times 1.0 \times 50 ksi = 50 ksi$$

Similarly the flexural resistance of the tension flange is $F_{nt} = F_y$.

$$\therefore F_y = 50 ksi$$

Flexural Resistance limit state of Compression Flanges

$$f_{bu} \le \phi_f \times F_y$$

The maximum stress developed in the compression flange due to factored loads is given by:

$$f_{bu} = \frac{M_{DC1}}{S_{bA}} + \frac{M_{DC2}}{S_{bB}} + \frac{M_{D3} + M_{DW}}{S_{bD}} + \frac{M_{LL}}{S_{bD}} \ge \frac{M_{DC1}}{S_{bA}} + \frac{M_{DC2}}{S_{bC}} + \frac{M_{D3} + M_{DW}}{S_{bE}} + \frac{M_{LL}}{S_{bD}}$$

$$\therefore f_{bu} = \frac{8170\ ft-kip}{8574\ in.^3} + \frac{15513\ ft-kip}{16551\ in.^3} + \frac{(3338\ +\ 2895)\ ft-kip}{11859\ in.^3} + \frac{18515\ ft-kip}{17312\ in.^3} = 46.90 ksi$$

$\therefore f_{bu} \le 1.0 \times 50ksi = 50ksi$

$\therefore f_{bu} \le \phi_f \times F_y$ is satisfied for the compression flange. Similarly, the tension flange can be checked using the same criteria. Calculations for the tension flange are shown in Appendix G.

## 10.12 Shear Design

The section must be checked for the maximum shear force. Since the maximum shear is at the interior support section, this section will be checked. Shear design of the web is in accordance with *Article 6.10.9 and 6.11.9*.

Table 10.10 indicates that the maximum factored shear is 1348 kips for Strength I limit state. This shear is not accounted for the impact at ultimate limit state. The total shear for ultimate limit state is 1348 kips. However, this shear is equally distributed to both webs of the box girder section.

Maximum shear for the single web $V_{us} = 674 \ kips$

The inclination of the web should also be taken into consideration.

$$V_u = \frac{V_{vs}}{\cos\theta} = \frac{674\,kips}{\cos 14.036} = 695\,kips$$

Therefore the maximum shear considered for design is 695 kips.

### 10.12.1 Nominal Shear Resistance of Unstiffened Webs

The nominal shear resistance for the unstiffened webs is calculated as per *Article 6.10.9* in this section. The resistance factor ($\Phi_v$) for shear design is 1.0 as per *Article 6.5.4.2*. The following steps show the shear design of the web.

1). Determine plastic shear force in accordance with *Article 6.10.9.2.*

$V_P = 0.58 \times F_y \times D \times t_w$ $\quad\quad$ $\therefore V_P = 0.58 \times 50ksi \times 72.15in \times 0.75in$

$\therefore V_P = 1569\,kips$

2). Determine the nominal shear resistance of the web.

$V_n = C \times V_p$, Where C is the ratio of shear buckling stress to the yield strength

C should be determined in accordance with *Article 6.10.9.3.2-6.*

If $\frac{D}{t_w} > 1.40\sqrt{\frac{E_s \times k}{F_y}}$ then $C = \frac{1.57}{\left(\frac{D}{t_w}\right)^2}\left(\frac{E_s \times k}{F_y}\right)$

Where, k = 5.0, shear buckling co-efficient.

In this case, $\frac{D}{t_w} = \frac{72.15\,in}{0.75\,in} = 96.2$ and $1.40\sqrt{\frac{E_s \times k}{F_y}} = 1.40 \times \sqrt{\frac{29000ksi \times 5}{50ksi}} = 75.392$

Since, $\frac{D}{t_w} > 1.40\sqrt{\frac{E_s \times k}{F_y}}$ hold true, the above equation for calculating C can be used.

$$\therefore C = \frac{1.57}{\left(\frac{72.15\,in.}{0.75\,in.}\right)^2}\left(\frac{29000\ ksi \times 5}{50\ ksi}\right) = 0.492$$

$$\therefore V_n = 0.492 \times 1569 = 772\ kips \qquad \therefore \phi_v \times V_n = 1.0 \times 772 = 772\ kips$$

Therefore, the nominal shear capacity of single web is 772 kips. Since, Vu = 695 kips is less than $\phi_v \times V_n = 772\ kips$, the section satisfies the nominal shear criteria.

## 10.13 Shear Connectors

There is no change in the design procedure of the shear connectors for the top flange in the negative flexure region. The shear connectors on the bottom flange are designed for the same provisions as the top flange in *Article 6.10.10* and *6.11.10*.

The fatigue life and nominal fatigue resistance of shear connecters are designed as per *Article 3.6.1.4* and *Article 6.6.1.2.5.* The detailed calculations for the design of shear connectors are presented in the Appendix G. However, the steps in the design of shear connectors are summarized below.

1) Ultimate resistance of shear connectors shall be calculated in accordance with *Article 6.10.10.4.*

2) Number of shear connectors shall be determined based on the ultimate resistance of the shear connectors.

3) Determine the fatigue life of the bridge in accordance with the *Article 3.6.1.4* and *Article 6.6.1.2.5.*

4) Determine the nominal fatigue resistance of shear connectors as per *Article 6.6.1.2.5* and *Article 6.10.10.2*.

5) Lateral spacing and longitudinal pitch of shear connector should be determined as per existing LRFD guidelines.

In this case, the total number of shear connectors required to connect the bottom slab to the bottom flange is 1940 with a longitudinal pitch of 18 in.

However the bottom flange should be checked for buckling between the shear stud lines. The spacing between two shear stud lines on bottom flange is 18 in. Classical theory on stability of plates is used to determine plate buckling. From the analysis it was found that the longitudinal spacing of 20 in. was adequate to prevent buckling failure. Refer Appendix G for the detailed calculations.

## 10.14 Temporary Bracing of Bottom Flange

Temporary bracing of the bottom flange should be considered by the designer to support the dead weight of the bottom concrete slab until it cures. The bottom flange deformation should follow the L/360 criteria for deflection and the through thickness bending stress in the bottom flange during construction should not exceed more than 20 ksi. The bottom flange should always be in accordance with the *Article 6.10.3* and *6.11.3* which describes the construction related guidelines. Lateral bracing of the bottom flange should be removed once the bottom slab hardens.

In this case, the bottom flange was braced with WT 8 × 13 members. The maximum spacing between the braced sections was 2 ft. and maximum stress was limited to 7.8 ksi. The maximum deflection of 0.287 in. was observed with bracing at 2 ft. Detailed calculations of the composite section properties, load, deflection and stress are included in the Appendix G.

## 10.15 Material Cost Comparison

The material (concrete and steel) cost of the double composite bridge was compared with the referenced AISI example having the overall dimensions, span configuration under the same loading. The difference in cost is due to the difference in the amount steel required by the negative moment region for the two designs. Several alternates with different concrete strength and different thickness of bottom flange and bottom slab were compared to select optimum section.

**Table 10.13** Cost Analysis of Materials used in Negative Flexure Region for Single Composite Section

| *Qty* | Single Composite Section | Dimensions | | | | Total | | Cost ($) |
|---|---|---|---|---|---|---|---|---|
| | | Length (ft.) | Width (in.) | Thickness (in.) | X-Sect Area ($in.^2$) | Volume ($ft.^3$) | Weight (lbs) | |
| 4 | Bottom Flange | 100.0 | 100.0 | 1.375 | - | 381.94 | 187153 | $402,378 |
| 4 | Stiffener (WT 12x34) | 100.0 | - | - | 10.0 | 27.78 | 13611 | $71,458 |
| Total | | | | | | | | $473,837 |

**Table 10.14** Cost Analysis of Materials Used in Negative Flexure Region for Double Composite Section

| *Qty* | Single Composite Section | Dimensions | | | | Total | | Cost ($) |
|---|---|---|---|---|---|---|---|---|
| | | Length (ft.) | Width (in.) | Thickness (in.) | X-Sect Area ($in.^2$) | Volume ($ft.^3$) | Weight (lbs) | |
| 4 | Bottom Flange | 100.0 | 100.0 | 1.0 | 100 | 278 | 136111 | $292,639 |
| 4 | Bottom Slab | 100.0 | 99 | 13 | 1290 | 3575 | 518375 | $105,926 |
| - | Reinforcing Steel | - | - | - | - | - | 17875 | $19,663 |
| 1940 | Shear Connectors | 0.5 | - | 0.75 (diameter) | - | 3.31 | 1620 | $2,430 |
| 204 | Temporary Bracing | 8.33 | - | - | 3.84 | 33.17 | 22213 | $19,437 |
| Total | | | | | | | | $440,094 |

In the comparison, costs are based on the FDOT cost data; these are $ 800 per cubic yard for structural concrete and $ 2.15 per pound of steel. The corresponding costs per cubic feet are $30 for structural concrete and $1053 for structural steel.

Table 10.14 and 10.15 shows the cost analysis of the materials used in negative flexure region for both ‘single’ and ‘double’ composite sections. The inspection of Table 10.14 and 10.15 shows that there is approximate saving of $ 33,743 in terms of materials used in negative flexure region for double composite section. In terms of the overall savings, 7 % can be saved by using double composite design.

**Table 10.15** Cost Comparison of Double Composite Sections

| Double Composite Sections | | | | | | |
|---|---|---|---|---|---|---|
| **Alternate** | **Concrete Strength (psi)** | **Bottom Slab Thickness** | **Bottom Flange Thickness** | **Cost Savings ($)** | **Cost Savings* ($/sq. ft.)** | **Cost Savings* (%)** |
| 1 | 6,500 | 13 | 1.0 | 33,743 | 1.3 | 0.70 |
| 2 | 7,500 | 10 | 1.0 | 62,215 | 2.39 | 1.30 |
| 3 | 8,500 | 9 | 0.875 | 107,375 | 4.12 | 2.23 |
| 4 | 10,000 | 7 | 0.875 | 126,860 | 4.87 | 2.63 |

***** Based on the estimated structural cost of $ 185/Sq. ft. and deck area of the 26026 sq.ft.

## 10.16 Summary

The thickness of the bottom flange in the referenced AISI example was 1.375 in. and the bottom flange was stiffened by WT sections with an approximate cross-sectional area of 10 sq. in. In contrast, in the double composite section, the bottom flange thickness reduced to 1.0 in. and no stiffeners were needed. The thickness of bottom concrete slab between the contraflexure points was maintained constant at 13 in. in the proposed design.

Several other alternates with high strength concrete were considered. Table 10.16 summarizes cost savings for all the different alternates for double composite section. In all the cases, stress in the bottom concrete slab was limited to 0.6f'c. Table 10.16 shows that by using high strength concrete, the thickness of bottom slab and steel bottom flange can be reduced. This increases the cost savings significantly for double composite sections in the negative flexure region. However, cost savings in terms of entire bridge is nominal.

The double composite design required the bottom slab to be checked for the new slab ductility requirement to avoid premature crushing of the concrete slab. Also, the section was designed as non-compact in the negative flexure region. The concrete slab continuously braces the compression flange and therefore eliminates the need for lateral bracing.

The bottom flange was temporarily braced every 2 ft to limit deflection and through thickness bending while it supported the weight of the concrete during construction.

## References

10.1 AASHTO LRFD Bridge Design Specifications (2004). 3rd Edition, Washington, D.C.

10.2 FDOT Structures Design Guidelines (2005). Tallahassee, FL.

10.3 AISI (1995). "Four LRFD Design Examples of Steel Highway Bridges." Vol. II, Ch 1A, Highway Structures Design Handbook. Prepared by HDR Engineering, Chicago, IL.

10.4 QConBridge (2005). http://www.wsdot.wa.gov/eesc/bridge/software.

10.5 AISC Manual of Steel Construction (2007). 13th Edition, Chicago, IL, pp 3-224–3-225.

# APPENDIX A

Design of Double Composite Box Girder Test Specimen

## A.1 Description

Design calculations for the double composite box girder test specimen are presented herein. The test specimen was designed using the Load and Resistance Factor Design (LRFD) method in accordance with *AASHTO LRFD Bridge Design Specifications, 3rd Edition, 2004* and *FDOT Structures Design Guidelines for LRFD, January 2005*.

The total length of the test specimen was 53 feet 0 inches. The test span arrangement included a simple span measuring 23 feet between supports, and a cantilever segment with loads applied near the tip, 25 feet from the adjacent support.

High performance structural steel (HPS) of grade 70 ksi (ASTM A709) and reinforcing steel of grade 60 ksi (ASTM A615) were used in the design. The specified concrete compressive strength was 5500 psi. The modulus of elasticity for the concrete was calculated with consideration of the effects of Florida limerock aggregates, as per the FDOT Standard Design Guidelines.

Hydraulic actuators were used to apply the test loads to the box girder system. Load factors were not considered for live loads since the actual values of the applied loads were known. However, load factors were applied to the dead loads calculated for the specimen.

The design of the test specimen included calculations for the following:

- Box Girder Section Properties using Design and Predicted Material Strengths
- Plastic Moment for Negative Flexure using Design Strengths
- Plastic Moment for Negative Flexure using Predicted Strengths
- Quantity and Layout of Shear Connectors based upon Predicted Fatigue Life
- Design of Double Composite Box Girder Test Specimen and all Components
- Natural Frequency of the Box Girder

## A.2 General Design Information

### Material Properties

Weight of Concrete, $w_c$ $w_c := 145 \cdot pcf$

Weight of Reinforced Concrete, $w_{rc}$ $w_{rc} := 150 \cdot pcf$

Design Concrete Strength, $f_{c\_des}$ $f_{c\_des} := 5500 \cdot psi$

Design Concrete Modulus of Elasticity, $E_{c\_des}$ $E_{c\_des} := 0.9 \cdot 33 \cdot \left( \frac{w_c}{pcf} \right)^{1.5} \cdot \sqrt{\left( f_{c\_des} \cdot psi \right)}$

$E_{c\_des} = 3845.83\ ksi$

Design HPS Steel Yield Strength, $F_{y\_des}$ $F_{y\_des} := 70 \cdot ksi$

Predicted Concrete Strength, $f_c$ $f_c := 7500 \cdot psi$

Predicted Concrete Modulus of Elasticity, $E_c$ $E_c := 0.9 \cdot 33 \cdot \left( \frac{w_c}{pcf} \right)^{1.5} \cdot \sqrt{\left( f_c \cdot psi \right)}$

$E_c = 4490.96\ ksi$

Predicted HPS Steel Yield Strength, $F_y$ $F_y := 80 \cdot ksi$

Steel Modulus of Elasticity, $E_s$ $E_s := 29000 \cdot ksi$

Steel Shear Modulus, $G_s$ $G_s := 11165 \cdot ksi$

Reinforcement Steel Yield Strength, $F_{yrebar}$ $F_{yrebar} := 60 \cdot ksi$

Reinforcement Ratio, $R_r$ $R_r := 0.01$

## Girder Geometry

| | | |
|---|---|---|
| Height of girder, $H_G$ | $H_G := 50.125 \cdot in$ | |
| Web depth (plumb), $D_w$ | $D_w := 48 \cdot in$ | |
| (inclination to vertical is 14.036 deg) | $\theta := 14.036 \cdot deg$ | |
| Web depth (inclined), D | $D := \frac{D_w}{\cos(\theta)}$ | $D = 49.477\ in$ |
| Web plate thickness, $t_w$ | $t_w := 0.75 \cdot in$ | |
| Top flange thickness, $t_{tf}$ | $t_{tf} := 1.75 \cdot in$ | |
| Top flange width, $b_{tf}$ | $b_{tf} := 16 \cdot in$ | |
| Bottom flange thickness, $t_{bf}$ | $t_{bf} := 0.375 \cdot in$ | |
| Bottom flange width, $b_{bf}$ | $b_{bf} := 76 \cdot in$ | |
| Top slab width, $b_{ts}$ | $b_{ts} := 192 \cdot in$ | |
| Top slab thickness, $t_{ts}$ | $t_{ts} := 8 \cdot in$ | |
| Bottom slab width, $b_{bs}$ | $b_{bs} := 72 \cdot in$ | |
| Bottom slab thickness, $t_{bs}$ | $t_{bs} := 7 \cdot in$ | |
| Total length of the test specimen, consists of simply supported span and cantilever span. $L_n$ | $L_n := 48 \cdot ft$ | |
| Simply supported span length, a | $a := 23 \cdot ft$ | |
| Cantilever span length, b | $b := 25 \cdot ft$ | |

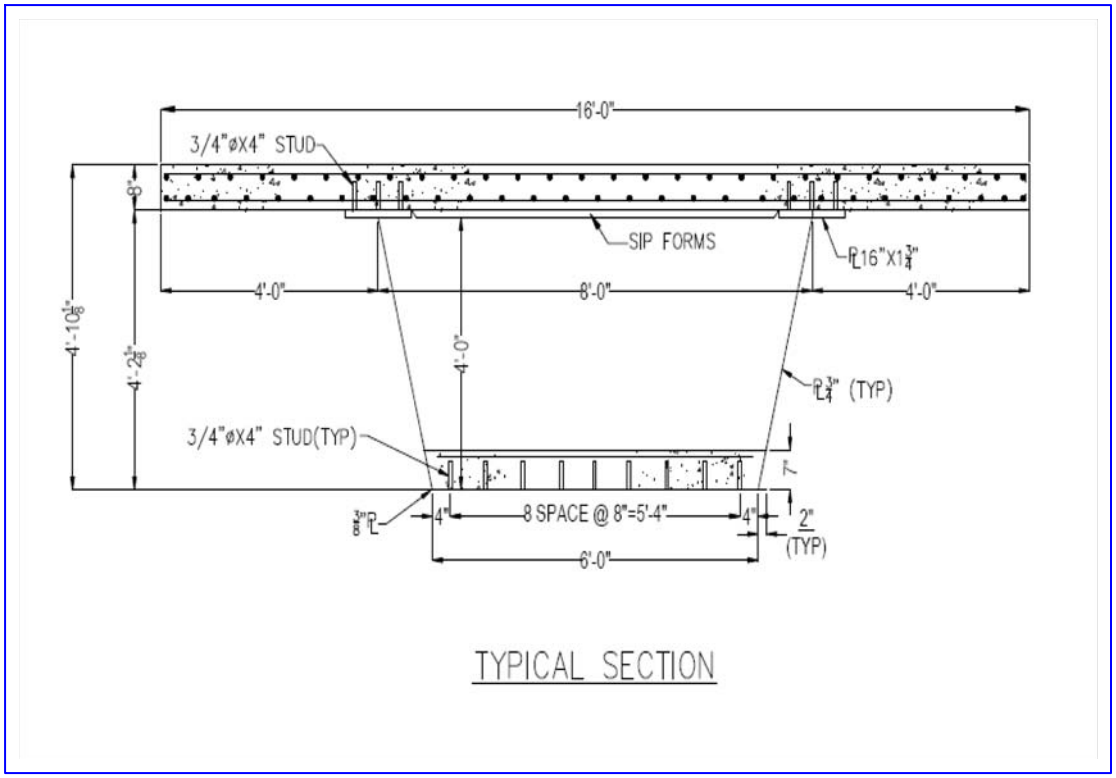


**Figure A.1** Typical Cross-Section of Double Composite Box Girder

## Section Properties

| | | |
|---|---|---|
| Area of steel box girder, $A_{gird}$ | $A_{gird} := 2 \cdot t_{tf} \cdot b_{tf} + t_{bf} \cdot b_{bf} + 2 \cdot D \cdot t_w$<br>$A_{gird} = 158.716\ in^2$ | |
| Moment of inertia of bare steel, $I_{st}$ | $I_{st} := 62469 \cdot in^4$ | (see pg-A.9) |
| Top fiber section modulus, $S_{t\_st}$ | $S_{t\_st} := 2930.5 \cdot in^3$ | (see pg-A.9) |
| Bottom fiber section modulus, $S_{b\_st}$ | $S_{b\_st} := 2168.4 \cdot in^3$ | (see pg-A.9) |
| Design SVC level composite moment of inertia, $I_{dc}$ | $I_{dc} := 208282 \cdot in^4$ | (see pg-A.11) |
| Design SVC level composite moment of inertia with bottom slab only, $I_{bsc}$ | $I_{bsc} := 92093 \cdot in^4$ | (see pg-A.15) |
| Predicted SVC level composite moment of inertia, $I_{pc}$ | $I_{pc} := 229010 \cdot in^4$ | (see pg-A.19) |
| Predicted ultimate level composite moment of inertia, $I_u$ | $I_u := 111354 \cdot in^4$ | (see pg-A.21) |

## A.3 Loads

### Dead Loads

| | | |
|---|---|---|
| Girder weight, $w_{gird}$ (klf) | $w_{gird} := 490 \cdot pcf \cdot A_{gird}$ | $w_{gird} = 0.54\,klf$ |
| steel details (10%) (klf) | $w_{det} := 0.10 \cdot w_{gird}$ | $w_{det} = 0.054\,klf$ |
| Top slab, $w_{ts}$ (klf) | $w_{ts} := b_{ts} \cdot t_{ts} \cdot w_{rc}$ | $w_{ts} = 1.6\,klf$ |
| Stay in place forms, $w_{sip}$ (klf) | $w_{sip} := 20 \cdot psf \cdot 6.667 \cdot ft$ | $w_{sip} = 0.133\,klf$ |
| Bottom slab, $w_{bs}$ (klf) | $w_{bs} := \left(72 \cdot in + \frac{7 \cdot in}{4}\right) \cdot 7in \cdot w_{rc}$ | $w_{bs} = 0.538\,klf$ |

### Actuator Loads

| | | |
|---|---|---|
| Service load, $P_f$ (kips) | $P_{svc} := 168 \cdot kip$ | |
| Ultimate load, $P_u$ (kips) | $P_u := \frac{27963 \cdot ft \cdot kip \cdot 1.15}{25 \cdot ft}$ | $P_u = 1286.298\,kip$ |
| Fatigue load, $P_f$ (kips) | $P_f := 100 \cdot kip$ | |

**Note:** Ultimate load was determined using the plastic moment calculated for the "predicted" material strengths (see pg-A.28). In addition, the ultimate load was increased 15% to ensure that the box girder failed before other test specimen components.

## A.4 Design Section Properties

### Non-Composite Section Properties (n=infinity) A (Uncracked)

**a.) Top Flange**

$t_{tf} = 1.75\,in$

$b_{tf} = 16\,in$

$A_{tf} := 2 \cdot t_{tf} \cdot b_{tf}$

$A_{tf} = 56\,in^2$

**b.) Bottom Flange**

$t_{bf} = 0.375\,in$

$b_{bf} = 76\,in$

$A_{bf} := t_{bf} \cdot b_{bf}$

$A_{bf} = 28.5\,in^2$

**c.) Web**

$t_w = 0.75\,in$

$D = 49.477\,in$

$A_w := 2 t_w \cdot D$

$A_w = 74.216\,in^2$

Total area of steel box girder, $A_s$

$A_s := A_{tf} + A_{bf} + A_w$ $\quad A_s = 158.716\,in^2$

**The distance from the extreme bottom fiber to the centroid of item center of gravity, h (inch)**

**a.) Top Flange**

$h_{tf} := t_{bf} + D_w + \frac{t_{tf}}{2}$

$h_{tf} = 49.25\,in$

$A_{tf} \cdot h_{tf} = 2758\,in^3$

**b.) Bottom Flange**

$h_{bf} := \frac{t_{bf}}{2}$

$h_{bf} = 0.187\,in$

$A_{bf} \cdot h_{bf} = 5.344\,in^3$

**c.) Web**

$h_w := t_{bf} + \frac{D_w}{2}$

$h_w = 24.375\,in$

$A_w \cdot h_w = 1809.011\,in^3$

$\Sigma Ah := A_{tf} \cdot h_{tf} + A_{bf} \cdot h_{bf} + A_w \cdot h_w$ $\quad \Sigma Ah = 4572.354\,in^3$

**Distance from bottom of section to the Neutral Axis (N.A.) of whole section, $Y_b$ (inch)**

$Y_b := \frac{\Sigma Ah}{A_s}$ $\quad Y_b = 28.808\,in$

**Distance from top of section to the Neutral Axis (N.A.) of whole section, $Y_t$ (inch)**

$Y_t := H_G - Y_b$ $\quad Y_t = 21.317\,in$

**Distance between Neutral Axis (N.A.) and Item center of gravity, d (inch)**

**a.) Top Flange**

$d_{tf} := h_{tf} - Y_b$

$d_{tf} = 20.442\ in$

**b.) Bottom Flange**

$d_{bf} := h_{bf} - Y_b$

$d_{bf} = -28.621\ in$

**c.) Web**

$d_w := h_w - Y_b$

$d_w = -4.433\ in$

**Moment of Inertia, $I_0$ ($in^4$)**

$I_{0tf} := 2 \cdot \frac{b_{tf} \cdot t_{tf}^3}{12}$

$I_{0tf} = 14.292\ in^4$

$I_{0bf} := \frac{b_{bf} \cdot t_{bf}^3}{12}$

$I_{0bf} = 0.334\ in^4$

$I_{0w} := 2 \cdot \frac{t_w \cdot D^3 \cdot \cos(\theta)^2}{12}$

$I_{0w} = 14249.438\ in^4$

$I_{0s} := I_{0tf} + I_{0bf} + I_{0w}$

$I_{0s} = 14264.064\ in^4$

$A_{tf} \cdot d_{tf}^2 = 23400.025\ in^4$

$A_{bf} \cdot d_{bf}^2 = 23346\ in^4$

$A_w \cdot d_w^2 = 1458.738\ in^4$

$\Sigma Ad := A_{tf} \cdot d_{tf}^2 + A_{bf} \cdot d_{bf}^2 + A_w \cdot d_w^2$

$\Sigma Ad = 48204.763\ in^4$

**Moment of Inertia of whole section with respect to Neutral Axis (N.A.) of whole section, $I_z$ ($in^4$)**

$I_{st} := I_{0s} + \Sigma Ad$

$I_{st} = 62468.826\ in^4$

**Section Modulus required for the weld, Q ($in^3$)**

$Q_{tf} := A_{tf} \cdot \left( Y_t - \frac{t_{tf}}{2} \right)$

$Q_{tf} = 1144.728\ in^3$

$Q_{bf} := A_{bf} \cdot \left( Y_b - \frac{t_{bf}}{2} \right)$

$Q_{bf} = 815.697\ in^3$

**Section Modulus of entire section, S ($in^3$)**

$S_{t\_st} := \frac{I_{st}}{Y_t}$

$S_{t\_st} = 2930.53\ in^3$

$S_{b\_st} := \frac{I_{st}}{Y_b}$

$S_{b\_st} = 2168.421\ in^3$

**Note:** St_st and Sb_st defines the section modulus of top fiber and bottom fiber of secction respectively.

## Short-term Composite Properties (n=7.5) B (Uncracked)

**Modular Ratio, n**

$$n := \text{round}\left(\frac{E_s}{E_{c\_des}}, 1\right) \qquad n = 7.5$$

**a.) Top Slab**

$$A_{tsB} := \frac{b_{ts} \cdot t_{ts}}{n}$$

$$A_{tsB} = 204.8\ \text{in}^2$$

**b.) Bottom Slab**

$$A_{bsB} := \frac{b_{bs} \cdot t_{bs}}{n}$$

$$A_{bsB} = 67.2\ \text{in}^2$$

**c.) Steel**

$$A_s = 158.716\ \text{in}^2$$

$$A_B := A_{tsB} + A_{bsB} + A_s \qquad A_B = 430.716\ \text{in}^2$$

**The distance from the extreme bottom fiber to the centroid of item center of gravity, h (inch)**

**a.) Top Slab**

$$h_{tsB} := t_{bf} + D_w + t_{tf} + \frac{t_{ts}}{2}$$

$$h_{tsB} = 54.125\ \text{in}$$

$$A_{tsB} \cdot h_{tsB} = 11084.8\ \text{in}^3$$

**b.) Bottom Slab**

$$h_{bsB} := t_{bf} + \frac{t_{bs}}{2}$$

$$h_{bsB} = 3.875\ \text{in}$$

$$A_{bsB} \cdot h_{bsB} = 260.4\ \text{in}^3$$

**c.) Steel**

$$A_s \cdot Y_b = 4572.354\ \text{in}^3$$

$$\Sigma Ah_B := A_{tsB} \cdot h_{tsB} + A_{bsB} \cdot h_{bsB} + A_s \cdot Y_b \qquad \Sigma Ah_B = 15917.554\ \text{in}^3$$

**Distance from bottom of section to the Neutral Axis (N.A.) of the whole section, $Y_b$ (inch)**

$$Y_{bB} := \frac{\Sigma Ah_B}{A_B} \qquad Y_{bB} = 36.956\ \text{in}$$

**Distance from top of section to the Neutral Axis (N.A.) of the whole section, $Y_t$ (inch)**

$$Y_{tB} := H_G + t_{ts} - Y_{bB} \qquad Y_{tB} = 21.169\ \text{in}$$

**Distance between Neutral Axis and Item center of gravity, d (inch).**

**a.) Top Slab**

$$d_{tsB} := h_{tsB} - Y_{bB}$$

$$d_{tsB} = 17.169\ \text{in}$$

**b.) Bottom Slab**

$$d_{bsB} := h_{bsB} - Y_{bB}$$

$$d_{bsB} = -33.081\ \text{in}$$

**c.) Steel**

$$d_{sB} := Y_b - Y_{bB}$$

$$d_{sB} = -8.148\ \text{in}$$

**Moment of Inertia, $I_0$ ($in^4$)**

$I_{0tsB} := \frac{b_{ts} \cdot t_{ts}^3}{12 \cdot n}$ $I_{0tsB} = 1092.267\ in^4$

$I_{0bsB} := \frac{b_{bs} \cdot t_{bs}^3}{12 \cdot n}$ $I_{0bsB} = 274.4\ in^4$

$I_{st} = 62468.826\ in^4$

$\Sigma I_{0B} := I_{0tsB} + I_{0bsB} + I_{st}$ $\Sigma I_{0B} = 63835.493\ in^4$

$A_{tsB} \cdot d_{tsB}^2 = 60369.496\ in^4$ $A_{bsB} \cdot d_{bsB}^2 = 73540.704\ in^4$ $A_s \cdot d_{sB}^2 = 10536.127\ in^4$

$\Sigma Ad_B := A_{tsB} \cdot d_{tsB}^2 + A_{bsB} \cdot d_{bsB}^2 + A_s \cdot d_{sB}^2$ $\Sigma Ad_B = 144446.326\ in^4$

**Moment of Inertia of whole section with respect to Neutral Axis (N.A.) of whole section, $I_{dc}$ ($in^4$)**

$I_{dc} := \Sigma I_{0B} + \Sigma Ad_B$ $I_{dc} = 208281.819\ in^4$

**Section Modulus required for the weld, Q ($in^3$).**

$Q_{tfB} := \left(H_G - Y_{bB} - \frac{t_{tf}}{2}\right) \cdot A_{tf} + \left(H_G + \frac{t_{ts}}{2} - Y_{bB}\right) \cdot A_{tsB}$ $Q_{tfB} = 4204.663\ in^3$

$Q_{bfB} := A_{bf} \cdot \left(Y_{bB} - \frac{t_{bf}}{2}\right) + A_{bsB} \cdot \left(Y_{bB} - t_{bf} - \frac{t_{bs}}{2}\right)$ $Q_{bfB} = 3270.95\ in^3$

$Q_{TslabB} := A_{tsB} \cdot \left(H_G + \frac{t_{ts}}{2} - Y_{bB}\right)$ $Q_{TslabB} = 3516.201\ in^3$

**Section Modulus of entire section, S ($in^3$)**

$S_{tslabB} := \frac{I_{dc} \cdot n}{Y_{tB}}$ $S_{tslabB} = 73792.676\ in^3$

$S_{tbeamB} := \frac{I_{dc}}{Y_{tB} - t_{ts}}$ $S_{tbeamB} = 15816.127\ in^3$

$S_{bbeamB} := \frac{I_{dc}}{Y_{bB}}$ $S_{bbeamB} = 5635.933\ in^3$

$S_{bslabB} := \frac{I_{dc} \cdot n}{Y_{bB} - t_{bf}}$ $S_{bslabB} = 42702.813\ in^3$

## Short-term Composite Section Properties (n=7.5) C (Negative Live Load Moment)

**Modular Ratio, n**

$n = 7.5$

**a.) Top Rebar**

$A_{rebarC} := R_r \cdot b_{ts} \cdot t_{ts}$

$A_{rebarC} = 15.36\ in^2$

**b.) Bottom Slab**

$A_{bsC} := \frac{b_{bs} \cdot t_{bs}}{n}$

$A_{bsC} = 67.2\ in^2$

**c.) Steel**

$A_s = 158.716\ in^2$

$A_C := A_{rebarC} + A_{bsC} + A_s$

$A_C = 241.276\ in^2$

**The distance from the extreme bottom fiber to the centroid of item center of gravity, h (inch)**

**a.) Top Rebar**

$h_{rebarC} := t_{bf} + D_w + t_{tf} + \frac{t_{ts}}{2}$

$h_{rebarC} = 54.125\ in$

$A_{rebarC} \cdot h_{rebarC} = 831.36\ in^3$

**b.) Bottom Slab**

$h_{bsC} := t_{bf} + \frac{t_{bs}}{2}$

$h_{bsC} = 3.875\ in$

$A_{bsC} \cdot h_{bsC} = 260.4\ in^3$

**c.) Steel**

$Y_b = 28.808\ in$

$A_s \cdot Y_b = 4572.354\ in^3$

$\Sigma Ah_C := A_{rebarC} \cdot h_{rebarC} + A_{bsC} \cdot h_{bsC} + A_s \cdot Y_b$

$\Sigma Ah_C = 5664.114\ in^3$

**Distance from bottom of section to the Neutral Axis (N.A.) of the whole section, $Y_b$ (inch)**

$Y_{bC} := \frac{\Sigma Ah_C}{A_C}$

$Y_{bC} = 23.476\ in$

**Distance from top of section to the Neutral Axis (N.A.) of the whole section, $Y_t$ (inch)**

$Y_{tC} := H_G + t_{ts} - Y_{bC}$

$Y_{tC} = 34.649\ in$

**Distance between Neutral Axis and Item center of gravity, d (inch)**

**a.) Top Rebar**

$d_{rebarC} := h_{rebarC} - Y_{bC}$

$d_{rebarC} = 30.649\ in$

**b.) Bottom Slab**

$d_{bsC} := h_{bsC} - Y_{bC}$

$d_{bsC} = -19.601\ in$

**c.) Steel**

$d_{sC} := Y_b - Y_{bC}$

$d_{sC} = 5.333\ in$

**Moment of Inertia, $I_0$ ($in^4$)**

$I_{rebarC} := 0.0 \cdot in^4$ $\quad I_{0bsC} := \frac{b_{bs} \cdot t_{bs}^3}{12 \cdot n}$

$I_{rebarC} = 0$ $\quad I_{0bsC} = 274.4\ in^4$ $\quad I_{st} = 62468.826\ in^4$

$\Sigma I_{0C} := I_{rebarC} + I_{0bsC} + I_{st}$ $\quad \Sigma I_{0C} = 62743.226\ in^4$

$A_{rebarC} \cdot d_{rebarC}^2 = 14428.888\ in^4$ $\quad A_{bsC} \cdot d_{bsC}^2 = 25817.348\ in^4$ $\quad A_s \cdot d_{sC}^2 = 4513.601\ in^4$

$\Sigma Ad_C := A_{rebarC} \cdot d_{rebarC}^2 + A_{bsC} \cdot d_{bsC}^2 + A_s \cdot d_{sC}^2$ $\quad \Sigma Ad_C = 44759.837\ in^4$

**Moment of Inertia of whole section with respect to Neutral Axis (N.A.) of whole section, $I_{zC}$ ($in^4$)**

$I_{zC} := \Sigma I_{0C} + \Sigma Ad_C$ $\quad I_{zC} = 107503.063\ in^4$

**Section Modulus required for the weld, Q ($in^3$).**

$Q_{tfC} := \left(H_G - Y_{bC} - \frac{t_{tf}}{2}\right) \cdot A_{tf} + \left(H_G + \frac{t_{ts}}{2} - Y_{bC}\right) \cdot A_{rebarC}$ $\quad Q_{tfC} = 1914.135\ in^3$

$Q_{bfC} := A_{bf} \cdot \left(Y_{bC} - \frac{t_{bf}}{2}\right) + A_{bsC} \cdot \left(Y_{bC} - t_{bf} - \frac{t_{bs}}{2}\right)$ $\quad Q_{bfC} = 1980.879\ in^3$

$Q_{BslabC} := A_{bsC} \cdot \left(Y_{bC} - t_{bf} - \frac{t_{bs}}{2}\right)$ $\quad Q_{BslabC} = 1317.166\ in^3$

**Section Modulus of entire section, S ($in^3$)**

$S_{trebarC} := \frac{I_{zC}}{Y_{tC} - \frac{t_{ts}}{2}}$ $\quad S_{trebarC} = 3507.519\ in^3$

$S_{tbeamC} := \frac{I_{zC}}{Y_{tC} - t_{ts}}$ $\quad S_{tbeamC} = 4033.989\ in^3$

$S_{bbeamC} := \frac{I_{zC}}{Y_{bC}}$ $\quad S_{bbeamC} = 4579.337\ in^3$

$S_{bslabC} := \frac{I_{zC} \cdot n}{Y_{bC} - t_{bf}}$ $\quad S_{bslabC} = 34902.562\ in^3$

## Short-term Composite Section Properties (n=7.5) D (For Bridge Deck Loading)

**Modular Ratio, n**

$n = 7.5$

**b.) Bottom Slab**

$A_{bsD} := \frac{b_{bs} \cdot t_{bs}}{n}$

$A_{bsD} = 67.2\ in^2$

**c.) Steel**

$A_s = 158.716\ in^2$

$A_D := A_{bsD} + A_s$

$A_D = 225.916\ in^2$

**The distance from the extreme bottom fiber to the centroid of item center of gravity, h (inch)**

**b.) Bottom Slab**

$h_{bsD} := t_{bf} + \frac{t_{bs}}{2}$

$h_{bsD} = 3.875\ in$

$A_{bsD} \cdot h_{bsD} = 260.4\ in^3$

**c.) Steel**

$Y_b = 28.808\ in$

$A_s \cdot Y_b = 4572.354\ in^3$

$\Sigma Ah_D := A_{bsD} \cdot h_{bsD} + A_s \cdot Y_b$

$\Sigma Ah_D = 4832.754\ in^3$

**Distance from bottom of section to the Neutral Axis (N.A.) of the whole section, $Y_b$ (inch)**

$Y_{bD} := \frac{\Sigma Ah_D}{A_D}$

$Y_{bD} = 21.392\ in$

**Distance from top of section to the Neutral Axis (N.A.) of the whole section, $Y_t$ (inch)**

$Y_{tD} := H_G + t_{ts} - Y_{bD}$

$Y_{tD} = 36.733\ in$

**Distance between Neutral Axis and Item center of gravity, d (inch)**

**b.) Bottom Slab**

$d_{bsD} := h_{bsD} - Y_{bD}$

$d_{bsD} = -17.517\ in$

**c.) Steel**

$d_{sD} := Y_b - Y_{bD}$

$d_{sD} = 7.417\ in$

**Moment of Inertia, $I_0$ ($in^4$)**

$$I_{0bsD} := \frac{b_{bs} \cdot t_{bs}^{3}}{12 \cdot n}$$

$I_{0bsD} = 274.4\ in^4$ $I_{st} = 62468.826\ in^4$

$\Sigma I_{0D} := I_{0bsD} + I_{st}$ $\Sigma I_{0D} = 62743.226\ in^4$

$A_{bsD} \cdot d_{bsD}^{2} = 20619.619\ in^4$ $A_s \cdot d_{sD}^{2} = 8730.311\ in^4$

$\Sigma Ad_D := A_{bsD} \cdot d_{bsD}^{2} + A_s \cdot d_{sD}^{2}$ $\Sigma Ad_D = 29349.93\ in^4$

**Moment of Inertia of whole section with respect to Neutral Axis (N.A.) of whole section, $I_{bsc}$ ($in^4$).**

$I_{bsc} := \Sigma I_{0D} + \Sigma Ad_D$ $I_{bsc} = 92093.156\ in^4$

**Section Modulus required for the weld, Q ($in^3$).**

$$Q_{tfD} := \left(H_G - Y_{bD} - \frac{t_{tf}}{2}\right) \cdot A_{tf}$$ $Q_{tfD} = 1560.057\ in^3$

$$Q_{bfD} := A_{bf} \cdot \left(Y_{bD} - \frac{t_{bf}}{2}\right) + A_{bsD} \cdot \left(Y_{bD} - t_{bf} - \frac{t_{bs}}{2}\right)$$ $Q_{bfD} = 1781.455\ in^3$

$$Q_{BslabD} := A_{bsD} \cdot \left(Y_{bD} - t_{bf} - \frac{t_{bs}}{2}\right)$$ $Q_{BslabD} = 1177.131\ in^3$

**Section Modulus of entire section, S ($in^3$)**

$$S_{tbeamD} := \frac{I_{bsc}}{Y_{tD} - t_{ts}}$$ $S_{tbeamD} = 3205.117\ in^3$

$$S_{bbeamD} := \frac{I_{bsc}}{Y_{bD}}$$ $S_{bbeamD} = 4305.061\ in^3$

$$S_{bslabD} := \frac{I_{bsc} \cdot n}{Y_{bD} - t_{bf}}$$ $S_{bslabD} = 32864.064\ in^3$

## A.5 Predicted Section Properties

### Non-Composite Section Properties (n=infinity) A (Uncracked)

**a.) Top Flange**

$t_{tf} = 1.75\,in$

$b_{tf} = 16\,in$

$A_{tf} := 2 \cdot t_{tf} \cdot b_{tf}$

$A_{tf} = 56\,in^2$

**b.) Bottom Flange**

$t_{bf} = 0.375\,in$

$b_{bf} = 76\,in$

$A_{bf} := t_{bf} \cdot b_{bf}$

$A_{bf} = 28.5\,in^2$

**c.) Web**

$t_w = 0.75\,in$

$D = 49.477\,in$

$A_w := 2 t_w \cdot D$

$A_w = 74.216\,in^2$

Total area of steel box girder, $A_s$

$A_s := A_{tf} + A_{bf} + A_w$ $\quad A_s = 158.716\,in^2$

**The distance from the extreme bottom fiber to the centroid of item center of gravity, h (inch)**

**a.) Top Flange**

$h_{tf} := t_{bf} + D_w + \frac{t_{tf}}{2}$

$h_{tf} = 49.25\,in$

$A_{tf} \cdot h_{tf} = 2758\,in^3$

**b.) Bottom Flange**

$h_{bf} := \frac{t_{bf}}{2}$

$h_{bf} = 0.187\,in$

$A_{bf} \cdot h_{bf} = 5.344\,in^3$

**c.) Web**

$h_w := t_{bf} + \frac{D_w}{2}$

$h_w = 24.375\,in$

$A_w \cdot h_w = 1809.011\,in^3$

$\Sigma Ah := A_{tf} \cdot h_{tf} + A_{bf} \cdot h_{bf} + A_w \cdot h_w$ $\quad \Sigma Ah = 4572.354\,in^3$

**Distance from bottom of section to the Neutral Axis (N.A.) of whole section, $Y_b$ (inch)**

$Y_b := \frac{\Sigma Ah}{A_s}$ $\quad Y_b = 28.808\,in$

**Distance from top of section to the Neutral Axis (N.A.) of whole section, $Y_t$ (inch)**

$Y_t := H_G - Y_b$ $\quad Y_t = 21.317\,in$

**Distance between Neutral Axis (N.A.) and Item center of gravity, d (inch)**

**a.) Top Flange** **b.) Bottom Flange** **c.) Web**

$d_{tf} := h_{tf} - Y_b$ $d_{bf} := h_{bf} - Y_b$ $d_w := h_w - Y_b$

$d_{tf} = 20.442\,in$ $d_{bf} = -28.621\,in$ $d_w = -4.433\,in$

**Moment of Inertia, $I_0$ ($in^4$)**

$I_{0tf} := 2 \cdot \frac{b_{tf} \cdot t_{tf}^3}{12}$ $I_{0bf} := \frac{b_{bf} \cdot t_{bf}^3}{12}$ $I_{0w} := 2 \cdot \frac{t_w \cdot D^3 \cdot \cos(\theta)^2}{12}$

$I_{0tf} = 14.292\,in^4$ $I_{0bf} = 0.334\,in^4$ $I_{0w} = 14249.438\,in^4$

$I_{0s} := I_{0tf} + I_{0bf} + I_{0w}$ $I_{0s} = 14264.064\,in^4$

$A_{tf} \cdot d_{tf}^2 = 23400.025\,in^4$ $A_{bf} \cdot d_{bf}^2 = 23346\,in^4$ $A_w \cdot d_w^2 = 1458.738\,in^4$

$\Sigma Ad := A_{tf} \cdot d_{tf}^2 + A_{bf} \cdot d_{bf}^2 + A_w \cdot d_w^2$ $\Sigma Ad = 48204.763\,in^4$

**Moment of Inertia of whole section with respect to Neutral Axis (N.A.) of whole section, $I_z$ ($in^4$)**

$I_{st} := I_{0s} + \Sigma Ad$ $I_{st} = 62468.826\,in^4$

**Section Modulus required for the weld, Q ($in^3$)**

$Q_{tf} := A_{tf} \cdot \left( Y_t - \frac{t_{tf}}{2} \right)$ $Q_{tf} = 1144.728\,in^3$

$Q_{bf} := A_{bf} \cdot \left( Y_b - \frac{t_{bf}}{2} \right)$ $Q_{bf} = 815.697\,in^3$

**Section Modulus of entire section, S ($in^3$)**

$S_{t\_st} := \frac{I_{st}}{Y_t}$ $S_{t\_st} = 2930.53\,in^3$

$S_{b\_st} := \frac{I_{st}}{Y_b}$ $S_{b\_st} = 2168.421\,in^3$

**Note:** St_st and Sb_st defines the section modulus of top fiber and bottom fiber of secction respectively.

## Short-term Composite Section Properties (n=6.5) B (Uncracked)

**Modular Ratio, n**

$$n := \text{round}\left(\frac{E_s}{E_c}, 1\right) \qquad n = 6.5$$

**a.) Top Slab** **b.) Bottom Slab** **c.) Steel**

$$A_{tsB} := \frac{b_{ts} \cdot t_{ts}}{n} \qquad A_{bsB} := \frac{b_{bs} \cdot t_{bs}}{n}$$

$$A_{tsB} = 236.308\ \text{in}^2 \qquad A_{bsB} = 77.538\ \text{in}^2 \qquad A_s = 158.716\ \text{in}^2$$

$$A_B := A_{tsB} + A_{bsB} + A_s \qquad A_B = 472.562\ \text{in}^2$$

**The distance from the extreme bottom fiber to the centroid of item center of gravity, h (inch)**

**a.) Top Slab** **b.) Bottom Slab** **c.) Steel**

$$h_{tsB} := t_{bf} + D_w + t_{tf} + \frac{t_{ts}}{2} \qquad h_{bsB} := t_{bf} + \frac{t_{bs}}{2}$$

$$h_{tsB} = 54.125\ \text{in} \qquad h_{bsB} = 3.875\ \text{in}$$

$$A_{tsB} \cdot h_{tsB} = 12790.154\ \text{in}^3 \qquad A_{bsB} \cdot h_{bsB} = 300.462\ \text{in}^3 \qquad A_s \cdot Y_b = 4572.354\ \text{in}^3$$

$$\Sigma Ah_B := A_{tsB} \cdot h_{tsB} + A_{bsB} \cdot h_{bsB} + A_s \cdot Y_b \qquad \Sigma Ah_B = 17662.97\ \text{in}^3$$

**Distance from bottom of section to the Neutral Axis (N.A.) of the whole section, $Y_b$ (inch).**

$$Y_{bB} := \frac{\Sigma Ah_B}{A_B} \qquad Y_{bB} = 37.377\ \text{in}$$

**Distance from top of section to the Neutral Axis (N.A.) of the whole section, $Y_t$ (inch).**

$$Y_{tB} := H_G + t_{ts} - Y_{bB} \qquad Y_{tB} = 20.748\ \text{in}$$

**Distance between Neutral Axis and Item center of gravity, d (inch)**

**a.) Top Slab** **b.) Bottom Slab** **c.) Steel**

$$d_{tsB} := h_{tsB} - Y_{bB} \qquad d_{bsB} := h_{bsB} - Y_{bB} \qquad d_{sB} := Y_b - Y_{bB}$$

$$d_{tsB} = 16.748\ \text{in} \qquad d_{bsB} = -33.502\ \text{in} \qquad d_{sB} = -8.569\ \text{in}$$

**Moment of Inertia, $I_0$ ($in^4$)**

$I_{0tsB} := \frac{b_{ts} \cdot t_{ts}^3}{12 \cdot n}$ $I_{0tsB} = 1260.308\ in^4$

$I_{0bsB} := \frac{b_{bs} \cdot t_{bs}^3}{12 \cdot n}$ $I_{0bsB} = 316.615\ in^4$

$I_{st} = 62468.826\ in^4$

$\Sigma I_{0B} := I_{0tsB} + I_{0bsB} + I_{st}$ $\Sigma I_{0B} = 64045.749\ in^4$

$A_{tsB} \cdot d_{tsB}^2 = 66282.897\ in^4$ $A_{bsB} \cdot d_{bsB}^2 = 87028.158\ in^4$ $A_s \cdot d_{sB}^2 = 11653.085\ in^4$

$\Sigma Ad_B := A_{tsB} \cdot d_{tsB}^2 + A_{bsB} \cdot d_{bsB}^2 + A_s \cdot d_{sB}^2$ $\Sigma Ad_B = 164964.139\ in^4$

**Moment of Inertia of whole section with respect to Neutral Axis (N.A.) of whole section, $I_{pc}$ ($in^4$).**

$I_{pc} := \Sigma I_{0B} + \Sigma Ad_B$ $I_{pc} = 229009.888\ in^4$

**Section Modulus required for the weld, Q ($in^3$).**

$Q_{tfB} := \left(H_G - Y_{bB} - \frac{t_{tf}}{2}\right) \cdot A_{tf} + \left(H_G + \frac{t_{ts}}{2} - Y_{bB}\right) \cdot A_{tsB}$ $Q_{tfB} = 4622.556\ in^3$

$Q_{bfB} := A_{bf} \cdot \left(Y_{bB} - \frac{t_{bf}}{2}\right) + A_{bsB} \cdot \left(Y_{bB} - t_{bf} - \frac{t_{bs}}{2}\right)$ $Q_{bfB} = 3657.599\ in^3$

$Q_{TslabB} := A_{tsB} \cdot \left(H_G + \frac{t_{ts}}{2} - Y_{bB}\right)$ $Q_{TslabB} = 3957.671\ in^3$

**Section Modulus of entire section, S ($in^3$)**

$S_{tslabB} := \frac{I_{pc} \cdot n}{Y_{tB}}$ $S_{tslabB} = 71745.105\ in^3$

$S_{tbeamB} := \frac{I_{pc}}{Y_{tB} - t_{ts}}$ $S_{tbeamB} = 17964.44\ in^3$

$S_{bbeamB} := \frac{I_{pc}}{Y_{bB}}$ $S_{bbeamB} = 6127.02\ in^3$

$S_{bslabB} := \frac{I_{pc} \cdot n}{Y_{bB} - t_{bf}}$ $S_{bslabB} = 40229.244\ in^3$

## Short-term Composite Section Properties (n=6.5) C (Negative Live Load Moment)

**Modular Ratio, n**

$n = 6.5$

**a.) Top Rebar**

$A_{rebarC} := R_r \cdot b_{ts} \cdot t_{ts}$

$A_{rebarC} = 15.36\ in^2$

**b.) Bottom Slab**

$A_{bsC} := \frac{b_{bs} \cdot t_{bs}}{n}$

$A_{bsC} = 77.538\ in^2$

**c.) Steel**

$A_s = 158.716\ in^2$

$A_C := A_{rebarC} + A_{bsC} + A_s$

$A_C = 251.614\ in^2$

**The distance from the extreme bottom fiber to the centroid of item center of gravity, h (inch)**

**a.) Top Rebar**

$h_{rebarC} := t_{bf} + D_w + t_{tf} + \frac{t_{ts}}{2}$

$h_{rebarC} = 54.125\ in$

$A_{rebarC} \cdot h_{rebarC} = 831.36\ in^3$

**b.) Bottom Slab**

$h_{bsC} := t_{bf} + \frac{t_{bs}}{2}$

$h_{bsC} = 3.875\ in$

$A_{bsC} \cdot h_{bsC} = 300.462\ in^3$

**c.) Steel**

$Y_b = 28.808\ in$

$A_s \cdot Y_b = 4572.354\ in^3$

$\Sigma Ah_C := A_{rebarC} \cdot h_{rebarC} + A_{bsC} \cdot h_{bsC} + A_s \cdot Y_b$

$\Sigma Ah_C = 5704.176\ in^3$

**Distance from bottom of section to the Neutral Axis (N.A.) of the whole section, $Y_b$ (inch).**

$Y_{bC} := \frac{\Sigma Ah_C}{A_C}$

$Y_{bC} = 22.67\ in$

**Distance from top of section to the Neutral Axis (N.A.) of the whole section, $Y_t$ (inch).**

$Y_{tC} := H_G + t_{ts} - Y_{bC}$

$Y_{tC} = 35.455\ in$

**Distance between Neutral Axis and Item center of gravity, d (inch)**

**a.) Top Rebar**

$d_{rebarC} := h_{rebarC} - Y_{bC}$

$d_{rebarC} = 31.455\ in$

**b.) Bottom Slab**

$d_{bsC} := h_{bsC} - Y_{bC}$

$d_{bsC} = -18.795\ in$

**c.) Steel**

$d_{sC} := Y_b - Y_{bC}$

$d_{sC} = 6.138\ in$

**Moment of Inertia, $I_0$ ($in^4$)**

$I_{rebarC} := 0.0 \cdot in^4$

$I_{0bsC} := \frac{b_{bs} \cdot t_{bs}^3}{12 \cdot n}$

$I_{rebarC} = 0$

$I_{0bsC} = 316.615\ in^4$

$I_{st} = 62468.826\ in^4$

$\Sigma I_{0C} := I_{rebarC} + I_{0bsC} + I_{st}$

$\Sigma I_{0C} = 62785.442\ in^4$

$A_{rebarC} \cdot d_{rebarC}^2 = 15197.138\ in^4$

$A_{bsC} \cdot d_{bsC}^2 = 27391.547\ in^4$

$A_s \cdot d_{sC}^2 = 5979.852\ in^4$

$\Sigma Ad_C := A_{rebarC} \cdot d_{rebarC}^2 + A_{bsC} \cdot d_{bsC}^2 + A_s \cdot d_{sC}^2$

$\Sigma Ad_C = 48568.537\ in^4$

**Moment of Inertia of whole section with respect to Neutral Axis (N.A.) of whole section, $I_u$ ($in^4$).**

$I_u := \Sigma I_{0C} + \Sigma Ad_C$

$I_u = 111353.979\ in^4$

**Section Modulus required for the weld, Q ($in^3$).**

$Q_{tfC} := \left(H_G - Y_{bC} - \frac{t_{tf}}{2}\right) \cdot A_{tf} + \left(H_G + \frac{t_{ts}}{2} - Y_{bC}\right) \cdot A_{rebarC}$

$Q_{tfC} = 1971.606\ in^3$

$Q_{bfC} := A_{bf} \cdot \left(Y_{bC} - \frac{t_{bf}}{2}\right) + A_{bsC} \cdot \left(Y_{bC} - t_{bf} - \frac{t_{bs}}{2}\right)$

$Q_{bfC} = 2098.12\ in^3$

$Q_{BslabC} := A_{bsC} \cdot \left(Y_{bC} - t_{bf} - \frac{t_{bs}}{2}\right)$

$Q_{BslabC} = 1457.36\ in^3$

**Section Modulus of entire section, S ($in^3$)**

$S_{trebarC} := \frac{I_u}{Y_{tC} - \frac{t_{ts}}{2}}$

$S_{trebarC} = 3540.14\ in^3$

$S_{tbeamC} := \frac{I_u}{Y_{tC} - t_{ts}}$

$S_{tbeamC} = 4055.92\ in^3$

$S_{bbeamC} := \frac{I_u}{Y_{bC}}$

$S_{bbeamC} = 4911.884\ in^3$

$S_{bslabC} := \frac{I_u \cdot n}{Y_{bC} - t_{bf}}$

$S_{bslabC} = 32464.253\ in^3$

## Short-term Composite Section Properties (n=6.5) D (For Bridge Deck Loading)

**Modular Ratio, n**

$n = 6.5$

**b.) Bottom Slab**

$A_{bsD} := \frac{b_{bs} \cdot t_{bs}}{n}$

$A_{bsD} = 77.538\ in^2$

**c.) Steel**

$A_s = 158.716\ in^2$

$A_D := A_{bsD} + A_s$

$A_D = 236.254\ in^2$

**The distance from the extreme bottom fiber to the centroid of item center of gravity, h (inch)**

**b.) Bottom Slab**

$h_{bsD} := t_{bf} + \frac{t_{bs}}{2}$

$h_{bsD} = 3.875\ in$

$A_{bsD} \cdot h_{bsD} = 300.462\ in^3$

**c.) Steel**

$Y_b = 28.808\ in$

$A_s \cdot Y_b = 4572.354\ in^3$

$\Sigma Ah_D := A_{bsD} \cdot h_{bsD} + A_s \cdot Y_b$

$\Sigma Ah_D = 4872.816\ in^3$

**Distance from bottom of section to the Neutral Axis (N.A.) of the whole section, $Y_b$ (inch).**

$Y_{bD} := \frac{\Sigma Ah_D}{A_D}$

$Y_{bD} = 20.625\ in$

**Distance from top of section to the Neutral Axis (N.A.) of the whole section, $Y_t$ (inch)**

$Y_{tD} := H_G + t_{ts} - Y_{bD}$

$Y_{tD} = 37.5\ in$

**Distance between Neutral Axis and Item center of gravity, d (inch)**

**b.) Bottom Slab**

$d_{bsD} := h_{bsD} - Y_{bD}$

$d_{bsD} = -16.75\ in$

**c.) Steel**

$d_{sD} := Y_b - Y_{bD}$

$d_{sD} = 8.183\ in$

**Moment of Inertia, $I_0$ ($in^4$)**

$$I_{0bsD} := \frac{b_{bs} \cdot t_{bs}^{3}}{12 \cdot n}$$

$I_{0bsD} = 316.615\ in^4$ $I_{st} = 62468.826\ in^4$

$\Sigma I_{0D} := I_{0bsD} + I_{st}$ $\Sigma I_{0D} = 62785.442\ in^4$

$A_{bsD} \cdot d_{bsD}^{2} = 21755.169\ in^4$ $A_s \cdot d_{sD}^{2} = 10628.193\ in^4$

$\Sigma Ad_D := A_{bsD} \cdot d_{bsD}^{2} + A_s \cdot d_{sD}^{2}$ $\Sigma Ad_D = 32383.362\ in^4$

**Moment of Inertia of whole section with respect to Neutral Axis (N.A.) of whole section, $I_{zD}$ ($in^4$)**

$I_{zD} := \Sigma I_{0D} + \Sigma Ad_D$ $I_{zD} = 95168.804\ in^4$

**Section Modulus required for the weld, Q ($in^3$).**

$$Q_{tfD} := \left(H_G - Y_{bD} - \frac{t_{tf}}{2}\right) \cdot A_{tf}$$ $Q_{tfD} = 1602.983\ in^3$

$$Q_{bfD} := A_{bf} \cdot \left(Y_{bD} - \frac{t_{bf}}{2}\right) + A_{bsD} \cdot \left(Y_{bD} - t_{bf} - \frac{t_{bs}}{2}\right)$$ $Q_{bfD} = 1881.27\ in^3$

$$Q_{BslabD} := A_{bsD} \cdot \left(Y_{bD} - t_{bf} - \frac{t_{bs}}{2}\right)$$ $Q_{BslabD} = 1298.793\ in^3$

**Section Modulus of entire section, S ($in^3$)**

$$S_{tbeamD} := \frac{I_{zD}}{Y_{tD} - t_{ts}}$$ $S_{tbeamD} = 3226.094\ in^3$

$$S_{bbeamD} := \frac{I_{zD}}{Y_{bD}}$$ $S_{bbeamD} = 4614.177\ in^3$

$$S_{bslabD} := \frac{I_{zD} \cdot n}{Y_{bD} - t_{bf}}$$ $S_{bslabD} = 30547.555\ in^3$

## A.6 Calculation of Design Plastic Moment

This section shows detailed calculation of Plastic Neutral Axis ($Y_{PNA}$) and Design Plastic Moment.

### Calculation of Forces

Force in top slab, $P_{re}$ $\quad P_{re} := A_{rebar} \cdot F_{yrebar}$ $\quad P_{re} = 921.6\,kip$

Force in top flange, $P_{tf}$ $\quad P_{tf} := 2 \cdot b_{tf} \cdot t_{tf} \cdot F_{y\_des}$ $\quad P_{tf} = 3920\,kip$

Force in web, $P_w$ $\quad P_w := 2 \cdot D \cdot t_w \cdot F_{y\_des}$ $\quad P_w = 5195\,kip$

Force in bottom flange, $P_{bf}$ $\quad P_{bf} := b_{bf} \cdot t_{bf} \cdot F_{y\_des}$ $\quad P_{bf} = 1995\,kip$

Force in bottom slab, $P_{bs}$ $\quad P_{bs} := 0.85 \cdot f_{c\_des} \cdot b_{bs} \cdot t_{bs}$ $\quad P_{bs} = 2356.2\,kip$

### Calculation of Center of Gravity of Forces

Height of rebar from bottom fiber, $h_{re}$ $\quad h_{re} := t_{bf} + D_w + t_{tf} + \frac{t_{ts}}{2}$ $\quad h_{re} = 54.125\,in$

Height of top flange from bottom fiber, $h_{tf}$ $\quad h_{tf} := t_{bf} + D_w + \frac{t_{tf}}{2}$ $\quad h_{tf} = 49.25\,in$

Height of web from bottom fiber, $h_w$ $\quad h_w := t_{bf} + \frac{D_w}{2}$ $\quad h_w = 24.375\,in$

Height of bottom slab from bottom fiber, $h_{bs}$ $\quad h_{bs} := t_{bf} + \frac{t_{bs}}{2}$ $\quad h_{bs} = 3.875\,in$

Height of bottom flange from bottom fiber, $h_{bf}$ $\quad h_{bf} := \frac{t_{bf}}{2}$ $\quad h_{bf} = 0.187\,in$

Assuming Plastic Neutral Axis to be in the web of box girder section.

$$Y_{pm} := \left(t_{bf} + \frac{D_w}{2}\right) \qquad Y_{pm} = 24.375\,in$$

$$\text{root}\left[P_{re} + P_{tf} + \left(\frac{P_w}{D_w}\right) \cdot \frac{\left(D_w + t_{bf}\right) - Y_{pm}}{\cos(\theta)} - P_{bf} - P_{bs} - \left(\frac{P_w}{D_w}\right) \cdot \frac{Y_{pm} - t_{bf}}{\cos(\theta)}, Y_{pm}\right] = 26.573\,in$$

$$Y_{PNA} := 26.573in$$

$Y_{PNA}$ is the actual position of Plastic Neutral Axis (P.N.A) from the bottom of the section.
$Y_{pm}$ was the trial value used for calculating actual position of neutral axis.

Tension force in the cross section, $T_c$

$$T_c := P_{re} + P_{tf} + \left(\frac{P_w}{D_w}\right)\cdot\left[\frac{\left(D_w + t_{bf}\right) - Y_{PNA}}{\cos(\theta)}\right] \qquad T_c = 7273.88\ \text{kip}$$

Compression force in the cross section, $C_c$

$$C_c := P_{bf} + P_{bs} + \left(\frac{P_w}{D_w}\right)\cdot\left(\frac{Y_{PNA} - t_{bf}}{\cos(\theta)}\right) \qquad C_c = 7273.908\ \text{kip}$$

## Calculation of Moment Arms

$$d_{re} := \left|h_{re} - Y_{PNA}\right| \qquad d_{re} = 27.552\ \text{in}$$

$$d_{tf} := \left|h_{tf} - Y_{PNA}\right| \qquad d_{tf} = 22.677\ \text{in}$$

$$d_w := \left|h_w - Y_{PNA}\right| \qquad d_w = 2.198\ \text{in}$$

$$d_{bs} := \left|h_{bs} - Y_{PNA}\right| \qquad d_{bs} = 22.698\ \text{in}$$

$$d_{bf} := \left|h_{bf} - Y_{PNA}\right| \qquad d_{bf} = 26.386\ \text{in}$$

**Case: 1** Plastic Neutral Axis is in the web.

$$M_{pm} := \left(\frac{P_w}{2\cdot D_w}\right)\cdot\left[\left(\frac{Y_{PNA} - t_{bf}}{\cos(\theta)}\right)^2 + \left(\frac{D + t_{bf} - Y_{PNA}}{\cos(\theta)}\right)^2\right] + P_{re}\cdot d_{re} + P_{tf}\cdot d_{tf} + P_{bs}\cdot d_{bs} + P_{bf}\cdot d_{bf}$$

$$M_{pm} = 24252.33\ \text{ft·kip}$$

## Web Slenderness (AASHTO 6.10.6.2.2)

The section satisfies the web slenderness limit if, $2\cdot\frac{D_{cp}}{t_w} \le 3.76\cdot\sqrt{\frac{E_s}{F_y}}$

$D_{cp}$ = Depth of web in compression at the plastic moment determined as specified in Article D6.3.2 (in)

$t_w$ = Web thickness of the box girder

$E_s$ = Elastic Modulus of the Steel

$F_y$ = Yield strength of the girder (flange and web)

$D_{cp} := Y_{PNA} - t_{bf}$ $\quad D_{cp} = 26.198\,in$

$2\cdot\frac{D_{cp}}{t_w} = 69.861$ $\quad 3.76\cdot\sqrt{\frac{E_s}{F_{y\_des}}} = 76.531$

$CHECK\_1 := if\left(2\cdot\frac{D_{cp}}{t_w} \le 3.76\cdot\sqrt{\frac{E_s}{F_y}}, "OK", "NG"\right)$ $\quad CHECK\_1 = "OK"$

Therefore, section satisfies web slenderness criteria.

## A.7 Calculation of Predicted Plastic Moment

This section shows calculation of Plastic Neutral Axis ($Y_{PNA}$) and Predicted Plastic Moment.

### Calculation of Forces

| | | |
|---|---|---|
| Force in top slab, $P_{re}$ | $P_{re} := A_{rebar} \cdot F_{yrebar}$ | $P_{re} = 921.6\,kip$ |
| Force in top flange, $P_{tf}$ | $P_{tf} := 2 \cdot b_{tf} \cdot t_{tf} \cdot F_y$ | $P_{tf} = 4480\,kip$ |
| Force in web, $P_w$ | $P_w := 2 \cdot D \cdot t_w \cdot F_y$ | $P_w = 5937\,kip$ |
| Force in bottom flange, $P_{bf}$ | $P_{bf} := b_{bf} \cdot t_{bf} \cdot F_y$ | $P_{bf} = 2280\,kip$ |
| Force in bottom slab, $P_{bs}$ | $P_{bs} := 0.85 \cdot f_c \cdot b_{bs} \cdot t_{bs}$ | $P_{bs} = 3213\,kip$ |

### Calculation of Center of Gravity of Forces

| | | |
|---|---|---|
| Height of rebar from Bottom fiber, $h_{re}$ | $h_{re} := t_{bf} + D_w + t_{tf} + \frac{t_{ts}}{2}$ | $h_{re} = 54.125\,in$ |
| Height of top flange from bottom fiber, $h_{tf}$ | $h_{tf} := t_{bf} + D_w + \frac{t_{tf}}{2}$ | $h_{tf} = 49.25\,in$ |
| Height of web from bottom fiber, $h_w$ | $h_w := t_{bf} + \frac{D_w}{2}$ | $h_w = 24.375\,in$ |
| Height of bottom slab from bottom fiber, $h_{bs}$ | $h_{bs} := t_{bf} + \frac{t_{bs}}{2}$ | $h_{bs} = 3.875\,in$ |
| Height of bottom flange from bottom fiber, $h_{bf}$ | $h_{bf} := \frac{t_{bf}}{2}$ | $h_{bf} = 0.187\,in$ |

Assuming Plastic Neutral Axis to be in the web of box girder section.

$$Y_{pm} := \left(t_{bf} + \frac{D_w}{2}\right) \qquad Y_{pm} = 24.375\,in$$

$$\text{root}\left[P_{re} + P_{tf} + \left(\frac{P_w}{D_w}\right) \cdot \frac{(D_w + t_{bf}) - Y_{pm}}{\cos(\theta)} - P_{bf} - P_{bs} - \left(\frac{P_w}{D_w}\right) \cdot \frac{Y_{pm} - t_{bf}}{\cos(\theta)}, Y_{pm}\right] = 24.017\,in$$

$$Y_{PNA} := 24.017in$$

$Y_{PNA}$ is the actual position of Plastic Neutral Axis (P.N.A) from the bottom of the section.
$Y_{pm}$ was the trial value used for calculating actual position of neutral axis.

Tension force in the cross section, $T_c$

$$T_c := P_{re} + P_{tf} + \left(\frac{P_w}{D_w}\right)\cdot\left[\frac{\left(D_w + t_{bf}\right) - Y_{PNA}}{\cos(\theta)}\right] \qquad T_c = 8507.238\,\text{kip}$$

Compression force in the cross section, $C_c$

$$C_c := P_{bf} + P_{bs} + \left(\frac{P_w}{D_w}\right)\cdot\frac{Y_{PNA} - t_{bf}}{\cos(\theta)} \qquad C_c = 8507.349\,\text{kip}$$

## Calculation of Moment Arms

$$d_{re} := \left|h_{re} - Y_{PNA}\right| \qquad d_{re} = 30.108\,\text{in}$$

$$d_{tf} := \left|h_{tf} - Y_{PNA}\right| \qquad d_{tf} = 25.233\,\text{in}$$

$$d_w := \left|h_w - Y_{PNA}\right| \qquad d_w = 0.358\,\text{in}$$

$$d_{bs} := \left|h_{bs} - Y_{PNA}\right| \qquad d_{bs} = 20.142\,\text{in}$$

$$d_{bf} := \left|h_{bf} - Y_{PNA}\right| \qquad d_{bf} = 23.83\,\text{in}$$

**Case: 1** Plastic Neutral Axis is in the web.

$$M_{pm} := \left(\frac{P_w}{2\cdot D_w}\right)\cdot\left[\left(\frac{Y_{PNA} - t_{bf}}{\cos(\theta)}\right)^2 + \left(\frac{D_w + t_{bf} - Y_{PNA}}{\cos(\theta)}\right)^2\right] + P_{re}\cdot d_{re} + P_{tf}\cdot d_{tf} + P_{bs}\cdot d_{bs} + P_{bf}\cdot d_{bf}$$

$$M_{pm} = 27963\,\text{ft·kip}$$

## Web Slenderness (AASHTO 6.10.6.2.2)

The section satisfies the web slenderness limit, if: $2\cdot\frac{D_{cp}}{t_w} \le 3.76\cdot\sqrt{\frac{E_s}{F_y}}$

$D_{cp}$ = Depth of web in compression at the plastic moment determined as specified in Article D6.3.2 (in)

$t_w$ = Web thickness of the box girder

$E_s$ = Elastic Modulus of the Steel

$F_y$ = Yield strength of the girder (flange and web)

$D_{cp} := Y_{PNA} - t_{bf}$ $\qquad D_{cp} = 23.642\,in$

$2\cdot\frac{D_{cp}}{t_w} = 63.045$ $\qquad 3.76\cdot\sqrt{\frac{E_s}{F_y}} = 71.588$

$CHECK\_1 := if\left(2\cdot\frac{D_{cp}}{t_w} \le 3.76\cdot\sqrt{\frac{E_s}{F_y}}, "OK", "NG"\right)$ $\qquad CHECK\_1 = "OK"$

Therefore, section satisfies web slenderness criteria.

## A.8 Design of Shear Connectors (AASHTO 6.10.10)

First moment of transformed short-term composite section, Q: $Q := 1317.459 \cdot in^3$ (see pg-A.13)

Diameter of shear stud, $d_{stud}$: $d_{stud} := 0.75 \cdot in$

Area of shear stud, $A_{sc}$: $A_{sc} := \frac{\pi \cdot d_{stud}^2}{4}$ $A_{sc} = 0.442\ in^2$

Ultimate strength of shear stud, $F_{us}$: $F_{us} := 60 \cdot ksi$

Resistance factor for shear studs, $\Phi_{sc}$: $\phi_{sc} := 0.85$ **(AASHTO C6.5.4.2)**

### Fatigue Limit State

Number of cycles, $N_s$: $N_s := 5650000$ (see Appendix D)

$\alpha := 34.5 - 4.28 \cdot \log(N_s)$ **(AASHTO 6.10.10.2-2)**

$\alpha = 5.601$

As per **(AASHTO 6.10.10.2-1)** $Z_r = \alpha \cdot d_{stud}^2 \geq \frac{5.5 \cdot d^2}{2}$. In this case

$\alpha \cdot d_{stud}^2 \cdot ksi = 3.151\ kip$ which is greater than $\frac{5.5 \cdot d_{stud}^2}{2} \cdot ksi = 1.547\ kip$.

Therefore,

$Z_r = \alpha \cdot d_{stud}^2 \cdot ksi = 3.151\ kip$

$Z_r := \alpha \cdot d_{stud}^2 \cdot ksi$ $Z_r = 3.151\ kip$

### Ultimate Limit State

Nominal shear resistance of one shear stud, $Q_n$ (kips): $Q_n := A_{sc} \cdot F_{us}$ **(AASHTO 6.10.10.4.3-1)**

$Q_n = 26.507\ kip$

As per **(AASHTO 6.10.10.4.3-1)** $Q_n = 0.5 A_{sc} \cdot \sqrt{f_c \cdot E_c} \leq A_{sc} \cdot F_{us}$. In this case

$0.5 A_{sc} \cdot \sqrt{f_c \cdot E_c} = 40.54\ kip$ which is greater than $A_{sc} \cdot F_{us} = 26.507\ kip$. Therefore,

$Q_n = A_{sc} \cdot F_{us}$. $Q_n = 26.507\ kip$

Therefore, design of shear stud is governed by Fatigue limit state and not by Ultimate limit state.

**Force in Top slab, $P_{tslab}$** **(AASHTO 6.10.10.4.2-6)**

$P_{tslab} := 0.45 \cdot f_{c\_des} \cdot t_{ts} \cdot b_{ts}$ $P_{tslab} = 3801.6\,kip$

**Number of shear studs in Top flange**

$n_{top} := round\left(\frac{P_{tslab}}{\phi_{sc} \cdot Q_n}\right)$ $n_{top} = 169$

**Force in Bottom slab, $P_{bslab}$** **(AASHTO 6.10.10.4.2-2)**

$P_{bslab} := 0.85 \cdot f_{c\_des} \cdot t_{bs} \cdot b_{bs}$ $P_{bslab} = 2356.2\,kip$

**Number of shear studs in Bottom flange**

$n_{bottom} := round\left(\frac{P_{bslab}}{\phi_{sc} \cdot Q_n}\right)$ $n_{bottom} = 105$

Distribute 169 on two top flanges equally. Distribute 105 connectors throughout the bottom flange.

**Pitch of the shear connectors along longitudinal axis (AASHTO 6.10.10.1.2).**

$P_{sc} \le \frac{n \cdot Z_r}{V_{sr}}$ **(AASHTO 6.10.10.1.2-1)**

where, $V_{sr}$ = horizontal fatigue shear range per unit length (kip/ft)

n = number of shear connectors across the width of cross-section $n := 9$

$Z_r$ = fatigue resistance of individual shear connectors

$P_{sc}$ = Pitch of shear connector along longitudinal axis

$V_{sr} := \frac{P_f \cdot Q}{I_u}$ $V_{sr} = 14.198\,klf$ **(AASHTO 6.10.10.1.2-2)**

where, $P_f$ = fatigue loading

Q = first moment of the transformed short-term area of the concrete slab about the neutral axis of the short term composite section

$I_u$ = moment of inertia of the short-term composite section.

$P_{sc} := \frac{n \cdot Z_r \cdot ksi}{V_{sr}}$ $P_{sc} = 287.606\,klf$ **(AASHTO 6.10.10.1.2-1)**

Provides shear connectors @ longitudinal pitch of 23 inch for both top and bottom flange.

## A.9 Tip Deflection

All the deflections are reported at the location of actuator load application. The deflections at the tip are 2 times the deflection of a fixed end supported cantilever beam. Neglect the reduction in section properties 1 feet prior to load application point. Deflection calculation assumes that the slab continues to the point of actuator.

Shear deflections are based on shape or form factors and the shear modulus of the beam. The formula for shear deflection comes from *Design of Welded Structures*, by *Blodgett.* However the simplified form factor comes from *Mechanics of Materials* by *Gere and Timoshenko.*

shape factor, $\alpha = \frac{A_{total}}{A_{web}}$ $A_{total} := 472.6 \cdot in^2$ $A_{web} := 2 \cdot D \cdot t_w$

$A_{web} = 74.216\ in^2$

$\alpha_{comp} := \frac{A_{total}}{A_{web}}$ $\alpha_{comp} = 6.368$

For Steel only: $\alpha_{stl} := \frac{A_{gird}}{A_{web}}$ $\alpha_{stl} = 2.139$

At Ultimate: $A_{ult} := 241.3 \cdot in^2$ $\alpha_{ult} := \frac{A_{ult}}{A_{web}}$ $\alpha_{ult} = 3.251$

### Dead Load Deflections (Bending and Shear)

Considering steel only

$$\Delta_{st} := 2 \cdot (w_{gird} + w_{det}) \cdot \left( \frac{b^4}{8 \cdot E_s \cdot I_{st}} + \frac{b^2 \cdot \alpha_{stl}}{2 \cdot A_{gird} \cdot G_s} \right) \qquad \Delta_{st} = 0.061\ in$$

Bottom slab on steel

$$\Delta_{bs} := 2 \cdot w_{bs} \cdot \left( \frac{b^4}{8 \cdot E_s \cdot I_{st}} + \frac{b^2 \cdot \alpha_{stl}}{2 \cdot A_{gird} \cdot G_s} \right) \qquad \Delta_{bs} = 0.055\ in$$

Top slab on steel with bottom slab

$$\Delta_{ts} := 2 \cdot w_{ts} \cdot \left( \frac{b^4}{8 \cdot E_s \cdot I_{bsc}} + \frac{b^2 \cdot \alpha_{stl}}{2 \cdot A_{gird} \cdot G_s} \right) \qquad \Delta_{ts} = 0.116\ in$$

Total Deadload Deflection

$\Delta_{DL} := \Delta_{st} + \Delta_{bs} + \Delta_{ts}$ $\Delta_{DL} = 0.231\ in$

## Actuator Load Deflections

Deflection considering only service load

$$\Delta_{svc} := 2 \cdot P_{svc} \cdot \left( \frac{b^3}{3 \cdot E_s \cdot I_{pc}} + \frac{b \cdot \alpha_{comp}}{A_{total} \cdot G_s} \right) \qquad \Delta_{svc} = 0.577 \text{ in}$$

Deflection considering only fatigue load

$$\Delta_{ftg} := 2 \cdot P_f \cdot \left( \frac{b^3}{3 \cdot E_s \cdot I_{pc}} + \frac{b \cdot \alpha_{comp}}{A_{total} \cdot G_s} \right) \qquad \Delta_{ftg} = 0.343 \text{ in}$$

Deflection considering only ultimate load

$$\Delta_{ult} := 2 \cdot P_u \cdot \left( \frac{b^3}{3 \cdot E_s \cdot I_u} + \frac{b \cdot \alpha_{ult}}{A_{ult} \cdot G_s} \right) \qquad \Delta_{ult} = 8.047 \text{ in}$$

**Note:** Maximum calculated deflection does not account for portion of deflection that occurs prior to the top slab cracking.

## A.10 Flange Bracing Requirements

### Bottom Flange in Compression (AASHTO 6.11.3.2)

Largest moment causing compression in an unbraced section of the bottom flange, $M_{bmb}$;

$$M_{bmb} := 1.25 \cdot \frac{(w_{gird} + w_{det} + w_{bs}) \cdot b^2}{2} \qquad M_{bmb} = 442.126\ ft \cdot kip$$

The stress in the bottom flange under this loading is defined as, $f_{bu}$ ;

$$f_{bu} := \frac{M_{bmb}}{S_{b\_st}} \qquad f_{bu} = 2.447\ ksi$$

**Nominal flexural resistance of the bottom flange in compression, $F_{nc}$**

The slenderness of the bottom flange is defined by $\lambda_f$;

$$\lambda_f := \frac{b_{bf}}{t_{bf}} \qquad \lambda_f = 202.667 \qquad \textbf{(AASHTO 6.11.8.2.2-4)}$$

For the case of zero torsion on the member; **(AASHTO 6.11.8.2.2)**

$f_v$ = St. Venant torsional shear stress in the flange due to the factored loads at the section under consideration. (ksi)

As there is no torsion in the member **(AASHTO 6.11.8.2.2-6)**

$f_v := 0 \cdot ksi$

$k_{BF}$ is the plate buckling coefficient for uniform normal stress

$k_{BF} := 4.0$

$k_s$ is the plate buckling coefficient for shear stress

$k_S := 5.34$

$$\Delta := \sqrt{1 - 3 \cdot \left(\frac{f_v}{F_{y\ des}}\right)} \qquad \Delta = 1 \qquad \textbf{(AASHTO 6.11.8.2.2-5)}$$

$R_1$ = constant which when multiplied by $\sqrt{\frac{k_{BF} \cdot E_s}{F_{y\_des}}}$ yields the slenderness ratio equal to 0.6 times the slenderness ratio for which $F_{nc}$ from Eq. 3 is equal to $R_b \cdot R_h \cdot F_{y\_des} \cdot \Delta$.

Where $R_b$ = web load shedding factor and $R_h$ = hybrid factor.

$$R_1 := \frac{0.57}{\sqrt{\frac{1}{2}\cdot\left[\Delta + \sqrt{\Delta^2 + 4\cdot\left(\frac{f_v}{F_{y\_des}}\right)^2\cdot\left(\frac{k_{BF}}{k_s}\right)^2}\right]}}$$ **(AASHTO 6.11.8.2.2-8)**

$R_1 = 0.57$ $\qquad R_1\cdot\sqrt{\frac{k_{BF}\cdot E_s}{F_{y\_des}}} = 23.204$

$F_{yr}$ = smaller of the compression-flange stress at the onset of the nominal yielding, with consideration of residual stress effects, or the specified minimum yield of the web (ksi)

$F_{yr} := (\Delta - 0.4)\cdot F_{y\_des}$ $\qquad F_{yr} = 42\,ksi$

$R_2$ = constant which when multiplied by $\sqrt{\frac{k_{BF}\cdot E_s}{F_{y\_des}}}$, yields the slenderness ratio for which $F_{nc}$ from Eq. 3 is equal to $F_{yr.}$

$$R_2 := \frac{1.23}{\sqrt{\frac{1}{1.2}\cdot\left[\frac{F_{yr}}{F_{y\_des}} + \sqrt{\left(\frac{F_{yr}}{F_{y\_des}}\right)^2 + 4\cdot\left(\frac{f_v}{F_{y\_des}}\right)^2\cdot\left(\frac{k_{BF}}{k_s}\right)^2}\right]}}$$

$R_2 = 1.23$ $\qquad R_2\cdot\sqrt{\frac{k_{BF}\cdot E_s}{F_{y\_des}}} = 50.071$

As $\lambda_f$ is less than $R_2\cdot\sqrt{\frac{k_{BF}\cdot E_s}{F_{y\_des}}}$, $F_{nc}$ is defined by **(AASHTO 6.11.8.2.2-3).**

$R_b := 1.0$

When computing the nominal flexural resistance of the compression flange for checking constructibility according to the provisions of Article 6.10.3.2, $R_b$ is always taken equal to 1.0. **(AASHTO C6.10.1.10.2)**

$$F_{nc} := \frac{0.9\cdot E_s\cdot R_b\cdot k_{BF}}{\lambda_f^2} - \frac{R_b\cdot f_v^2\cdot k_{BF}}{0.9\cdot E_s\cdot k_s^2}\cdot\lambda_f^2$$ **(AASHTO 6.11.8.2.2-3)**

$F_{nc} = 2.542\,ksi$

$CHECK\_3 := \text{if}\left(F_{nc} > f_{bu}, \text{"OK"}, \text{"NG"}\right)$ $\qquad CHECK\_3 = \text{"OK"}$

## Top Flange in Compression (AASHTO 6.10.3.2)

Largest moment causing compression in an unbraced section of top flange, $M_{bmt}$
Worst case would be loading only the specimen between the supports

$$M_{bmt} := 1.25 \cdot \frac{(w_{gird} + w_{det} + w_{bs} + w_{ts}) \cdot a^2}{8} \qquad M_{bmt} = 225.804\ \text{ft·kip}$$

The top and bottom fiber stresses in the girder are based on the section with a composite bottom flange (see pg-A.15).

$$S_{t\_bsc} := 3205 \cdot in^3 \qquad S_{b\_bsc} := 4305 \cdot in^3$$

Stresses in Tension and Compression respectively

$$f_t := \frac{M_{bmt}}{S_{b\_bsc}} \qquad f_t = 0.629\ \text{ksi}$$

$$f_{cm} := \frac{M_{bmt}}{S_{t\_bsc}} \qquad f_{cm} = 0.845\ \text{ksi}$$

The depth of web in compression

$$D_c := \left(\frac{f_{cm}}{f_{cm} + f_t}\right) \cdot H_G - t_{tf} \qquad D_c = 26.983\ \text{in}$$

Top flange bracing requirements are given by **(AASHTO 6.10.1.6)**

The limiting flexural unbraced length to achieve nominal flexural resistance of $F_y$ is $L_p$. In order to calculate $L_p$ we must calculate effective radius of gyration for lateral torsional buckling, $r_t$.

$$r_t := \frac{b_{tf}}{\sqrt{12\left(1 + \frac{D_c \cdot t_w}{3 b_{tf} \cdot t_{tf}}\right)}} \qquad r_t = 4.146\ \text{in}$$

$$L_p := r_t \cdot \sqrt{\frac{E_s}{F_{y\_des}}} \qquad L_p = 84.393\ \text{in} \qquad \textbf{(AASHTO 6.10.8.2.3-4)}$$

$$L_r := \pi \cdot r_t \cdot \sqrt{\frac{E_s}{0.7 \cdot F_{y\_des}}} \qquad L_r = 316.889\ \text{in} \qquad \textbf{(AASHTO 6.10.8.2.3-5)}$$

$$L_{b\_max} := 1.2 \cdot L_p \cdot \sqrt{\frac{1}{\frac{f_{cm}}{F_{y\_des}}}} \qquad L_{b\_max} = 921.499\ in \qquad \textbf{(AASHTO 6.10.1.6-2)}$$

We will use intermediate diaphragms at 12.5 feet each side of the center support.

Therefore

$L_b := 12.5 \cdot ft$

## Lateral Bending Moment Due to Placement of Top Slab

Conservatively the vertical reaction at one brace,

$$V_b := \frac{1}{2} \cdot w_{rc} \cdot 8 \cdot in \cdot 12.5 \cdot ft \cdot 4 \cdot ft \qquad V_b = 2.5\ kip$$

The slope of the bracing is approximately 1:1. This make the lateral force equal to the vertical force.

The distributed lateral force on each top flange due to deck placement is defined as $w_{lat.}$

$$w_{lat} := \frac{V_b}{L_b} \qquad w_{lat} = 0.2\ klf$$

The maximum factored lateral moment experienced by the top flange is $M_{lat}$

$$M_{lat} := 1.25 \cdot \frac{w_{lat} \cdot L_b^{\,2}}{8} \qquad M_{lat} = 4.883\ ft \cdot kip$$

The lateral section modulus of the top flange is defined by $S_{TF\_I}$

$$S_{TF\_1} := \frac{t_{tf} \cdot b_{tf}^{\,2}}{6} \qquad S_{TF\_1} = 74.667\ in^3$$

The lateral stress in top flange is defined by $f_l$

$$f_l := \frac{M_{lat}}{S_{TF\_1}} \qquad f_l = 0.785\ ksi$$

The nominal flexural resistance of top flange is $F_{nc\_t}$

$$F_{nc\_t} := \left[1 - (1 - 0.7) \cdot \left(\frac{L_b - L_p}{L_r - L_p}\right)\right] \cdot F_{y\_des} \qquad \textbf{(AASHTO 6.10.8.2.3-2)}$$

$F_{nc\_t} = 64.074\ ksi$

$$CHECK\_2 := if\left(F_{nc\_t} > f_{cm} + \frac{f_l}{3}, "OK", "NG"\right) \qquad \textbf{(AASHTO 6.10.3.2.1-2)}$$

$CHECK\_2 = "OK"$

## A.11 Design of Loading Cross Frame

### Design of Diagonal Members

The fatigue loading at the mid point of the cross frame will control design of the diagonals. The top tie of the cross frame will not experience any bending during loading. The angle of the diagonals with the top tie is defined as $\theta_{d\_lcf.}$ The angle of the diagonal with the top tie is approximately 40 degrees.

$\theta_{d\_lcf} := 40 \cdot deg$

Fatigue force in the diagonal is defined as $F_{d\_lcf.}$

$F_{d\_lcf} := 1.75 \cdot P_f \cdot \frac{1}{2 \cdot \sin(\theta_{d\_lcf})}$ $F_{d\_lcf} = 136.126\ kip$

Try double angle (6 x 4 x 1/2) with $F_y$= 50 ksi

$F_{y\_cf} := 50 \cdot ksi$

The maximum length of the diagonal is 4.5 feet depending on the size of member chosen for the top tie.

The length of the diagonal member is defined as $L_{d\_lcf.}$
The gross cross sectional area of the double angle section is defined as $As_{d\_lcf.}$
The minimum radius of gyration is defined as $r_{min\_lcf.}$

$L_{d\_lcf} := 4.5 \cdot ft$ $As_{d\_lcf} := 9.5 \cdot in^2$ $r_{min\_lcf} := 1.91 \cdot in$

$k := 0.75$ **(AASHTO 4.6.2.5)**

$\frac{k \cdot L_{d\_lcf}}{r_{min\_lcf}} = 21.204$

Calculate the factored resistance in pure compression which is defined as $P_{r\_lcf.}$

Resistance factor in pure compression is defined as $\phi_c$

$\phi_c := 0.9$ **(AASHTO 6.5.4.2)**

Nominal compressive resistance is defined as $P_{n.}$ **(AASHTO 6.9.4)**

$\lambda := \left(\frac{k \cdot L_{d\_lcf}}{r_{min\_lcf} \cdot \pi}\right)^2 \cdot \frac{F_{y\_cf}}{E_s}$ **(AASHTO 6.9.4.1-3)**

$\lambda = 0.079$

As $\lambda \le 2.25$, then $P_n := 0.66^{\lambda} \cdot F_{y\_cf} \cdot As_{d\_lcf}$ from **(AASHTO 6.9.4.1-1)**

$P_n = 459.748\ kip$

$P_r := \phi_c \cdot P_n$ $\quad P_r = 413.773\ kip$ **(AASHTO 6.9.2.1-1)**

$CHECK\_4 := if\left(F_{d\_lcf} < P_r, "OK", "NG"\right)$ $\quad CHECK\_4 = "OK"$

**Check the number of 7/8 inch diameter A325 bolts required to resist the compression in the double angle diagonals.**

**Minimum number of bolts required**

$d_{bolt} := 0.875 \cdot in$

Tensile strength of A325 bolts is defined as $F_{ub.}$

$F_{ub} := 120 \cdot ksi$

Area of bolt is defined as $A_{bolt.}$

$A_{bolt} := \pi \cdot \frac{d_{bolt}^2}{4}$ $\quad A_{bolt} = 0.601\ in^2$

Number of shear planes is defined as $N_{sh.}$

$N_{sh} := 2$

**Minimum numbers of bolts required based on Shear capacity of bolts.** **(AASHTO 6.13.2.7)**

Nominal shear resistance of the bolt is defined as $R_{n\_bolt.}$

$R_{n\_bolt} := 0.48 \cdot A_{bolt} \cdot F_{ub} \cdot N_{sh}$ **(AASHTO 6.13.2.7-1)**

$R_{n\_bolt} = 69.272\ kip$

$N_{b\_min} := round\left(\frac{F_{d\_lcf}}{R_{n\_bolt}}\right)$ $\quad N_{b\_min} = 2$

**Minimum number of bolts required based on bearing strength of the bolt holes.** **(AASHTO 6.13.2.9)**

Assume for Grade 50 Angles

$F_u := 70 \cdot ksi$

The minimum material thickness is defined by t = 0.5 inch and the clear edge distance is $L_c$ = 0.781 inch. This value is used since the top tie will likely use same connection and will be in tension.

$L_c := 0.781 \cdot in$ $\quad t := 0.5 \cdot in$

Assuming that the angles control :

$R_{n\_hole} := 1.2 \cdot F_u \cdot t \cdot L_c$ **(AASHTO 6.13.2.9-4)**

$R_{n\_hole} = 32.802\,kip$

$N_{bh\_min} := ceil\left(\frac{0.5 \cdot F_{d\_lcf}}{R_{n\_hole}}\right)$ $N_{bh\_min} = 3$

Assuming that connection plate controls.
Length and thickness of connection plate are defined as $L_{c\_conpl}$ and $t_{conpl}$ respectively.

$L_{c\_conpl} := 1 \cdot in$ $t_{conpl} := 0.75 \cdot in$

$R_{nc\_hole} := 1.2 \cdot L_{c\_conpl} \cdot t_{conpl} \cdot F_u$ $R_{nc\_hole} = 63\,kip$

$N_{bc\_min} := ceil\left(\frac{F_{d\_lcf}}{R_{nc\_hole}}\right)$ $N_{bc\_min} = 3$

**Use double angle (6 x 4 x 1/2) inch connected with three 7/8 inch diameter High Strength bolts at each end. Use 3/4 inch minimum connection plates.**

**Note:** A doule angle (8 x 8 x 1/2) inch member was used in the final design to accommodate the top bearing plate and fatigue load bearing stiffeners.

## Design of Top Tie

The top tie of the loading cross frame will be controlled by the ultimate loading which is applied equally to each flange. The load experienced by the top tie is due to angle of the web. The inclination of web is 1 : 4.

The horizontal tension load that must be carried by Top Tie is defined as $T_{lcf.}$

$T_{lcf} := 0.25 \cdot \frac{P_u}{2}$ $T_{lcf} = 159.706\,kip$

By inspection, double angle (L8 x 8 x 1/2) inch are more than adequate to carry the tension required for the ultimate loading. Therefore only design of connection is considered.

Minimum number of bolts required based on the shear capacity of the bolts :

$N_{bt\_min} := ceil\left(\frac{T_{lcf}}{R_{n\_bolt}}\right)$ $N_{bt\_min} = 3$

Minimum number of bolts required based on the bearing strength of the bolt. **(AASHTO 6.13.9.2)**

Assume that angle controls:

$L_{ct} := 1 \cdot in$

$R_{nt\_hole} := 1.2 \cdot L_{ct} \cdot t \cdot F_u$ $\quad R_{nt\_hole} = 42\,kip$

$N_{btb\_min} := ceil\left(\frac{0.5 \cdot T_{lcf}}{R_{n\_hole}}\right)$ $\quad N_{btb\_min} = 3$

**Use double angle (8 x 8 x 1/2) with four 7/8 inch diameter high strength bolts per end and use 5 bolts spaced at 6 inch max to connect the top and middle 7/8 inch thick connection plate to the cross frame to the angles.**

## Design of Connection Plate Welds

Assume that the top flange to connection plate weld carries the horizontal force. The minimum weld thickness assuming welds on both sides of the connection plate is defined by $t_{w\_dmin.}$

$$t_{w\_dmin} := \frac{T_{lcf}}{2 \cdot 0.48 \cdot 70 \cdot ksi \cdot 0.707 \cdot (8 \cdot in - 0.375 \cdot in - 1.5 \cdot in - 0.5 \cdot in - 0.5 \cdot in)}$$

$t_{w\_dmin} = 0.656\,in$

**Use 11/16 inch welds for top flange to the connection plate.**

**Check fatigue in the weld.**

$N_{cycles} := 5.65 \cdot 10^6$

Welds loaded longitudinally are category 'E' Details on the weld metal.

Allowable fatigue stress is defined as $F_{f.}$

$F_f := \left(\frac{11 \cdot 10^8 \cdot ksi^3}{N_{cycles}}\right)^{\frac{1}{3}}$ $\quad F_f = 5.796\,ksi$

The actual longitudinal stress in the weld is based on the angle of the diagonal with the web.

$T_{fatigue} := 0.25 \cdot \frac{P_f}{2}$ $\quad T_{fatigue} = 12.5\,kip$

$$\sigma_{weld} := \frac{T_{fatigue}}{2 \cdot 0.707 \cdot 0.6875 \cdot in \cdot (8 \cdot in - 0.375 \cdot in - 1.5 \cdot in - 0.5 \cdot in - 0.5 \cdot in)}$$

$\sigma_{weld} = 2.509\,ksi$

$CHECK\_5 := \text{if}(\sigma_{weld} < F_f, \text{"OK"}, \text{"NG"})$ $CHECK\_5 = \text{"OK"}$

Assuming that connection plate to web weld transfers the vertical force from the diagonals. This vertical force is defined as $T_{wcf.}$

$T_{wcf} := 1.75 \cdot \frac{P_f}{2}$ $T_{wcf} = 87.5\,\text{kip}$

The minimum thickness of weld required to resist this force is defined as $t_{w\_min.}$

$$t_{w\_min} := \frac{T_{wcf}}{2 \cdot 0.48 \cdot 0.707 \cdot 70 \cdot \text{ksi} \cdot (33 \cdot \text{in} - 4 \cdot \text{in} - 0.5 \cdot \text{in} - 0.5 \cdot \text{in})}$$

$t_{w\_min} = 0.066\,\text{in}$

Try 5/16 inch weld and check fatigue.

$$\sigma_{weld\_w} := \frac{\frac{T_{wcf}}{1.75}}{2 \cdot 0.707 \cdot 0.3125 \cdot \text{in} \cdot (33 \cdot \text{in} - 4 \cdot \text{in} - 0.5 \cdot \text{in} - 0.5 \cdot \text{in})}$$

$\sigma_{weld\_w} = 4.041\,\text{ksi}$

$CHECK\_6 := \text{if}(\sigma_{weld\_w} < F_f, \text{"OK"}, \text{"NG"})$ $CHECK\_6 = \text{"OK"}$

**Use 5/16 inch weld for connection plate and web.**

## Design of Bottom Tie

The ultimate force in the bottom tie is defined as $T_{bot\_tie.}$

$T_{bot\_tie} := 1.75 \cdot P_f \cdot \frac{1}{2 \cdot \tan(\theta_{d\_lcf})}$ $T_{bot\_tie} = 104.278\,\text{kip}$

By inspection, the double angles (L4 x 4 x 1/2) inch have sufficient section area to resist tension force.

The number of bolts required to transfer the forces into the bottom flange is defined as $N_{bb\ min.}$

$N_{bb\_min} := \text{ceil}\left(\frac{T_{bot\_tie}}{0.5 \cdot R_{n\_bolt}}\right)$ $N_{bb\_min} = 4$

Based on the bearing strength of the bolt holes **(AASHTO 6.13.2.9)**

Assuming that bottom flange controls

$R_{nb\_hole} := 2.4 \cdot 0.875 \cdot \text{in} \cdot t_{bf} \cdot F_u$ $R_{nb\_hole} = 55.125\,\text{kip}$

$$N_{bs\_min} := \text{ceil}\left(\frac{T_{bot\_tie}}{R_{nb\_hole}}\right) \qquad N_{bs\_min} = 2$$

Use 2 L4 x 4 x 1/2 angles with 13 numbers of 7/8 inch dia HS bolts to connect to the connection plate. Use 15 bolts (per angle 30 total) to connect angles to the bottom flange of the box girder.

## Design of Loading Plate Stiffeners

The bearing area required for Loading plate is defined as $A_{bearing}$.

$$A_{bearing} := \frac{1.75 \cdot P_f}{1.4 \cdot F_{y\_cf}} \qquad A_{bearing} = 2.5\,in^2$$

For four, two sided stiffeners, the minium thickness required is $t_{bearing}$.

$$t_{bearing} := \frac{A_{bearing}}{(8 \cdot in - 0.5 \cdot in) \cdot 4 \cdot 2} \qquad t_{bearing} = 0.042\,in$$

The minimum thickness based on b = 8 inch is defined as $t_{abearing}$.

$$t_{abearing} := \frac{8 \cdot in}{0.48 \cdot \sqrt{\frac{E_s}{F_{y\_cf}}}} \qquad t_{abearing} = 0.692\,in$$

Design of weld for stiffeners. The minimum thickness required of weld is defined as $t_{weldmin}$.

$$t_{weldmin} := \frac{\frac{1.75 \cdot P_f}{8}}{2 \cdot 0.48 \cdot 0.707 \cdot 70 \cdot ksi \cdot (8 \cdot in - 0.5 \cdot in - 0.5 \cdot in - 0.5 \cdot in)}$$

$$t_{weldmin} = 0.071\,in$$

Try 5/16 inch weld and Check for Fatigue.

Allowable stress in the weld for the stiffeners is defined as $\sigma_{sweld}$.

$$\sigma_{sweld} := \frac{\frac{P_f}{8}}{2 \cdot 0.707 \cdot 0.3125 \cdot in \cdot (8 \cdot in - 0.5 \cdot in - 0.5 \cdot in - 0.5 \cdot in} \qquad \sigma_{sweld} = 4.352\,ksi$$

$$CHECK\_7 := \text{if}\left(\sigma_{sweld} < F_f, \text{"OK"}, \text{"NG"}\right) \qquad CHECK\_7 = \text{"OK"}$$

**Use 3/4 inch Stiffeners and 5/16 inch welds**

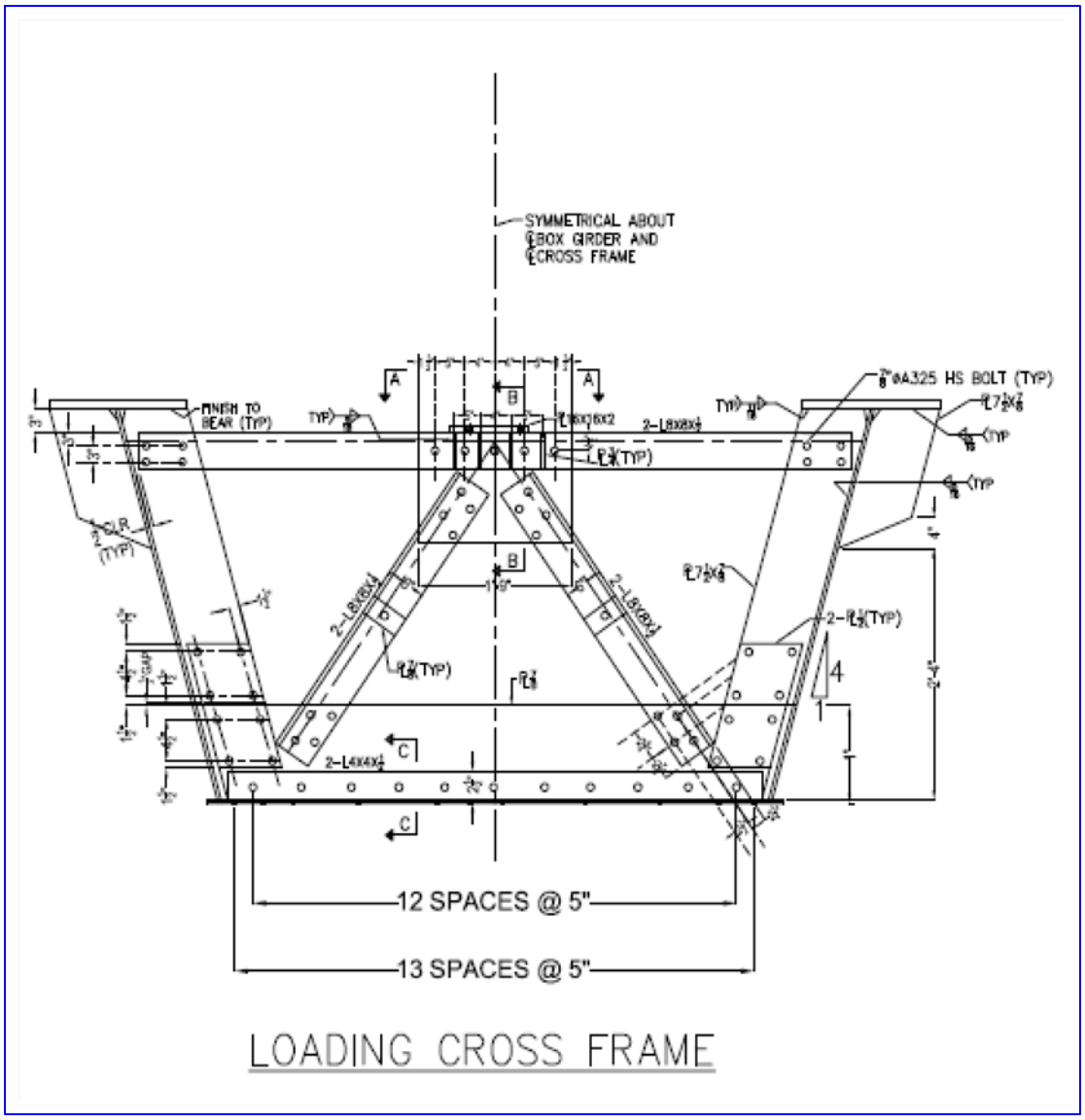


**Figure A.2** Loading Cross Frame

## A.12 Design of Intermediate Cross-Frame

The intermediate cross frames are primarily used to brace the top flanges during the placement of the concrete deck slab. However, they will also help to maintain the shape of the box as it is loaded.

The force in the top member of an intermediate cross frame is defined as $F_{top.}$

The force in the two diagonal members is defined as $F_{d,}$ as the force in both members is the same.

The angle of inclination between the top horizontal member and the diagonal members is defined as $\theta_{lcf.}$

$\theta_{lcf} := 45.67 \cdot deg$

$F_{top} := 1.25 \cdot w_{lat} \cdot L_b$ $\quad F_{top} = 3.125\ kip$

$F_d := \frac{F_{top}}{\cos(\theta_{lcf})}$ $\quad F_d = 4.472\ kip$

Assume that the cross frame members are L4 x 4 x 1/4 angles with two 7/8 inch diameter bolts at each ends.

The maximum length of each diagonal is approximately 4.5 feet. This is also the maximum unbraced length for all cross frame members. The length is defined as $L_{d\_cf.}$

The gross cross-sectional area of the section is defined as $As_{d\_cf.}$

The minimum radius of gyration is defined as $r_{min\_cf.}$

The section modulus is defined as $S_{d\_cf.}$

$L_{d\_cf} := 4.5 \cdot ft$ $\quad As_{d\_cf} := 1.94 \cdot in^2$ $\quad r_{min\_cf} := 0.78 \cdot in$

$S_{d\_cf} := 1.05 \cdot in^3$

$k = 0.75$ **(AASHTO 4.6.2.5)**

$\frac{k \cdot L_{d\_cf}}{r_{min\_cf}} = 51.923$

Calculate the factored resistance in pure compression which is defined as $P_{r\_cf.}$

Resistance factor in pure compression is defined as $\phi_c$

$\phi_c = 0.9$ **(AASHTO 6.5.4.2)**

Nominal compressive resistance is defined as **(AASHTO 6.9.4)**

$$\lambda_{cf} := \left(\frac{k \cdot L_{d\_cf}}{r_{min\_cf} \cdot \pi}\right)^2 \cdot \frac{F_{y\_cf}}{E_s}$$ **(AASHTO 6.9.4.1-3)**

$\lambda_{cf} = 0.471$

As $\lambda_{cf} \le 2.25$, then $P_{n\_cf} := 0.66^{\lambda_{cf}} \cdot F_{y\_cf} \cdot As_{d\_cf}$ from **( AASHTO 6.9.4.1-1)**

$P_{n\_cf} = 79.759\,kip$

$P_{r\_cf} := \phi_c \cdot P_{n\_cf}$ $P_{r\_cf} = 71.784\,kip$ **(AASHTO 6.9.2.1-1)**

$CHECK\_8 := if(F_d < P_{r\_cf}, "OK", "NG")$ $CHECK\_8 = "OK"$

Moments applied due to the eccentricity of the connection are defined as $M_x$ and $M_{y.}$

$M_x := F_d \cdot (1.5 - 1.18) \cdot in$ $M_x = 0.119\,ft \cdot kip$

$M_y := F_d \cdot (1.18 - 0.25) \cdot in$ $M_y = 0.347\,ft \cdot kip$

The maximum resisting moment of the angle is defined as $M_{r.}$

$M_r := F_{y\_cf} \cdot S_{d\_cf}$ $M_r = 4.375\,ft \cdot kip$

Check beam/column interaction :

$$CHECK\_9 := if\left(\frac{F_d}{P_{r\_cf}} + \frac{M_x + M_y}{M_r} < 1.0, "OK", "NG"\right)$$ $CHECK\_9 = "OK"$

**Use L4 x 4 x 1/2 inch angles for all members of the intermediate cross frame and connect them using two 7/8 inch diameter HS bolts per end. Use 3/4 inch connection plate thickness to match the plates used elsewhere.**

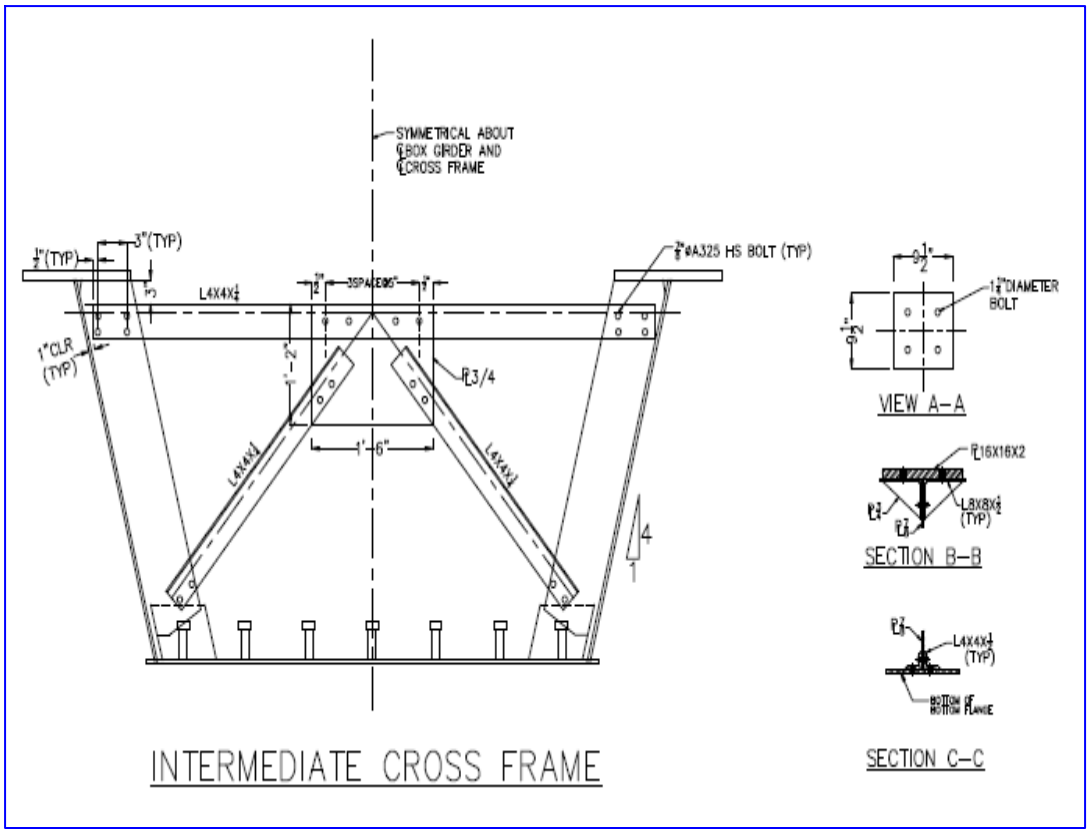


**Figure A.3** Intermediate Cross Frame

## A.13 Design of the Bearing Diaphragms

The "pier" diaphragm shall be fully designed since it is subjected to the largest loads and the end diaphragm shall use the same design.

The bearing diaphragm plate should be sized to meet the D/t ratio of the stiffened vertical web of an I girder as per AASHTO LRFD 6.10.6.2.

The thickness of the diaphragm plate is defined as $t_d$.

The depth of the diaphragm plate is defined as $D_d$.

Assuming that the thickness of the diaphragm plate is $t_d := 0.75 \cdot in$ and the depth of the diaphragm plate is $D_d := 48 \cdot in$.

$$CHECK\_10 := if\left(\frac{2 \cdot D_d}{t_d} < 5.7 \cdot \sqrt{\frac{E_s}{F_{y\_cf}}}, "OK", "NG"\right) \qquad \textbf{(AASHTO 6.10.6.2.3-1)}$$

$CHECK\_10 = "OK"$

Since the bearings being used are rated at 800 kips and are 27 inches wide, three bearings would be required when the member is fully loaded. However, the three bearings are wider than the bottom flange which would lead to uneven loading of the bearings and the concrete floor.

In order to better distribute the load, four bearings will be used and we will add diaphragm extensions on the exterior of the box to distribute reactions over the full width of the bearings. To prevent the extensions from influencing the bending capacity of the box girder, the extension will not be attached to the bottom flange.

Due to the support condition at the "pier", the bearing diaphragm web plate need only be sized for the slenderness criteria above. It is present to essentially maintain the shape of the box and distribute the reaction load to the bearing stiffeners. Each stiffener uses a tributary area of the diaphragm plate to carry the reaction load.

### Size Bearing Stiffeners (AASHTO 6.10.11.2)

Thickness of the stiffener plates is defined by $t_p$.

Assume that the stiffener plates are 3/4 inch thick.

$t_p := 0.75 \cdot in$

The maximum projecting width of each stiffener plate is defined by $b_{t\_max}$.

$$b_{t\_max} := 0.48 \cdot t_p \cdot \sqrt{\frac{E_s}{F_{y\_cf}}} \quad b_{t\_max} = 8.67\ in \qquad \textbf{(AASHTO 6.10.11.2.2-1)}$$

Assuming that each of the 4 interior stiffeners carry 20% of the reaction and that the outside full height stiffeners carry 5% each, the bearing reaction carried by one interior stiffeners is defined by $R_{bi.}$

$R_{bi} := 0.20 \cdot 2 \cdot P_u$ $\quad R_{bi} = 511.06\,kip$

**Check the bearing resistance of fitted end of the stiffeners**

The end of the bearing stiffener will need to be clipped by 1-1/2 inch to be clear of the flange and diaphragm weld and leave room to weld the bearing stiffener to the flanges.

The area required for each bearing stiffener plate is defined by $A_{pn\_min.}$

$A_{pn\_min} := \frac{R_{bi}}{2 \cdot 1.4 \cdot F_{y\_cf}}$ $\quad A_{pn\_min} = 3.65\,in^2$

Therefore, for two-sided stiffeners, the minimum width is defined as $b_{t\_min.}$

$b_{t\_min} := \frac{A_{pn\_min}}{t_p} + 1.5 \cdot in$ $\quad b_{t\_min} = 6.367\,in$

**<u>Use 0.75 inch thick by 7.5 inch wide stiffener plates on each side of the bearing diaphragms.</u>**

**Check that the nominal axial resistance of the stiffener to diaphragm plate is greater than $R_{bi.}$**

By AASHTO LRFD 6.10.11.2.4b, the effective portion of the diaphragm plate is $2 \cdot 9 \cdot 0.75 \cdot in = 13.5\,in$ However, since the stiffeners are approximately one foot apart, use 12 inches as the tributary width of the diaphragm plate for the column element to be analyzed.

The width of the bearing stiffener is defined as $b_{t.}$

$b_t := 7.5 \cdot in$

$t_p = 0.75\,in$

The area of the diaphragm plate is defined by $A_{cs.}$

$A_{cs} := 12 \cdot in \cdot t_d + 2 \cdot b_t \cdot t_p$ $\quad A_{cs} = 20.25\,in^2$

The inertia of the diaphragm plate is defined by $I_{cs.}$

$I_{cs} := \frac{1}{12} \cdot \left(12 \cdot in \cdot {t_d}^3 + 2 \cdot t_p \cdot {b_t}^3\right) + 2 \cdot b_t \cdot t_p \cdot \left(\frac{b_t + t_d}{2}\right)^2$ $\quad I_{cs} = 244.582\,in^4$

The radius of gyration of diaphragm plate is defined by $r_{cs.}$

$r_{cs} := \sqrt{\frac{I_{cs}}{A_{cs}}}$ $\quad r_{cs} = 3.475\,in$

$$\lambda_{cs} := \left(\frac{k \cdot 48 \cdot in}{r_{cs} \cdot \pi}\right)^2 \cdot \frac{F_{y\_cf}}{E_s} \qquad \lambda_{cs} = 0.019 \qquad \textbf{(AASHTO 6.9.4.1-3)}$$

The nominal compressive resistance of the diaphragm plate is defined as $P_{n\_cs}$.

Since $\lambda_{cs} < 2.25$ ;

$$P_{n\_cs} := 0.66^{\lambda_{cs}} \cdot F_{y\_cf} \cdot A_{cs} \qquad \textbf{(AASHTO 6.9.4.1-1)}$$

$$P_{n\_cs} = 1004.645\,kip$$

The factored compressive resistance of the diaphragm plate is defined as $P_{r\_cs}$.

$$\phi_c = 0.9$$

$$P_{r\_cs} := \phi_c \cdot P_{n\_cs} \qquad \textbf{(AASHTO 6.9.2.1-1)}$$

$$P_{r\_cs} = 904.18\,kip$$

$$CHECK\_11 := if\left(R_{bi} < P_{r\_cs}, "OK", "NG"\right) \qquad CHECK\_11 = "OK"$$

## Diagphragm Top Flange Plate

There is no bending force in the top flange. Therefore, the plate width will be based upon what is necessary to engage the full width of the bearing stiffeners and the plate thickness will match the top flanges of the box for ease of connection.

**Use 16 inch wide by 0.75 inch thick top flange plate for diaphragm. In order to maintain continuity with the composite box girder section, place shear studs at 1 foot spacing along the diaphragm top flange.**

### Connection of diaphragm top flange to top flange of girder

Design the top flange of the diaphragm connection to top flange of box to carry the horizontal component of maximum web shear that is introduced into the diaphragm at the "pier".

The forces to be resisted by bolts and splices is defined as $P_{splice}$.

$$P_{splice} := \frac{P_u}{4} \qquad P_{splice} = 319.412\,kip$$

**Minimum number of bolts required :**

The diameter of A325 bolts is defined by $d_{bolt}$.

$$d_{bolt} = 0.875\,in$$

Tensile Strength of A325 bolts is defined by $F_{ub}$.

$$F_{ub} = 120\,ksi$$

Area of A325 bolts is defined by $A_{bolt.}$

$A_{bolt} = 0.601\ in^2$

Number of shear planes is defined by $N_{sh.}$

$N_{sh} = 2$

**Based on shear capacity of bolt :** **(AASHTO 6.13.2.7)**

The nominal resistance offered by the bolt is defined as $R_{ns\_bolt.}$

$R_{ns\_bolt} := 0.48 \cdot A_{bolt} \cdot F_{ub} \cdot N_{sh}$ $R_{ns\_bolt} = 69.272\ kip$

The minimum number of bolts required to resist $P_{splice}$ is defined by $N_{bsplice\_min.}$

$N_{bsplice\_min} := ceil\left(\frac{P_{splice}}{R_{ns\_bolt}}\right)$ $N_{bsplice\_min} = 5$

**Based on bearing strength of the bolt holes :** **(AASHTO 6.13.2.9)**

Assuming Grade 50 ksi plates, $F_u = 70\ ksi$ the minimum material thickness of the plate is defined as $t_{tfd}$, and the clear edge distance is defined as $L_{c\_tfd}$ in inches.

$t_{tfd} := 0.5 \cdot in$

$L_{c\_tfd} := 1.5 \cdot in - 0.4375 \cdot in$ $L_{c\_tfd} = 1.063\ in$

$R_{n\_sp\_hole} := 1.2 \cdot L_{c\_tfd} \cdot t_{tfd} \cdot F_u$ $R_{n\_sp\_hole} = 44.625\ kip$

$N_{sp\_min} := ceil\left(\frac{0.5 \cdot P_{splice}}{R_{n\_sp\_hole}}\right)$ $N_{sp\_min} = 4$

For "sealing bolts" maximum spacing is 6 inches. **(AASHTO 6.13.2.6)**

**Use 2 rows of 4 bolts each side of splice and use 1/2 inch splice plates for the connection of top flange of diaphragms to top flange of girder, as shown below.**

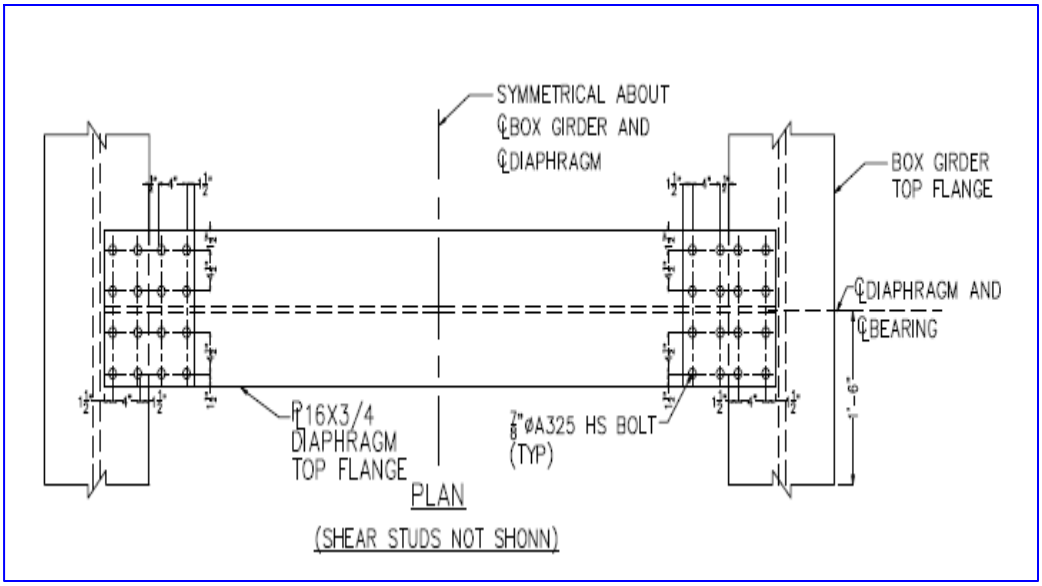


**Figure A.4** Plan View of Pier Diaphragm

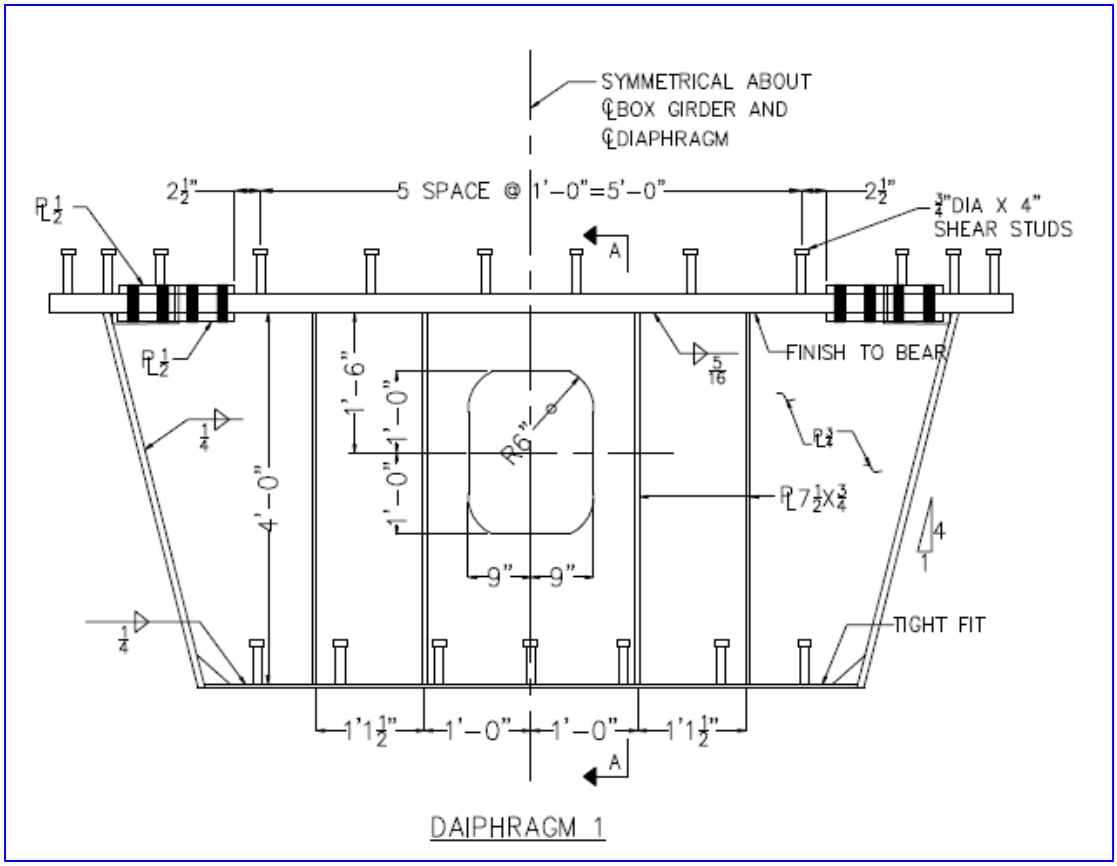


**Figure A.5** Pier Diaphragm

## A.14 Design of Welds

### Design of Bottom Flange to Web Welds

The minimum weld size from the bottom flange to web is 1/4 inch. However, the minimum size for the top flange to web weld is 5/16 inch. **(AASHTO 6.13.3.4)**

The first moment of the bottom flange and slab at the section over the "pier" is defined as $Q_{n,}$ as calculated on pg-A.21. The value used is based on predicted material properties, since we want to ensure that the welds do not fail prior to the predicted plastic moment being reached.

$Q_w := 2098.120 \cdot in^3$ (see pg-A.21)

The required weld strength for the four web to bottom flange welds is defined by $R_{w\_bot.}$

$$R_{w\_bot} := \frac{P_u \cdot Q_w}{I_u} \qquad R_{w\_bot} = 288.88\ klf$$

Four 1/4 inch welds have a resistance which is defined as $R_{r\_bot.}$

$R_{r\_bot} := 4 \cdot (0.6 \cdot 0.8 \cdot F_u \cdot 0.707 \cdot 0.25 \cdot in)$ $R_{r\_bot} = 285.062\ klf$

$CHECK\_12 := if(R_{w\_bot} < R_{r\_bot}, "OK", "NG")$ $CHECK\_12 = "NG"$

Say "OK", only 0.8 % over limit.

**Use 1/4 inch fillet welds for all bottom flange to web and diaphragm welds.**

### Top Flange to Web Welds

The first moment of the top flange and slab at the end of the girder is $Q_p$ (see pg-A.19). The value used is based on predicted material properties, since we want to ensure that the welds do not fail prior to the predicted plastic moment being reached.

$Q_p := 4623 \cdot in^3$

The required weld strength for the four web to top flange weld is defined as $R_{w\_top.}$

$$R_{w\_top} := \frac{P_u \cdot Q_p}{I_{pc}} \qquad R_{w\_top} = 309.501\ klf$$

The resistance of four 5/16 inch weld is defined as $R_{r\_top.}$

$R_{r\_top} := 4 \cdot (0.6 \cdot 0.8 \cdot F_u \cdot 0.707 \cdot 0.3125 \cdot in)$ $R_{r\_top} = 356.328\ klf$

$CHECK\_13 := if(R_{w\_top} < R_{r\_top}, "OK", "NG")$ $CHECK\_13 = "OK"$

**Use 5/16 inch fillet welds for all top flange to web and diaphragm welds**

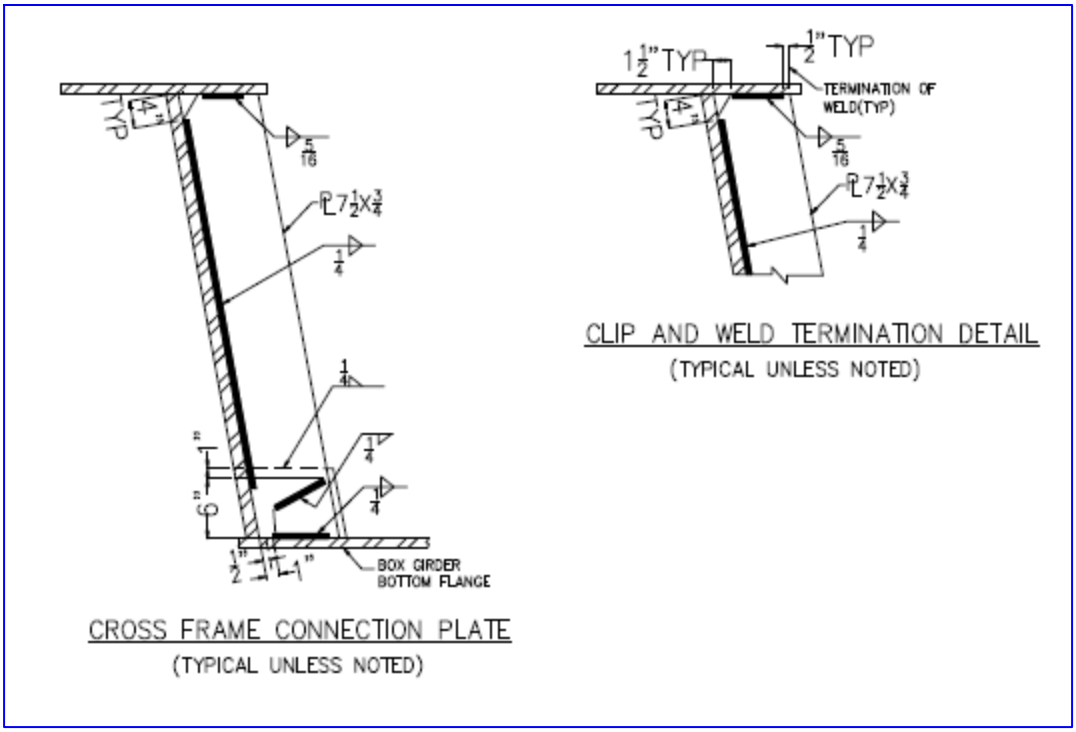


**Figure A.6** Typical Cross Frame Connection Plate

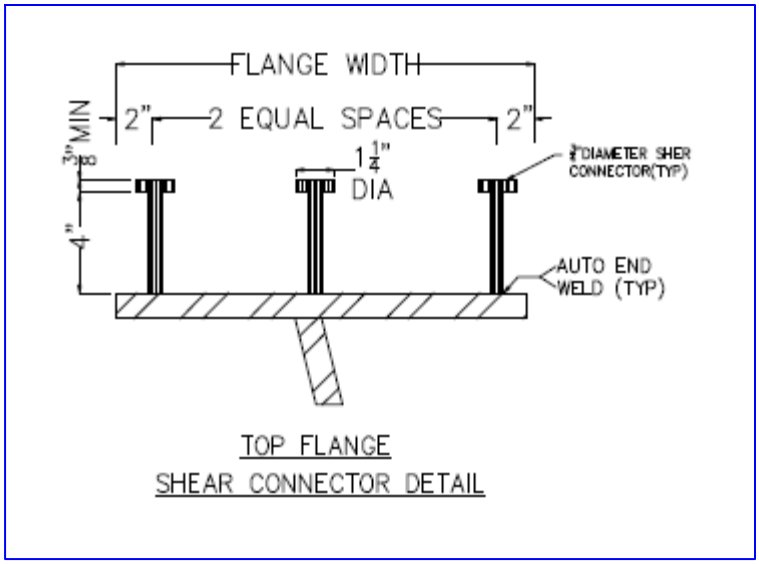


**Figure A.7** Top Flange Shear Connector Detail

## A.15 Design of Loading End Bearing Stiffeners

**Size Bearing Stiffeners** **(AASHTO 6.10.11.2)**

The thickess of the stiffener plates is defined by $t_{lbs.}$

Assume that stiffener plates are 7/8 inch thick.

$t_{lbs} := 0.875 \cdot in$

The maximum projecting width of each stiffener plate is $b_{lbs\_max.}$

$$b_{lbs\_max} := 0.48 \cdot t_{lbs} \cdot \sqrt{\frac{E_s}{F_{y\_cf}}} \qquad b_{lbs\_max} = 10.115\ in$$

Each pair of stiffeners carries the load imparted by one actuator. In order to allow maximum load application, size the stiffeners to carry the capacity of the load cell which is $R_u := 600 \cdot kip$

**Check the bearing resistance of the fitted ends of the stiffeners :**

The end of the bearing stiffener will need to be clipped by 1-1/2 inch to be clear of the weld and leave room to weld the bearing stiffener to the flanges.

The area required for each bearing stiffener plate is defined as $A_{ps\_min.}$

$$A_{ps\_min} := \frac{\frac{P_u}{2}}{2 \cdot 1.4 \cdot F_{y\_cf}} \qquad A_{ps\_min} = 4.563\ in^2$$

Therefore, for two-sided stiffeners, minimum width is defined by $b_{lbs\_min.}$

$$b_{lbs\_min} := \frac{A_{ps\_min}}{t_{lbs}} + 1.5 \cdot in \qquad b_{lbs\_min} = 6.715\ in$$

**<u>Use 7/8 inch thick by 7.5 inch wide (normal to web) stiffener plate on each side of the web.</u>**

**Check that the nominal axial resistance to the stiffener/web plate is greater than $R_{u.}$**

By AASHTO 6.10.11.2.4b, the effective portion of the web plate is $2 \cdot 9 \cdot 0.75 \cdot in = 13.5\ in$

$b_{lbs} := 7.5 \cdot in$

The area of the bearing stiffener plate is defined by $A_{bs.}$

$$A_{bs} := 13.5 \cdot in \cdot t_w + 2 \cdot b_{lbs} \cdot t_{lbs} \qquad A_{bs} = 23.25\ in^2$$

$$I_{bs} := \frac{1}{12} \cdot \left(12 \cdot in \cdot t_{lbs}^{\ 3} + 2 \cdot 0.75 \cdot in \cdot b_{lbs}^{\ 3}\right) + 2 \cdot b_{lbs} \cdot 0.75 \cdot in \cdot \left(\frac{b_{lbs} + t_{lbs}}{2}\right)^2$$

$I_{bs} = 250.675\ in^4$

$r_{bs} := \sqrt{\frac{I_{bs}}{A_{bs}}}$ $r_{bs} = 3.284\ in$

As per AASHTO 6.9.4: maximum length is 48 inches, though actual stiffeners are not full height.

$\lambda_{bs} := \left(\frac{0.75 \cdot 48 \cdot in}{r_{bs} \cdot \pi}\right)^2 \cdot \frac{F_{y\_cf}}{E_s}$ **(AASHTO 6.9.4.1-3)**

$\lambda_{bs} = 0.021$

$P_{n\_bs} := 0.66^{\lambda_{bs}} \cdot F_{y\_cf} \cdot A_{bs}$ **(AASHTO 6.9.4.1-1)**

$P_{n\_bs} = 1152.401\ kip$

$P_{r\_bs} := \phi_c \cdot P_{n\_bs}$ $P_{r\_bs} = 1037.161\ kip$

$CHECK\_14 := if\left(R_u < P_{r\_bs}, "OK", "NG"\right)$ $CHECK\_14 = "OK"$

## A.16 Bracing System for Bottom Flange

### Non-Composite Section Properties

Area of the bottom flange, $A_{BF}$ $A_{BF} := 12in \cdot t_{bf}$

**Note:** Transverse section properties are calculated on per foot basis. $A_{BF} = 4.5\,in^2$

Moment of inertia of the bottom flange, $I_{BF}$ $I_{BF} := \frac{12in \cdot t_{bf}^3}{12}$ $I_{BF} = 0.053\,in^4$

Section modulus of the bottom flange, $S_{BF}$ $S_{BF} := \frac{I_{BF}}{0.5 \cdot t_{bf}}$ $S_{BF} = 0.281\,in^3$

### Composite Section Properties

Modular ratio, n $n := round\left(\frac{E_s}{E_{c\_des}}, 1\right)$ $n = 7.5$

Location of Neutral Axis of composite bottom fiber section, $Y_{b\_comp}$

$$Y_{b\_comp} := \frac{A_{BF} \cdot 0.5 \cdot t_{bf} + \left(\frac{12 \cdot in \cdot 7 \cdot in}{n}\right) \cdot (t_{bf} + 3.5i}{A_{BF} + \left(\frac{12in \cdot 7in}{n}\right)}$$

$Y_{b\_comp} = 2.818\,in$

Moment of inertia of composite bottom slab section, $I_{bslab}$ $I_{bslab} := \frac{12in \cdot t_{bs}^3}{12 \cdot n}$ $I_{bslab} = 45.733\,in^4$

Area of bottom slab, $A_{bslab}$ $A_{bslab} := 12in \cdot t_{bs}$ $A_{bslab} = 84\,in^2$

Moment of inertia of composite bottom fiber section, $I_{comp}$

$$I_{comp} := I_{BF} + I_{bslab} + A_{BF} \cdot \left(Y_{b\_comp} - \frac{t_{bf}}{2}\right)^2 + \left(\frac{A_{bslab}}{n}\right) \cdot (Y_{b\_comp} - 3.875in)^2$$

$I_{comp} = 89.437\,in^4$

**Note:** 3.875 inch is the distance from extreme bottom fiber to centroid of bottom slab.

Bottom section modulus of composite bottom fiber, $S_{b\_comp}$

$$S_{b\_comp} := \frac{I_{comp}}{Y_{b\_comp}}$$

$$S_{b\_comp} = 31.737\,in^3$$

Top section modulus of composite top fiber, $S_{t\_comp}$

$$S_{t\_comp} := \frac{I_{comp}}{t_{bf} + t_{bs} - Y_{b\_comp}}$$

$$S_{t\_comp} = 19.627\,in^3$$

## Loads

Dead load of steel bottom flange, $DL_{stl}$

$$DL_{stl} := 490 \cdot pcf \cdot A_{BF}$$

**Note:** 490 pcf is the unit weight of steel.

$$DL_{stl} = 0.015\,klf$$

Dead load of concrete bottom slab, $DL_{conc}$

$$DL_{conc} := w_{rc} \cdot A_{bslab}$$

$$DL_{conc} = 0.087\,klf$$

Total factored loading used in the analysis, $DL_{tot}$

$$DL_{tot} := 1.25 \cdot \left(DL_{stl} + DL_{conc}\right)$$

$$DL_{tot} = 0.129\,klf$$

If we consider entire flange the pressure acting on the plate is $P_{DL}$

$$P_{DL} := \frac{DL_{tot}}{12 \cdot in}$$

$$P_{DL} = 8.925 \times 10^{-4}\,ksi$$

## Calculate Stress Without Bracing

For the unbraced bottom flange, the bottom flange will span between webs like a sinple beam under its own self-weight and weight of wet concrete.

Using the rectangular plate tables from *Design of Welded Structures* by *Blodgett,* the stress in the plate can be calculated from the loading and plate thickness.

Stress in the bottom plate, $\sigma_1$

$$\sigma_1 := \frac{0.75 \cdot P_{DL} \cdot (72in)^2}{t_{bf}^2} \quad \sigma_1 = 24.675\,ksi$$

$CHECK\_1 := if(\sigma_1 > 20ksi, "OK", "NG")$ $CHECK\_1 = "OK"$

We need to provide bracing along bottom flange to temporarily support concrete until it cures.

## Calculate Stress With Bracing

Assume bracing at every 10 feet in the form of back-to-back angles supported from two inch bottom flange extension to the exterior of box girder.

The width of the panel, w (feet) $w := 6 \cdot ft$

The length of the panel, L (feet) $L_{br} := 10 \cdot ft$

$$\frac{L_{br}}{w} = 1.667$$

The stress considering bracing, $\sigma_{braced}$ $$\sigma_{braced} := \frac{0.5448 \cdot P_{DL} \cdot (72in)^2}{t_{bf}^2}$$

$$\sigma_{braced} = 17.924\,ksi$$

The maximum deflection of plate, $\Delta_{braced}$ $$\Delta_{braced} := \frac{0.0964 \cdot P_{DL} \cdot (72in)^4}{E_s \cdot t_{bf}^3}$$

$$\Delta_{braced} = 1.512\,in$$

Deflection criteria $$\frac{w}{\Delta_{braced}} = 47.624$$

Once the braces are removed the bracing force is applied back to the composite section.

Conservatively, if the entire load is then reapplied to the section and that stress is added to the non-composite stress, we will have the upper bound of the solution.

Stress due to bracing, $\sigma_{braced\_2}$ $$\sigma_{braced\_2} := \frac{0.75 \cdot P_{DL} \cdot (72in)^2}{\left(t_{bf} + \frac{7in}{n}\right)^2}$$

$$\sigma_{braced\_2} = 2.027\,ksi$$

Total stress in the composite bottom flange, $\sigma_{total}$ $$\sigma_{total} := \sigma_{braced} + \sigma_{braced\_2}$$

$\sigma_{total} = 19.951\ ksi$

$CHECK\_2 := if(20ksi > \sigma_{total}, "OK", "NG")$ $CHECK\_2 = "OK"$

The stress is within the limits required by AASHTO, however the deflection is not. The bracing would have to be moved even closer to limit the deflection of the bottom plate to L/360

The allowable deflection, $\Delta_{allowable}$ $\Delta_{allowable} := \frac{w}{360}$ $\Delta_{allowable} = 0.2\ in$

Deflection for bracing at 4 feet, $\Delta_{4ft}$ $\Delta_{4ft} := \frac{0.0843 \cdot P_{DL} \cdot (48in)^4}{E_s \cdot t_{bf}^3}$

$\Delta_{4ft} = 0.261\ in$

Deflection for bracing at 3 feet, $\Delta_{3ft}$ $\Delta_{3ft} := \frac{0.1106 \cdot P_{DL} \cdot (36in)^4}{E_s \cdot t_{bf}^3}$

$\Delta_{3ft} = 0.108\ in$

Composite deflection after removal of braces, $\Delta_{abrace}$ $\Delta_{abrace} := \frac{0.1422 \cdot P_{DL} \cdot (72in)^4}{E_s \cdot \left(t_{bf} + \frac{7in}{n}\right)^3}$

$\Delta_{abrace} = 0.053\ in$

## Calculate Deflection for Selected Bracing Member

The actual member selected as a bottom flange brace is a WT5 x 9.5 based on less assembly than the double channel option.

Inertia of WT5 x 9.5, $I_{brace}$ $I_{brace} := 6.68in^4$

Deflection of WT5 x 9.5, $\Delta_{wbrace}$ $\Delta_{wbrace} := \frac{5 \cdot (P_{DL} \cdot 3ft + 9 \cdot plf) \cdot (6ft)^4}{384 \cdot E_s \cdot I_{brace}}$

$\Delta_{wbrace} = 0.059\ in$

Conservatively, the maximum deflection after removal of braces, $D_{tot\_max}$

$$\Delta_{tot\_max} := \Delta_{3ft} + \Delta_{abrace} + \Delta_{wbrace}$$

$$\Delta_{tot\_max} = 0.22\ in$$

This the composite deflection assuming the full load is applied to the composite section.

Check deflection criteria

$$\frac{6 \cdot ft}{\Delta_{tot\_max}} = 326.809$$

**Since the above conservative estimate basically negates the portion of the slab supported by the bottom flange under the braced case, in reality maximum deflection should be below 0.2 inch.**

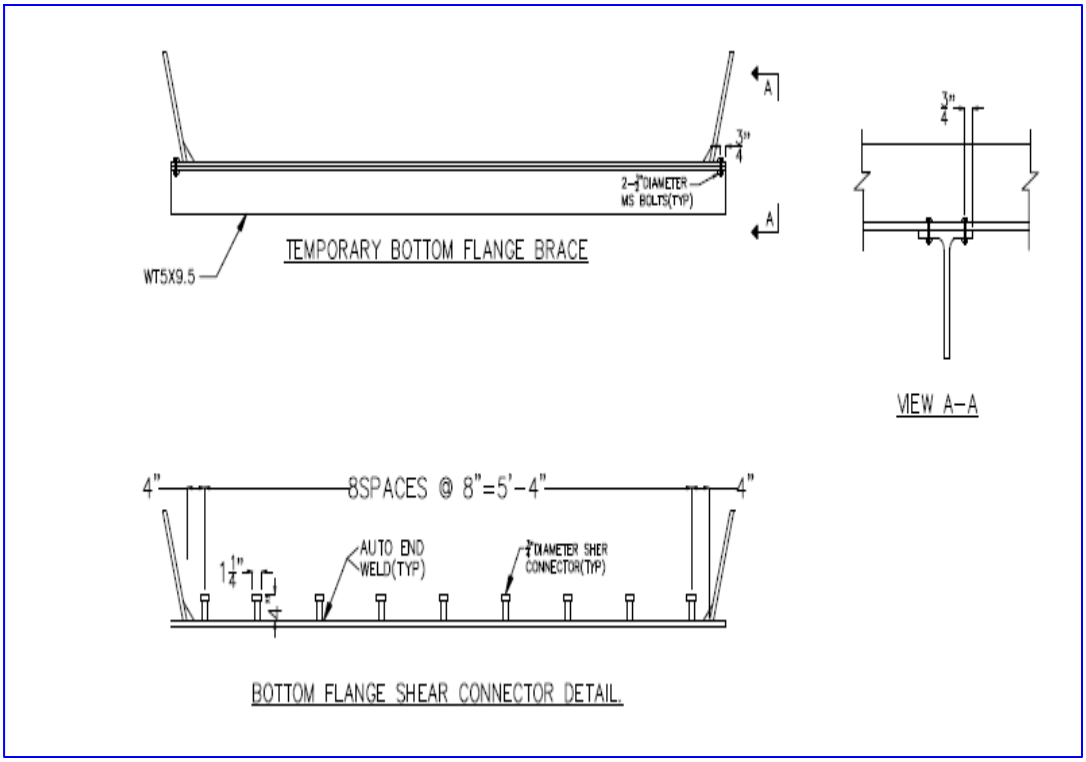


**Figure A.8** Temporary Bracing System of Bottom Flange

## A.17 Calculate Beam Natural Frequency

To ensure the safety of testing equipment and lab personnel, compare the loading frequency for fatigue to the natural frequency of the test specimen and assure they are not equal.

From *Theory of Vibration with Application, 3rd Edition* by *Thomson*, the natural frequency of a cantilever beam is determined as follows.

Mass per unit Length of the beam, $\rho$ (plf)

$$\rho := \frac{1}{g}\cdot\left(w_{gird} + w_{det} + w_{ts} + w_{sip} + w_{bs}\right)$$

$$\rho = 2865\,\frac{lb}{ft}$$

$(\beta_n*L)^2$ is selected from the chart in Fig 8.4-2 on page 223

$$(\beta_n*L)^2 = 3.52$$

The fundamental natural frequency, $\omega_1$ –

$$\omega_1 := 3.52\cdot\sqrt{\frac{E_s\cdot I_{pc}}{\rho\cdot(b)^4}}$$

$$\omega_1 = 128.17\,\frac{1}{s}$$

The frequency of second and third mode are even higher than the fundamental frequency. The fatigue loading is 3 Hz, well below the natural frequency of the test specimen.

# APPENDIX B

Material Test Data

## B.1 Concrete Compressive Strength of Top Slab (6 × 12) cylinders

Table B.1 summarizes information on the compressive strength of concrete for the top slab. Average compressive strength of concrete for the top slab prior to service and ultimate load test was 10124 psi for truck # 1 (*actuator end*) and 7650 psi for truck # 2 (*hold down frame end*).

**Table B.1** Compressive Strength of Top Slab

| Cast Date | Test Date | Compressive Strength (psi) | | | | Average Compressive Strength (psi) | |
|---|---|---|---|---|---|---|---|
| | | Truck # 1 | | Truck # 2 | | | |
| | | Cy # 1 | Cy # 2 | Cy # 1 | Cy # 2 | Truck # 1 | Truck # 2 |
| 12/12/2007 | 3/7/2008 | 8522 | 8759 | 6245 | 6517 | 8641 | 6381 |
| 12/21/2007 | 5/15/2008 | 9776 | 9724 | 6909 | 7121 | 9750 | 7015 |
| 12/21/2007 | 8/14/2008 | 9856 | 9955 | 7606 | 7574 | 9905 | 7590[1] |
| 12/21/2007 | 10/3/2008 | 9817 | 10430 | 7487 | 7814 | 10124 | 7650[2] |

1. Compressive strength after fatigue test was completed.
2. Compressive strength prior to commencement of service and ultimate load test.

**Note:** The concrete with high compressive strength (truck # 1) is towards actuator end and concrete with low compressive strength (truck # 2) is towards hold down frame end.

## B.2 Concrete Compressive Strength of Bottom Slab (4 × 8) cylinders

Table B.2 summarizes information on the compressive strength of concrete for the bottom slab provided by FDOT. Compressive strength was corrected to account for the 4 x 8 cylinder size, that is, values were reduced by dividing by 1.05. The corrected values are presented in Table B.3. The average compressive strength of the concrete for the bottom slab prior to commencement of service and ultimate load test was 8118 psi.

FDOT also tested 6×12 cylinders for the bottom slab only for service and ultimate load test dated 10/03/08. The data for the 6×12 cylinders is also presented in Table B.3.

**Table B.2** Compressive Strength of Bottom Slab (FDOT)

| Cast Date | Test Date | Compressive Strength (psi) | | | | Cylinders |
|---|---|---|---|---|---|---|
| | | Cy # 1 | Cy # 2 | Cy # 3 | Average | |
| 7/17/2007 | 5/15/2008 | 8492 | 8536 | 8719 | 8514 | 4×8 |
| 7/17/2007 | 8/14/2008 | 8473 | 8032 | 8237 | 8253[1] | 4×8 |
| 7/17/2007 | 10/3/2008 | 8317 | 8764 | 8480 | 8541[2] | 4×8 |
| 7/17/2007 | 10/3/2008 | 8543 | 8421 | 8468 | 8482[2] | 4×8 |
| 7/17/2007 | 10/3/2008 | 8884 | 8679 | 8772 | 8778[2] | 6×12 |

1. Compressive strength after fatigue test was completed.
2. Compressive strength prior to commencement of service and ultimate load test

**Table B.3** Compressive Strength of Bottom Slab with Correction

| Cast Date | Test Date | Compressive Strength (psi) | | | | Cylinders |
|---|---|---|---|---|---|---|
| | | Cy # 1 | Cy # 2 | Cy # 3 | Average | |
| 7/17/2007 | 5/15/2008 | 8091 | 8133 | 8308 | 8178 | 4×8 |
| 7/17/2007 | 8/14/2008 | 8074 | 7653 | 7849 | 7859[1] | 4×8 |
| 7/17/2007 | 10/3/2008 | 7925 | 8351 | 8080 | 8118[2] | 4×8 |
| 7/17/2007 | 10/3/2008 | 8140 | 8024 | 8069 | 8078[2] | 4×8 |
| 7/17/2007 | 10/3/2008 | 8884 | 8679 | 8772 | 8778[2] | 6×12 |

## B.3 Yield Strength of Rebars

Table B.4 summarizes the information on yield strength of rebars from mill certificates.

**Table B.4** Yield Strength of slab rebars

| Location | Yield Stress (ksi) | Tensile Stress (ksi) | Elongation % in 8 in |
|---|---|---|---|
| Bottom Slab | 72.9 | 110 | 10% |
| Top Slab | 73.1 | 112.9 | 9% |

## B.4 HPS Steel Testing Data

This section summarizes the information on coupon tests from HPS steel plates and important material parameters obtained from the testing. Values of elastic modulus, yield strength and ultimate tensile strength are summarized in Table B.5-B.7. Corresponding plots of the respective stress-strain curves are appended. Table B.8-B.10 summarizes information on yield strength and ultimate tensile strength from mill certificates.


**Figure B.1** Photograph of Coupon Test Specimens Tested at Gainesville – August 2008

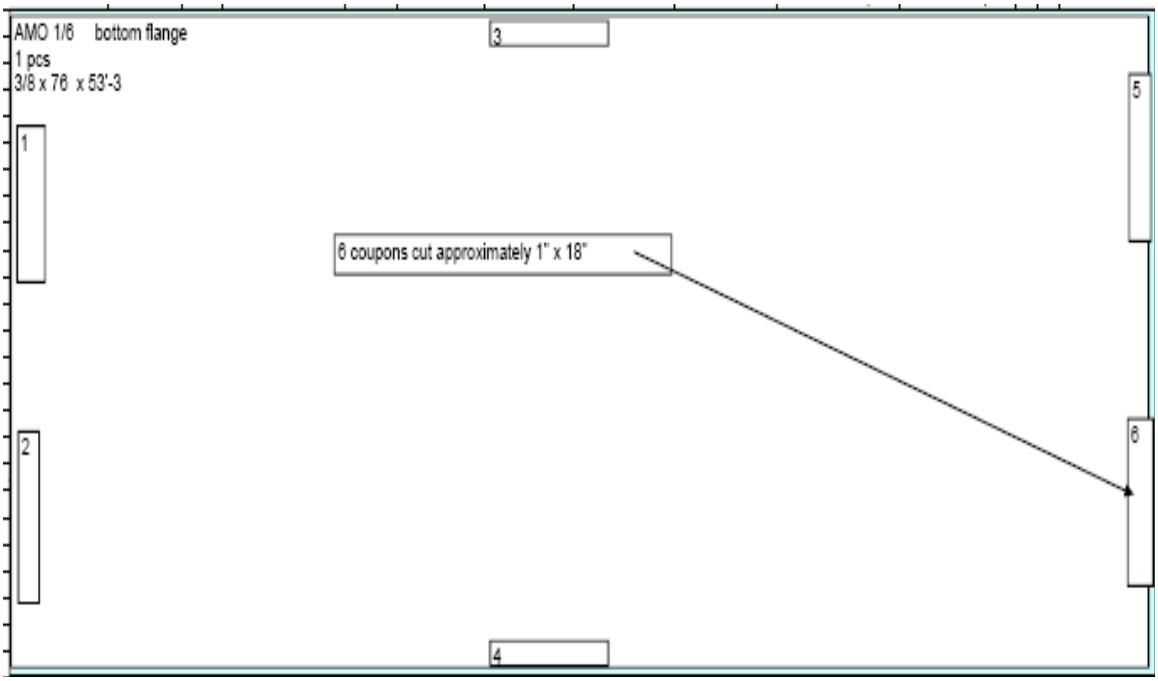


**Figure B.2** Location of Coupons Test Specimen in Plates

**Table B.5** Coupon Test Data of HPS Steel of Bottom Flange

| Sample no. | Thickness (inch) | Modulus of Elasticity (Mpsi) | Yield Strength (psi) | Tensile Strength (psi) | Comments |
|---|---|---|---|---|---|
| 1-A | 0.375 | 32.2 | 81,500 | 81,500 | Fig. B.3 |
| 2-A | 0.375 | 30.4 | 80,900 | 81,000 | Fig. B.4 |
| 3-A | 0.375 | 29.8 | 80,700 | 80,800 | Fig. B.5 |
| 4-A | 0.375 | 29.3 | 78,200 | 78,300 | Fig. B.6 |
| 5-A | 0.375 | 32.2 | 79,600 | 79,800 | Fig. B.7 |
| 6-A | 0.375 | 32 | 82,400 | 82,400 | Fig. B.8 |
| 1-B | 0.375 | 33.6 | 81,900 | 82,000 | Fig. B.9 |
| 2-B | 0.375 | 28.6 | 80,400 | 80,400 | Fig. B.10 |
| 3-B | 0.375 | 30.4 | 81,600 | 81,800 | Fig. B.11 |
| 4-B | 0.375 | 30.3 | 79,500 | 79,500 | Fig. B.12 |
| 5-B | 0.375 | 31.5 | 82,500 | 82,300 | Fig. B.13 |
| 6-B | 0.375 | 30.2 | 81,300 | 81,200 | Fig. B.14 |
| Average | - | 30.875 | 80,875 | 81,000 | - |

**Table B.6** Coupon Test Data of HPS Steel of Top flange

| Sample no. | Thickness (inch) | Modulus of Elasticity (Mpsi) | Yield Strength (psi) | Tensile Strength (psi) | Comments |
|---|---|---|---|---|---|
| 2-A | 1.75 | 30.6 | 82,000 | 82,100 | Fig. B.15 |
| 3-A | 1.75 | 26.1 | 76,000 | 76,800 | Fig. B.16 |
| 4-A | 1.75 | 28.6 | 83,000 | 83,000 | Fig. B.17 |
| 5-A | 1.75 | 31 | 80,700 | 80,800 | Fig. B.18 |
| 3-B | 1.75 | 30.2 | 81,100 | 81,200 | Fig. B.29 |
| 4-B | 1.75 | 23.4 | 77,600 | 77,600 | Fig. B.20 |
| 5-B | 1.75 | 28.9 | 81,900 | 82,000 | Fig. B.21 |
| Average | - | 28.4 | 80,471 | 80,500 | - |

**Table B.7** Coupon Test Data of HPS Steel of Web Plates

| Sample no. | Thickness (inch) | Modulus of Elasticity (Mpsi) | Yield Strength (psi) | Tensile Strength (psi) | Comments |
|---|---|---|---|---|---|
| 1-A | 0.75 | 33.6 | 78,000 | 78,700 | Fig. B.22 |
| 2-A | 0.75 | 30.1 | 77,800 | 78,200 | Fig. B.23 |
| 3-A | 0.75 | 34.1 | 86,000 | 87,100 | Fig. B.24 |
| 4-A | 0.75 | 31.5 | 84,500 | 85,700 | Fig. B.25 |
| 5-A | 0.75 | 32.6 | 78,300 | 79,200 | Fig. B.26 |
| 6-A | 0.75 | 30.3 | 75,900 | 76,600 | Fig. B.27 |
| 1-B | 0.75 | 27.7 | 77,800 | 78,100 | Fig. B.28 |
| 2-B | 0.75 | 32.3 | 77,800 | 78,500 | Fig. B.29 |
| 3-B | 0.75 | 28.7 | 88,200 | 88,100 | Fig. B.30 |
| 4-B | 0.75 | 34.7 | 83,200 | 85,400 | Fig. B.31 |
| 5-B | 0.75 | 31 | 80,100 | 80,600 | Fig. B.32 |
| 6-B | 0.75 | 33.7 | 78,000 | 78,700 | Fig. B.33 |
| Average | - | 31.69 | 80,458 | 81,242 | - |

**Table B.8** Yield Strength of Bottom Flange (Mill Certificate)

| Sample | Thickness of plate (inch) | Yield Strength (psi) | Ultimate Strength (psi) |
|---|---|---|---|
| 1 | ⅜ | 81600 | 102900 |
| 2 | ⅜ | 80200 | 102200 |

**Table B.9** Yield Strength of Top Flange (Mill Certificate)

| Sample | Thickness of plate (inch) | Yield Strength (psi) | Ultimate Strength (psi) |
|---|---|---|---|
| 1 | 1.75 | 78400 | 92500 |
| 2 | 1.75 | 77100 | 91400 |

**Table B.10** Yield Strength of Web Plates (Mill Certificates)

| Sample | Thickness of plate (inch) | Yield Strength (psi) | Ultimate Strength (psi) |
|---|---|---|---|
| 1 | ¾ | 79800 | 97700 |
| 2 | ¾ | 75700 | 98900 |

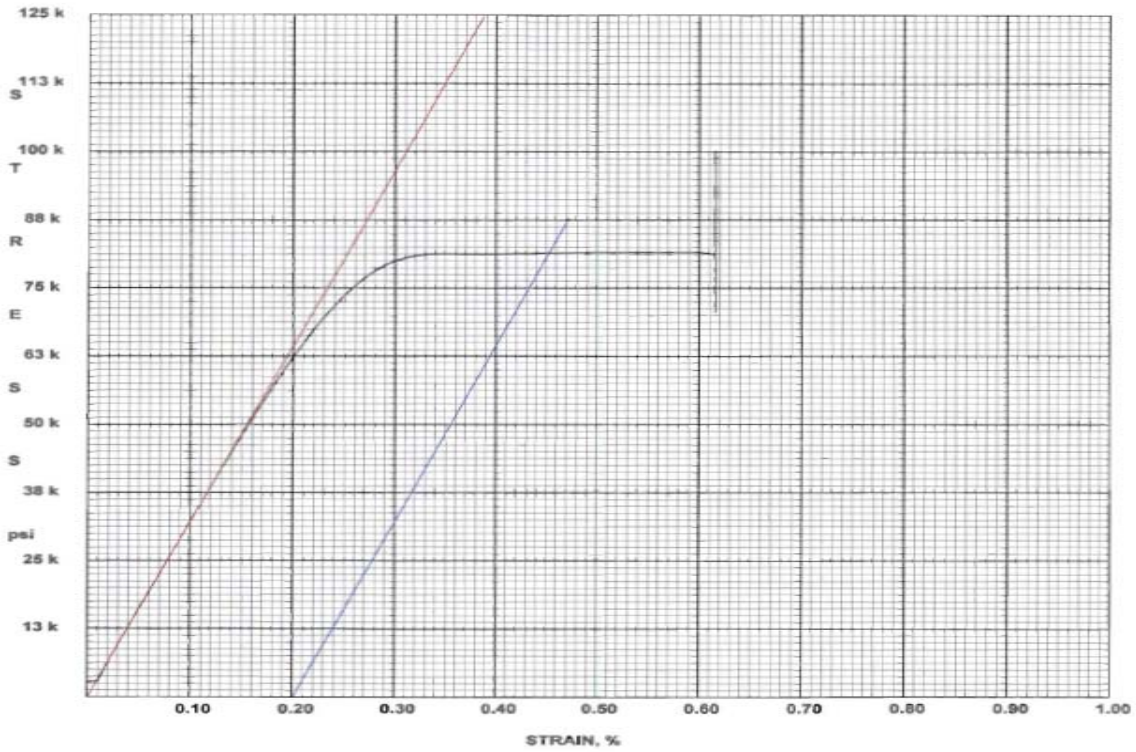


**Figure B.3** Stress – Strain Plot for Bottom Flange Sample 1-A

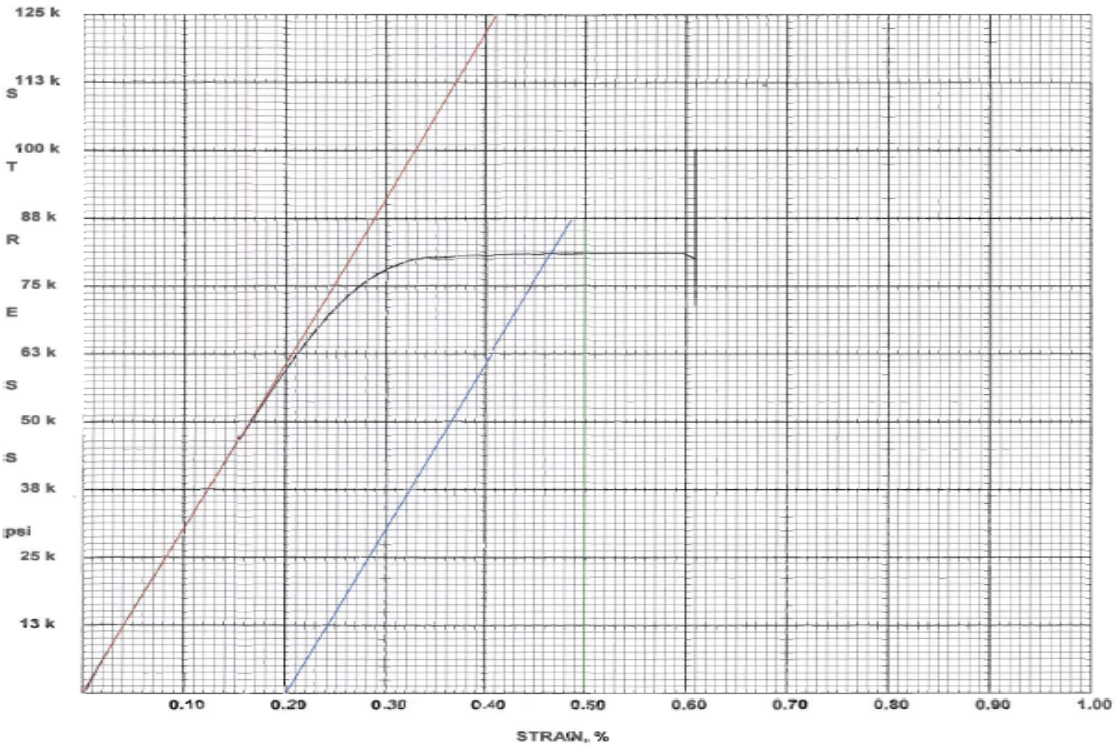


**Figure B.4** Stress – Strain Plot for Bottom Flange Sample 2-A

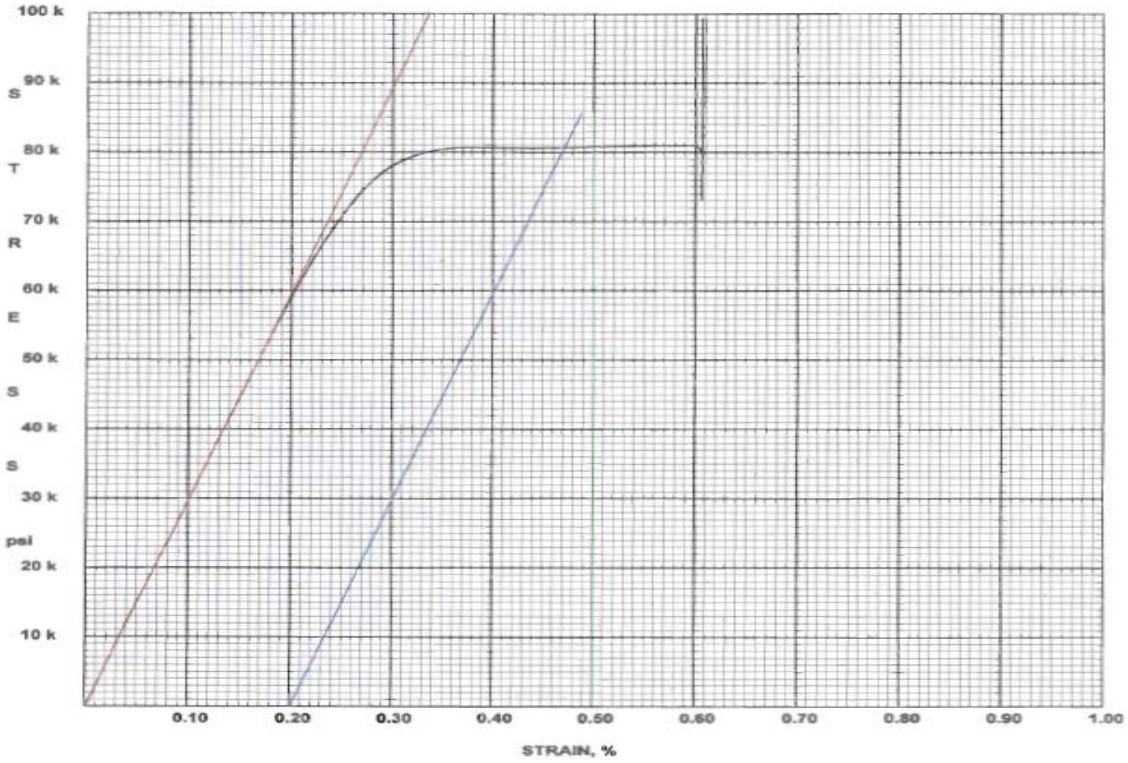


**Figure B.5** Stress – Strain Plot for Bottom Flange Sample 3-A

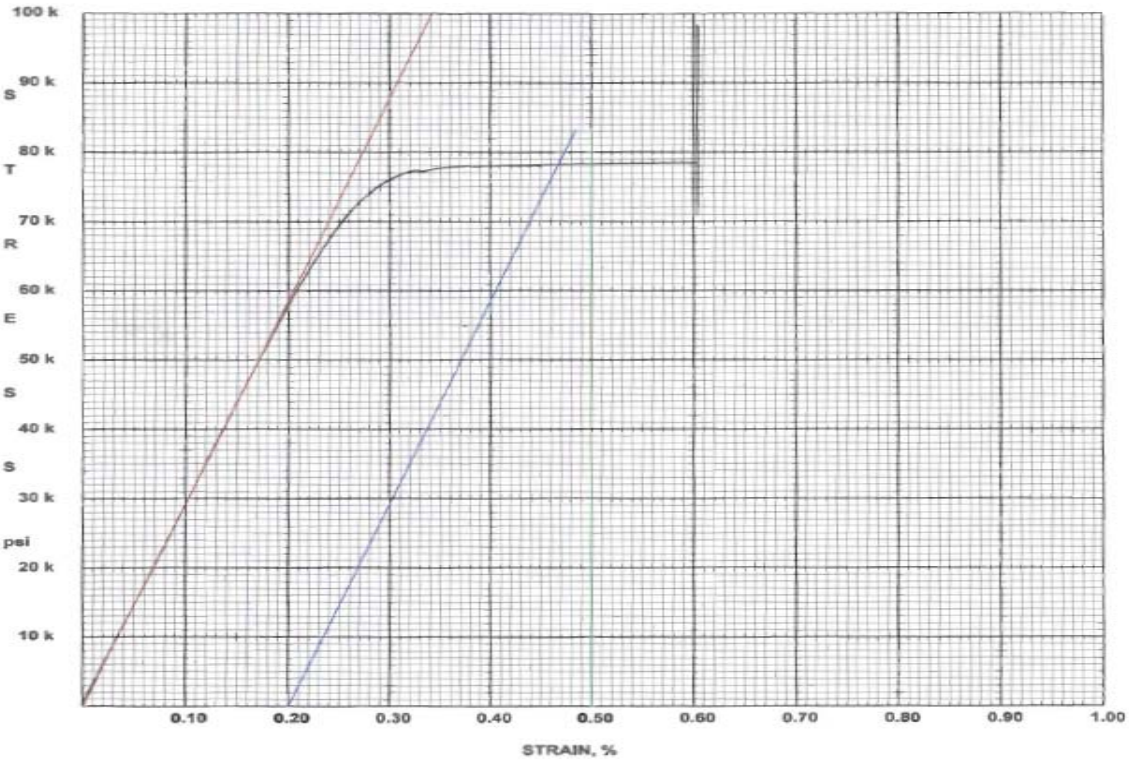


**Figure B.6** Stress – Strain Plot for Bottom Flange Sample 4-A

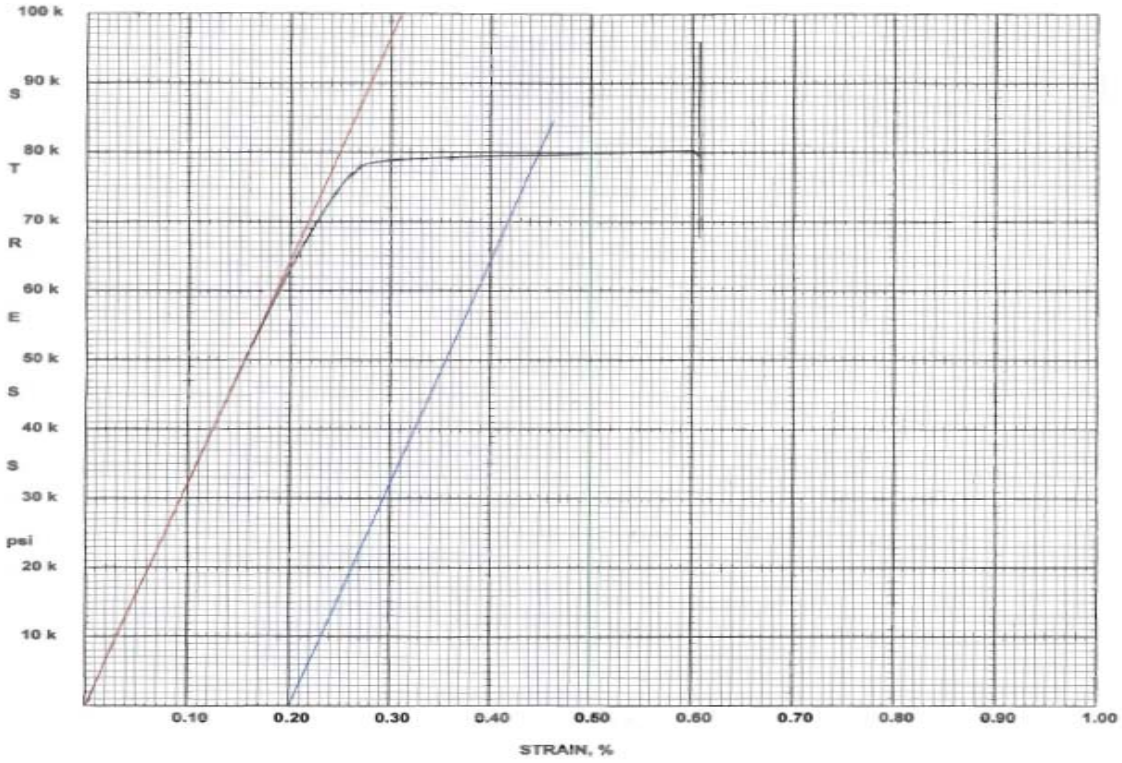


**Figure B.7** Stress – Strain Plot for Bottom Flange Sample 5-A

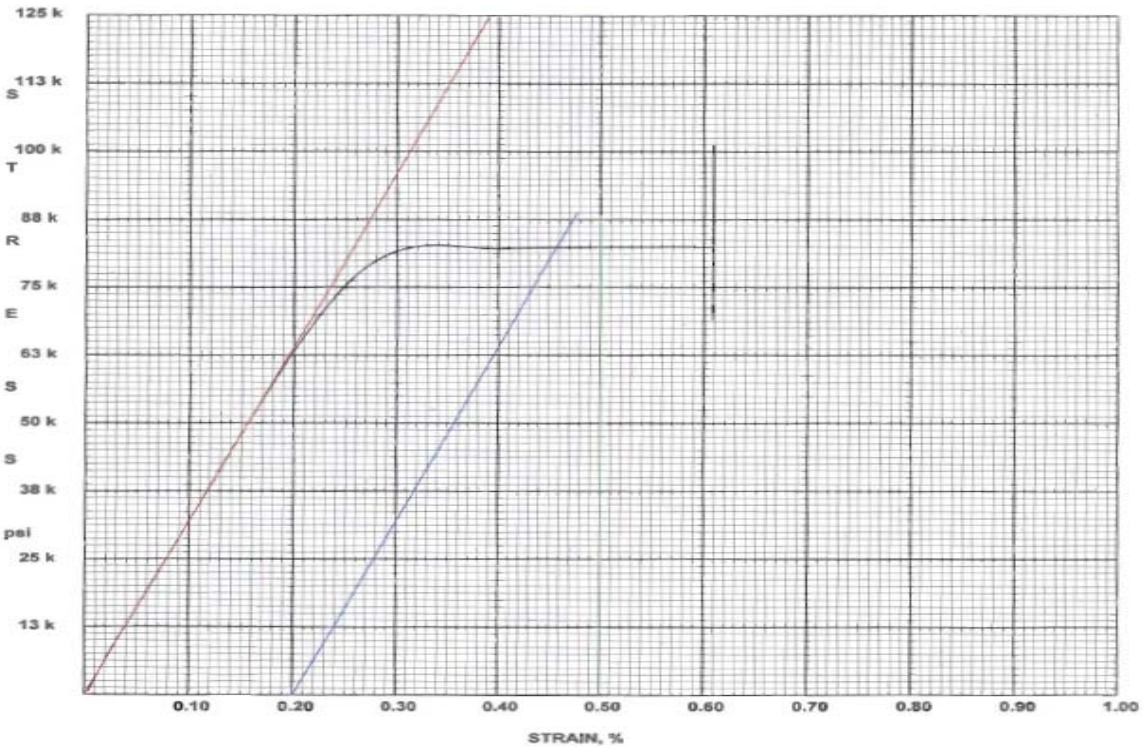


**Figure B.8** Stress – Strain Plot for Bottom Flange Sample 6-A

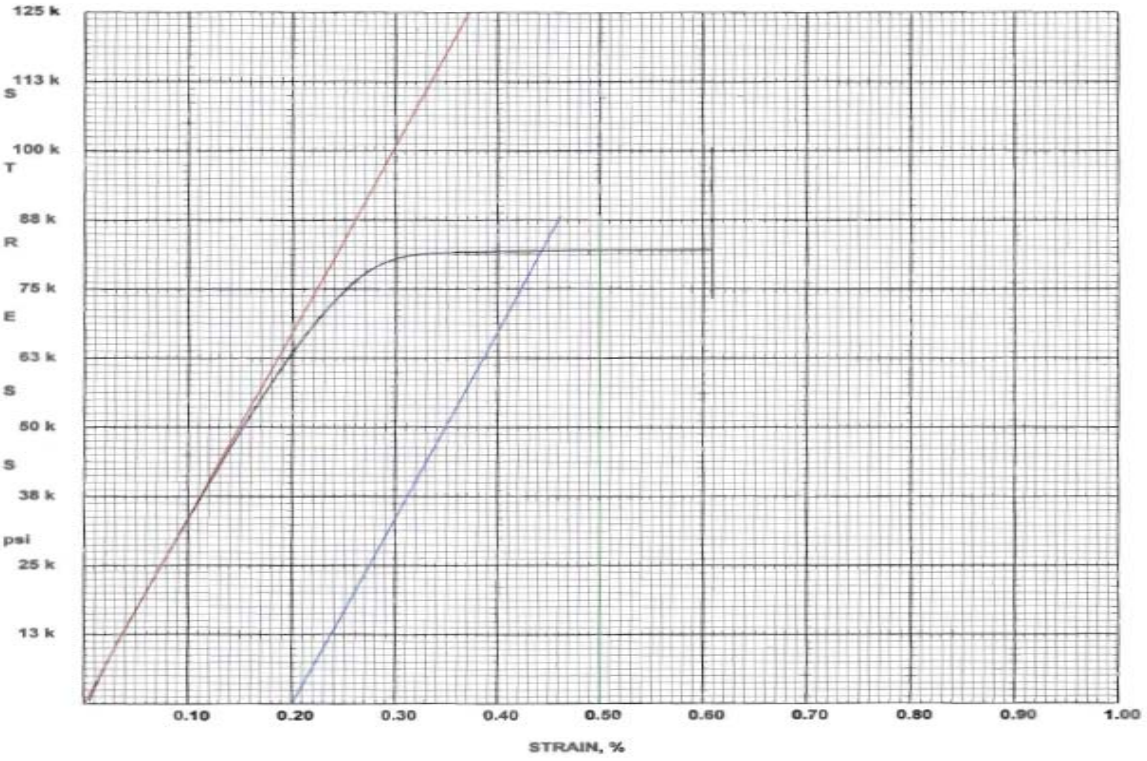


**Figure B.9** Stress – Strain Plot for Bottom Flange Sample 1-B

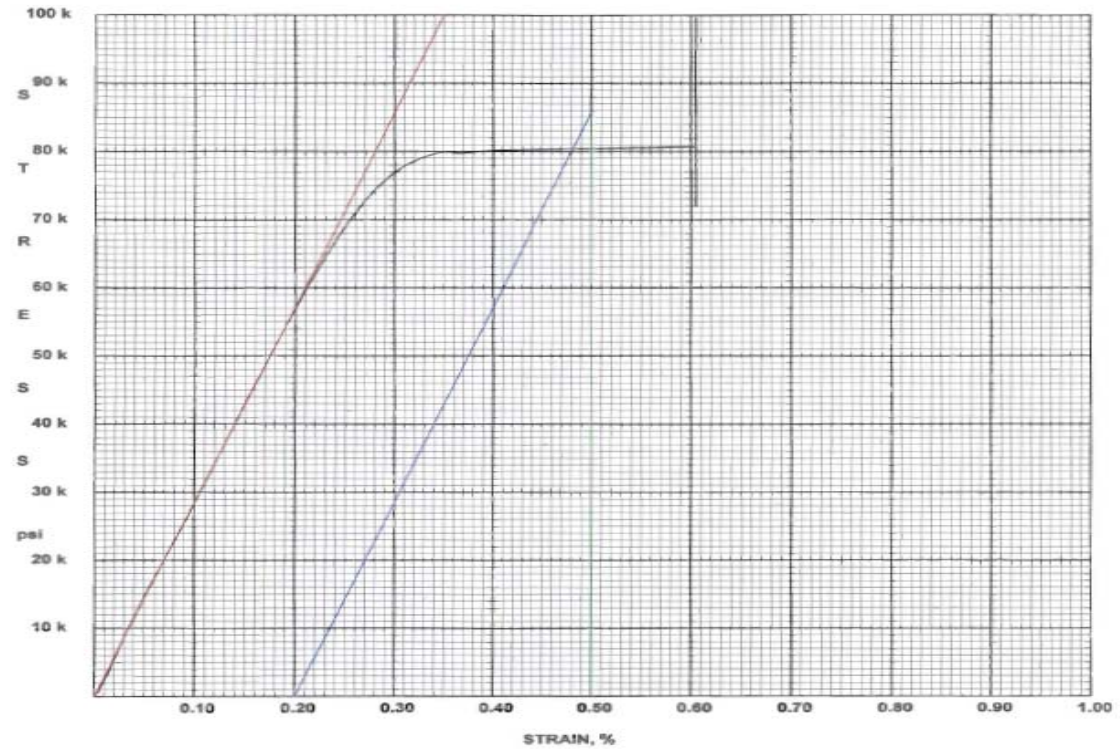


**Figure B.10** Stress – Strain Plot for Bottom Flange Sample 2-B

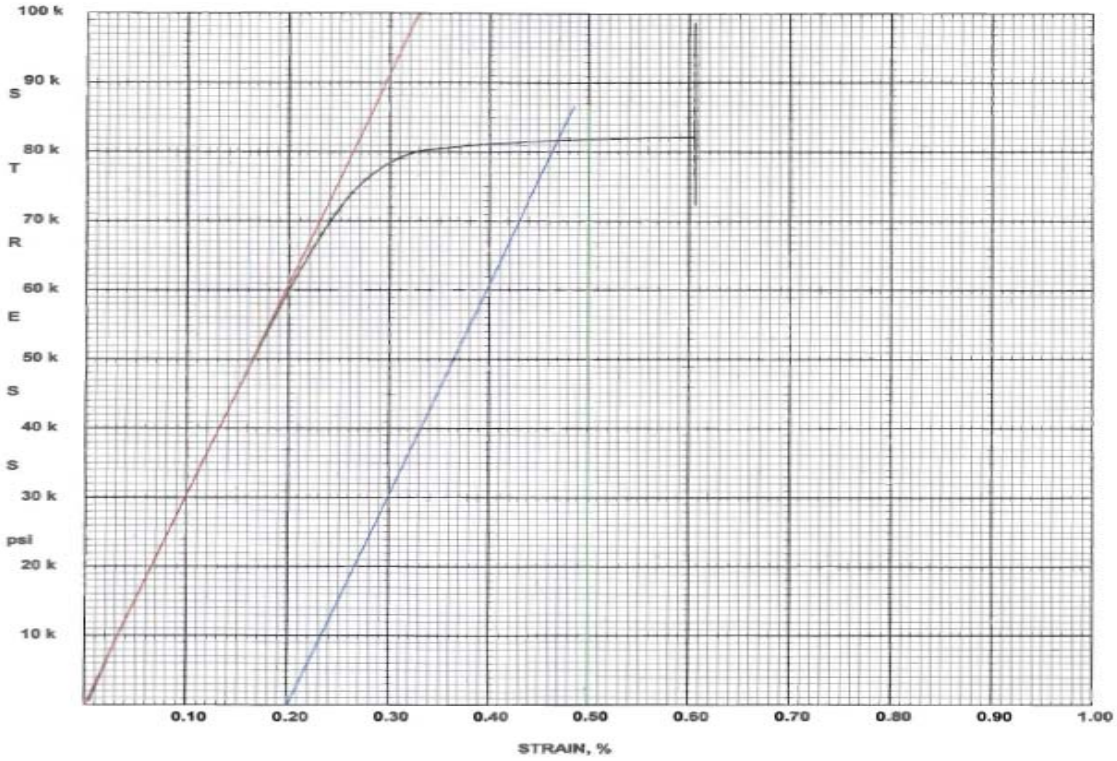


**Figure B.11** Stress – Strain Plot for Bottom Flange Sample 3-B

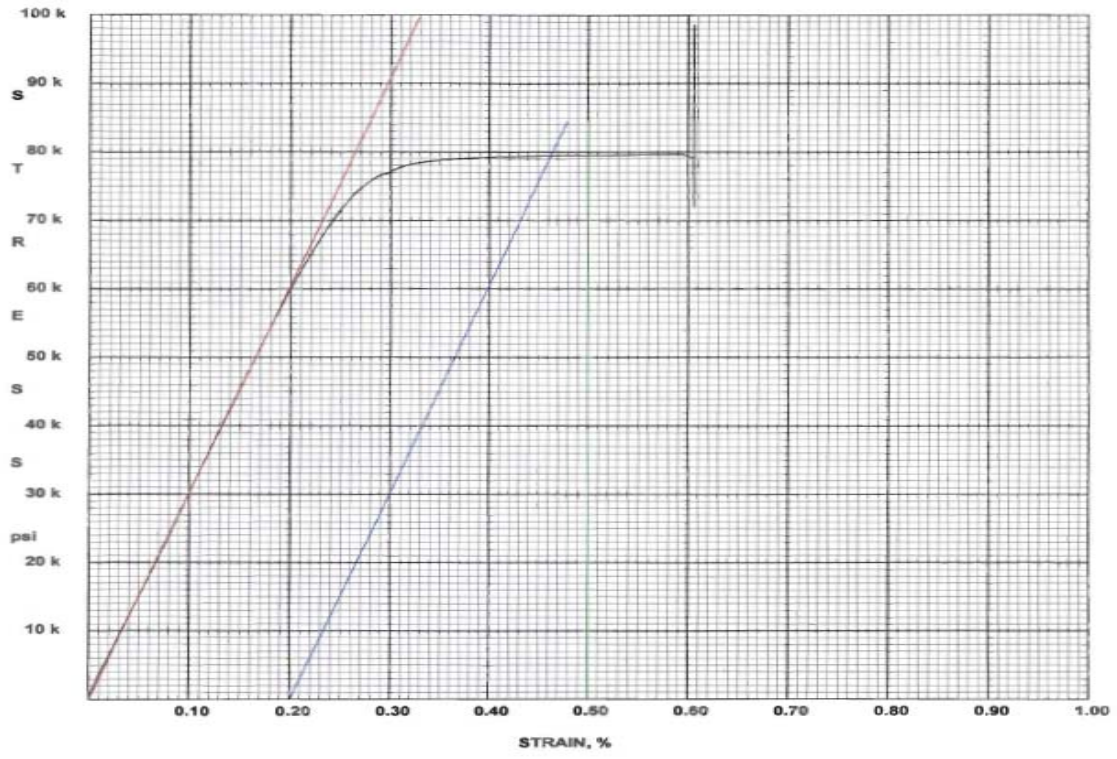


**Figure B.12** Stress – Strain Plot for Bottom Flange Sample 4-B

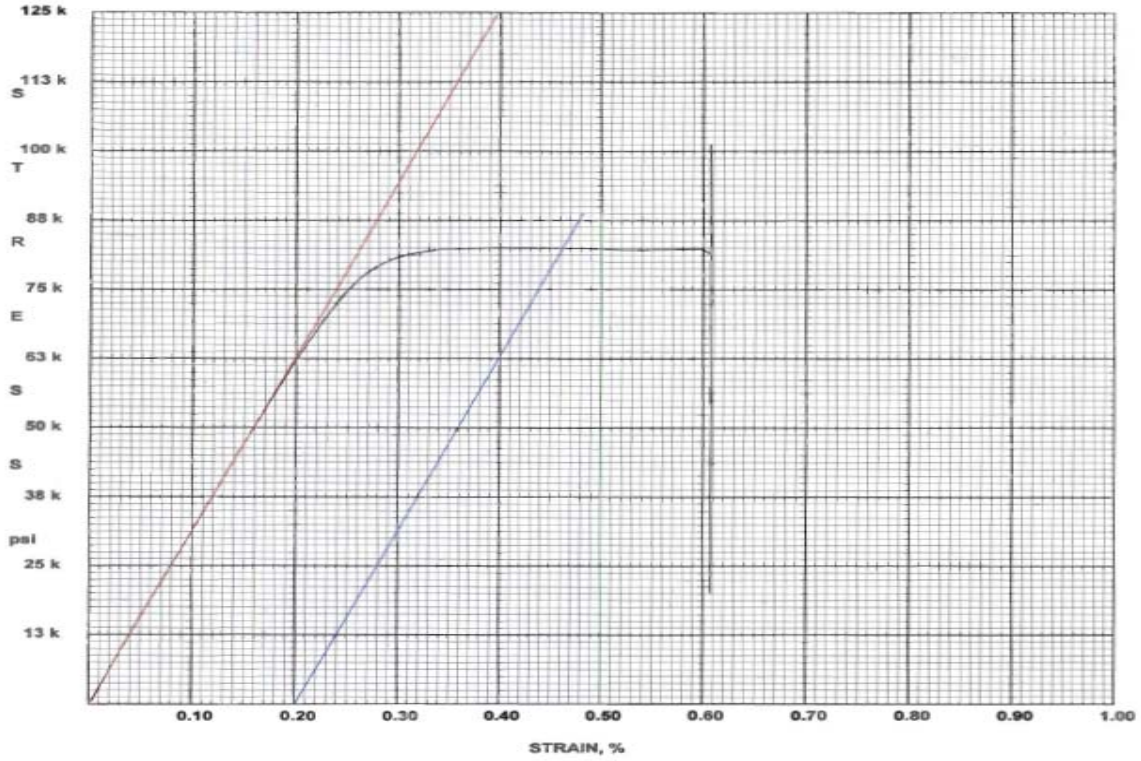


**Figure B.13** Stress – Strain Plot for Bottom Flange Sample 5-B

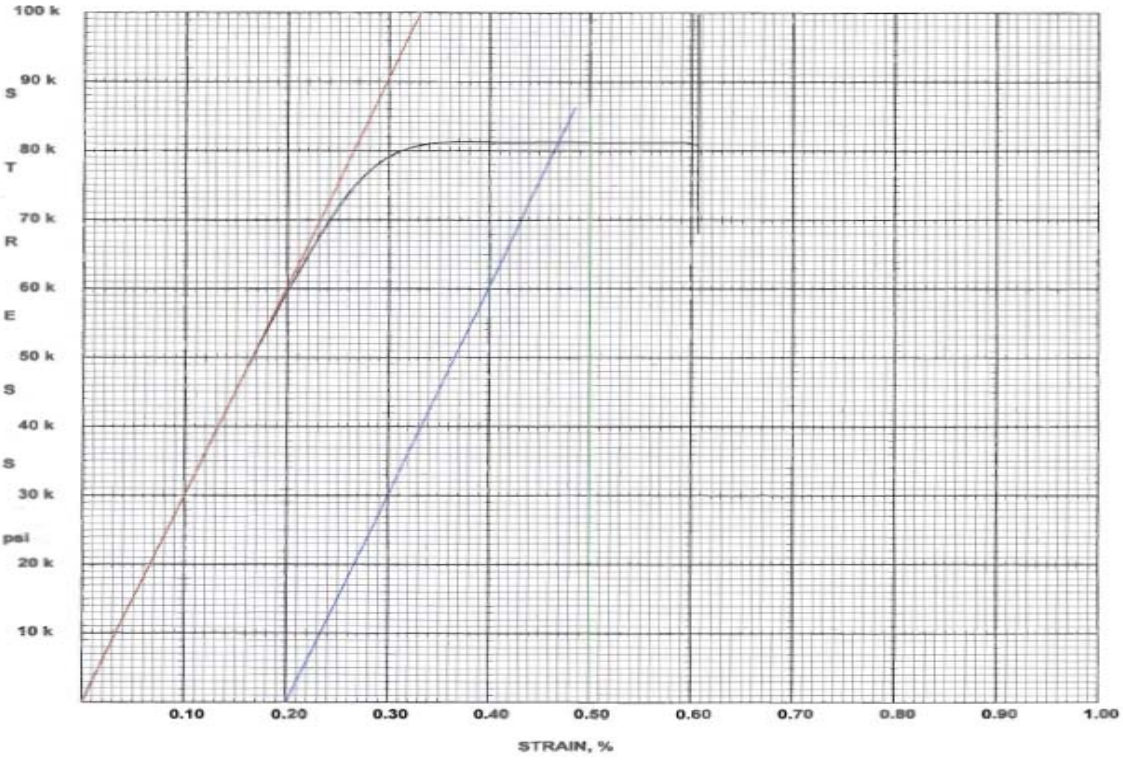


**Figure B.14** Stress – Strain Plot for Bottom Flange Sample 6-B

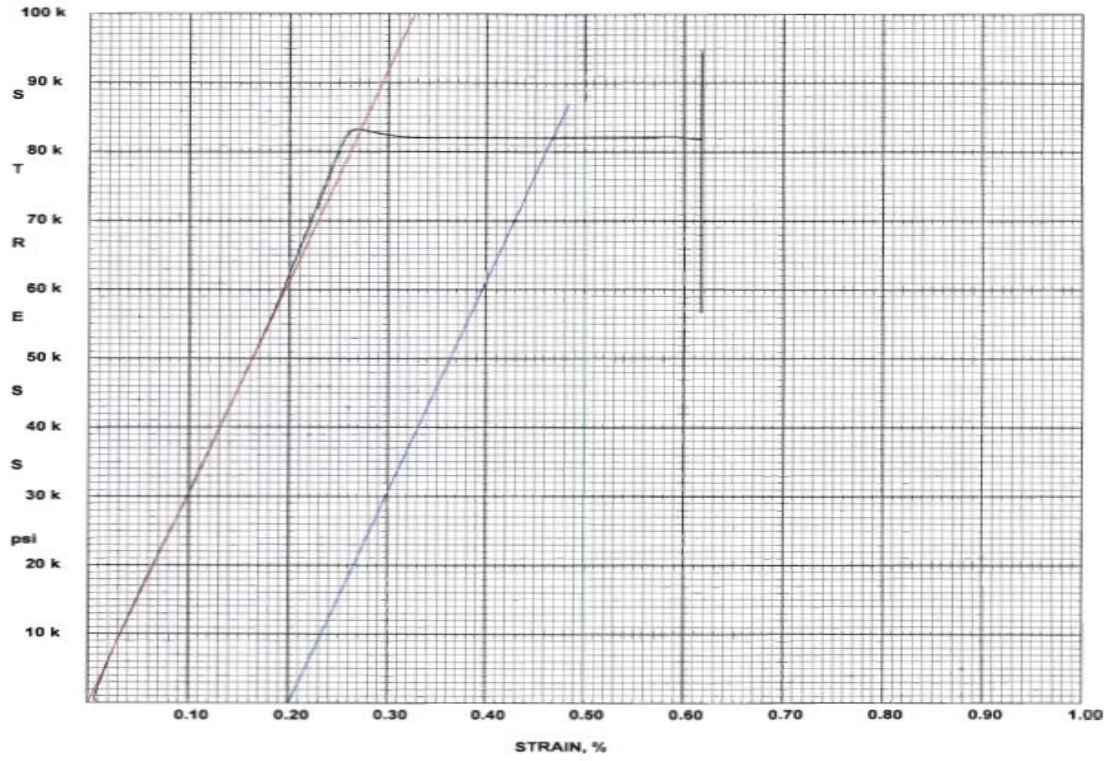


**Figure B.15** Stress – Strain Plot for Top Flange Sample 2-A

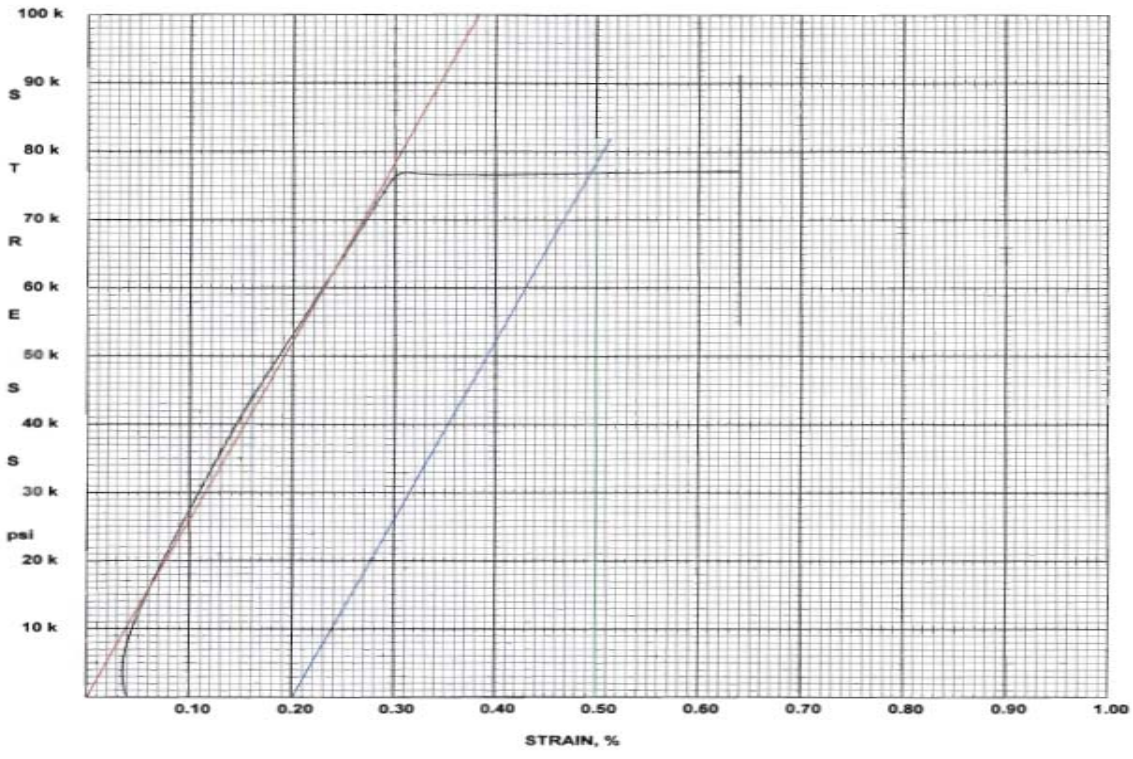


**Figure B.16** Stress – Strain Plot for Top Flange Sample 3-A

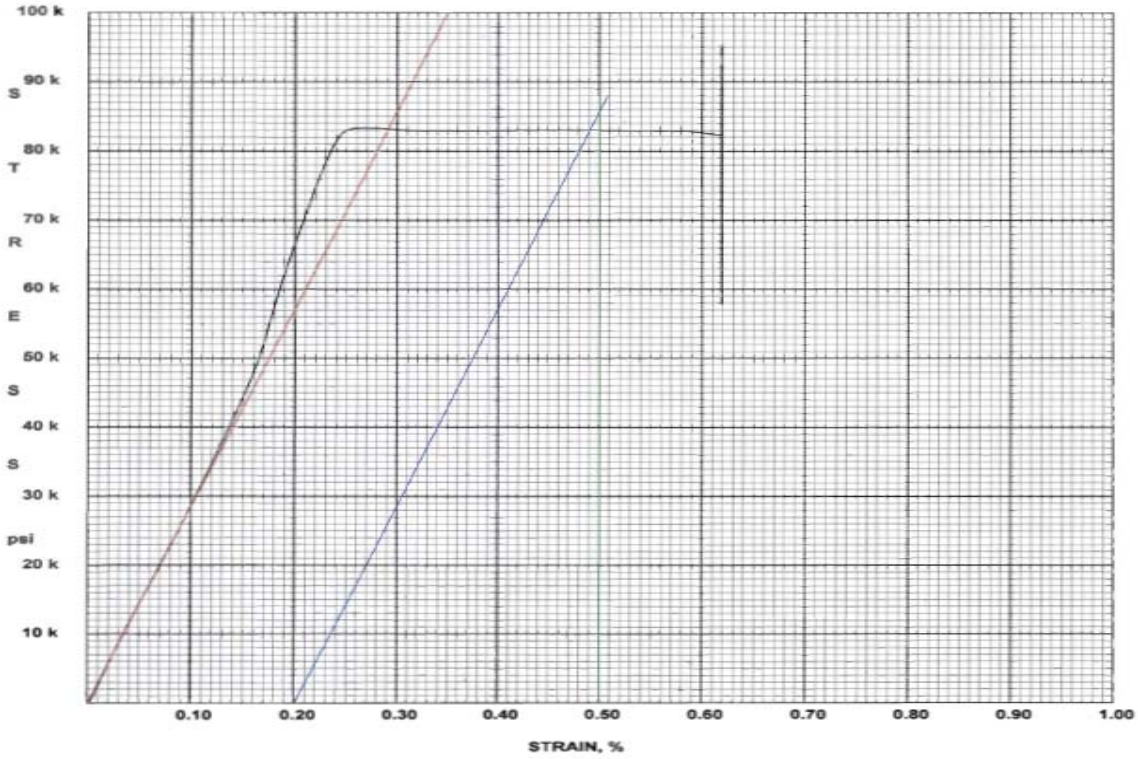


**Figure B.17** Stress – Strain Plot for Top Flange Sample 4-A

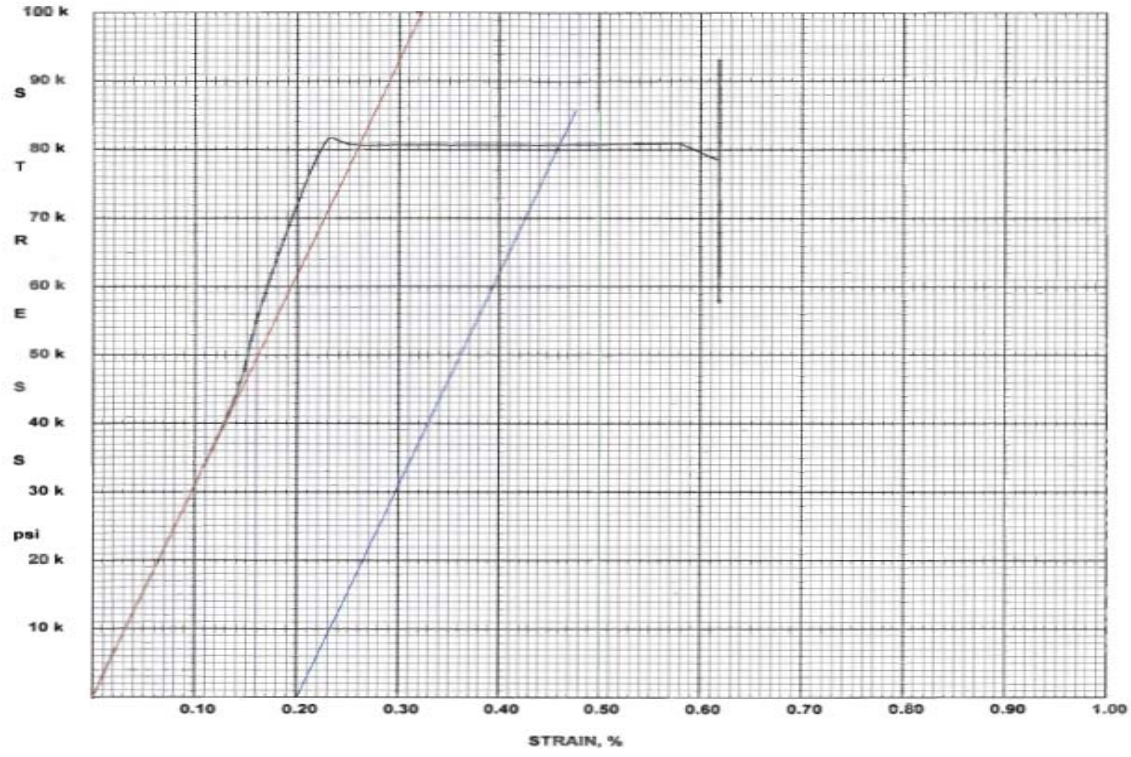


**Figure B.18** Stress – Strain Plot for Top Flange Sample 5-A

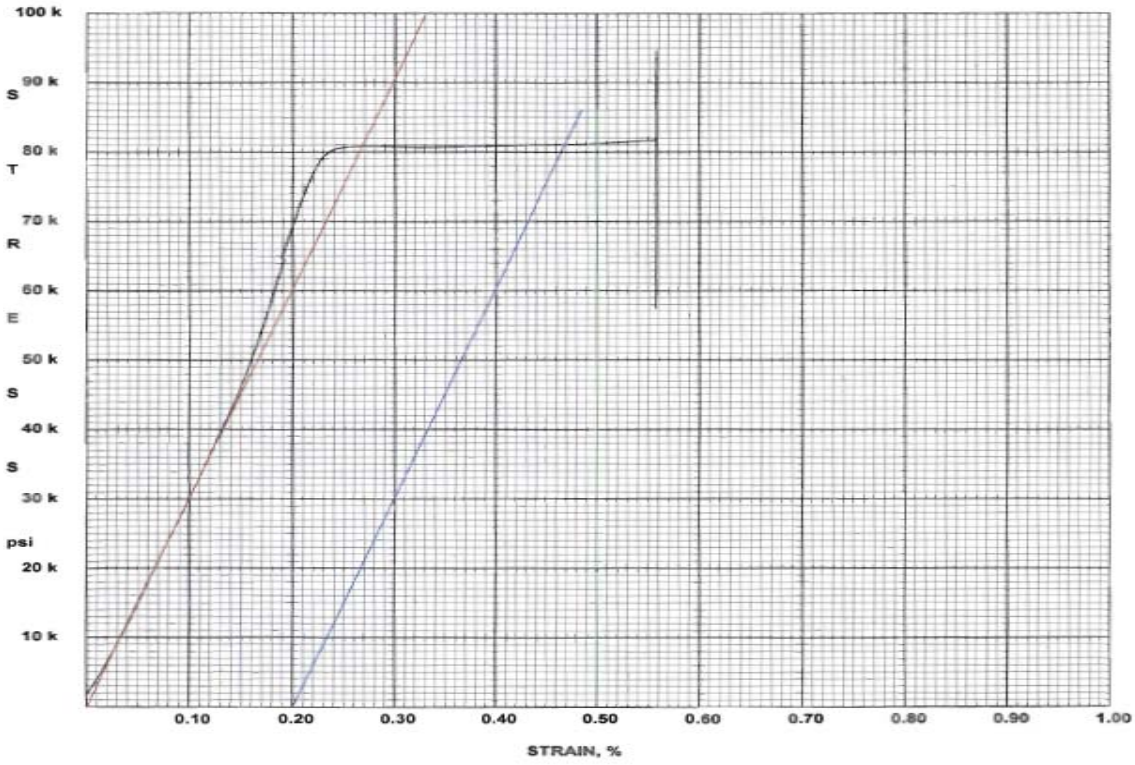


**Figure B.19** Stress – Strain Plot for Top Flange Sample 3-B

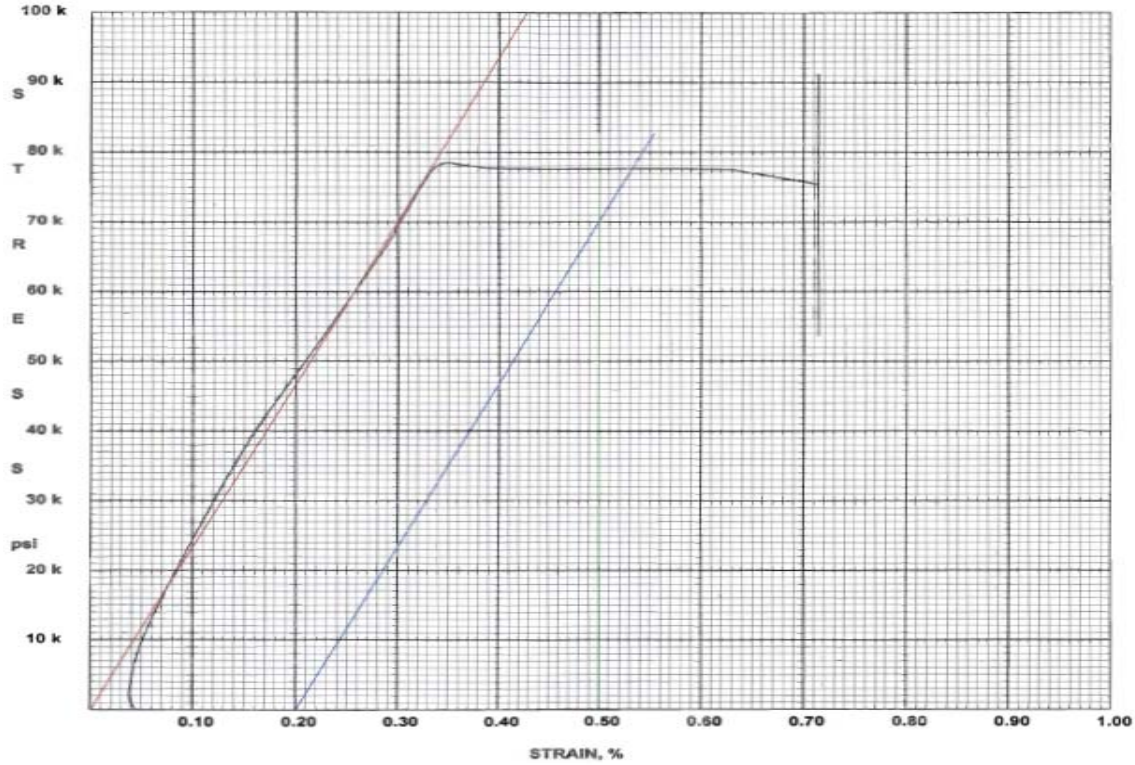


**Figure B.20** Stress – Strain Plot for Top Flange Sample 4-B

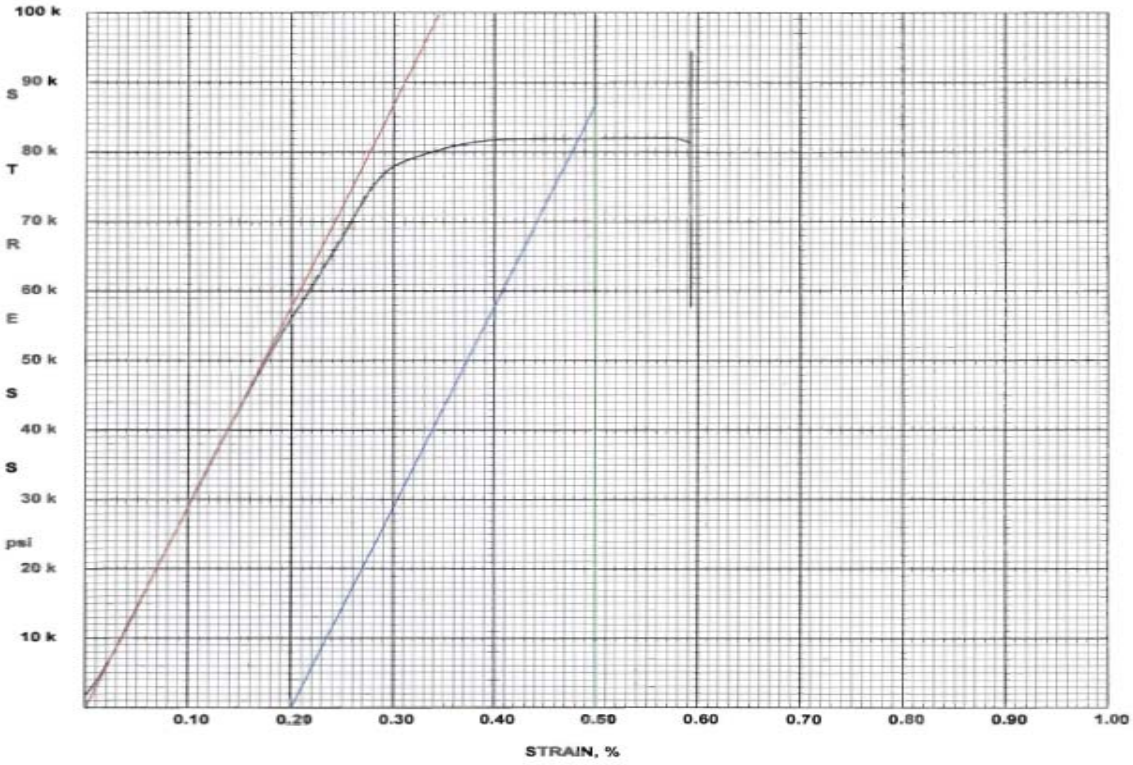


**Figure B.21** Stress – Strain Plot for Top Flange Sample 5-B

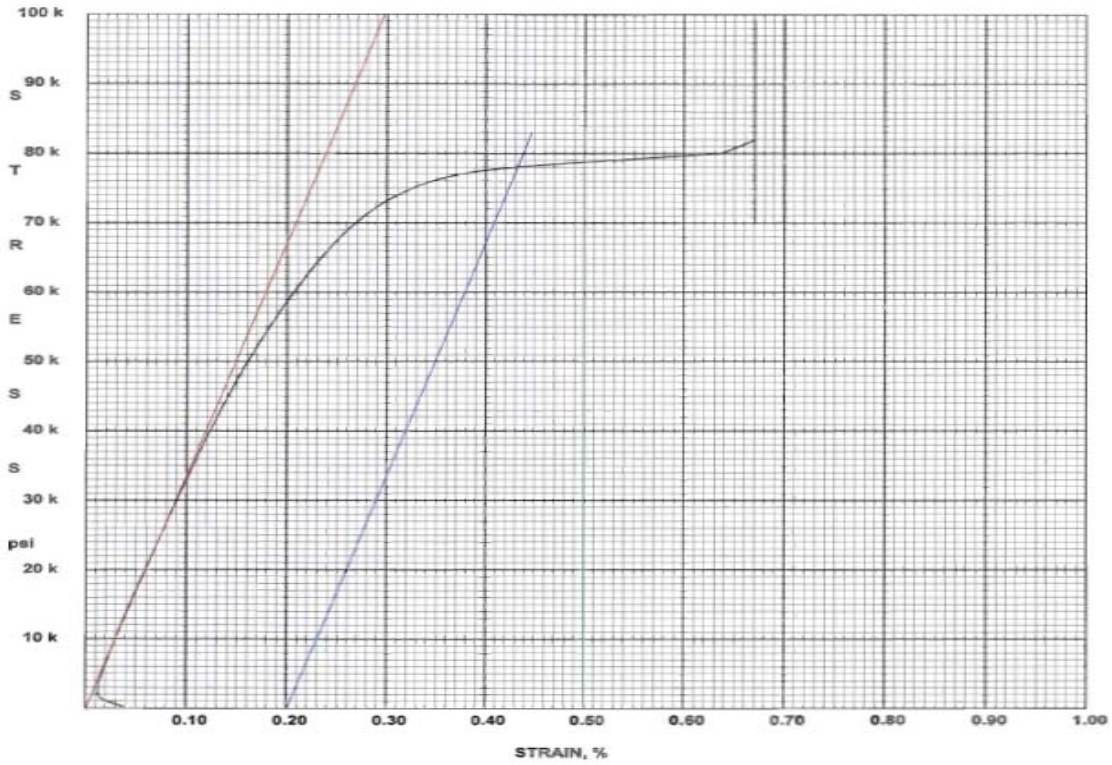


**Figure B.22** Stress – Strain Plot for Web Plates Sample 1-A

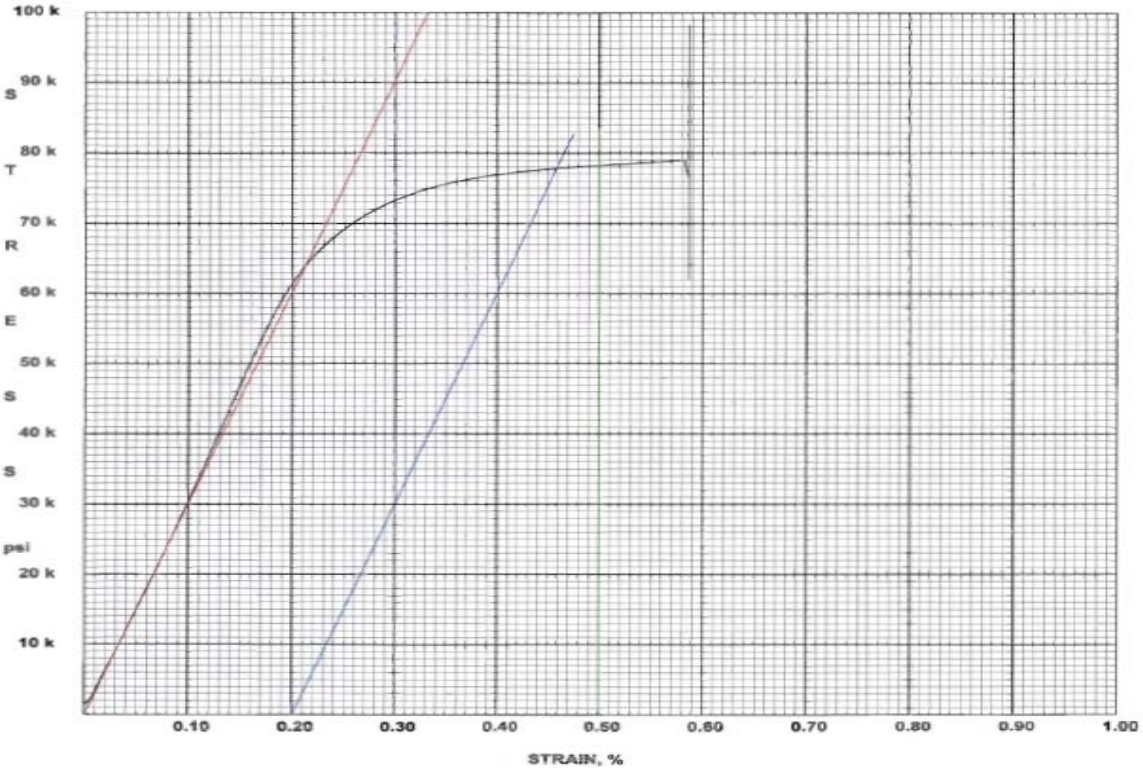


**Figure B.23** Stress – Strain Plot for Web Plates Sample 2-A

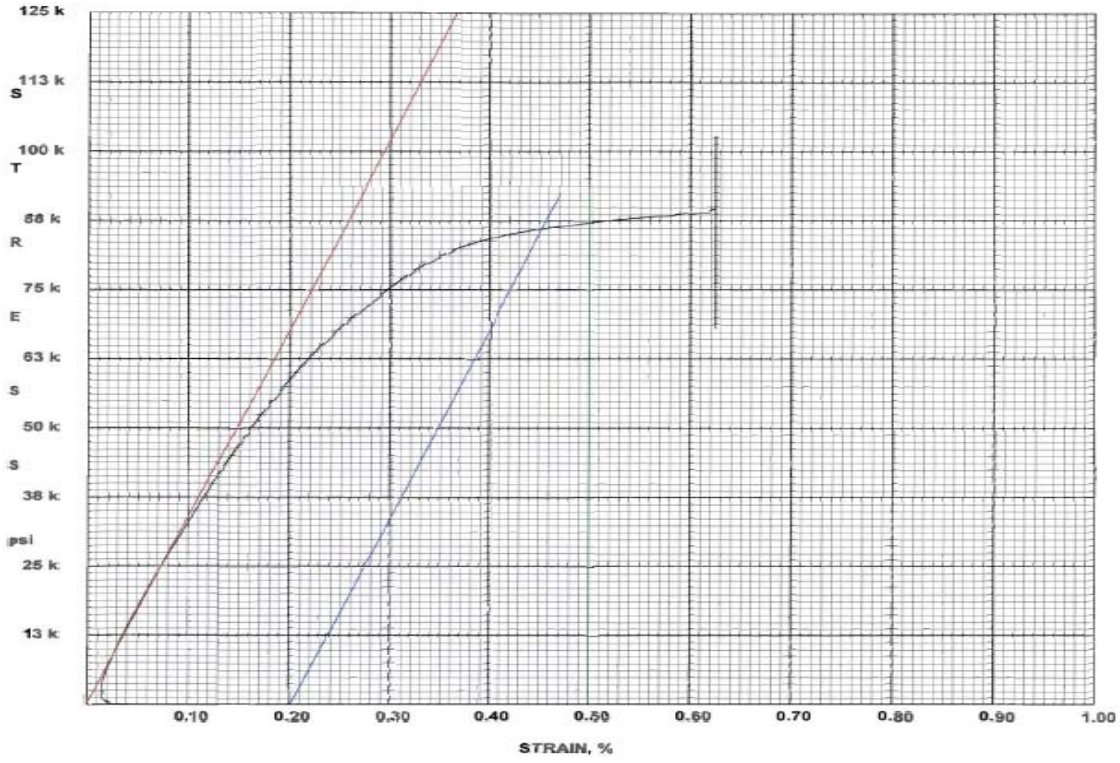


**Figure B.24** Stress – Strain Plot for Web Plates Sample 3-A

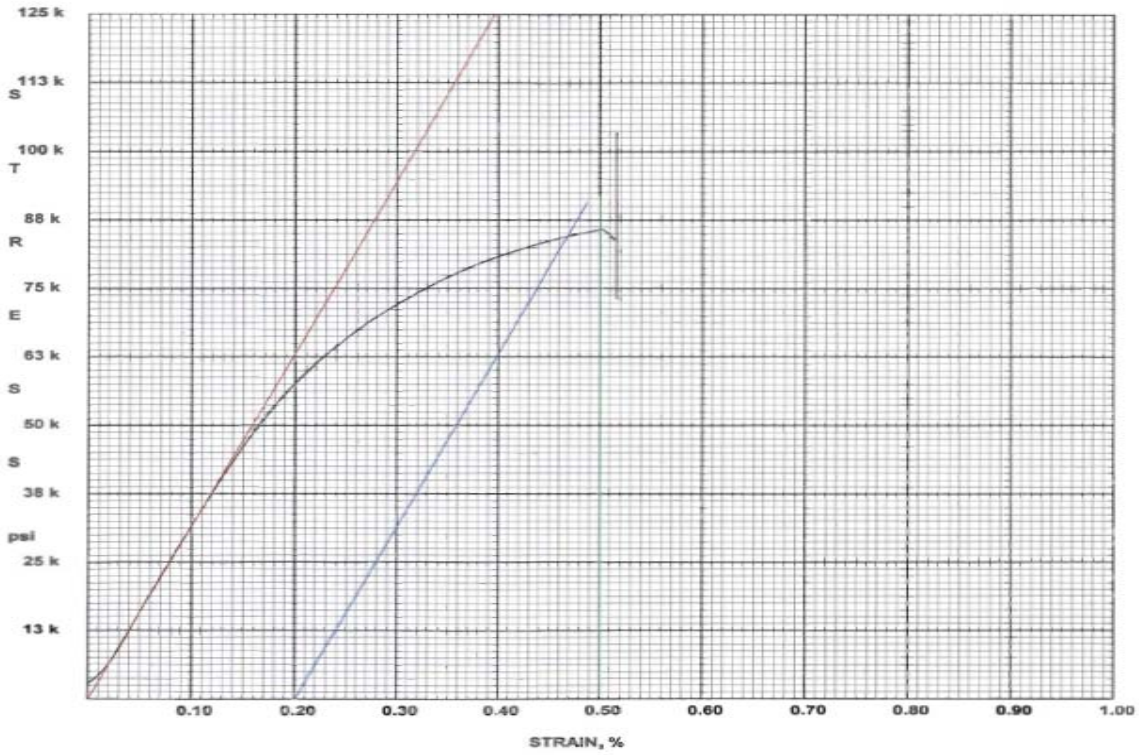


**Figure B.25** Stress – Strain Plot for Web Plates Sample 4-A

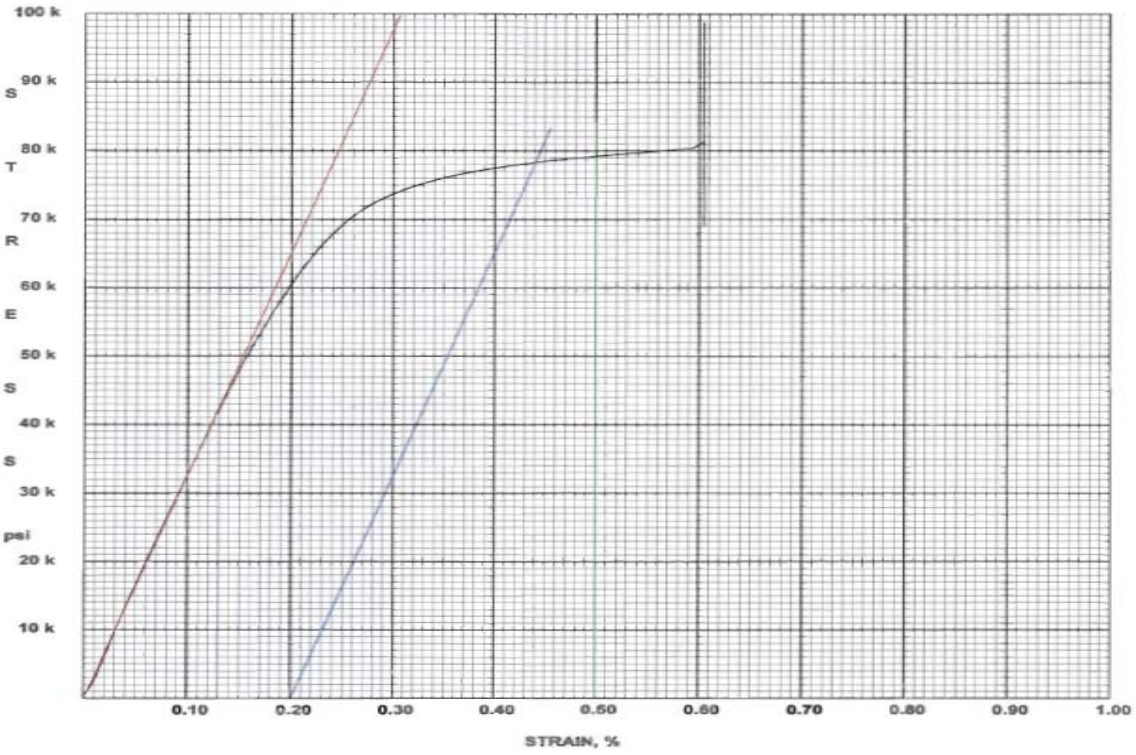


**Figure B.26** Stress – Strain Plot for Web Plates Sample 5-A

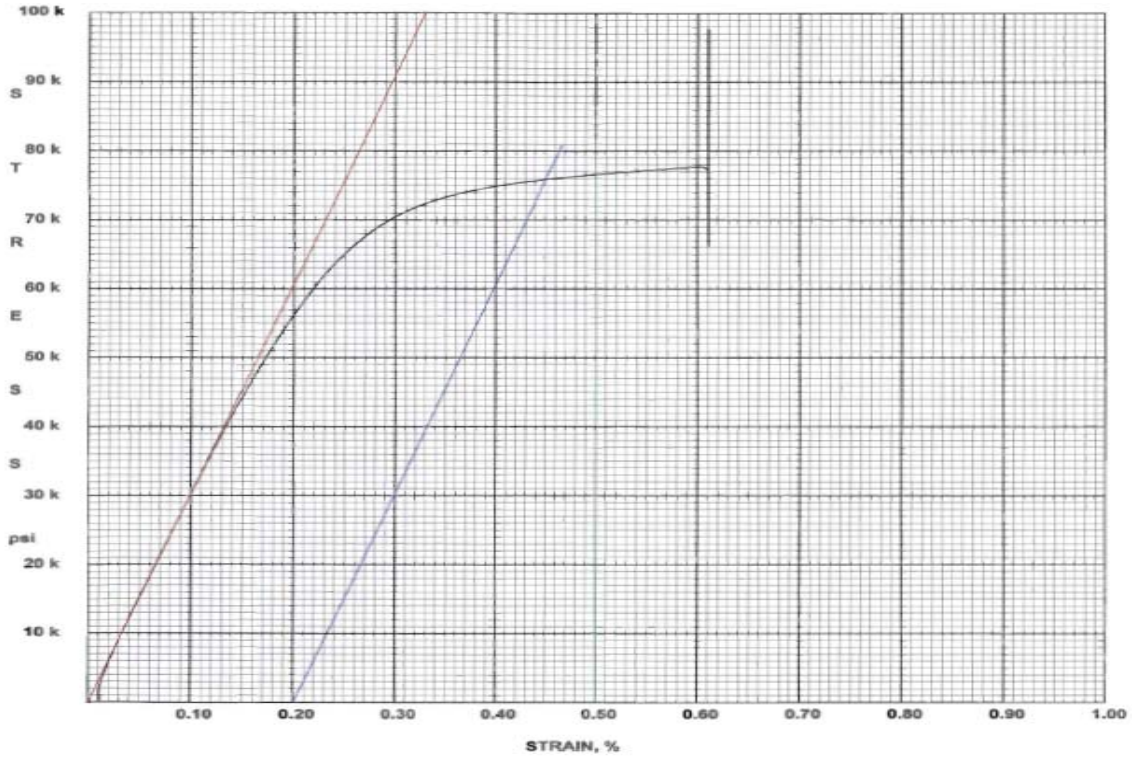


**Figure B.27** Stress – Strain Plot for Web Plates Sample 6-A

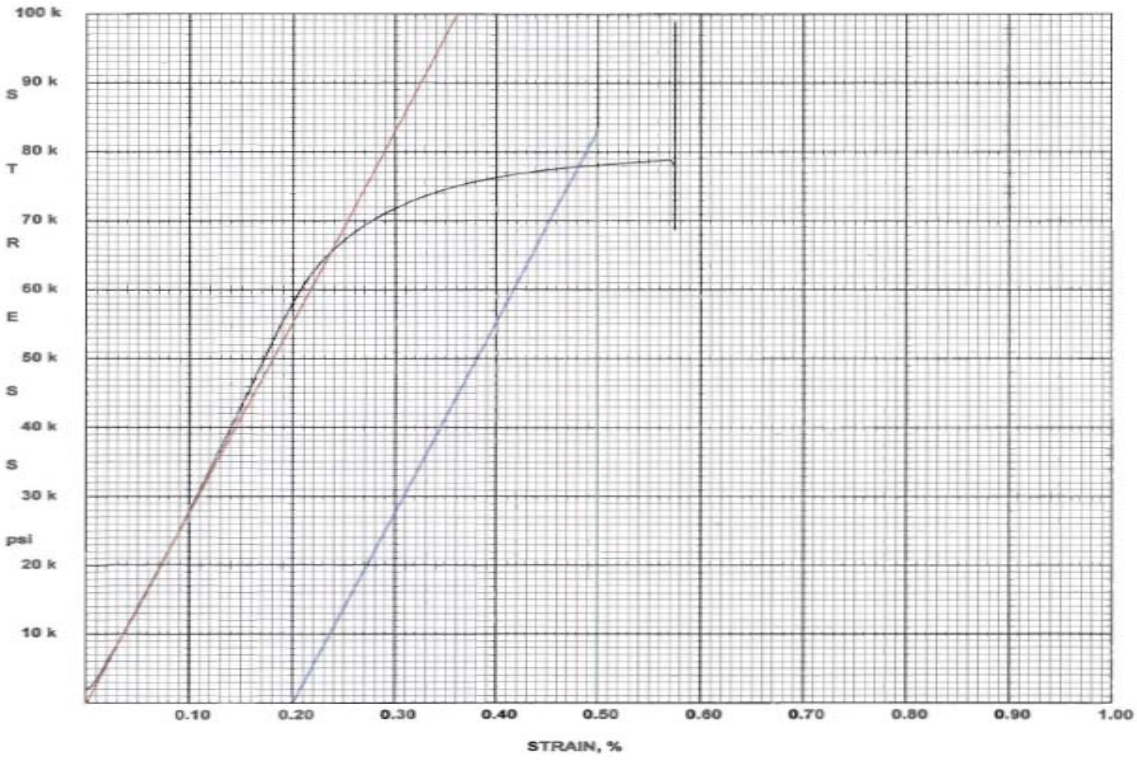


**Figure B.28** Stress – Strain Plot for Web Plates Sample 1-B

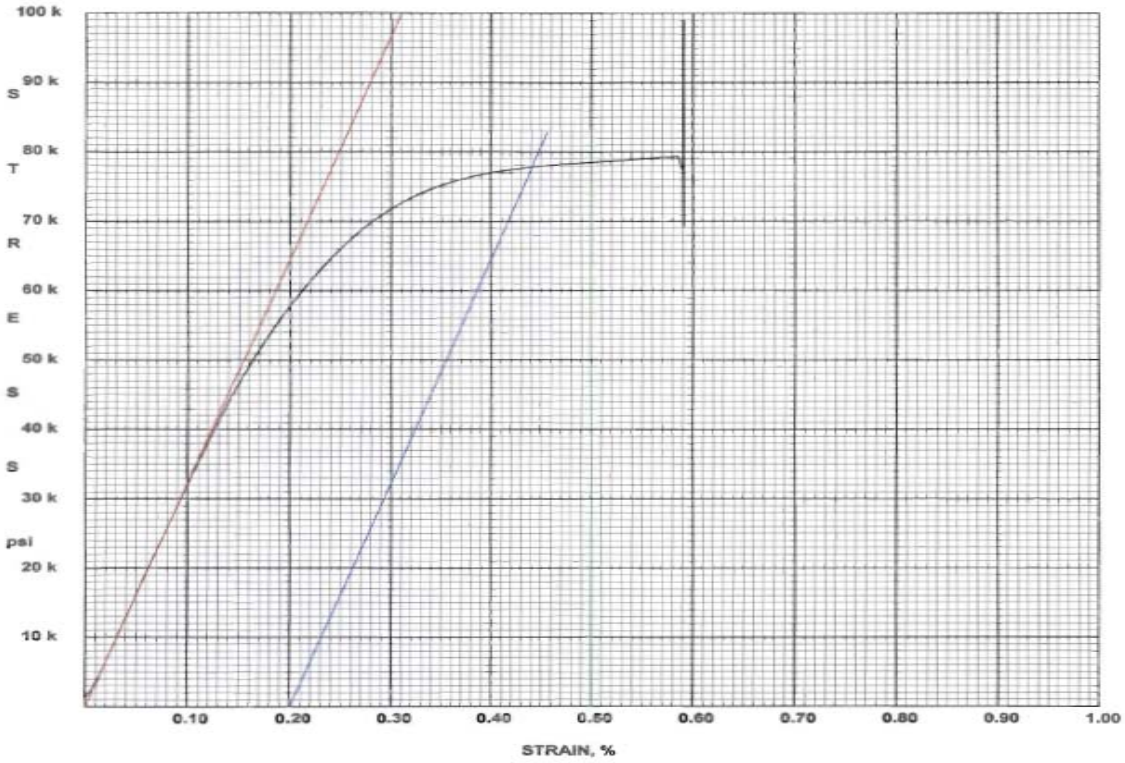


**Figure B.29** Stress – Strain Plot for Web Plates Sample 2-B

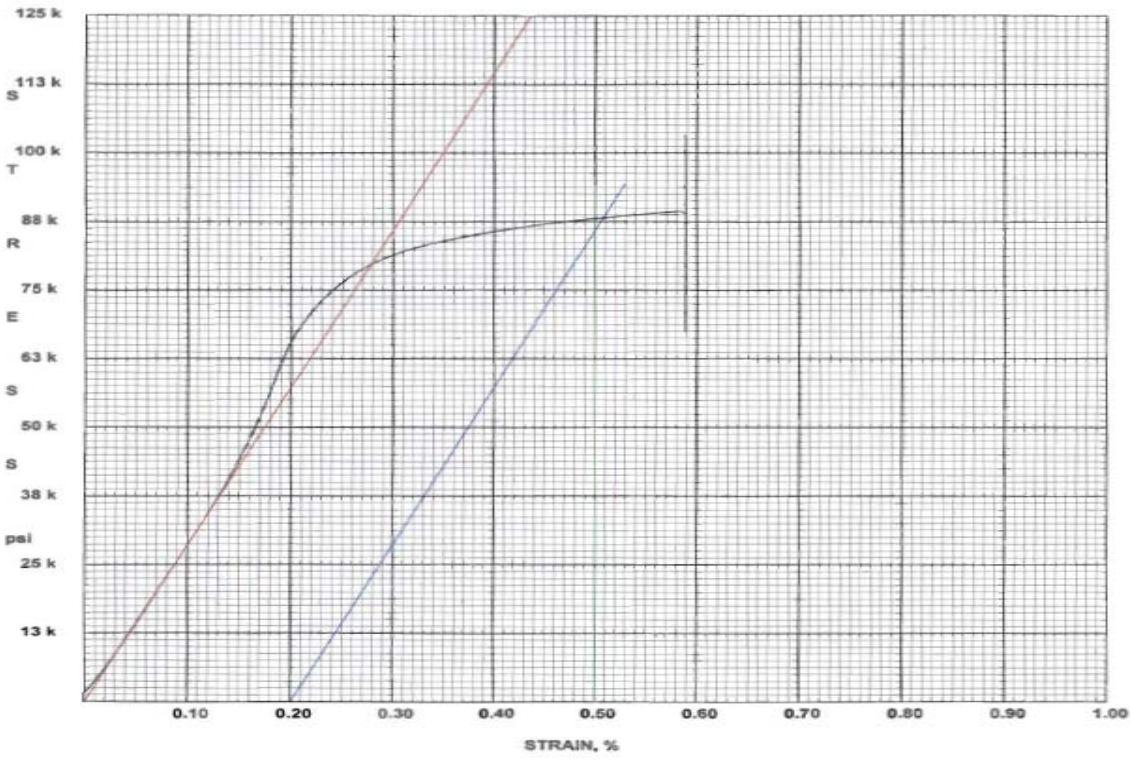


**Figure B.30** Stress – Strain Plot for Web Plates Sample 3-B

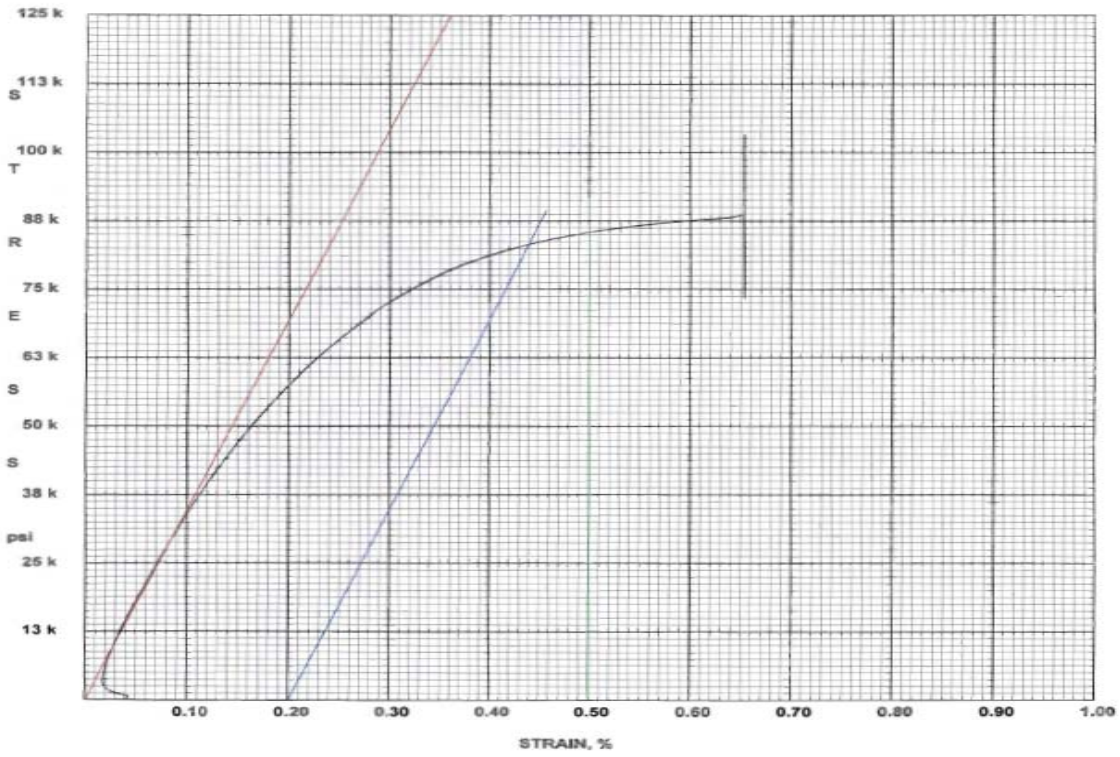


**Figure B.31** Stress – Strain Plot for Web Plates Sample 4-B

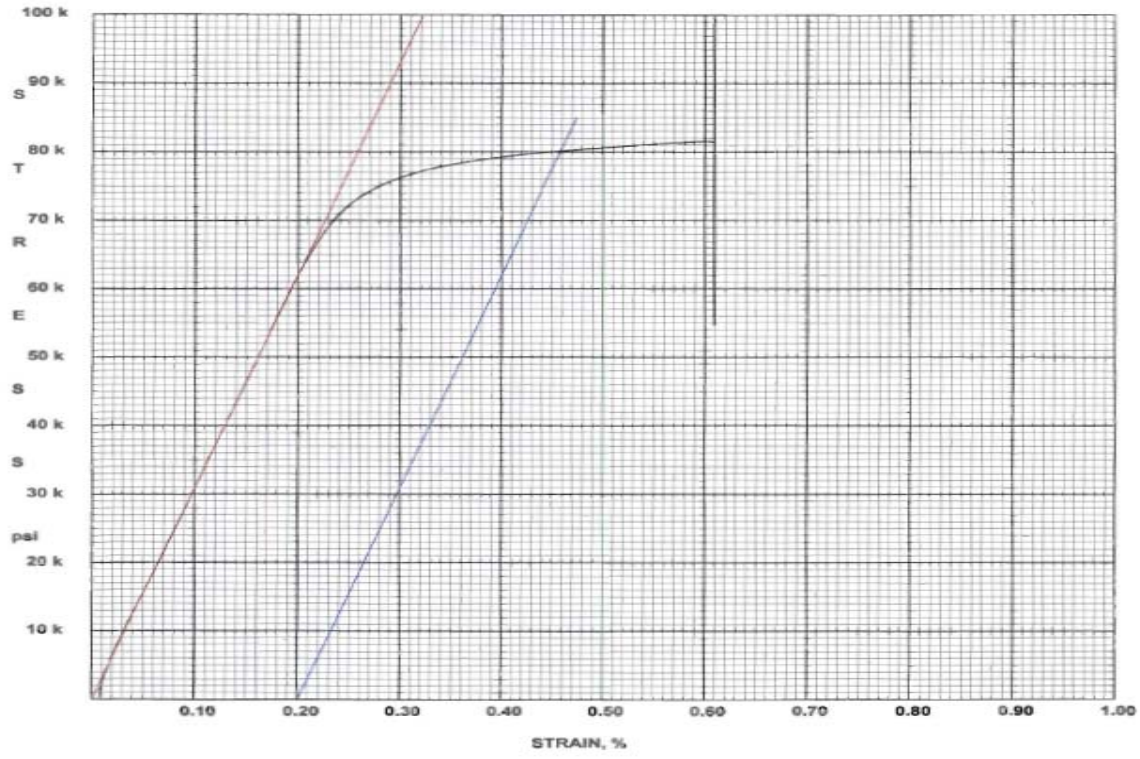


**Figure B.32** Stress – Strain Plot for Web Plates Sample 5-B

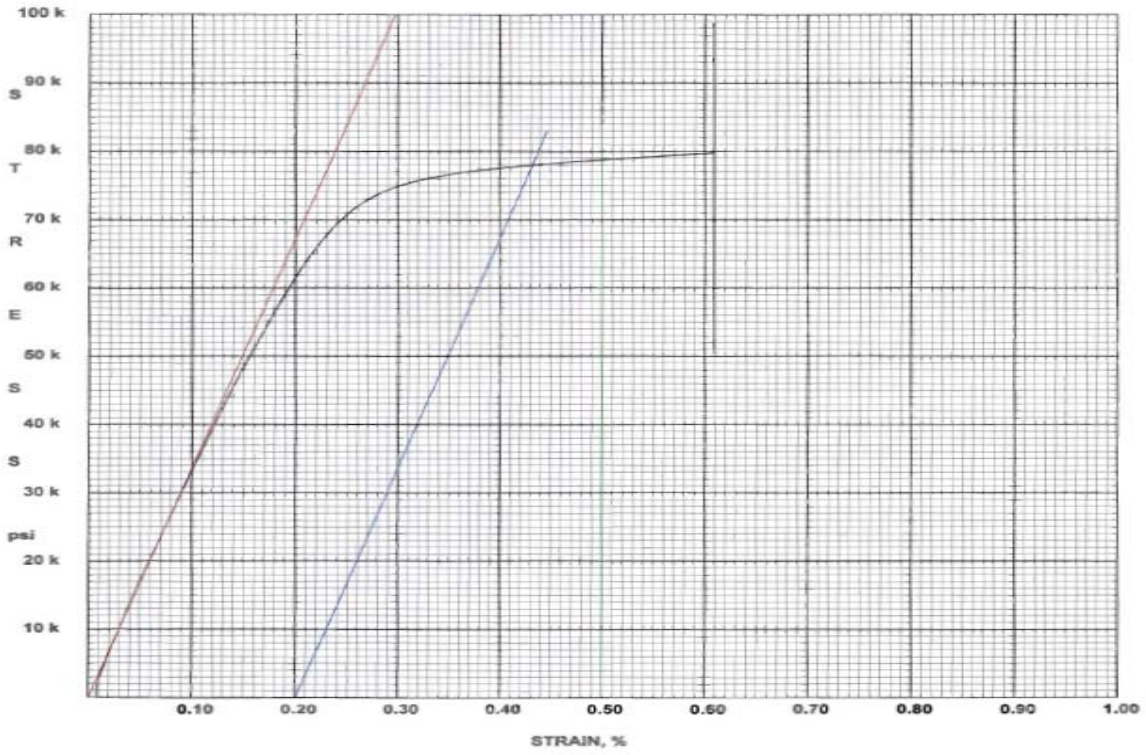


**Figure B.33** Stress – Strain Plot for Web Plates Sample 6-B

## References

B.1 Mehta, P.K. and Monteiro, P.J.M. (1993), *"Concrete: Structure, Properties, and Materials"* 2nd Ed. (Prentice-Hall, Englewood Cliffs, New Jersey, 1993), pp. 60.

B.2 Potter W. (FDOT), 03/07/08, 05/15/08 and 10/03/08, *"Compressive strength data"*, e-mail correspondence.

B.3 Nucor Steel Birmingham, Inc., Birmingham, AL., 03/13/07 and 11/12/07, *"Certified Mill Test Report"*.

B.4 Potter W. (FDOT) and FDOT's State Materials Office, FL, 08/18/08, *"Coupon test data"*, e-mail correspondence.

# Appendix C

Instrumentation Specifications

## C.1 Introduction

This appendix describes the Instrumentation specifications of all the sensors used in the fatigue, service and ultimate load tests.

## C.2 Instrumentation Specifications of Sensors Used in Fatigue Test

This section describes the instrumentation specifications for sensors used in Fatigue test.

### C.2.1 Electronic Hardware and Software

DAQ Software

- National Instruments LabVIEW Professional Development Version 8.5
- Measurement and Automation Explorer Version 4.3
- DAQmx Version 8.6.0f5

DAQ Hardware

- Embedded Controller: National Instruments PXI-8106
- Main Chassis: National Instruments PXI-1052
- Expansion Chassis: National Instruments SCXI-1001
- ADC (Analog to Digital Converter): National Instruments PXI-6251
- Signal Conditioning: National Instruments SCXI-1520 with SCXI-1314 terminal block for load, displacement and strain and SCXI-1112 for temperature

Filtering

- 10 Hz Butterworth low pass hardware filter was applied to each channel on the signal conditioning module before the ADC.

Sampling and Recording

Fatigue

Data was acquired at 200 samples per second with a recording duration of 4 seconds. Recording was triggered based on cycle count and the record increment was set at every 20000 cycles. Files were recorded to a LabVIEW TDM (Test Data Management) file (.tdm) which is a binary file

that is described with an XML header. The files can be viewed in Excel using the TDM add-in for Excel which can be downloaded here: http://zone.ni.com/devzone/cda/epd/p/id/2944

Static

Each static test was ran and recorded at an increment of 500000 cycles. Data was acquired continuously at 1000 samples per second. The first 250 samples of each 1 second window of the 1000 points were averaged, resulting in 1 sample per second recorded to disk. Files were recorded to a LabVIEW Measurement File (.lvm) which is an ASCII tab delimited file that can be directly imported into Excel or many other analysis packages for review.

### C.2.2 Strain Gages

### Steel

Nomenclature of Sensors

- SG_69–SG_78 (Top Flange)
- SG_79–SG_102, SG_129–SG_140 (Webs)
- SG_115–SG_128 (Bottom Flange)
- SG_57 AB–SG_68 AB (Top Slab Reinforcement)

Instrumentation Specifications

- Manufacturer: TML
- Model Number: FLA-5-11-3LT
- Gauge Length: 5mm
- Gauge Factor: 2.11
- Gauge Resistance: 120 Ω
- Excitation Voltage Used: 1 Volt
- Surface Preparation: surface sanded using 120 grit sandpaper, then cleaned with acetone before application
- Surface Pre-coating: None
- Adhesive: TML CN
- Environmental Coating: TML SB tape

- Cable connection at gage: TYCO S01-02-R solder sleeve
- Cable connection at DAQ: screwed into 1314 terminal block

**Concrete**

Nomenclature of Sensors

- SG_40–SG_56 (Not used in fatigue test as slab cracked in initial static test.)
- SG_103–SG_114 (Bottom Slab)

Instrumentation Specifications

- Manufacturer: TML
- Model Number: PL-60-11-1L
- Gauge Length: 60mm
- Gauge Factor: 2.09
- Gauge Resistance: 120 Ω
- Excitation Voltage Used: 1 Volt
- Surface Preparation: surface ground using concrete grinding disk, ground surface sanded using 120 grit sandpaper, then cleaned with acetone before application
- Surface Pre-coating: TML PS
- Adhesive: TML RP-2
- Environmental Coating: TML SB tape
- Cable connection at gage: TYCO S01-02-R solder sleeve
- Cable connection at DAQ: screwed into 1314 terminal block

### C.2.3 Displacement

**Slip**

Nomenclature

- (LV_30-LV_38)

Instrumentation Specifications

- TML Model# CDP-50
- ±1 inch range

**Deflection**

Nomenclature

- (LV_07-LV_08)

Instrumentation Specifications

- Omega Model# LD620-50
- ±2 inch range

**Deflection**

Nomenclature

- (LV_21-LV_24, LV_28, LV_29)

Instrumentation Specifications

- Omega Model# LD620-15
- ±0.5 inch range

## C.2.4 Loading Apparatus

**Hydraulic Actuator System**

Actuator Load: MTS, 110 kip capacity

**Load Cells**

Nomenclature

- (LC_03-LC_04) (Hold Down End)

Instrumentation Specifications

- Interface Model# 1232
- 100 kip capacity

### C.2.5 Thermocouples

Instrumentation Specifications

- Omega Part# SA1-T-SRTC Type T fine wire surface mount thermocouple

## C.3 Instrumentation Specifications of Sensor Used in Service and Ultimate Test

A complete instrumentation specification of all the sensors used in Service and Ultimate load test is described in this section.

### C.3.1 Electronic Hardware and Software

DAQ Software

- National Instruments LabVIEW Professional Development Version 8.5
- Measurement and Automation Explorer Version 4.3
- DAQmx Version 8.6.0f5

DAQ Hardware

- Chassis: National Instruments PXI-1052 combination PXI/SCXI signal conditioning chassis with SCXI-1001 expansion chassis
- Embedded controller: National Instruments PXI-8106
- ADC (Analog to Digital Converter): National Instruments PXI-6251
- Signal Conditioning:
- Strain, displacement, load cells: National Instruments SCXI-1520 Wheatstone bridge module with SCXI-1314/SCXI-1314T terminal block

Filtering

- A 10Hz Butterworth low pass hardware filter was applied to all channels on the signal conditioning module before the ADC.

Sampling and Recording

Data was sampled at 1000 samples per second. Every 100 samples were averaged in real time resulting in 10 samples per second recorded to disk. Files were recorded to a LabVIEW measurement file (.lvm) which is an ASCII tab delimited file.

## C.3.2 Strain Gages

### Girder Steel

Nomenclature of Sensors

- SG_69–SG_78 (Top Flange)
- SG_79–SG_102, SG_129–SG_140 (Webs)
- SG_115–SG_128 (Bottom Flange)

Instrumentation Specifications

- Manufacturer: TML
- Model Number: FLA-5-11-3LT
- Gauge Length: 5mm
- Gauge Factor: 2.11
- Gauge Resistance: 120 Ω
- Excitation Voltage Used: 1 Volt
- Surface Preparation: surface sanded using 120 grit sandpaper, then cleaned with acetone before application
- Surface Pre-coating: None
- Adhesive: TML CN
- Environmental Coating: TML SB tape
- Cable connection at gage: TYCO S01-02-R solder sleeve
- Cable connection at DAQ: screwed into 1314 terminal block

### Reinforcing Steel

Nomenclature of Sensors

- SG_57A–SG_68A, (A – indicates actuator Span)
- SG_57B–SG_68B, (B – indicates Hold Down Span)

*Note*

The nomenclature of strain gages on rebars was modified from (SG_57 AB–SG_68 AB) to (1 AB–16 AB) for simplicity in presenting results.

Instrumentation Specification

- Manufacturer: TML
- Model Number: FLA-5-11-3LT
- Gauge Length: 5mm
- Gauge Factor: 2.11
- Gauge Resistance: 120 Ω
- Excitation Voltage Used: 1 Volt
- Surface Preparation: cross ribs ground in gage area and surface sanded using 120 grit sandpaper, then cleaned with acetone before application
- Surface Pre-coating: None
- Adhesive: TML CN
- Environmental Coating: 1 layer of TML SB tape, then overwrapped with Scotch 2228 rubber mastic tape.
- Cable connection at gage: TYCO S01-02-R solder sleeve
- Cable connection at DAQ: screwed into 1314 terminal block

**Concrete**

Nomenclature of Sensors

- SG_40–SG_56, (Not used in service and ultimate load test as top slab was cracked.)
- SG_103–SG_114 (Bottom Slab)

Instrumentation Specifications

- Manufacturer: TML
- Model Number: PL-60-11-1L
- Gauge Length: 60mm

- Gauge Factor: 2.09
- Gauge Resistance: 120 Ω
- Excitation Voltage Used: 1 Volt
- Surface Preparation: surface ground using concrete grinding disk, ground surface sanded using 120 grit sandpaper, then cleaned with acetone before application
- Surface Pre-coating: TML PS
- Adhesive: TML RP-2
- Environmental Coating: TML SB tape
- Cable connection at gage: TYCO S01-02-R solder sleeve
- Cable connection at DAQ: screwed into 1314 terminal block

### C.3.3 Displacement

### Slip

Nomenclature

- LV_30–LV_38

Instrumentation Specifications

- Manufacturer:  TML
- Electrical Circuit: 350 Ω Wheatstone full bridge
- Mechanical: Shaft, spring return
- Model Number: CDP-50
- Gauge Length: 50mm
- Rated Output: 5mV/V Full Scale
- Non-linearity: 0.3% Rated Output
- Excitation Voltage Used: 5.0 Volts

## Deflection

Nomenclature

- LV_09–LV_14 (Top Flange)
- LV_A–LV_D (Center Support)
- LV_21–LV_24 (Bottom Flange)

Instrumentation Specifications

- Manufacturer: TML
- Electrical Circuit: 350 Ω Wheatstone bridge
- Mechanical: Shaft, spring return
- Model Number: CDP-100
- Gauge Length: 100mm
- Rated Output: 5mV/V Full Scale
- Non-linearity: 0.3% Rated Output
- Excitation Voltage Used: 5.0 Volts

**Deflection**

Nomenclature

- LV_07–LV_08 (Cantilevered End)
- LV_28–LV_29 (Hold Down End)
- LV_18–LV_20, LV_25–LV_27 (Bottom Flange)

Instrumentation Specifications

- Manufacturer: Psi-Tronix
- Electrical Circuit: “B” circuit Wheatstone bridge
- Mechanical: stainless cable, spring return
- Model Number: DT-40-B
- Gauge Length: 40 inches
- Rated Output: 1mV/V/inch

- Non-linearity: 0.05% Rated Output
- Excitation Voltage Used: 10.0 Volts

### C.3.4 Load Cells

**Cantilevered End (South End)**

Nomenclature

- LC_01–LC_02 (Cantilevered End)

Instrumentation Specifications

- Manufacturer: Interface
- Model Number: 1260CHG-600K-B
- Range: 600 kips
- Rated Output: approx. 4mV/V Full Scale
- Non-linearity: 1% Full scale
- Excitation Voltage Used: 10.0 Volts

**Hold Down End (North End)**

Nomenclature

- LC_03–LC_04 (Hold Down End)

Instrumentation Specifications

- Manufacturer: Geokon
- Model Number: 3000-1500-8
- Range: 1000 kips
- Rated Output: approx. 0.800mV/V/full scale
- Non-linearity: 1% Full scale
- Excitation Voltage Used: 10.0 Volts

*General Note*

The reaction load cells, manufactured by Geokon, were found to have disparities between each other at the same loads. For this reason, the raw voltage was recorded from the two load cells during the testing (without using excitation for scaling) in order to investigate the disparity at a later date. As of 11/10/08, discussion has begun with Geokon on re-calibrating the load cells using more points. Hopefully, this will yield a more accurate characterization of the load cell output at known loads.

### C.3.5 Hydraulic Test System

Manually controlled at a rate of approximately 1 kip/second using V-182 flow valves

Enerpac 10000 psi hydraulic power unit

(2) Enerpac RRH-40018 400 ton hydraulic cylinders

## References

C.1 Potter, W. (FDOT), 03/04/09, *"Double Composite Test Note_Fatigue"*, word file, e-mail correspondence.

C.2 Potter, W. (FDOT), 03/04/09, *"Double Composite Test Note_Ultimate"*, word file, e-mail correspondence.

# APPENDIX D

Fatigue Test Results

## D.1 Predicted Fatigue Life

In order to yield results, the life of shear connectors was based on the fatigue limit state and not on the ultimate limit state criteria of the AASHTO LRFD Bridge Design Specifications 2004. The predicted fatigue life was calculated to be 5.65 million cycles. It is an iterative procedure. In this case, shear connectors were designed for the fatigue limit state.

Number of cycles to be applied is calculated based on AASHTO 6.10.10.2-2. Number of cycles are assumed and substituted in the following equation.

$$\alpha = 34.5 - 4.28(\log(N_c)) \qquad \textbf{(AASHTO 6.10.10.2-2)}$$

$$N_c = 10^{(34.5-\alpha)/4.28}$$

Where, $N_c = Number\ of\ fatigue\ cycles$

These calculations are given below:

**Input Parameters**

Effective length of the girder, $L_{eff} = 25\ feet$

Diameter of shear stud, $d = 0.75\ in$

Ultimate strength of shear connector, $F_u = 60\ ksi$

Compressive strength of concrete, $f'_c = 7.5\ ksi$

Elastic modulus of concrete, $E_c = 4491\ ksi$

Width of the top slab, $w_{ts} = 16\ feet$

Thickness of the top slab, $t_{ts} = 8\ in$

Width of the bottom slab, $w_{bs} = 6\ feet$

Thickness of the bottom slab, $t_{bs} = 8\ in$

Thickness of the top flange, $t_{tf} = 1.75\ in$

Width of the top flange, $b_{tf} = 16\ in$

Thickness of the bottom flange, $t_{bf} = 0.375\ in$

Width of the bottom flange, $b_{bf} = 72\ in$

Vertical shear force, $V_f = 108.7\ kips$

Modular ratio, $n = 6.5$

Moment of Inertia of the composite box girder section (For Negative Live-Load Moment), I

$$I = I_{ts} + I_{bs} + I_{st} + \left(A_{ts} \times d_{ts}^{\ 2}\right) + \left(A_{bs} \times d_{bs}^{\ 2}\right) + \left(A_s \times d_s^{\ 2}\right)$$

$$= 1260.31 + 316.62 + 62468.415 + \left(236.31 \times 16.75^2\right) + \left(77.54 \times 33.50^2\right) + \left(158.71 \times 8.57^2\right)$$

$$= 229009.19 \ \ in^4$$

Where,

$I_{ts} = Inertia\ \ of\ top\ slab,\ I_{bs} = Inertia\ of\ \ bottom\ slab,\ \ I_{st} = Inertia\ of\ \ steel$

$A_{ts} = Area\ \ of\ rebar,\ \ A_{bs} = Area\ of\ bottom\ slab,\ A_s = Area\ of\ \ steel$

$d_{ts} = distance\ between\ centroid\ \ of\ \ top\ slab\ and\ neutral\ axis\ of\ \ composite\ \ section$

$d_{bs} = distance\ between\ centroid\ \ of\ \ bottom\ slab\ and\ neutral\ axis\ of\ \ composite\ \ section$

$d_{st} = distancebe\,tween\ centroid\ \ of\ \ steel\ and\ neutral\ \ axis\ of\ \ composite\ \ section$

First moment of area of the transformed short-term area of the concrete of bottom slab about the neutral axis of the short-term composite section, $Q_b$

$$Q_b = A_{bs} \times \left(Y_b - t_{bf} - \frac{t_{bs}}{2}\right) = 77.538\ in^2 \times \left(37.377\ in - 0.375\ in - \frac{7\ in}{2}\right)$$

$$\therefore Q_b = 2597.67\ \ in^3$$

First moment of area of the transformed short-term area of the concrete of top slab about the neutral axis of the short-term composite section, $Q_t$

$$Q_t = A_{ts} \times \left(Y_t - \frac{t_{ts}}{2}\right) = 236\ in^2 \times \left(20.748\ in - \frac{8\ in}{2}\right)$$

$$\therefore Q_t = 3952.528\ in^2$$

Where,

$Y_b = distance\ of\ \ neutral\ axis\ (N.A)\ from\ the\ extreme\ bottom\ \ fiber\ of\ \ the\ box\ girder\ section.$

$Y_t = distance\ of\ \ neutral\ axis\ (N.A.)\ from\ the\ extreme\ top\ \ fiber\ of\ \ the\ box\ girder\ section.$

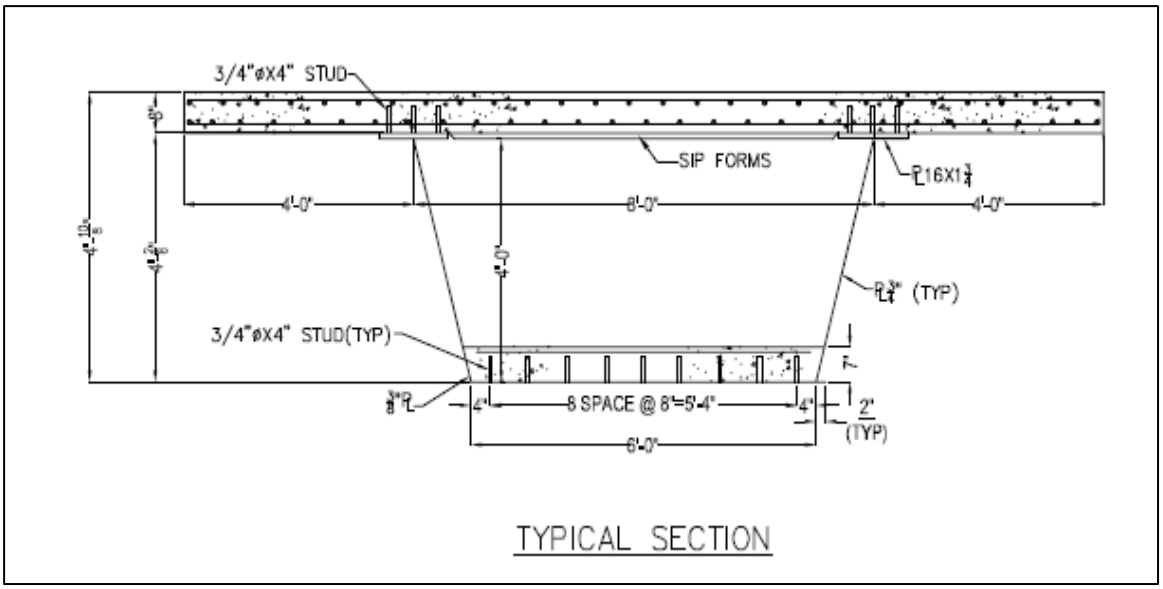


**Figure 1.1** Typical Cross-section of Double Composite Box Girder Test Specimen

**Calculations:**

**Step 1 Calculate area of shear stud**

Area of shear stud, $A_{sc} = \frac{\pi \times d^2}{4} = \frac{\pi \times 0.75^2}{4}$

$$\therefore A_{sc} = 0.44 \ in^2$$

**Step 2 Calculate value of α based on assumed Number of cycles**

Let, Number of cycles $N_c = 5{,}650{,}000$

$$\alpha = 34.5 - 4.28(\log(N_c)) \qquad \textbf{(AASHTO 6.10.10.2-2)}$$

$$\therefore \alpha = 34.5 - 4.28(\log(5{,}650{,}000))$$

$$\therefore \alpha = 5.60$$

**Step 3 Fatigue Resistance of individual shear stud**

$$Z_r = \alpha \times d^2 \geq \frac{5.5 \times d^2}{2} \qquad \textbf{(AASHTO 6.10.10.2-1)}$$

$$\therefore Z_r = 5.60 \times 0.75^2 \geq \frac{5.5 \times 0.75^2}{2}$$

$$\therefore Z_r = 3.15 \geq 1.54$$

$$\therefore Z_r = 3.15\ kips$$

**Step 4 Horizontal fatigue shear per unit length (kip/in)**

**Horizontal fatigue shear for the top slab**

$$V_{srt} = \frac{V_f \times Q_t}{I} \qquad \textbf{(AASHTO 6.10.10.1.2-2)}$$

$$\therefore V_{srt} = \frac{108.7\ kips \times 3952.528\ in^3}{229009.19\ in^4} = 1.876\ \frac{kip}{in}$$

**Horizontal fatigue shear for the bottom slab**

$$V_{srb} = \frac{V_f \times Q_b}{I} \qquad \textbf{(AASHTO 6.10.10.1.2-2)}$$

$$\therefore V_{srb} = \frac{108.7\ kips \times 2597.67\ in^3}{229009.19\ in^4} = 1.23\ \frac{kip}{in}$$

**Step 5 Pitch of shear connectors along longitudinal axis for top and bottom slab**

Pitch of the shear connectors along longitudinal axis for top and bottom slab are based on assumed number of shear connectors across the width of cross section

**Pitch for the shear connectors of the top slab**

Assumed number of shear connectors for top flange $n_t = 6$

$$P \leq \frac{n_t \times Z_r}{V_{sr}} = \frac{6 \times 3.15\ kip}{1.876\ \frac{kip}{in}} \qquad \textbf{(AASHTO 6.10.10.1.2-1)}$$

$$\therefore P \leq 10\ in$$

Provide shear connectors at the pitch of 10 inch in longitudinal direction for top flange.

**Pitch for the shear connectors of the bottom slab**

Assumed number of shear connectors for bottom flange $n_b = 9$

$$P \leq \frac{n_b \times Z_r}{V_{sr}} = \frac{9 \times 3.15\ kip}{1.23\ \frac{kip}{in}} \qquad \textbf{(AASHTO 6.10.10.1.2-1)}$$

$$\therefore P \leq 23.05\,in$$

Provide shear connectors at the pitch of 23 inch in longitudinal direction for bottom flange.

**Step 6 Nominal Resistance of one shear connector (Ultimate Limit State)**

$$Q_n = 0.5 \times A_{sc} \times \sqrt{f'_c \times E_c} \leq A_{sc} \times F_u \qquad \textbf{(AASHTO 6.10.10.4.3-1)}$$

$$\therefore Q_n = 0.5 \times 0.44\,in^2 \times \sqrt{7.5\,ksi \times 4491\,ksi} \leq 0.44\,in^2 \times 60\,ksi$$

$$\therefore Q_n = 40.54\,kip \leq 26.51\,kip$$

$$\therefore Q_n = 26.51\,kip$$

Minimum of the two is considered as the nominal resistance. Fatigue limit state governs the design of shear connectors.

**Step 7 Number of shear connectors in top flange and bottom flange**

Number of shear connector on both, top and bottom slab are governed by fatigue limit state criteria. Therefore, number of shear connectors are calculated based on pitch and number of shear connectors provided across the width of the cross section.

**Number of shear connectors in top flange**

Pitch of shear connectors in the top slab $p_{ts} = 10\,in$

$$n_t = \frac{n_{ts} \times L_{eff}}{p_{ts}} = \frac{6 \times 25ft \times 12\,in}{10\,in}$$

$$\therefore n_t = 180$$

Number of shear connectors provided in the top flange is 185. Distribute 185 shear connectors equally on both the top flanges.

**Number of shear connectors in bottom flange**

Pitch of shear connectors in the top slab $p_{bs} = 23\,in$

$$n_b = \frac{n_{bs} \times L_{eff}}{p_{bs}} = \frac{9 \times 25ft \times 12\,in}{23\,in}$$

$$\therefore n_t = 117$$

Therefore, the number of shear connectors provided in the bottom flange is 117 at longitudinal pitch of 23 inch and 9 shear connectors across the width of the cross section.

## D.2 Deflection

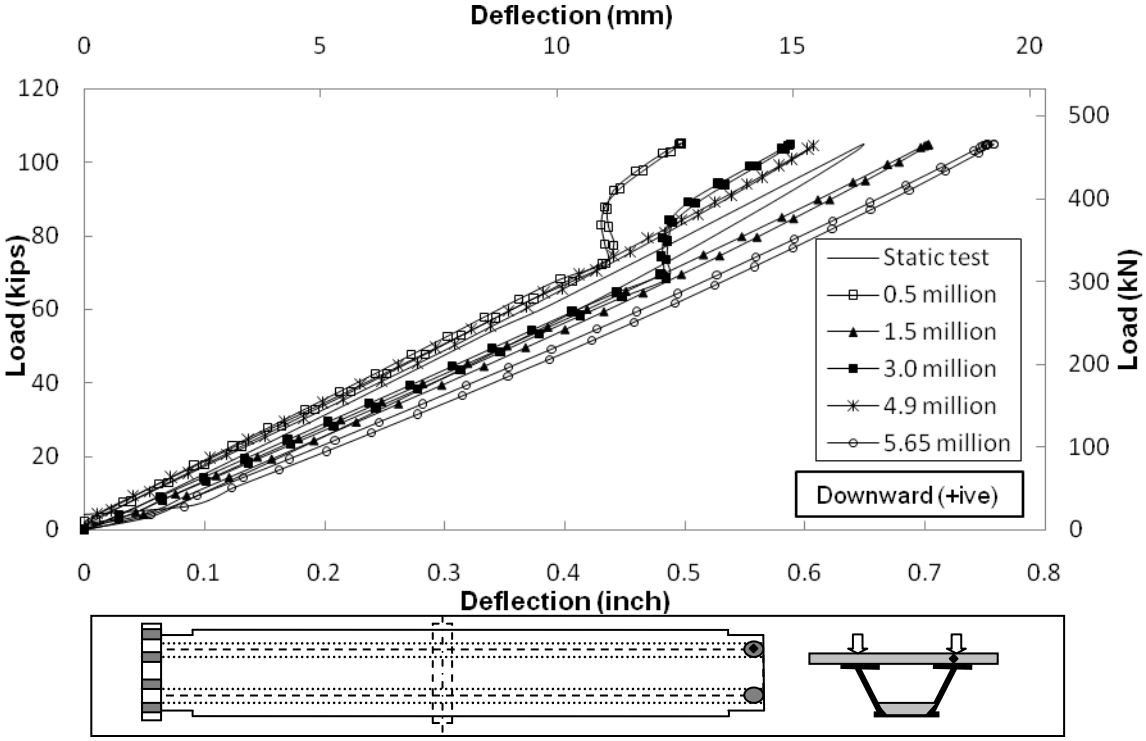


**Figure D.1** Deflection at Actuator End LVDT # 7

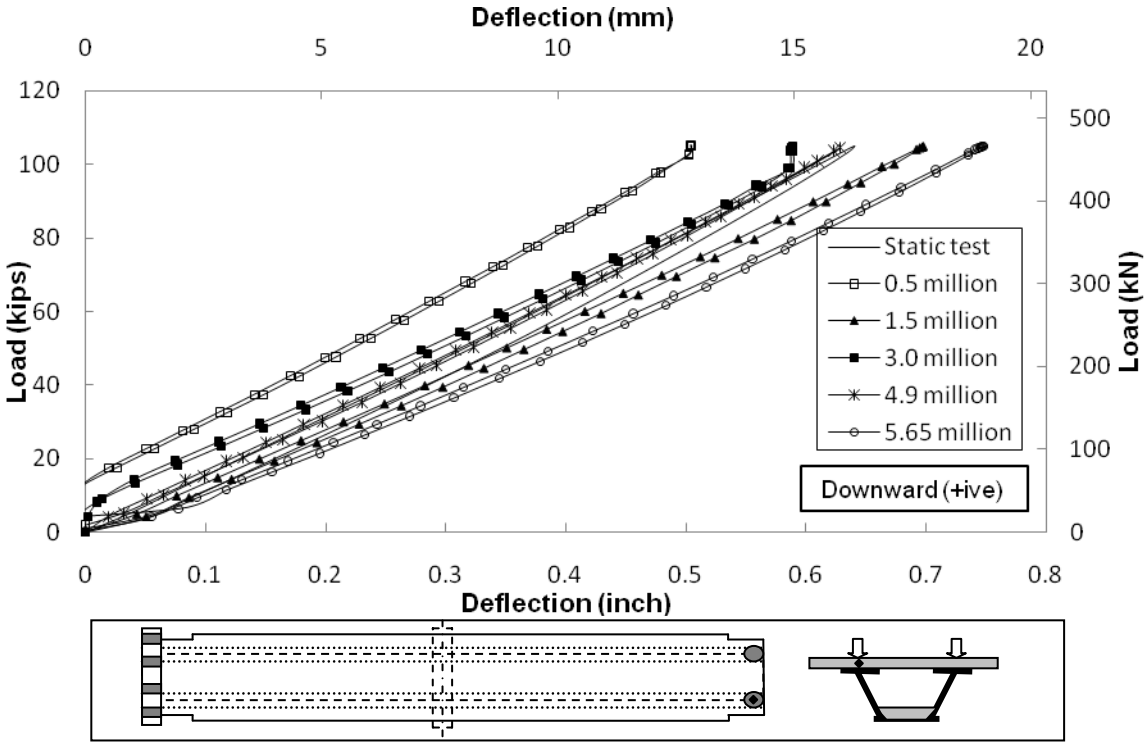


**Figure D.2** Deflection at Actuator End LVDT # 8

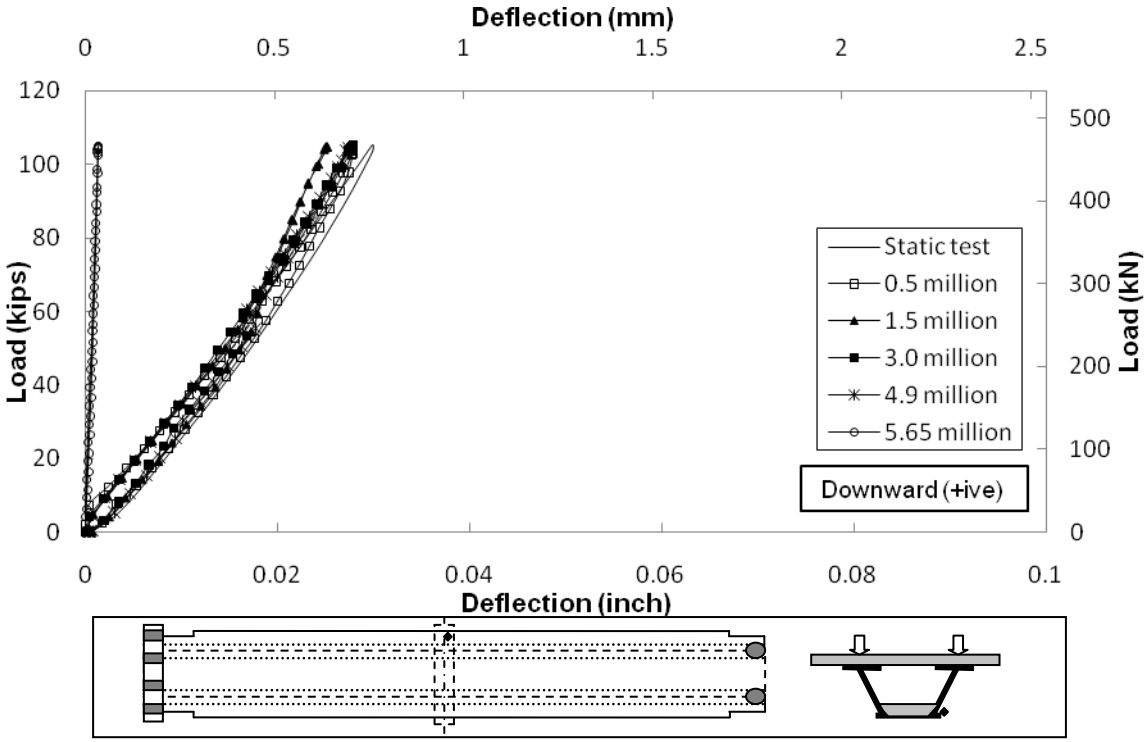


**Figure D.3** Deflection at Center End LVDT # 21

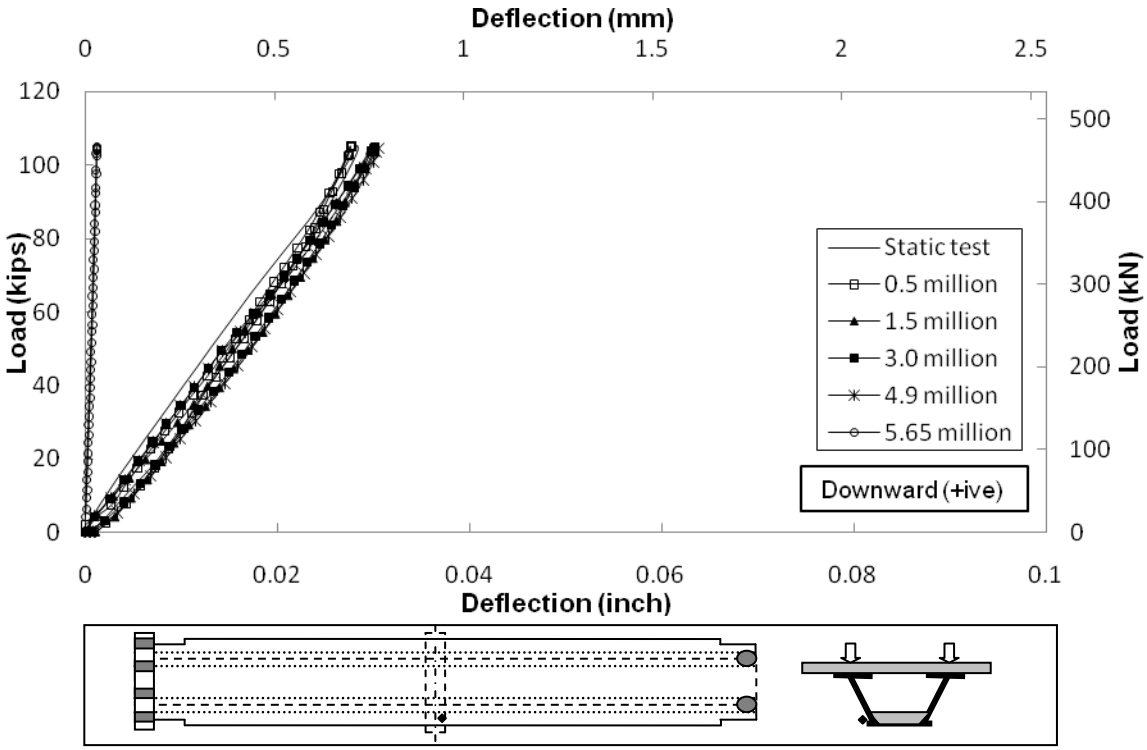


**Figure D.4** Deflection at Center End LVDT # 22

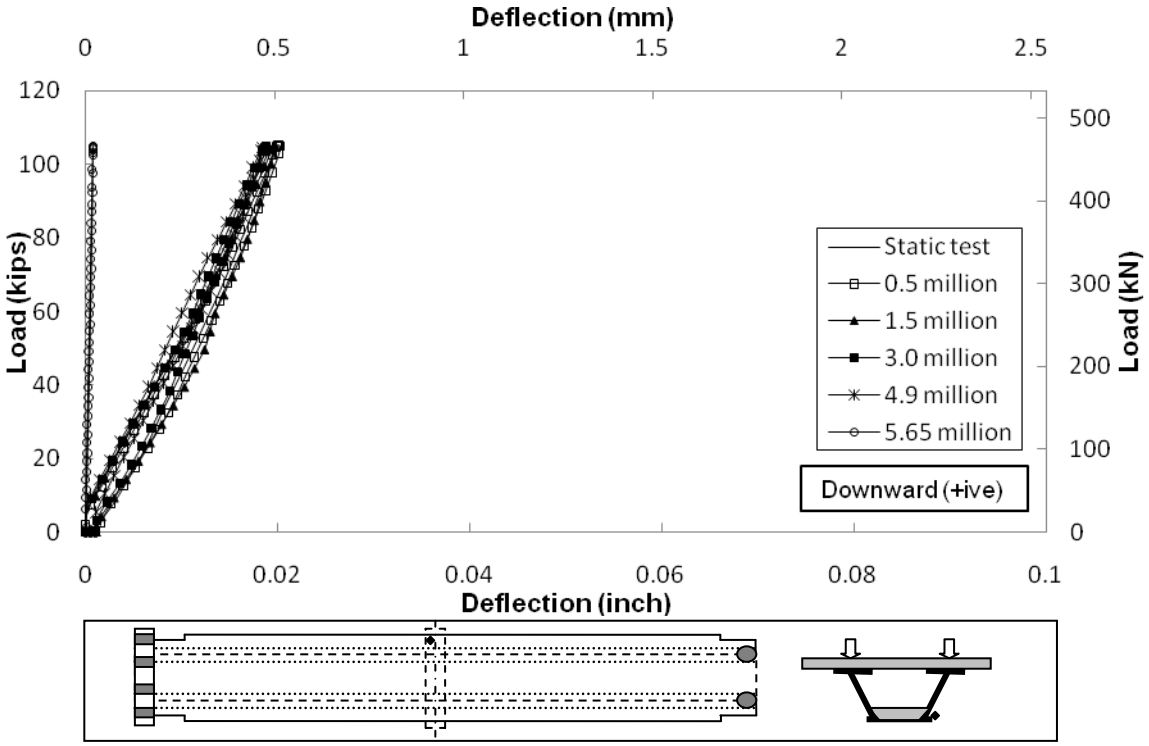


**Figure D.5** Deflection at Center End LVDT # 23

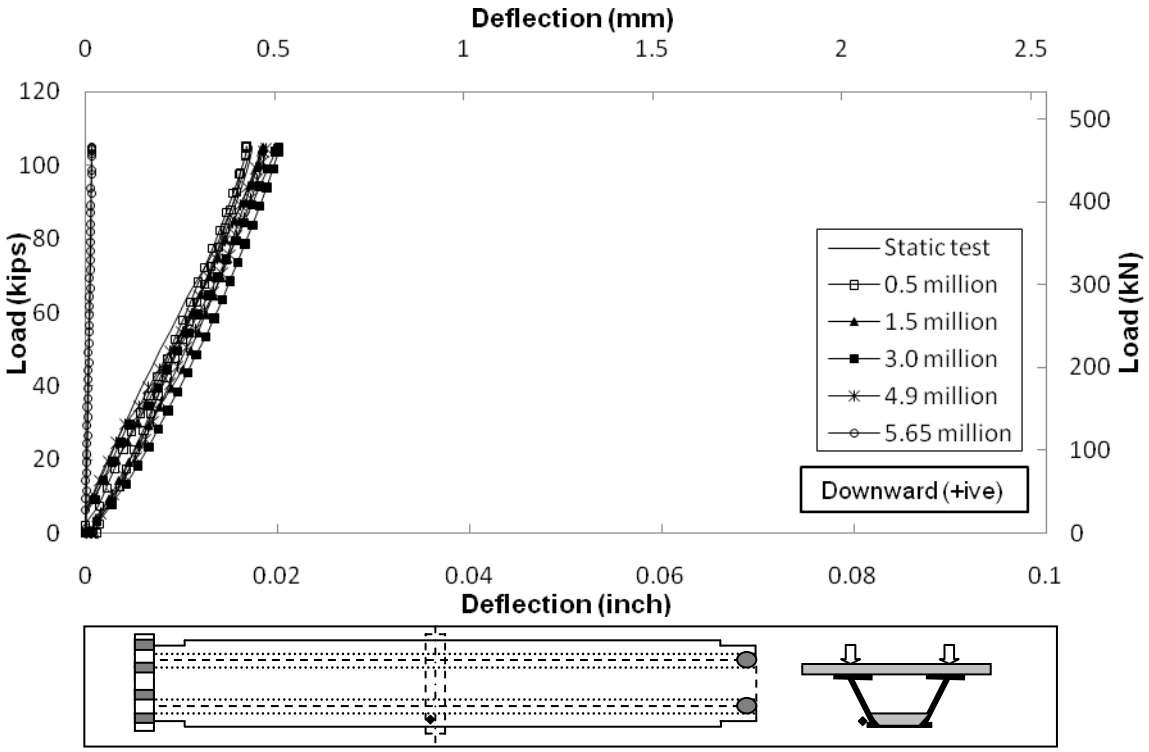


**Figure D.6** Deflection at Center End LVDT # 24

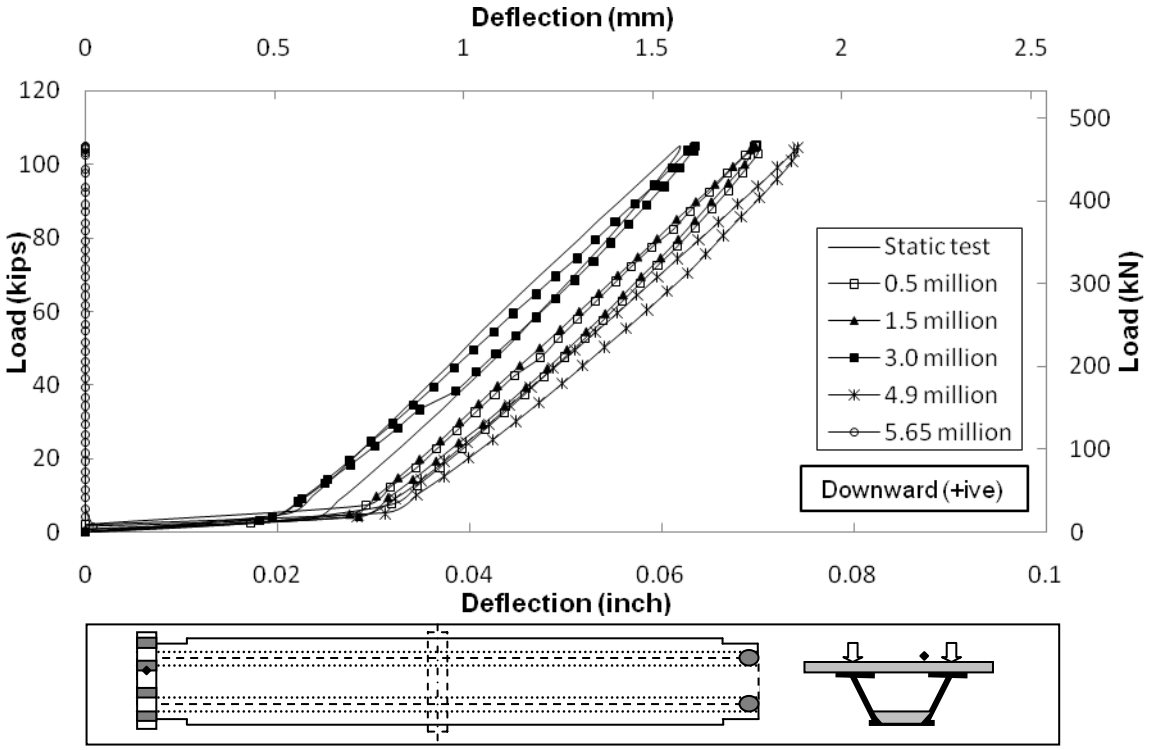


**Figure D.7** Deflection at Hold Down End LVDT # 28

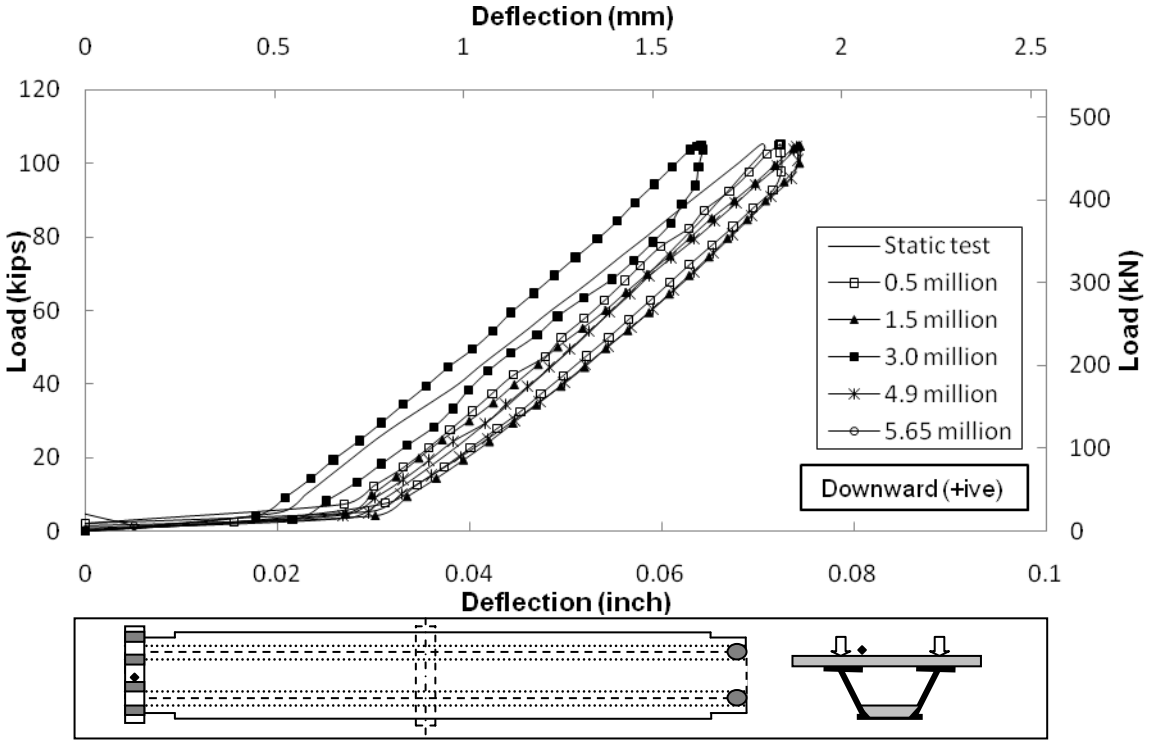


**Figure D.8** Deflection at Hold Down End LVDT # 29

## D.3 Slip

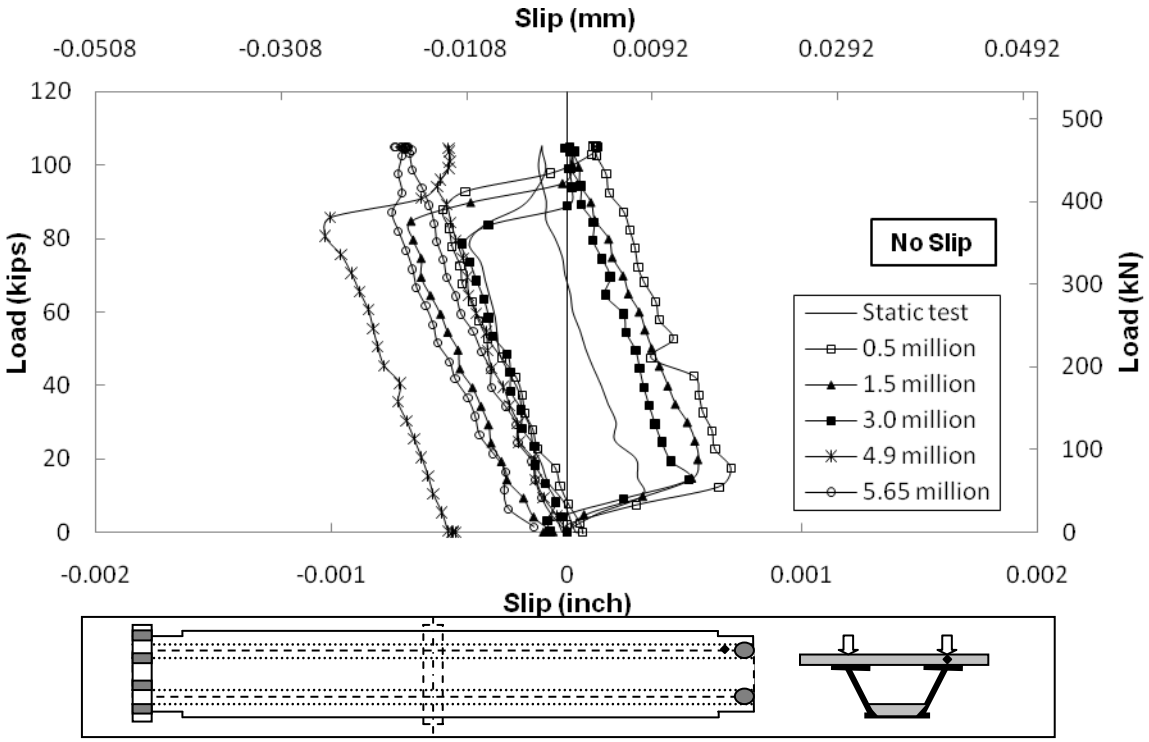


**Figure D.9** Slip at Actuator End in Top Slab LVDT # 30

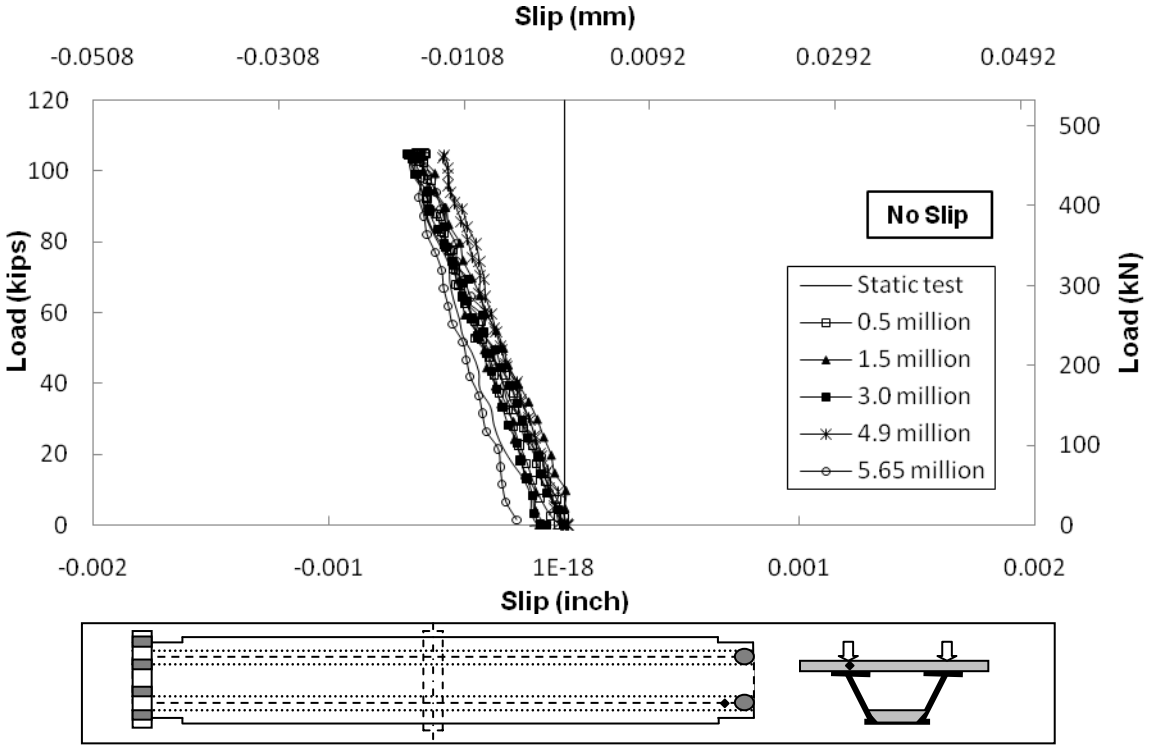


**Figure D.10** Slip at Actuator End in Top Slab LVDT # 31

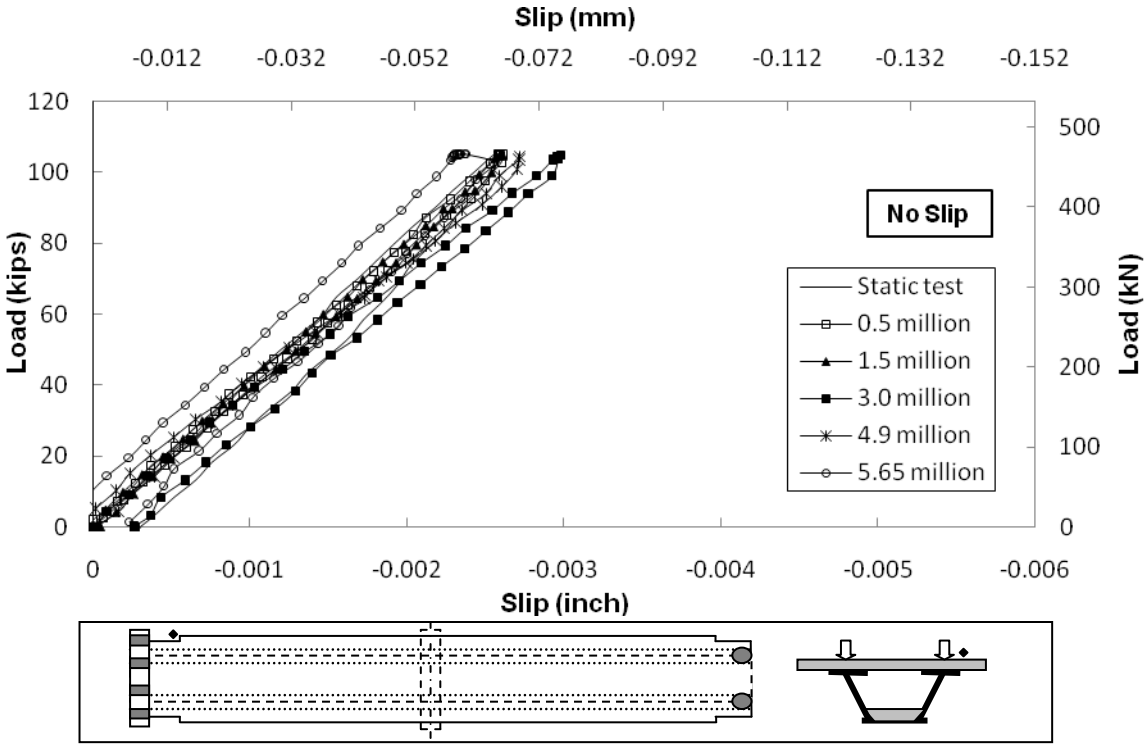


**Figure D.11** Slip at Hold Down End in Top Slab LVDT # 32

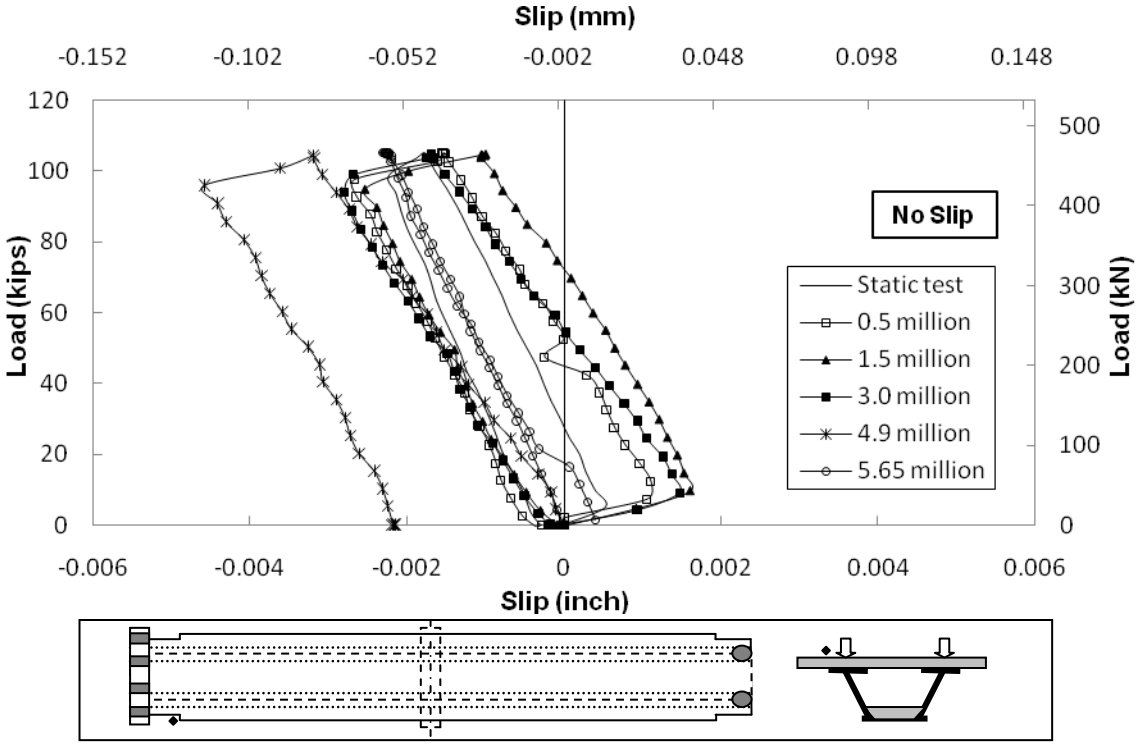


**Figure D.12** Slip at Hold Down End in Top Slab LVDT # 33

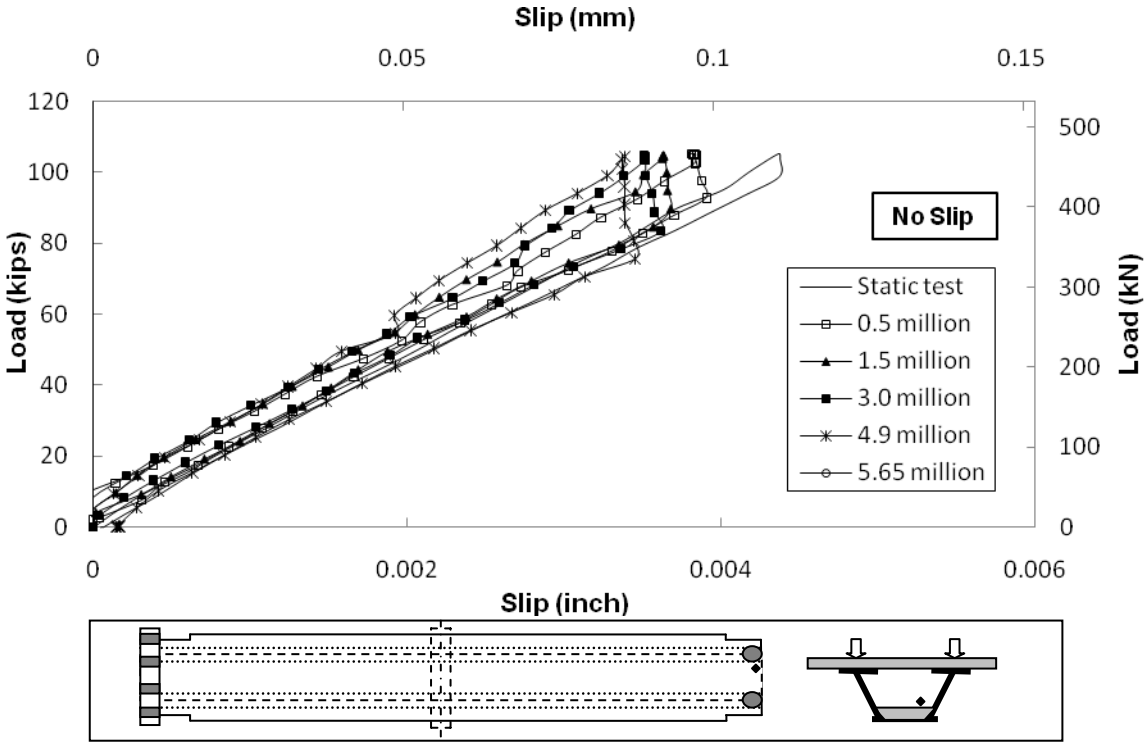


**Figure D.13** Slip at Actuator End in Bottom Slab LVDT # 34

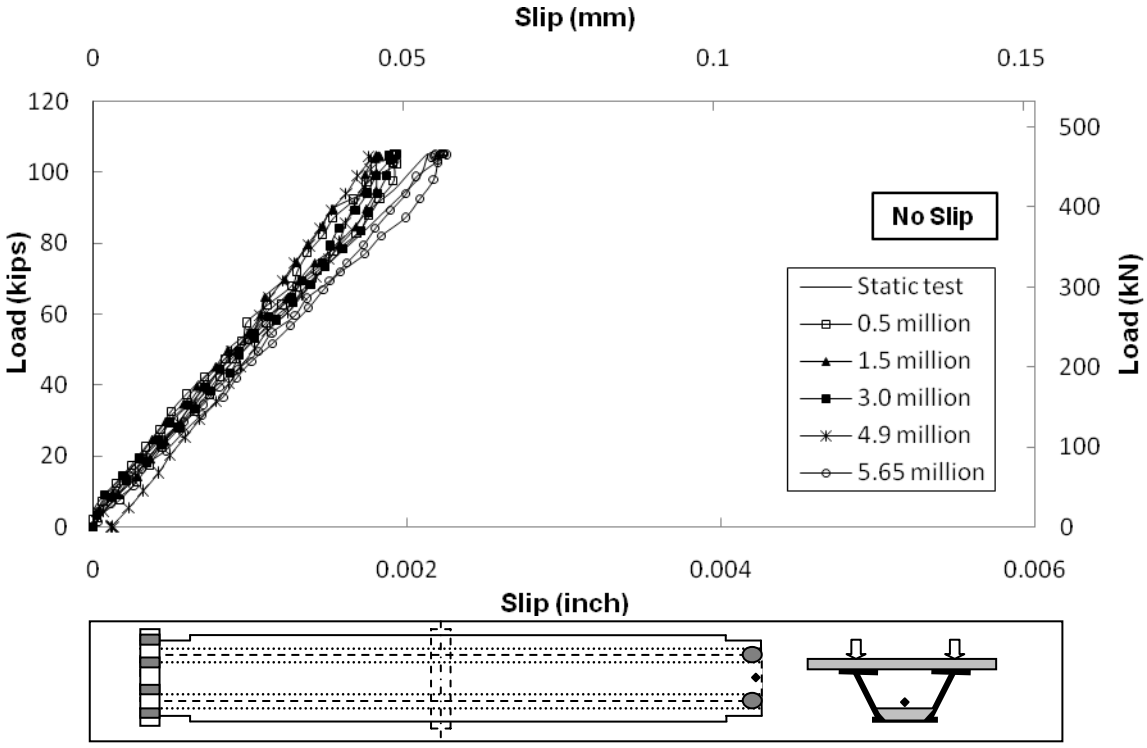


**Figure D.14** Slip at Actuator End in Bottom Slab LVDT # 35

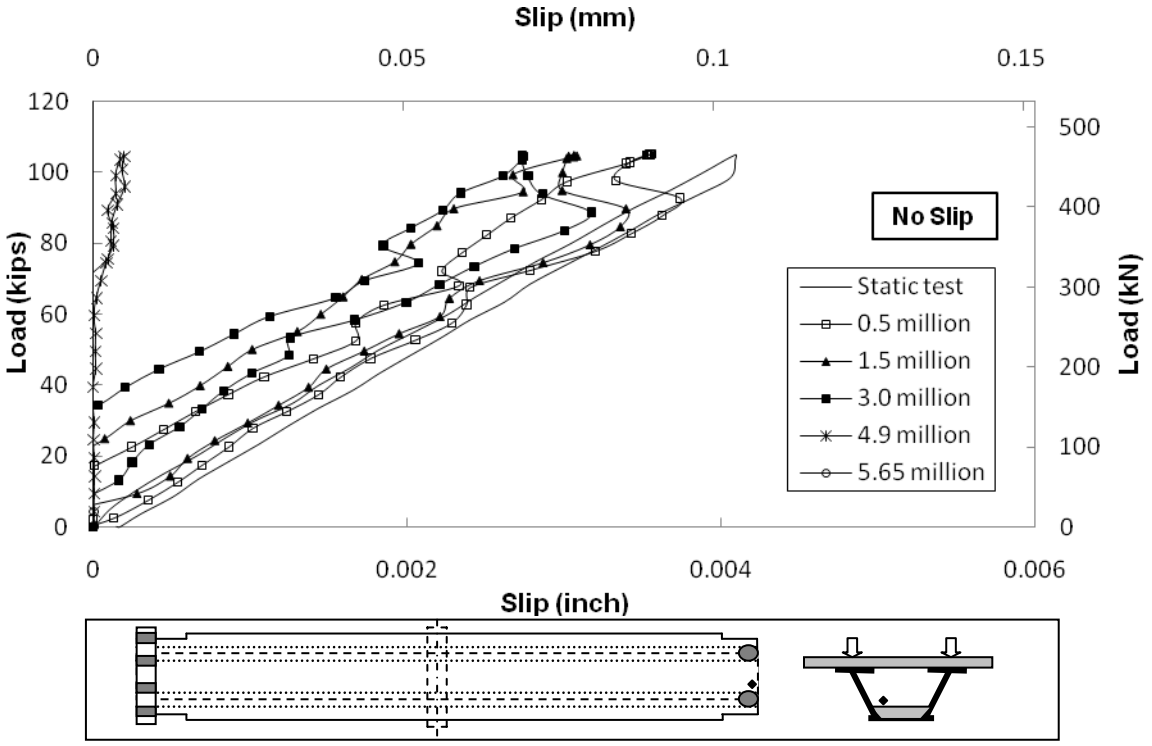


**Figure D.15** Slip at Actuator End in Bottom Slab LVDT # 36

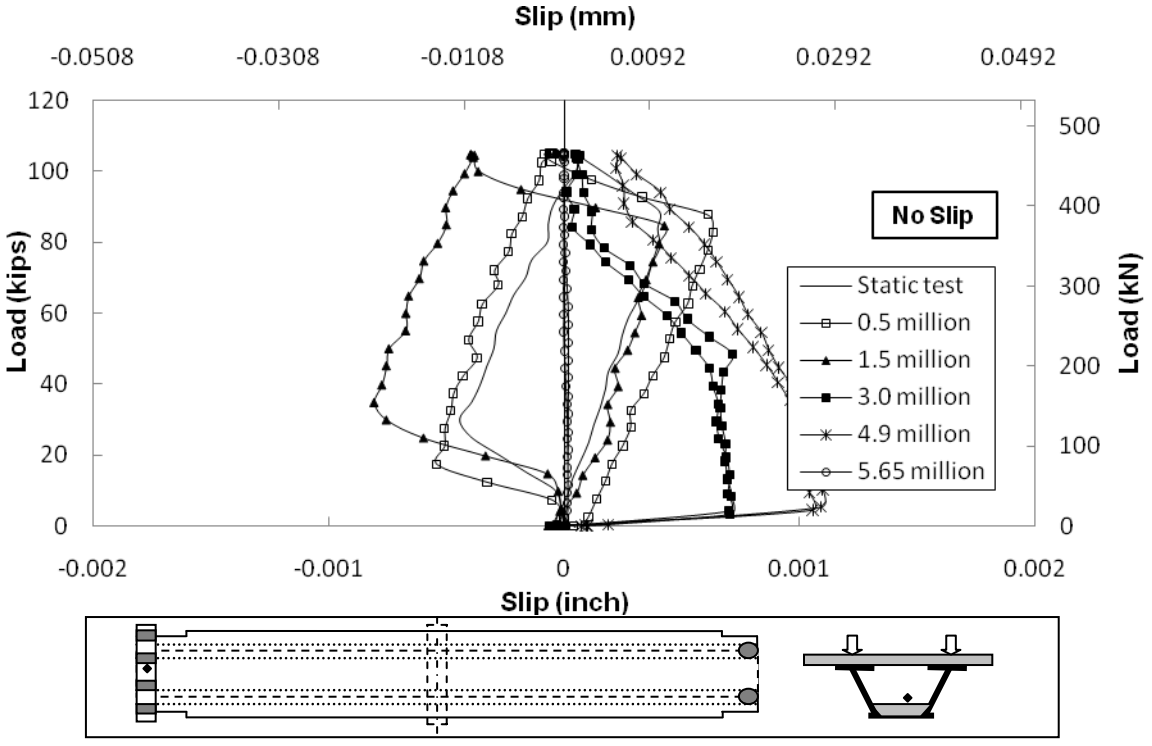


**Figure D.16** Slip at Hold Down End in Bottom Slab LVDT # 37

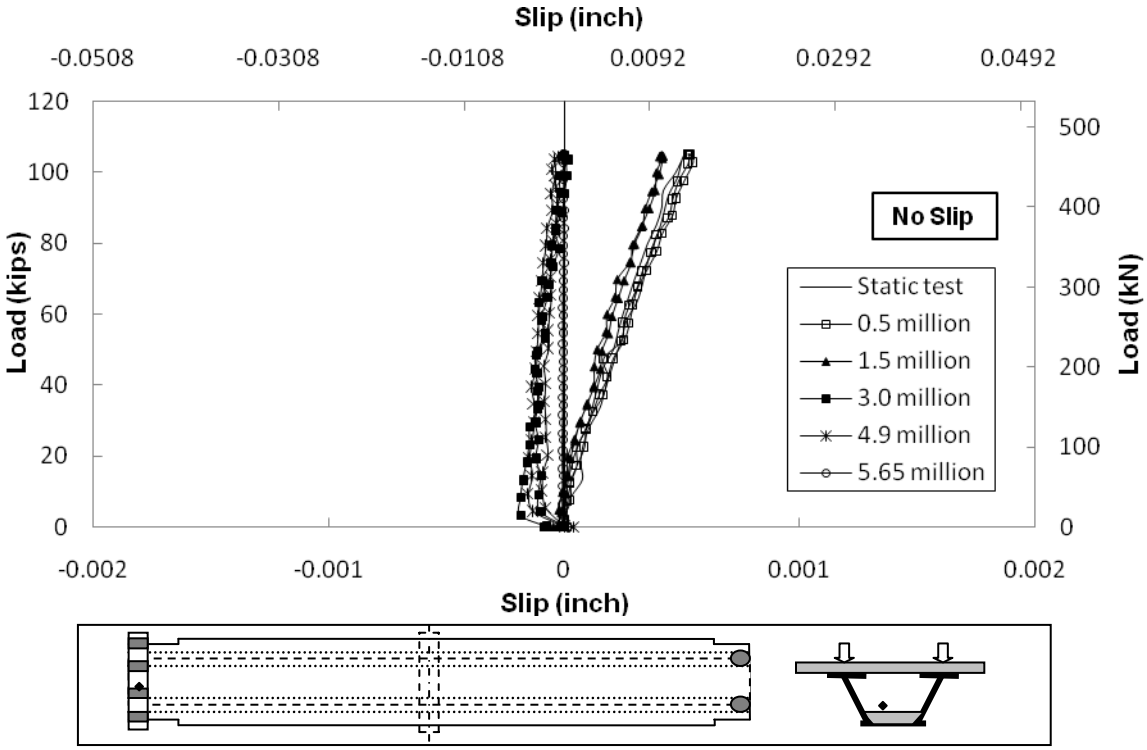


**Figure D.17** Slip at Hold Down End in Bottom Slab LVDT # 38

## D.4 Strain in Top Slab Rebars

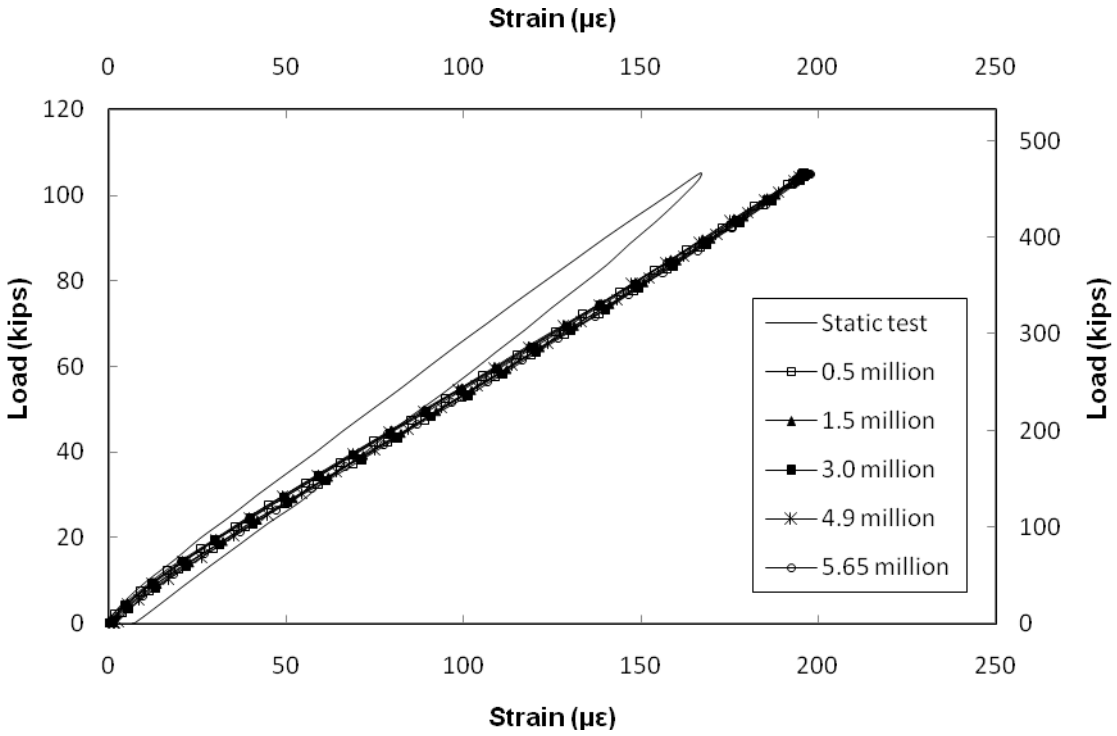


**Figure D.18** Strain in Rebars on Actuator Side SG # 57A

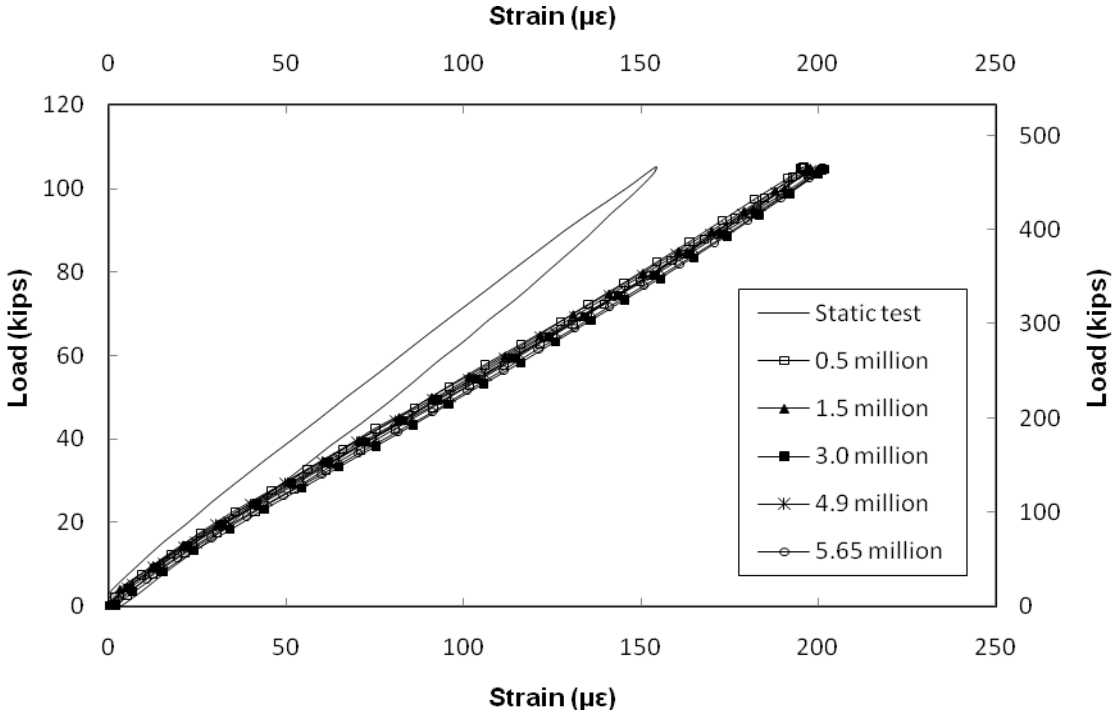


**Figure D.19** Strain in Rebars on Actuator Side SG # 58A

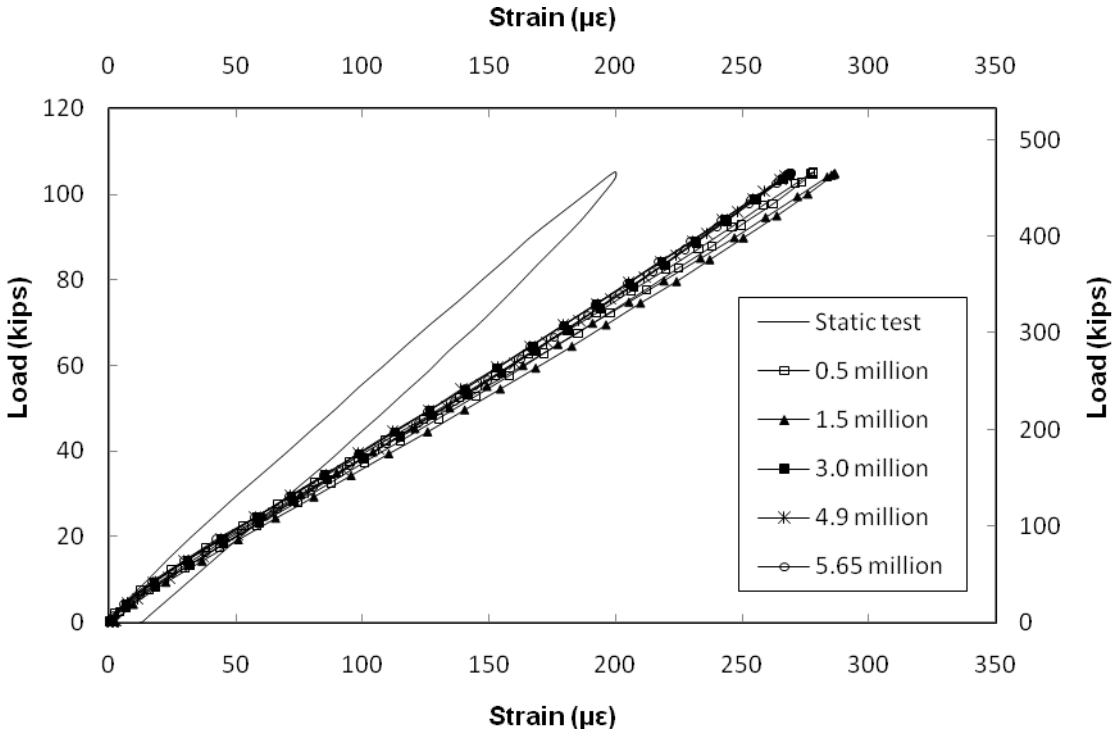


**Figure D.20** Strain in Rebars on Actuator Side SG # spare1A

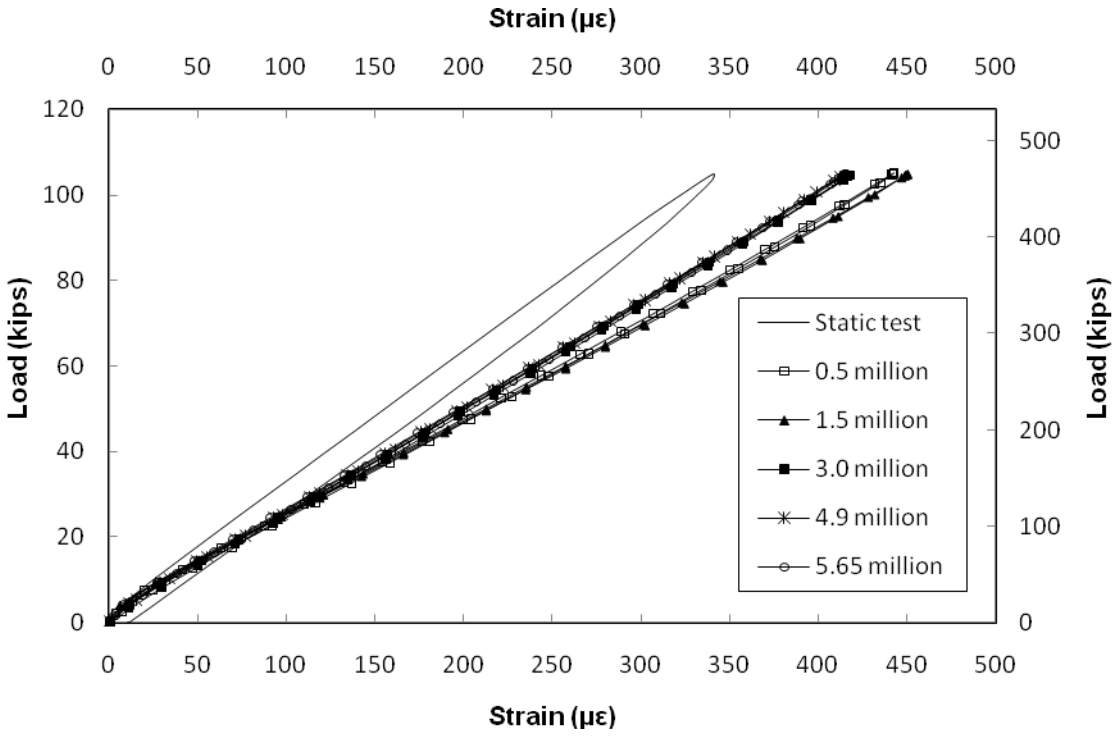


**Figure D.21** Strain in Rebars on Actuator Side SG # 59A

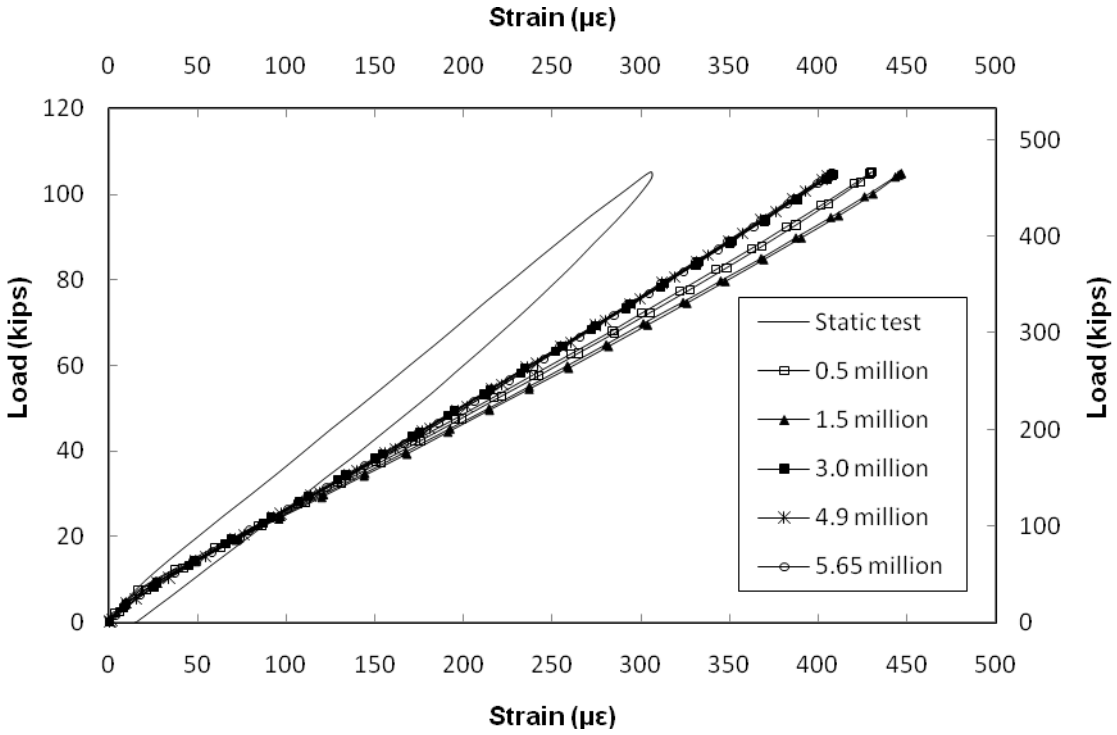


**Figure D.22** Strain in Rebars on Actuator Side SG # 60A

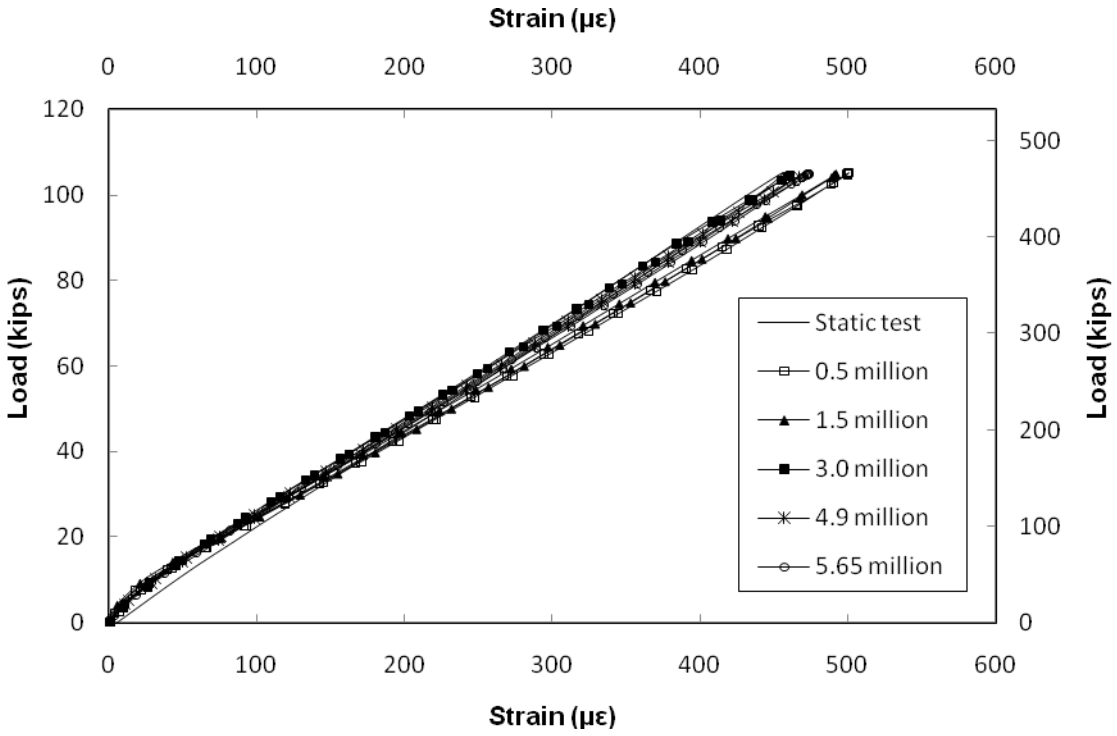


**Figure D.23** Strain in Rebars on Actuator Side SG # 61A

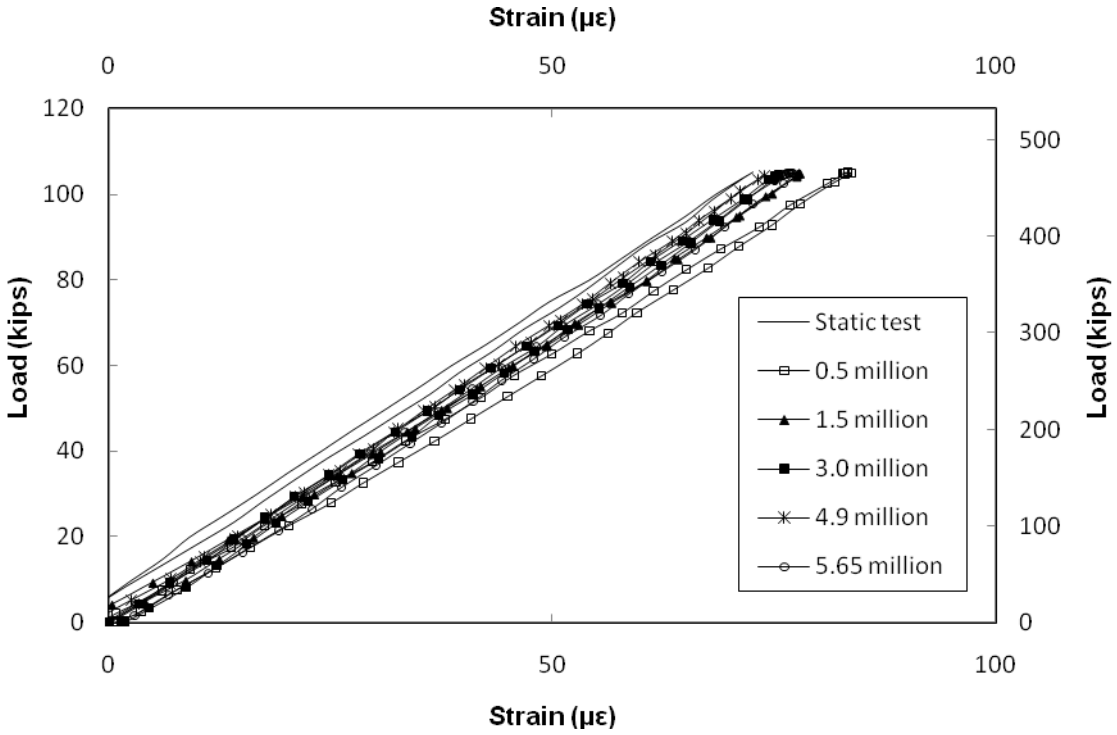


**Figure D.24** Strain in Rebars on Actuator Side SG # 62A

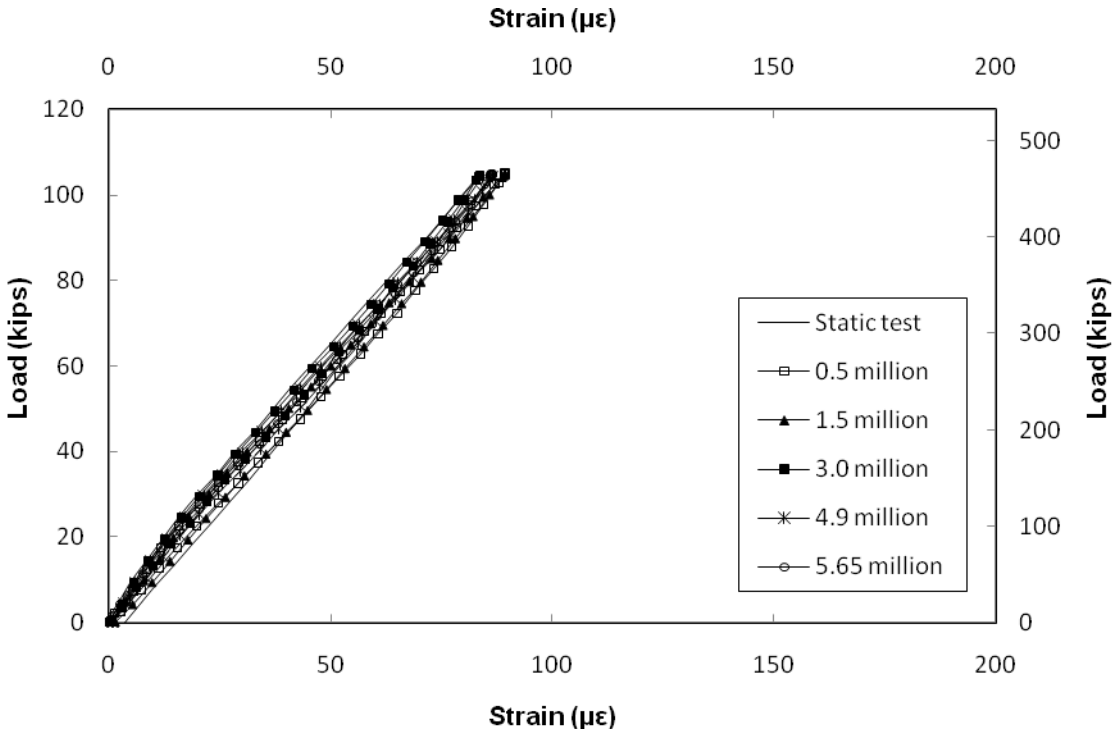


**Figure D.25** Strain in Rebars on Actuator Side SG # spare2A

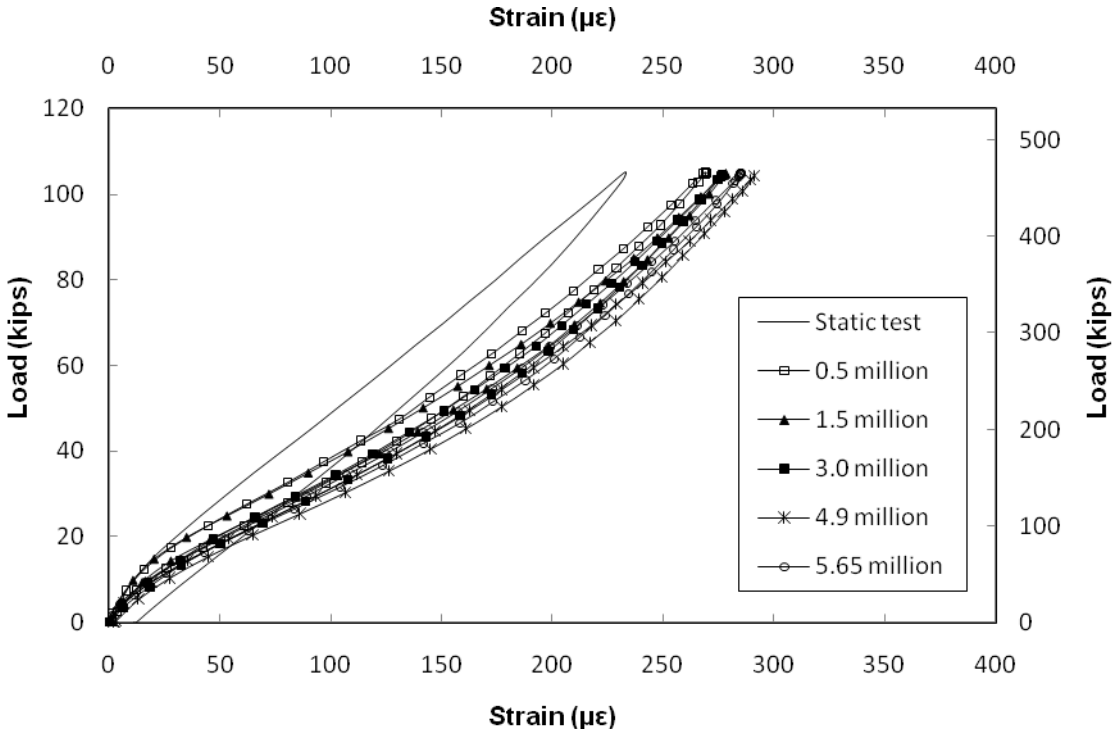


**Figure D.26** Strain in Rebars on Actuator Side SG # spare3A

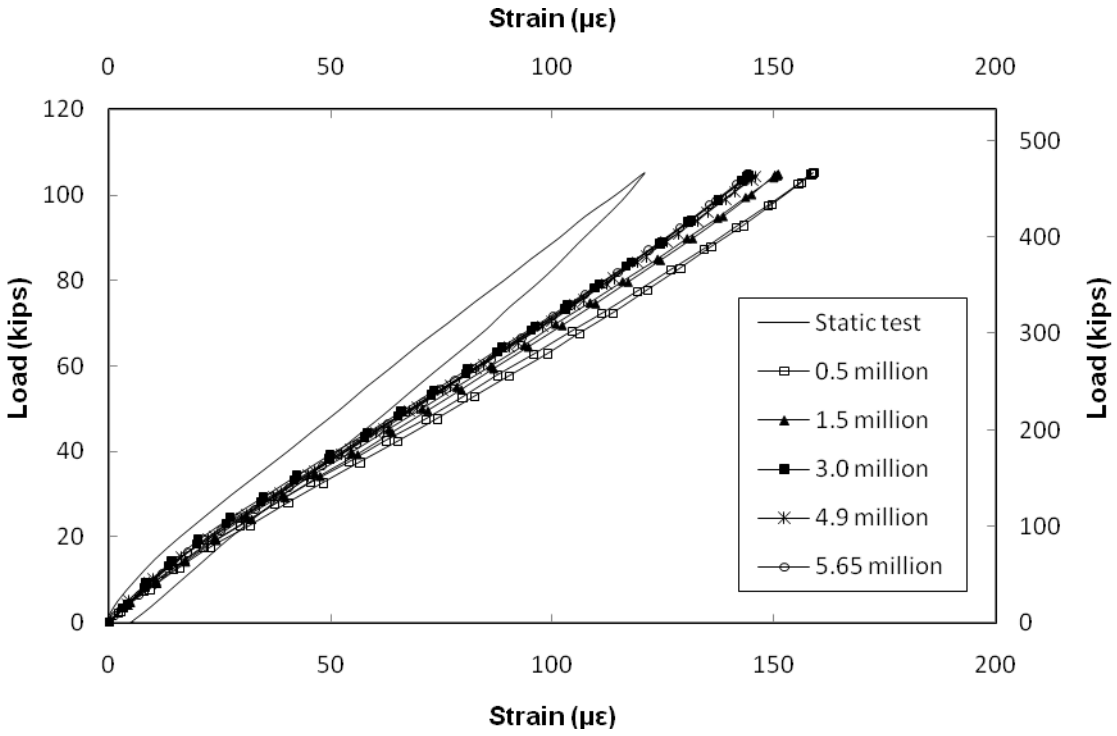


**Figure D.27** Strain in Rebars on Actuator Side SG # 63A

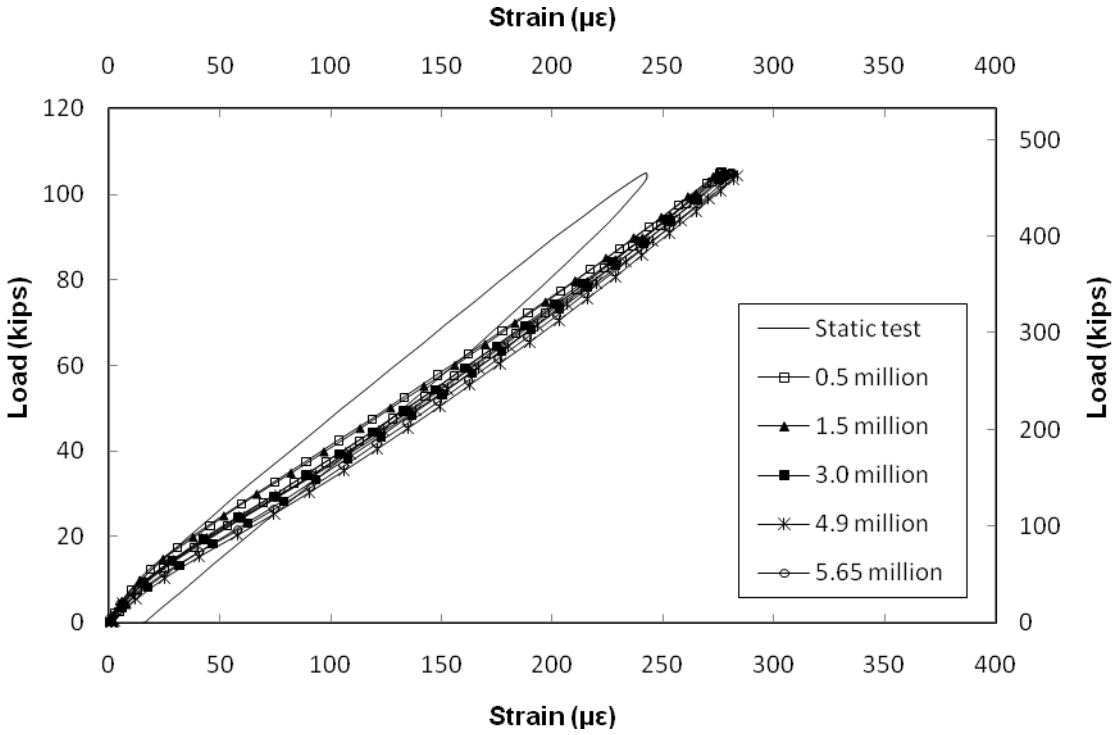


**Figure D.28** Strain in Rebars on Actuator Side SG # 64A

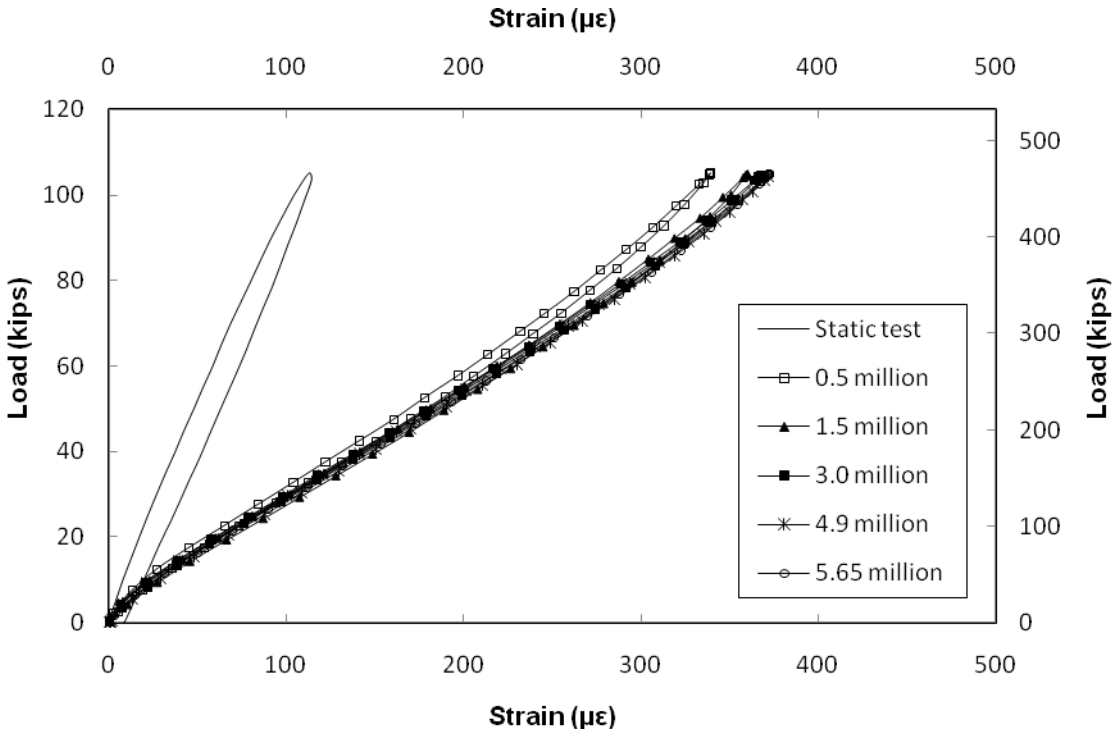


**Figure D.29** Strain in Rebars on Actuator Side SG # 65A

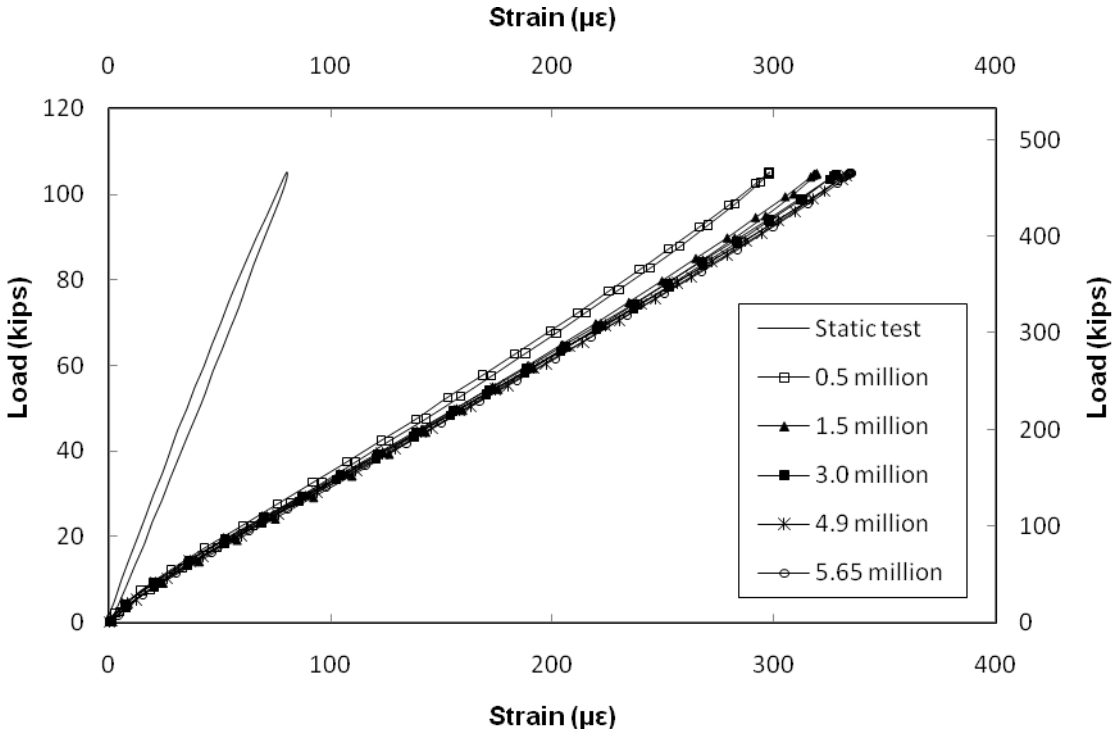


**Figure D.30** Strain in Rebars on Actuator Side SG # 66A

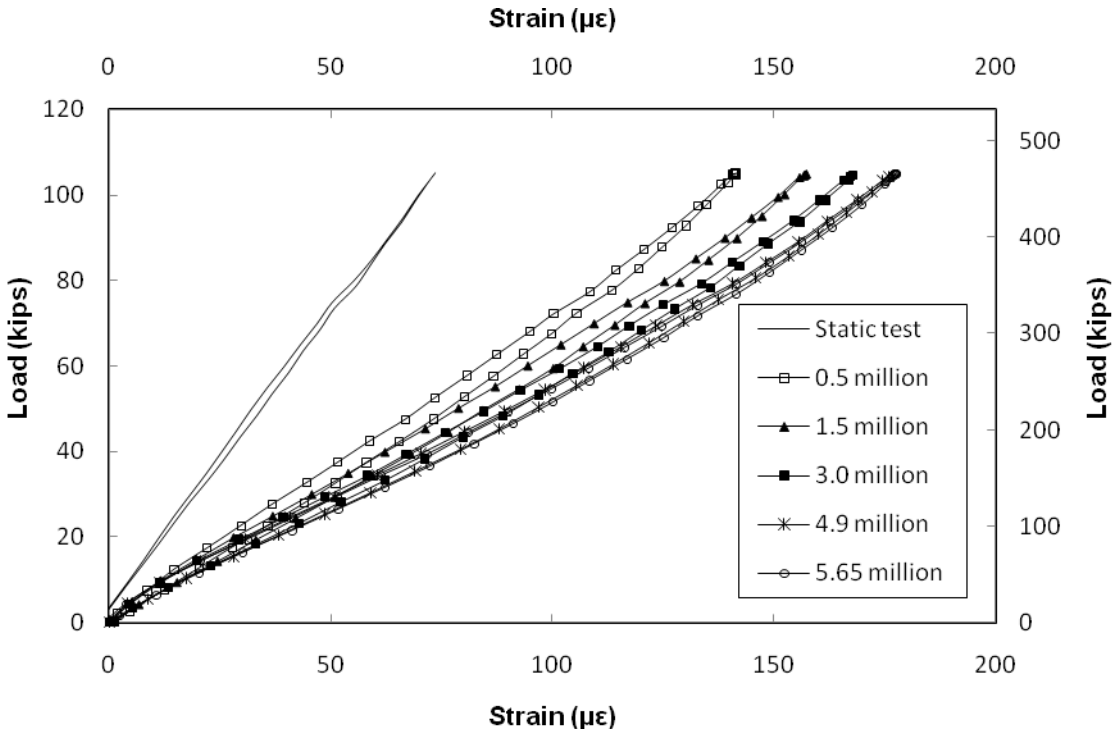


**Figure D.31** Strain in Rebars on Actuator Side SG # spare4A

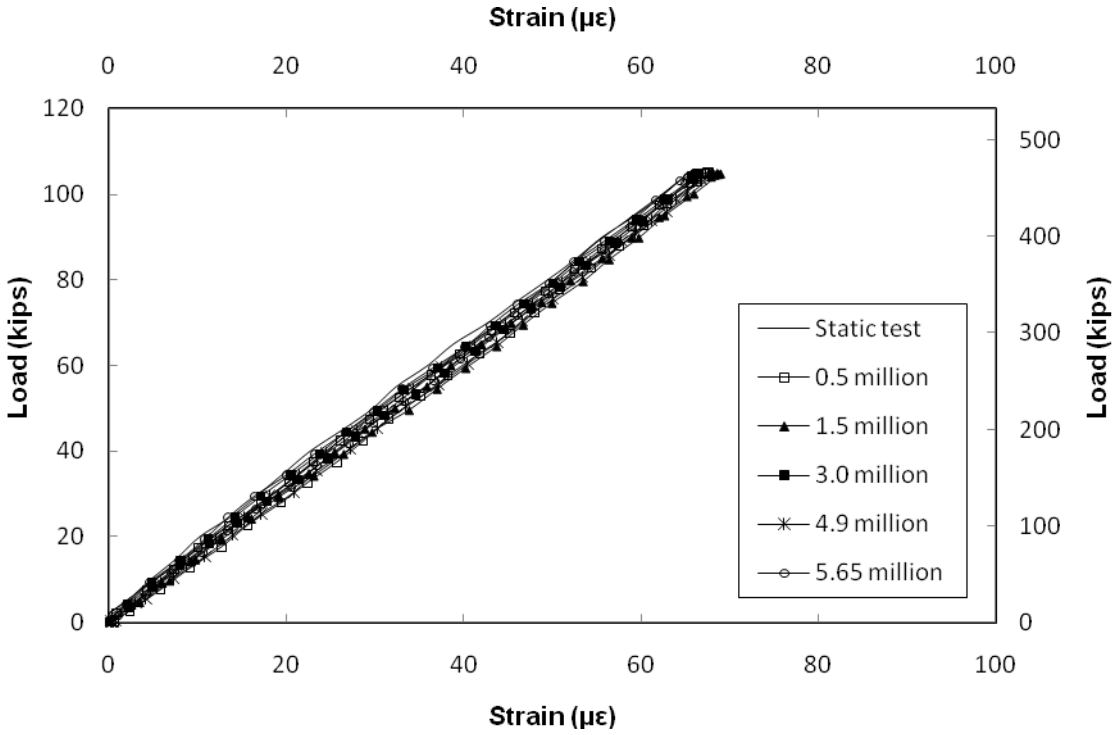


**Figure D.32** Strain in Rebars on Actuator Side SG # 67A

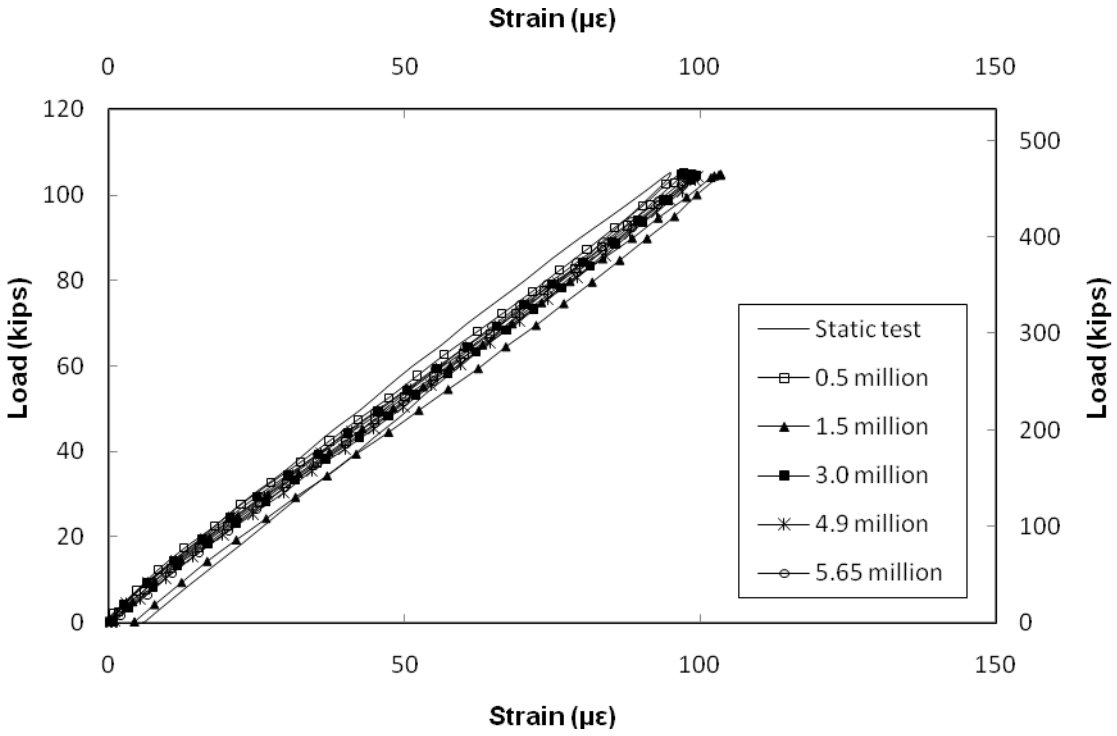


**Figure D.33** Strain in Rebars on Actuator Side SG # 68A

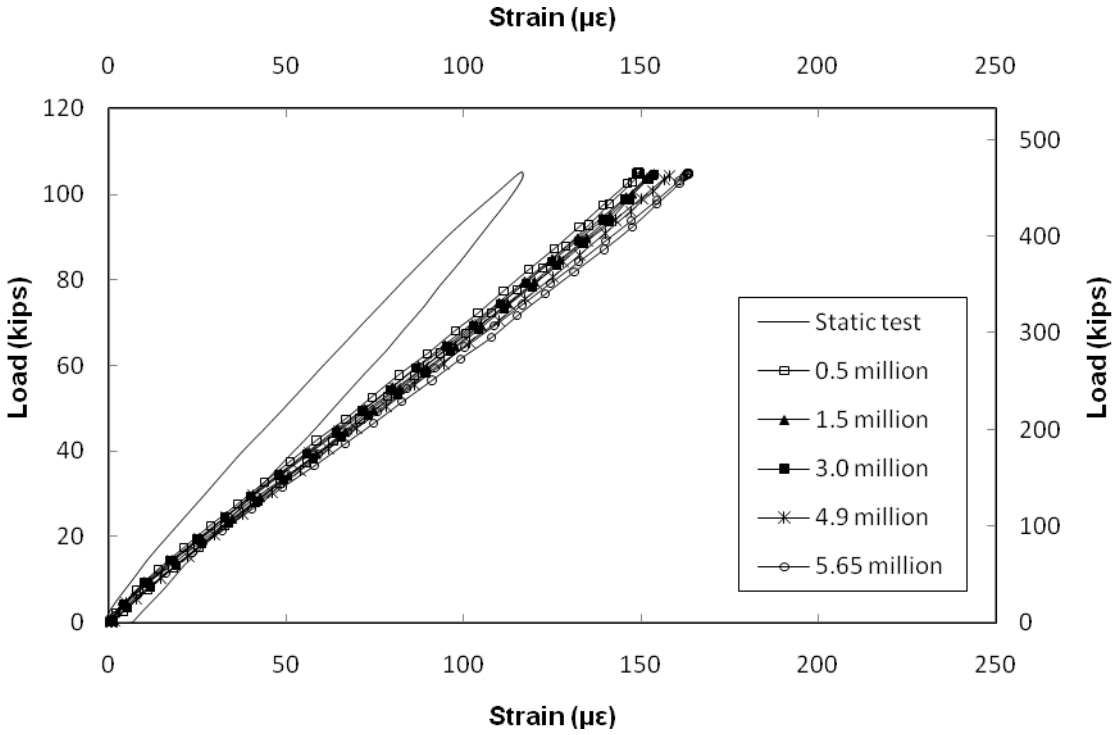


**Figure D.34** Strain in Rebars on Hold Down Side SG # 57B

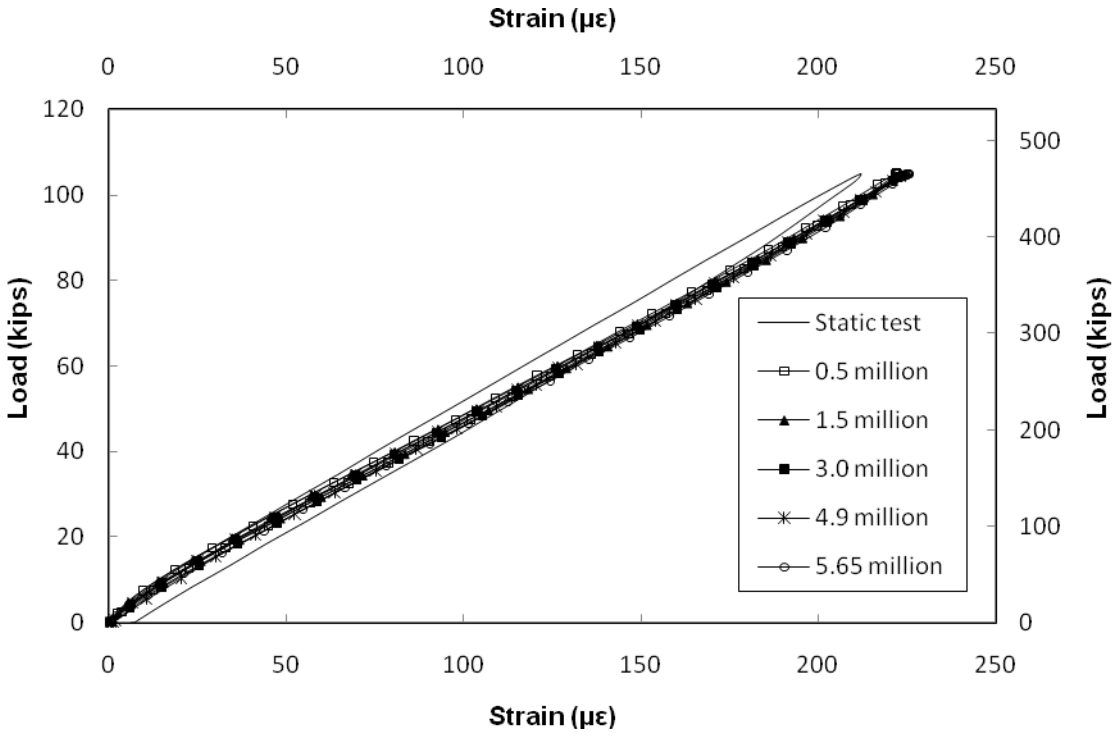


**Figure D.35** Strain in Rebars on Hold Down Side SG # 58B

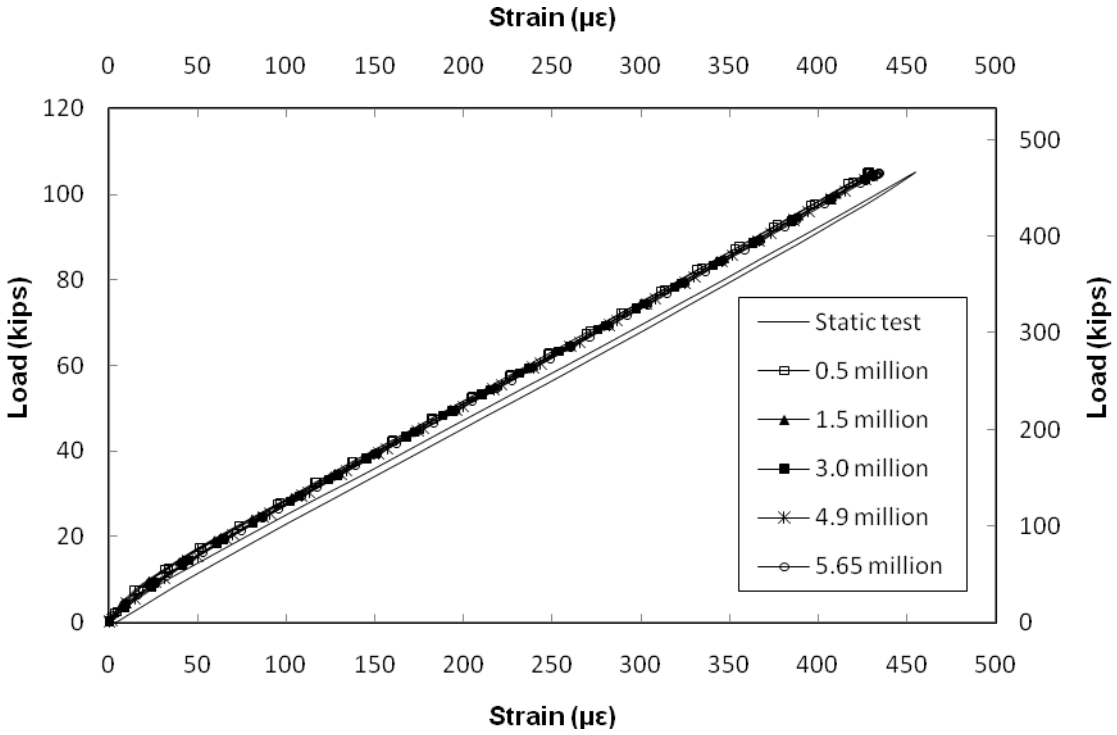


**Figure D.36** Strain in Rebars on Hold Down Side SG # spare1B

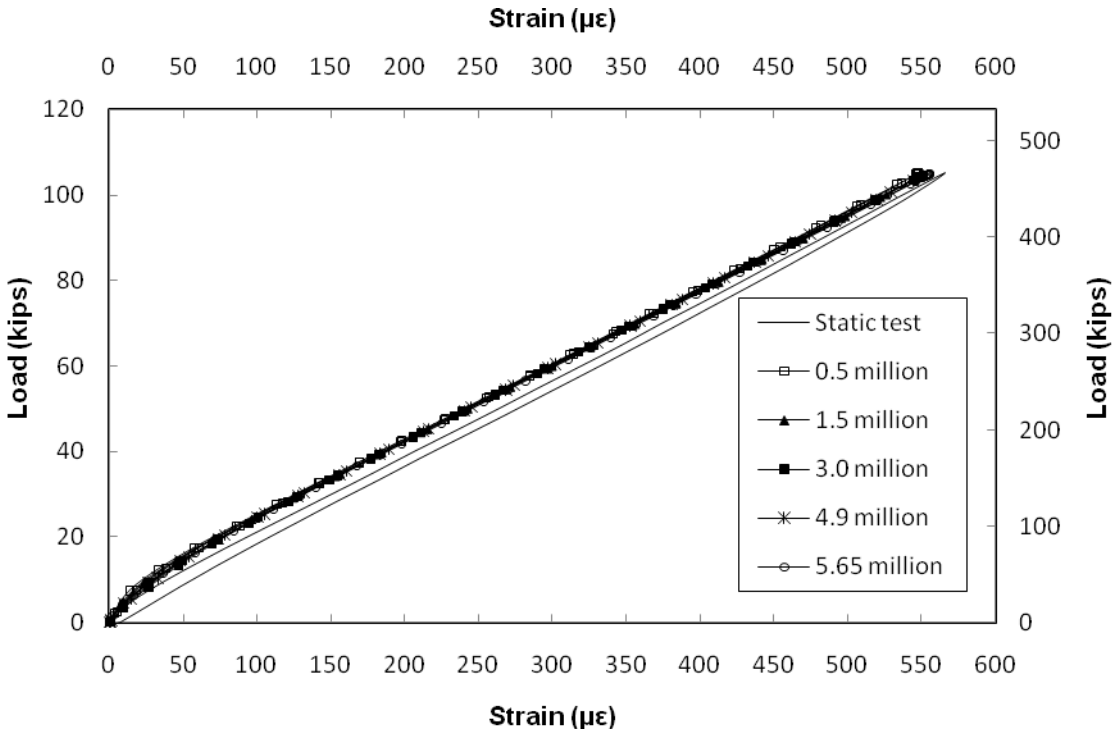


**Figure D.37** Strain in Rebars on Hold Down Side SG # 59B

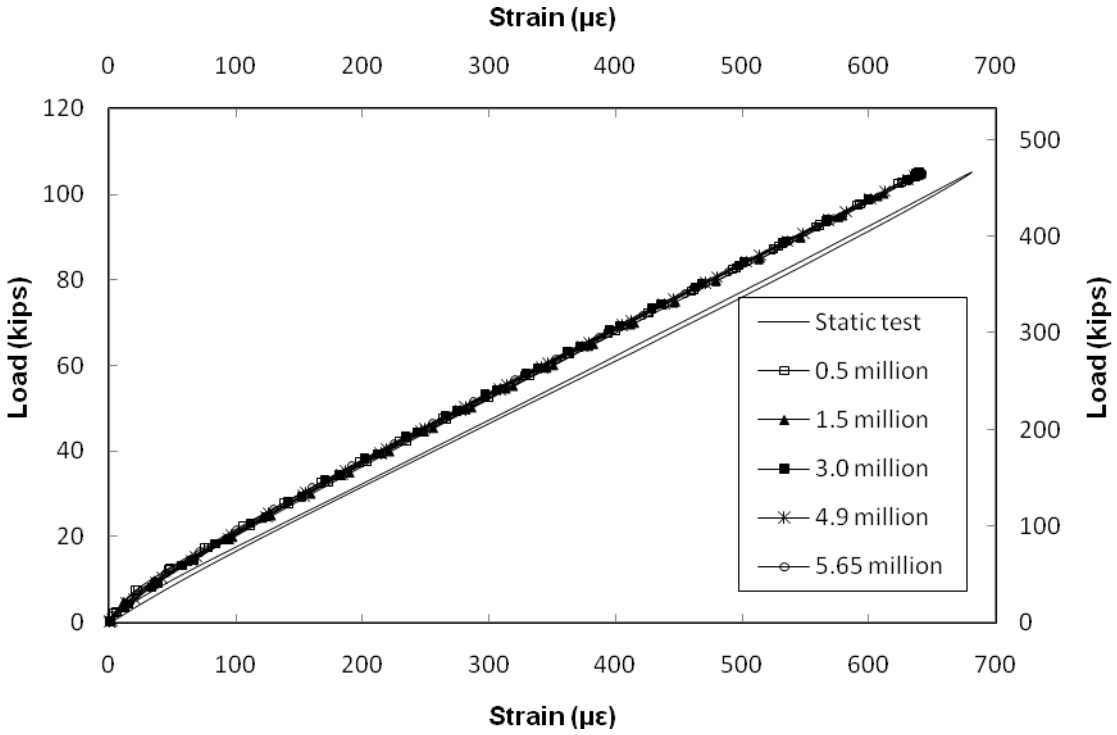


**Figure D.38** Strain in Rebars on Hold Down Side SG # 60B

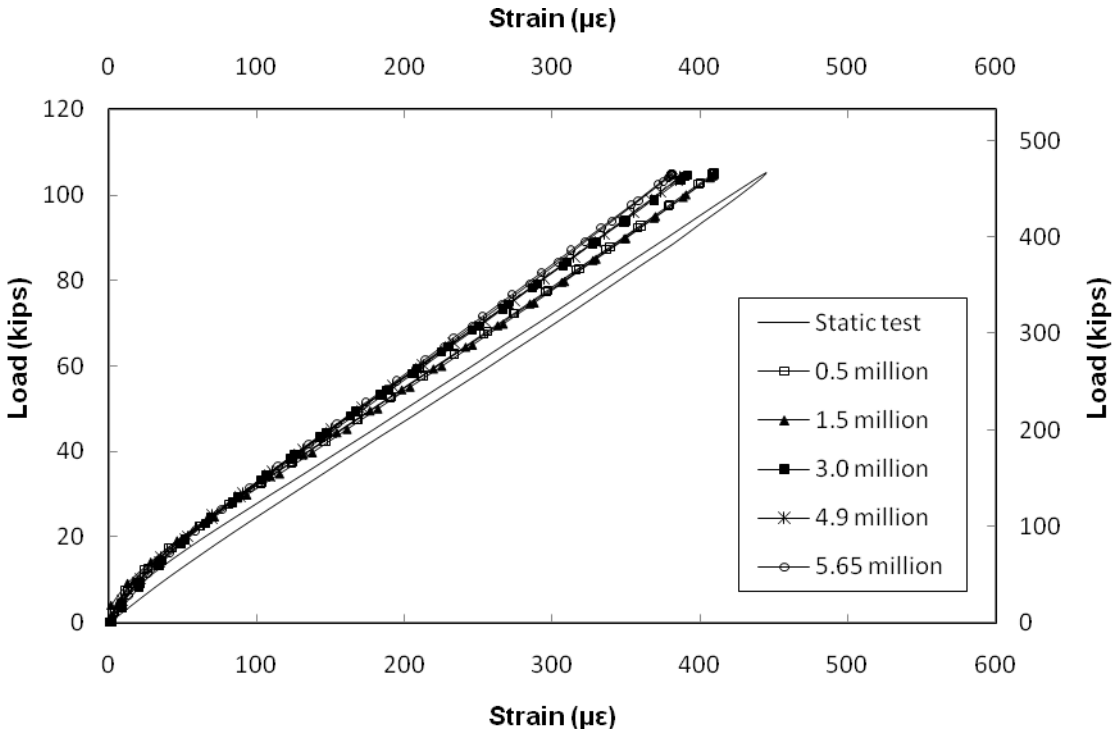


**Figure D.39** Strain in Rebars on Hold Down Side SG # 61B

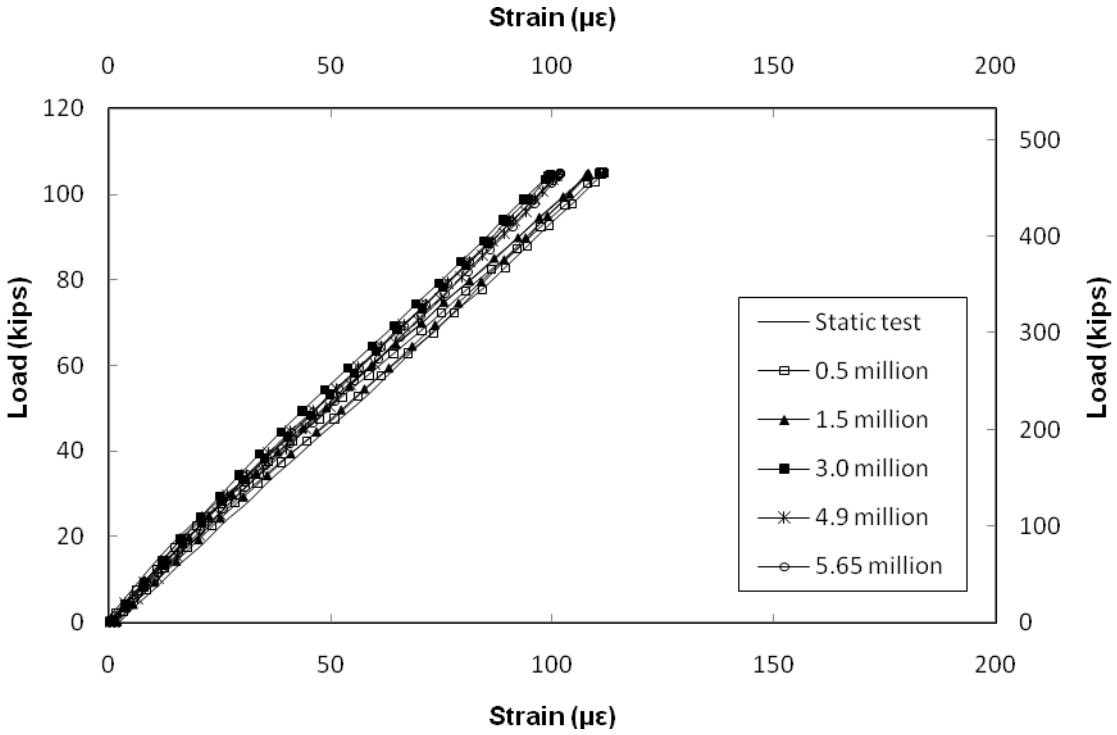


**Figure D.40** Strain in Rebars on Hold Down Side SG # 62B

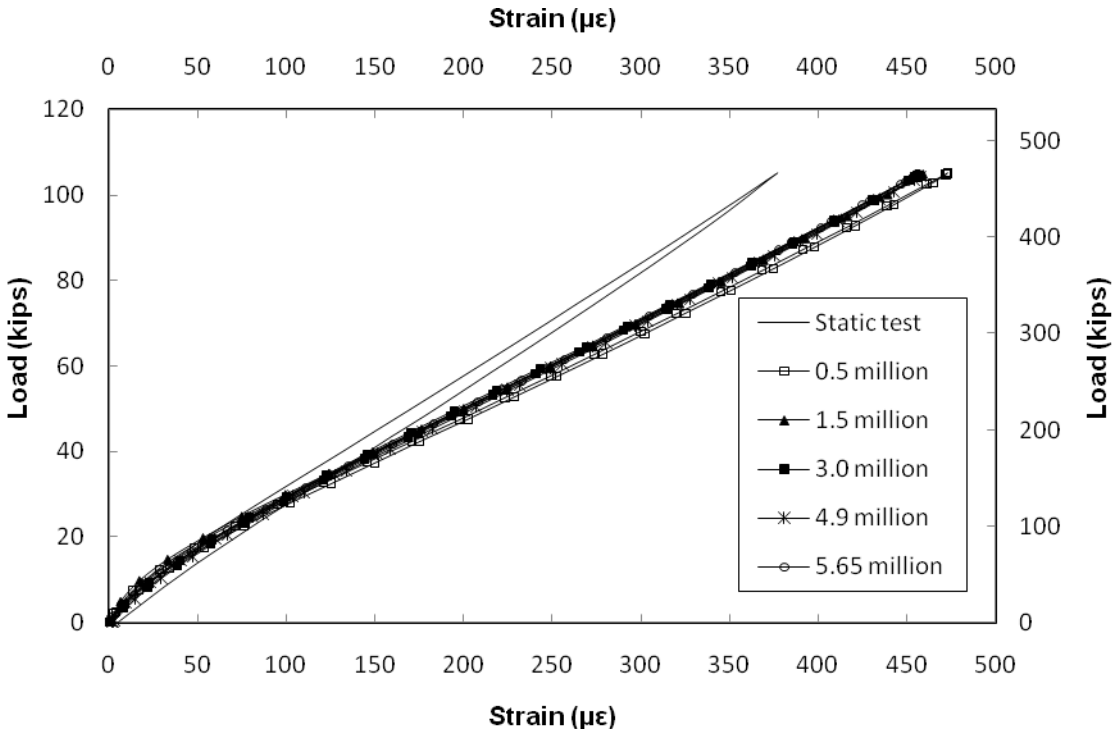


**Figure D.41** Strain in Rebars on Hold Down Side SG # spare2B

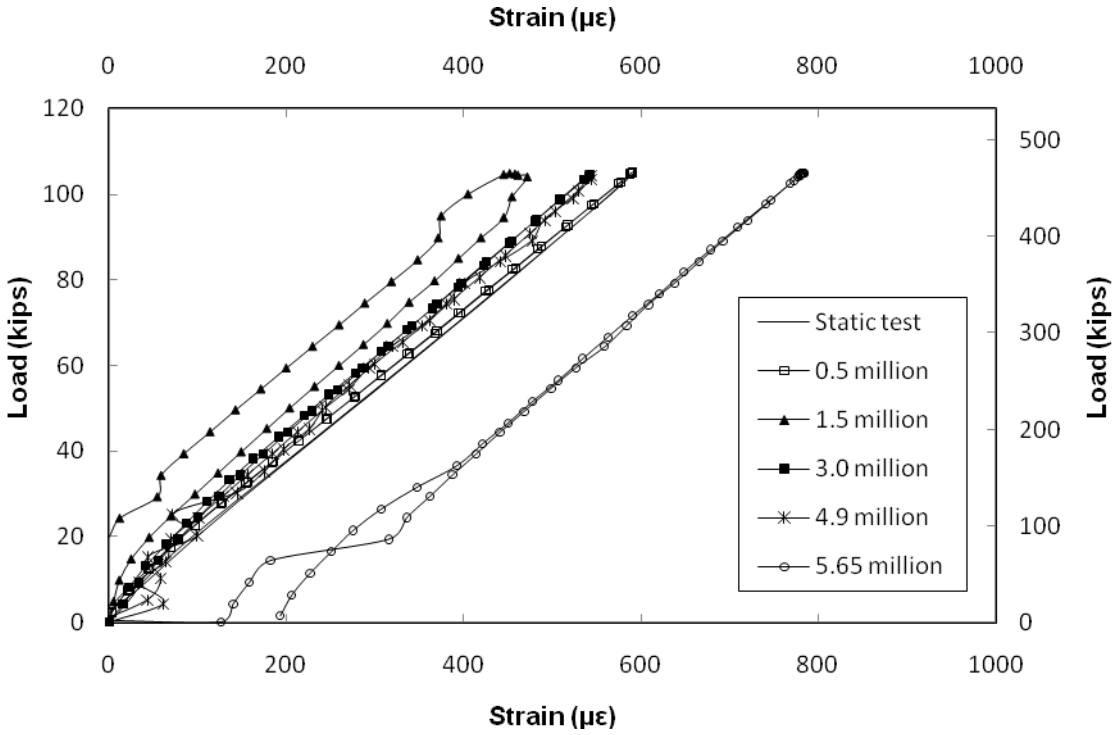


**Figure D.42** Strain in Rebars on Hold Down Side SG # spare3B

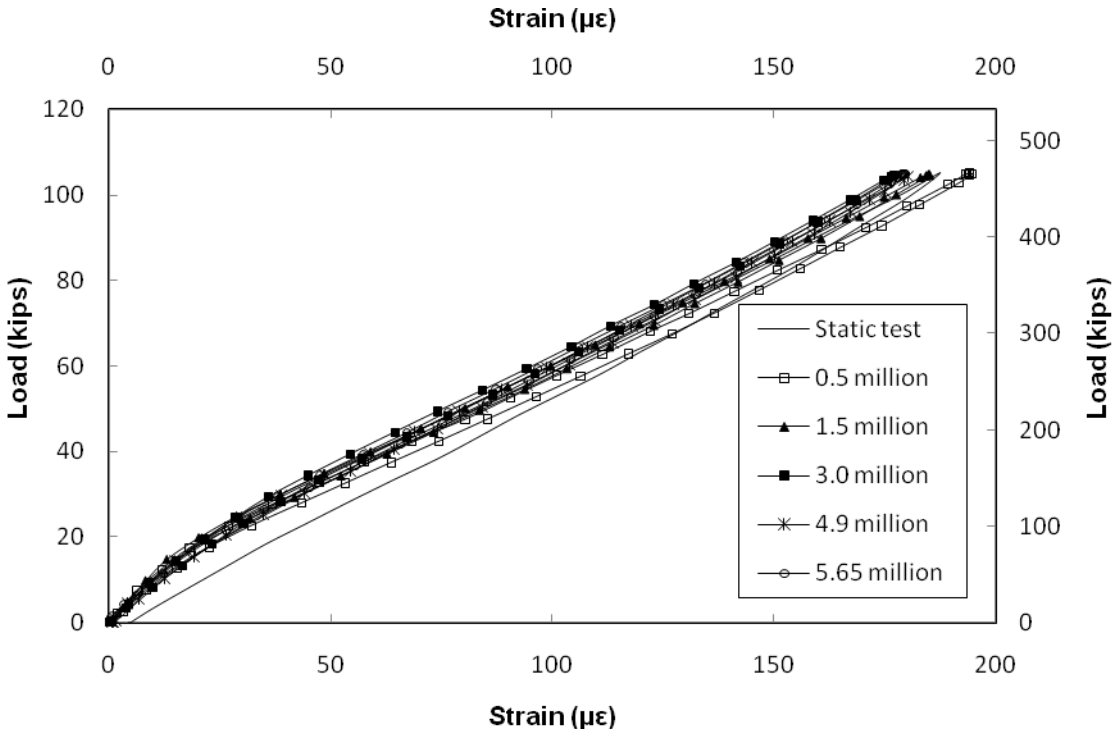


**Figure D.43** Strain in Rebars on Hold Down Side SG # 63B

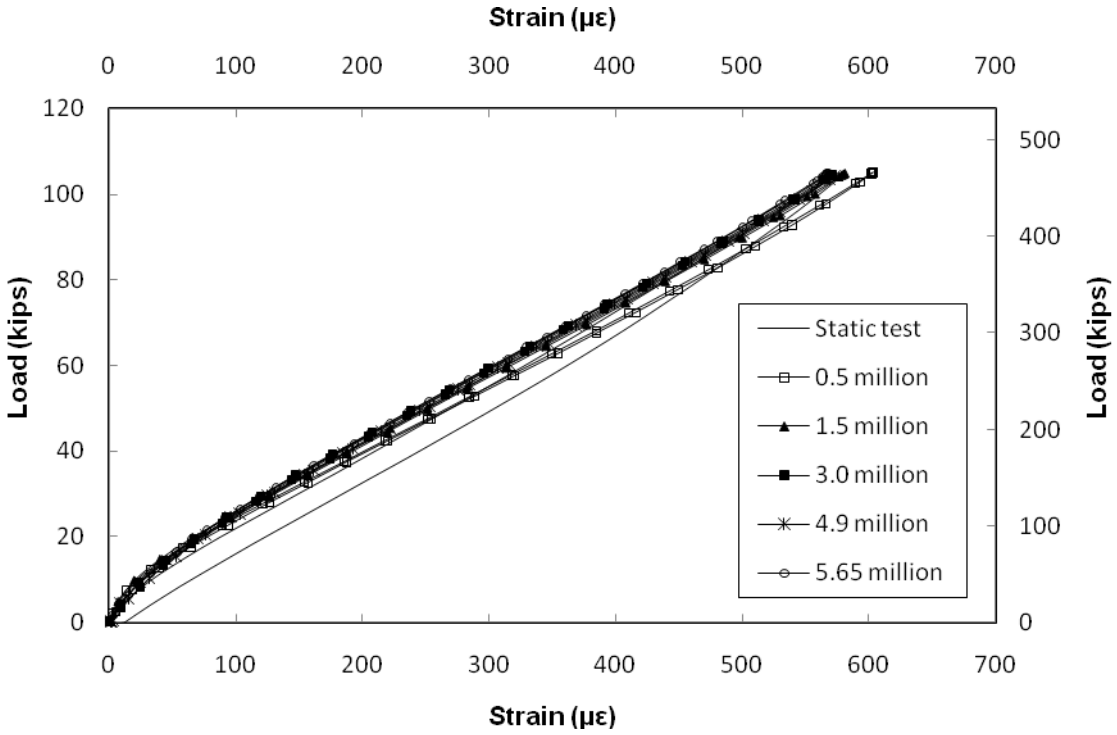


**Figure D.44** Strain in Rebars on Hold Down Side SG # 64B

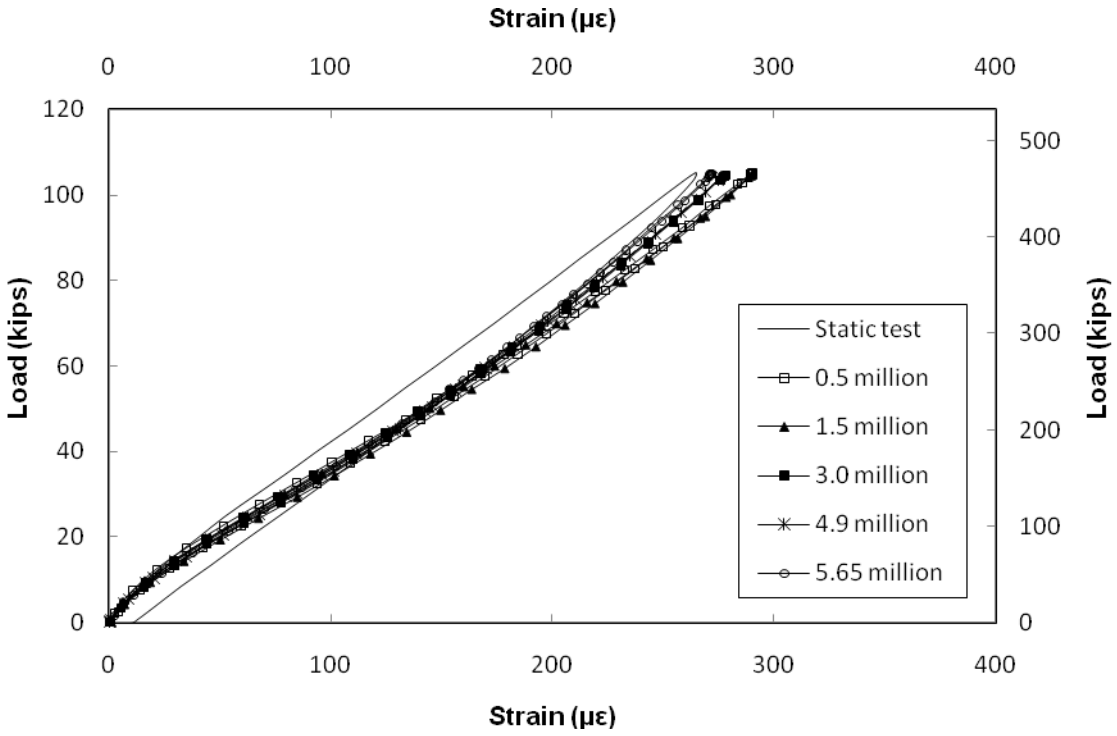


**Figure D.45** Strain in Rebars on Hold Down Side SG # 65B

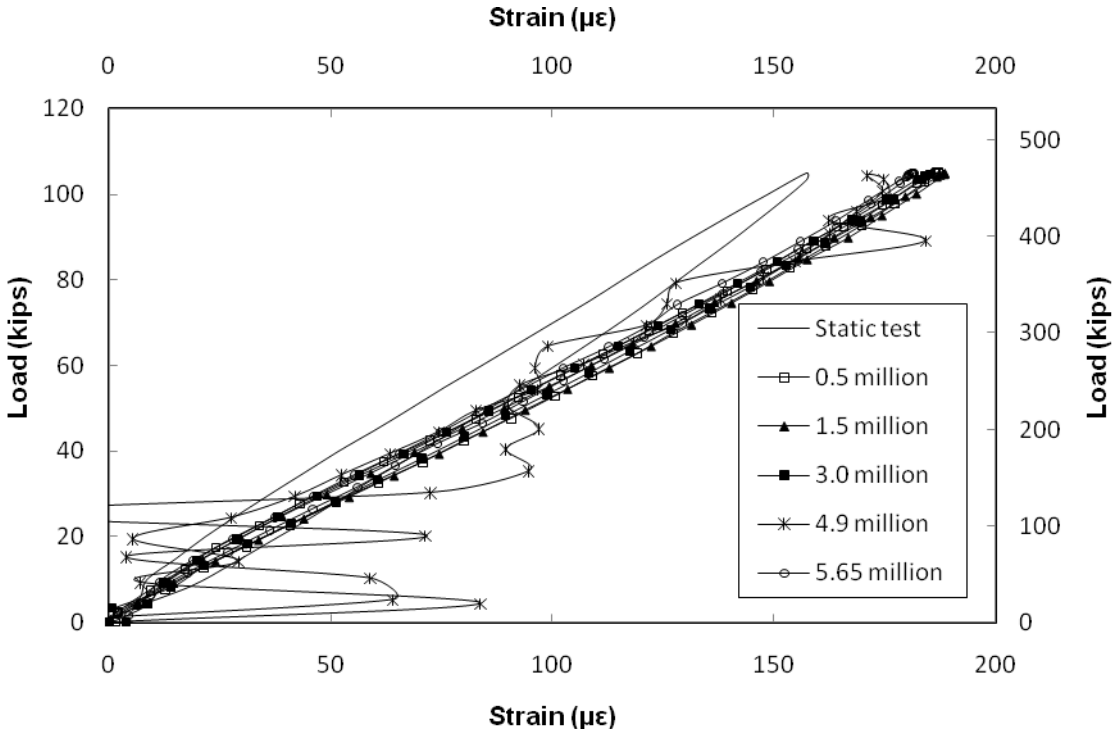


**Figure D.46** Strain in Rebars on Hold Down Side SG # 66B

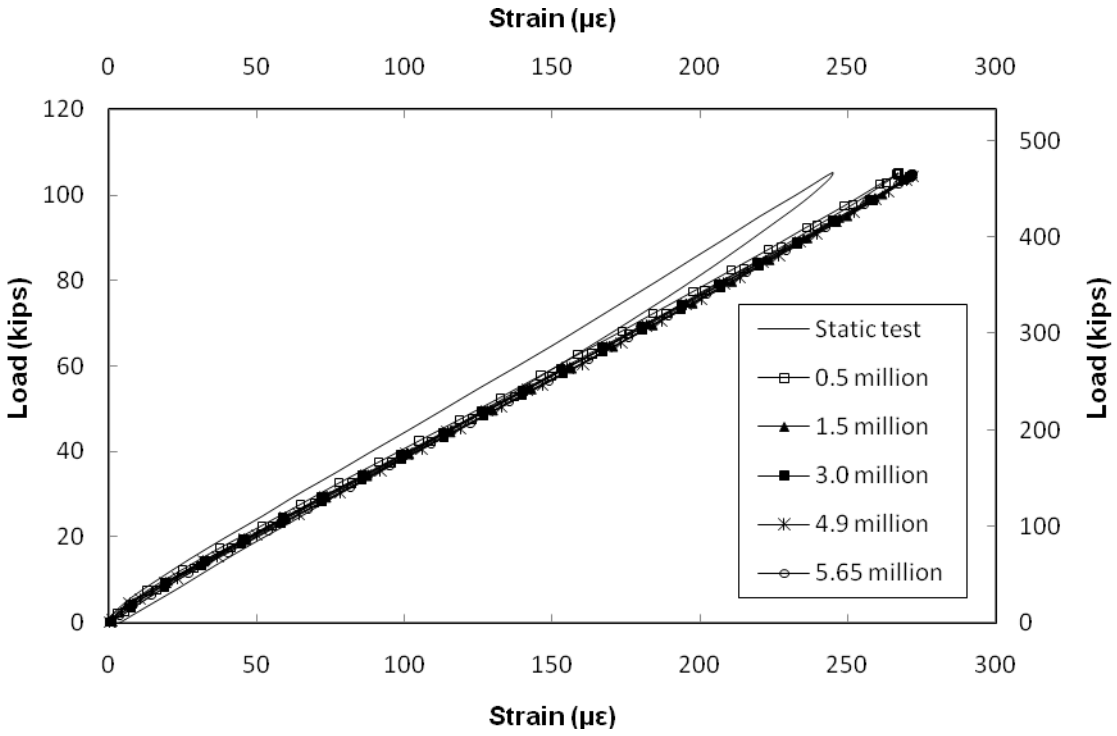


**Figure D.47** Strain in Rebars on Hold Down Side SG # spare4B

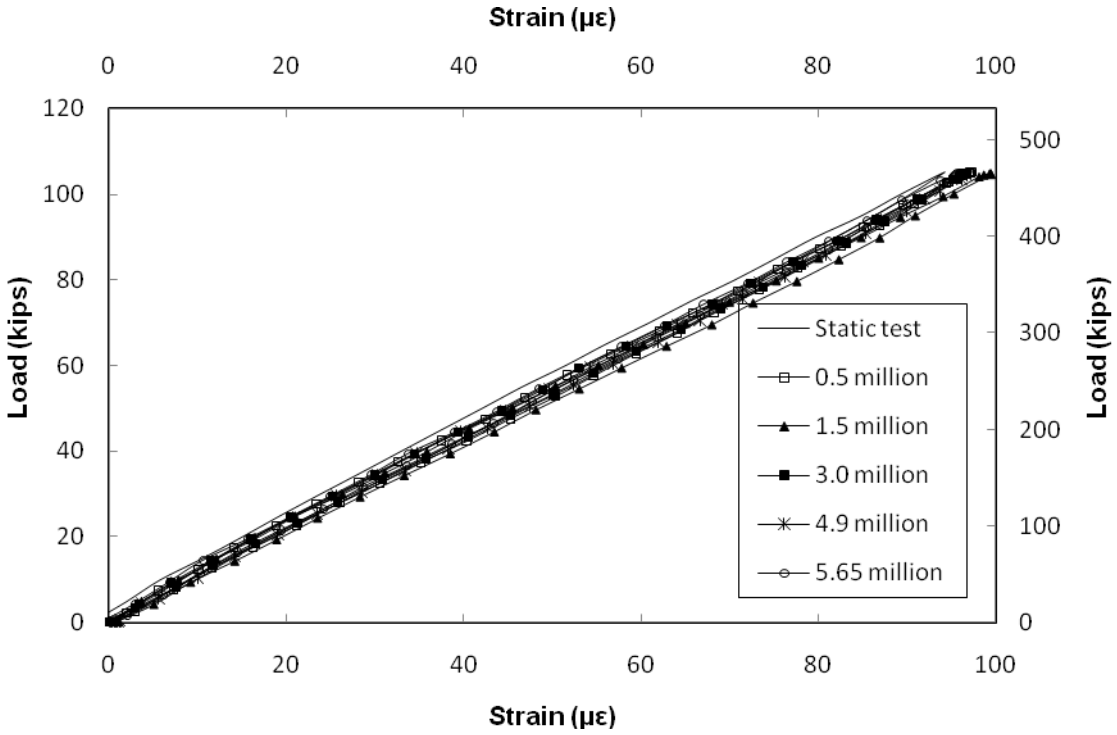


**Figure D.48** Strain in Rebars on Hold Down Side SG # 67B

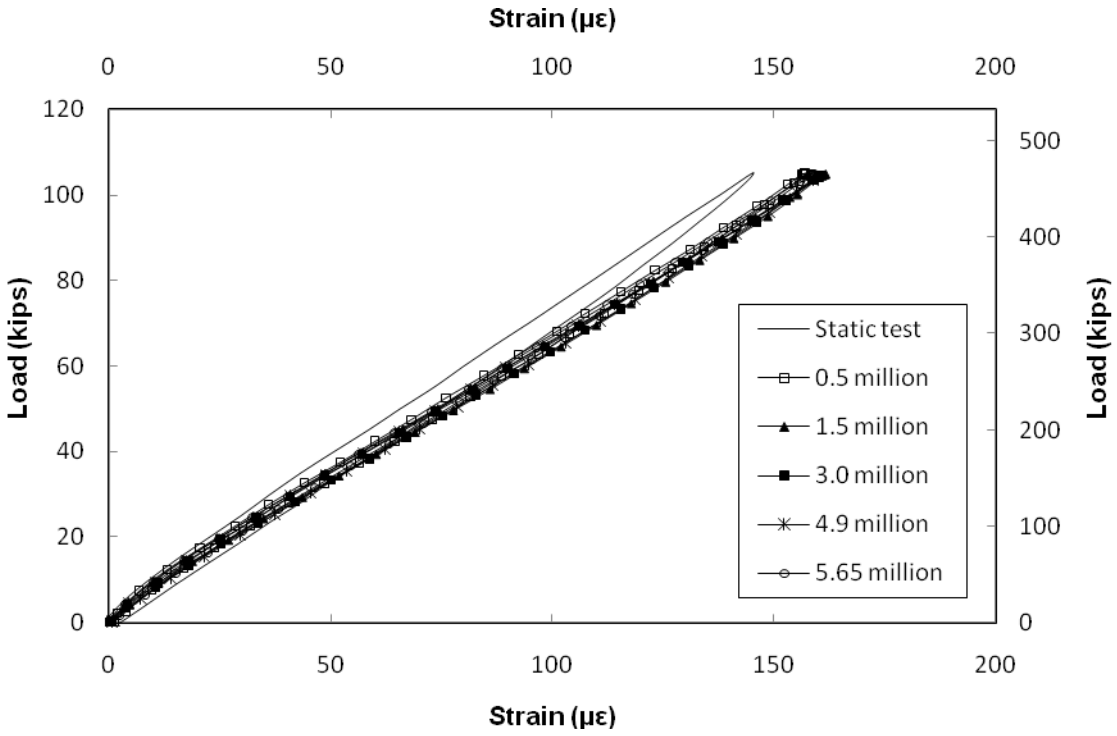


**Figure D.49** Strain in Rebars on Hold Down Side SG # 68B

## D.5 Strain in Steel

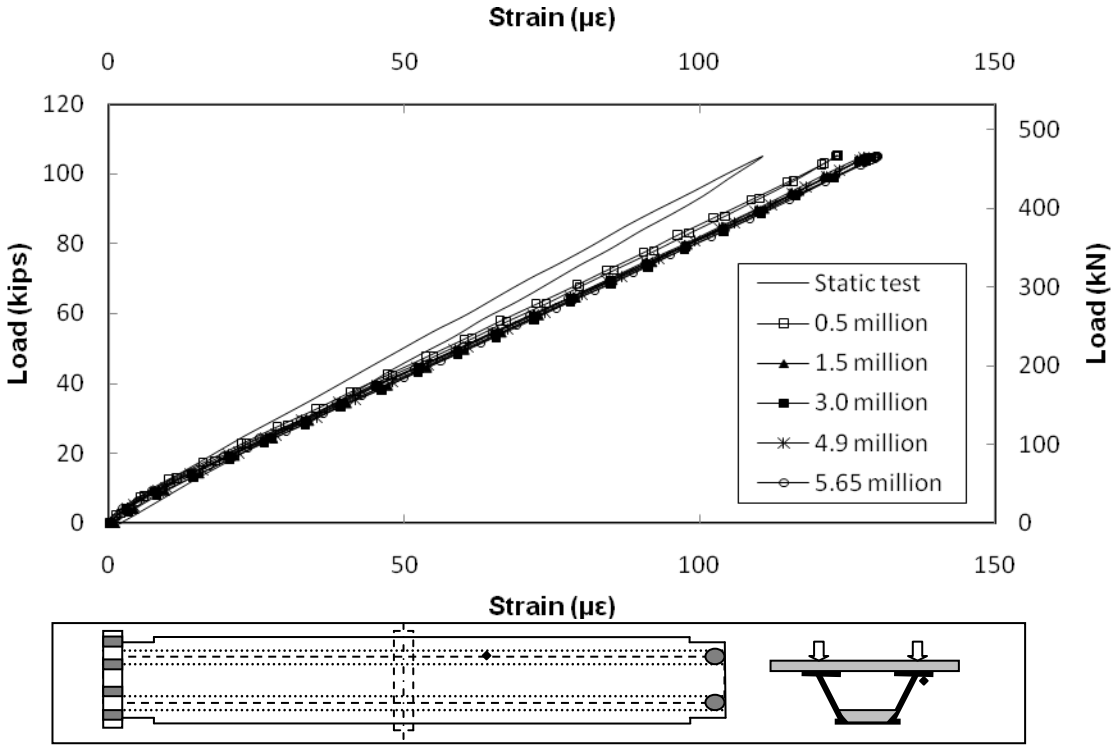


**Figure D.50** Strain in Top Flange on Actuator Side SG # 71

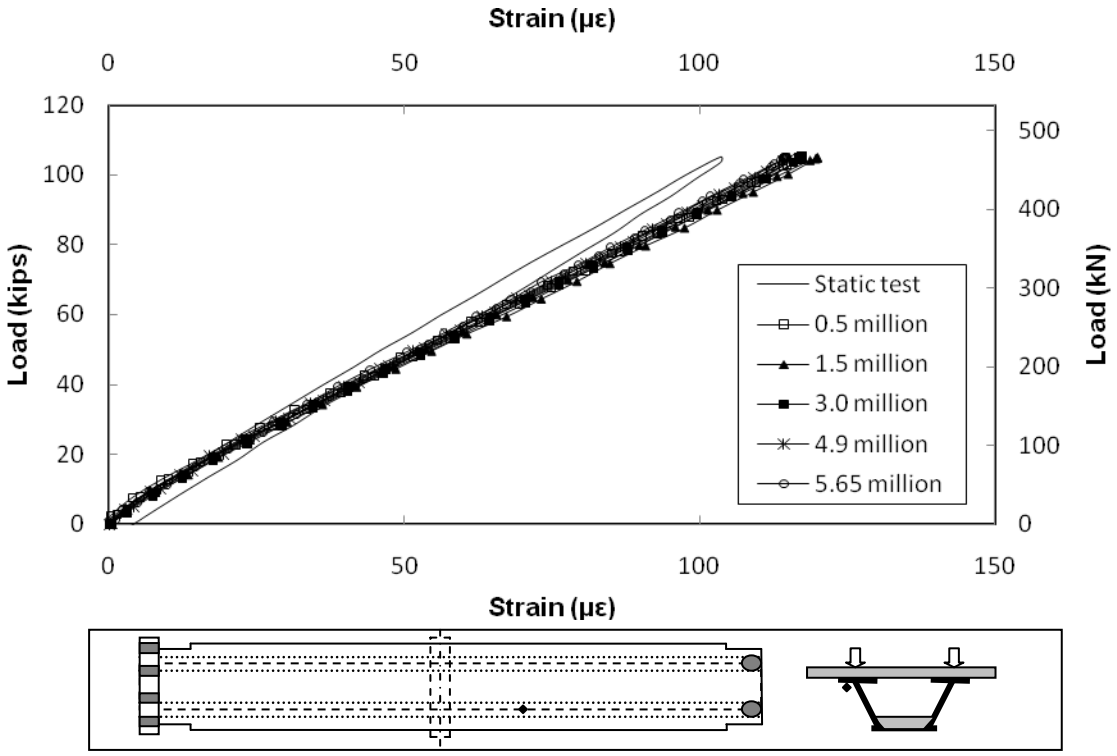


**Figure D.51** Strain in Top Flange on Actuator Side SG # 72

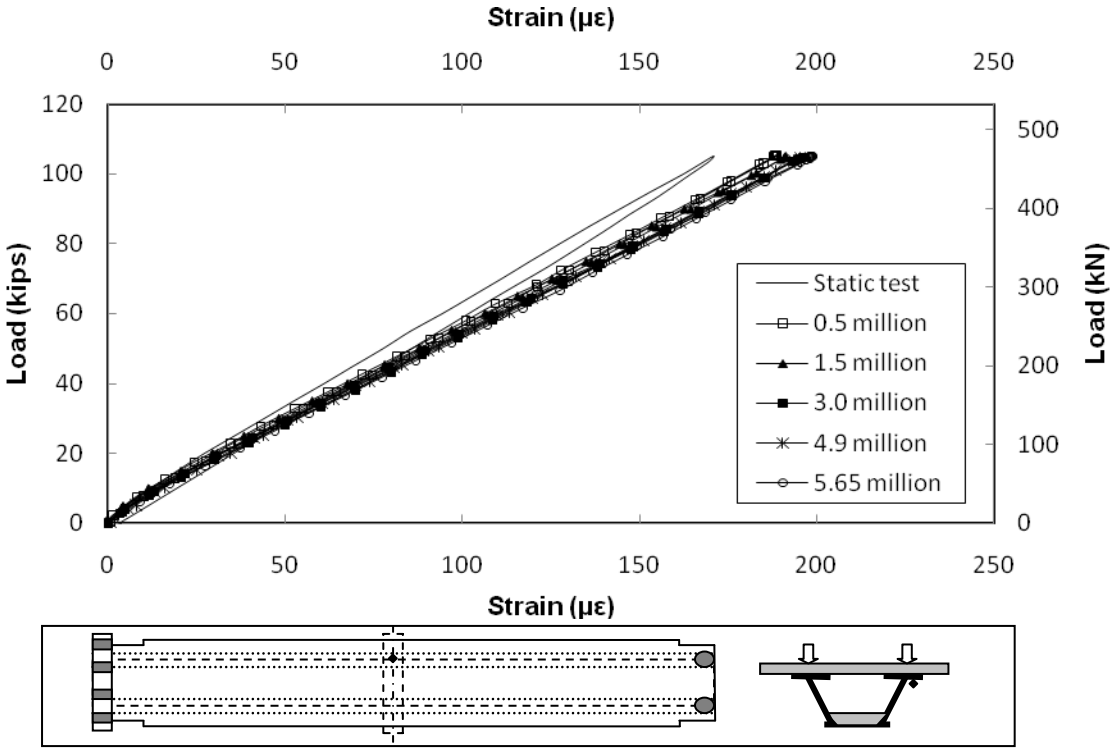


**Figure D.52** Strain in Top Flange at Center Support SG # 73

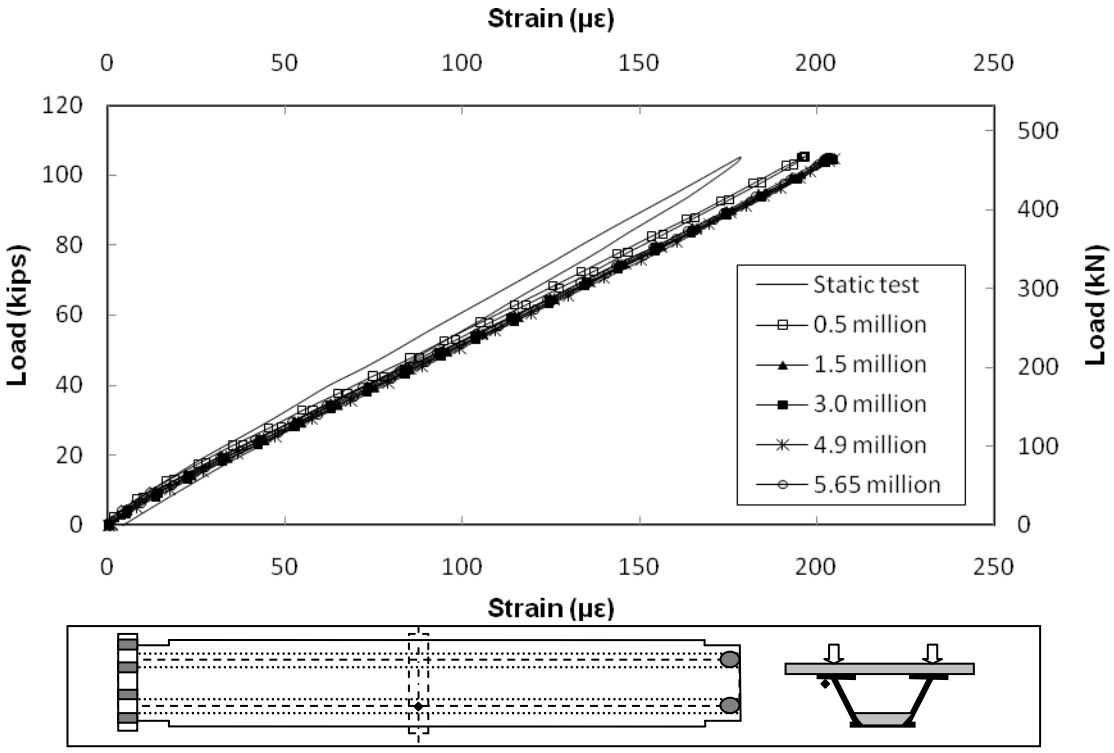


**Figure D.53** Strain in Top Flange at Center Support SG # 74

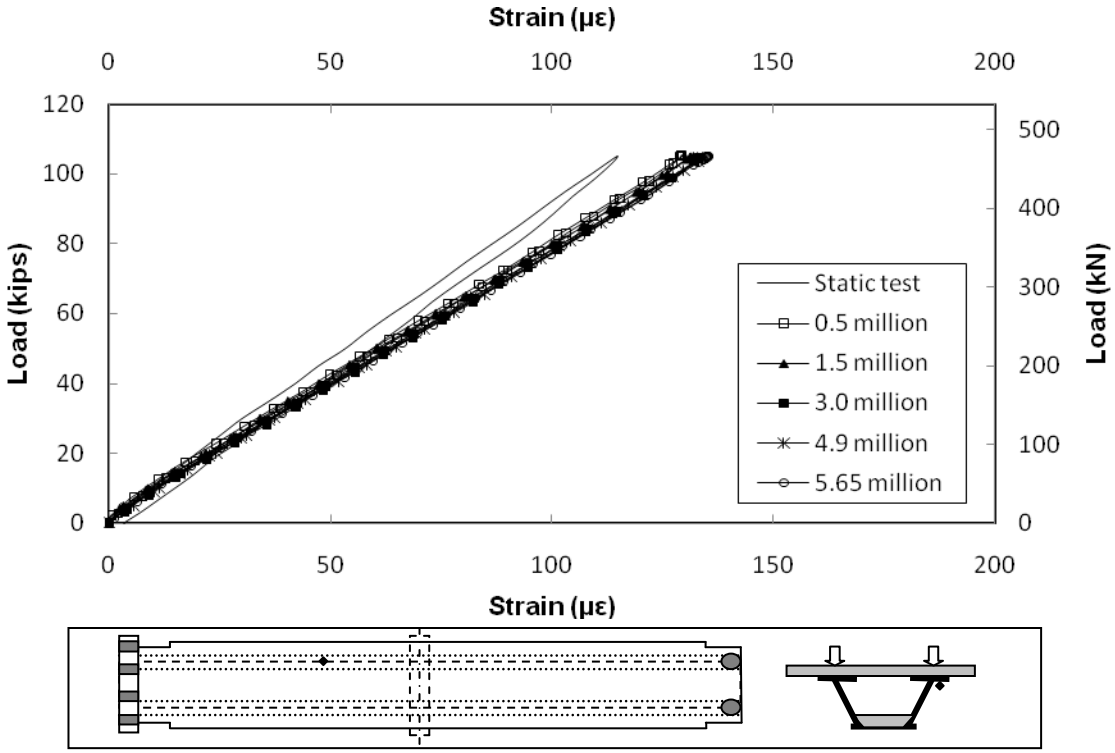


**Figure D.54** Strain in Top Flange at 4 ft 10⅛ in. on Hold Down Side SG # 75

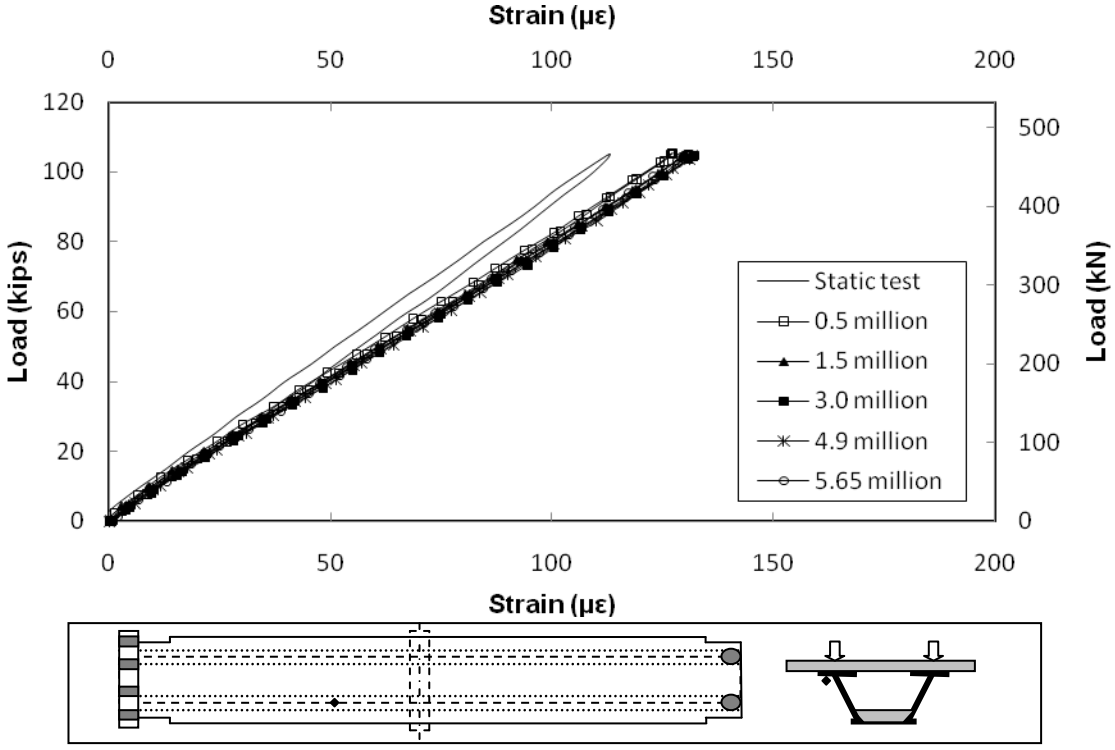


**Figure D.55** Strain in Top Flange (at 4 ft 10⅛ in.) on Hold Down Side SG # 76

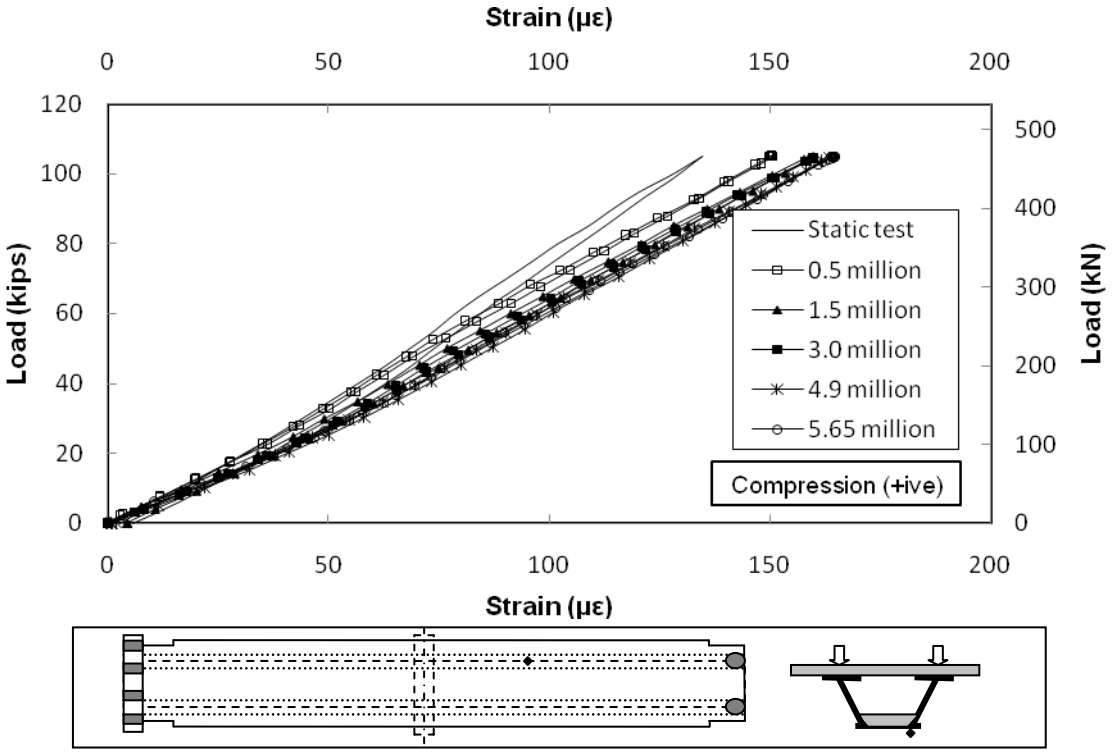


**Figure D.56** Strain in Bottom Flange (at 4 ft 10⅛ in.) on Actuator Side SG # 118

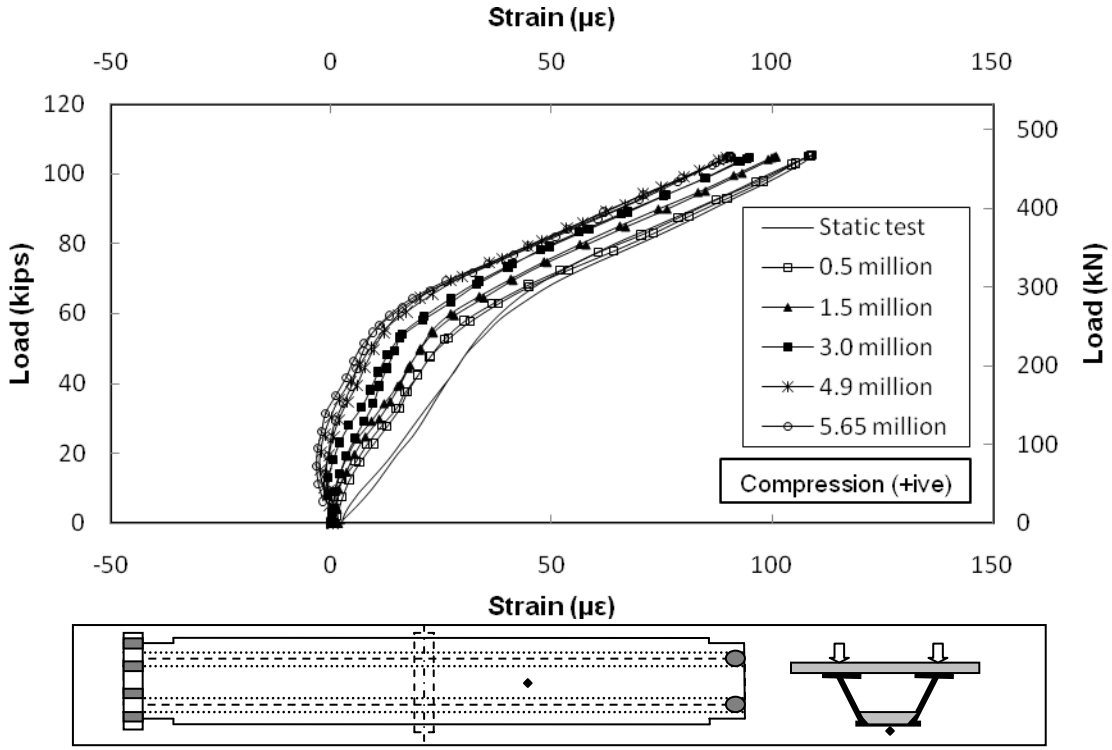


**Figure D.57** Strain in Bottom Flange (at 4 ft 10⅛ in.) on Actuator Side SG # 119

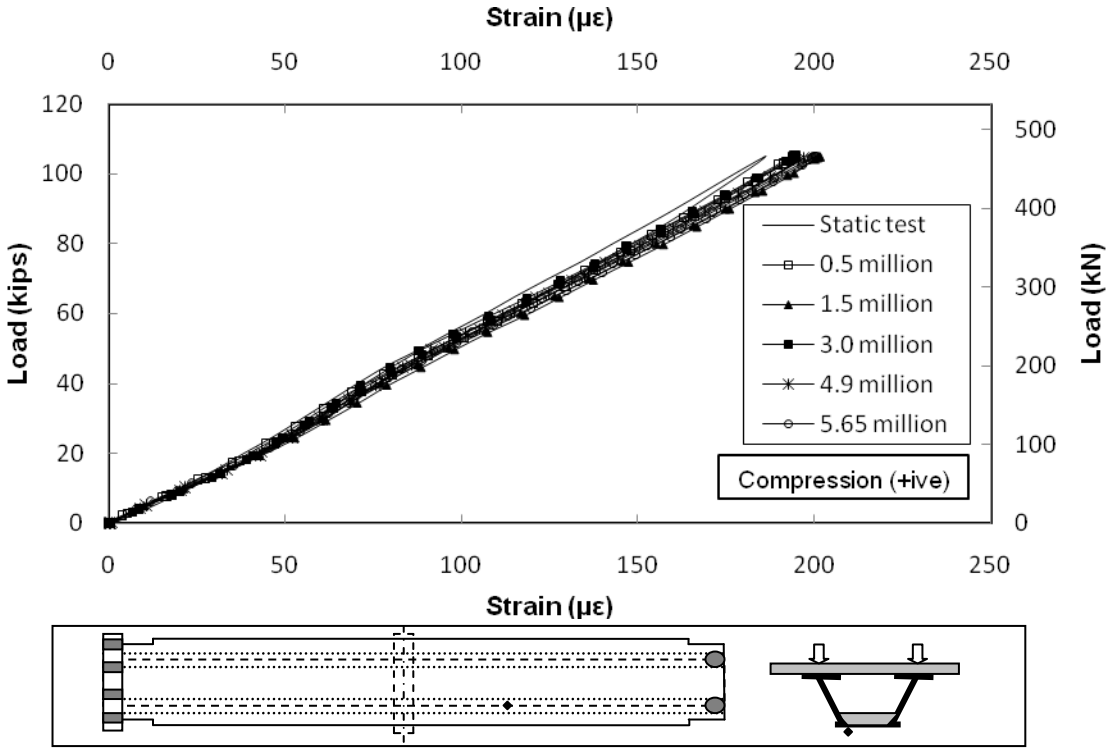


**Figure D.58** Strain in Bottom Flange (at 4 ft 10⅛ in.) on Actuator Side SG # 120

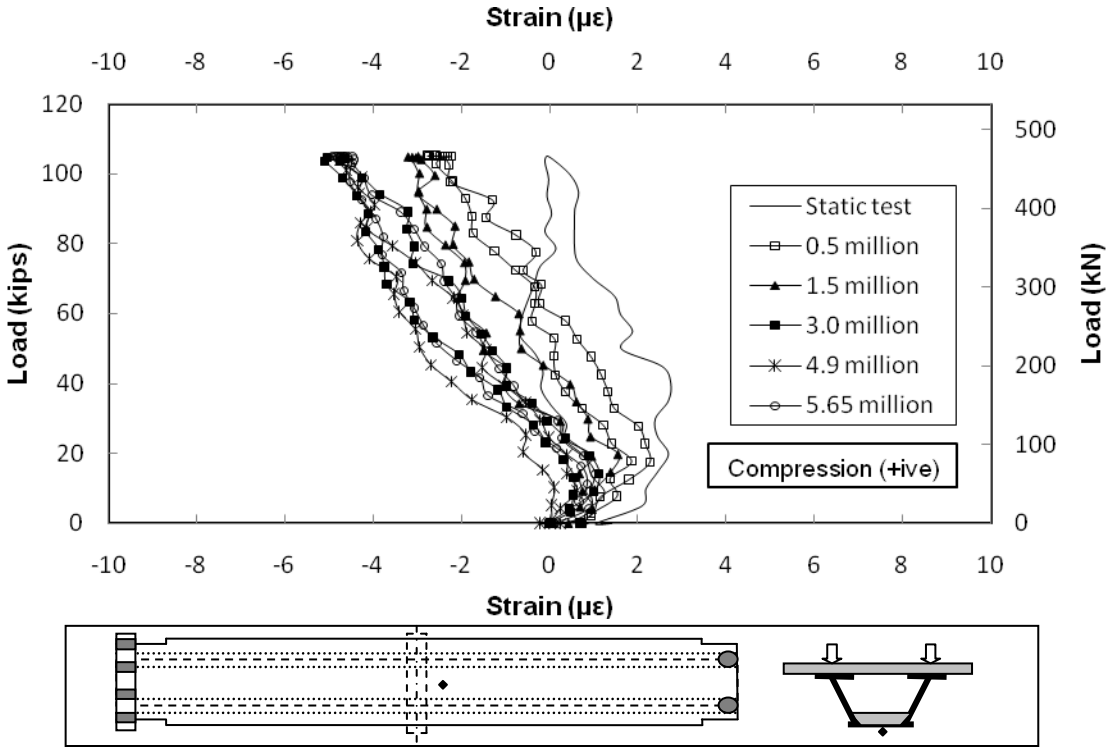


**Figure D.59** Strain in Bottom Flange (at 2 ft ¼ in.) on Actuator Side SG # 121

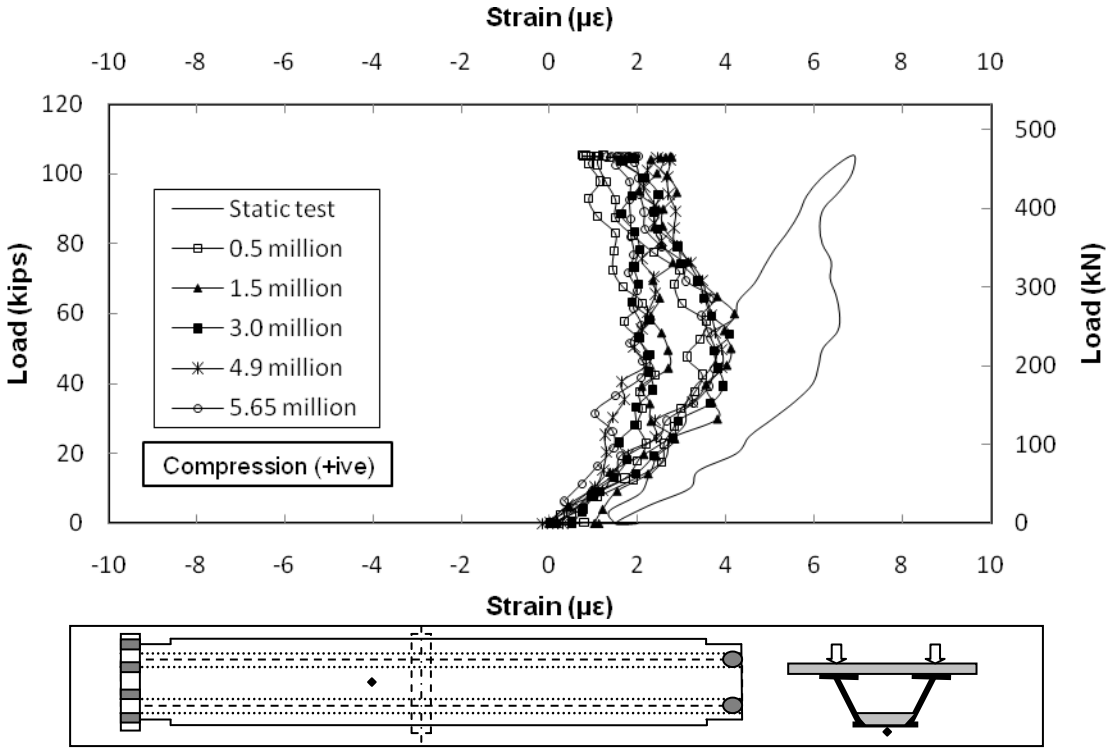


**Figure D.60** Strain in Bottom Flange (at 2 ft ¼ in.) on Hold Down Side SG # 122

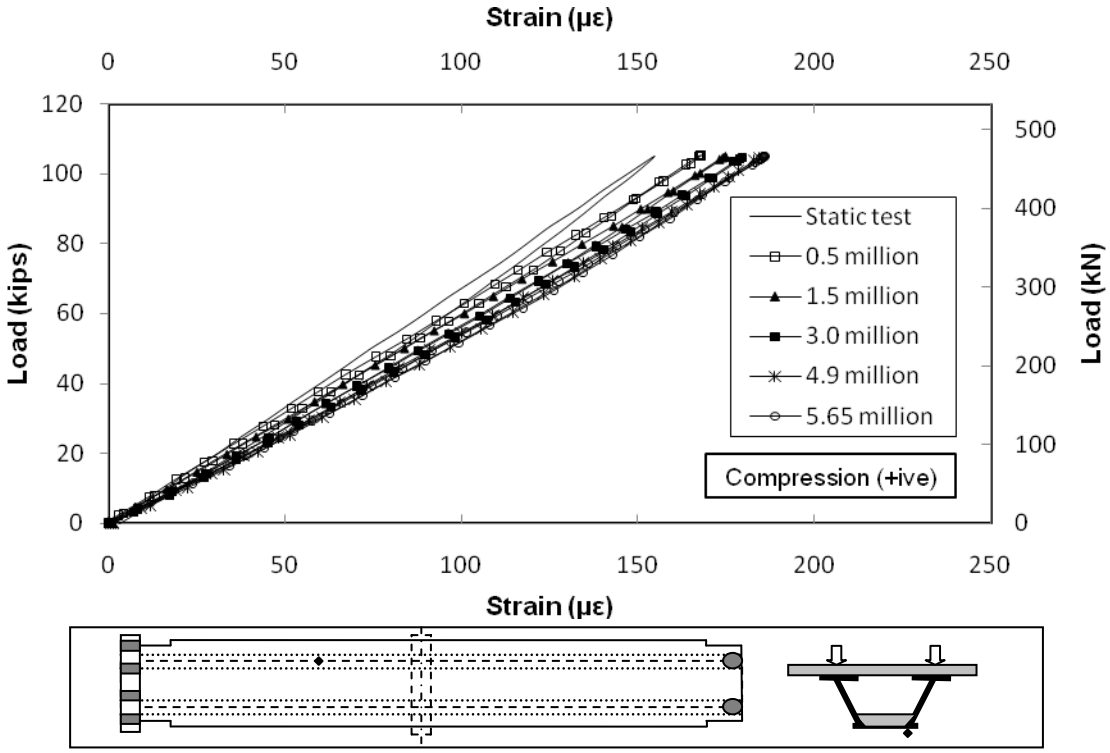


**Figure D.61** Strain in Bottom Flange (at 4 ft 10⅛ in.) on Hold Down Side SG # 123

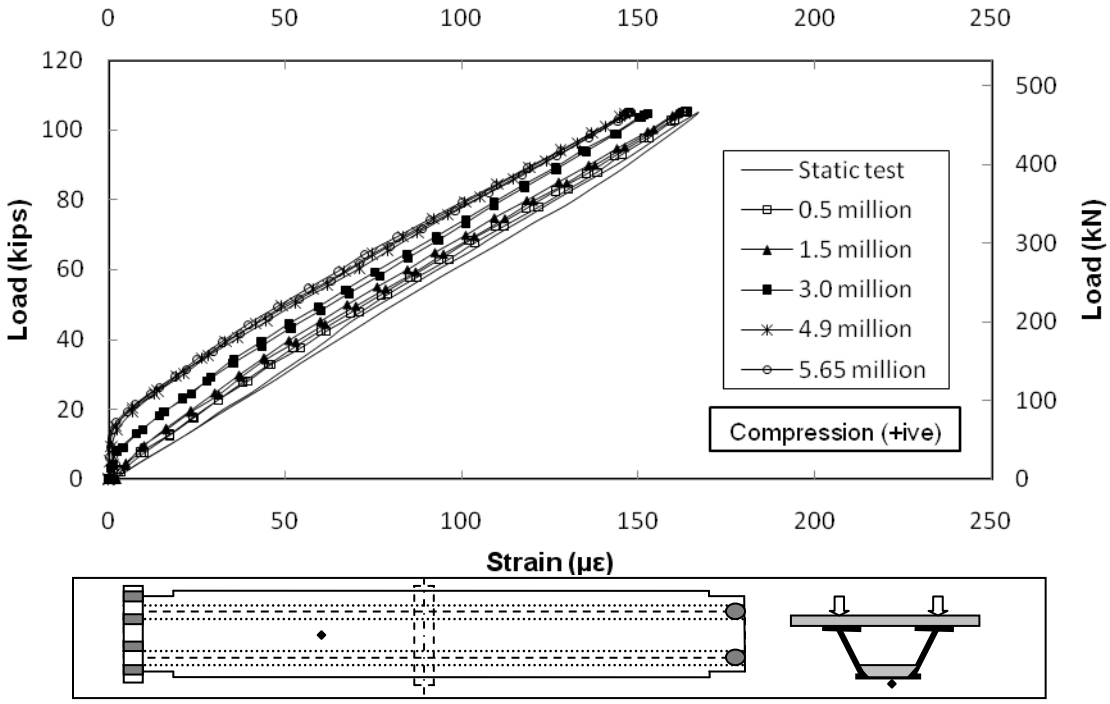


**Figure D.62** Strain in Bottom Flange (at 4 ft 10⅛ in.) on Hold Down Side SG # 124

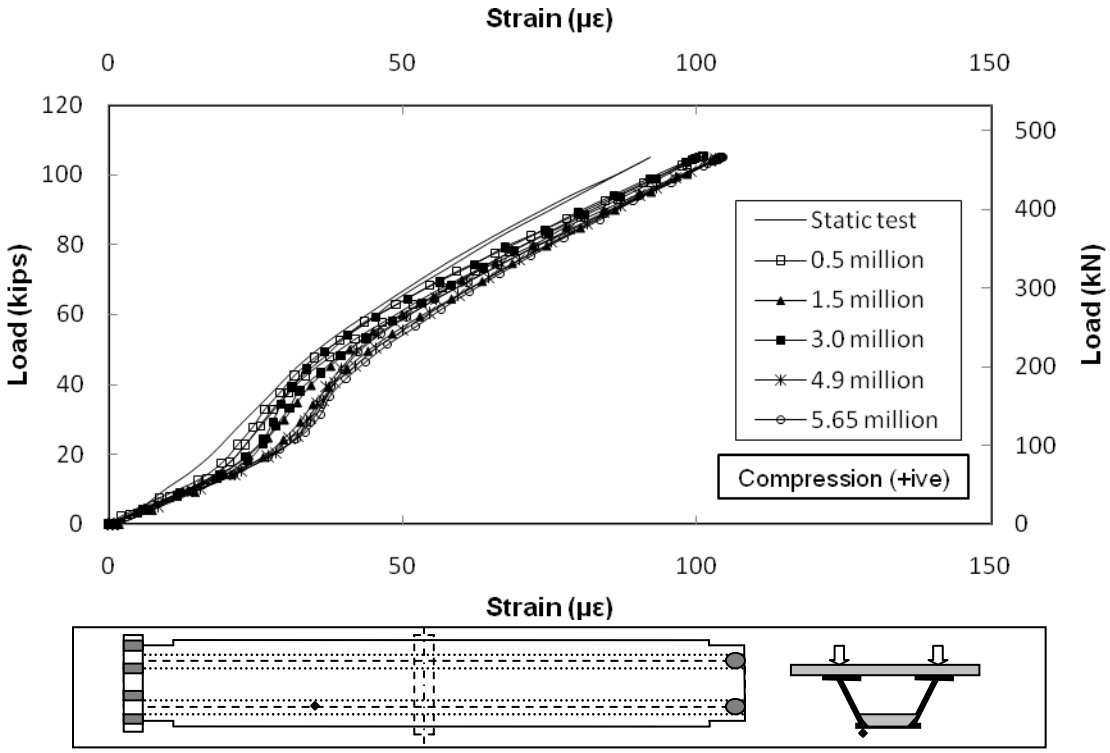


**Figure D.63** Strain in Bottom Flange (at 4 ft 10⅛ in.) on Hold Down Side SG # 125

## D.6 Strain in Concrete

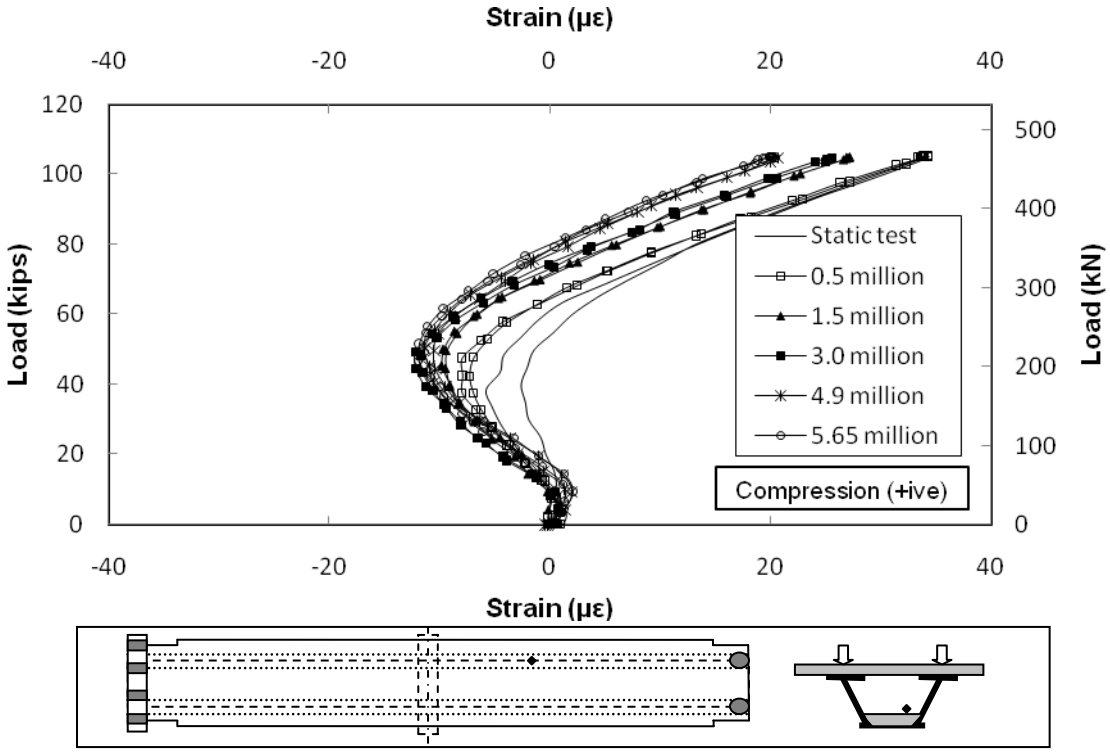


**Figure D.64** Strain in Bottom Flange (at 4 ft 10⅛ in.) on Actuator Side SG # 106

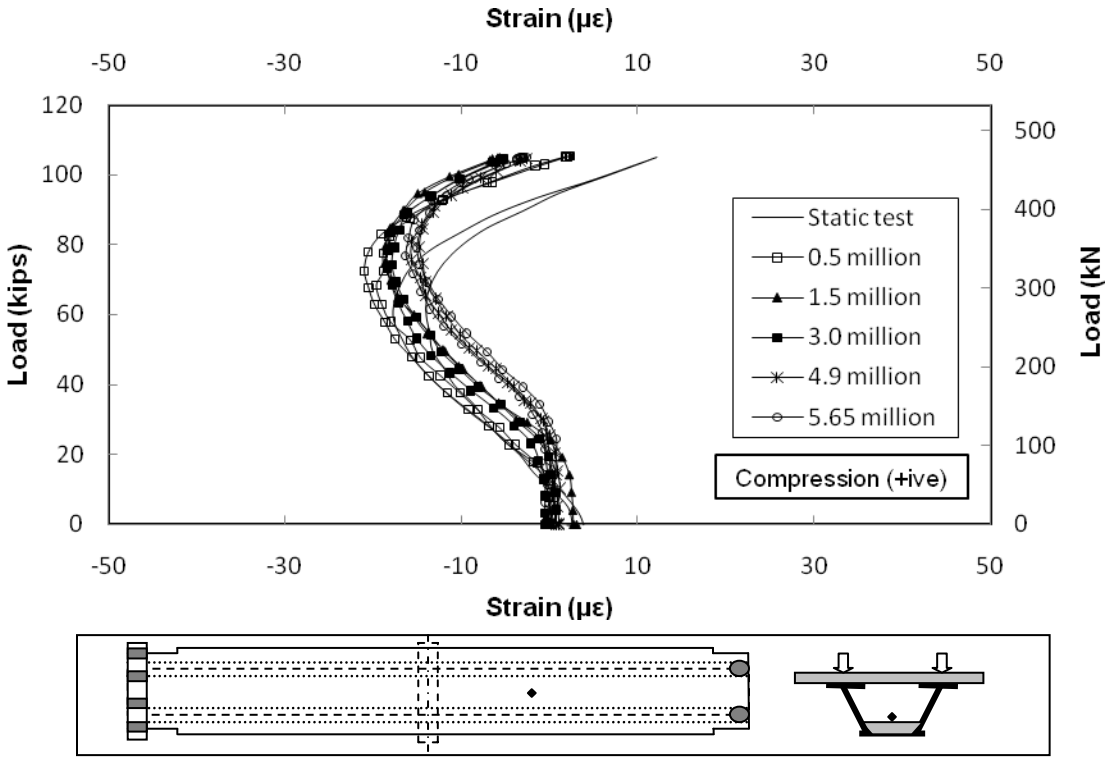


**Figure D.65** Strain in Bottom Flange (at 4 ft 10⅛ in.) on Actuator Side SG # 107

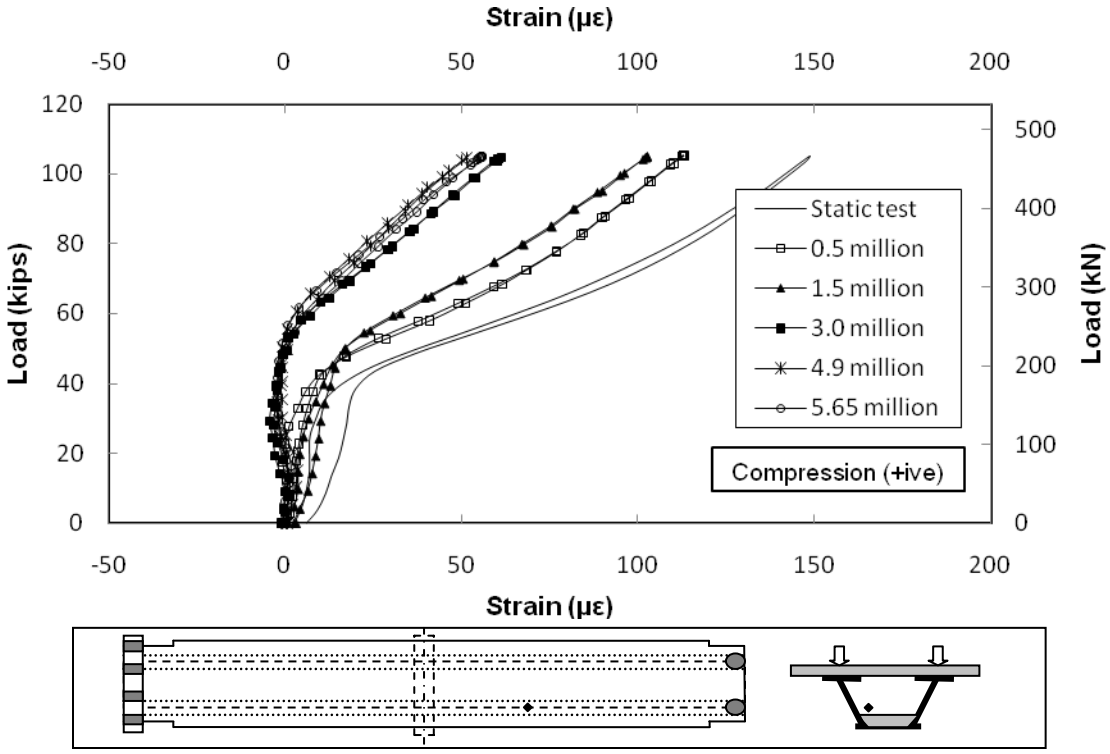


**Figure D.66** Strain in Bottom Flange (at 4 ft 10⅛ in.) on Actuator Side SG # 108

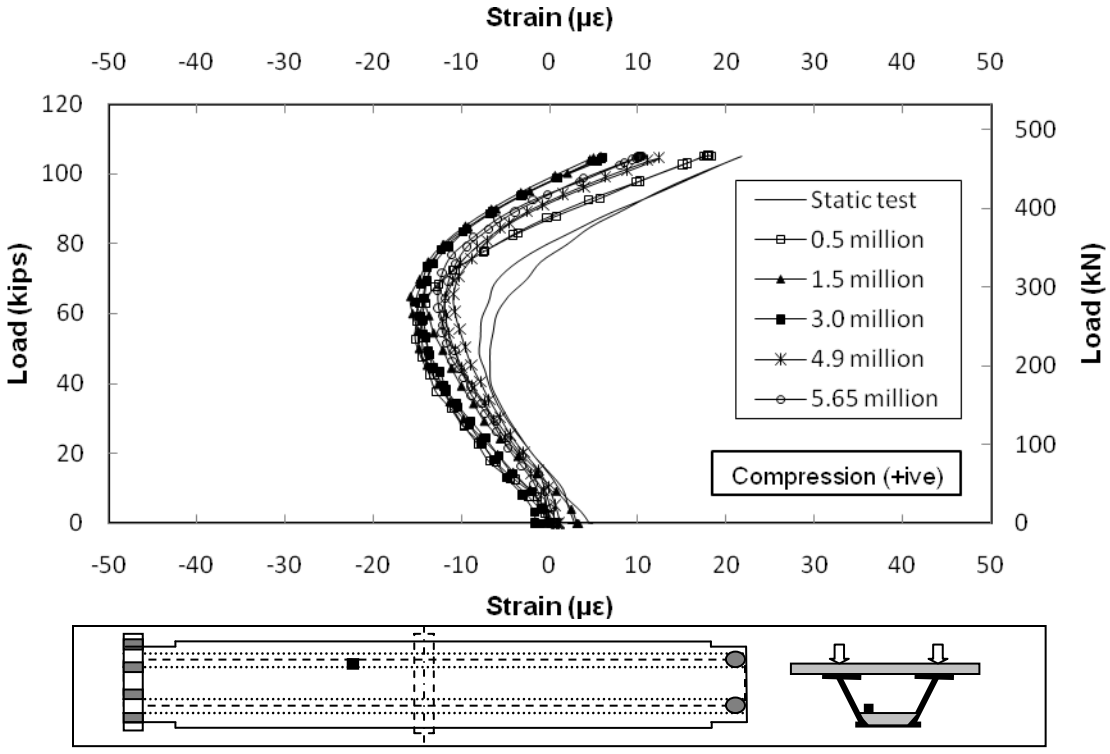


**Figure D.67** Strain in Bottom Flange (at 4 ft 10⅛ in.) on Hold Down Side SG # 109

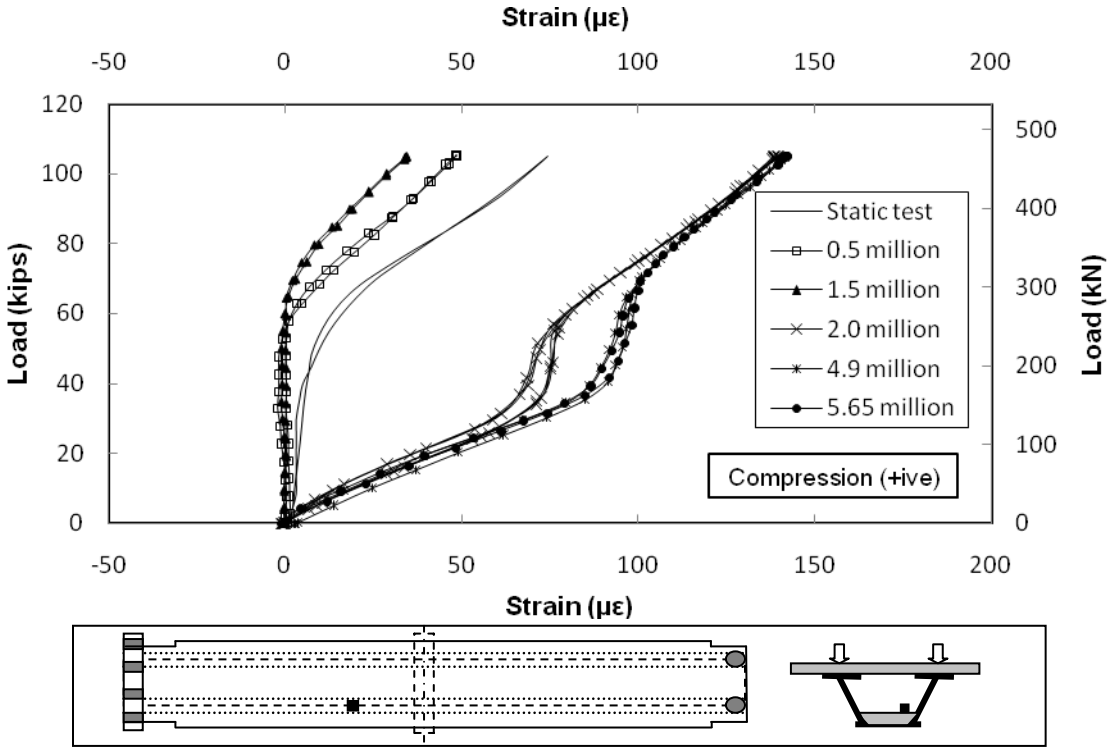


**Figure D.68** Strain in Bottom Flange (at 4 ft 10⅛ in.) on Hold Down Side SG # 111

## D.7 Neutral Axis

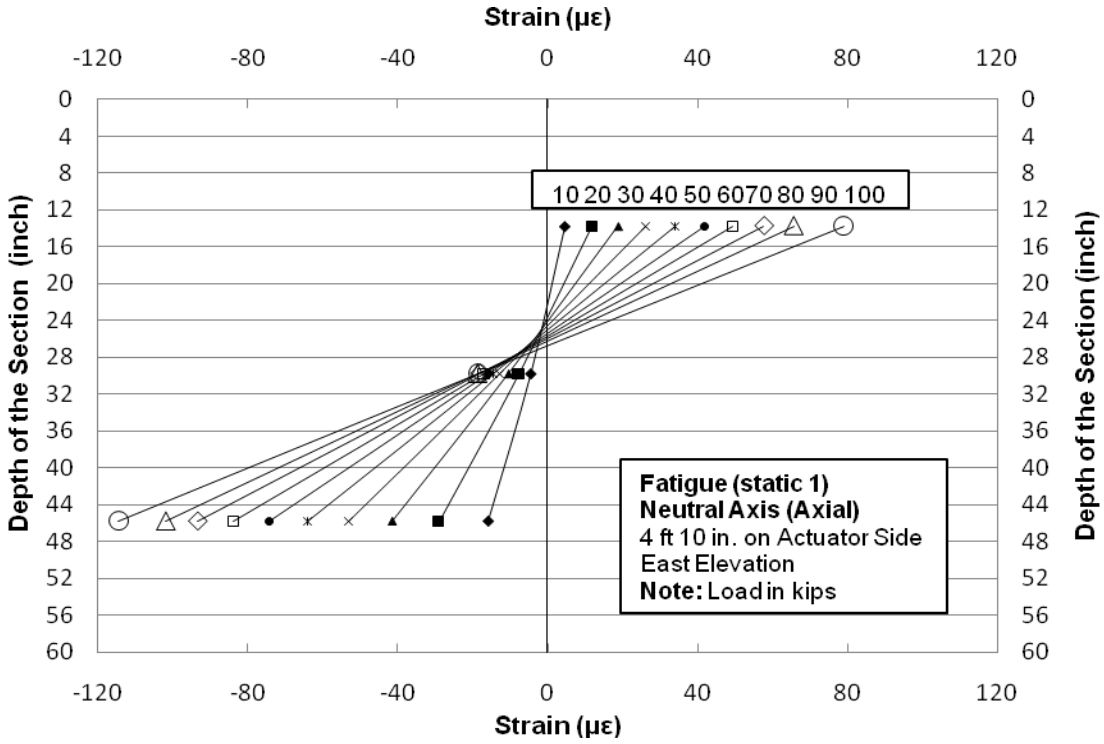


**Figure D.69** Neutral Axis on Actuator Side after 1st Static Cycle (East Elevation)

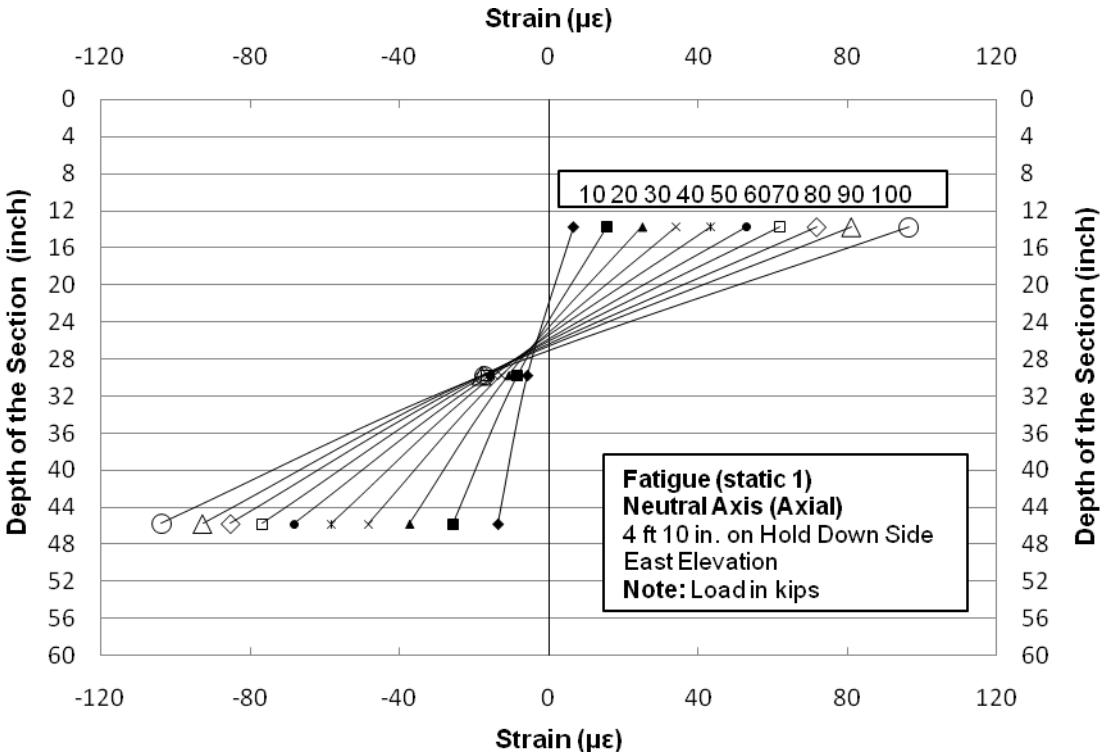


**Figure D.70** Neutral Axis on Hold Down Side after 1st Static Cycle (East Elevation)

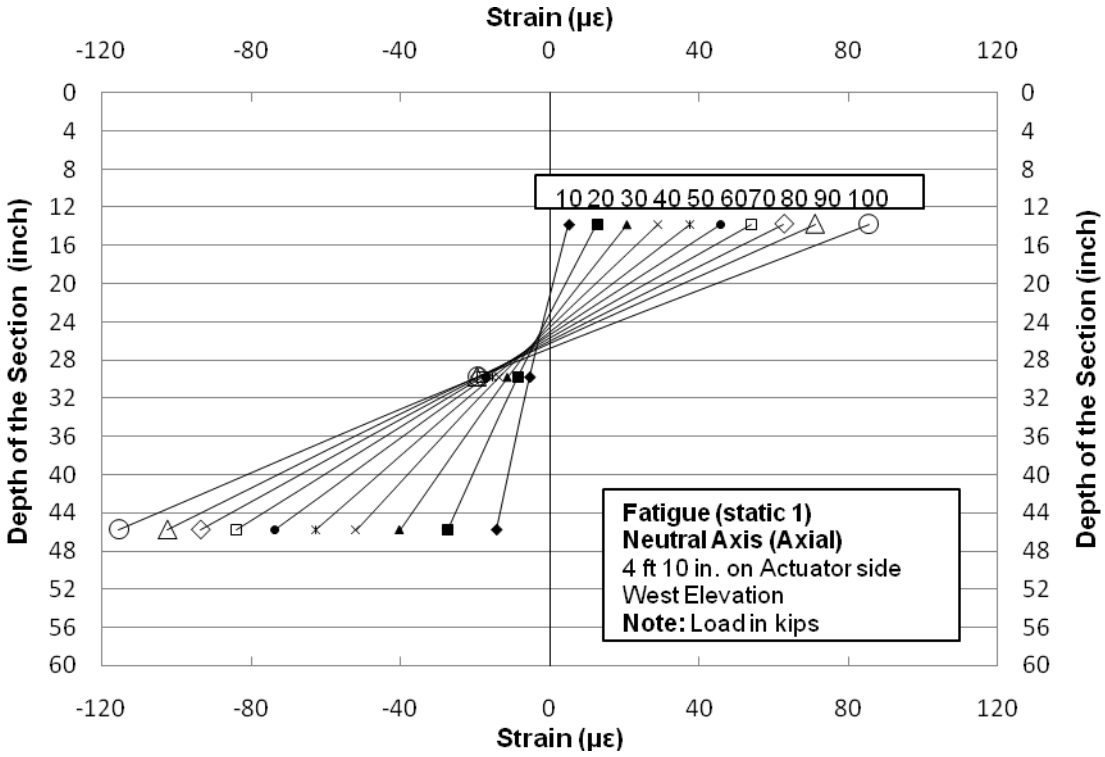


**Figure D.71** Neutral Axis on Actuator Side after 1st Static Cycle (West Elevation)

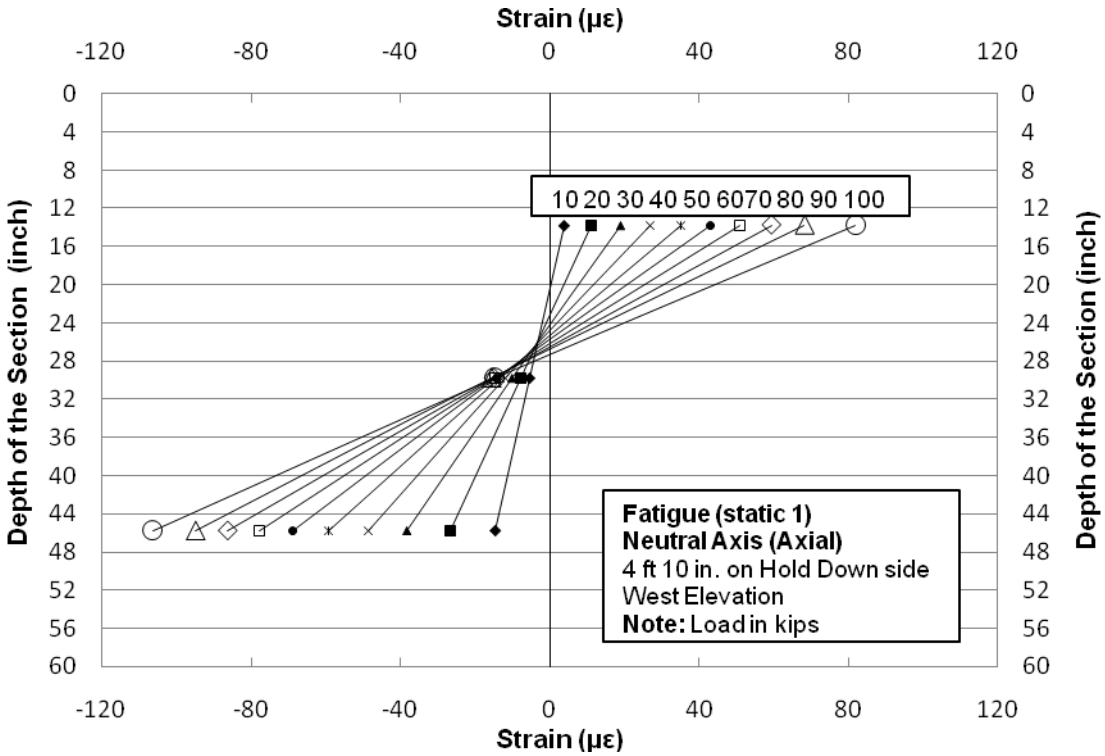


**Figure D.72** Neutral Axis on Hold Down Side after 1st Static Cycle (West Elevation)

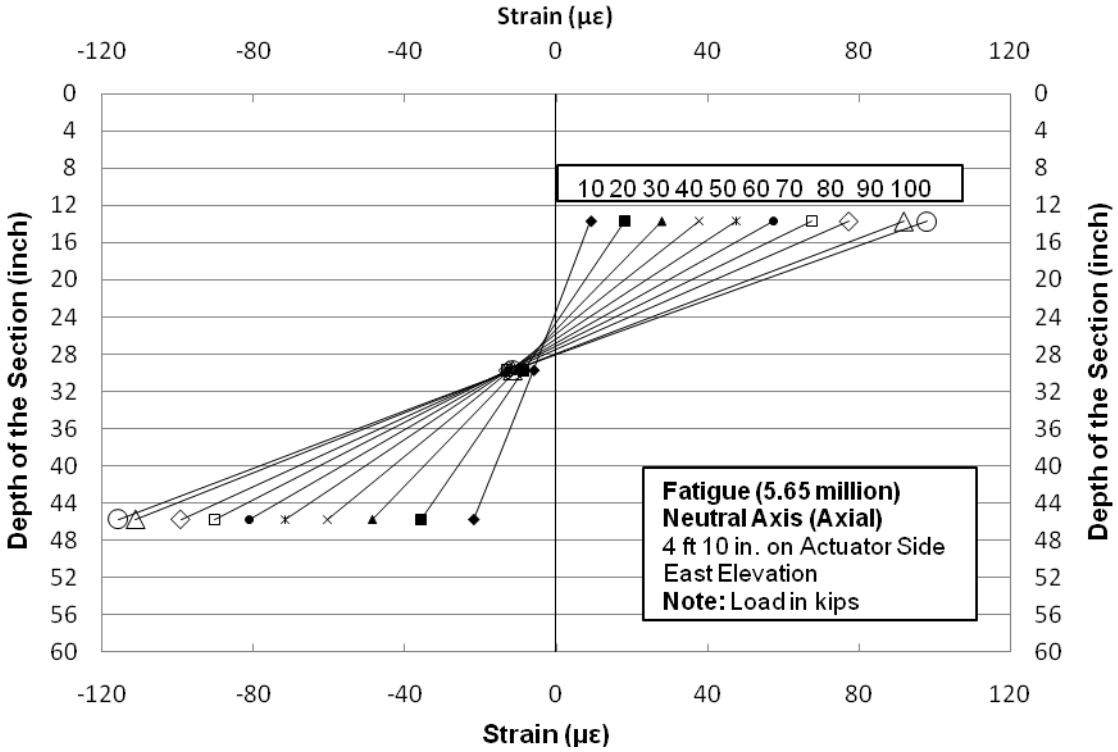


**Figure D.73** Neutral Axis on Actuator Side after 5.65 Million Cycles (East Elevation)

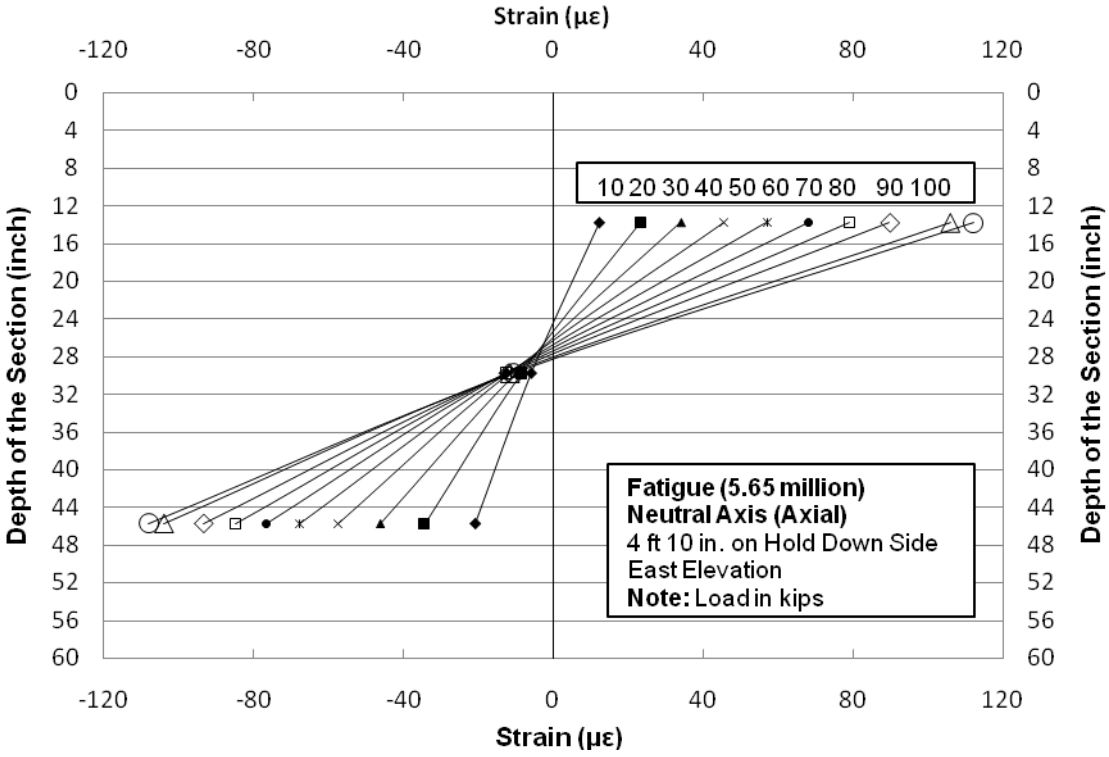


**Figure D.74** Neutral Axis on Hold Down Side after 5.65 Million Cycles (East Elevation)

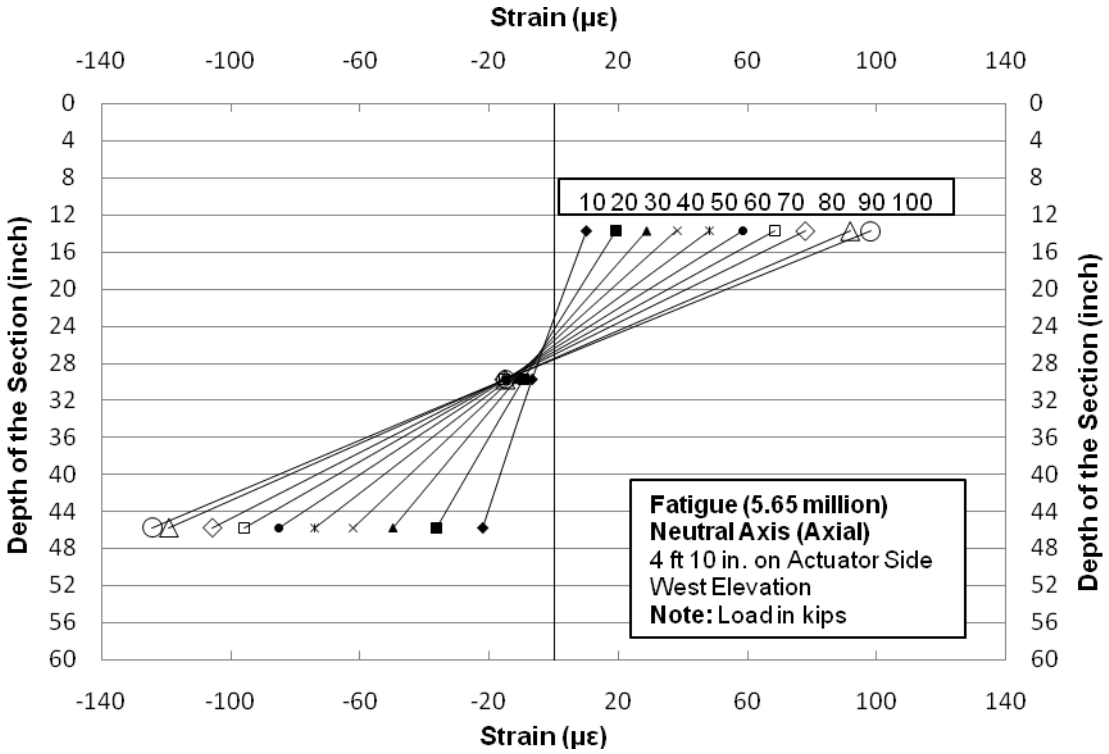


**Figure D.75** Neutral Axis on Actuator Side after 5.65 Million Cycles (West Elevation)

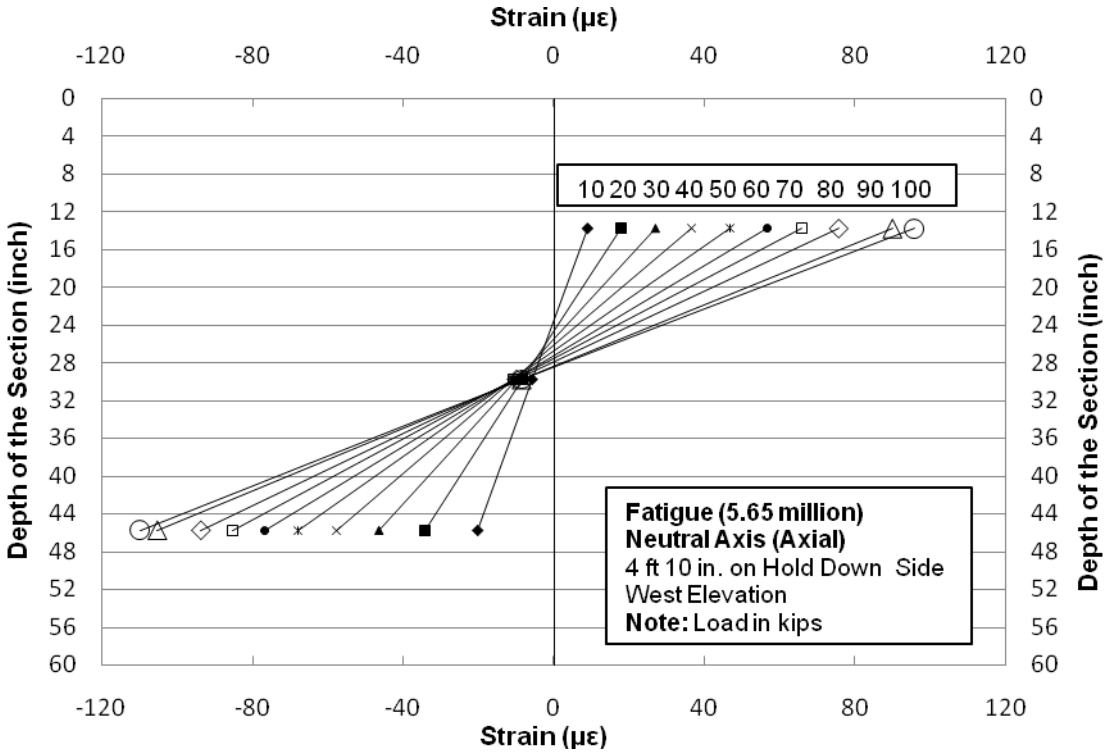


**Figure D.76** Neutral Axis on Hold Down Side after 5.65 Million Cycles (West Elevation)

# APPENDIX E

Service Test Results

## E.1 Predicted Service Load

The service load was predicted for three load cases based on AASHTO LRFD provisions and section properties of the box girder section. Table 2.1 gives information on the predicted service load for the different load cases of the service load test. This section provides detailed calculations of the predicted service load for all the three cases. The predicted service load was calculated based on the design material and section properties rather than predicted material and section properties.

**Table E.1** Service Load Cases

| Load Case | Load per Actuator (kips) | Total Load (kips) | Comments |
|---|---|---|---|
| 1 | 210.5 | 421 | Stressing top slab rebars upto $0.6*f_y$ |
| 2 | 319.4 | 638.8 | Stressing top flange upto $0.95*F_y$ ($F_y$=50 ksi) |
| 3 | 447.1 | 894.14 | Stressing top flange upto $0.95*F_y$ ($F_y$=70 ksi) |

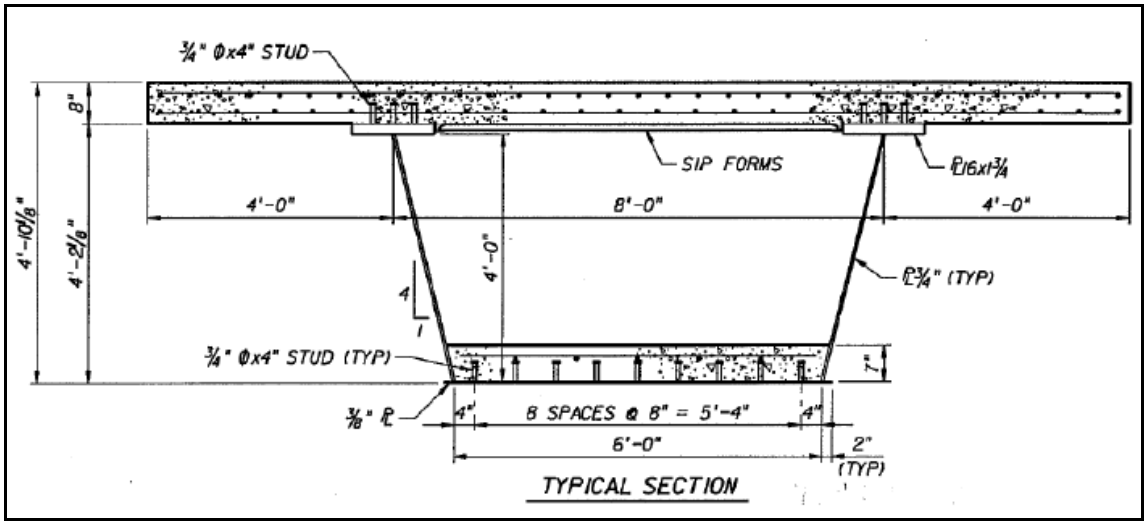


Typical Cross-Section of Double Composite Box Girder

**Material Properties**

Design yield strength of the structural steel, $f_{yd} = 70\ ksi$

Design yield strength of the rebars, $f_{red} = 60\ ksi$

Design compressive strength of concrete, $f_{cd} = 5.5\ ksi$

Design elastic modulus of concrete, $E_{cd} = 3845.83\ ksi$

Elastic modulus of steel, $E_s = 29000\ ksi$

**Design Section Properties**

Top slab section modulus (uncracked), $S_{ts} = 73793\ in^3$

Top flange section modulus (cracked), $S_{tfd} = 4034\ in^3$

Bottom flange section modulus (cracked), $S_{bfd} = 4579\ in^3$

Top rebar section modulus, $S_{tred} = 3508\ in^3$

Bottom slab section modulus (cracked), $S_{bsd} = 34903\ in^3$

Length of the cantilevered span, $L_c = 25ft$

## Load Case I

In this load case, the stress developed in the top slab rebars is limited to $0.6*f_y$ (36 ksi).

Moment required for developing stress in reinforcements to 36 ksi,

$$M_1 = 0.6 \times S_{tred} \times f_{red}$$

$$\therefore M_1 = \frac{0.6 \times 3508\ in^3 \times 60\ ksi}{12}$$

$$\therefore M_1 = 10524\ ft - kip$$

Total load applied by the actuators,

$$P_1 = \frac{M_1}{L_c} = \frac{10524\ ft - kip}{25\ ft} = 420.96\ kips \approx 421\ kips$$

Therefore, the load applied by each actuator is 210.5 kips (assuming 2 actuators).

**Check top slab stress is above modulus of rupture for concrete**

The stress developed in the concrete due to the Moment $M_{1,}$

$$\sigma_{tsd} = \frac{M_1}{S_{ts}} = \frac{10524\ ft-kip \times 12\ {}^{in}\!/\!_{ft}}{73793\ in^3} = 1.71\ ksi$$

Modulus of rupture of the concrete,

$$f_{cr} = 7.5 \times \sqrt{f_c} = \frac{7.5 \times \sqrt{5500}}{1000} = 0.556\ ksi$$

Therefore, stress in the concrete due to applied load of 421 kips exceed the modulus of rupture.

**Check top flange stress**

$$\sigma_{tf1} = \frac{M_1}{S_{tfd}} = \frac{10524\ ft-kip \times 12\ {}^{in}\!/\!_{ft}}{4034\ in^3} = 31.31\ ksi$$

The stress developed in the top flange is less than less than yield strength of the flange.

## Load Case II

In this load case, the stress developed in the top flange is limited to $0.95*F_{y,}$ considering grade 50 ksi steel. Therefore, the maximum stress developed in the top flange is limited to 47.5 ksi.

Moment required for developing stress in top flange to 47.5 ksi,

$$M_2 = 0.95 \times 50\ ksi \times S_{tfd}$$

$$\therefore M_2 = \frac{0.95 \times 50\ ksi \times 4034\ in^3}{12\ {}^{in}\!/\!_{ft}}$$

$$\therefore M_2 = 15967.92\ ft-kip$$

The total load applied by the actuators,

$$P_2 = \frac{M_2}{L_c} = \frac{15967.92\ ft-kip}{25\ ft} = 638.72\ kips$$

Therefore, the load applied by each actuator is 319.36 kips (assuming 2 actuators).

**Check stress in rebars**

$$\sigma_{rebar2} = \frac{M_2}{S_{tred}} = \frac{15967.92\ ft-kip \times 12\ {}^{in}\!/\!_{ft}}{3508\ in^3} = 54.62ksi$$

Therefore, the stress in the rebars is less than the yield stress.

## Load Case III

In this load case, the stress developed in the top flange is limited to 0.95*$F_y$ considering grade 70 ksi steel. Therefore, the maximum stress developed in the top flange is limited to 66.5 ksi.

Moment required for developing stress in top flange to 66.5 ksi,

$$M_3 = 0.95 \times F_y \times S_{tfd}$$

$$\therefore M_3 = \frac{0.95 \times 70\ ksi \times 4034\ in^3}{12\ {}^{in}\!/\!_{ft}}$$

$$\therefore M_3 = 22355.08\ ft-kip$$

The total load applied by the actuators,

$$P_3 = \frac{M_3}{L_c} = \frac{22355.08\ ft-kip}{25\ ft} = 894.20\ kips$$

Therefore, the load applied by each actuator is 447.10 kips (assuming 2 actuators).

**Check stress in top rebars (assuming elastic response)**

$$\sigma_{rebar3} = \frac{M_3}{S_{tred}} = \frac{22355.08\ ft-kip \times 12\ {}^{in}\!/\!_{ft}}{3508\ in^3} = 76.47\ ksi$$

**Check stress in bottom flange**

$$\sigma_{bf3} = \frac{M_3}{S_{bf}} = \frac{22355.08\ ft-kip \times 12\ {}^{in}\!/\!_{ft}}{4579\ in^3} = 58.59\ ksi$$

Therefore, the stress in the bottom flange is within the elastic range.

## E.2 Deflection for Service I Load Test

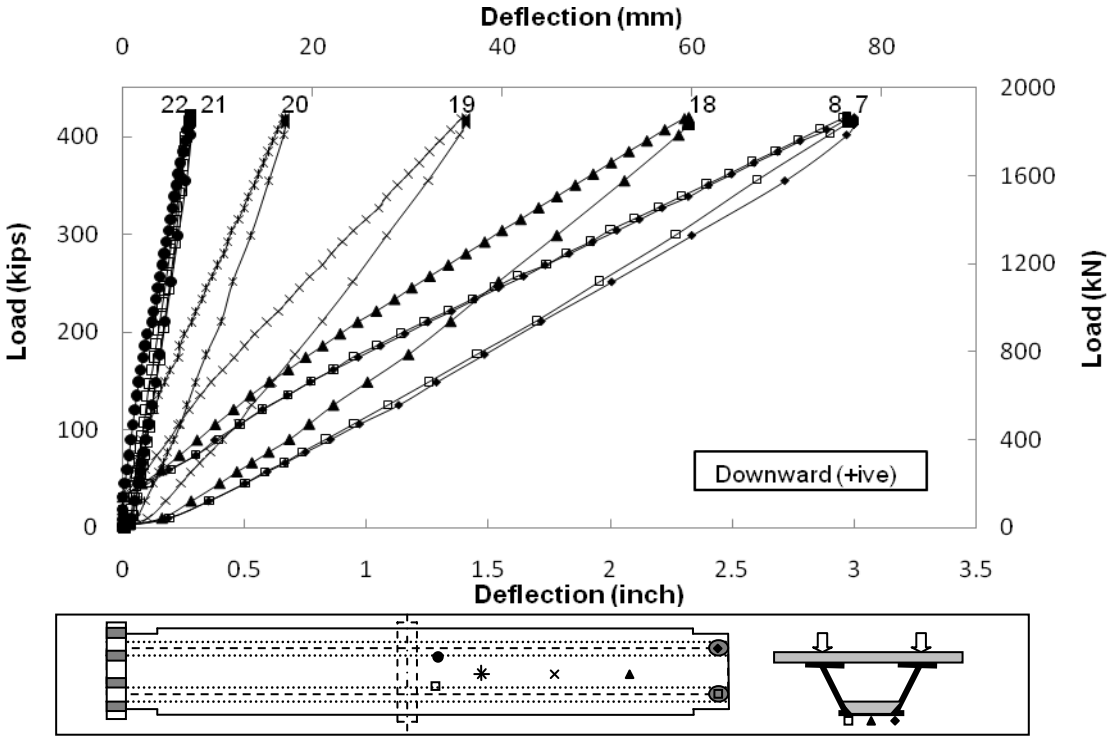


**Figure E.1** Deflection of Bottom Flange on Actuator Side (1st Cycle)

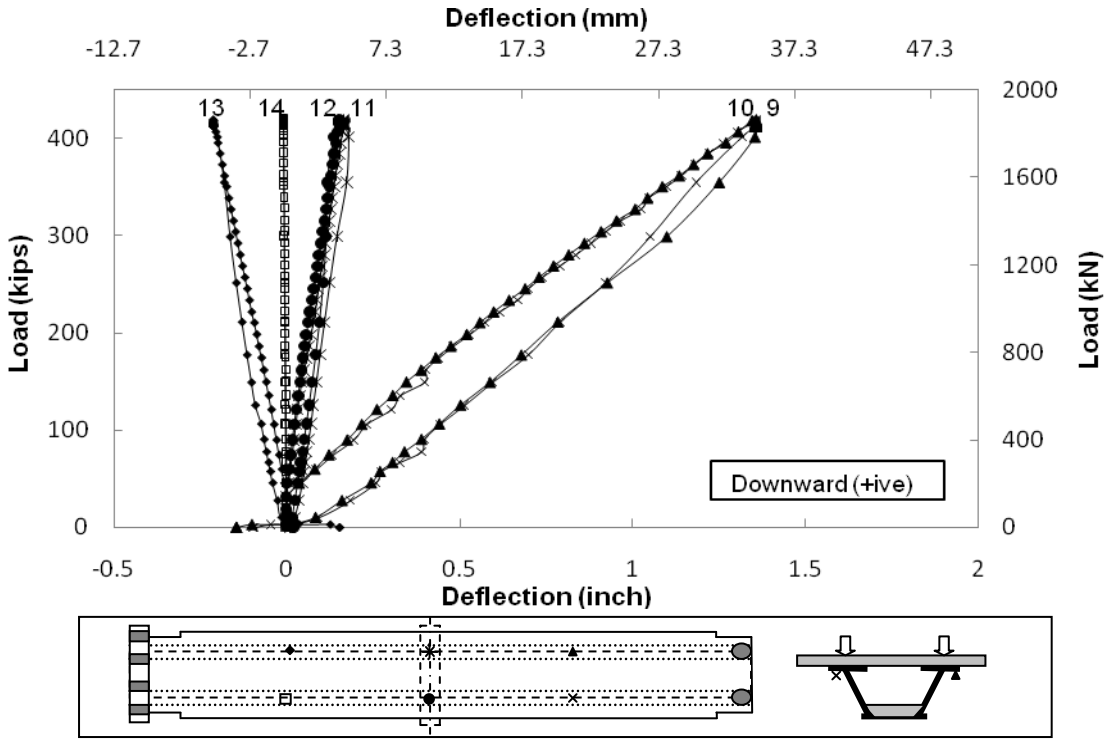


**Figure E.2** Deflection of Top Flange (1st Cycle)

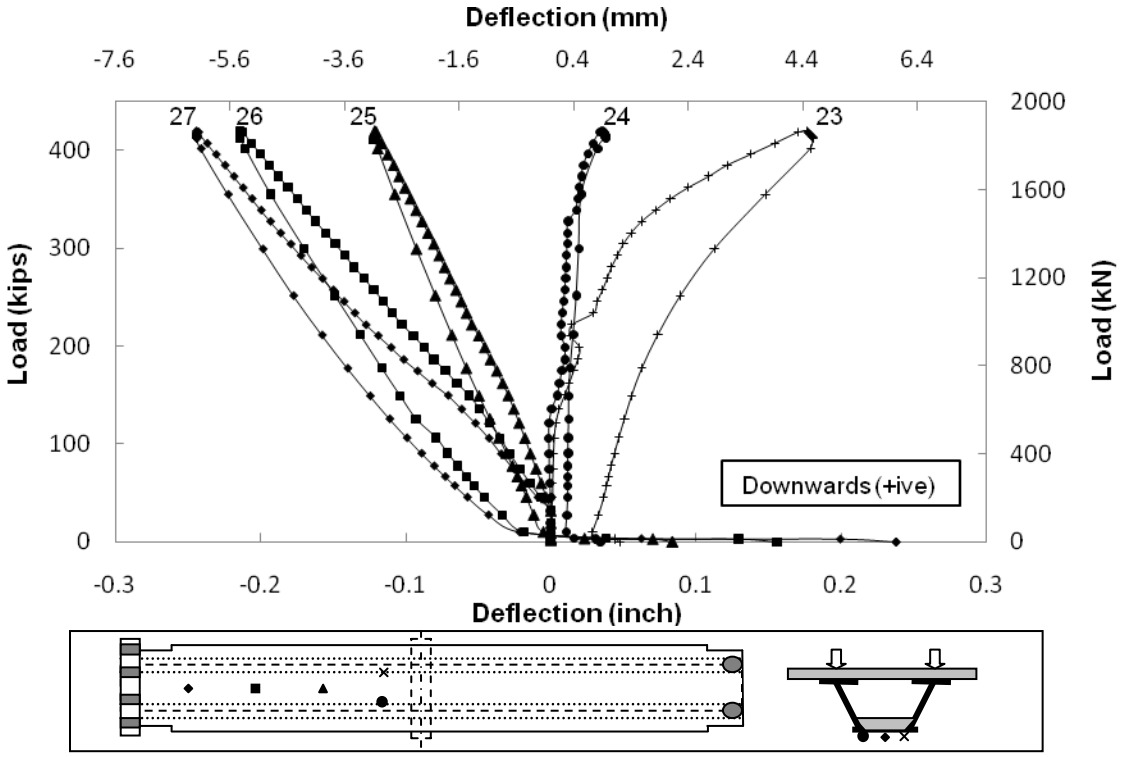


**Figure E.3** Deflection of Bottom Flange on Hold Down Side (1st Cycle)

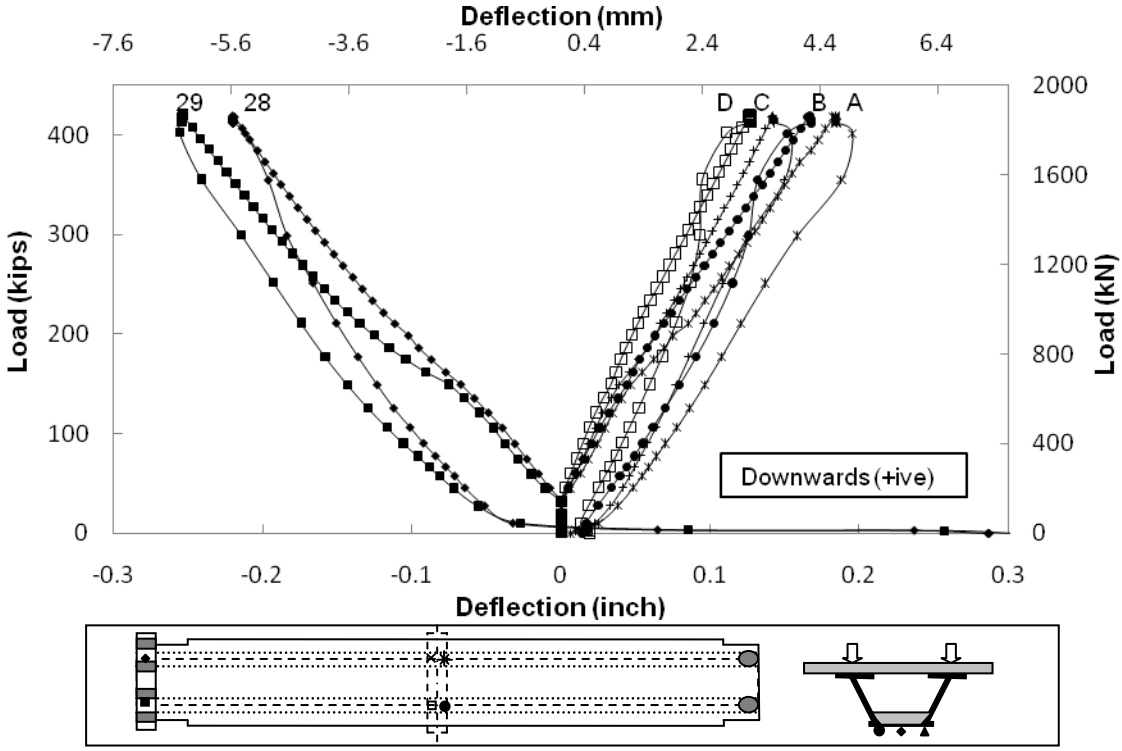


**Figure E.4** Deflection at Hold Down End and Center Support (1st Cycle)

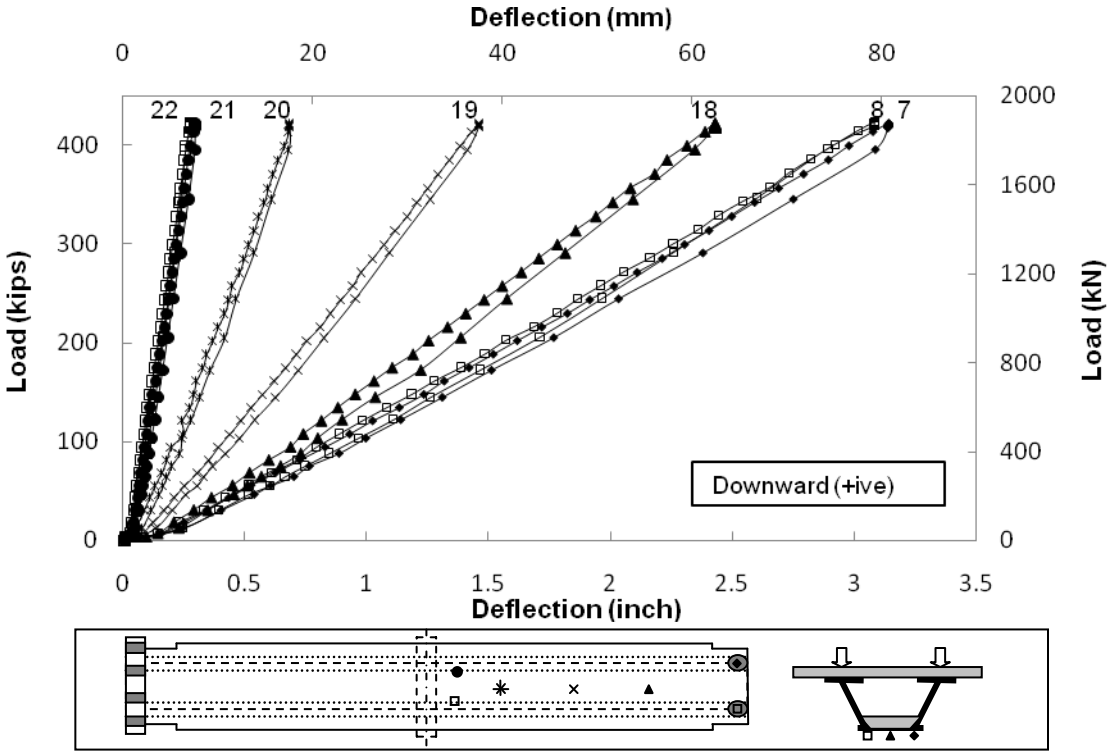


**Figure E.5** Deflection of Bottom Flange on Actuator Side (5th Cycle)

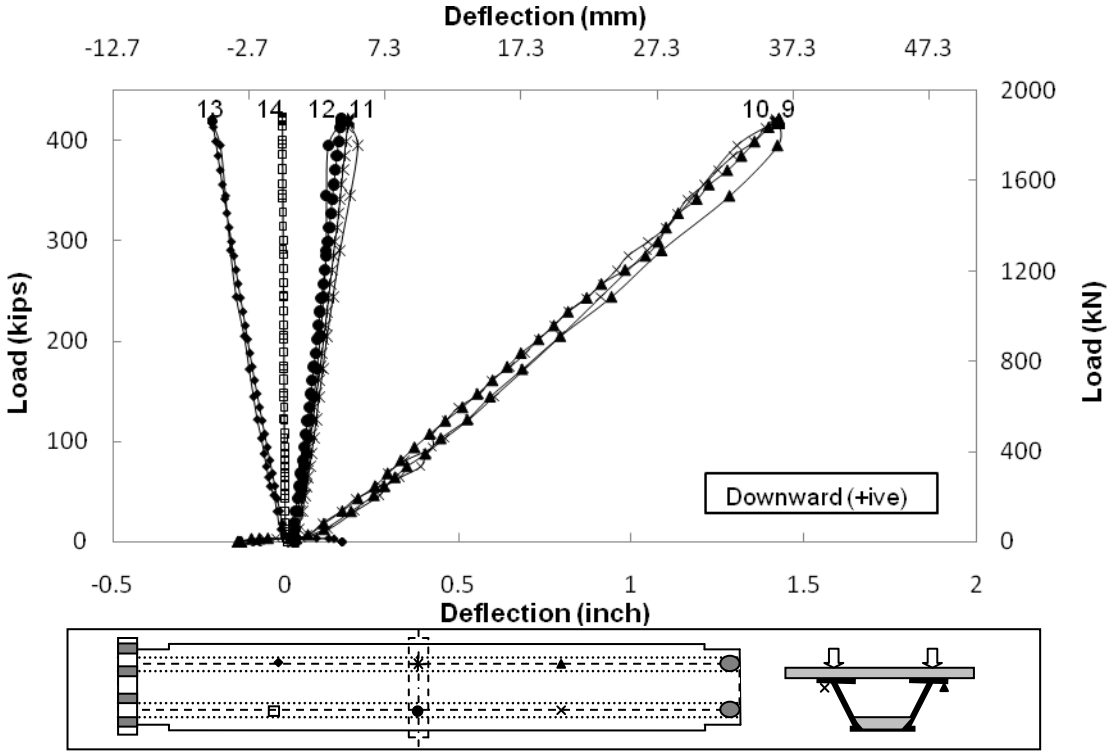


**Figure E.6** Deflection of Top Flange (5th Cycle)

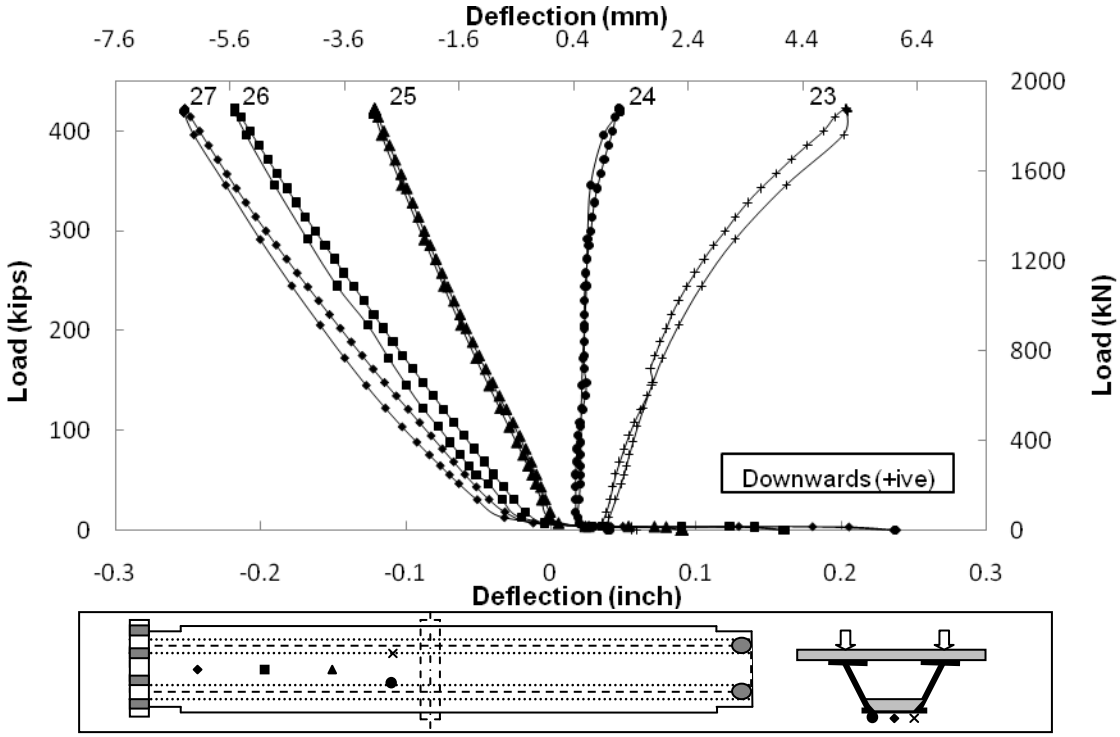


**Figure E.7** Deflection of Bottom Flange on Hold Down Side (5th Cycle)

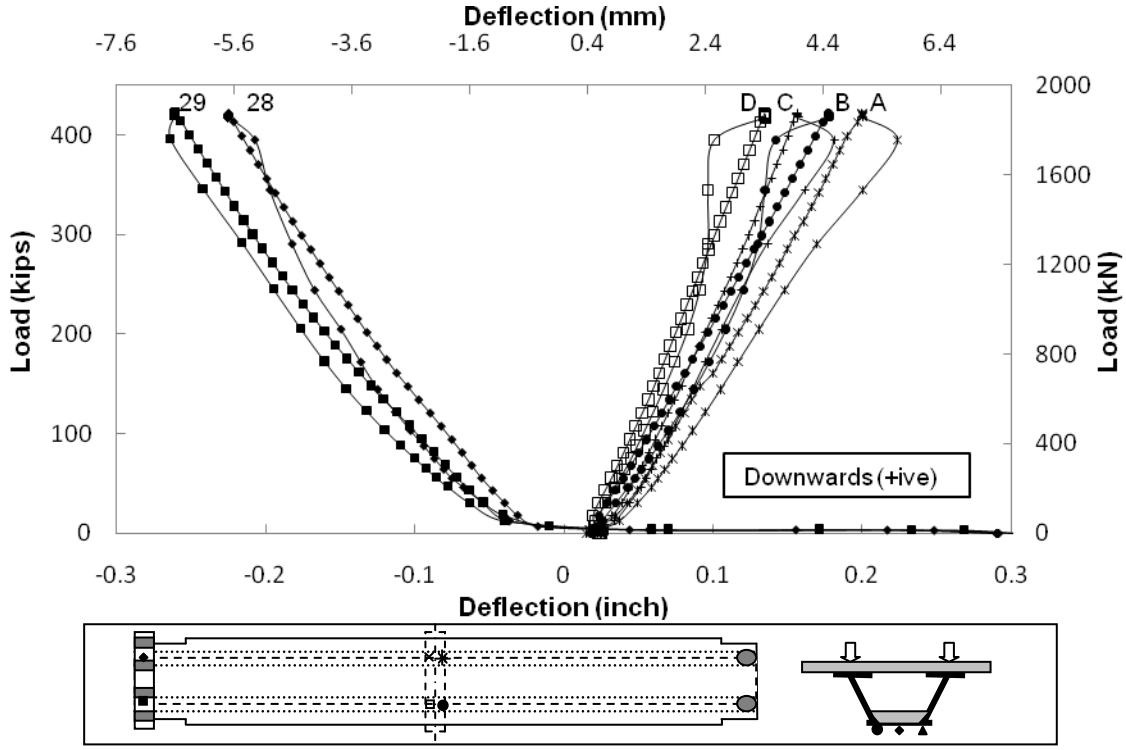


**Figure E.8** Deflection at Hold Down End and Center Support (5th Cycle)

## E.3 Slip for Service I Load Test

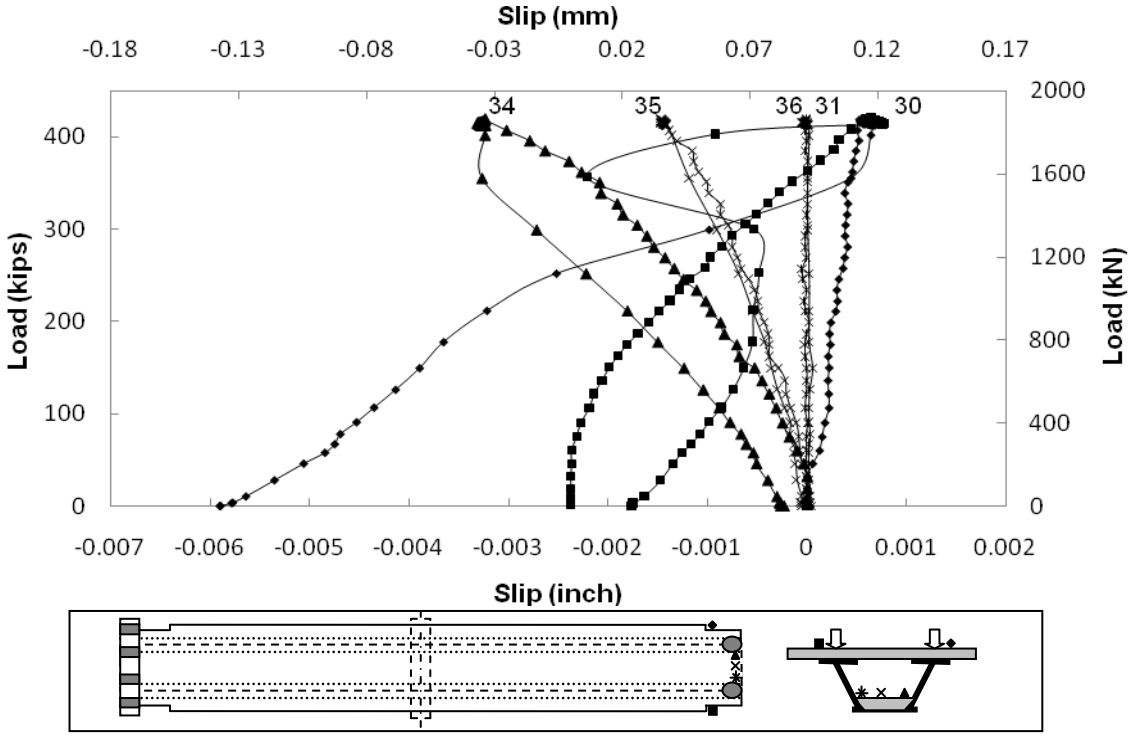


**Figure E.9** Slip at Actuator End (1st Cycle)

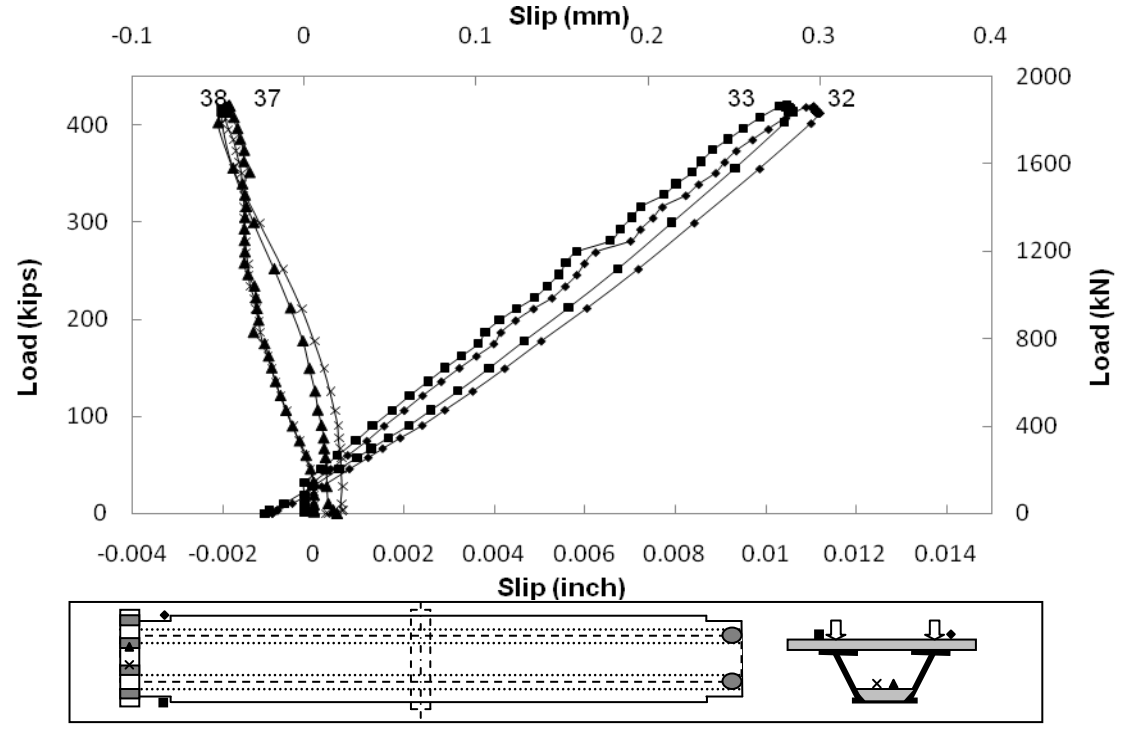


**Figure E.10** Slip at Hold Down End (1st Cycle)

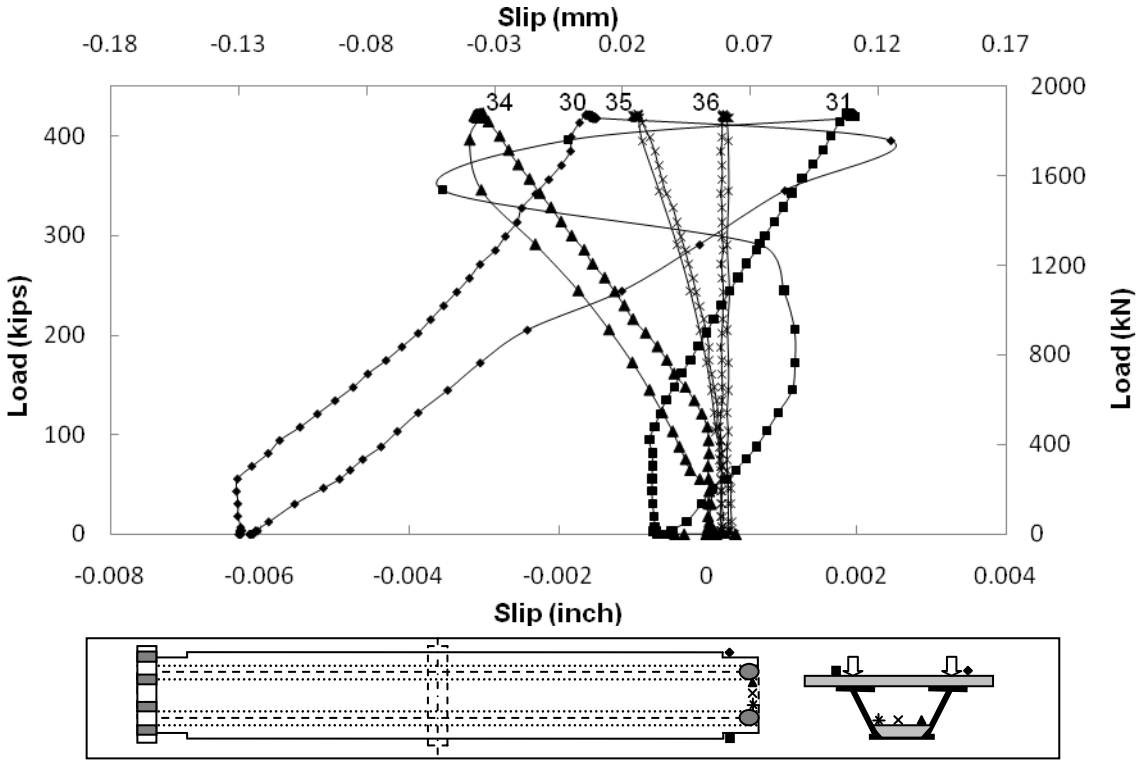


**Figure E.11** Slip at Actuator End (5th Cycle)

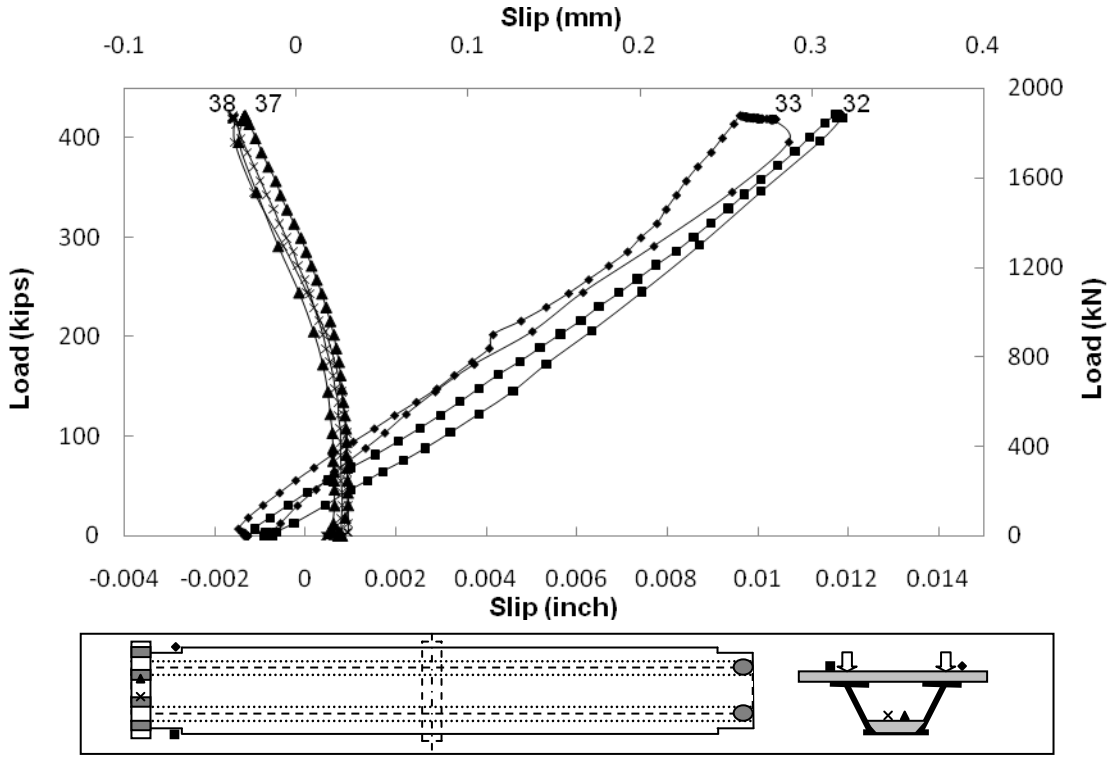


**Figure E.12** Slip at Hold Down End (5th Cycle)

## E.4 Strain in Top Slab Rebars for Service I Load Case

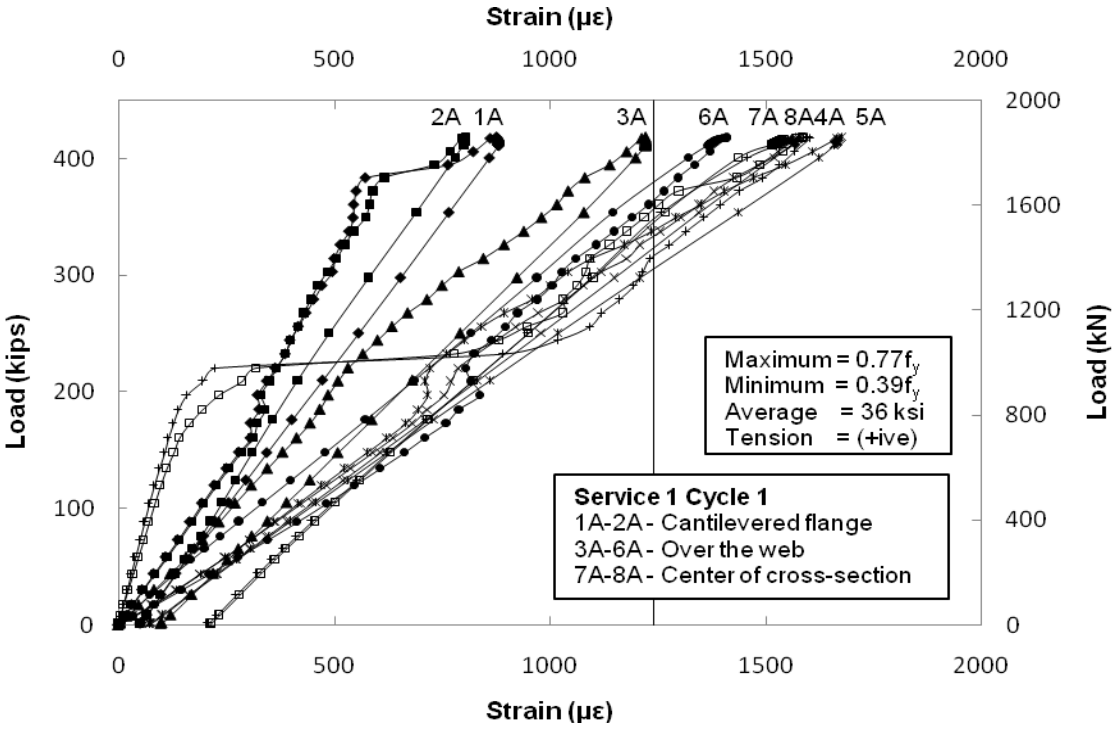


**Figure E.13** Strain in Rebars on Actuator Side (1st Cycle)

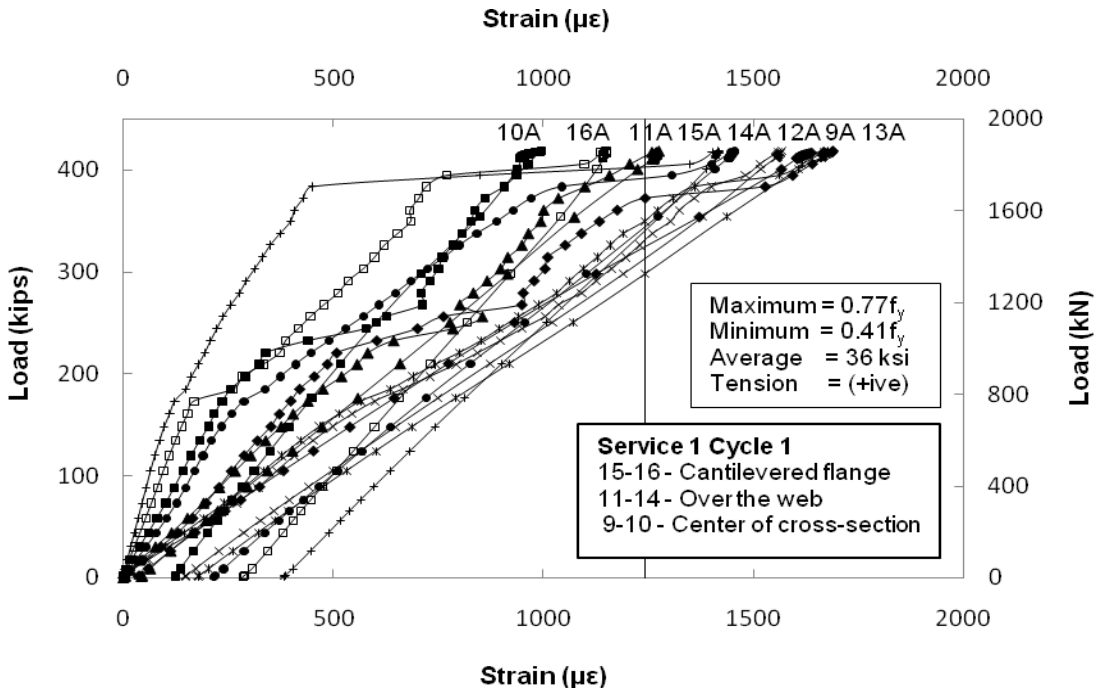


**Figure E.14** Strain in Rebars on Actuator Side (1st Cycle)

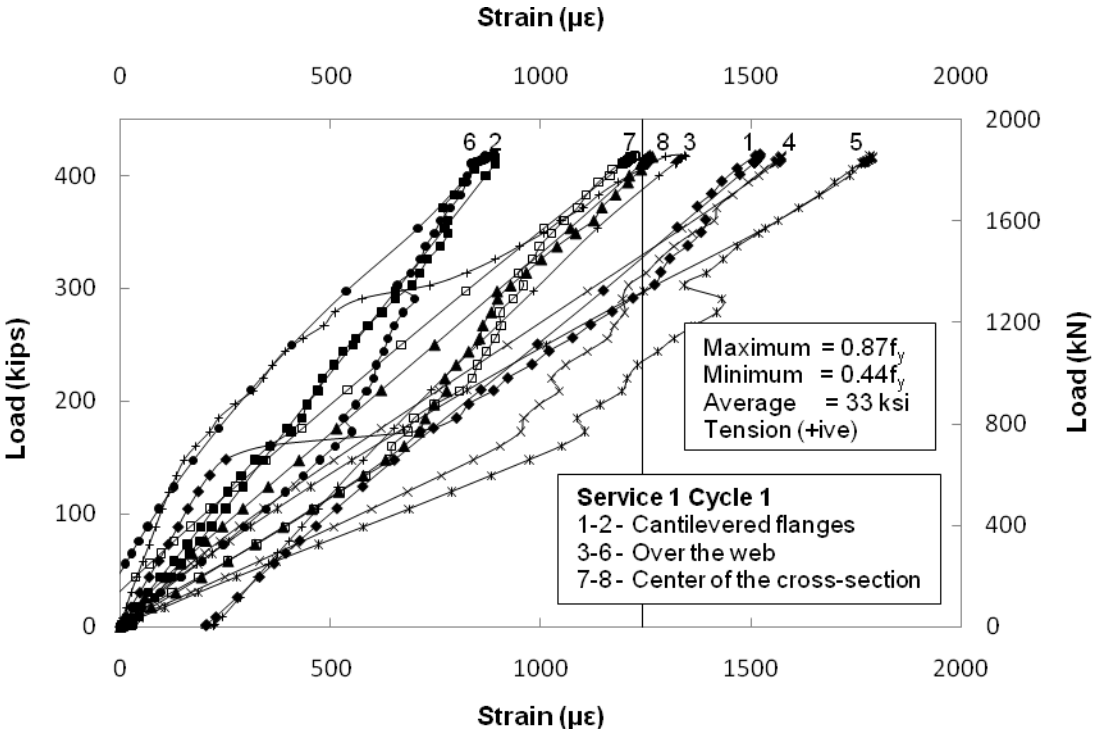


**Figure E.15** Strain in Rebars on Hold Down Side (1st Cycle)

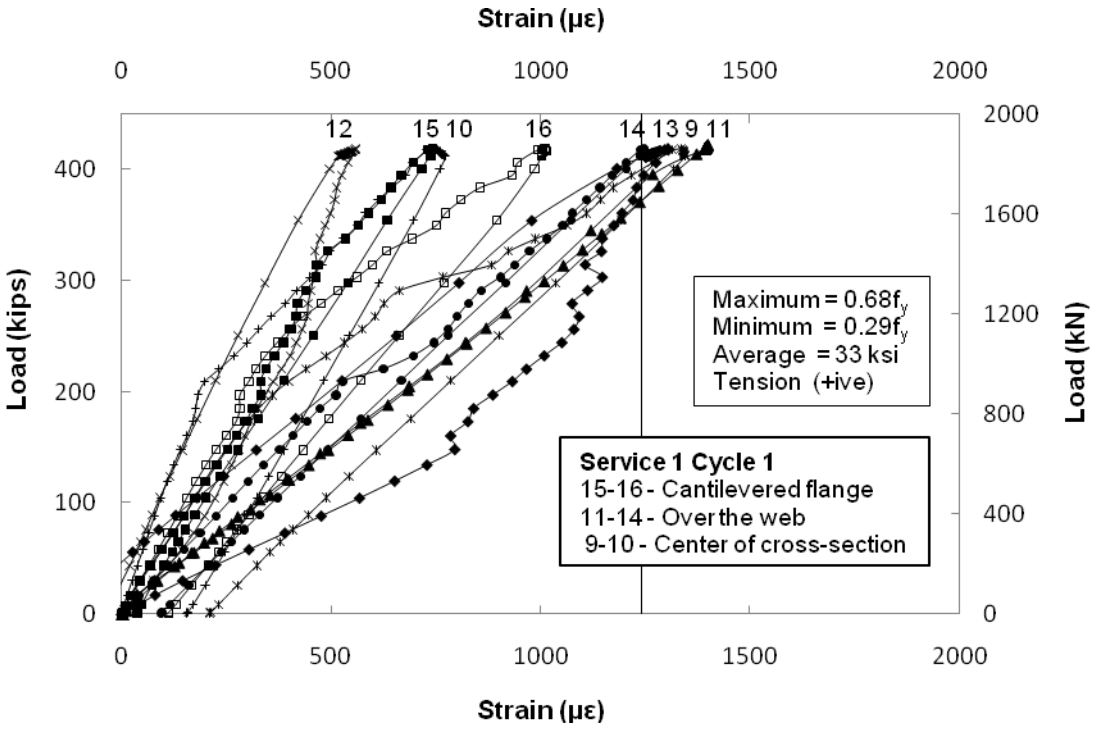


**Figure E.16** Strain in Rebars on Hold Down Side (1st Cycle)

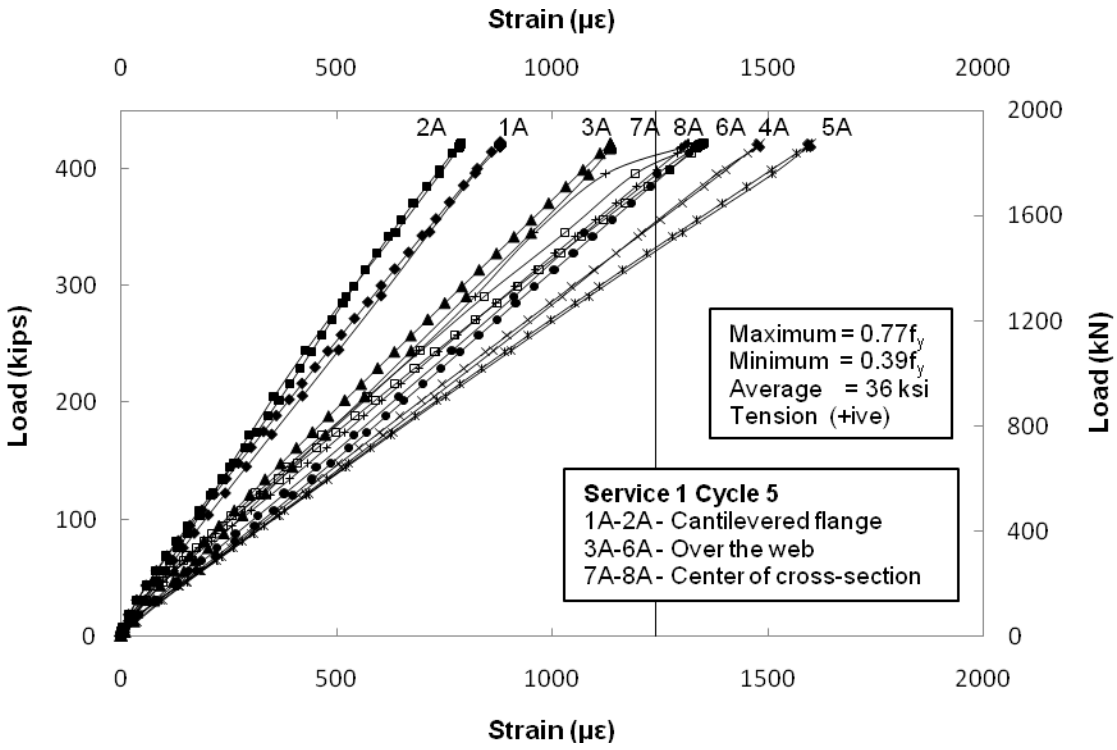


**Figure E.17** Strain in Rebars on Actuator Side (5th Cycle)

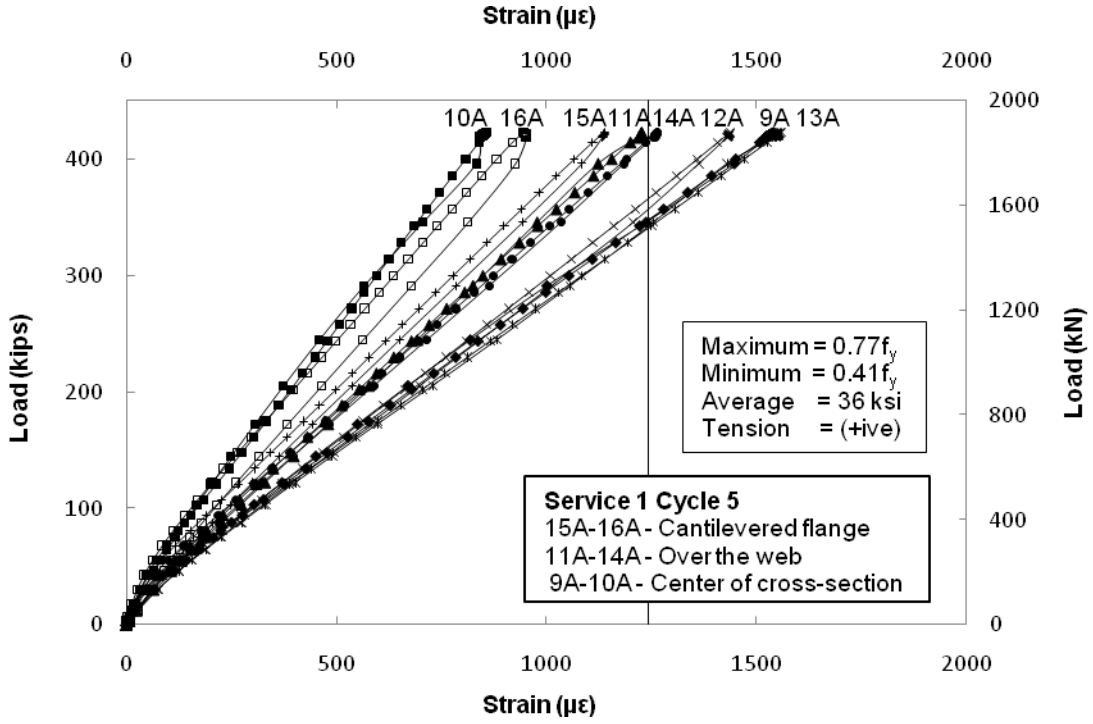


**Figure E.18** Strain in Rebars on Actuator Side (5th Cycle)

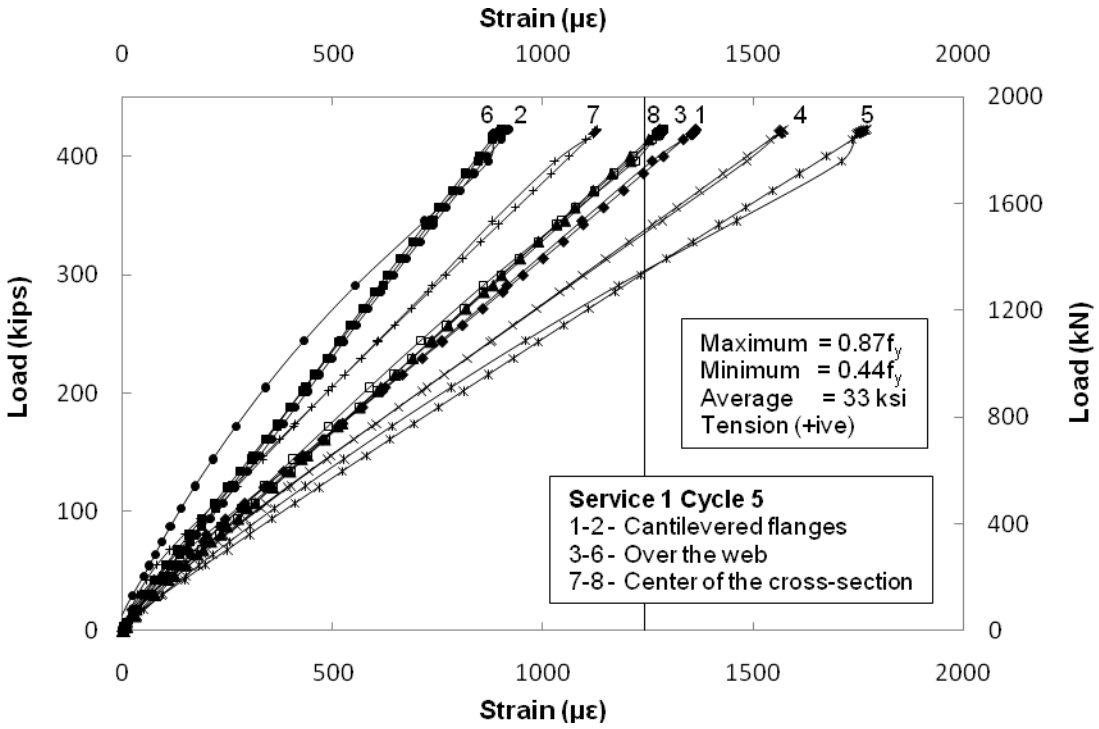


**Figure E.19** Strain in Rebars on Hold Down Side (5th Cycle)

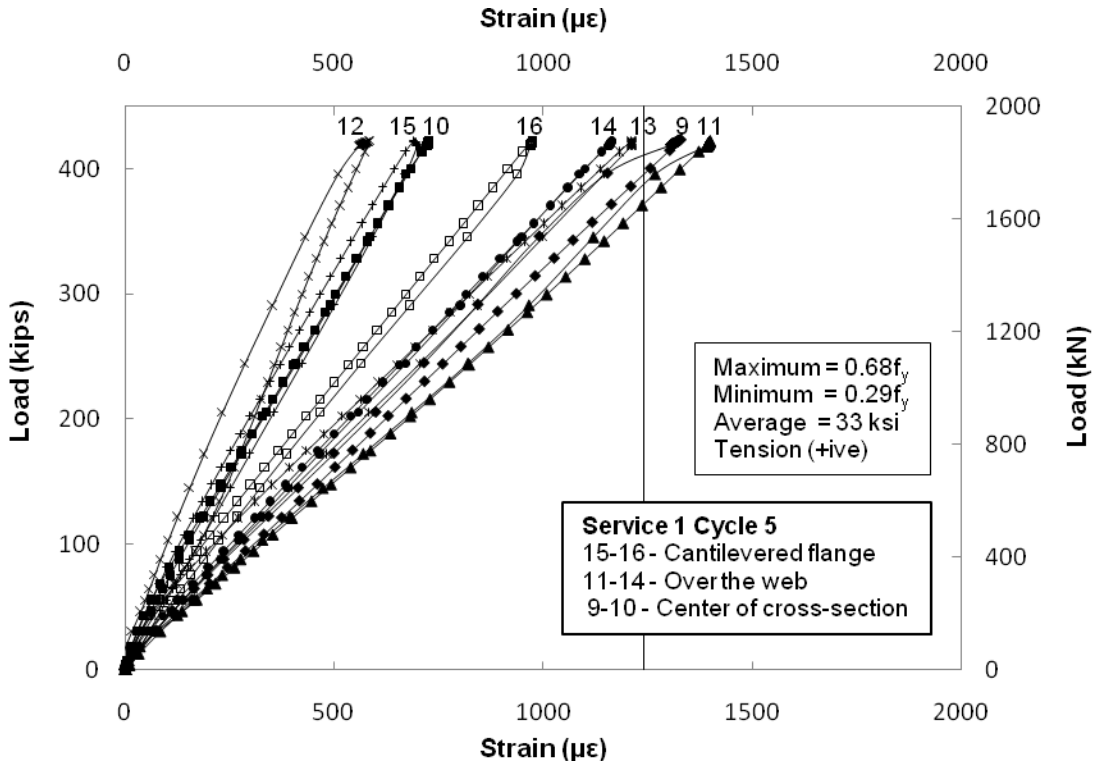


**Figure E.20** Strain in Rebars on Hold Down Side (5th Cycle)

## E.5 Strain in Steel for Service I Load Case

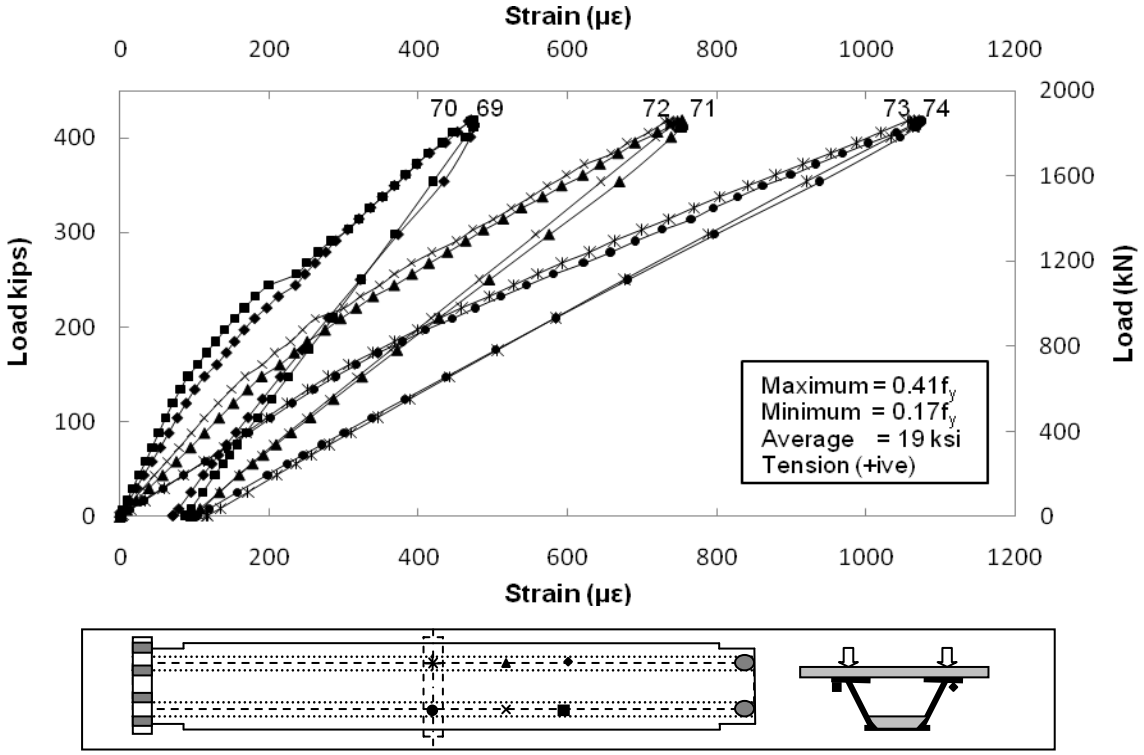


**Figure E.21** Strain in Top Flange on Actuator Side (1st Cycle)

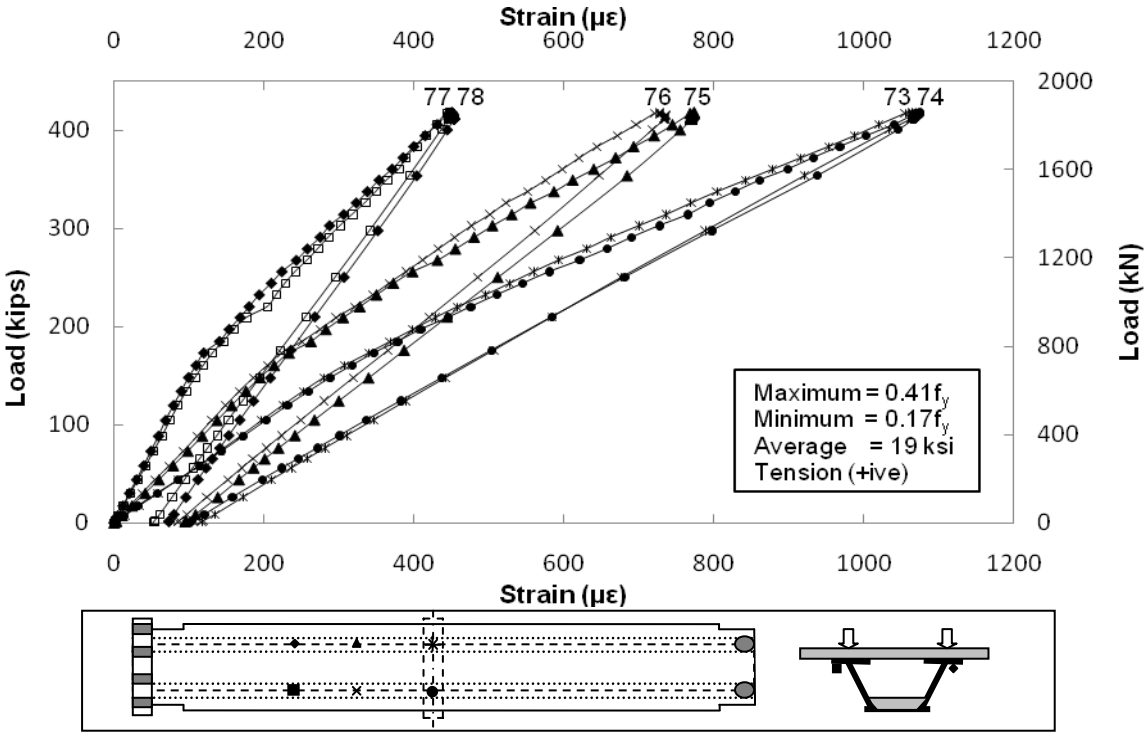


**Figure E.22** Strain in Top Flange on Hold Down Side (1st Cycle)

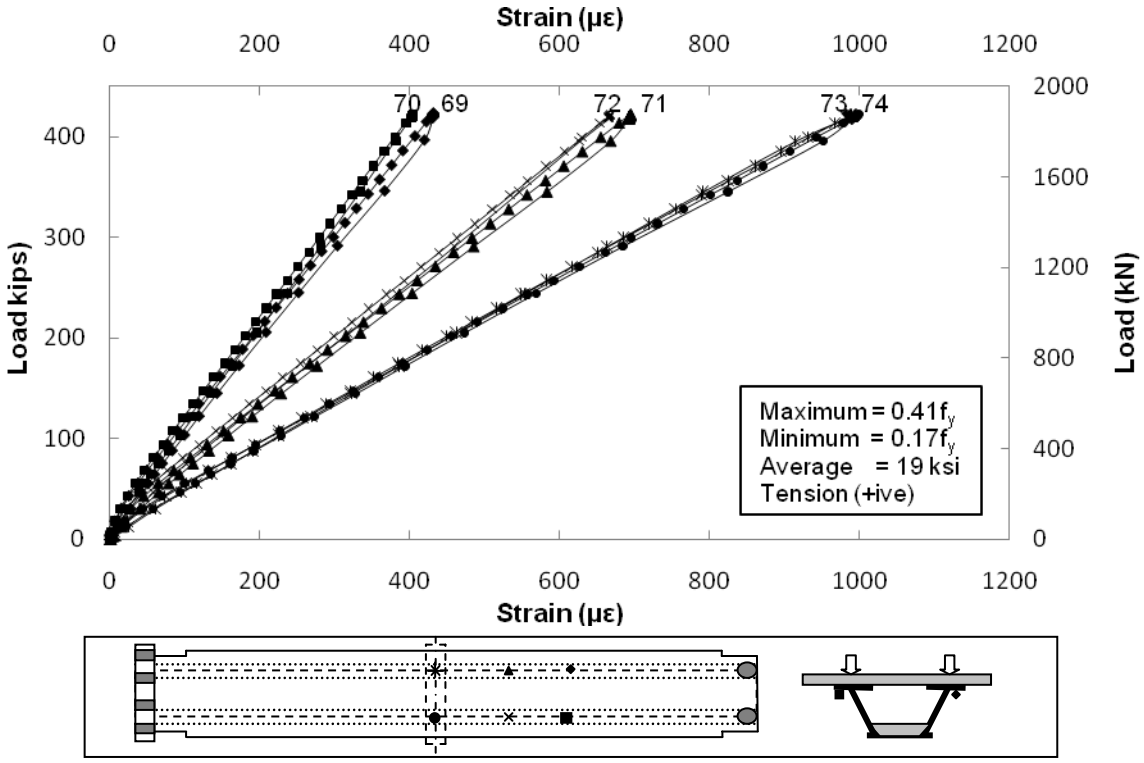


**Figure E.23** Strain in Top Flange on Actuator Side (5th Cycle)

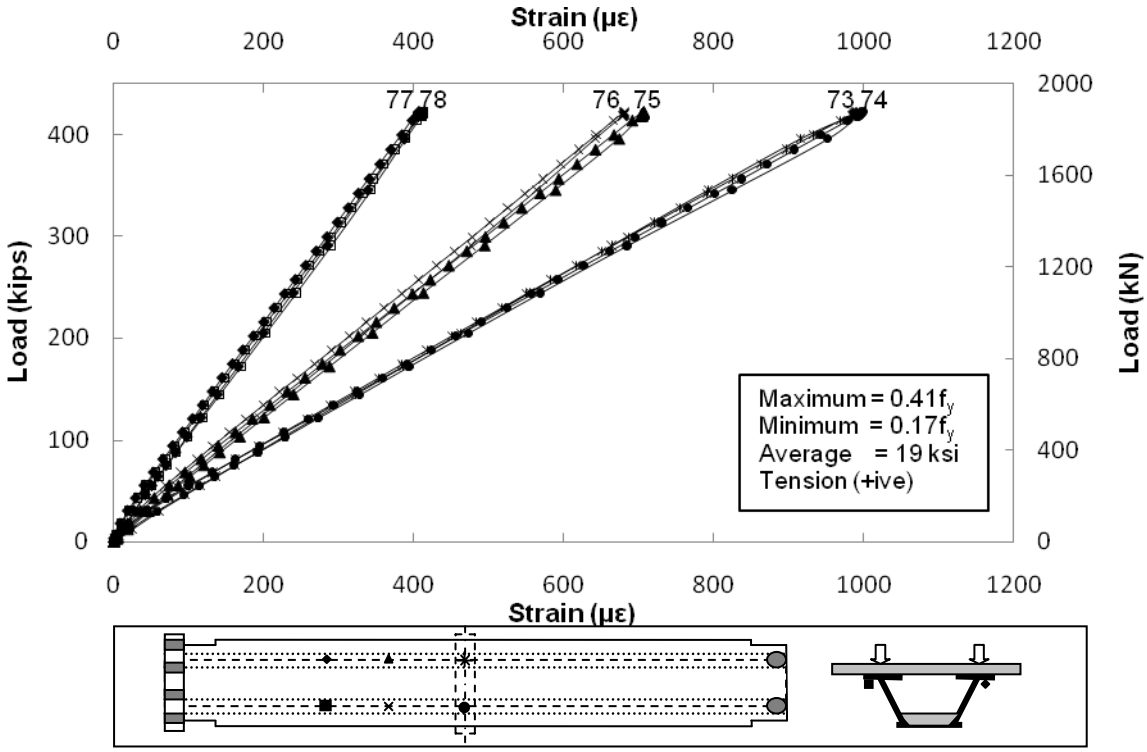


**Figure E.24** Strain in Top Flange on Hold Down Side (5th Cycle)

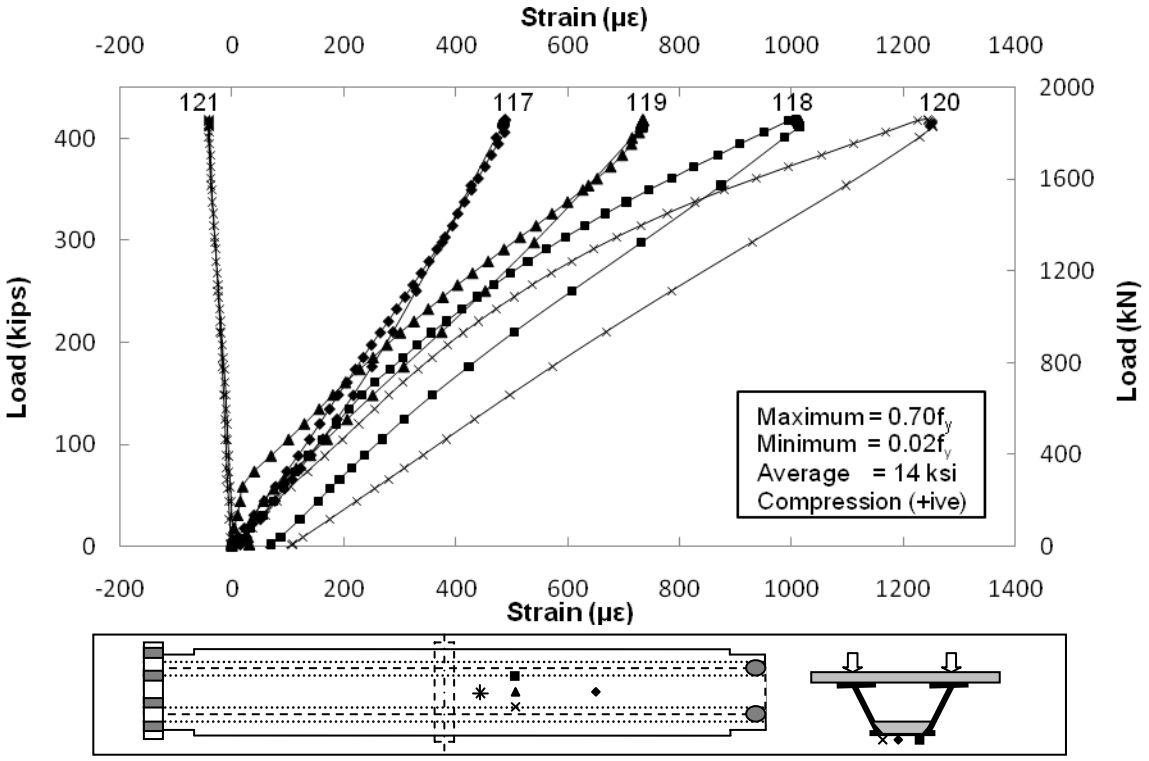


**Figure E.25** Strain in Bottom Flange on Actuator Side (1st Cycle)

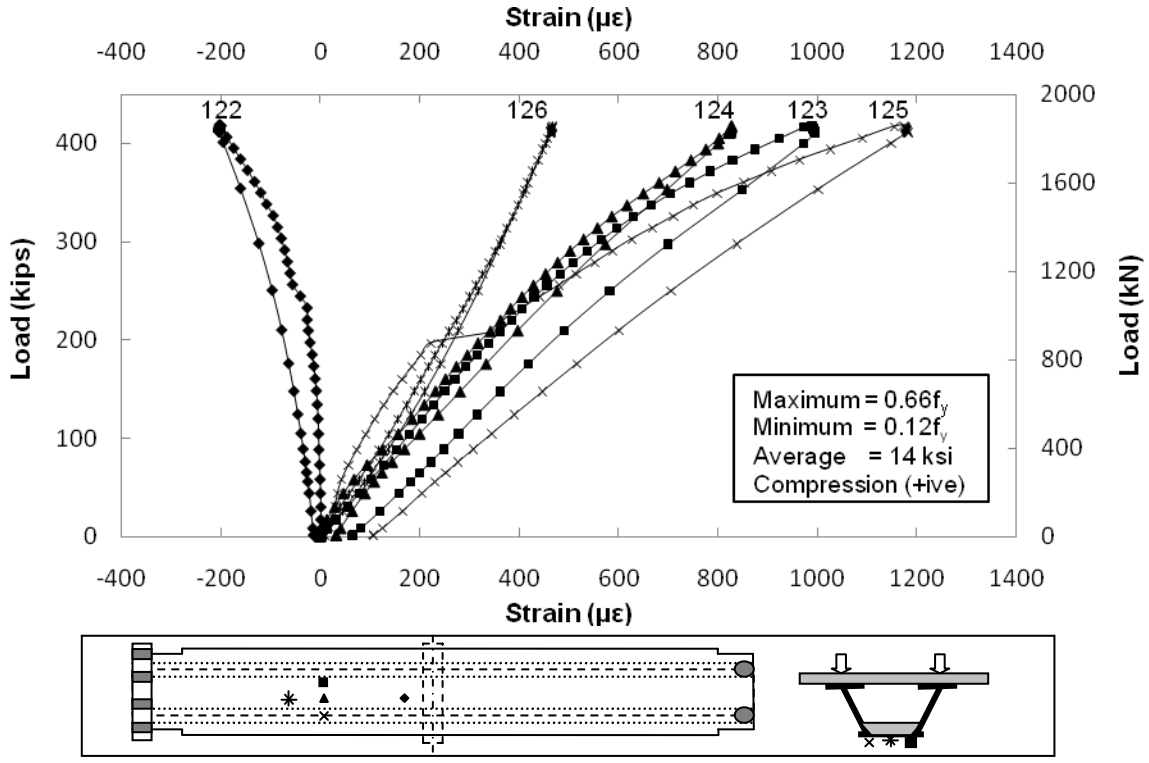


**Figure E.26** Strain in Bottom Flange on Hold Down Side (1st Cycle)

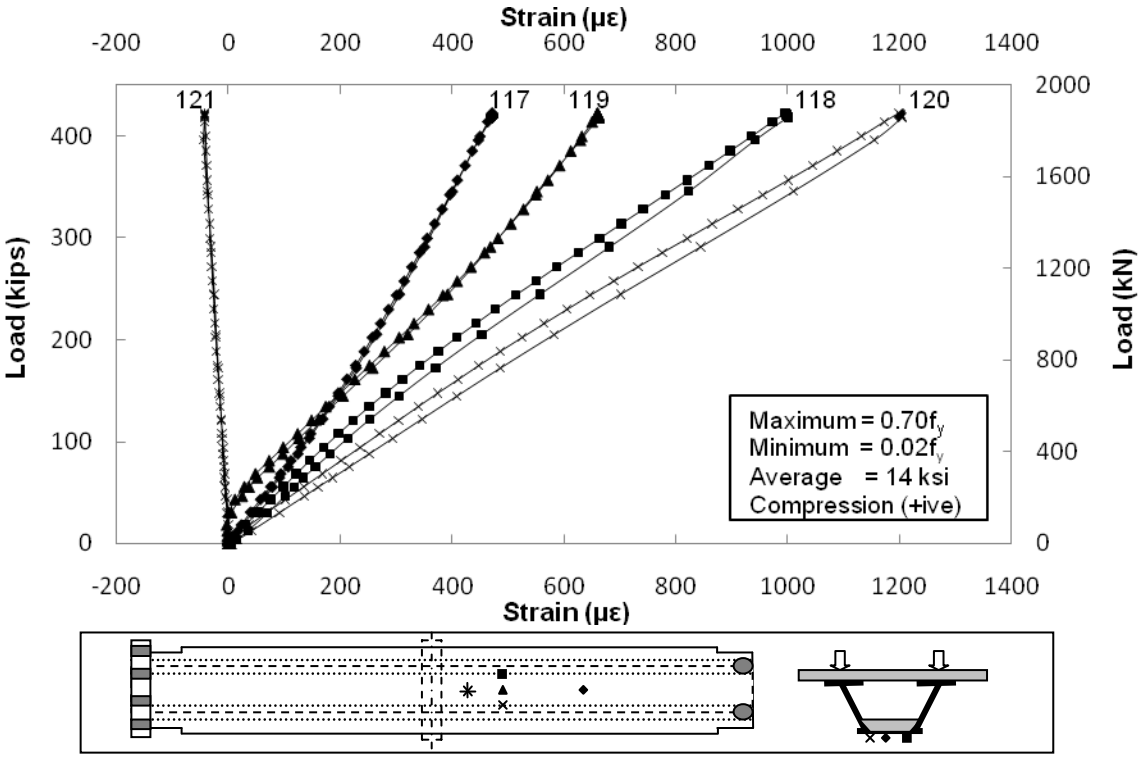


**Figure E.27** Strain in Bottom Flange on Actuator Side (5th Cycle)

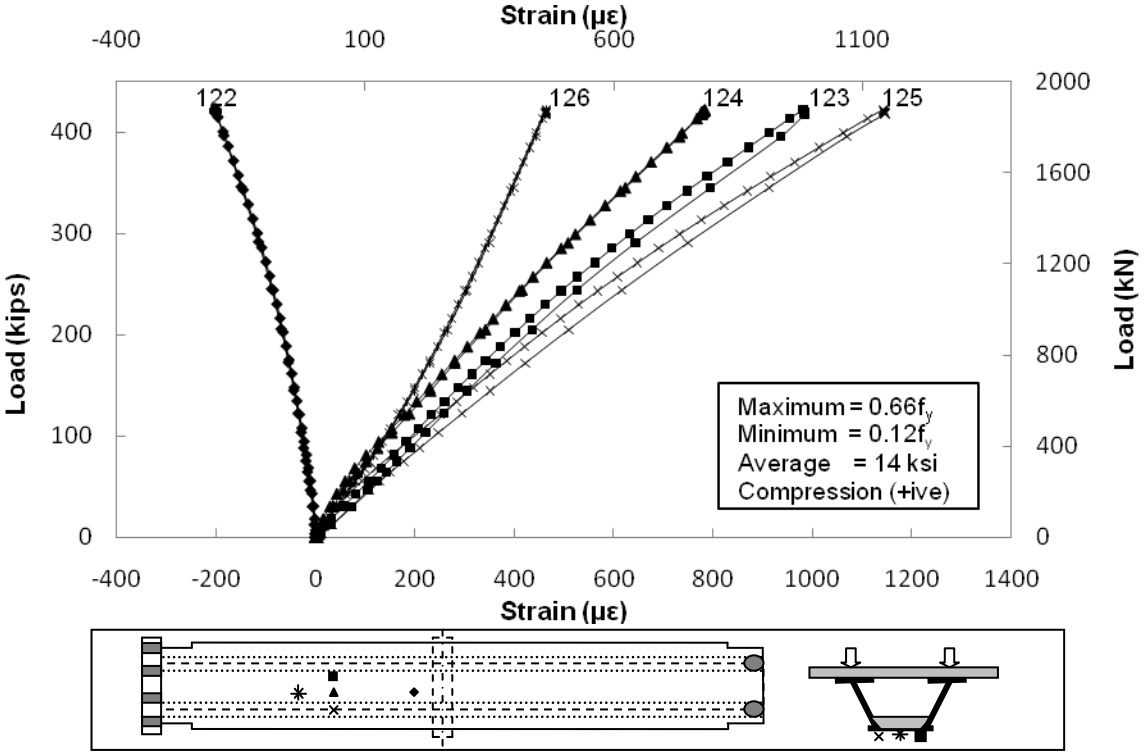


**Figure E.28** Strain in Bottom Flange on Hold Down Side (5th Cycle)

## E.6 Strain in Concrete for Service I Load Case

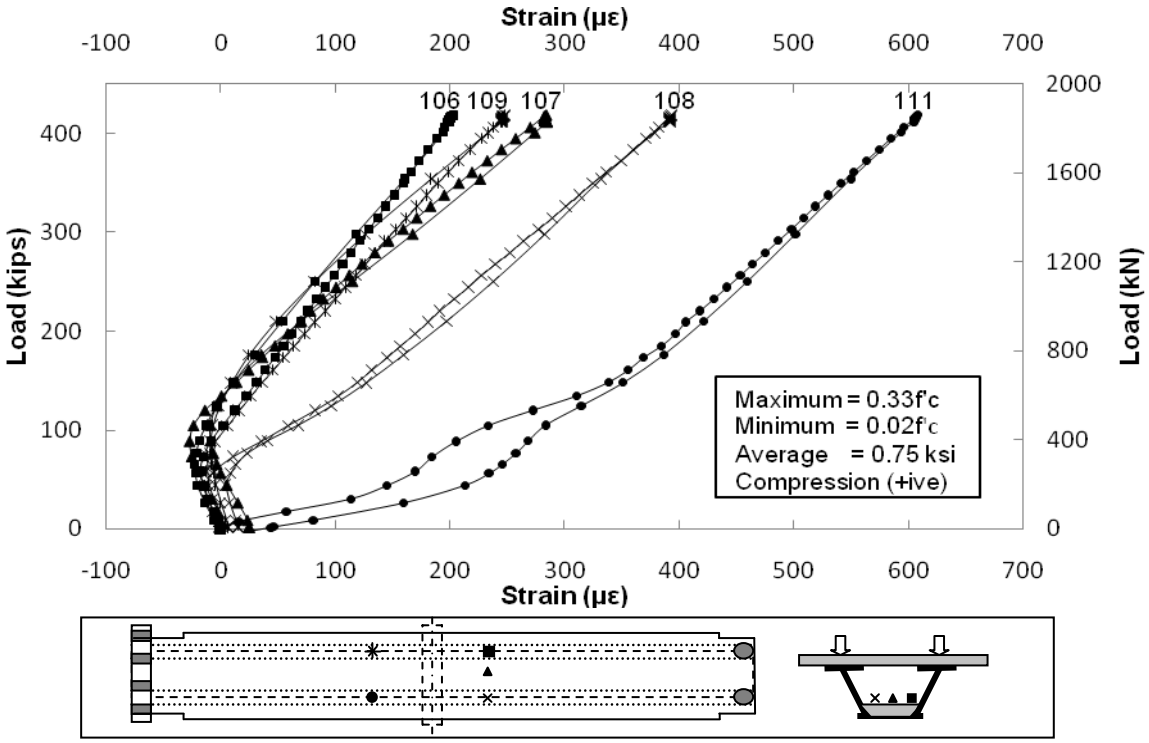


**Figure E.29** Strain in Bottom Concrete Slab (1st Cycle)

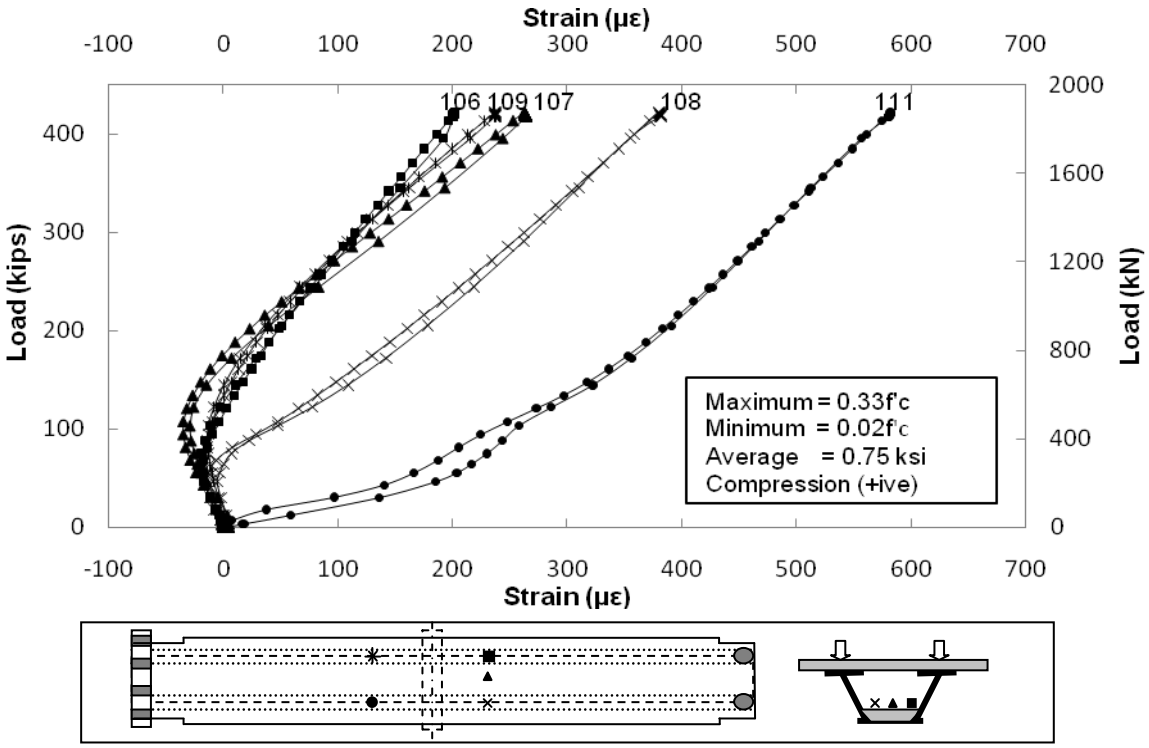


**Figure E.30** Strain in Bottom Concrete Slab (5th Cycle)

## E.7 Crack Width on Top Slab for Service I Load Case

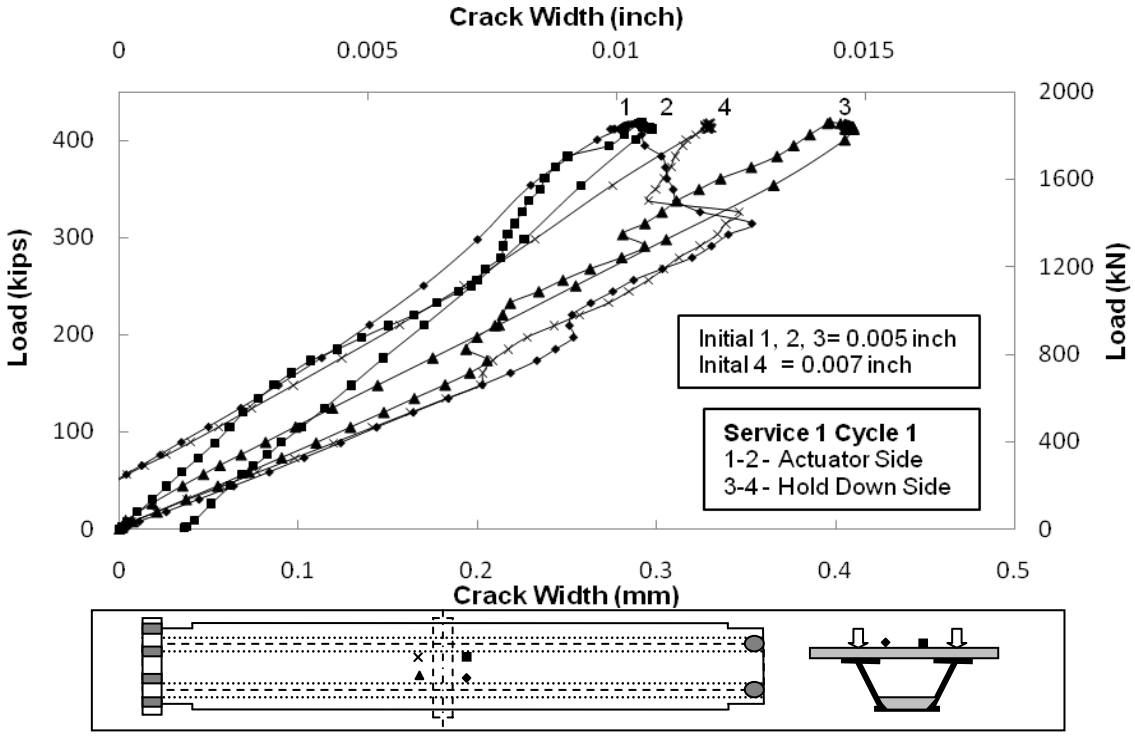


**Figure E.31** Crack Width on Top Slab (1st Cycle)

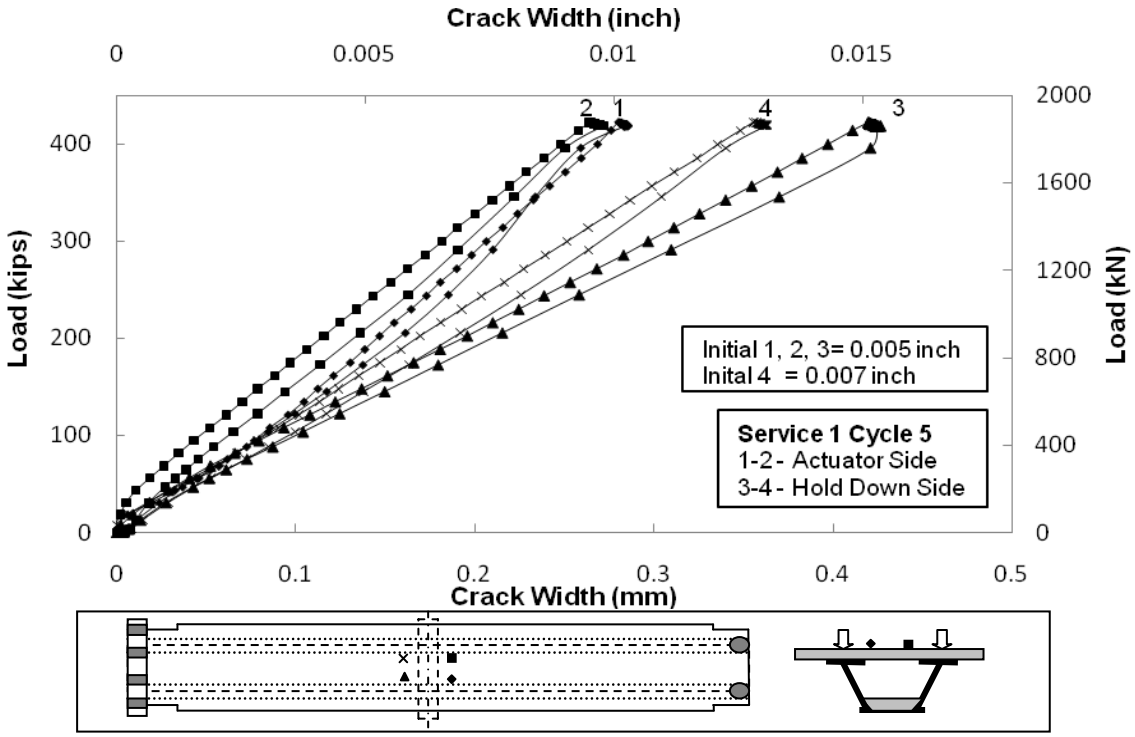


**Figure E.32** Crack Width on Top Slab (5th Cycle)

## E.8 Neutral Axis for Service I Load Case

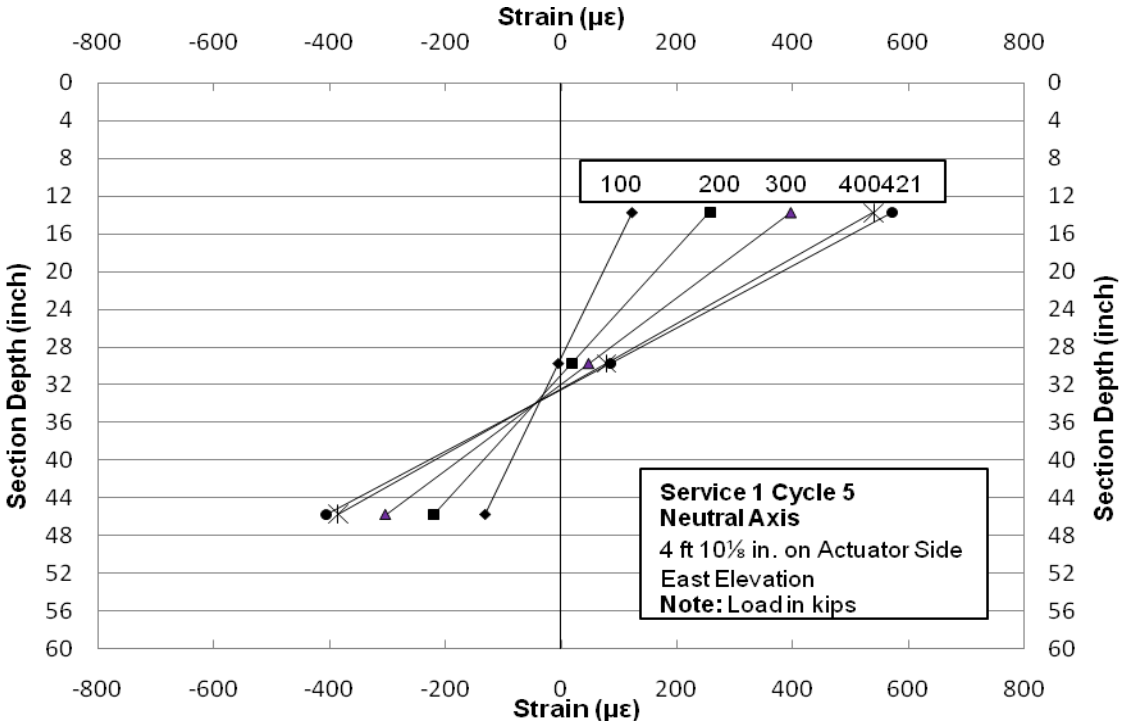


**Figure E.33** Neutral Axis on Actuator Side (East Elevation)

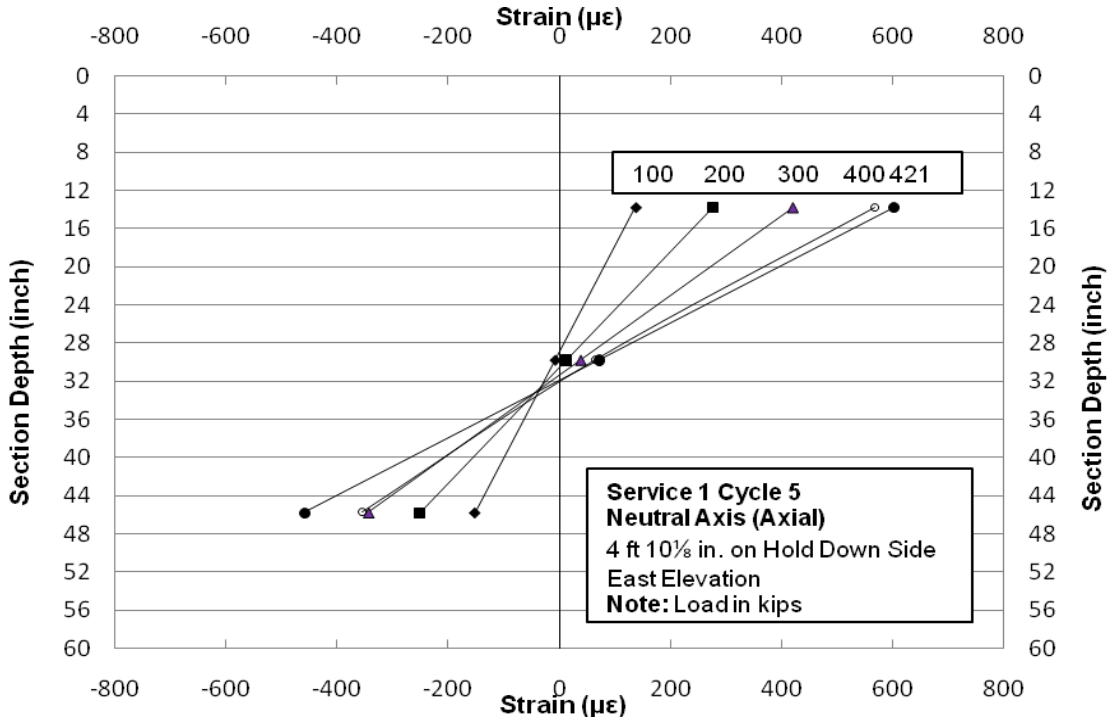


**Figure E.34** Neutral Axis on Hold Down Side (East Elevation)

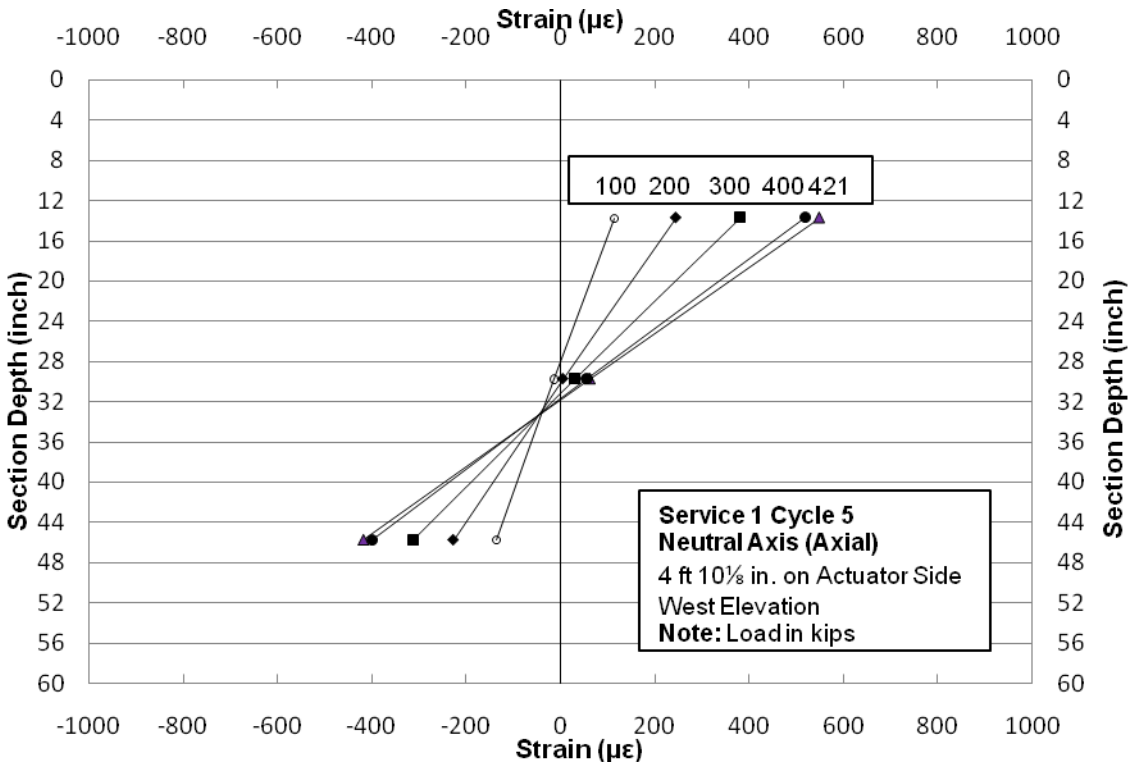


**Figure E.35** Neutral Axis on Actuator Side (West Elevation)

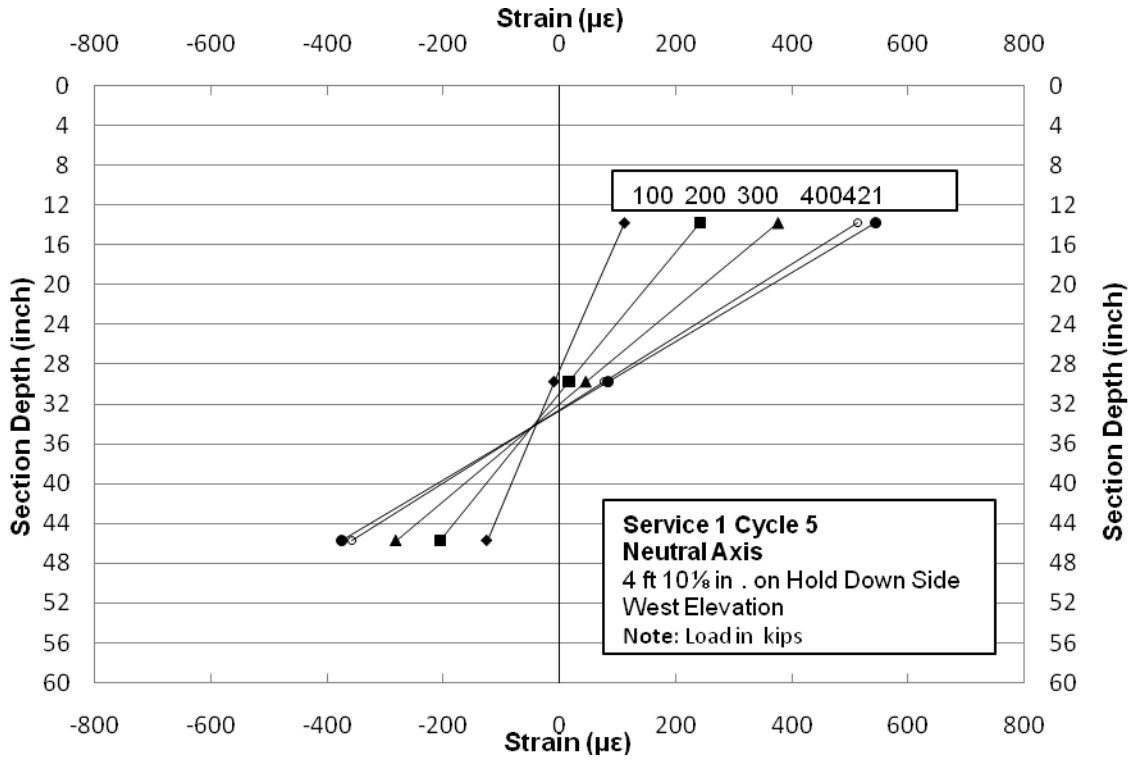


**Figure E.36** Neutral Axis on Hold Down Side (West Elevation)

## E.9 Deflection for Service II Load Case

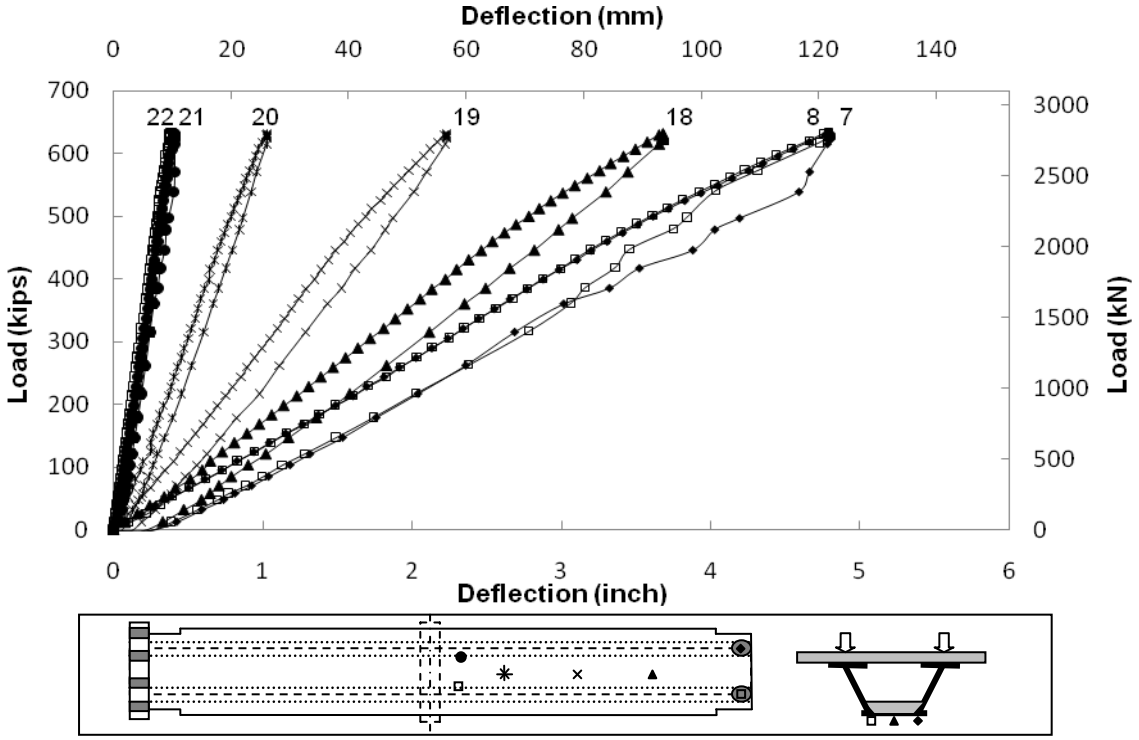


**Figure E.37** Deflection of Bottom Flange on Actuator Side (1st Cycle)

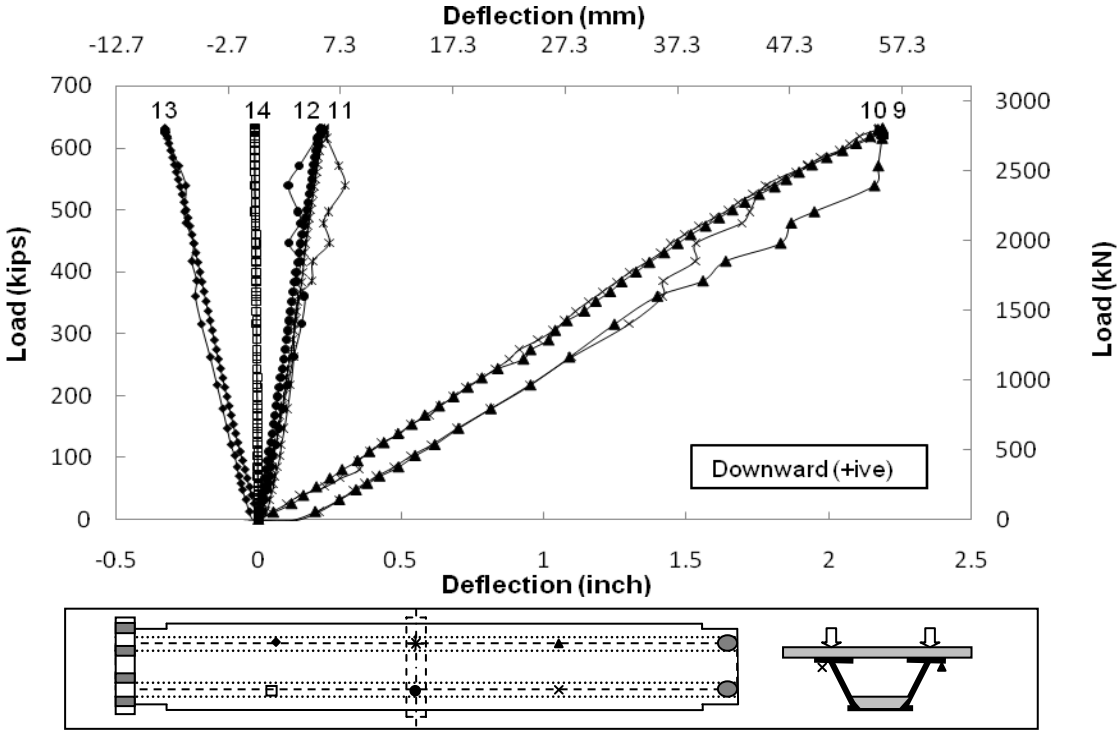


**Figure E.38** Deflection of Top Flange (1st Cycle)

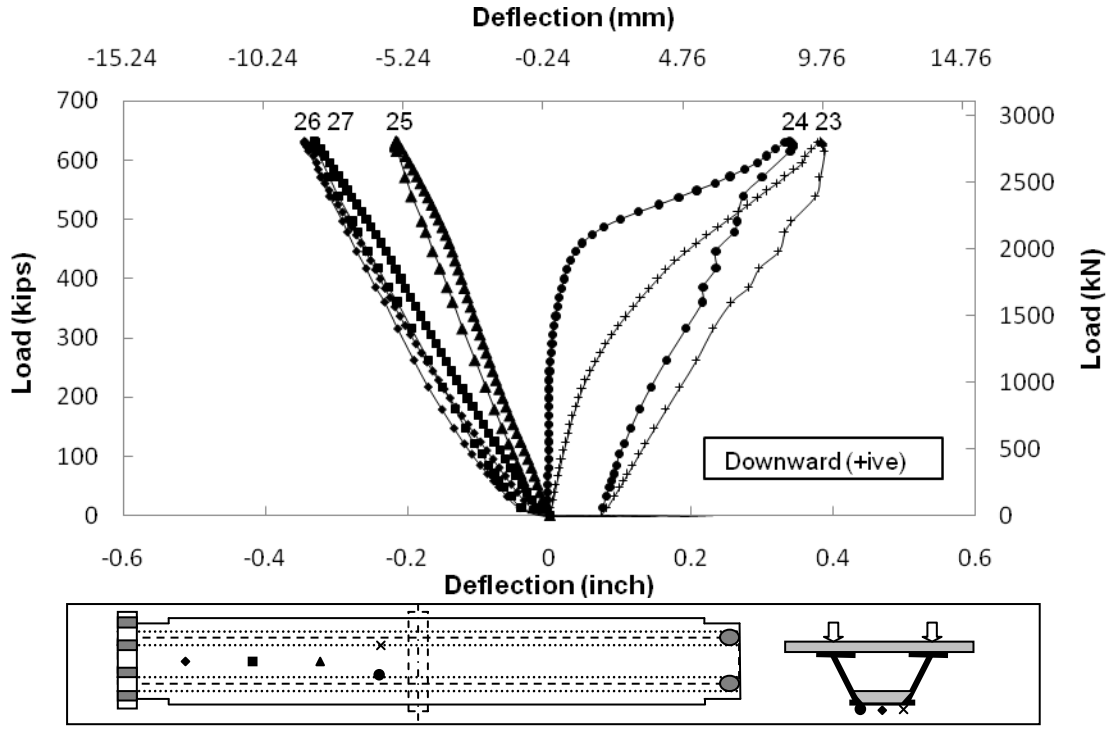


**Figure E.39** Deflection of Bottom Flange on Hold Down Side (1st Cycle)

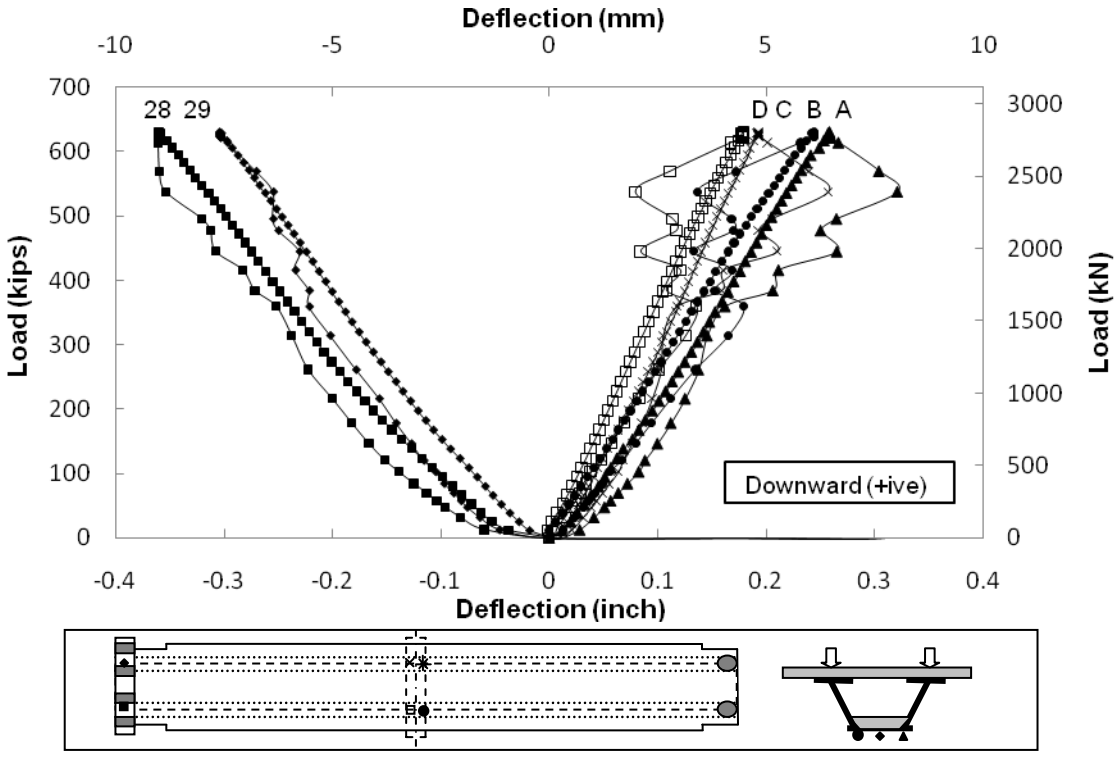


**Figure E.40** Deflection at Hold Down End and Center Support (1st Cycle)

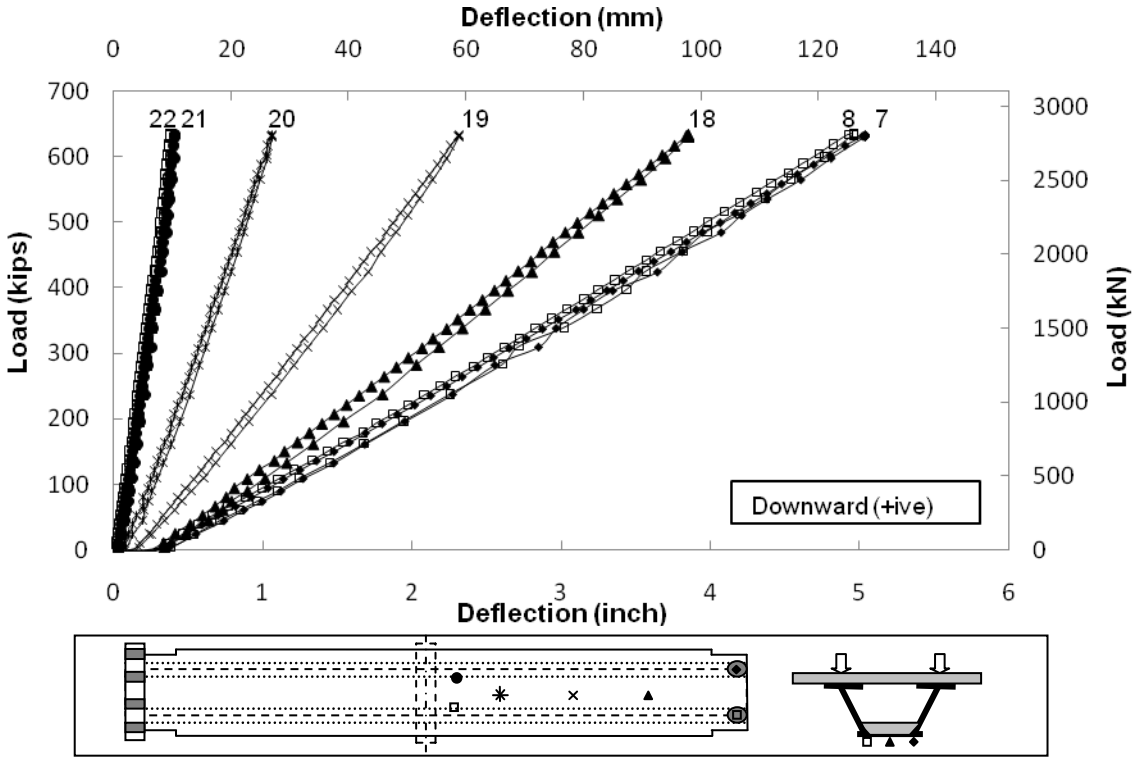


**Figure E.41** Deflection of Bottom Flange on Actuator Side (5th Cycle)

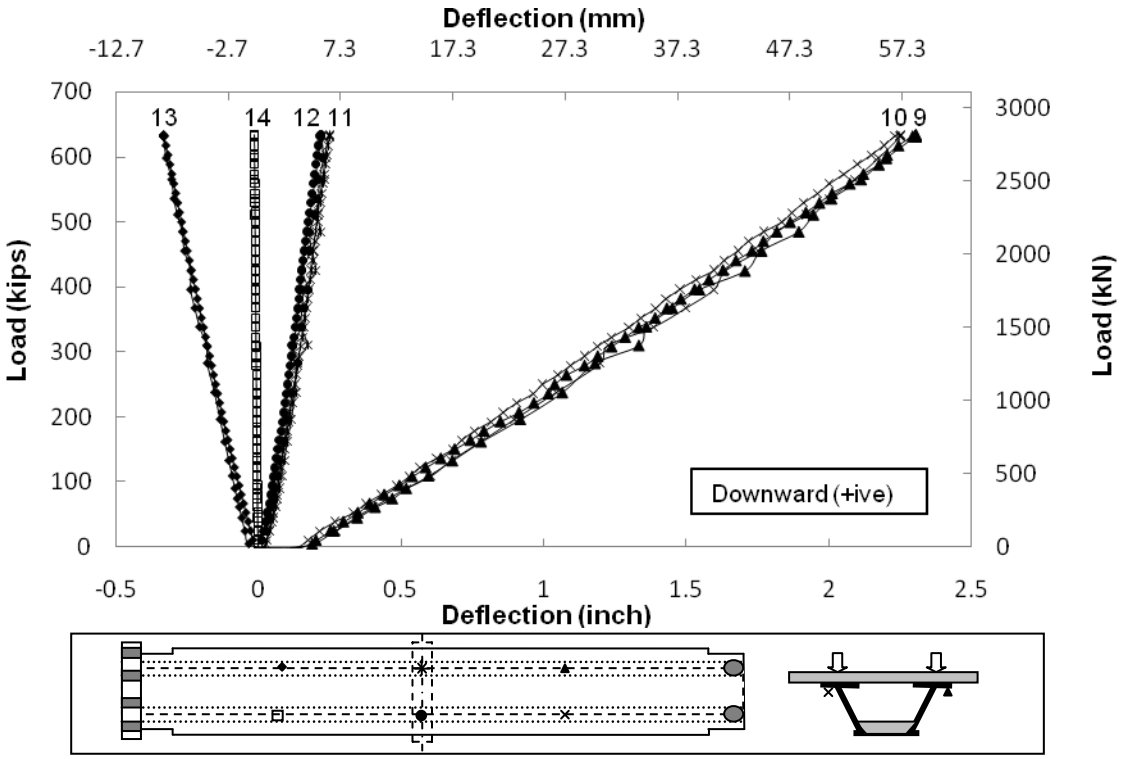


**Figure E.42** Deflection of Top Flange (5th Cycle)

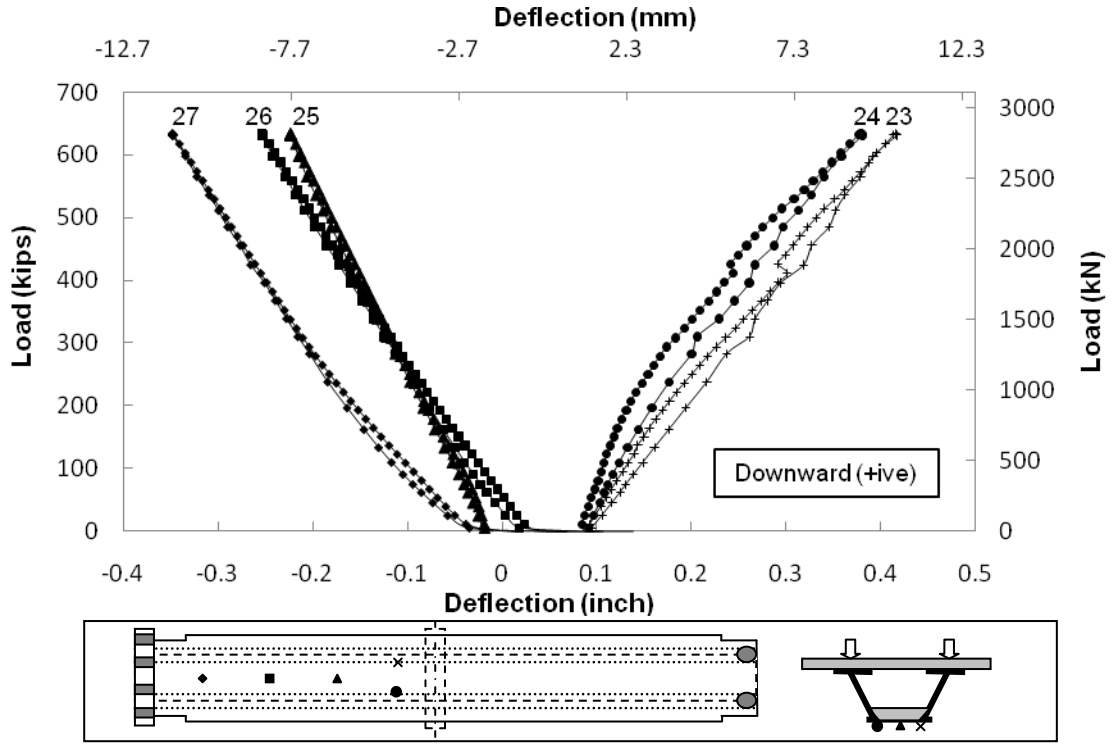


**Figure E.43** Deflection of Bottom Flange on Hold Down Side (5th Cycle)

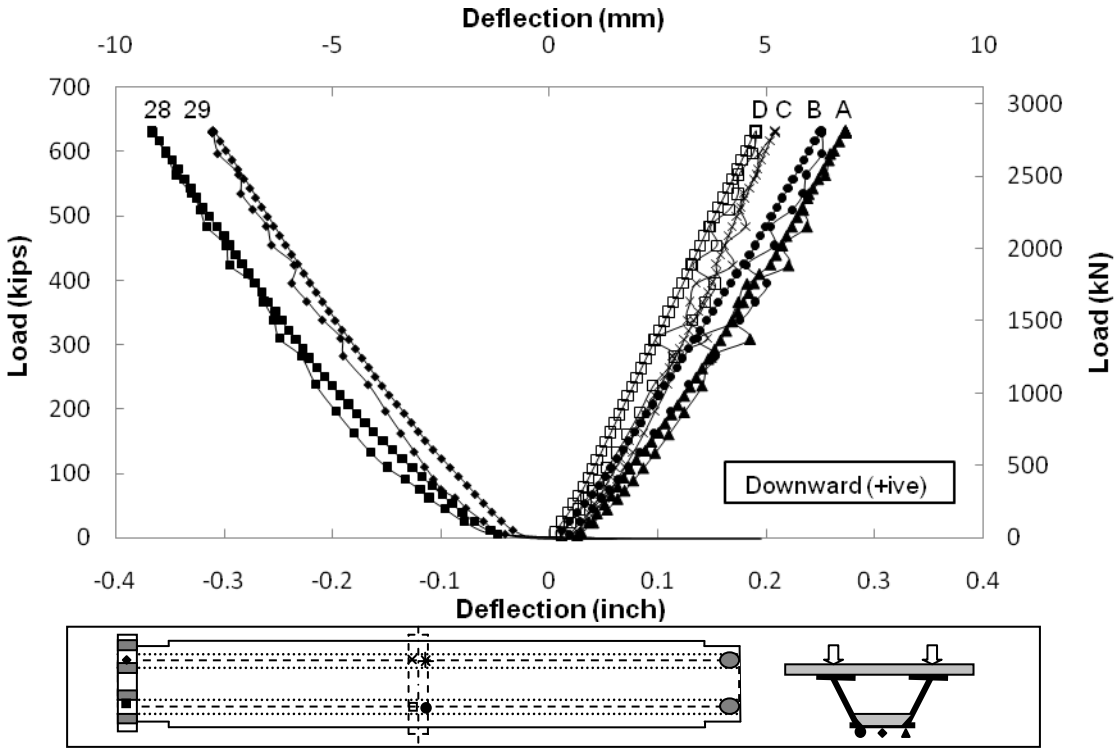


**Figure E.44** Deflection at Hold Down End and Center Support (5th Cycle)

## E.10 Slip for Service II Load Case

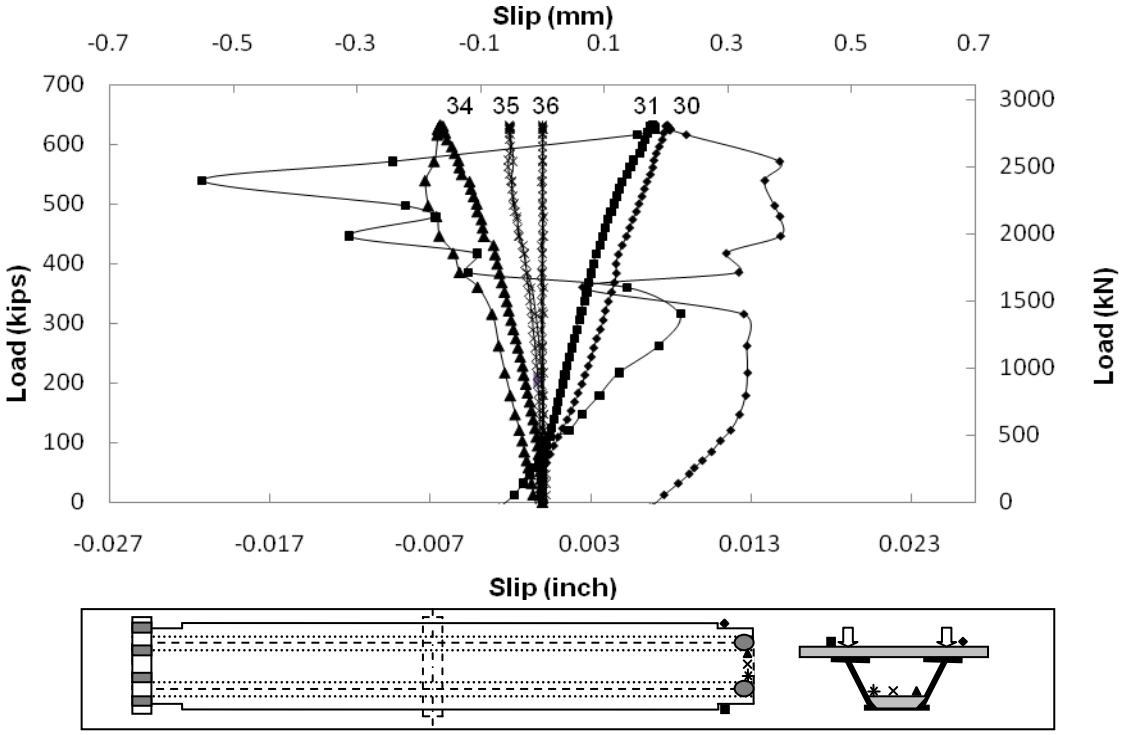


**Figure E.45** Slip at Actuator End (1st Cycle)

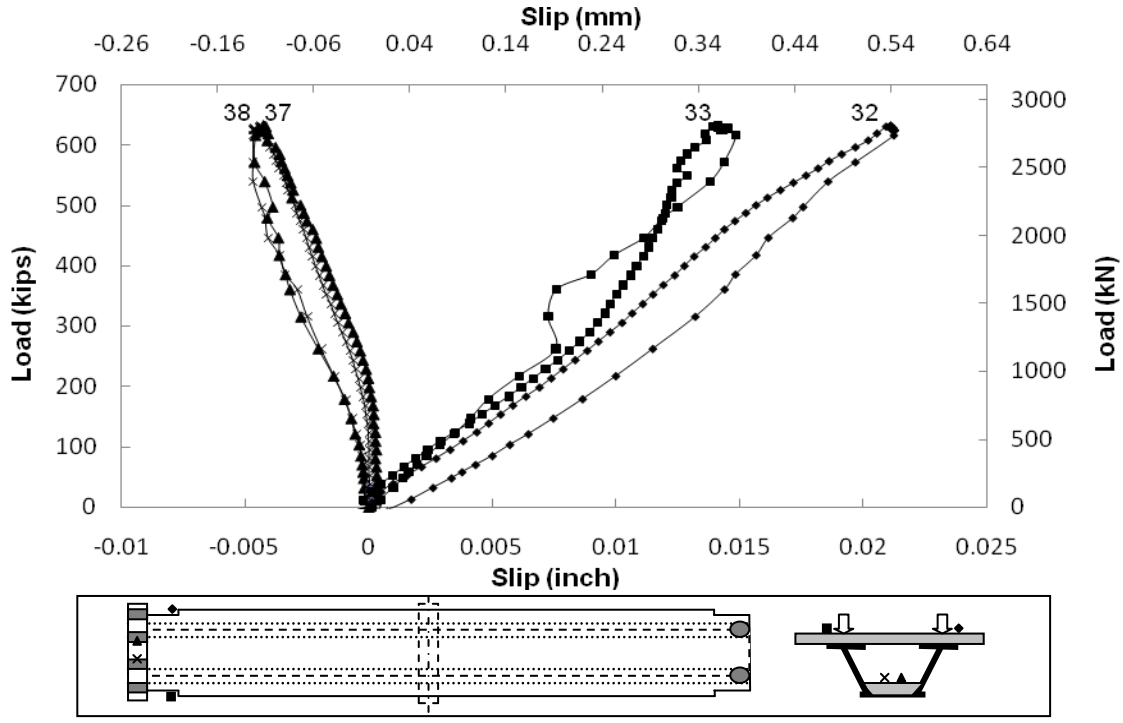


**Figure E.46** Slip at Hold Down End (1st Cycle)

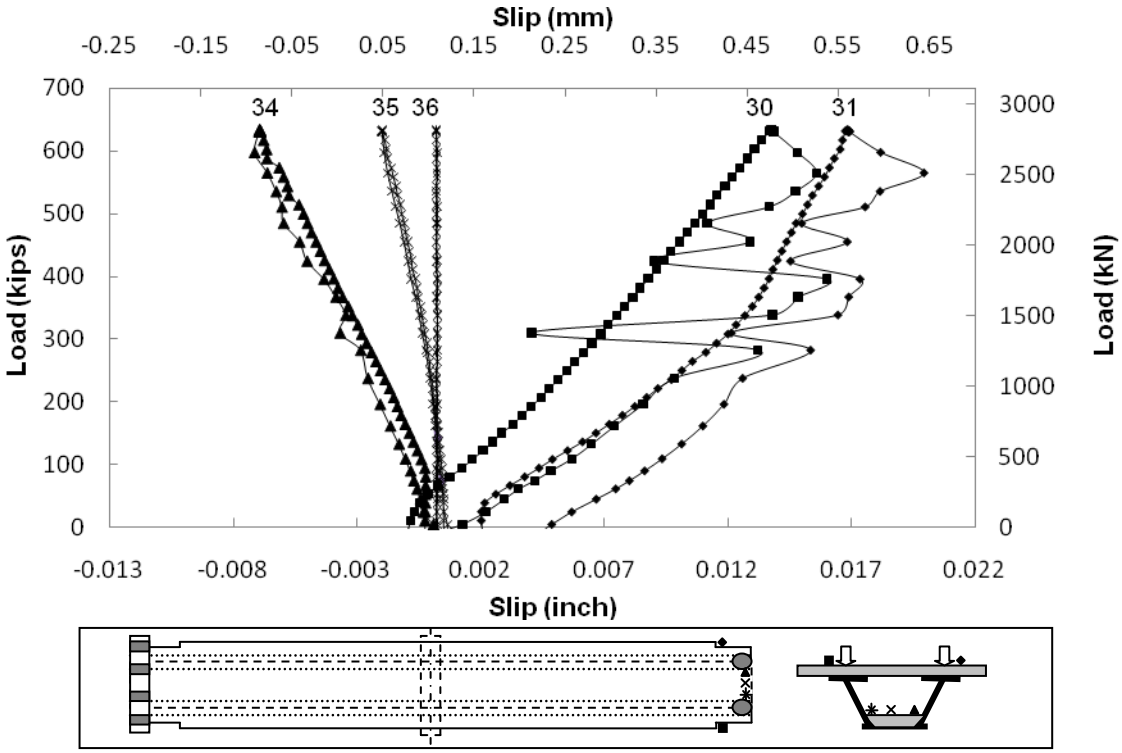


**Figure E.47** Slip at Actuator End (5th Cycle)

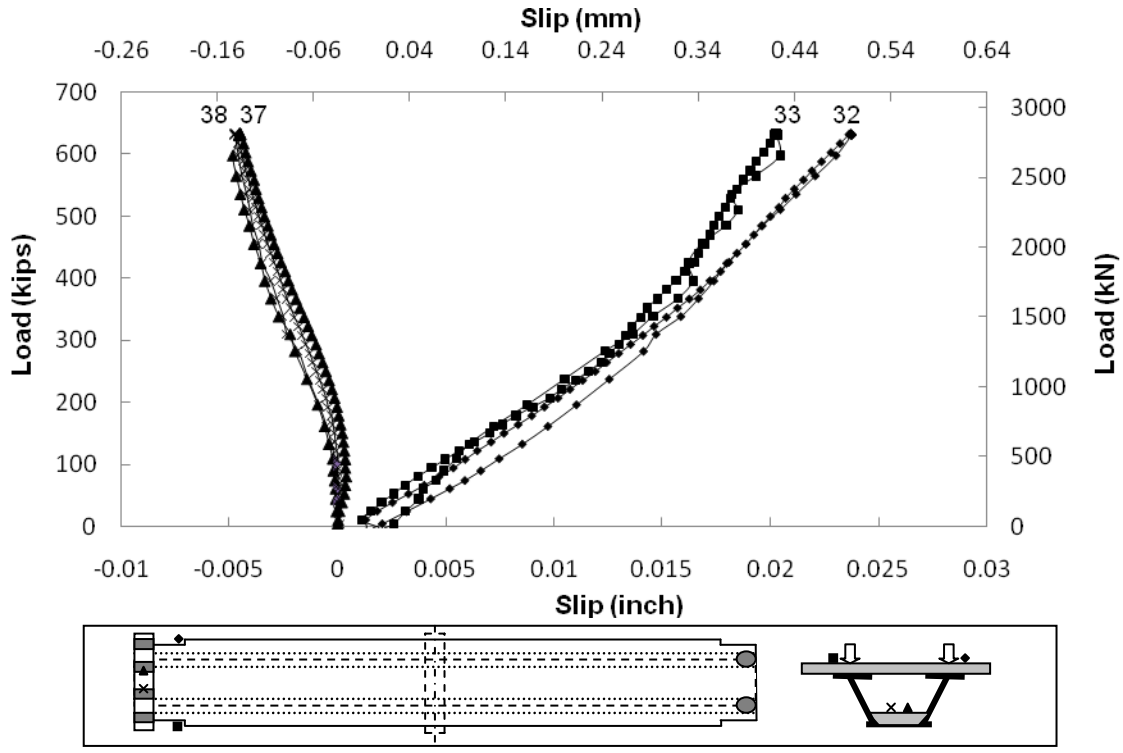


**Figure E.48** Slip at Hold Down End (5th Cycle)

## E.11 Strain in Top Slab Rebars for Service II Load Case

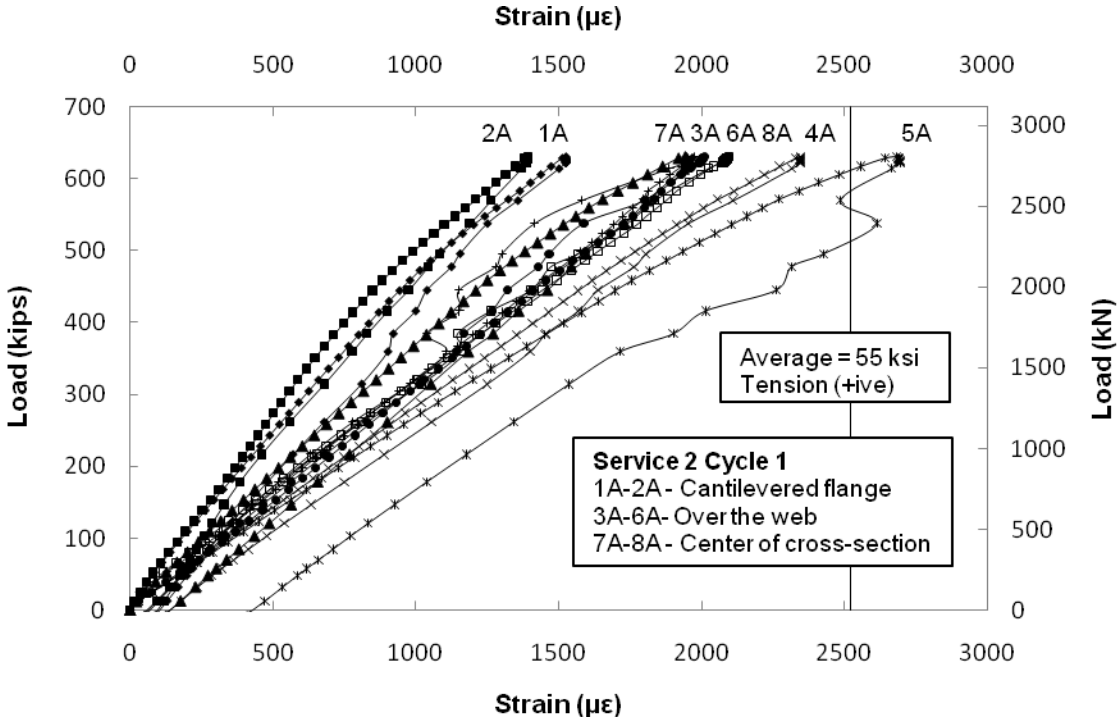


**Figure E.49** Strain in Rebars on Actuator Side (1st Cycle)

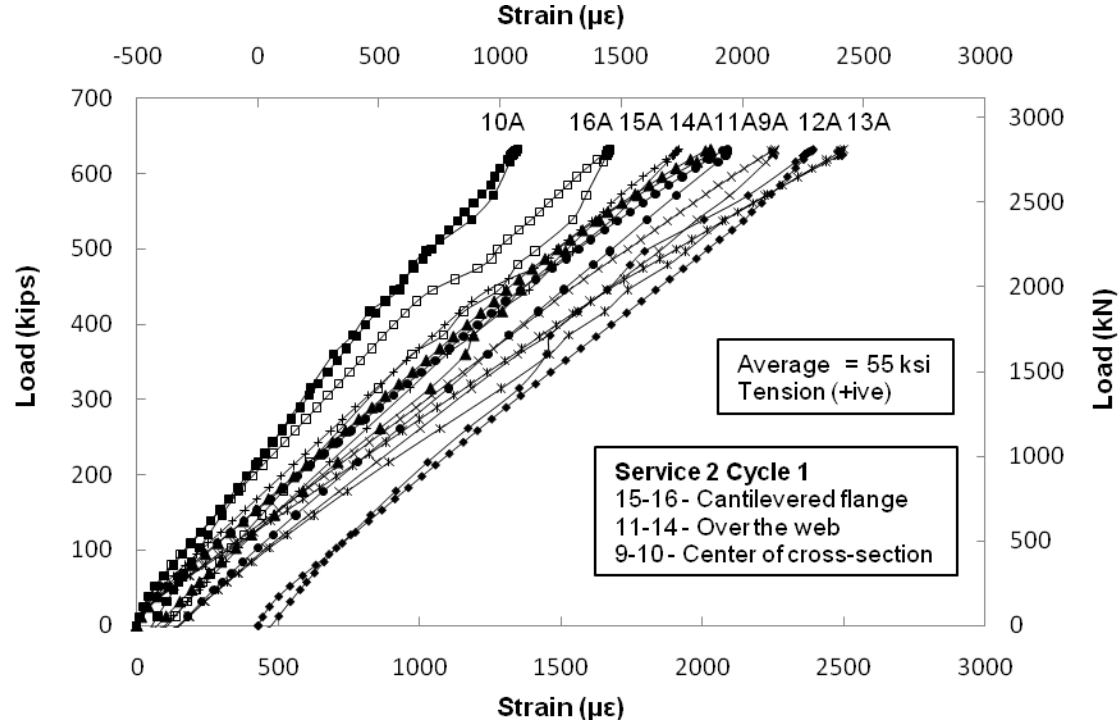


**Figure E.50** Strain in Rebars on Actuator Side (1st Cycle)

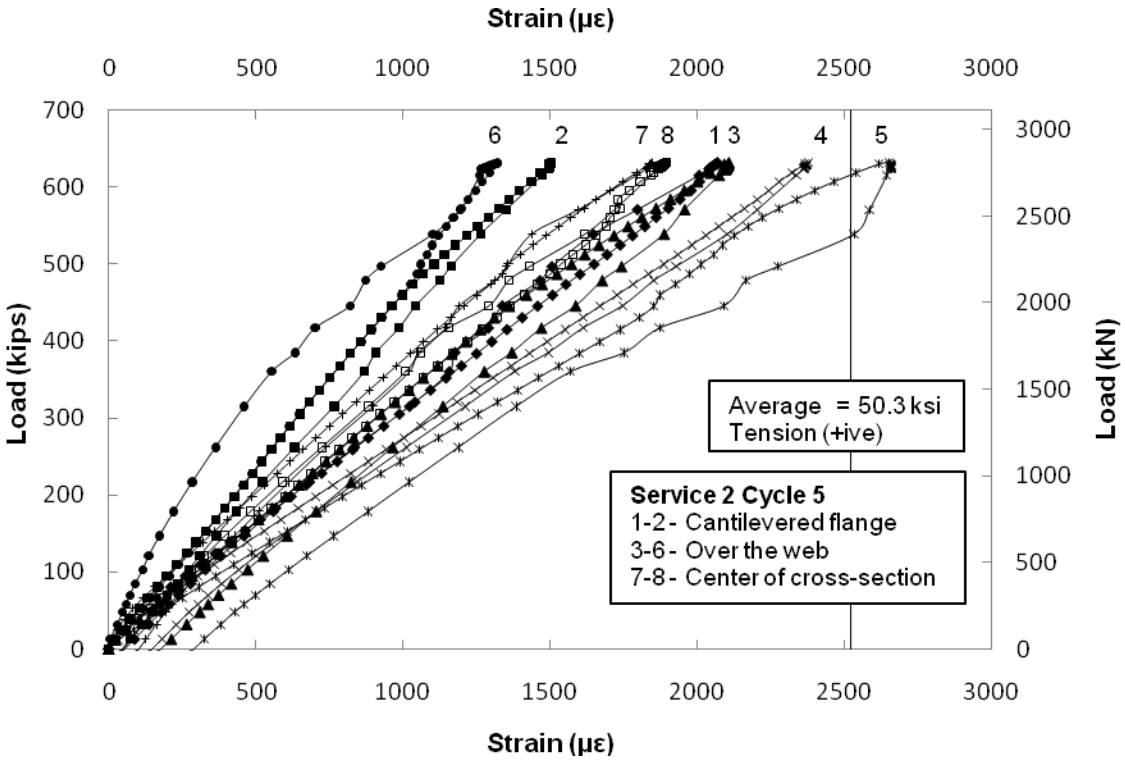


**Figure E.51** Strain in Rebars on Hold Down Side (1st Cycle)

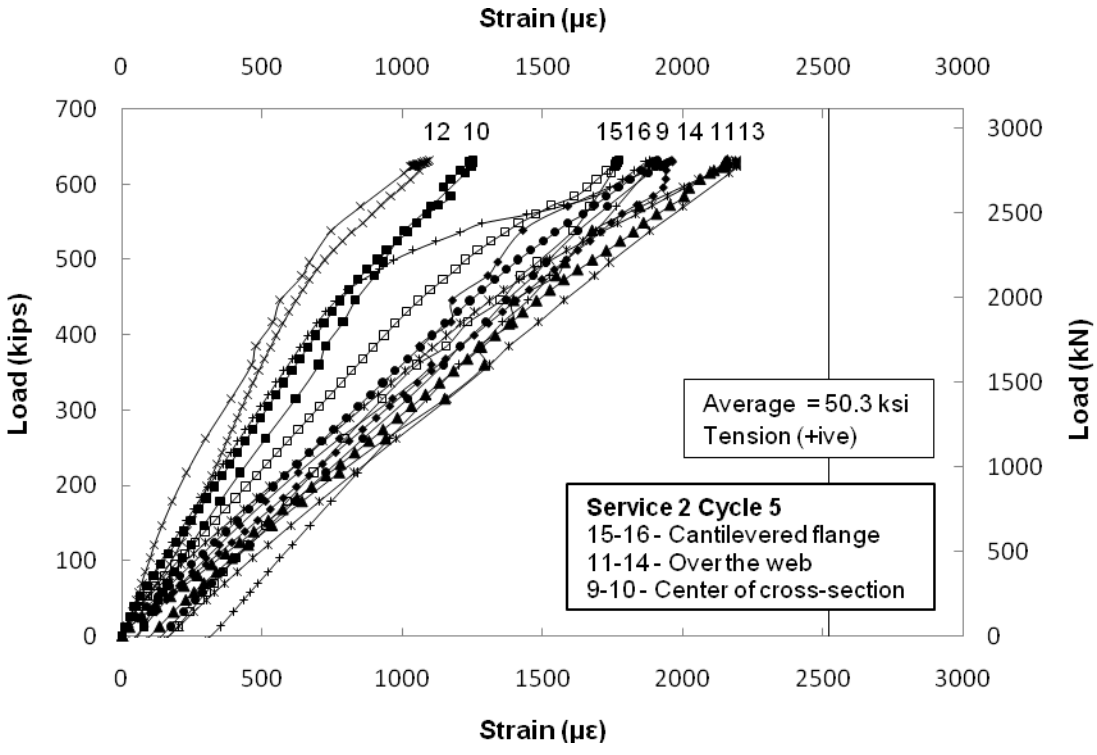


**Figure E.52** Strain in Rebars on Hold Down Side (1st Cycle)

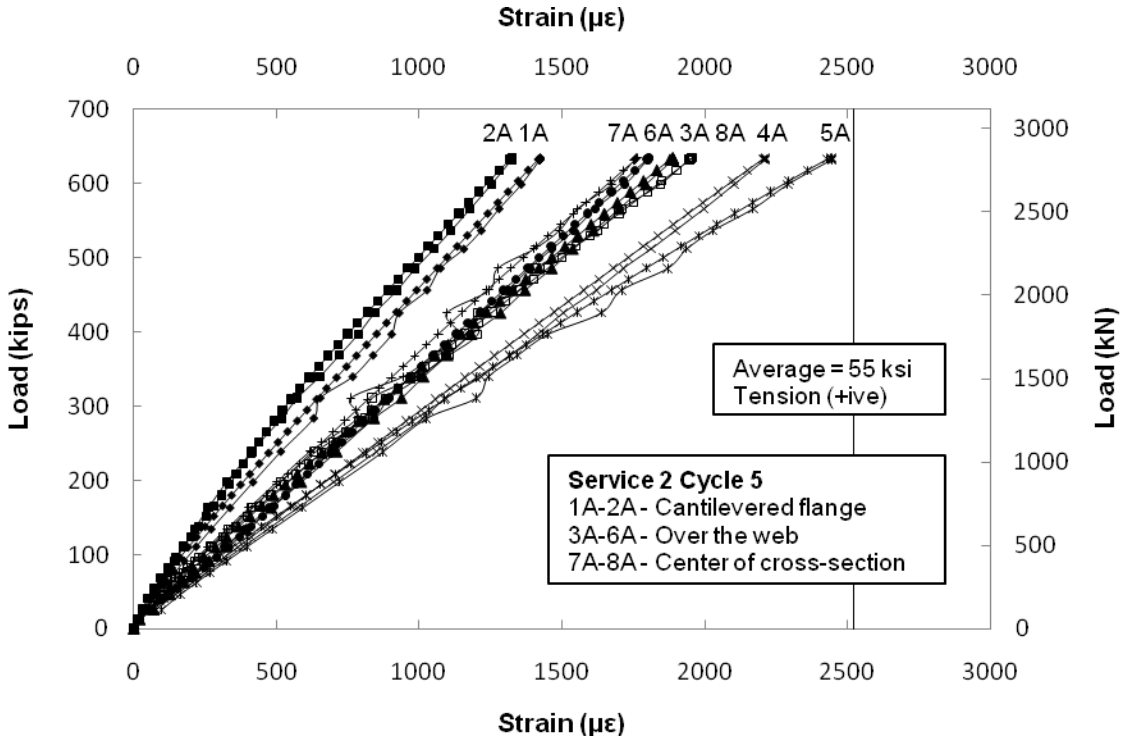


**Figure E.53** Strain in Rebars on Actuator Side (5th Cycle)

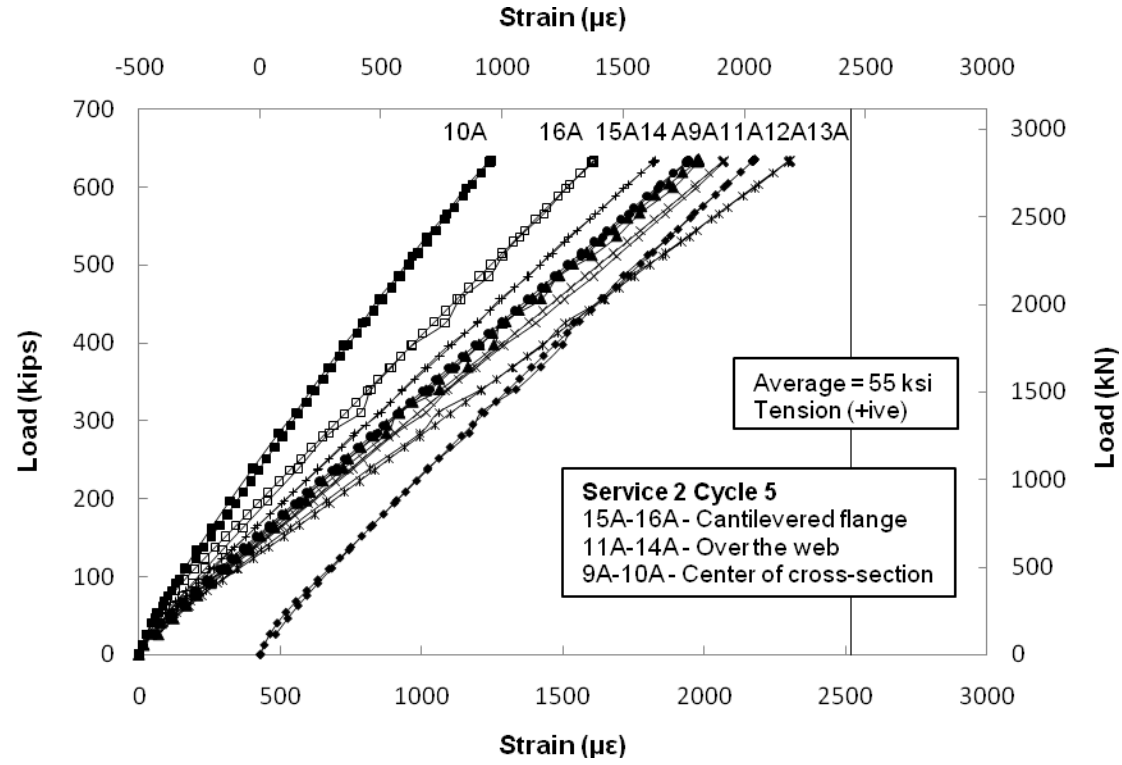


**Figure E.54** Strain in Rebars on Actuator Side (5th Cycle)

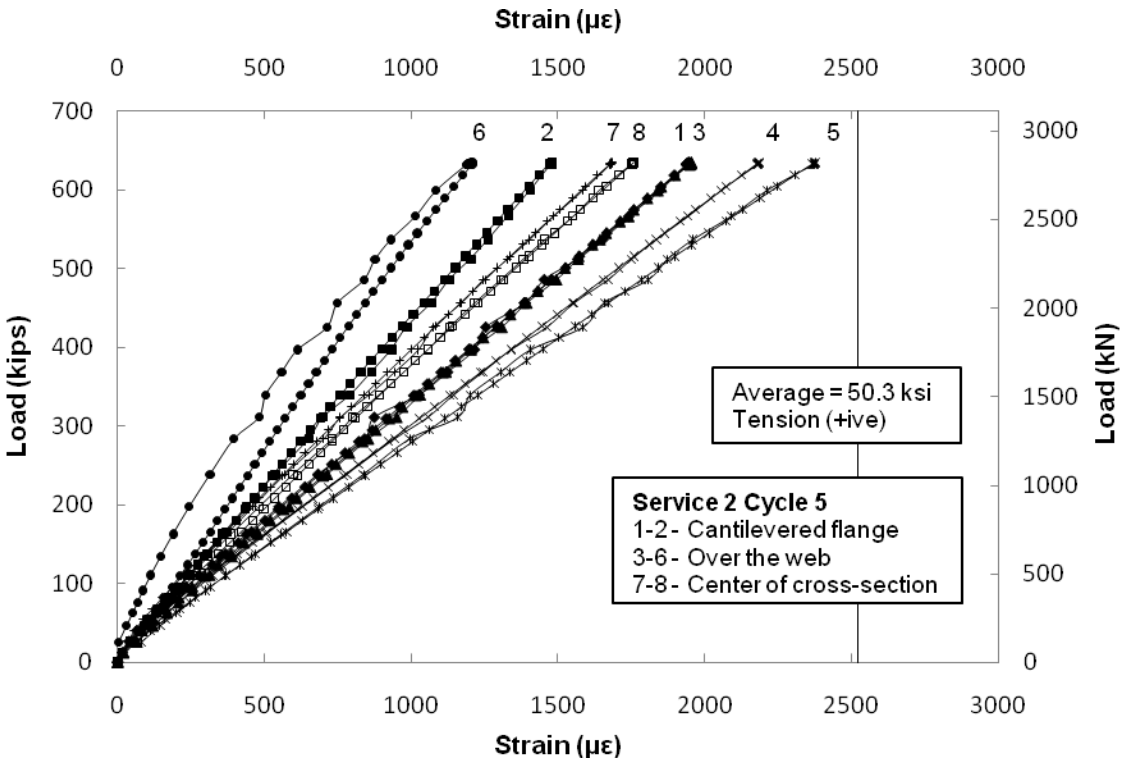


**Figure E.55** Strain in Rebars on Hold Down Side (5th Cycle)

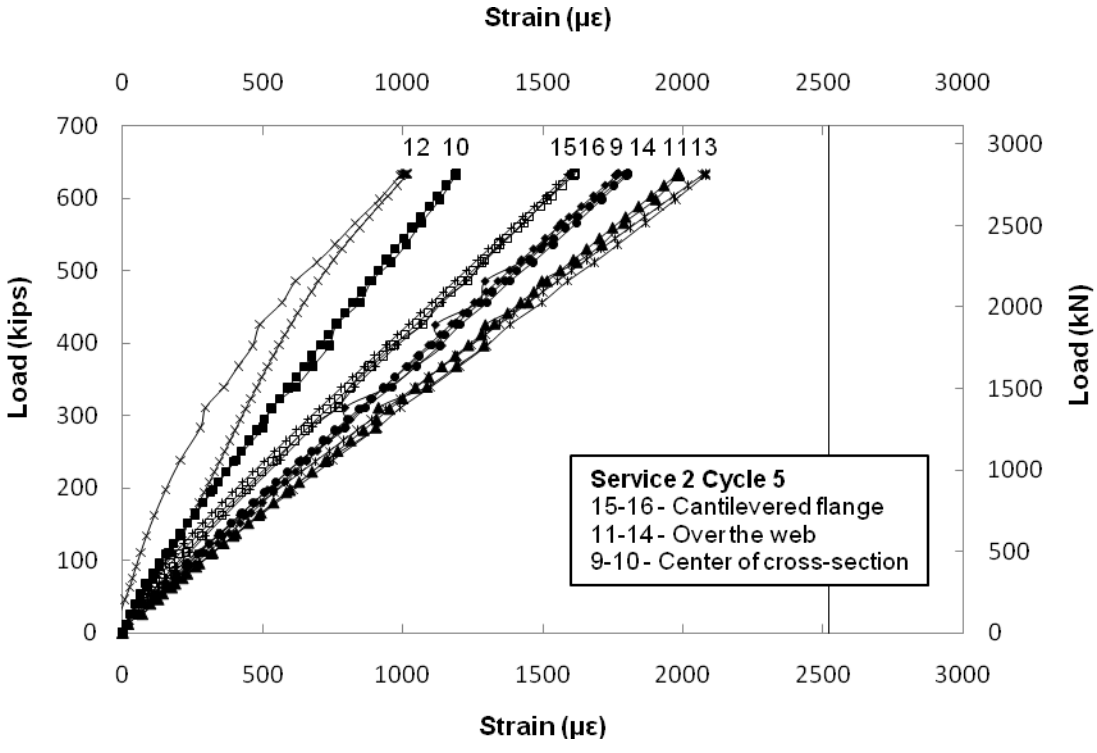


**Figure E.56** Strain in Rebars on Hold Down Side (5th Cycle)

## E.12 Strain in Steel for Service II Load Case

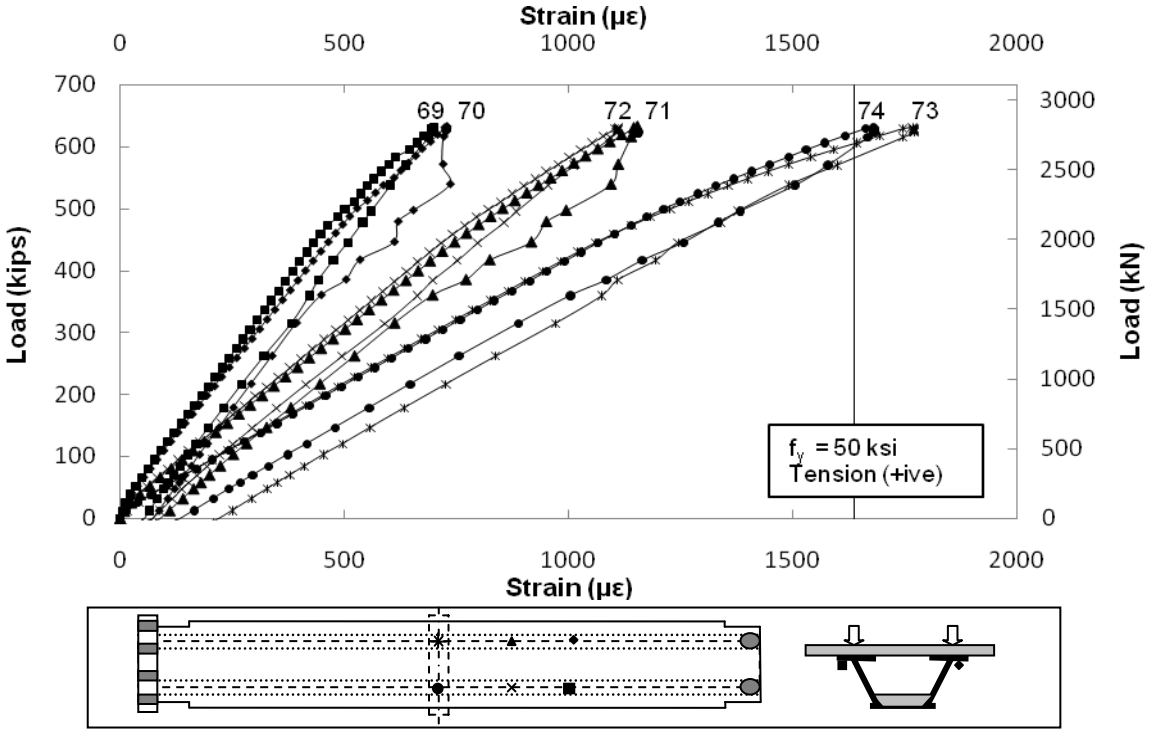


**Figure E.57** Strain in Top Flange on Actuator Side (1st Cycle)

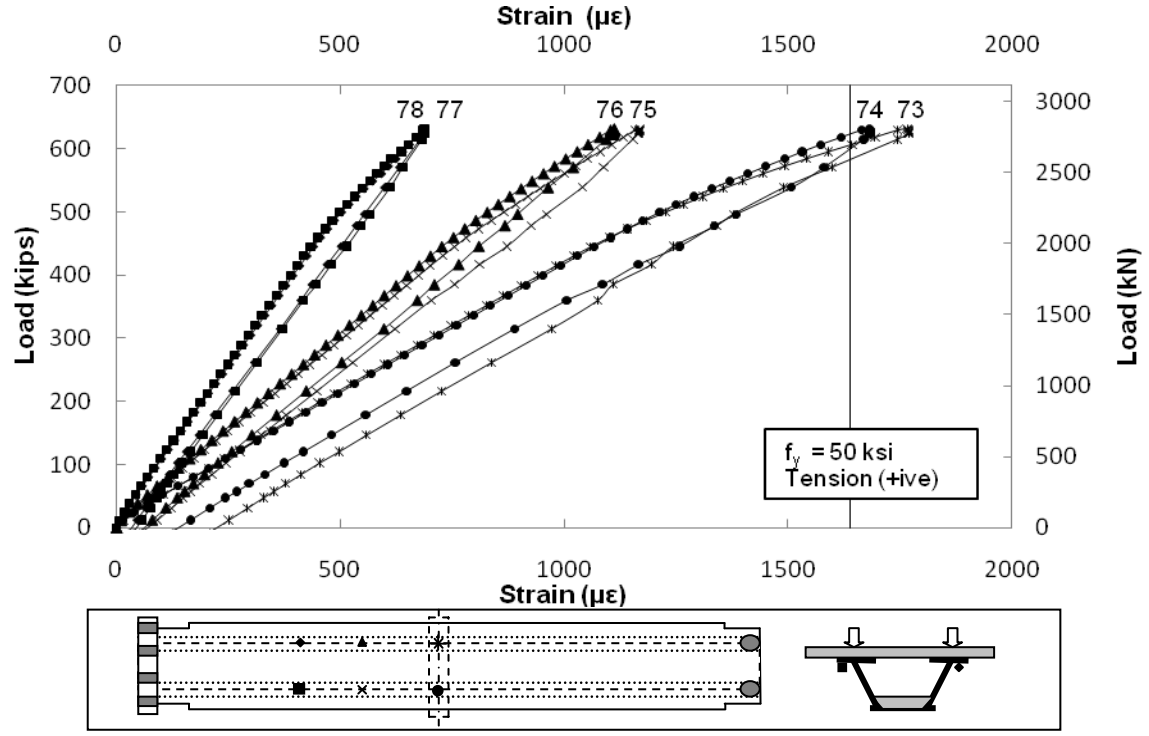


**Figure E.58** Strain in Top Flange on Hold Down Side (1st Cycle)

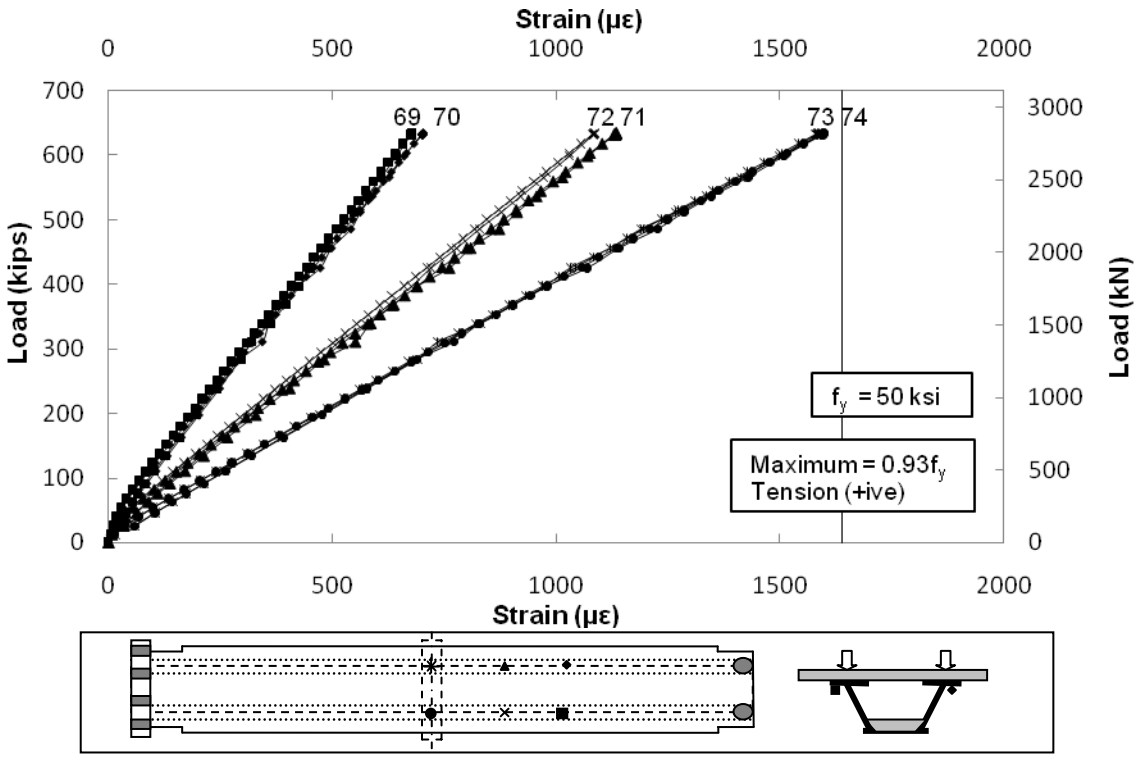


**Figure E.59** Strain in Top Flange on Actuator Side (5th Cycle)

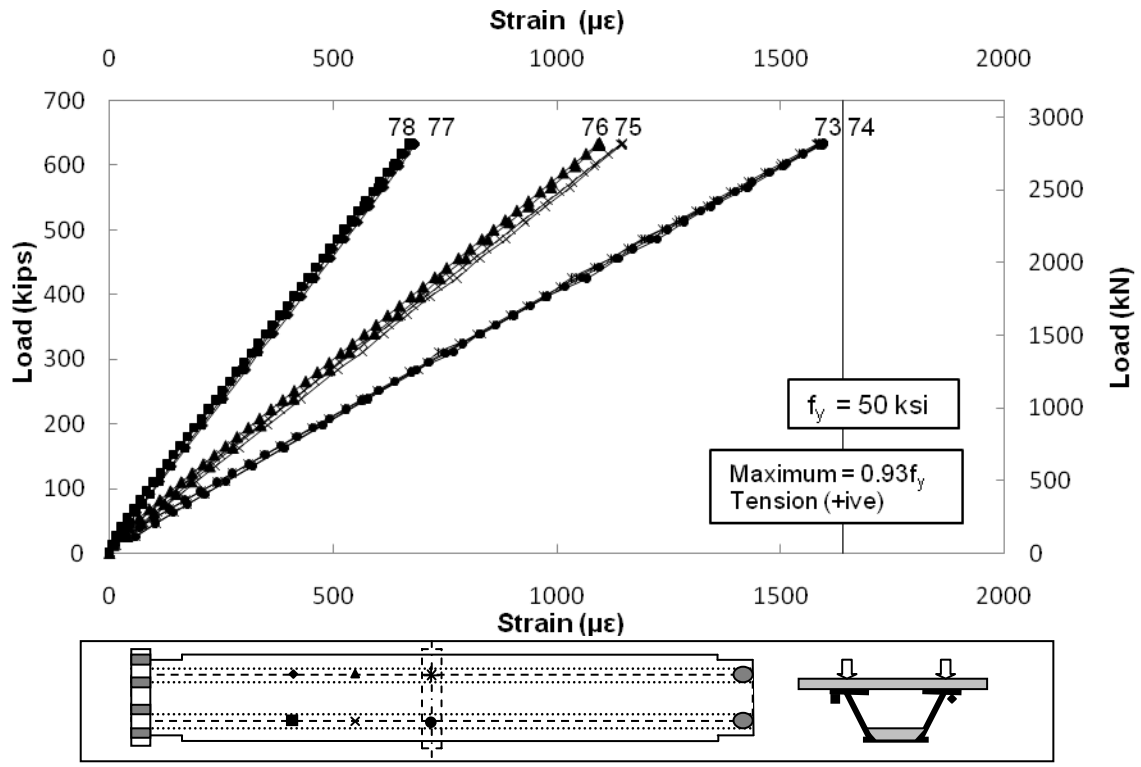


**Figure E.60** Strain in Top Flange on Hold Down Side (5th Cycle)

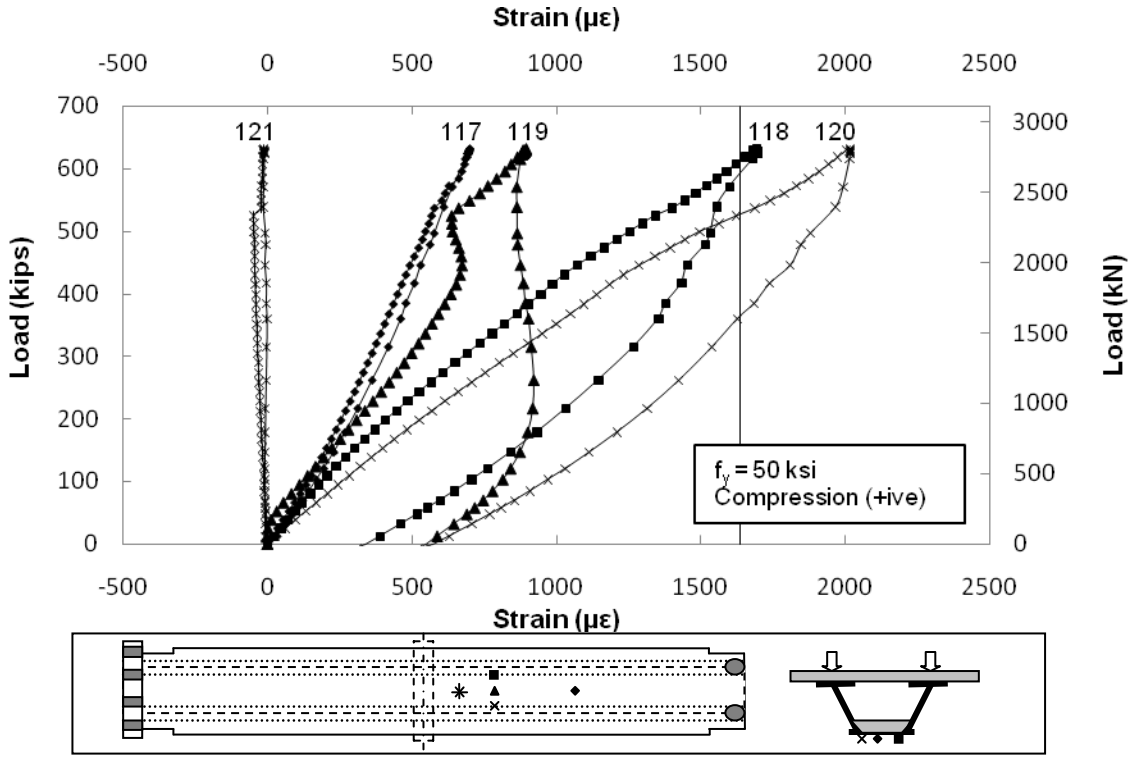


**Figure E.61** Strain in Bottom Flange on Actuator Side (1st Cycle)

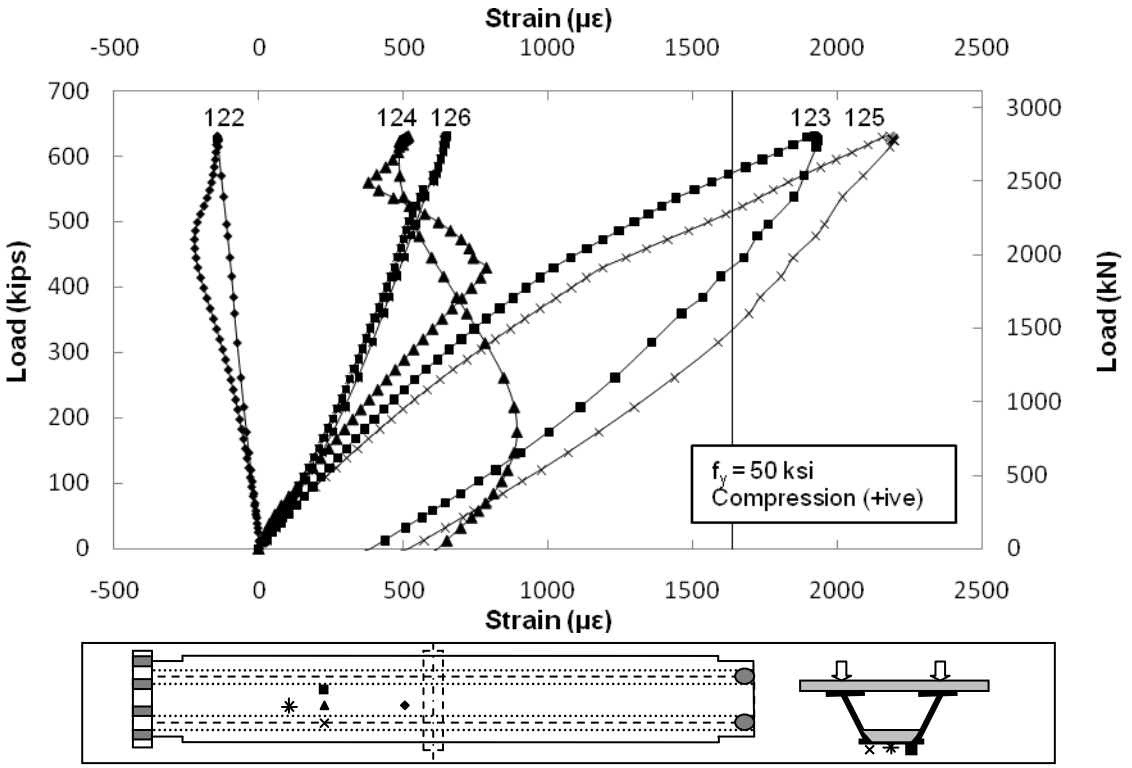


**Figure E.62** Strain in Bottom Flange on Hold Down Side (1st Cycle)

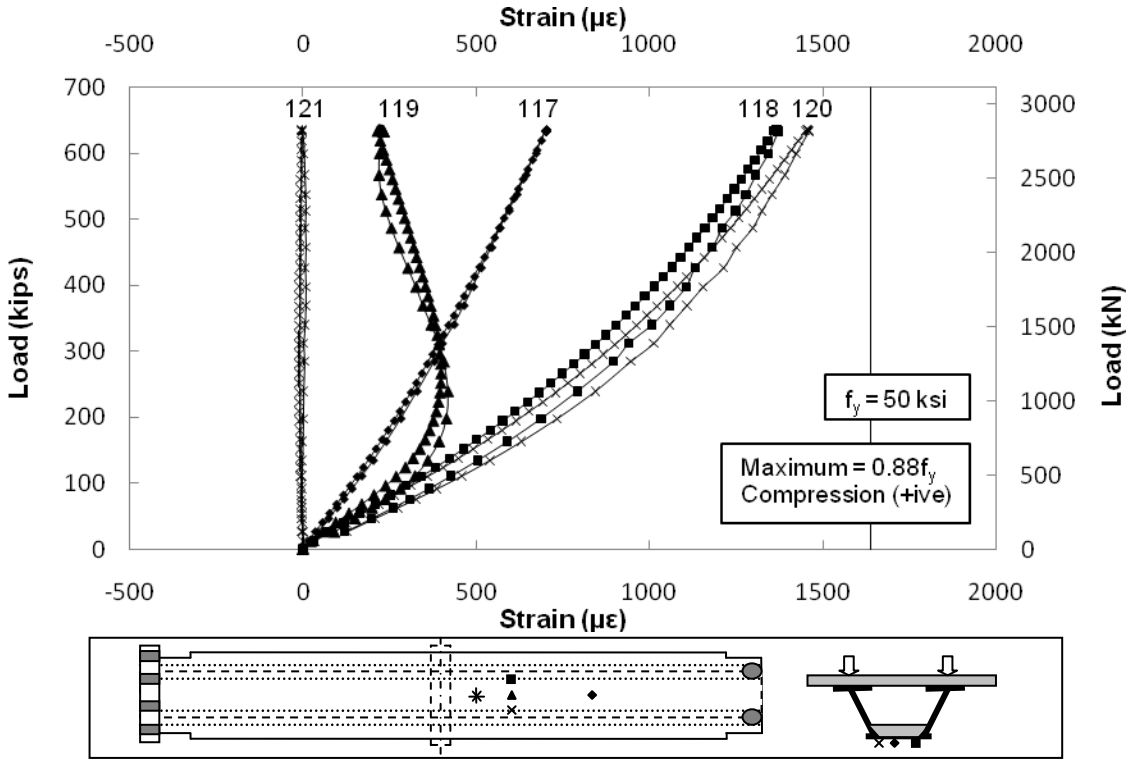


**Figure E.63** Strain in Bottom Flange on Actuator Side (5th Cycle)

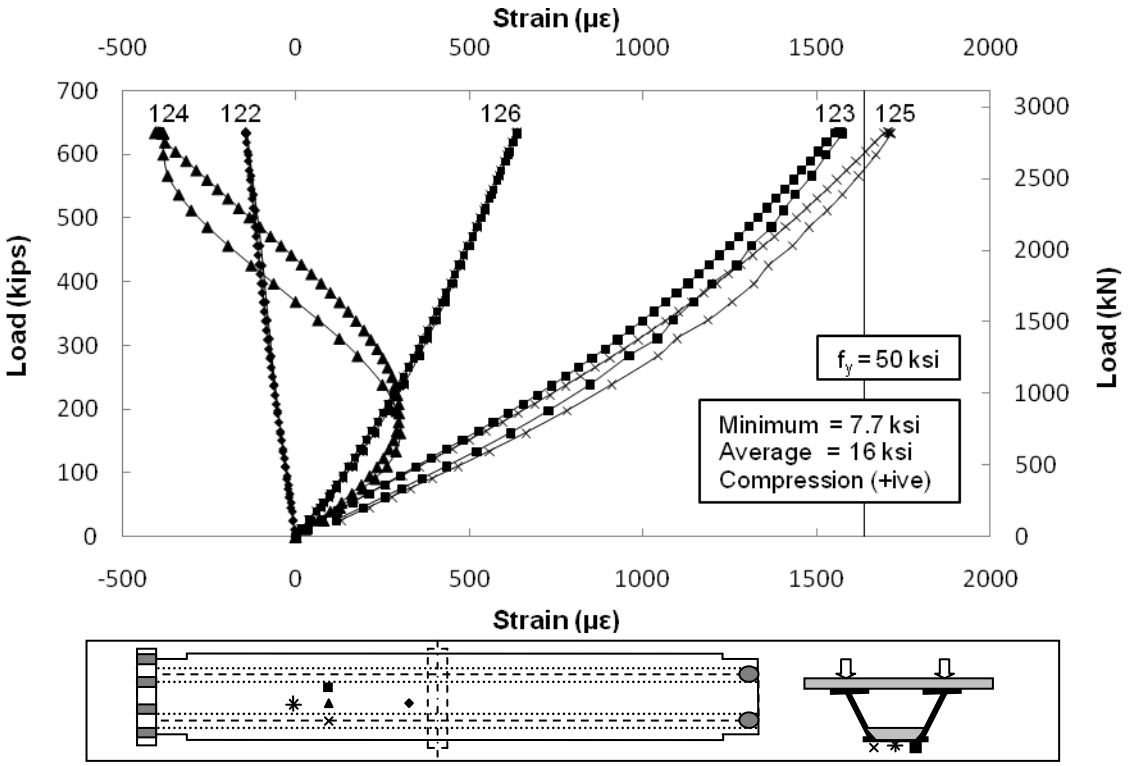


**Figure E.64** Strain in Bottom Flange on Hold Down Side (5th Cycle)

## E.13 Strain in Concrete for Service II Load Case

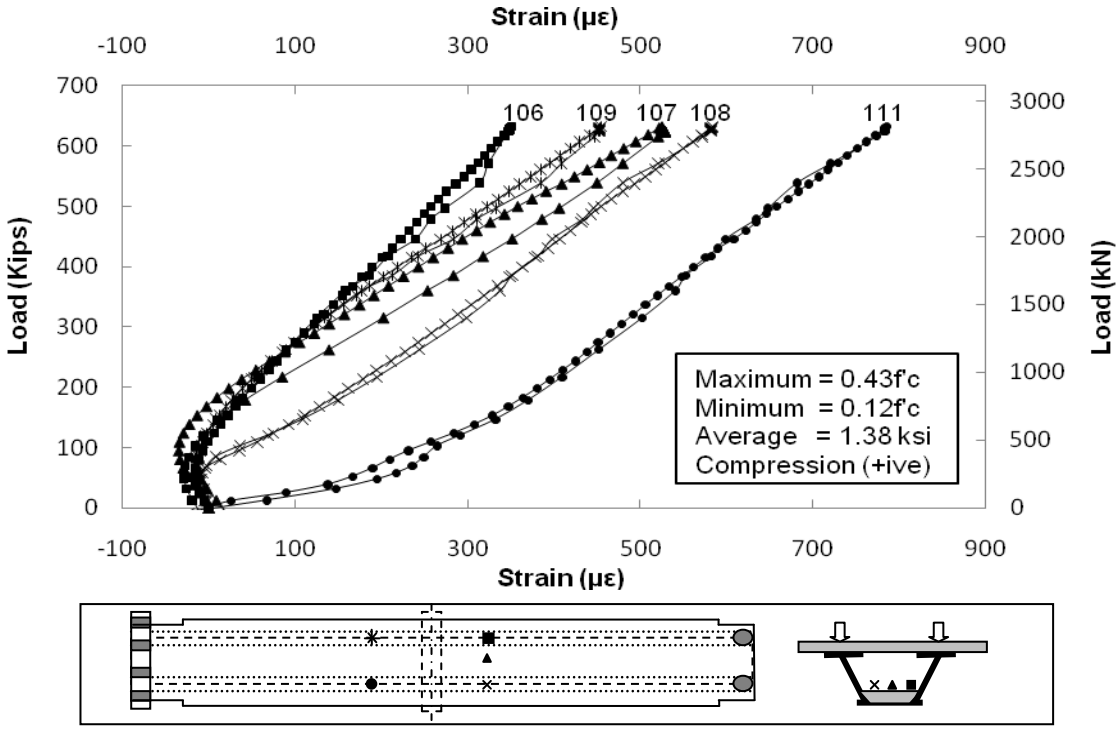


**Figure E.65** Strain in Bottom Concrete Slab (1st Cycle)

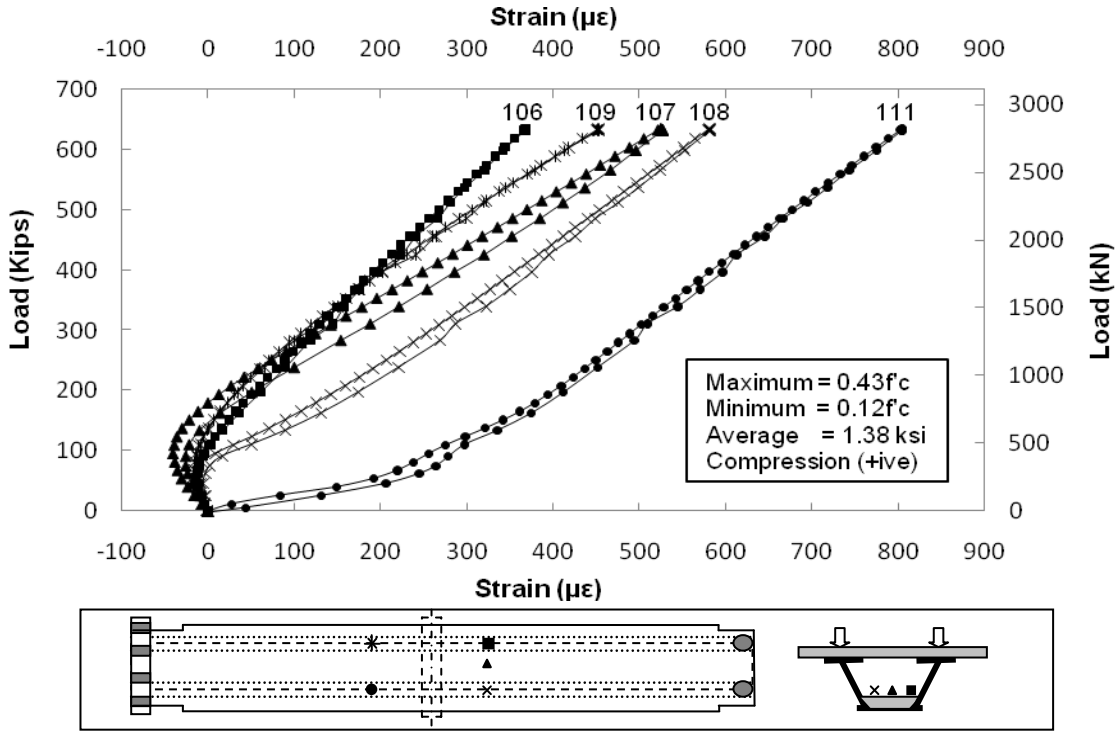


**Figure E.66** Strain in Bottom Concrete Slab (5th Cycle)

## E.14 Crack Width for Service II Load Case

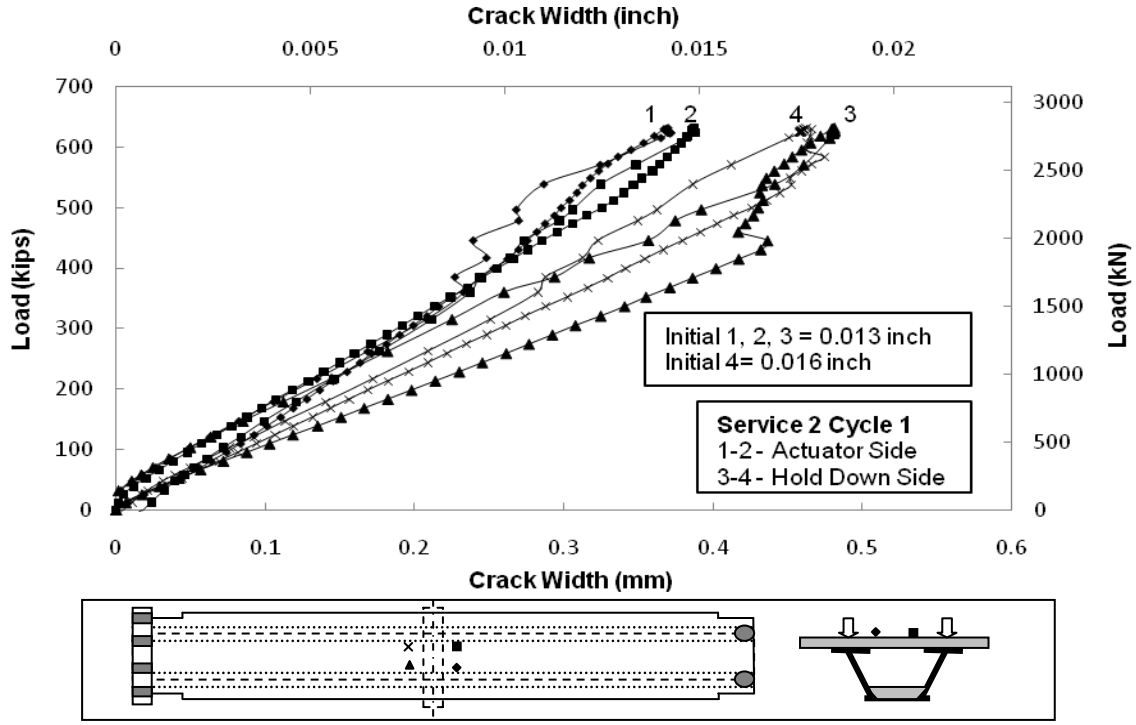


**Figure E.67** Crack Width on Top Slab (1st Cycle)

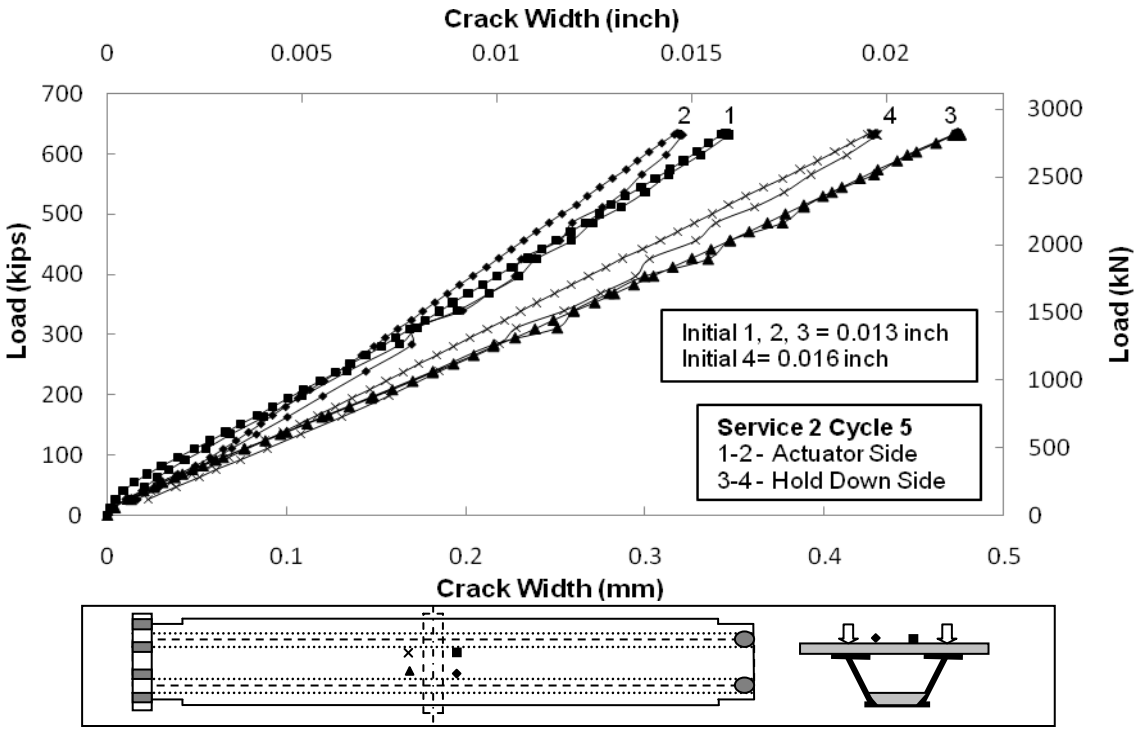


**Figure E.68** Crack Width on Top Slab (5th Cycle)

## E.15 Neutral Axis for Service II Load Case

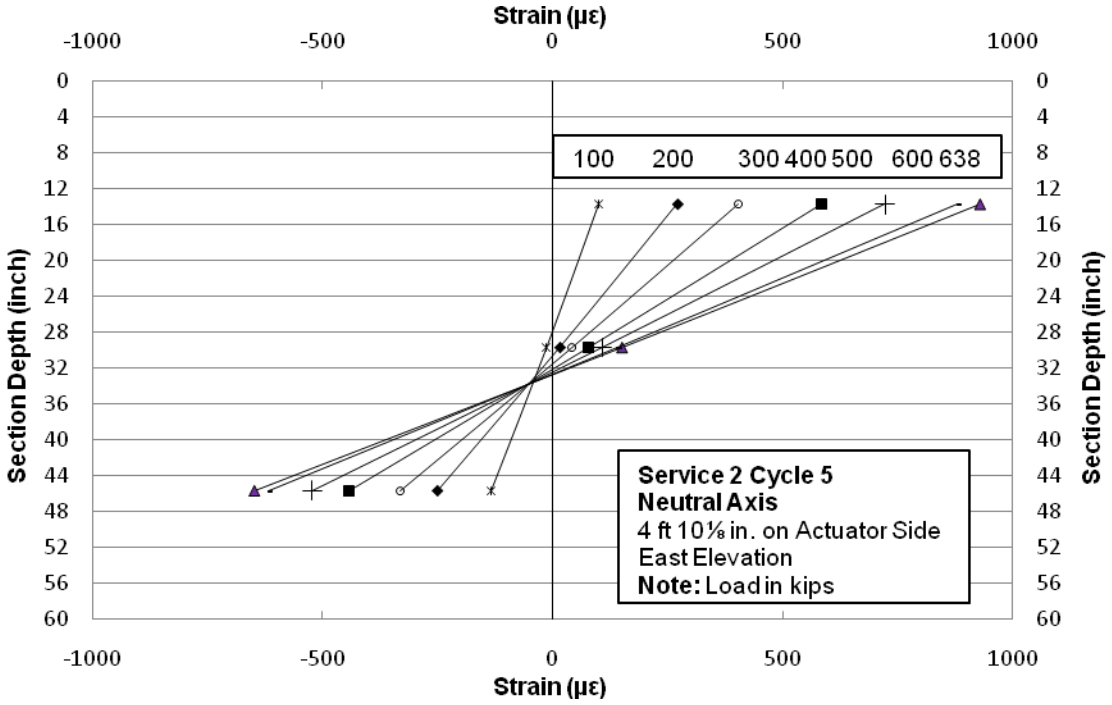


**Figure E.69** Neutral Axis on Actuator Side (East Elevation)

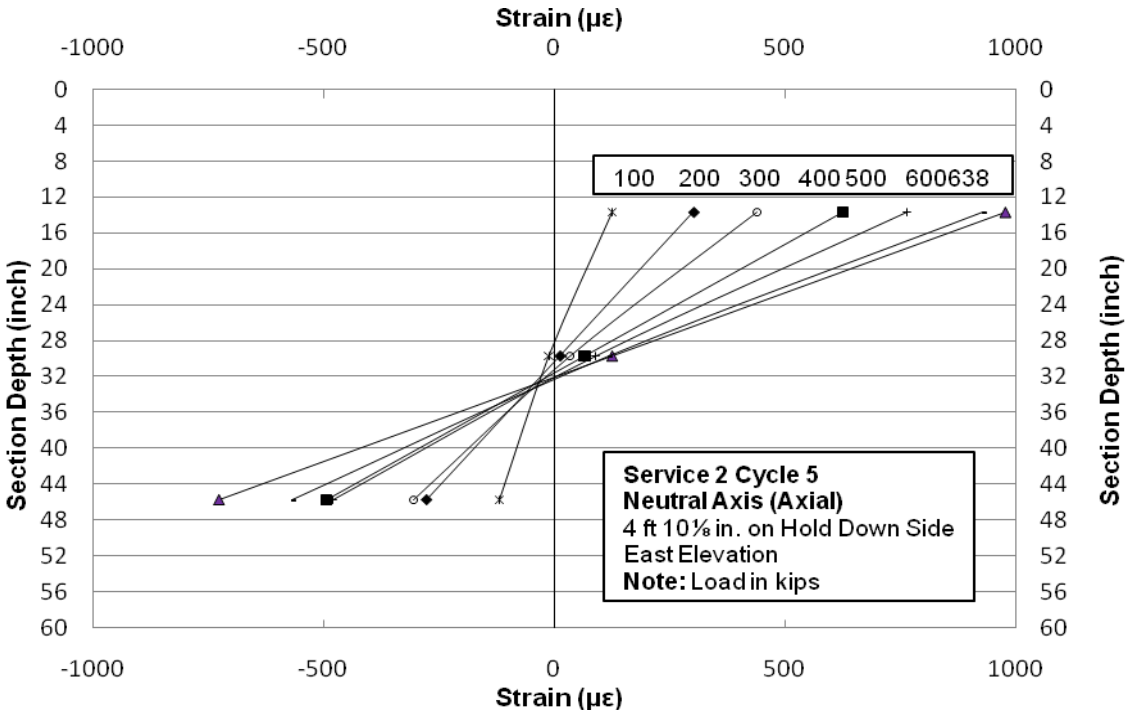


**Figure E.70** Neutral Axis on Hold Down Side (East Elevation)

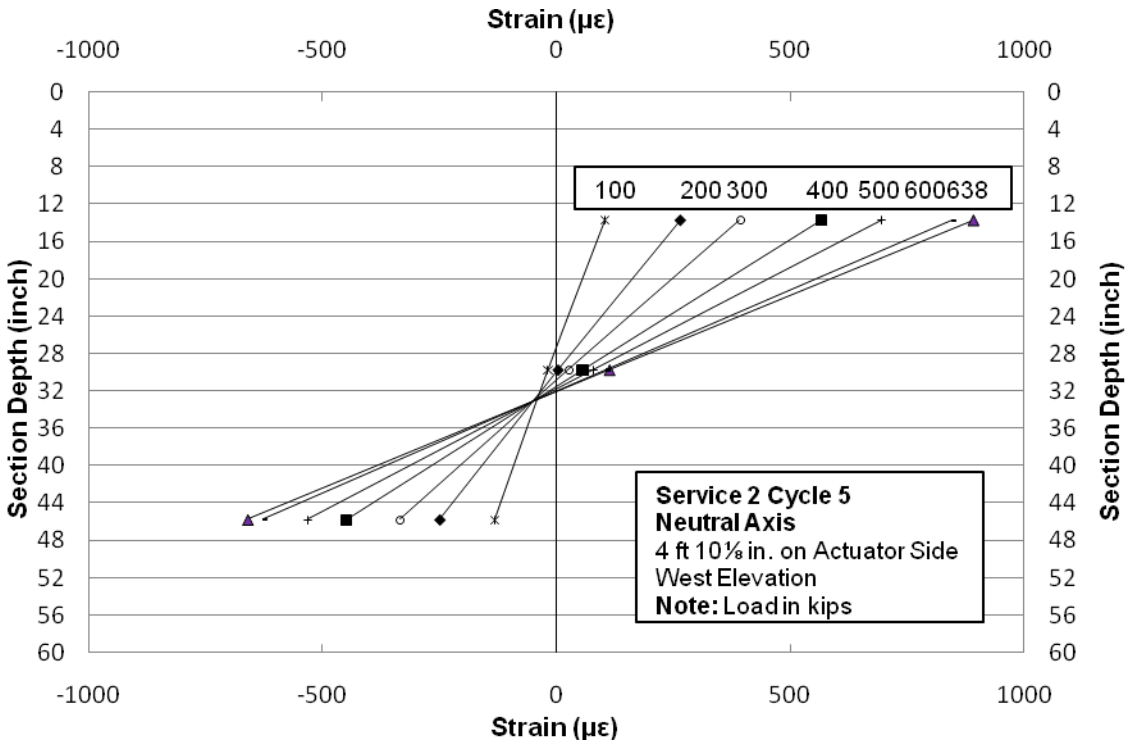


**Figure E.71** Neutral Axis on Actuator Side (West Elevation)

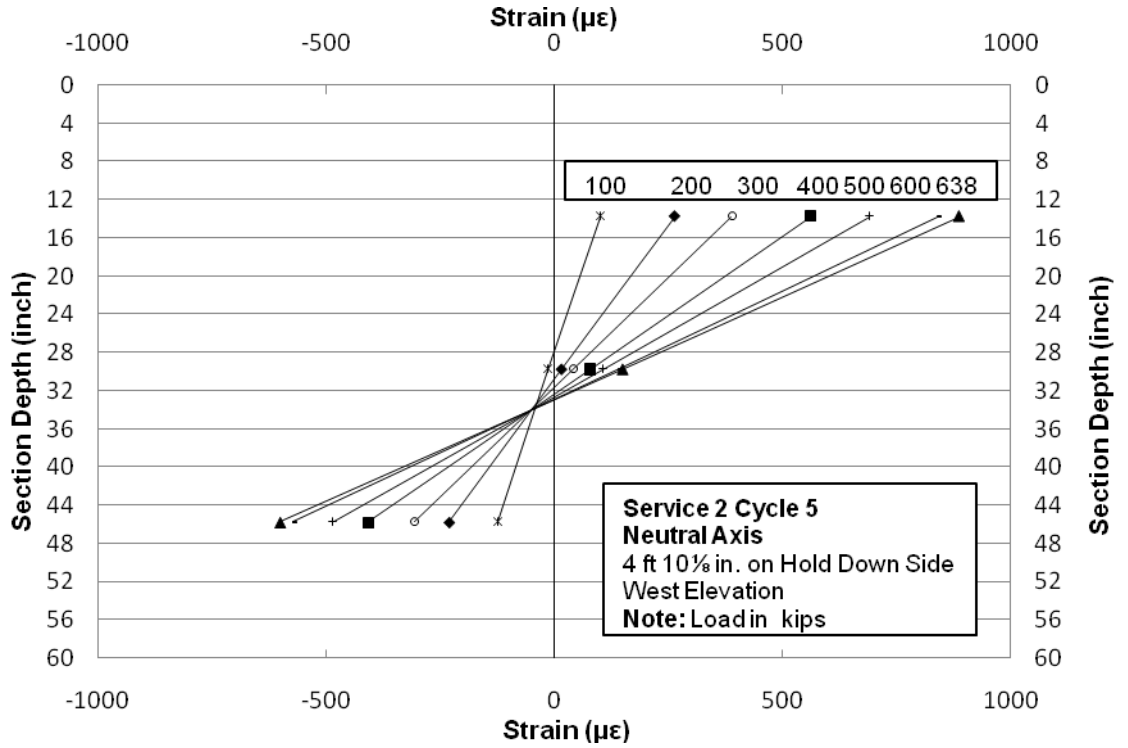


**Figure E.72** Neutral Axis on Actuator Side (West Elevation)

**Table E.2** Initial Data Points for Service Load Tests

| Channels | Service I (1st Cycle) | Service II (1st Cycle) | Service I (5th Cycle) | Service II (5th Cycle) | Service III |
|---|---|---|---|---|---|
| LV_07 | -0.02906 | 0.709657 | -0.31504 | 0.065449 | -0.610507 |
| LV_08 | -0.033262 | 0.621176 | -0.27077 | 0.024974 | -0.520441 |
| LV_09 | -0.013791 | 0.346909 | -0.1505 | 0.027821 | -0.292689 |
| LV_10 | -0.00187 | 0.277385 | -0.13166 | 0.006674 | -0.220715 |
| LV_11 | -0.001141 | 0.053552 | -0.04729 | 0.019979 | -0.069867 |
| LV_12 | 0.000236 | 0.025367 | -0.02328 | 0.010666 | -0.039821 |
| LV_13 | 0.00742 | -0.150068 | -0.01042 | 0.101018 | -0.012711 |
| LV_14 | 0.005004 | -0.170289 | 0.015432 | 0.080509 | 0.037238 |
| LV_18 | -0.016049 | 0.552232 | -0.25832 | 0.070296 | -0.508897 |
| LV_19 | -0.004488 | 0.321068 | -0.1475 | 0.022747 | -0.260648 |
| LV_20 | 0.001112 | 0.152951 | -0.07518 | -0.00645 | -0.123228 |
| LV_21 | -0.000557 | 0.0767 | -0.04823 | 0.005362 | -0.072559 |
| LV_22 | -0.000339 | 0.064771 | -0.03831 | -0.00011 | -0.057155 |
| LV_A | -0.001386 | 0.053452 | -0.04397 | 0.014676 | -0.062756 |
| LV_B | 0.000187 | 0.028259 | -0.02247 | 0.00733 | -0.037233 |
| LV_C | -0.001192 | 0.043145 | -0.04195 | 0.017987 | -0.059054 |
| LV_D | 0.000262 | 0.016753 | -0.01823 | 0.009142 | -0.029704 |
| LV_23 | -0.000125 | 0.02315 | -0.04117 | 0.106695 | -0.137989 |
| LV_24 | 0.000153 | -0.001338 | -0.0172 | 0.103119 | -0.110947 |
| LV_25 | 0.003396 | -0.07467 | -0.00665 | 0.045685 | -0.003416 |
| LV_26 | 0.006931 | -0.162949 | 0.003012 | 0.09825 | 0.003082 |
| LV_27 | 0.011526 | -0.249371 | 0.005353 | 0.153345 | 0.002694 |
| LV_28 | 0.014039 | -0.289422 | -0.01162 | 0.193874 | -0.019266 |
| LV_29 | 0.014408 | -0.319495 | 0.014512 | 0.192234 | 0.009789 |
| LV_30 | 0.000631 | 0.005339 | -0.00553 | -0.0021 | -0.00077 |
| LV_31 | 0.000535 | -0.00188 | 0.00205 | -0.00307 | 0.006329 |
| LV_32 | 0.000656 | -0.000791 | 0.000601 | -0.00131 | 0.002272 |
| LV_33 | 0.000484 | -0.0005 | -0.00086 | -0.00031 | 0.001905 |
| LV_34 | 0.00017 | -0.000576 | 0.000192 | 0.000245 | 0.000645 |
| LV_35 | 0.000139 | -0.000618 | 0.000311 | -0.00051 | 0.001305 |
| LV_36 | 0.000174 | -0.000541 | 0.000381 | -0.00024 | 0.000855 |
| LV_37 | -0.000214 | -0.000862 | 0.000886 | 0.000058 | 0.001063 |
| LV_38 | 0.000263 | -0.001196 | 0.000839 | 0.000072 | 0.000825 |
| SG_57A | 1.747673 | 57.453696 | 50.6624 | 149.9607 | 143.6403 |
| SG_57B | -0.417489 | 182.686514 | 180.9806 | 212.7629 | 205.40161 |
| SG_58A | 0.523307 | 49.355084 | 45.86604 | 132.733 | 127.23938 |
| SG_58B | 1.854485 | 28.665419 | 22.59084 | 62.92316 | 55.439932 |
| SGSPARE_1A | 3.347566 | 101.692943 | 94.04238 | 237.6522 | 230.85683 |

| | | | | | |
|---|---|---|---|---|---|
| SGSPARE_1B | 3.609177 | 19.475737 | 7.684594 | 212.2119 | 208.83535 |
| SG_59A | 3.630337 | 64.54109 | 60.6091 | 195.2031 | 188.28883 |
| SG_59B | 2.455307 | 26.314714 | 16.37947 | 178.4489 | 172.99986 |
| SG_60A | 3.349256 | 85.281649 | 75.19828 | 735.3305 | 747.89195 |
| SG_60B | 6.093487 | 12.445681 | 0.36586 | 356.4892 | 358.7302 |
| SG_61A | 2.552306 | -4.225651 | -11.1422 | 53.87867 | 48.285478 |
| SG_61B | 0.18913 | -67.243686 | -75.4633 | -66.752 | -62.64844 |
| SG_62A | -1.640996 | 188.511853 | 189.1862 | 245.4965 | 240.78849 |
| SG_62B | 0.01579 | 212.211233 | 206.7457 | 303.7192 | 300.0917 |
| SGSPARE_2A | 0.243964 | 205.216015 | 200.6816 | 267.8509 | 264.25566 |
| SGSPARE_2B | 1.001432 | -80.582985 | -88.0025 | -38.6315 | -41.87467 |
| SGSPARE_3A | -0.626654 | 18.419453 | 15.88245 | 71.49119 | 67.445445 |
| SGSPARE_3B | 2.616272 | -122.935123 | -131.313 | -64.0946 | -40.72792 |
| SG_63A | -0.092187 | 129.745294 | 123.1137 | 180.8688 | 182.52371 |
| SG_63B | -1.245363 | 35.756732 | 32.36981 | 88.14323 | 85.956662 |
| SG_64A | 0.53525 | 33.735715 | 30.35 | 106.8149 | 102.30628 |
| SG_64B | 0.36613 | -104.777706 | -114.181 | -8.92591 | -13.35094 |
| SG_65A | 1.844874 | 154.797526 | 147.6163 | 312.9003 | 310.69919 |
| SG_65B | -2.335328 | -19.651019 | -28.8264 | -1.89327 | 3.847191 |
| SG_66A | 0.648652 | 179.840815 | 173.8448 | 327.0604 | 323.4958 |
| SG_66B | -0.179104 | 216.585259 | 212.0237 | 382.0049 | 377.92141 |
| SGSPARE_4A | -0.8031 | 203.762061 | 202.1337 | 352.1077 | 348.61019 |
| SGSPARE_4B | 0.235819 | 97.599544 | 90.5993 | 239.0195 | 235.72027 |
| SG_67A | -0.847707 | 367.14749 | 366.7877 | 444.988 | 438.4414 |
| SG_67B | -0.496959 | 174.09408 | 165.0536 | 471.526 | 462.32853 |
| SG_68A | 1.368349 | 301.280436 | 296.7691 | 397.1331 | 388.84703 |
| SG_68B | 0.235858 | 107.058126 | 106.5346 | 256.9715 | 249.58298 |
| SG_69 | 0.382463 | 78.261094 | 76.45246 | 142.9667 | 140.13049 |
| SG_70 | -1.243063 | 85.33699 | 83.49322 | 135.4244 | 133.26471 |
| SG_71 | 1.309569 | 100.107924 | 96.58267 | 183.8512 | 180.8993 |
| SG_72 | 0.163362 | 98.594064 | 95.91288 | 167.2058 | 166.09528 |
| SG_73 | 1.564142 | 119.239278 | 113.8496 | 353.7399 | 353.20324 |
| SG_74 | 0.851056 | 102.501903 | 98.70391 | 250.8361 | 249.76778 |
| SG_75 | 1.367228 | 95.344205 | 91.59637 | 161.651 | 157.77668 |
| SG_76 | 3.28712E-07 | 84.281823 | 80.25425 | 143.0769 | 140.79134 |
| SG_77 | 0.066782 | 74.767632 | 72.12115 | 115.2102 | 113.26294 |
| SG_78 | -1.153396 | 48.530935 | 46.97862 | 78.40454 | 76.498729 |
| SG_79 | 0.766502 | 84.312931 | 82.50204 | 149.2381 | 146.80857 |
| SG_80 | 0.069383 | 53.111715 | 56.87139 | 88.6531 | 86.337852 |
| SG_81 | -2.11981 | 33.039369 | 37.2226 | 48.25417 | 48.644781 |
| SG_82 | -3.003104 | 9.658963 | 14.80855 | 1.400781 | 4.465201 |

| | | | | | |
|---|---|---|---|---|---|
| SG_83 | -14.431599 | -31.401249 | -19.2981 | -69.4484 | -66.12668 |
| SG_84 | -5.566107 | -40.310335 | -31.4372 | -86.3236 | -79.01289 |
| SG_85 | 1.106957 | 80.775288 | 77.20043 | 133.3104 | 130.8134 |
| SG_86 | -1.050056 | 47.012512 | 48.24317 | 72.80644 | 71.645143 |
| SG_87 | -3.299619 | 24.42849 | 27.77694 | 29.65967 | 28.933114 |
| SG_88 | -4.325561 | 7.932192 | 10.87663 | -3.08085 | -0.850456 |
| SG_89 | -7.591325 | -18.569186 | -10.6432 | -49.5152 | -45.46107 |
| SG_90 | -6.412299 | -36.578529 | -27.7776 | -77.1277 | -71.45237 |
| SG_91 | -0.697975 | 82.713005 | 82.8139 | 135.0318 | 133.31637 |
| SG_92 | -1.797857 | 52.816038 | 55.76337 | 80.22626 | 78.831409 |
| SG_93 | -3.308647 | 25.981799 | 33.30469 | 29.22379 | 28.384905 |
| SG_94 | -3.583514 | 5.760448 | 13.89868 | -8.60898 | -7.137961 |
| SG_95 | -4.782723 | -19.477666 | -9.98553 | -53.804 | -51.59337 |
| SG_96 | -4.749062 | -42.680649 | -30.2998 | -91.6715 | -88.72792 |
| SG_97 | -0.038491 | 74.678986 | 72.44487 | 121.339 | 119.33191 |
| SG_98 | -2.602556 | 46.008157 | 47.3222 | 72.71294 | 71.891618 |
| SG_99 | -2.008513 | 24.109745 | 28.76057 | 31.52458 | 32.048355 |
| SG_100 | -2.28287 | 3.822432 | 11.09854 | -6.04672 | -4.215151 |
| SG_101 | -4.562342 | -19.322755 | -8.76256 | -41.4625 | -38.86198 |
| SG_102 | -5.299873 | -42.666158 | -30.2908 | -78.8463 | -72.9801 |
| SG_103 | -1.722756 | -3.087017 | 1.640273 | 4.67022 | 8.962871 |
| SG_104 | -0.262547 | 14.945143 | 12.49717 | 32.72821 | 33.736611 |
| SG_105 | -1.270032 | 8.995147 | 9.544845 | 0.053052 | -2.84878 |
| SG_106 | -2.124715 | 1.906704 | 0.487641 | 14.89132 | 15.065482 |
| SG_107 | -2.329382 | -36.991288 | -33.6611 | -62.471 | -66.87271 |
| SG_108 | -0.673914 | -21.535188 | -19.538 | -26.9082 | -29.33056 |
| SG_109 | -2.595421 | -16.239774 | -14.4428 | -24.6855 | -27.19478 |
| SG_111 | -3.719608 | -32.389859 | -29.2101 | -6.20576 | 4.927401 |
| SG_112 | -1.720775 | 12.120136 | 11.77957 | -6.97045 | -9.951887 |
| SG_113 | -3.976731 | -8.088796 | -1.95261 | -14.4739 | -10.13205 |
| SG_114 | -6.882731 | -22.797485 | -11.367 | -30.6494 | -21.94276 |
| SG_115 | -1.675058 | -13.262242 | -10.9927 | -48.2869 | -48.34364 |
| SG_116 | -1.53153 | -8.596186 | -5.61264 | -33.7884 | -34.26148 |
| SG_117 | -3.193726 | -13.626966 | -7.85528 | -19.2914 | -13.77205 |
| SG_118 | -4.117074 | -85.814309 | -72.1412 | -462.865 | -458.0002 |
| SG_119 | -3.131773 | -40.866735 | -39.5036 | -665.693 | -664.3 |
| SG_120 | -4.195221 | -127.168894 | -113.537 | -741.542 | -735.5653 |
| SG_121 | -1.480833 | 1.853416 | 1.499783 | 11.30058 | 11.546864 |
| SG_122 | -2.235646 | 11.895678 | 12.19823 | 5.138812 | 4.275301 |
| SG_123 | -3.726559 | -78.100421 | -67.2844 | -508.549 | -503.7098 |
| SG_124 | -2.86257 | -36.327308 | -28.7964 | -792.499 | -800.9364 |

| | | | | | |
|---|---|---|---|---|---|
| SG_125 | -2.547269 | -113.017216 | -102.748 | -673.491 | -668.3661 |
| SG_126 | -3.90161 | -12.58715 | -7.15398 | -19.5203 | -13.84774 |
| SG_127 | -2.534658 | -13.124569 | -12.2647 | -45.8222 | -45.85385 |
| SG_128 | -0.732466 | -9.071911 | -8.492 | -27.5468 | -27.37029 |
| SG_129 | 0.930354 | 89.382546 | 87.57516 | 154.651 | 152.36431 |
| SG_130 | -1.467174 | 30.139356 | 35.00061 | 41.31079 | 41.533199 |
| SG_131 | -14.341127 | -37.043772 | -25.648 | -93.2869 | -91.39099 |
| SG_132 | 1.075721 | 81.618856 | 77.99239 | 136.8751 | 135.34697 |
| SG_133 | -3.159799 | 19.298192 | 25.01124 | 24.28124 | 23.563929 |
| SG_134 | -5.67092 | -20.026986 | -13.5177 | -53.1553 | -50.07513 |
| SG_135 | -1.17232 | 74.743107 | 77.66804 | 118.6189 | 114.51603 |
| SG_136 | -3.664359 | 19.772516 | 29.33554 | 17.36592 | 14.197347 |
| SG_137 | -4.951793 | -27.549183 | -16.6182 | -75.1296 | -74.64803 |
| SG_138 | 0.451233 | 71.490553 | 69.5201 | 116.6669 | 114.83611 |
| SG_139 | -2.914473 | 24.054132 | 28.70711 | 27.19218 | 27.516811 |
| SG_140 | -2.929629 | -16.813591 | -8.9524 | -48.6691 | -45.26498 |
| CR_01 | 0.00351 | -0.053773 | -0.05065 | -0.07009 | -0.072711 |
| CR_02 | 0.002562 | 0.030676 | 0.032899 | 0.037326 | 0.031362 |
| CR_03 | -0.000399 | -0.009437 | -0.01115 | -0.02734 | -0.03465 |
| CR_04 | 0.002906 | -0.051173 | -0.04805 | -0.05679 | -0.063185 |

# APPENDIX F

Ultimate Load Test Results

## F.1 Deflection

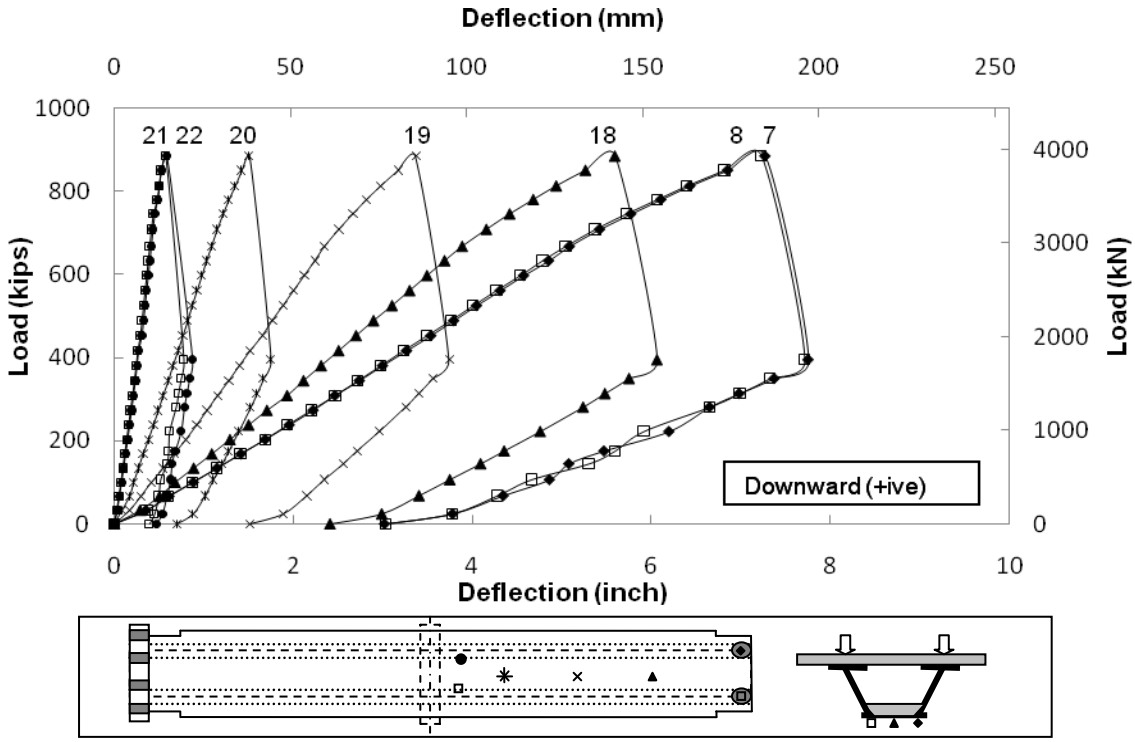


**Figure F.1** Deflection of Bottom Flange on Actuator Side

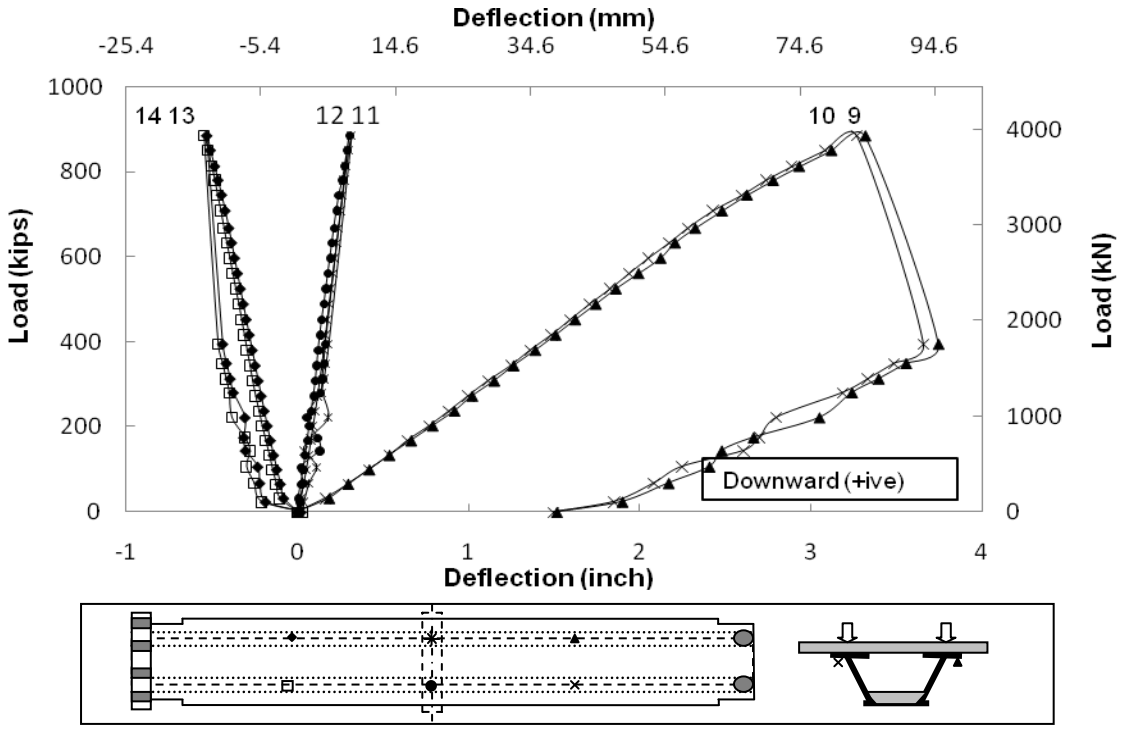


**Figure F.2** Deflection of Top Flange on Actuator Side

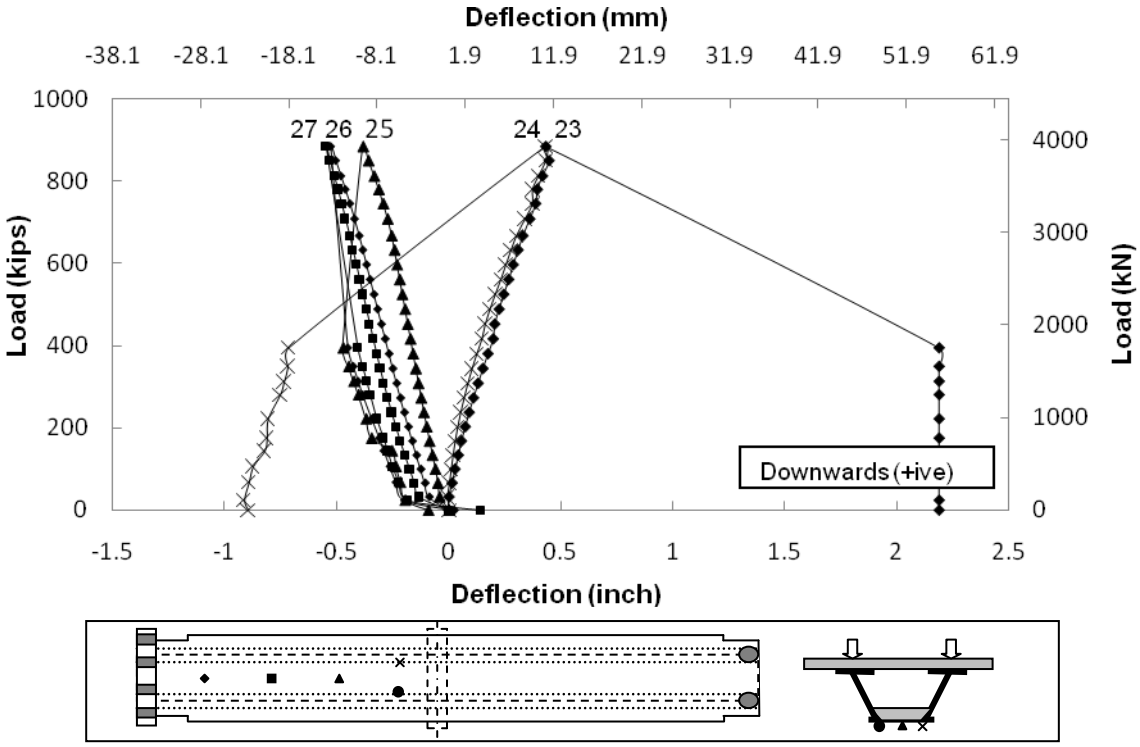


**Figure F.3** Deflection of Bottom Flange on Hold Down Side

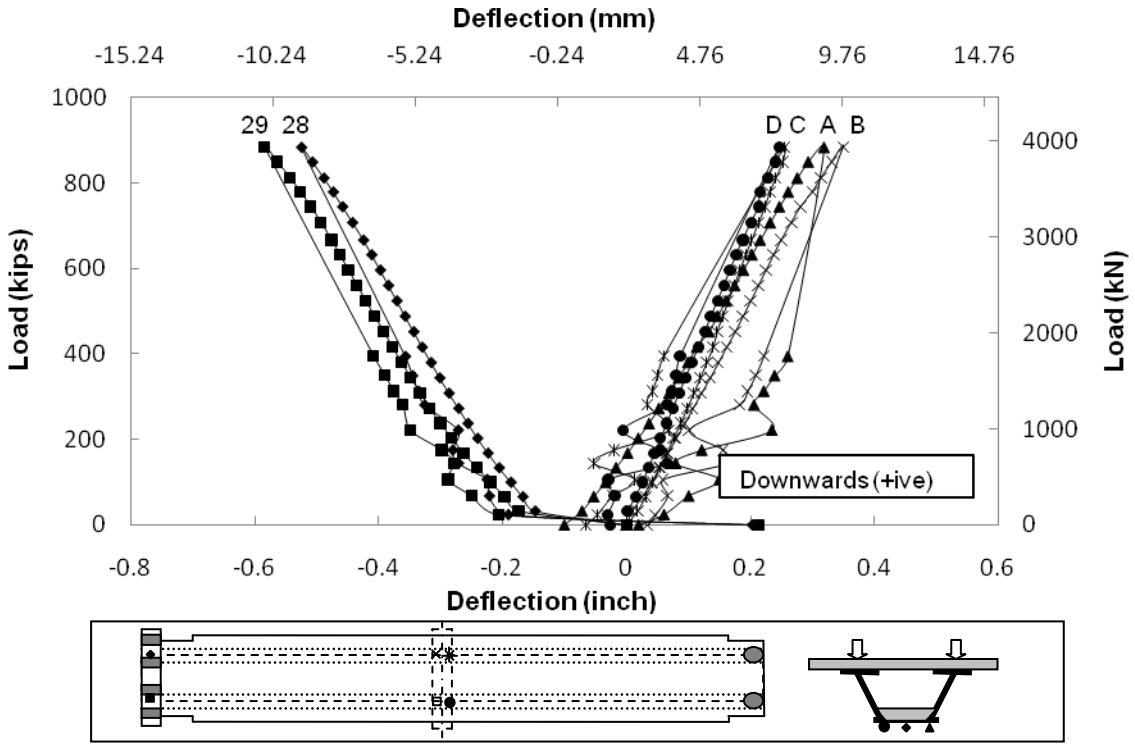


**Figure F.4** Deflection at Hold Down End and Center Support

## F.2 Slip

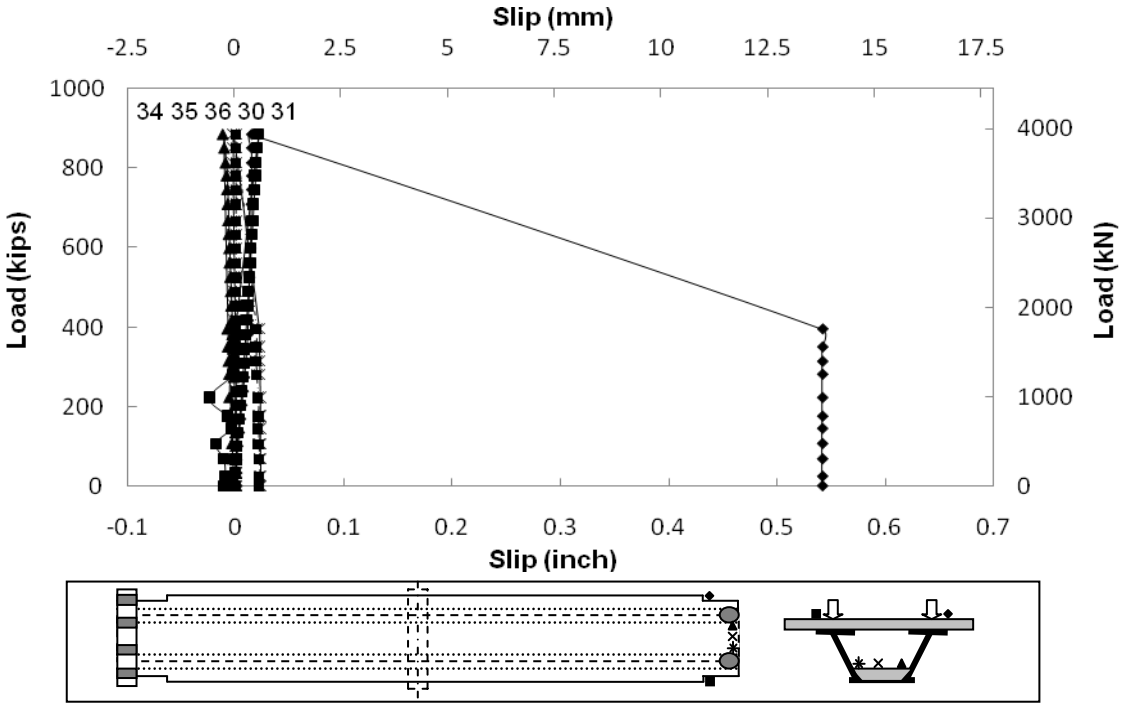


**Figure F.5** Slip at Actuator End

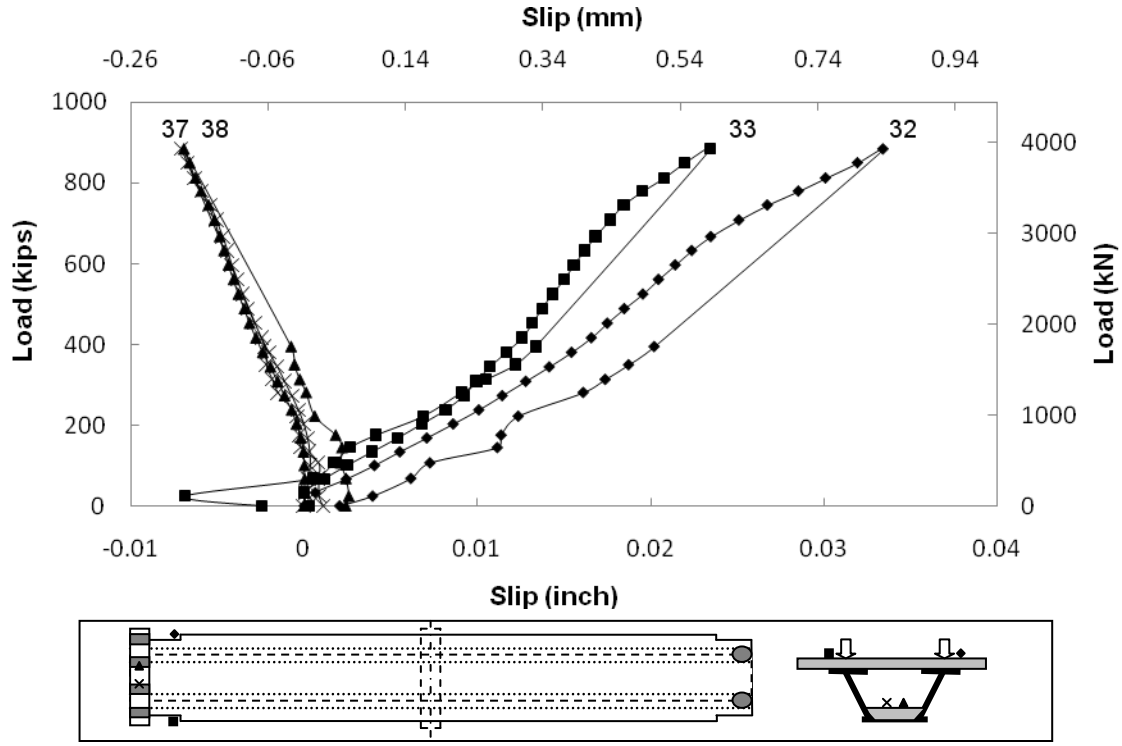


**Figure F.6** Slip at Hold Down End

## F.3 Strain in Top Slab Rebars

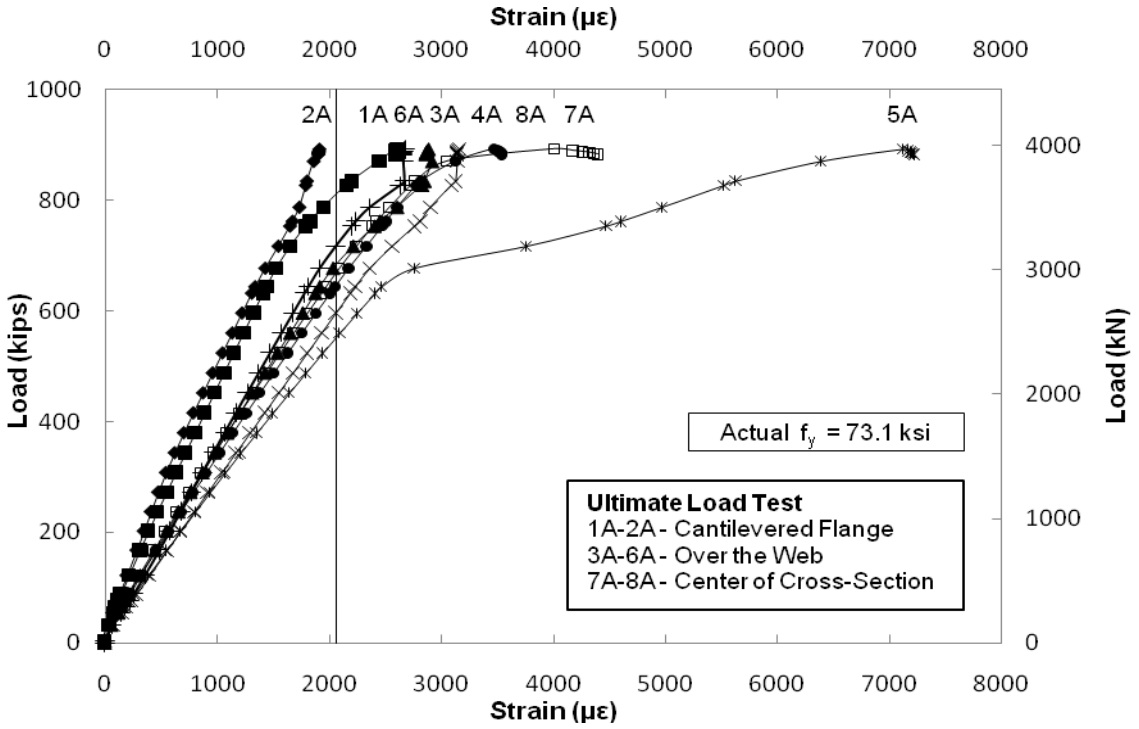


**Figure F.7** Strain in Rebars on Actuator Side

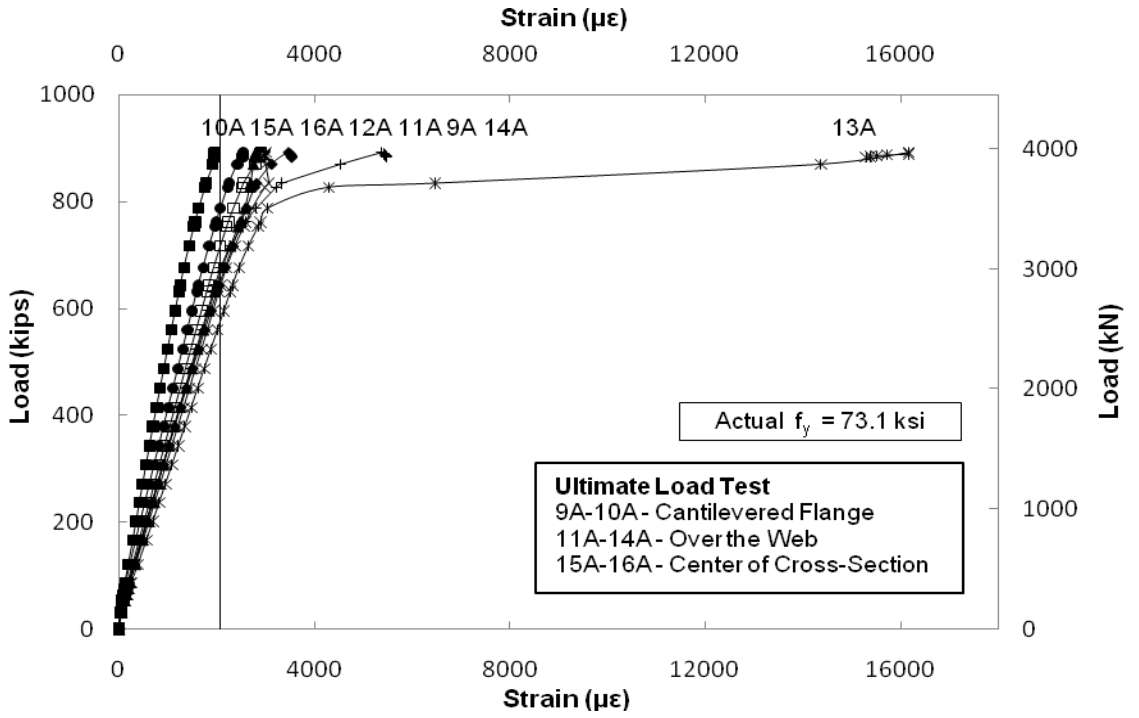


**Figure F.8** Strain in Rebars on Actuator Side

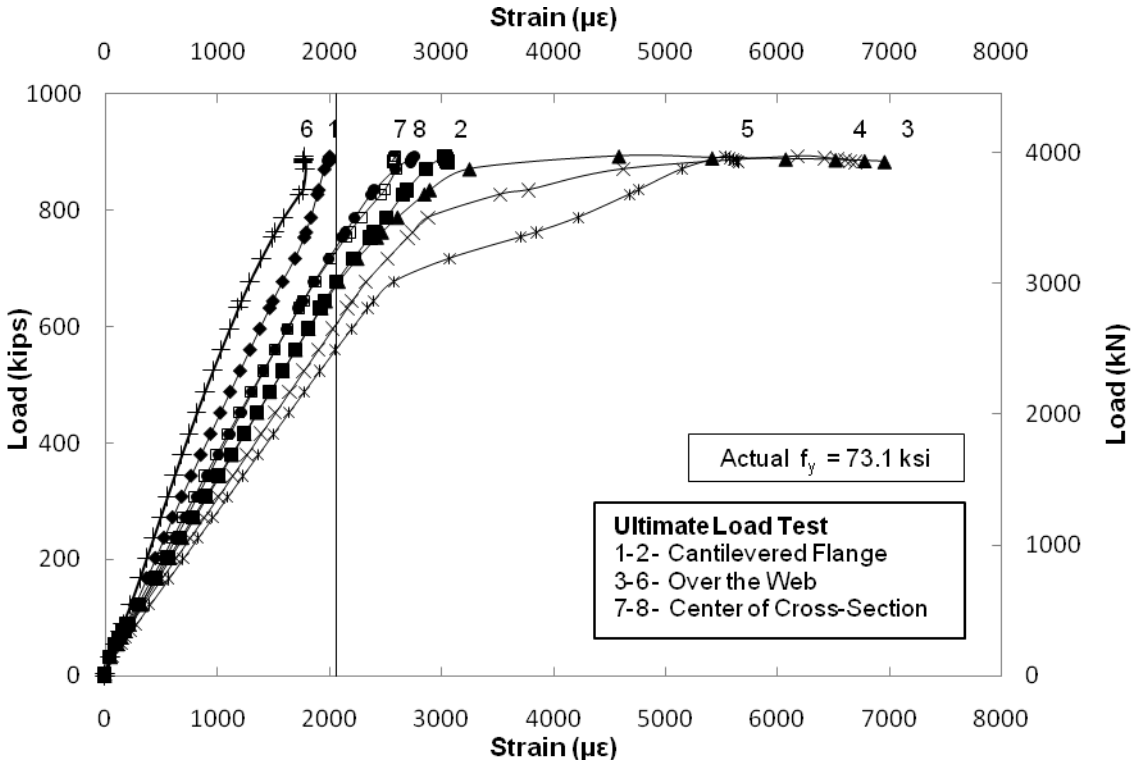


**Figure F.9** Strain in Rebars on Hold Down Side

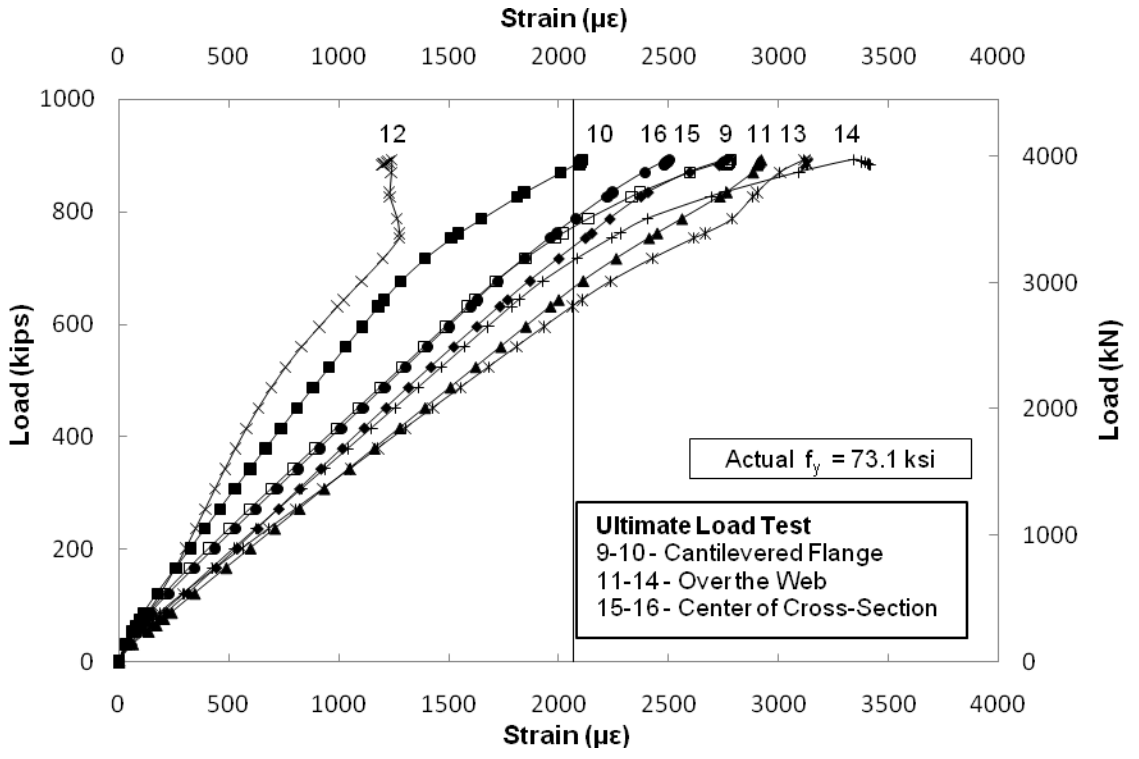


**Figure F.10** Strain in Rebars on Hold Down Side

## F.4 Strain in Steel

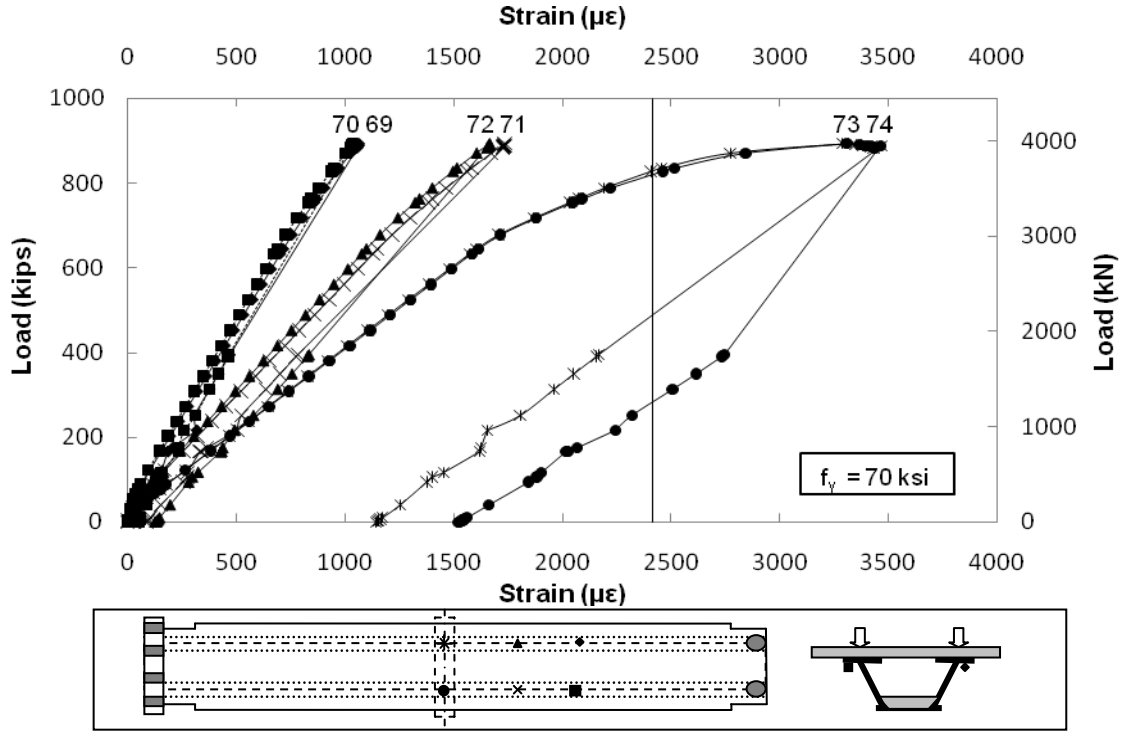


**Figure F.11** Strain in Top Flange on Actuator Side

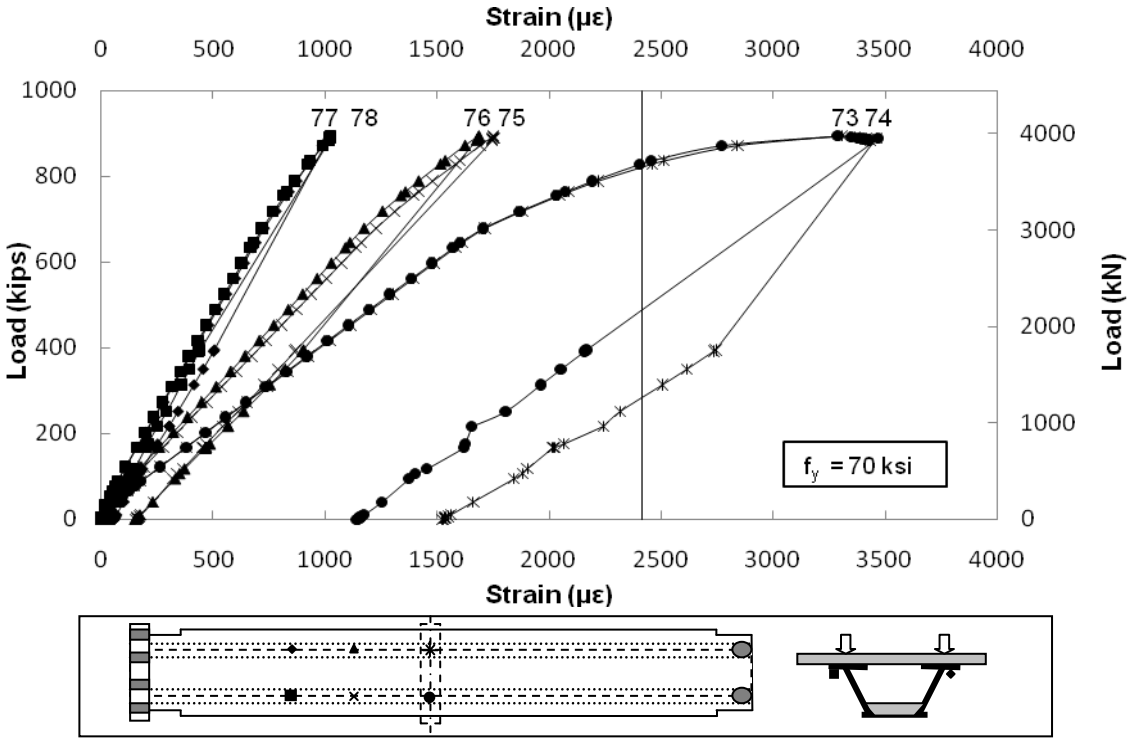


**Figure F.12** Strain in Top Flange on Hold Down Side

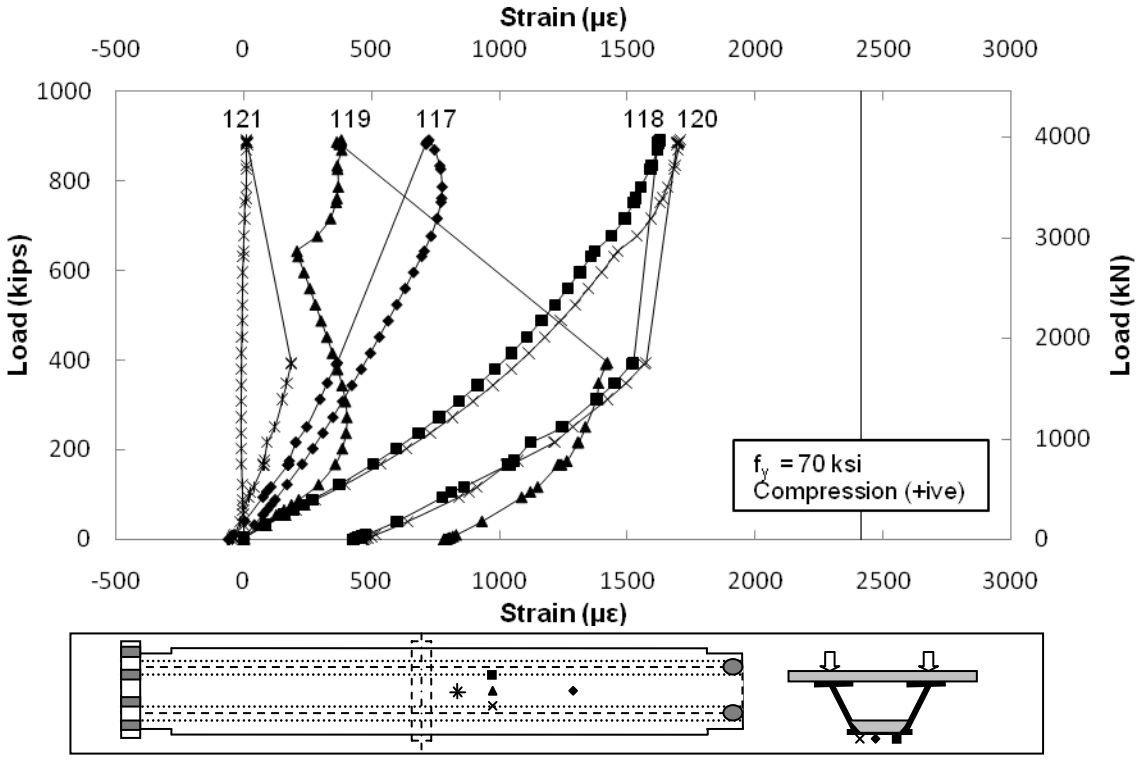


**Figure F.13** Strain in Bottom Flange on Actuator Side

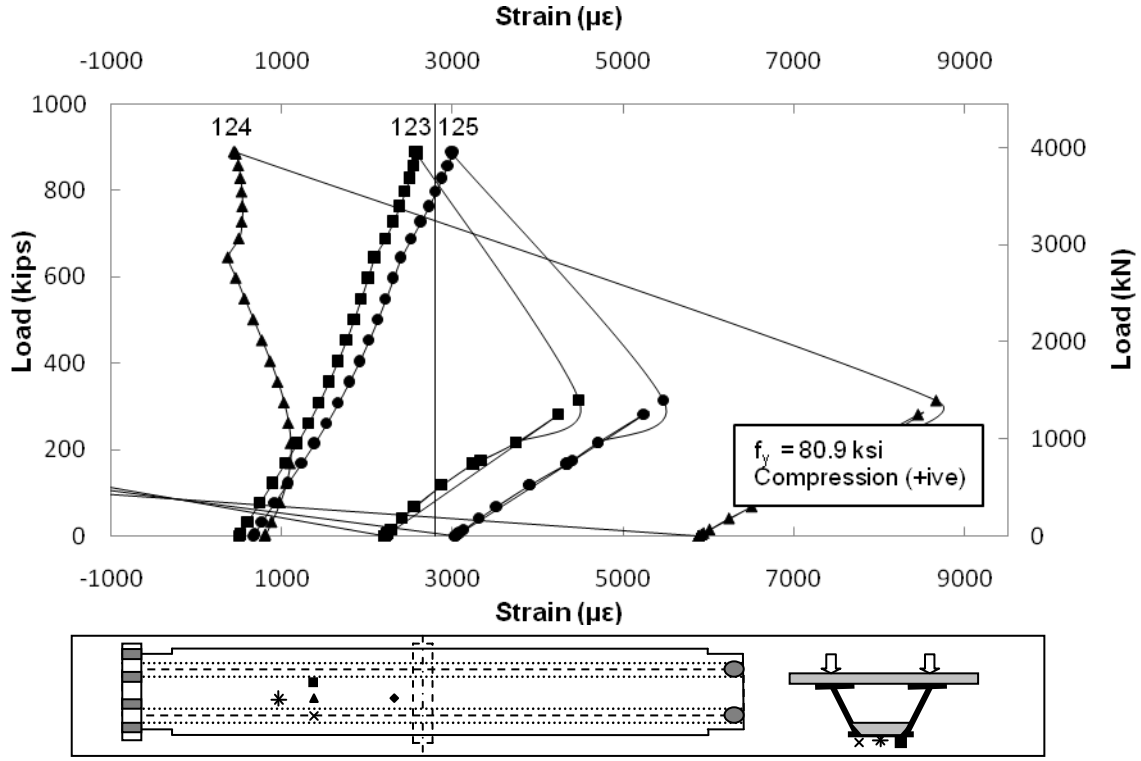


**Figure F.14** Strain in Bottom Flange on Hold Down Side

## F.5 Strain in Concrete

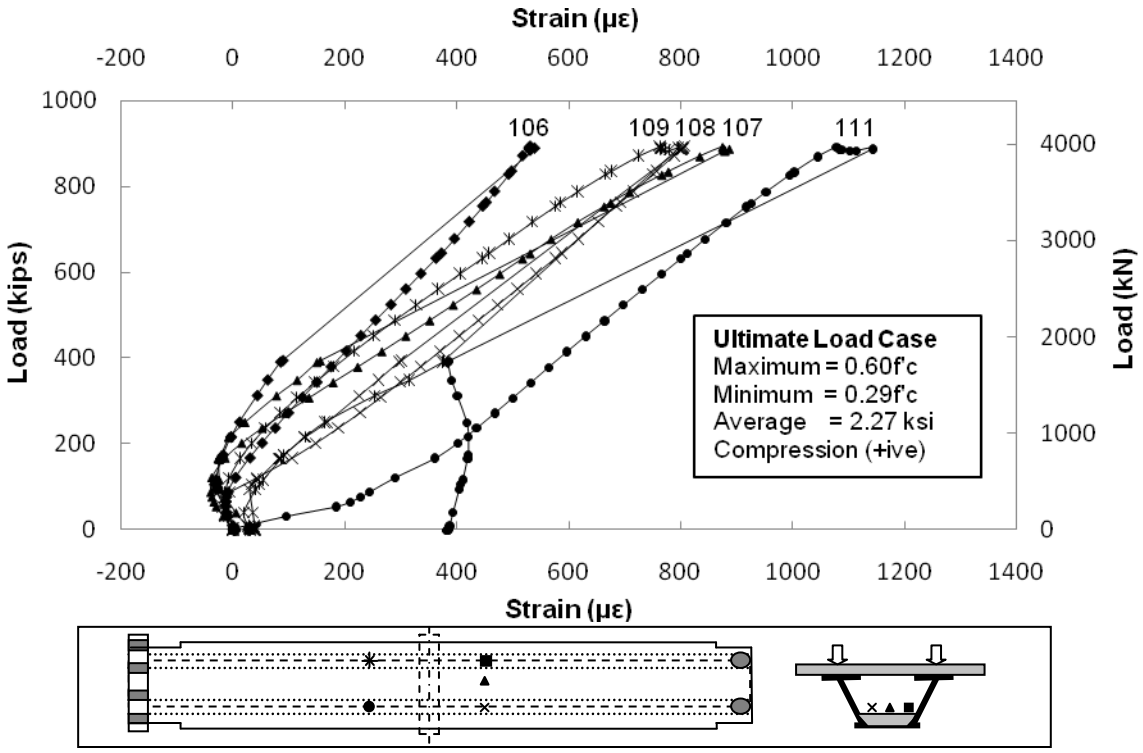


**Figure F.15** Strain in Bottom Concrete Slab

## F.6 Crack Width on Top Slab

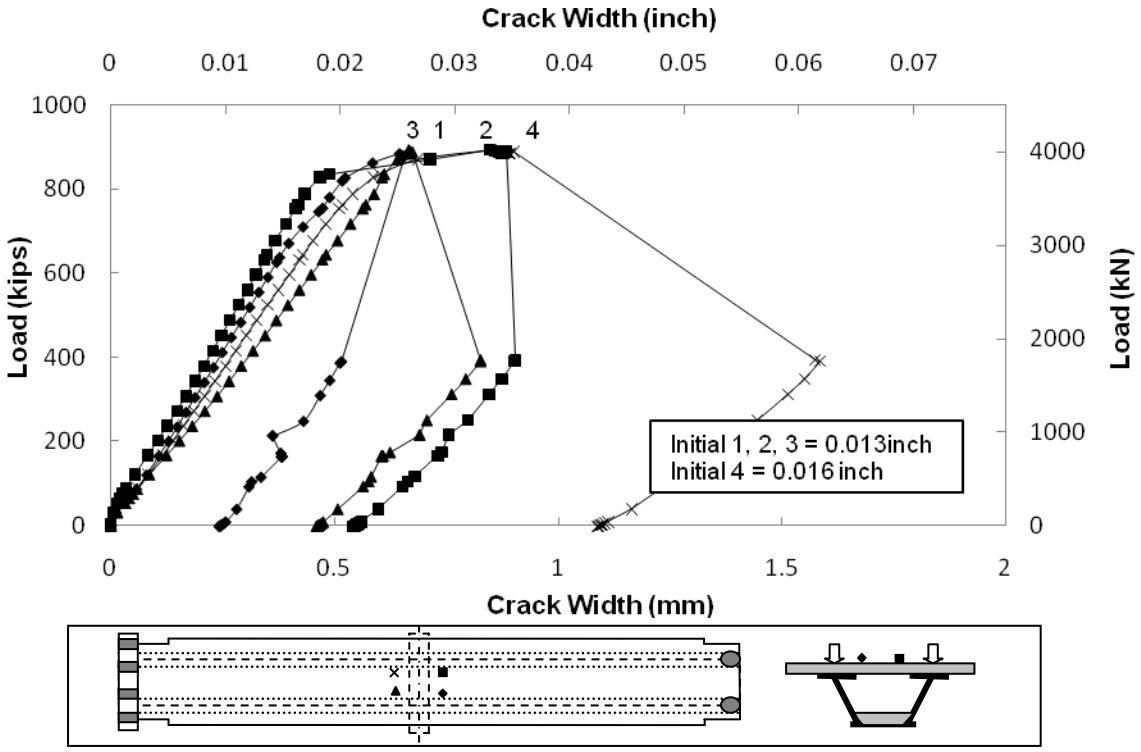


**Figure F.16** Crack Width on Top Slab

## F.6 Neutral Axis

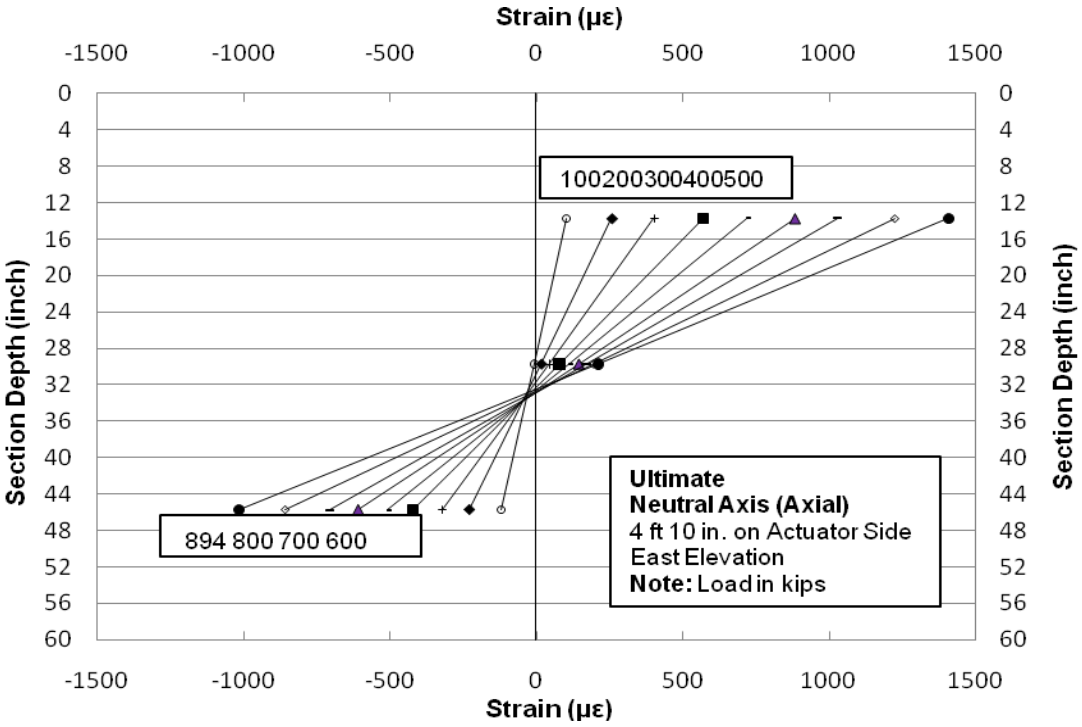


**Figure F.17** Neutral Axis on Actuator Side (East Elevation)

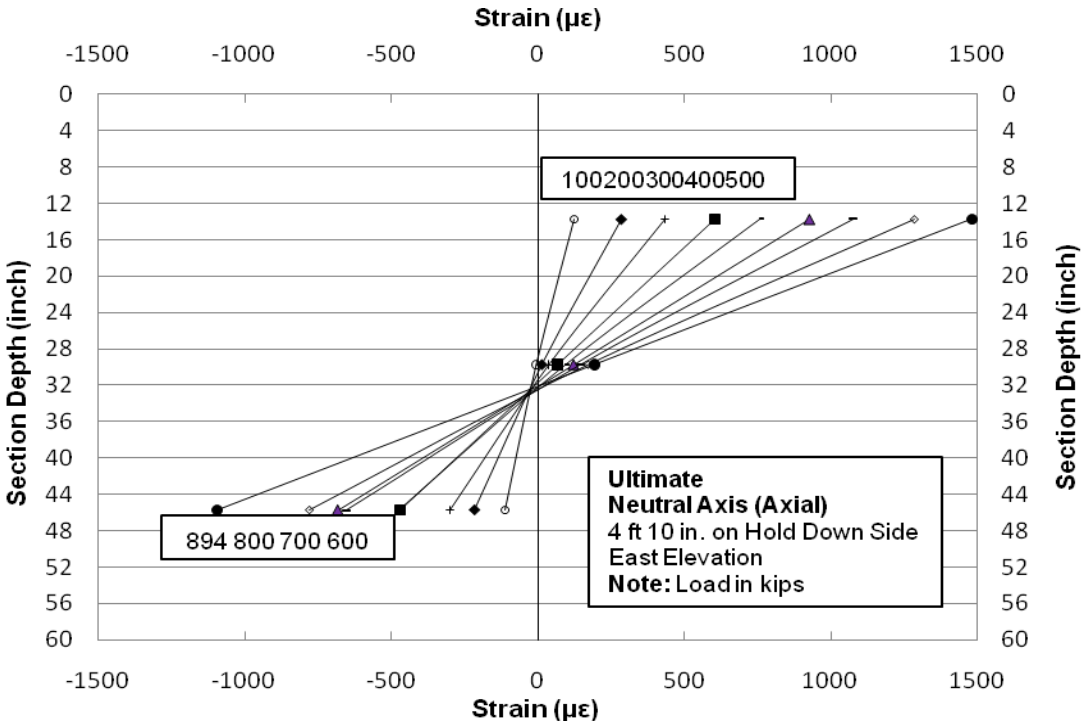


**Figure F.18** Neutral Axis on Hold Down Side (East Elevation)

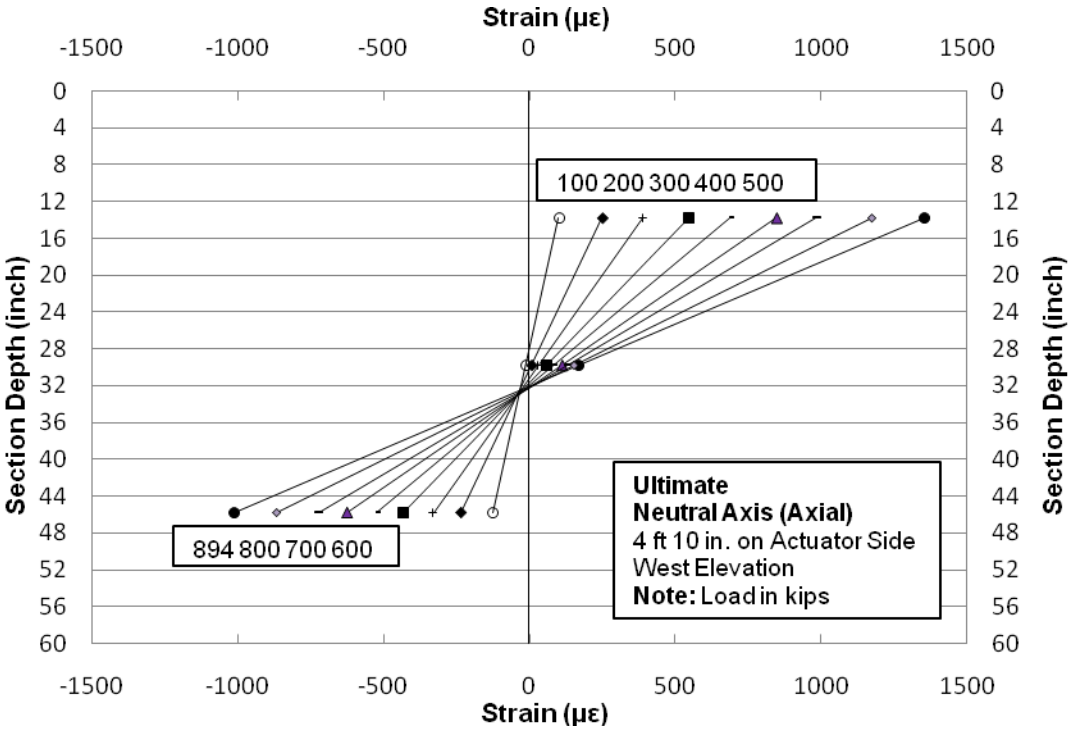


**Figure F.19** Neutral Axis on Actuator Side (West Elevation)

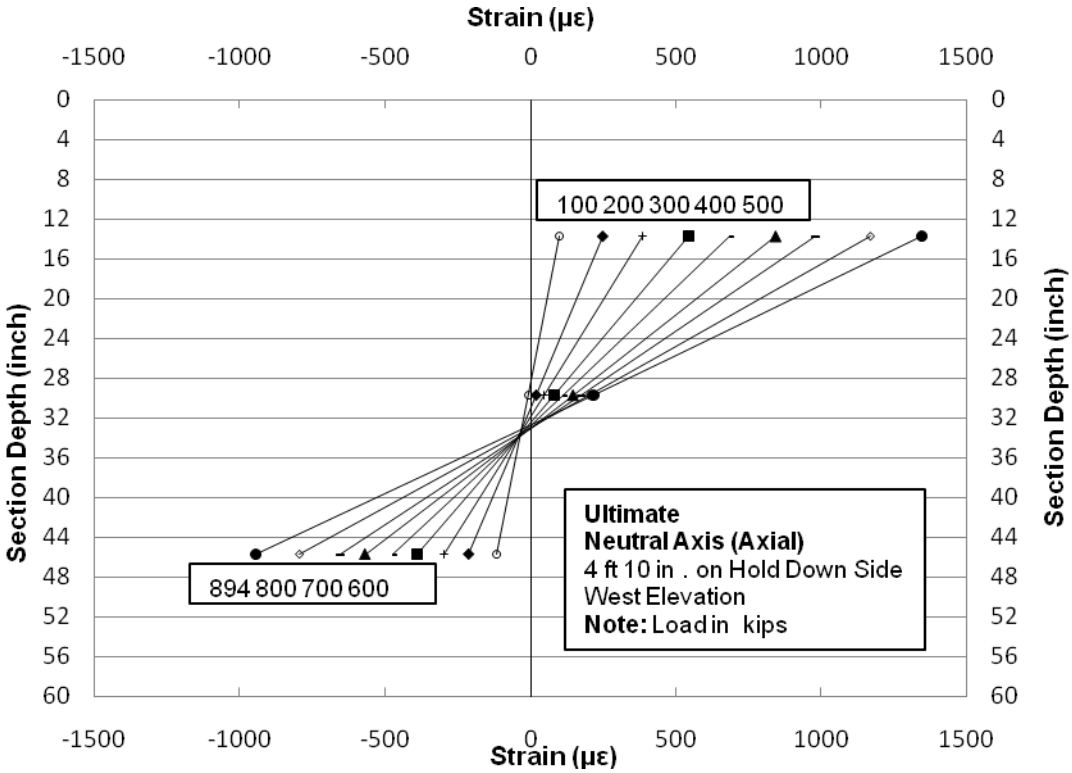


**Figure F.20** Neutral Axis on Hold Down Side (West Elevation)

# Appendix G

Double Composite Box Girder Design Example

## Description

A Model design of double composite box girder bridge is presented in this Appendix. The double composite box girder section was designed using *Load and Resistance Factored Design* (LRFD) method of *AASHTO LRFD Bridge Design Specifications, 3rd Edition, 2004* and *Florida Structures Design Guidelines, January 2005*.

Design calculations of a three span continuous box girder bridge with double composite action are presented herein. The span arrangement consists of 190 ft – 236 ft – 190 ft span lengths. Specifically this example illustrates the flexure design at interior pier section (i.e. region of maximum negative moment), including flexural design of the double composite section, shear design of the webs, and design of shear connectors.

This design is based on the results gathered from experimental testing of a full-scale box girder test specimen. New design guidelines were developed for the design of such box girder sections after evaluations of the test results. These guidelines were used in this example.

For this example, only the section for maximum negative flexure is considered, including composite action provided by the steel bottom flange and concrete bottom slab. The stress in the bottom slab was limited to 0.6f'c for strength design. The section is designed and checked for the LRFD Strength I limit state.

Construction sequence plays a critical role in determining the ultimate stresses experienced by the double composite section. For this, example the steel box section is cured is erected first followed by the pouring of the bottom concrete slab. Once the bottom slab is cured, normal construction procedures are followed, including the placement of the concrete deck and traffic barriers. Temporary bracing will be used to support the bottom flange until the bottom slab cures. Stress due to self-weight of the bottom flange and slab shall be limited to 20 ksi and a deflection limit of L/360 shall be met at all times.

This example contains the following sections.

# THREE-SPAN CONTINUOUS BOX GIRDER BRIDGE WITH DOUBLE COMPOSITE ACTION

# DESIGN OF NEGATIVE FLEXURE SECTION

## G.1 Given Requirements

| | |
|---|---|
| Number of girders | $N_g := 2$ |
| Number of spans | $N_{sp} := 3$ |
| Number of design lanes | $N_L := 3$ |
| Length of middle span | $L_2 := 236\ ft$ |
| Length of side span (equal length) | $L_1 := 190\ ft$ |
| Girder spacing | $GS := 11.375\ ft$ |
| Roadway width | $RW := 40\ ft$ |
| Concrete deck thickness (structural) | $T_{ts} := 9\ in$ |
| Concrete deck overhang | $OH_c := 4.5\ ft$ |
| Haunch thickness | $t_h := 3\ in$ |
| Reinforcement Ratio | $R_r := 0.01$ |

## G.2 Materials

This section provides the information about the materials used in the design of box girder bridge

### Concrete

Compressive strength of concrete, $f_c$ — $f_c := 6500\ psi$

Unit weight of reinforced concrete, $\gamma_{rc}$ — $\gamma_{rc} := 150\ pcf$

Unit weight of concrete, $\gamma_c$ — $\gamma_c := 145$

**Note:** Unit weight of concrete is for calculation of Elastic modulus only

### Reinforcing steel

ASTM 615, Grade 60 (ksi) — $f_{yrebar} := 60\ ksi$

### Structural steel

ASTM A709, Grade 50 (ksi) — $f_y := 50\ ksi$

Unit weight of steel, $\gamma_s$ — $\gamma_s := 490\ pcf$

### Stay in place forms

Surface area density,$\gamma_{sip}$ — $\gamma_{sip} := 20\ psf$

### Future wearing surface

Surface area density, $\gamma_{ws}$ — $\gamma_{ws} := 21\ psf$

### Barrier

Weight per unit length — $m_{barr} := 0.581 klf$

Width of the barrier — $w_{barr} := 1.50\ ft$

Number of barriers — $n_b := 2$

## G.3 Geometry of the Box Girder Section

This section provides information on geometry of the cross-section and design parameters.

### G.3.1 Girder Geometry

Web Depth (plumb), $D_w$ $D_w := 70\ in$

(inclination to vertical is 14.03 deg) $\theta := 14.03\ deg$ $D := \frac{D_w}{\cos(\theta)}$

Web Depth (inclined), D $D = 72.152\ in$

Web plate thickness, $t_w$ $t_w := 0.75\ in$

Area of web plate, $A_w$ $A_w := 2D\ t_w$ $A_w = 108.229\ in^2$

Top flange thickness, $t_{tf}$ $t_{tf} := 2.65\ in$

Top flange width, $b_{tf}$ $b_{tf} := 25\ in$

Area of top flanges, $A_{tf}$ $A_{tf} := 2\ b_{tf}\ t_{tf}$ $A_{tf} = 132.5\ in^2$

Bottom flange thickness, $t_{bf}$ $t_{bf} := 1.00in$

Bottom flange width, $b_{bf}$ $b_{bf} := 100\ in$

Area of bottom flange, $A_{bf}$ $A_{bf} := b_{bf}\ t_{bf}$ $A_{bf} = 100\ in^2$

Height of girder, $H_G$ $H_G := t_{tf} + D_w + t_{bf}$ $H_G = 73.65\ in$

Top slab width, $b_{ts}$ $b_{ts} := 507\ in$

Top slab thickness, $t_{ts}$ $t_{ts} := 9\ in$

Bottom slab thickness, $t_{bs}$ $t_{bs} := 13\ in$

Bottom slab width, $b_{bs}$ $b_{bs} := \left(96\ in + \frac{t_{bs}}{4}\right)$ $b_{bs} = 99.25\ in$

Area of steel section, $A_{sec}$ $A_{sec} := A_{tf} + A_w + A_{bf}$ $A_{sec} = 340.729\ in^2$

### G.3.2 Design Parameters

Design concrete strength $f_c = 6.5\ ksi$

Modulus of Elasticity of concrete $E_c := 0.9\ 33\ (\gamma_c)^{1.5}\ \sqrt{f_c\ psi}$

(0.9 is a factor for florida's limerocks) $E_c = 4180.855\ ksi$

Yield strength of steel $f_y = 50\ ksi$

Modulus of Elasticity of steel $E_s := 29000\ ksi$

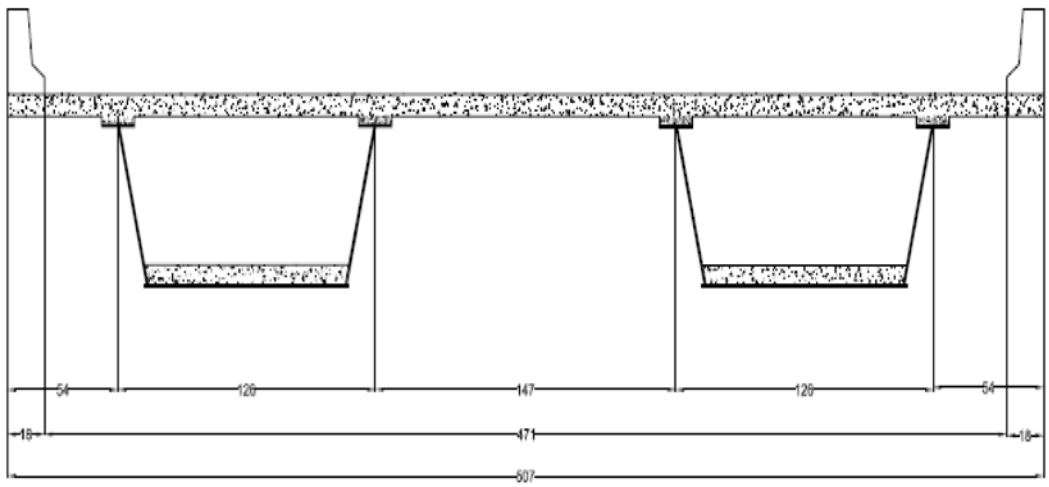


**NOTE:** All the dlmenslons are In Inches except as noted

**TYPICAL CROSS-SECTION OF DOUBLE COMPOSİTE BOX GİRDER BRİDGE**

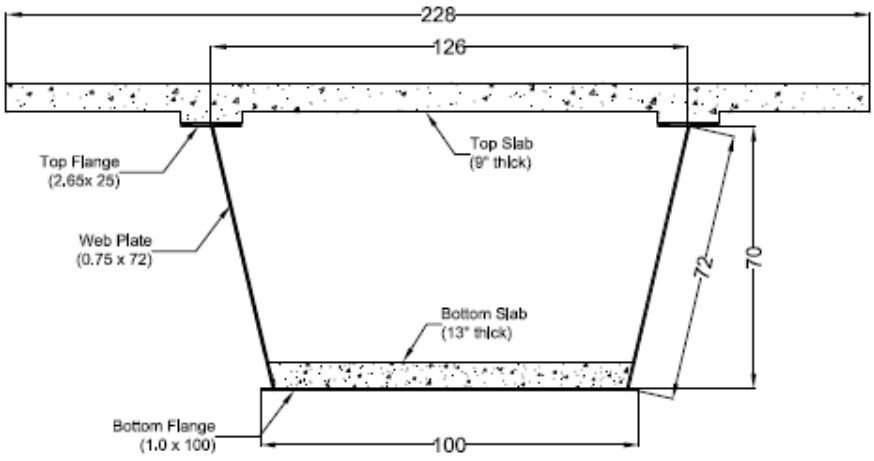


**TYPICAL CROSS-SECTION OF DOUBLE COMPOSITE BOX GIRDER**

Note: 1). Drawlng not to scale
2). All Dlmenslon are In Inches.

## G.4 Load Calculation Per Girder

This section provides information on design loads for single box girder section.

### Non Composite Dead Load

Dead load due to top slab, $w_{ts}$ (klf) $w_{ts} := t_{ts} \frac{b_{ts}}{2} \gamma_{rc}$ $w_{ts} = 2.377\ klf$

Dead load due to haunch, $w_h$ (klf) $w_h := 2b_{tf}\ t_h\ \gamma_{rc}$ $w_h = 0.156\ klf$

Dead Load due to bottom slab, $w_{bs}$ (klf) $w_{bs} := b_{bs}\ t_{bs}\ \gamma_{rc}$ $w_{bs} = 1.344\ klf$

Stay in Place forms, $w_{sip}$ (klf) $w_{sip} := \left[\left(126in - b_{tf}\right) + \left(\frac{147\ in - b_{tf}}{2}\right)\right] \gamma_{sip}$ $w_{sip} = 0.27\ klf$

**Note:** 126 inch is the c/c distance between top flanges of box girder

Dead load of steel section, $w_s$ (klf) $w_s := A_{sec}\ \gamma_s$ $w_s = 1.159\ klf$

Dead load of steel details, $w_{sd}$ (klf) $w_{sd} := 0.1\ w_s$ $w_{sd} = 0.116\ klf$

(Assumed 10 % of the steel weight)

Total non composite dead load, $DC_1$ $DC_1 := w_s + w_{sd} + w_{bs}$

$DC_1 = 2.619\ klf$

Total composite dead load, $DC_2$ $DC_2 := w_{ts} + w_h + w_{sip}$ $DC_2 = 2.803\ klf$

### Long Term Composite Dead Load

Dead load due to barrier, $w_b$ (klf) $w_b := \frac{m_{barr}\ n_b}{N_g}$ $w_b = 0.581\ klf$

Dead load of wearing surface, $w_{dw}$ (klf) $w_{dw} := \frac{\gamma_{ws}\ RW}{N_g}$ $w_{dw} = 0.42\ klf$

Total long term dead load, $DC_3$ (klf) $DC_3 := w_b$ $DC_3 = 0.581\ klf$

Total dead Load, DC (klf) $DC := DC_1 + DC_2 + DC_3 + w_{dw}$

$DC = 6.423\ klf$

### Live Load

Design vehicular live load and fatigue load are based on HS20 truck model of AASHTO LRFD 2004 Bridge Design Specifications, 3rd Edition.

Design vehicular live load is HL93 model.

Live load are assumed to be carried in full by the short term composite section.

## G.5 Load Factors

### Load Modification Factors for Strength Limit States

Ductility factor, $\eta 1_D$ $\eta 1_D := 1.0$

Redundancy factor, $\eta 1_R$ $\eta 1_R := 1.0$

Operational importance factor, $\eta 1_I$ $\eta 1_I := 1.0$

Load modification factor, $\eta 1$ $\eta 1 := \eta 1_D \, \eta 1_R \, \eta 1_I$

$\eta 1 = 1$

### Load Modification Factors for All Other Limit States Except Extreme Event Limit States

Ductility factor, $\eta 2_D$ $\eta 2_D := 1.0$

Redundancy factor, $\eta 2_R$ $\eta 2_R := 1.0$

Operational importance factor, $\eta 2_I$ $\eta 2_I := 1.0$

Load modification factor, $\eta 2$ $\eta 2 := \eta 1_D \, \eta 1_R \, \eta 1_I$

$\eta 2 = 1$

### Load Factors

Strength I $\gamma 1_{DC} := 1.25$ $\gamma 1_{DW} := 1.50$ $\gamma 1_{LL} := 1.75$

Fatigue $\gamma 3_{LL} := 0.75$

## G.6 Distribution Factors

This section provides information on distribution factors used for moments and shear.

### Live Load Lateral Distribution Factors

In this example, live load distributed to individual girders according to the approximate methods specified in **AASHTO 4.6.2.2**

For concrete deck on multiple box girders following condition shall be satisfied for the use of approximate method.

**Conditions for application of approximate methods.**

a.) Width of the deck is constant.

b.) Number of beams is not less than four unless otherwise specified.

c.) Beams are parallel and have approximately the same stiffness.

d.) The roadway part of the overhang ($d_e$) does not exceed 36 inch, unless otherwise specified.

e.) The cross-section is consistent with one of the cross-section shown in Table 4.6.2.2.1-1.

Conditions specified above are met, thus permanent loads of and on the deck may be uniformly distributed among the beams.

$$DF_{LL} := 0.05 + 0.85\frac{N_L}{N_g} + \frac{0.425}{N_L} \qquad DF_{LL} = 1.467 \quad \textbf{(AASHTO 4.6.2.2.2b-1)}$$

where,
$N_L$ = number of design lanes
$N_g$ = number of girders in the cross section

$$CHECK\_1 := \text{if}\left(0.5 \le \frac{N_L}{N_g} \le 1.5, \text{"OK"}, \text{"NG"}\right) \qquad CHECK\_1 = \text{"OK"}$$

As the ratio of $N_L/N_g$ increases beyond the upper limit of 1.5 and lesser girders per lane are used, the effects of torsion will increase and a more refined analysis is required. Where there are no depth or deflection limitations, the most effective designs are those having the largest ratios of $N_L/N_g$.

It should be noted that as per AASHTO 6.11.2.2.2 shear connectors should be provided throughout the negative flexure region of the box girder bridges.

## Distribution Factor for Fatigue Load

When checking fatigue, fatigue load is placed in single lane. Therefore, the distribution factor for one lane loaded when computing stress and shear ranges due to the fatigue load.

$$DF_{FL} := 0.05 + 0.85\left(\frac{1}{N_g}\right) + \frac{0.425}{1} \qquad DF_{FL} = 0.9$$

## Dynamic Load Allowance Factor (AASHTO 3.6.2)

For strength limit state checks:

$IM_{strength} := 33\%$ **(AASHTO 3.6.2.1-1)**

$$IM_{st} := 1 + \frac{33}{100} \qquad IM_{st} = 1.33$$

For fatigue limit state checks:

$IM_{fatigue} := 15\%$ **(AASHTO 3.6.2.1-1)**

$$IM_f := 1 + \frac{15}{100} \qquad IM_f = 1.15$$

## G.7 Load Combinations

Maximum negative moment exists at 1st pier from the exterior support. This is the maximum negative moment in all the three spans. Thus the negative section will be designed and checked for this moment.

**Table G.1** Unfactored and Distributed Moments for Single Box Girder

| Span | x/L | DC1 | DC2 | DC3 | Total DC | DW | Distributed LL + IM | |
|---|---|---|---|---|---|---|---|---|
| | | | | | | | M+ | M- |
| 1 | 0 | 0 | 0 | 0 | 0 | 0 | 0 | 0 |
| 1 | 0.1 | 1525 | 3145 | 677 | 5347 | 489.24 | 4288 | -682 |
| 1 | 0.2 | 2603 | 5315 | 1144 | 9062 | 826.87 | 7389 | -1363 |
| 1 | 0.3 | 3233 | 6511 | 1401 | 11145 | 1012 | 9345 | -2044 |
| 1 | 0.4 | 3416 | 6732 | 1449 | 11597 | 1047 | 10266 | -2725 |
| 1 | 0.5 | 3151 | 5978 | 1286 | 10415 | 930.00 | 10194 | -3407 |
| 1 | 0.6 | 2439 | 4250 | 914 | 7603 | 661.16 | 9214 | -4090 |
| 1 | 0.7 | 1279 | 1547 | 333 | 3159 | 240.67 | 7345 | -4771 |
| 1 | 0.8 | -448 | -2130 | -459 | -3037 | -331 | 4699 | -6724 |
| 1 | 0.9 | -3048 | -6782 | -1460 | -11290 | -1055 | 2069 | -8130 |
| 1 | 1 | -6536 | -12410 | -2670 | -21616 | -1930 | 1491 | -10580 |
| 2 | 0 | -6536 | -12410 | -2670 | -21616 | -1930 | 1491 | -10580 |
| 2 | 0.1 | -2792 | -5643 | -1214 | -9649 | -877 | 2213 | -6536 |
| 2 | 0.2 | -312 | -379 | -81 | -772 | -59.00 | 5084 | -4885 |
| 2 | 0.3 | 1410 | 3379 | 727 | 5516 | 525.73 | 8100 | -3577 |
| 2 | 0.4 | 2443 | 5635 | 1212 | 9290 | 876.72 | 9999 | -3198 |
| 2 | 0.5 | 2785 | 6387 | 1374 | 10546 | 993.00 | 10610 | -2820 |

**Note:** Moments are in unit of ft-kip.

**Table G.2** Factored Moments for Single Box Girder

| | | | | | | Total Factored and Distributed STRENGTH I Moments | |
|---|---|---|---|---|---|---|---|
| | | 1.25 | 1.5 | 1.75(LL+IM) | | | |
| Span | x/L | DC | DW | M+ | M- | M+ | M- |
| 1 | 0 | 0 | 0 | 0 | 0 | 0 | 0 |
| 1 | 0.1 | 6684 | 734 | 7504 | -1193 | 14922 | 6225 |
| 1 | 0.2 | 11328 | 1240 | 12931 | -2386 | 25499 | 10182 |
| 1 | 0.3 | 13931 | 1518 | 16354 | -3577 | 31804 | 11872 |
| 1 | 0.4 | 14496 | 1571 | 17965 | -4769 | 34031 | 11297 |
| 1 | 0.5 | 13019 | 1395 | 17839 | -5962 | 32253 | 8452 |
| 1 | 0.6 | 9504 | 992 | 16124 | -7157 | 26620 | 3338 |
| 1 | 0.7 | 3949 | 361 | 12854 | -8349 | 17164 | -4040 |
| 1 | 0.8 | -3796 | -497 | 8223 | -11767 | 3931 | -16059 |
| 1 | 0.9 | -14113 | -1583 | 3620 | -14228 | -12075 | -29923 |
| 1 | 1 | -27020 | -2895 | 2610 | -18515 | -27305 | -48430 |
| 2 | 0 | -27020 | -2895 | 2610 | -18515 | -27305 | -48430 |
| 2 | 0.1 | -12061 | -1316 | 3872 | -11438 | -9505 | -24814 |
| 2 | 0.2 | -965 | -89 | 8896 | -8549 | 7843 | -9603 |
| 2 | 0.3 | 6895 | 789 | 14176 | -6260 | 21859 | 1424 |
| 2 | 0.4 | 11613 | 1315 | 17498 | -5596 | 30425 | 7332 |
| 2 | 0.5 | 13183 | 1490 | 18567 | -4935 | 33239 | 9737 |

**Note:** Moments are in unit of ft-kip.

**Unfactored Maximum Negative Moments**

| | |
|---|---|
| Total DC maximum negative moment (at pier) | $MDCn := 21616\ kip\ ft$ |
| DC1 maximum negative moment (at pier) | $MDC1n := 6536\ kip\ ft$ |
| DC2 maximum negative moment (at pier) | $MDC2n := 12410\ kip\ ft$ |
| DC3 maximum negative moment (at pier) | $MDC3n := 2670\ kip\ ft$ |
| WDW maximum negative moment (at pier) | $MDWn := 1930\ kip\ ft$ |
| LL maximum negative moment (at pier) | $MLLn := 10580\ kip\ ft$ |

## Strength I

$\Sigma MSTn_{max} := \gamma 1_{DC}\ MDCn + \gamma 1_{DW}\ MDWn + \gamma 1_{LL}\ MLLn$ $\Sigma MSTn_{max} = 48430\ ft{\cdot}kip$

## Fatigue

LL range for negative moment span $MLL_{nf} := 2075\ ft\ kip$

$\Sigma MFn_{max} := \gamma 3_{LL}\ DF_{FL}\ IM_f\ MLL_{nf}$ $\Sigma MFn_{max} = 1610.719\ ft{\cdot}kip$

**Note :** Calculated design moments compare favourably with the design moments used in the AISI example (< 2 % difference)

## G.8 Section Properties

This section provides calculation of section properties for negative section.

### G.8.1 Non-Composite Section Properties (n=infinity) A

**a.) Top Flange**

$t_{tf} = 2.65\ in$

$b_{tf} = 25\ in$

$A_{tf} = 132.5\ in^2$

**b.) Bottom Flange**

$t_{bf} = 1\ in$

$b_{bf} = 100\ in$

$A_{bf} = 100\ in^2$

**c.) Web**

$t_w = 0.75\ in$

$D = 72.152\ in$

$A_w = 108.229\ in^2$

Total area of steel box girder, $A_s$

$A_s := A_{tf} + A_{bf} + A_w$

$A_s = 340.729\ in^2$

**The distance from the extreme bottom fiber to the centroid of item center of gravity, h (inch)**

**a.) Top Flange**

$h_{tf} := t_{bf} + D_w + \frac{t_{tf}}{2}$

$h_{tf} = 72.325\ in$

$A_{tf}\ h_{tf} = 9583.063\ in^3$

**b.) Bottom Flange**

$h_{bf} := \frac{t_{bf}}{2}$

$h_{bf} = 0.5\ in$

$A_{bf}\ h_{bf} = 50\ in^3$

**c.) Web**

$h_w := t_{bf} + \frac{D_w}{2}$

$h_w = 36\ in$

$A_w\ h_w = 3896.229\ in^3$

$\Sigma Ah := A_{tf}\ h_{tf} + A_{bf}\ h_{bf} + A_w\ h_w$

$\Sigma Ah = 13529.291\ in^3$

**Distance from bottom of section to the Neutral Axis (N.A.) of whole section, $Y_b$ (inch)**

$Y_b := \frac{\Sigma Ah}{A_s}$

$Y_b = 39.707\ in$

**Distance from top of section to the Neutral Axis (N.A.) of whole section, $Y_t$ (inch)**

$Y_t := H_G - Y_b$

$Y_t = 33.943\ in$

**Distance between Neutral Axis (N.A.) and Item center of gravity, d (inch)**

**a.) Top Flange**

$d_{tf} := h_{tf} - Y_b$

$d_{tf} = 32.618\ in$

**b.) Bottom Flange**

$d_{bf} := h_{bf} - Y_b$

$d_{bf} = -39.207\ in$

**c.) Web**

$d_w := h_w - Y_b$

$d_w = -3.707\ in$

**Moment of Inertia, $I_0$ ($in^4$)**

**a.) Top Flange**

$I_{0tf} := 2\ \frac{b_{tf}\ t_{tf}^3}{12}$

$I_{0tf} = 77.54\ in^4$

**b.) Bottom Flange**

$I_{0bf} := \frac{b_{bf}\ t_{bf}^3}{12}$

$I_{0bf} = 8.333\ in^4$

**c.) Web**

$I_{0w} := 2\ \frac{t_w\ D^3\ \cos(\theta)^2}{12}$

$I_{0w} = 44193.335\ in^4$

$I_{0s} := I_{0tf} + I_{0bf} + I_{0w}$ $I_{0s} = 44279.208\ in^4$

$A_{tf}\ d_{tf}^2 = 140971.71\ in^4$ $A_{bf}\ d_{bf}^2 = 153718.463\ in^4$ $A_w\ d_w^2 = 1487.218\ in^4$

$\Sigma Ad := A_{tf}\ d_{tf}^2 + A_{bf}\ d_{bf}^2 + A_w\ d_w^2$ $\Sigma Ad = 296177.391\ in^4$

**Moment of Inertia of whole section with respect to Neutral Axis (N.A.) of whole section, $I_{st}$ ($in^4$)**

$I_{st} := I_{0s} + \Sigma Ad$ $I_{st} = 340456.599\ in^4$

**Section Modulus of Entire Section, S ($in^3$)**

$S_{t\_st} := \frac{I_{st}}{Y_t}$ $S_{t\_st} = 10030.229\ in^3$

$S_{b\_st} := \frac{I_{st}}{Y_b}$ $S_{b\_st} = 8574.233\ in^3$

**Note:** St_st and Sb_st defines the section modulus of top fiber and bottom fiber of section respectively.

## G.8.2 Short-term Composite Section Properties (n=6.9) B

**(With Bottom Slab only)**

**Modular Ratio, n**

$$n := \text{round}\left(\frac{E_s}{E_c}, 1\right) \qquad n = 6.9$$

**a.) Bottom Slab** **b.) Steel**

$$A_{bsB} := \frac{b_{bs}\, t_{bs}}{n}$$

$$A_{bsB} = 186.993\ \text{in}^2 \qquad A_s = 340.729\ \text{in}^2$$

$$A_B := A_{bsB} + A_s \qquad A_B = 527.721\ \text{in}^2$$

**The distance from the extreme bottom fiber to the centroid of item center of gravity, h (inch)**

**a.) Bottom Slab** **b.) Steel**

$$h_{bsB} := t_{bf} + \frac{t_{bs}}{2}$$

$$h_{bsB} = 7.5\ \text{in}$$

$$A_{bsB}\, h_{bsB} = 1402.446\ \text{in}^3 \qquad A_s\, Y_b = 13529.291\ \text{in}^3$$

$$\Sigma Ah_B := A_{bsB}\, h_{bsB} + A_s\, Y_b \qquad \Sigma Ah_B = 14931.737\ \text{in}^3$$

**Distance from bottom of section to the Neutral Axis (N.A.) of the whole section, $Y_b$ (inch).**

$$Y_{bB} := \frac{\Sigma Ah_B}{A_B} \qquad Y_{bB} = 28.295\ \text{in}$$

**Distance from top of section to the Neutral Axis (N.A.) of the whole section, $Y_t$ (inch).**

$$Y_{tB} := H_G - Y_{bB} \qquad Y_{tB} = 45.355\ \text{in}$$

**Distance between Neutral Axis and Item center of gravity, d (inch)**

**a.) bottom Slab** **b.) Steel**

$$d_{bsB} := h_{bsB} - Y_{bB} \qquad d_{sB} := Y_b - Y_{bB}$$

$$d_{bsB} = -20.795\ \text{in} \qquad d_{sB} = 11.412\ \text{in}$$

**Moment of Inertia, $I_0$ ($in^4$)**

$$I_{0bsB} := \frac{b_{bs}\ t_{bs}^{3}}{12\ n}$$

$I_{0bsB} = 2633.481\ in^4$ $I_{st} = 340456.599\ in^4$

$\Sigma I_{0B} := I_{0bsB} + I_{st}$ $\Sigma I_{0B} = 343090.08\ in^4$

$A_{bsB}\ d_{bsB}^{2} = 80859.619\ in^4$ $A_s\ d_{sB}^{2} = 44375.975\ in^4$

$\Sigma Ad_B := A_{bsB}\ d_{bsB}^{2} + A_s\ d_{sB}^{2}$ $\Sigma Ad_B = 125235.595\ in^4$

**Moment of Inertia of whole section with respect to Neutral Axis (N.A.) of whole section, $I_{stB}$ ($in^4$).**

$I_{stB} := \Sigma I_{0B} + \Sigma Ad_B$ $I_{stB} = 468325.675\ in^4$

**Section Modulus required for the weld, Q ($in^3$).**

$$Q_{tfB} := \left(H_G - Y_{bB} - \frac{t_{tf}}{2}\right) A_{tf}$$ $Q_{tfB} = 5834.01\ in^3$

**Section Modulus of entire section, S ($in^3$)**

$$S_{bslabB} := \frac{I_{stB}\ n}{Y_{bB} - t_{bf}}$$ $S_{bslabB} = 118390.846\ in^3$

$$S_{tbeamB} := \frac{I_{stB}}{Y_{tB}}$$ $S_{tbeamB} = 10325.719\ in^3$

$$S_{bbeamB} := \frac{I_{stB}}{Y_{bB}}$$ $S_{bbeamB} = 16551.688\ in^3$

## G.8.3 Long-term Composite Section Properties ($n_c$=20.7) C

**(With bottom slab only)**

**Modular Ratio, $n_c$**

$n = 6.9$ $\quad n_c := 3n \quad$ $n_c = 20.7$

**a.) Bottom Slab** **b.) Steel**

$$A_{bsC} := \frac{b_{bs}\, t_{bs}}{n_c}$$

$A_{bsC} = 62.331\ in^2$ $\quad A_s = 340.729\ in^2$

$A_C := A_{bsC} + A_s$ $\quad A_C = 403.059\ in^2$

**The distance from the extreme bottom fiber to the centroid of item center of gravity, h (inch)**

**a.) Bottom Slab** **b.) Steel**

$$h_{bsC} := t_{bf} + \frac{t_{bs}}{2}$$

$h_{bsC} = 7.5\ in$

$A_{bsC}\, h_{bsC} = 467.482\ in^3$ $\quad A_s\, Y_b = 13529.291\ in^3$

$\Sigma Ah_C := A_{bsC}\, h_{bsC} + A_s\, Y_b$ $\quad \Sigma Ah_C = 13996.773\ in^3$

**Distance from bottom of section to the Neutral Axis (N.A.) of the whole section, $Y_b$ (inch).**

$$Y_{bC} := \frac{\Sigma Ah_C}{A_C}$$ $\quad Y_{bC} = 34.726\ in$

**Distance from top of section to the Neutral Axis (N.A.) of the whole section, $Y_t$ (inch).**

$Y_{tC} := H_G - Y_{bC}$ $\quad Y_{tC} = 38.924\ in$

**Distance between Neutral Axis and Item center of gravity, d (inch)**

**a.) Bottom Slab** **b.) Steel**

$d_{bsC} := h_{bsC} - Y_{bC}$ $\quad d_{sC} := Y_b - Y_{bC}$

$d_{bsC} = -27.226\ in$ $\quad d_{sC} = 4.981\ in$

**Moment of Inertia, $I_0$ ($in^4$)**

$$I_{0bsC} := \frac{b_{bs}\, t_{bs}^{\,3}}{12\, n_c}$$

$I_{0bsC} = 877.827\ in^4$ $I_{st} = 340456.599\ in^4$

$\Sigma I_{0C} := I_{0bsC} + I_{st}$ $\Sigma I_{0C} = 341334.426\ in^4$

$A_{bsC}\ d_{bsC}^2 = 46204.197\ in^4$ $A_s\ d_{sC}^2 = 8452.329\ in^4$

$\Sigma Ad_C := A_{bsC}\ d_{bsC}^2 + A_s\ d_{sC}^2$ $\Sigma Ad_C = 54656.526\ in^4$

**Moment of Inertia of whole section with respect to Neutral Axis (N.A.) of whole section, $I_{ltC}$ ($in^4$).**

$I_{ltC} := \Sigma I_{0C} + \Sigma Ad_C$ $I_{ltC} = 395990.951\ in^4$

**Section Modulus of entire section, S ($in^3$)**

$S_{tbeamC} := \frac{I_{ltC}}{Y_{tC}}$ $S_{tbeamC} = 10173.523\ in^3$

$S_{bbeamC} := \frac{I_{ltC}}{Y_{bC}}$ $S_{bbeamC} = 11403.194\ in^3$

$S_{bbslabC} := \frac{I_{ltC}}{Y_{bC} - t_{bf}}\ n_c$ $S_{bbslabC} = 243044.975\ in^3$

## G.8.4 Short-term Composite Section Properties (n=6.9) D

**(Negative Live Load)**

**Modular Ratio, n**

$n = 6.9$

**Effective flange width (AASHTO 4.6.2.6)**

For an interior web, $b_{eff}$ is lesser of:

$L_{eff} := 136.4\ ft$ $\quad \frac{L_{eff}}{4} = 409.2\ in$ $\quad 12\ t_{ts} + \frac{b_{tf}}{2} = 120.5\ in$

Here $L_{eff}$ is taken as the distance between the inflection points of permanent load.

$b_{eff\_int} := if\left[\frac{L_{eff}}{4} < \left(12\ t_{ts} + \frac{b_{tf}}{2}\right), \frac{L_{eff}}{4}, 12\ t_{ts} + \frac{b_{tf}}{2}\right]$ $\quad b_{eff\_int} = 120.5\ in$

For an exterior web, beff is lesser of:

$\frac{L_{eff}}{8} = 204.6\ in$ $\quad 6\ t_{ts} + \frac{b_{tf}}{4} = 60.25\ in$ $\quad OH_c = 54\ in$ (Governs)

By inspection overhang governs the effective width of the top slab.

$b_{eff\_ext} := OH_c + \frac{b_{eff\_int}}{2}$ $\quad b_{eff\_ext} = 114.25\ in$

Thus total beff of the entire box girder

$b_{eff} := b_{eff\_int} + b_{eff\_ext}$ $\quad b_{eff} = 234.75\ in$

**a.) Top Rebar** **b.) Bottom Slab** **c.) Steel**

$A_{rebarD} := R_r\ b_{eff}\ t_{ts}$ $\quad A_{bsD} := \frac{b_{bs}\ t_{bs}}{n}$

$A_{rebarD} = 21.127\ in^2$ $\quad A_{bsD} = 186.993\ in^2$ $\quad A_s = 340.729\ in^2$

$A_D := A_{rebarD} + A_{bsD} + A_s$ $\quad A_D = 548.849\ in^2$

**The distance from the extreme bottom fiber to the centroid of item center of gravity, h (inch)**

**a.) Top Rebar** **b.) Bottom Slab** **c.) Steel**

$h_{rebarD} := t_{bf} + D_w + t_{tf} + t_h + \frac{t_{ts}}{2}$ $\quad h_{bsD} := t_{bf} + \frac{t_{bs}}{2}$

$h_{rebarD} = 81.15\ in$ $h_{bsD} = 7.5\ in$ $Y_b = 39.707\ in$

$A_{rebarD}\ h_{rebarD} = 1714.497\ in^3$ $A_{bsD}\ h_{bsD} = 1402.446\ in^3$ $A_s\ Y_b = 13529.291\ in^3$

$\Sigma Ah_D := A_{rebarD}\ h_{rebarD} + A_{bsD}\ h_{bsD} + A_s\ Y_b$ $\Sigma Ah_D = 16646.233\ in^3$

**Distance from bottom of section to the Neutral Axis (N.A.) of the whole section, $Y_b$ (inch).**

$$Y_{bD} := \frac{\Sigma Ah_D}{A_D}$$ $Y_{bD} = 30.329\ in$

**Distance from top of section to the Neutral Axis (N.A.) of the whole section, $Y_t$ (inch).**

$Y_{tD} := H_G + t_{ts} + t_h - Y_{bD}$ $Y_{tD} = 55.321\ in$

**Distance between Neutral Axis and Item center of gravity, d (inch)**

**a.) Top Rebar** **b.) Bottom Slab** **c.) Steel**

$d_{rebarD} := h_{rebarD} - Y_{bD}$ $d_{bsD} := h_{bsD} - Y_{bD}$ $d_{sD} := Y_b - Y_{bD}$

$d_{rebarD} = 50.821\ in$ $d_{bsD} = -22.829\ in$ $d_{sD} = 9.378\ in$

**Moment of Inertia, $I_0$ ($in^4$)**

$I_{rebarD} := 0.0\ in^4$ $$I_{0bsD} := \frac{b_{bs}\ t_{bs}^3}{12\ n}$$

$I_{rebarD} = 0$ $I_{0bsD} = 2633.481\ in^4$ $I_{st} = 340456.599\ in^4$

$\Sigma I_{0D} := I_{rebarD} + I_{0bsD} + I_{st}$ $\Sigma I_{0D} = 343090.08\ in^4$

$A_{rebarD}\ d_{rebarD}^2 = 54566.786\ in^4$ $A_{bsD}\ d_{bsD}^2 = 97456.82\ in^4$ $A_s\ d_{sD}^2 = 29963.375\ in^4$

$\Sigma Ad_D := A_{rebarD}\ d_{rebarD}^2 + A_{bsD}\ d_{bsD}^2 + A_s\ d_{sD}^2$ $\Sigma Ad_D = 181986.981\ in^4$

**Moment of Inertia of whole section with respect to Neutral Axis (N.A.) of whole section, $I_{stD}$ ($in^4$).**

$I_{stD} := \Sigma I_{0D} + \Sigma Ad_D$ $I_{stD} = 525077.061\ in^4$

**First Moment of Area for Transformed Bottom Slab, Q ($in^3$).**

$$Q_{BslabD} := A_{bsD}\left(Y_{bD} - t_{bf} - \frac{t_{bs}}{2}\right) \qquad Q_{BslabD} = 4268.925\ in^3$$

**Section Modulus of entire section, S ($in^3$)**

$$S_{trebarD} := \frac{I_{stD}}{Y_{tD} - \frac{t_{ts}}{2}} \qquad S_{trebarD} = 10331.965\ in^3$$

$$S_{tbeamD} := \frac{I_{stD}}{Y_{tD} - t_{ts} - t_h} \qquad S_{tbeamD} = 12120.713\ in^3$$

$$S_{bbeamD} := \frac{I_{stD}}{Y_{bD}} \qquad S_{bbeamD} = 17312.501\ in^3$$

$$S_{bslabD} := \frac{I_{stD}\ n}{Y_{bD} - t_{bf}} \qquad S_{bslabD} = 123529.179\ in^3$$

## G.8.5 Long-term Composite Section Properties ($n_e$=20.7) E

**(Negative Service Dead Load Moment)**

**Modular Ratio, $n_e$**

$n = 6.9$ $\quad n_e := 3n \quad$ $n_e = 20.7$

**a.) Top rebar** **b.) Bottom Slab** **c.) Steel**

$A_{rebarE} := R_r\, b_{eff}\, t_{ts}$ $\quad A_{bsE} := \dfrac{b_{bs}\, t_{bs}}{n_e}$

$A_{rebarE} = 21.127\ in^2$ $\quad A_{bsE} = 62.331\ in^2$ $\quad A_s = 340.729\ in^2$

$A_E := A_{rebarE} + A_{bsE} + A_s$ $\quad A_E = 424.187\ in^2$

**The distance from the extreme bottom fiber to the centroid of item center of gravity, h (inch)**

**a.) Top Rebar** **b.) Bottom Slab** **c.) Steel**

$h_{rebarE} := t_{bf} + D_w + t_{tf} + t_h + \dfrac{t_{ts}}{2}$ $\quad h_{bsE} := t_{bf} + \dfrac{t_{bs}}{2}$

$h_{rebarE} = 81.15\ in$ $\quad h_{bsE} = 7.5\ in$

$A_{rebarE}\, h_{rebarE} = 1714.497\ in^3$ $\quad A_{bsE}\, h_{bsE} = 467.482\ in^3$ $\quad A_s\, Y_b = 13529.291\ in^3$

$\Sigma Ah_E := A_{rebarE}\, h_{rebarE} + A_{bsE}\, h_{bsE} + A_s\, Y_b$ $\quad \Sigma Ah_E = 15711.27\ in^3$

**Distance from bottom of section to the Neutral Axis (N.A.) of the whole section, $Y_b$ (inch).**

$Y_{bE} := \dfrac{\Sigma Ah_E}{A_E}$ $\quad Y_{bE} = 37.039\ in$

**Distance from top of section to the Neutral Axis (N.A.) of the whole section, $Y_t$ (inch).**

$Y_{tE} := H_G + t_{ts} + t_h - Y_{bE}$ $\quad Y_{tE} = 48.611\ in$

**Distance between Neutral Axis and Item center of gravity, d (inch)**

**a.) Top Slab** **b.) Bottom Slab** **c.) Steel**

$d_{rebarE} := h_{rebarE} - Y_{bE}$ $\quad d_{bsE} := h_{bsE} - Y_{bE}$ $\quad d_{sE} := Y_b - Y_{bE}$

$d_{rebarE} = 44.111\ in$ $\quad d_{bsE} = -29.539\ in$ $\quad d_{sE} = 2.668\ in$

**Moment of Inertia, $I_0$ ($in^4$)**

$I_{rebarE} := 0.0\ in^4$

$I_{0bsE} := \frac{b_{bs}\ t_{bs}^3}{12\ n_e}$

$I_{rebarE} = 0$

$I_{0bsE} = 877.827\ in^4$

$I_{st} = 340456.599\ in^4$

$\Sigma I_{0E} := I_{rebarE} + I_{0bsE} + I_{st}$

$\Sigma I_{0E} = 341334.426\ in^4$

$A_{rebarE}\ d_{rebarE}^2 = 41110.319\ in^4$ $A_{bsE}\ d_{bsE}^2 = 54385.33\ in^4$ $A_s\ d_{sE}^2 = 2426.109\ in^4$

$\Sigma Ad_E := A_{rebarE}\ d_{rebarE}^2 + A_{bsE}\ d_{bsE}^2 + A_s\ d_{sE}^2$

$\Sigma Ad_E = 97921.758\ in^4$

**Moment of Inertia of whole section with respect to Neutral Axis (N.A.) of whole section, $I_{ltE}$ ($in^4$).**

$I_{stE} := \Sigma I_{0E} + \Sigma Ad_E$

$I_{stE} = 439256.184\ in^4$

**Section Modulus required for the weld, Q ($in^3$).**

$Q_{tfE} := \left(H_G - Y_{bE} - \frac{t_{tf}}{2}\right) A_{tf} + \left(H_G + \frac{t_{ts}}{2} - Y_{bE}\right) A_{rebarE}$

$Q_{tfE} = 5544.037\ in^3$

$Q_{bfE} := A_{bf}\left(Y_{bE} - \frac{t_{bf}}{2}\right) + A_{bsE}\left(Y_{bE} - t_{bf} - \frac{t_{bs}}{2}\right)$

$Q_{bfE} = 5495.019\ in^3$

$Q_{BslabE} := A_{bsE}\left(Y_{bE} - t_{bf} - \frac{t_{bs}}{2}\right)$

$Q_{BslabE} = 1841.165\ in^3$

**Section Modulus of entire section, S ($in^3$)**

$S_{trebarE} := \frac{I_{stE}}{Y_{tE} - \frac{t_{ts}}{2}}$

$S_{trebarE} = 9957.871\ in^3$

$S_{tbeamE} := \frac{I_{stE}}{Y_{tE} - t_{ts} - t_h}$

$S_{tbeamE} = 11997.781\ in^3$

$S_{bbeamE} := \frac{I_{stE}}{Y_{bE}}$

$S_{bbeamE} = 11859.434\ in^3$

$S_{bslabE} := \frac{I_{stE}\ n_e}{Y_{bE} - t_{bf}}$

$S_{bslabE} = 252302.156\ in^3$

## G.9 Calculation of Plastic Neutral Axis

This section shows detailed calculation of Plastic Neutral Axis, $Y_{PNA.}$

### Calculation of Forces

| | | |
|---|---|---|
| Force in top rebars of top slab, $P_{rt}$ | $P_{rt} := 0.0067\ b_{eff}\ t_{ts}\ f_{yrebar}$ | $P_{rt} = 849.326\ kip$ |
| Force in bottom rebars of top slab, $P_{rb}$ | $P_{rb} := 0.0033\ b_{eff}\ t_{ts}\ f_{yrebar}$ | $P_{rb} = 418.325\ kip$ |
| Total force in rebars of top slab, $P_{re}$ | $P_{re} := P_{rt} + P_{rb}$ | $P_{re} = 1267.65\ kip$ |
| Force in Top flange, $P_{tf}$ | $P_{tf} := 2\ b_{tf}\ t_{tf}\ f_y$ | $P_{tf} = 6625\ kip$ |
| Force in Web, $P_w$ | $P_w := 2\ D\ t_w\ f_y$ | $P_w = 5411.429\ kip$ |
| Force in Bottom flange, $P_{bf}$ | $P_{bf} := b_{bf}\ t_{bf}\ f_y$ | $P_{bf} = 5000\ kip$ |
| Force in Bottom slab, $P_{bs}$ | $P_{bs} := 0.85\ f_c\ b_{bs}\ t_{bs}$ | $P_{bs} = 7128.631\ kip$ |

$P_{bf} + P_{bs} = 12128.631\ kip$

Therefore, plastic neutral axis is located in the steel section.

| | |
|---|---|
| Clear cover to the top rebars of top slab, CLrt | $CL_{rt} := 2in$ |
| Clear cover to the bottom rebars of top slab, CLrb | $CL_{rb} := 2in$ |
| Diameter of top rebar of top slab, DIArt | $DIA_{rt} := 0.625in$ |
| Diameter of bottom rebar of top slab, DIArb | $DIA_{rb} := 0.625in$ |

Assuming Plastic Neutral Axis to be in the top flange of box girder section.

## Calculation of Center of Gravity of Forces

Height of top rebar from bottom fiber, $h_{rt}$

$$h_{rt} := t_{bf} + D_w + t_{tf} + t_{ts} + t_h - CL_{rt} - \frac{DIA_{rt}}{2} \qquad h_{rt} = 83.337\ in$$

Height of bottom rebar from top fiber, $h_{rb}$

$$h_{rb} := t_{bf} + D_w + t_{tf} + t_h + CL_{rb} + \frac{DIA_{rb}}{2} \qquad h_{rb} = 78.963\ in$$

Height of centroid of rebars from bottom fiber, $h_{re}$

$$h_{re} := \frac{P_{rt}\, h_{rt} + P_{rb}\, h_{rb}}{P_{re}} \qquad h_{re} = 81.894\ in$$

Height of top flange from bottom fiber, $h_{ytf}$

$$h_{ytf} := t_{bf} + D_w + \frac{t_{tf}}{2} \qquad h_{tf} = 72.325\ in$$

Height of web from bottom fiber, $h_{yw}$

$$h_{yw} := t_{bf} + \frac{D_w}{2} \qquad h_w = 36\ in$$

Height of bottom slab from bottom fiber, $h_{bs}$

$$h_{bs} := t_{bf} + \frac{t_{bs}}{2} \qquad h_{bs} = 7.5\ in$$

Height of bottom flange from bottom fiber, $h_{ybf}$

$$h_{ybf} := \frac{t_{bf}}{2} \qquad h_{bf} = 0.5\ in$$

## Location of Plastic Neutral Axis for the Critical Negative Section

Assuming Plastic Neutral Axis to be in the web of box girder section.

$$Y_{pm} := \left(t_{bf} + \frac{D_w}{2}\right) \qquad Y_{pm} = 36\ in$$

$$\text{root}\left[P_{re} + P_{tf} + \left(\frac{P_w}{D}\right)\frac{(D_w + t_{bf}) - Y_{pm}}{\cos(\theta)} - P_{bf} - P_{bs} - \left(\frac{P_w}{D}\right)\frac{Y_{pm} - t_{bf}}{\cos(\theta)}, Y_{pm}\right] = 8.603\ in$$

$$Y_{PNA} := 8.603\ in$$

Thus, Plastic Neutral axis is located inside bottom slab from the bottom of the bottom, flange. Since bottom slab is located in the web, the equation will not change.

$$Y_{PNA} = 8.603\ in$$

$Y_{PNA}$ is the actual position of Plastic Neutral Axis (P.N.A) from the bottom of the section.

Tension force in the cross section, $T_c$

$$T_c := P_{re} + P_{tf} + \left(\frac{P_w}{D}\right)\left(\frac{D_w + t_{bf} - Y_{PNA}}{\cos(\theta)}\right) \qquad T_c = 12716.32\,\text{kip}$$

Compression force in the cross section, $C_c$

$$C_c := P_{bf} + P_{bs} + \left(\frac{P_w}{D}\right)\left(\frac{Y_{PNA} - t_{bf}}{\cos(\theta)}\right) \qquad C_c = 12716.39\,\text{kip}$$

The equilibrium equation used here does not account for the loss of compressive force for the bottom slab concrete above the plastic neutral axis. However the result is adequate for design.

## G.10 Design and Stress Checks

This section provides information on design and stress checks.

### Web Slenderness (AASHTO 6.10.6.2.3)

The section satisfies the web slenderness limit if:

$$\text{if } 2\frac{D_c}{t_w} \le 5.7\sqrt{\frac{E_s}{F_y}} \qquad \textbf{(AASHTO 6.10.6.2.3-1)}$$

$D_c$ = Depth of web in compression in the elastic range determined as specified in Article D6.3.1 (in)

$t_w$ = Web thickness of the box girder

$E_s$ = Elastic Modulus of the Steel

$F_y$ = Yield strength of the girder (flange and web)

$f_{cf\_s}$ = Stress in compression flange at strength limit state for DC1, DC2, DC3, DW, LL.

$f_{tf\_s}$ = Stress in tension flange at strength limit state for DC1, DC2, DC3, DW, LL.

$$f_{cf\_s} := -\left(\frac{\gamma 1_{DC}\,MDC1n}{S_{b\_st}} + \frac{\gamma 1_{DC}\,MDC2n}{S_{bbeamC}} + \frac{\gamma 1_{DC}\,MDC3n + \gamma 1_{DW}\,MDWn}{S_{bbeamE}} + \frac{\gamma 1_{LL}\,MLLn}{S_{bbeamD}}\right)$$

$$f_{cf\_s} = -46.899\,\text{ksi}$$

$$f_{tf\_s} := \frac{\gamma 1_{DC}\,MDC1n}{S_{t\_st}} + \frac{\gamma 1_{DC}\,MDC2n}{S_{tbeamC}} + \frac{\gamma 1_{DC}\,MDC3n + \gamma 1_{DW}\,MDWn}{S_{tbeamE}} + \frac{\left(\gamma 1_{LL}\,MLLn\right)}{S_{tbeamD}}$$

$$f_{tf\_s} = 52.636\,\text{ksi}$$

$$D_c := \frac{-f_{cf\_s}}{\left|f_{cf\_s}\right| + f_{tf\_s}} D_w - t_{tf} \qquad D_c = 30.332\,\text{in}$$

$$2\frac{D_c}{t_w} = 80.886 \qquad 5.7\sqrt{\frac{E_s}{f_y}} = 137.274$$

$$CHECK\_4 := \text{if}\left(2\frac{D_c}{t_w} \le 5.7\sqrt{\frac{E_s}{f_y}}, \text{"OK"}, \text{"NG"}\right) \qquad CHECK\_4 = \text{"OK"}$$

Therefore, section satisfies web slenderness criteria.

## Slab Ductility Requirement (AASHTO 6.11.6.2.2)

$$\frac{D_p}{D_t} \le 0.42$$

$D_p$ = Distance from bottom of the bottom concrete slab to the neutral axis of the composite section.

$D_t$ = Total depth of composite section

$D_p := Y_{PNA} - t_{bf}$ $\quad D_p = 7.603\ in$

$D_t := t_{ts} - CL_{rt} + t_h + t_{tf} + D_w$ $\quad D_t = 82.65\ in$ $\quad \frac{D_p}{D_t} = 0.092$

$CHECK\_5 := if\left(\frac{D_p}{D_t} \le 0.42, "OK", "NG"\right)$ $\quad CHECK\_5 = "OK"$

Therefore, section does satisfies Slab Ductility requirement by **AASHTO 6.10.7.3.** Section is a compact section.

### Nominal Flexural Resistance of Box Flanges in Compression (AASHTO 6.11.8)

Assume that there exist negligible torsional shear stresses in the flange due to the factored loads.Therefore, St. Venant torsional stresses can be taken as zero.

Flange stress reduction factor for homogeneous section **(AASHTO 6.10.1.10.1)** $\quad R_h := 1.0$ $\quad R_b := 1.0$

The resistance factor for flexure $\quad \phi_f := 1.0$

St. Venant torsional shear stresses in the flange $\quad f_v := 0\ ksi$

Nominal yield strength of the compression flange $\quad F_{yc} := f_y$ $\quad F_{yc} = 50\ ksi$

Plate buckling co-efficient for uniform normal stress $\quad k := 4.0$

Plate buckling co-efficient for shear stress $\quad k_s := 5.34$

$\Delta := \sqrt{1 - 3\left(\frac{f_v}{F_{yc}}\right)^2}$ $\quad \Delta = 1$

Nominal flexure resistance of the compression flange $\quad F_{nc} := R_b R_h F_{yc} \Delta$ $\quad F_{nc} = 50\ ksi$

The stress developed in the compression flange due to Factored loads.

$$f_{bu} := \frac{MDC1n\ \gamma 1_{DC}}{S_{b\_st}} + \frac{MDC2n\ \gamma 1_{DC}}{S_{bbeamC}} + \frac{MDC3n\ \gamma 1_{DC} + MDWn\ \gamma 1_{DW}}{S_{bbeamE}} + \frac{MLLn\ \gamma 1_{LL}}{S_{bbeamD}}$$

$$f_{bu} = 46.899\ ksi$$

$$CHECK\_6 := if\left(f_{bu} \le \phi_f\ F_{nc}, "OK", "NG"\right) \qquad CHECK\_6 = "OK"$$

**Nominal Flexural Resistance of Box Flanges in Tension (AASHTO 6.11.7.2)**

Nominal flexure resistance of the tension flange $F_{nt} := f_y$ $F_{nt} = 50\ ksi$

$$f_{bt} := \frac{MDC1n\ \gamma 1_{DC}}{S_{t\_st}} + \frac{MDC2n\ \gamma 1_{DC}}{S_{tbeamC}} + \frac{MDWn\ \gamma 1_{DW} + MDC3n\ \gamma 1_{DC}}{S_{tbeamE}} + \frac{MLLn\ \gamma 1_{LL}}{S_{tbeamD}}$$

$$f_{bt} = 52.636\ ksi$$

$$\frac{F_{nt} - f_{bt}}{F_{nt}}\ 100 = -5.272$$

Since the stress in top flange exceeds the yield stress, the top flange would need to be resized. however, for the purpose of this example size is acceptable.

**Stress in Bottom Concrete Slab**

Stress in bottom concrete slab at Strength I limit state should not exceed 0.6f'c.

$$f_{DC2bs} := \frac{\gamma 1_{DC}\ MDC2n}{S_{bslabB}} \qquad f_{DC2bs} = 1.572\ ksi$$

$$f_{DC3bs} := \frac{MDC3n\ \gamma 1_{DC}}{S_{bslabD}} \qquad f_{DC3bs} = 0.324\ ksi$$

$$f_{DWbs} := \frac{MDWn\ \gamma 1_{DW}}{S_{bslabD}} \qquad f_{DWbs} = 0.281\ ksi$$

$$f_{LLbs} := \frac{MLLn\ \gamma 1_{LL}}{S_{bslabD}} \qquad f_{LLbs} = 1.799\ ksi$$

$$f_{cbs} := f_{DC2bs} + f_{DC3bs} + f_{DWbs} + f_{LLbs}$$

$$f_{cbs} = 3.976\ ksi$$

$$CHECK\_7 := if\left(f_{cbs} \le 0.60\ f_c, "OK", "NG"\right) \qquad CHECK\_7 = "NG"$$

$$f_{clim} := 0.60 f_c \qquad f_{clim} = 3.9\ ksi$$

$$\frac{f_{cbs} - f_{clim}}{f_{clim}}\ 100 = 1.959$$

Eventhough the stress exceeds the 0.6f'c limit by 2 %, for the purpose of this example bottom slab is acceptable.

## G.11 Shear

Section will be checked for the maximum shear force at the end bearings. Since maximum shear force is observed at interior support, section will be checked at interior support.

**Table G.3** Unfactored Shear for Negative section in kips

| Span | x/L | DC1 | DC2 | DC3 | Total DC | DW | Distributed LL + IM | |
|---|---|---|---|---|---|---|---|---|
| | | | | | | | V- | V+ |
| 1 | 0 | 92 | 191 | 41 | 324 | 29 | -35 | 258 |
| 1 | 0.1 | 68 | 140 | 30 | 238 | 21 | -37 | 216 |
| 1 | 0.2 | 44 | 89 | 19 | 152 | 13 | -54 | 179 |
| 1 | 0.3 | 21 | 37 | 8 | 66 | 6 | -83 | 144 |
| 1 | 0.4 | -2 | -14 | -3 | -19 | -2 | -111 | 112 |
| 1 | 0.5 | -25 | -65 | -15 | -105 | -10 | -140 | 84 |
| 1 | 0.6 | -49 | -116 | -26 | -191 | -18 | -172 | 60 |
| 1 | 0.7 | -72 | -167 | -37 | -276 | -26 | -205 | 39 |
| 1 | 0.8 | -113 | -219 | -47 | -379 | -33 | -239 | 23 |
| 1 | 0.9 | -160 | -270 | -58 | -488 | -41 | -270 | 11 |
| 1 | 1 | -206 | -321 | -70 | -597 | -49 | -302 | 7 |
| 2 | 0 | 187 | 319 | 69 | 575 | 48 | -30 | 306 |
| 2 | 0.1 | 129 | 255 | 55 | 439 | 39 | -30 | 272 |
| 2 | 0.2 | 87 | 191 | 41 | 319 | 29 | -39 | 232 |
| 2 | 0.3 | 58 | 127 | 27 | 212 | 19 | -61 | 193 |
| 2 | 0.4 | 29 | 63 | 15 | 107 | 9 | -88 | 155 |
| 2 | 0.5 | 0 | 0 | 0 | 0 | 0 | -119 | 121 |

**Table G.4** Factored and Distributed Shear for Negative Section in kips

| | | Max | Max | | | Total Factored and Distributed STRENGTH I Shears | |
|---|---|---|---|---|---|---|---|
| | | 1.25 | 1.5 | 1.75(LL+IM) | | | |
| Span | x/L | DC | DW | V- | V+ | V- | V+ |
| 1 | 0 | 405 | 44 | -61 | 452 | 387 | 900 |
| 1 | 0.1 | 298 | 32 | -65 | 378 | 264 | 707 |
| 1 | 0.2 | 190 | 20 | -95 | 313 | 114 | 523 |
| 1 | 0.3 | 83 | 9 | -144 | 252 | -53 | 343 |
| 1 | 0.4 | -24 | -3 | -194 | 197 | -220 | 170 |
| 1 | 0.5 | -131 | -15 | -246 | 148 | -392 | 1 |
| 1 | 0.6 | -239 | -27 | -301 | 104 | -567 | -161 |
| 1 | 0.7 | -345 | -39 | -360 | 68 | -744 | -316 |
| 1 | 0.8 | -474 | -50 | -418 | 40 | -941 | -483 |
| 1 | 0.9 | -610 | -62 | -473 | 18 | -1145 | -653 |
| 1 | 1 | -746 | -74 | -529 | 12 | -1348 | -807 |
| 2 | 0 | 719 | 72 | -52 | 535 | 739 | 1325 |
| 2 | 0.1 | 549 | 59 | -52 | 476 | 555 | 1084 |
| 2 | 0.2 | 399 | 44 | -68 | 406 | 375 | 848 |
| 2 | 0.3 | 265 | 29 | -108 | 338 | 186 | 632 |
| 2 | 0.4 | 134 | 14 | -154 | 270 | -6 | 418 |

**Maximum shear force due to unfactored loads**

Maximum shear force due to total DC $V_{DCn} := 597\ kip$

Maximum Shear force due to DC1 $V_{DC1n} := 206\ kip$

Maximum shear force due to DC2 $V_{DC2n} := 321\ kip$

Maximum shear force due to DC3 $V_{DC3n} := 70$

Maximum shear force due to DW $V_{DWn} := 49\ kip$

Maximum shear force due to LL $V_{LLn} := 302\ kip$

Maximum shear force for fatigue $V_{fn} := 80\ kip$

**Strength I Limit State**

$\Sigma VSTn_{max} := \gamma 1_{DC}\ V_{DCn} + \gamma 1_{DW}\ V_{DWn} + \gamma 1_{LL}\ V_{LLn}$ $\Sigma VSTn_{max} = 1348.25\ kip$

**Fatigue Limit State**

$V_{nf} := IM_f\ DF_{FL}\ \gamma 3_{LL}\ V_{fn}$ $V_{nf} = 62.1\ kip$

**Maximum shear per web**

$\Sigma VSTn_{maxw} := \frac{\Sigma VSTn_{max}}{2}$ $\Sigma VSTn_{maxw} = 674.125\ kip$

Inclination of webs needs to be taken into consideration.

$V_u := \frac{\Sigma VSTn_{maxw}}{\cos(\theta)}$ $V_u = 694.853\ kip$

## Nominal Resistance of Unstiffened Webs (AASHTO 6.10.9.2)

$V_u \le \phi_v\ V_n$

Resistance factor for shear $\phi_v := 1.0$

Nominal shear resistance, $V_n$

$V_n = C\ V_p$ **(AASHTO 6.10.9.2-1)**

Plastic shear force, $V_p$

$V_p := 0.58\ f_y\ D\ t_w$ $V_p = 1569.314\ kip$ **(AASHTO 6.10.9.2-2)**

Shear buckling co-efficient, $k_{sh}$ $k_{sh} := 5$

$\frac{D}{t_w} = 96.203$ $1.40\sqrt{\frac{E_s\ k_{sh}}{f_y}} = 75.392$

$$C_w := \begin{cases} \dfrac{1.57}{\left(\dfrac{D}{t_w}\right)^2}\left(\dfrac{E_s\, k_{sh}}{f_y}\right) & \text{if } \dfrac{D}{t_w} > 1.40\sqrt{\dfrac{E_s\, k_{sh}}{f_y}} \\ \text{"NG"} & \text{otherwise} \end{cases}$$ **(AASHTO 6.10.9.3.2-6)**

$C_w = 0.492$

$V_n := C_w\, V_p$ $V_n = 772.02\ \text{kip}$

$\phi_v\, V_n = 772.02\ \text{kip}$ $V_u = 694.853\ \text{kip}$

$\text{CHECK\_8} := \text{if}\left(V_u < \phi_v\, V_n, \text{"OK"}, \text{"NG"}\right)$ $\text{CHECK\_8} = \text{"OK"}$

Thus, section satisfies nominal shear criteria.

## G.12 Shear Connectors

This section provides information on design of shear connectors and fatigue limit state.

Assume diameter of shear connectors $d_{sc} := 0.75in$

Area of shear connectors $A_{sc} := \pi \frac{d_{sc}^2}{4}$ $A_{sc} = 0.442\ in^2$

## G.12.1 Ultimate Resistance of Shear Connectors (AASHTO 6.10.10.4.3)

Minimum tensile strength of shear connectors $F_u := 60ksi$

Nominal resistance of one stud shear connectors in concrete deck, $Q_n$

$0.5\ A_{sc} \sqrt{f_c\ E_c} = 36.414\ kip$ $A_{sc}\ F_u = 26.507\ kip$

$Q_n := if\left(0.5\ A_{sc} \sqrt{f_c\ E_c} \le A_{sc}\ F_u, 0.5 A_{sc} \sqrt{f_c\ E_c}, A_{sc}\ F_u\right)$ $Q_n = 26.507\ kip$

Resistance factor of shear connectors $\phi_{sc} := 0.85$
From **(AASHTO 6.5.4.2)**

Factored resistance of one stud shear connector, $Q_r$ $Q_r := \phi_{sc}\ Q_n$

$Q_r = 22.531\ kip$

Maximum shear force in the concrete deck for negative section as per **AASHTO 6.10.10.4.2**

$P_{1p} := 0.60\ f_c\ b_{bs}\ t_{bs}$ $P_{1p} = 5031.975\ kip$ **(AASHTO 6.10.10.4.2-2)**

$P_{2p} := 2 f_y\ D\ t_w + 2 f_y\ b_{tf}\ t_{tf} + f_y\ b_{bf}\ t_{bf}$ $P_{2p} = 17036.429\ kip$ **(AASHTO 6.10.10.4.2-3)**

Maximum shear force is lesser of the two values.

$P_p := if\left(P_{1p} < P_{2p}, P_{1p}, P_{2p}\right)$ $P_p = 5031.975\ kip$

Number of shear connector in the bottom flange, $n_{sc}$

$n_{sc} := round\left(\frac{P_p}{Q_r}, 0\right)$ $n_{sc} = 223$

**Transverse Spacing of Shear Connectors (AASHTO 6.11.10)**

$$S_t \le \frac{R_1\ t_{bf}}{\sqrt{\frac{f_y}{k\ E_s}}}$$

Where

$R_1 := 0.57$ $\quad k = 4$ $\quad E_s = 29000\ ksi$

$f_y = 50\ ksi$ $\quad t_{bf} = 1\ in$

$$S_t := \frac{R_1\ t_{bf}}{\sqrt{\frac{f_y}{k\ E_s}}}$$

$S_t = 27.455\ in$

$n_{sh} := 7$

The maximum allowable transverse spacing is 27 in. Try 7 shear connectors at the spacing of 14 in.

## G.12.2 Fatigue Resistance of Shear Connectors

$ADTT_{SL} = p\ ADTT$ **(AASHTO 3.6.1.4.2-1)**

Where:

ADTT = number of trucks per day in one direction averaged over the design life.

$ADTT_{SL}$ = the number of trucks per day in a single-lane averaged over the design life.

p = fraction of truck traffic in single lane **(Table 3.6.1.4.2-1)**

For 3 or more lanes $p := 0.8$

Assuming one-way traffic $ADTT := 4000$

The number of trucks per day in a single-lane averaged over the design life.

$ADTT_{SL} := p\ ADTT$

$ADTT_{SL} = 3200$

Therefore, the number of trucks per day in a single lane averaged is 3200.

Considering Category **C type** of detail.

Number of stress range cycles per truck passage $n_s := 1.5$

(From Table 6.6.1.2.5-2)

Number of stress cycle in entire life span of bridge $N_s := 365\ 75\ n_s\ ADTT_{SL}$ **(AASHTO 6.6.1.2.5-2)**

$N_s = 131400000$

### Nominal Fatigue Resistance

Nominal fatigue resistance shall be as per **AASHTO 6.6.1.2.5**

$$\Delta F_n = \left(\frac{A_f}{N_s}\right)^{\frac{1}{3}} \geq \frac{1}{2}\Delta F_{TH}$$ **(AASHTO 6.6.1.2.5-1)**

where,

$\Delta F_n$ = Nominal fatigue resistance

$A_f$ = Constant from Table 6.6.1.2.5-1

$N_s$ = Number of stress cycles in entire life span of bridge

$\Delta F_{TH}$ = Constant amplitude fatigue threshold from Table-6.6.1.2.5-3

$A_f := 44 \times 10^8$

$N_s = 131400000$

$\Delta F_{TH} := 10.0$

$$\Delta F_n := \text{if}\left[\left(\frac{A_f}{N_s}\right)^{\frac{1}{3}} \geq \frac{1}{2}\Delta F_{TH}, \left(\frac{A_f}{N_s}\right)^{\frac{1}{3}}, \frac{1}{2}\Delta F_{TH}\right] \qquad \Delta F_n \text{ ksi} = 5 \text{ ksi}$$

Fatigue stress in bottom flange

$$\sigma_{bffatigue} := \frac{\Sigma MFn_{max}}{S_{bbeamD}} \qquad \sigma_{bffatigue} = 1.116 \text{ ksi}$$

$$\text{Check\_bf} := \text{if}\left(\sigma_{bffatigue} \leq \Delta F_n \text{ ksi}, \text{"OK"}, \text{"NG"}\right) \qquad \text{Check\_bf} = \text{"OK"}$$

## Fatigue Resistance of Shear Connectors

Fatigue resistance of individual shear connectors, $Z_r$

$$Z_r = \alpha\, d_{sc}^{\,2} \geq \frac{5.5\, d_{sc}^{\,2}}{2} \qquad \alpha := 34.5 - 4.28 \log(N_s) \qquad \textbf{(AASHTO 6.10.10.2-1)}$$

$\alpha = -0.248$

Where,

$d_{sh}$ = diameter of the stud

$$Z_r := \text{if}\left(\alpha\, d_{sc}^{\,2} \geq \frac{5.5\, d_{sc}^{\,2}}{2}, \alpha\, d_{sc}^{\,2}, \frac{5.5\, d_{sc}^{\,2}}{2}\right) \qquad Z_r \text{ ksi} = 1.547 \text{ kip}$$

Maximum horizontal shear per unit length

$$V_{sr} := \frac{V_{nf}\ Q_{BslabD}}{I_{stD}} \qquad V_{sr} = 6.059\ klf \qquad \textbf{(AASHTO 6.10.10.1.2-2)}$$

Therefore, horizontal shear is 0.505 kip/inch.

Pitch of shear connectors for strength limit state

$$P_{sc} := \frac{n_{sh}\ Z_r\ ksi}{V_{sr}} \qquad P_{sc} = 21.447\ in$$

In any case pitch of shear conenectors shall not exceed 24 inches as per AASHTO LRFD Bridge Design Specifications, 2004.

Thus provide shear connectors at longitudinal pitch of 18 inch center to center throughout the negative moment region for connecting bottom slab to bottom flange of the entire bridge.

Thus provide total of 1940 shear connectors in the negative region of bottom flange to connect bottom slab.

## G.13 Buckling of Bottom Steel Plate

The buckling stress of bottom flange is determined using classical theory on stability of plates

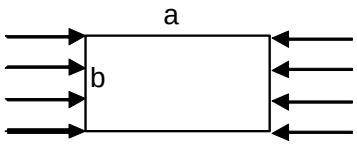


$a := 20\ in \qquad b := 96\ in$

$\frac{a}{b} = 0.208 \qquad \nu := 0.3$

$ab := \begin{pmatrix} 0.2 \\ 0.3 \\ 0.4 \\ 0.6 \\ 0.8 \\ 1.0 \\ 1.2 \\ 1.4 \\ 1.6 \\ 1.8 \\ 2.0 \\ 2.2 \\ 2.4 \\ 2.7 \\ 3.0 \end{pmatrix} \qquad K_s := \begin{pmatrix} 22.2 \\ 10.9 \\ 6.92 \\ 4.23 \\ 3.45 \\ 3.29 \\ 3.4 \\ 3.68 \\ 3.45 \\ 3.32 \\ 3.29 \\ 3.32 \\ 3.40 \\ 3.32 \\ 3.29 \end{pmatrix}$

$K_{s\_s} := \text{linterp}\left(ab, K_s, \frac{a}{b}\right)$

$K_{s\_s} = 21.258$

$K_{s\_sm} := \text{if}\left(K_{s\_s} > 22.2, 22.2, K_s\right)$

The stress that will cause buckling in the bottom flange can be determined using the formula given below.

$$\sigma_b := K_{s\_s} \frac{E_s}{1 - \nu^2} \left(\frac{t_{bf}}{b}\right)^2$$

The longitudinal spacing of 20 in. or less is adequate because the stress is above the yield.

## G.14 Temporary Bracing of Bottom Flange

### Non-Composite Section Properties

Area of the bottom flange, $A_{BF}$

$A_{BF} := 12in\ t_{bf}$

**Note:** Transverse section properties are calculated on per foot basis.

$A_{BF} = 12\ in^2$

Area of bottom slab, $A_{bslab}$

$A_{bslab} := 12in\ t_{bs}$ $A_{bslab} = 156\ in^2$

### Loads

Dead load of steel bottom flange, $DL_{stl}$

$DL_{stl} := 490\ pcf\ A_{BF}$

**Note:** 490 pcf is the unit weight of steel.

$DL_{stl} = 0.041\ klf$

Dead load of concrete bottom slab, $DL_{conc}$

$DL_{conc} := \gamma_{rc}\ A_{bslab}$

$DL_{conc} = 0.162\ klf$

Total factored loading used in the analysis, $DL_{tot}$

$DL_{tot} := 1.25\ (DL_{stl} + DL_{conc})$

$DL_{tot} = 0.254\ klf$

If we consider entire flange the pressure acting on the plate is $P_{DL}$

$$P_{DL} := \frac{DL_{tot}}{12\ in}$$

$P_{DL} = 1.765 \times 10^{-3}\ ksi$

### Calculate Stress Without Bracing

For the unbraced bottom flange, the bottom flange will span between webs like a simple beam under its own self-weight and weight of wet concrete.

Using the rectangular plate tables from *Design of Welded Structures* by *Blodgett*, the stress in the plate can be calculated from the loading and plate thickness.

Stress in the bottom plate, $\sigma_1$

$$\sigma_1 := \frac{0.75\ P_{DL}\ (b_{bf})^2}{t_{bf}^{\ 2}}$$ $\sigma_1 = 13.238\ ksi$

$CHECK\_16 := if(\sigma_1 < 20ksi, "OK", "NG")$ $CHECK\_16 = "OK"$

**Deflection Check**

$$\Delta_d := \frac{0.1422\ P_{DL}\ b_{bf}^{4}}{E_s\ t_{bf}^{3}} \qquad \Delta_d = 0.865\ in$$

$$\Delta_{allow} := \frac{b_{bf}}{360} \qquad \Delta_{allow} = 0.278\ in$$

We need to provide bracing along bottom flange to temporarily support concrete until it cures.

## Calculate Deflection With Bracing

Assume bracing at every 10 feet in the form of WT's supported from two inch bottom flange extension to the exterior of box girder.

The width of the panel, w (feet) $\quad w := b_{bf}$

The length of the panel, L (feet) $\quad L_{br} := 10\ ft$

$$\frac{L_{br}}{w} = 1.2$$

The maximum deflection of plate, $\Delta_{braced}$ $\quad \Delta_{braced} := \frac{0.0616\ P_{DL}\ (b_{bf})^{4}}{E_s\ t_{bf}^{3}}$

$$\Delta_{braced} = 0.375\ in$$

The deflecion is within the limits required by AASHTO, however the deflection is not. The bracing would have to be moved even closer to limit the deflection of the bottom plate to L/360

Deflection for bracing at 5 feet, $\Delta_{5ft}$ $\quad \Delta_{5ft} := \frac{0.0964\ P_{DL}\ (60in)^{4}}{E_s\ t_{bf}^{3}}$

$$\Delta_{5ft} = 0.076\ in$$

Deflection for bracing at 2 feet, $\Delta_{2ft}$ $\quad \Delta_{2ft} := \frac{0.1422\ P_{DL}\ (24in)^{4}}{E_s\ t_{bf}^{3}}$

$$\Delta_{2ft} = 0.003\ in$$

Once the braces are removed the bracing force is applied back to the composite section.

Conservatively, if the entire load is then reapplied to the section and that deflection is added to the non-composite deflection, we will have the upper bound of the solution.

Composite deflection after removal of braces, $\Delta_{abrace}$

$$\Delta_{abrace} := \frac{0.1422\ P_{DL}\ (b_{bf})^4}{E_s \left(t_{bf} + \frac{t_{bs}}{3n}\right)^3}$$

$$\Delta_{abrace} = 0.201\ in$$

## Calculate Deflection for Selected Bracing Member

Try a bottom flange brace of a WT8 x 13

Inertia of WT8 x 13, $I_{brace}$

$$I_{brace} := 23.5 in^4$$

Deflection of WT8 x 13, $\Delta_{wbrace}$

$$\Delta_{wbrace} := \frac{5\ (P_{DL}\ 2ft + 13\ plf)\ (b_{bf})}{384\ E_s\ I_{brace}}$$

$$\Delta_{wbrace} = 0.083\ in$$

Conservatively, the maximum deflection after removal of braces, $D_{tot\_max}$

$$\Delta_{tot\_max} := \Delta_{2ft} + \Delta_{abrace} + \Delta_{wbrace}$$

$$\Delta_{tot\_max} = 0.286\ in$$

The above estimate is conservative, in reality, the maximum deflection should be less than 0.28 inch.

# APPENDIX H

Supplementary on Finite Element Model

## H.1 Introduction

This Appendix contains additional information about the finite element model that was omitted for brevity from Chapter 8.

## H.2 Finite Element Model

### H.2.1 Finite Element Mesh

#### H.2.1.1 Pre-Test Mesh

There were several finite element models created over the course of the project to model the double composite test specimen. At the design stage (prior to testing), the primary goal of the finite element analysis was to include non-linear behavior of the steel and concrete in the analysis. The finite element mesh used for analysis during the design phase is shown in Figure H.1. The model was simplified to maintain a reasonable run time. Due to geometric symmetry only one half of the section was modeled and symmetry boundary conditions were used at the symmetry plane [H.1]. Steel bottom flange and web were modeled with 4 node shell elements (SHELL181) with 6 degrees of freedom (DOF) (3 displacements and 3 rotations) at each node, while steel top flange was modeled with 8 node brick elements (SOLID185) with 3 DOF (3 displacements). To allow for load transfer at the interface between the steel web (shell) and the top flange (solid element), the shell elements were embedded through the depth of the solid element. This results in fairly accurate transfer of loads from the shells to the solids [H.1]. Top and bottom concrete slabs were modeled with 8 node concrete brick element (SOLID65) with 3 DOF at each node (3 displacements), which is capable of modeling concrete cracking, crushing and effect of steel reinforcing by smearing the stiffness [H.1]. To prevent numerical instability from localized cracking, all concrete elements were modeled with smeared reinforcement in three mutually perpendicular directions with reinforcement ratio of 0.001%. Reinforcing steel provided per design was not modeled using smeared reinforcing, but instead was discretely modeled with 2 node link (spar) element (LINK8) with 3 displacement DOFs at each node. Strain compatibility between the reinforcing steel elements and concrete elements was modeled by using common nodes. Reinforcing elements were distributed uniformly along all the nodes located at the appropriate layer of nodes and the area of the spar elements are set so that the total reinforcement area in the model matched the area of rebar provided in the specimen.

Design calculations and current finite element modeling practice [H.2] for composite design assumes strain compatibility at interface between the concrete and steel. This was modeled by using shared nodes for steel and concrete members at the interface. Shell elements used in the model have the capability to have the nodes defined at an offset from the centroid, therefore permitting accurate modeling of the location of the interface nodes. At the interface between the bottom of the bottom concrete slab and the top of the bottom steel flange, the concrete element nodes do not possess rotational DOFs of the shell elements used for the bottom flange. However, studies with shell elements have shown the impact of this type of incompatibility is small if an adequate mesh density is used [H.2].

All elements were modeled with non-linear material properties (see Section H.2.2). Shear studs and diaphragm members were not explicitly modeled, but their effect was approximated with coupling DOF to simulate rigid behavior. Coupling DOF results in specific DOF (say horizontal displacement) in specified nodes, to have the same value. The model comprised of 14K nodes and 21K elements and needed approximately 14 hrs of run time on a 3GHz Pentium 4 PC with 2.5 GB RAM running Windows XP (32 bits).

### H.2.1.2 Post-Test Mesh

Pre-test analysis performed assuming perfect composite action between the bottom flange and bottom slab failed to predict the observed failure load as well as failure mode (bottom flange buckling). During the design phase, the model idealization was based on prevailing standard practice [H.2] and the anticipated full composite behavior of the structure. However, once the failure mode was found to be a result of bottom flange buckling, the finite element model was refined several times until the numerical results were found to capture the experimental observations.

Figure H.2 shows the final post-test finite element mesh. The mesh density of typical cross-section (see Figure H.1) remained similar to the pre-test model, however number of elements along the length of the specimen was more than doubled to better capture buckling deformation. As shown in Figure H.2, the geometry of the top slab at hold down and actuator end was modified to match that of the actual test specimen. In addition, diaphragms, cross-frames and loading frame were explicitly modeled. To better compute the stresses in the bottom flange (since it impacts bottom flange buckling response), temporary bracing members used prior to curing of bottom slab were also explicitly modeled and used at the initial construction stages.

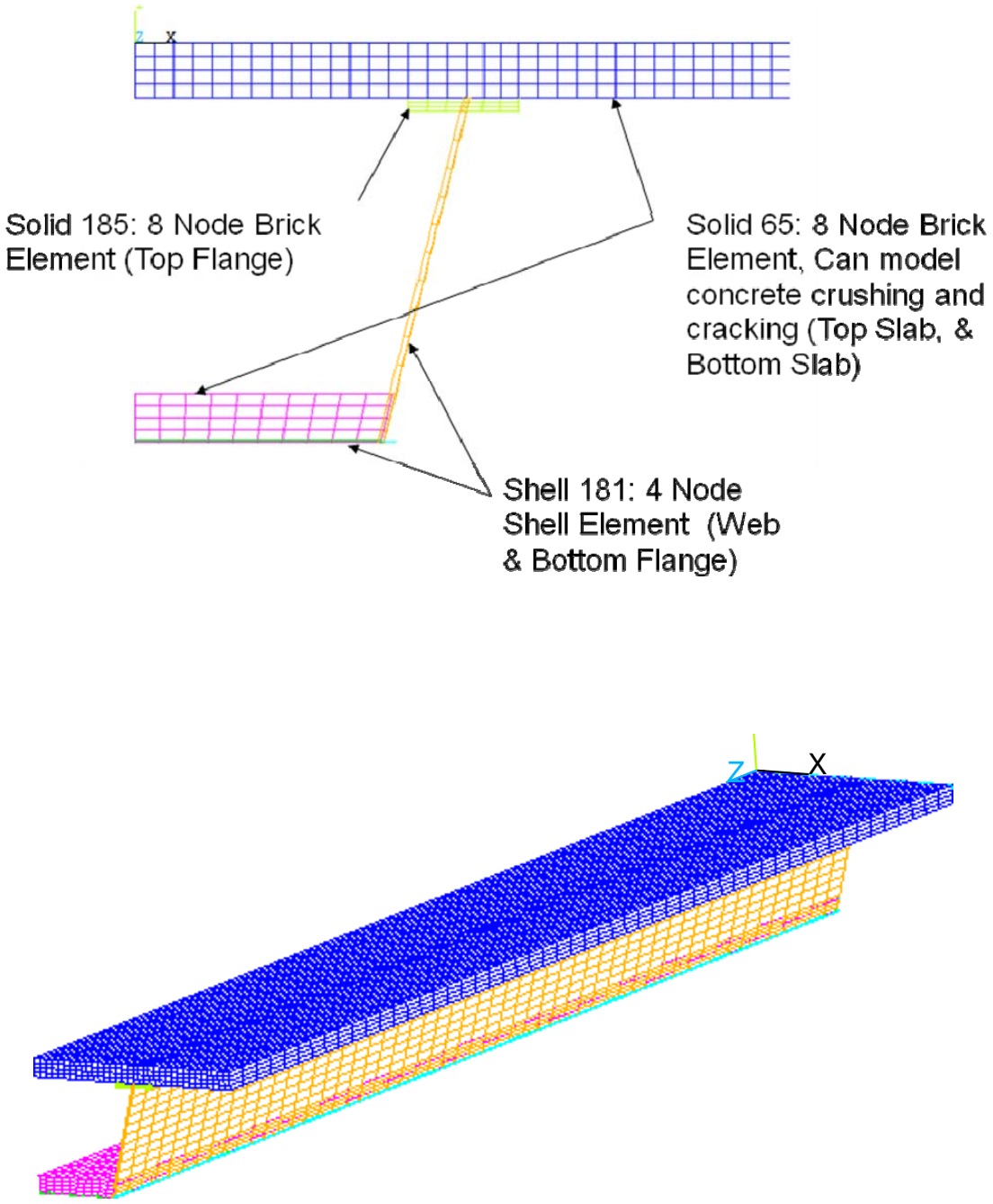


**Figure H.1** Finite element mesh - pre-test.

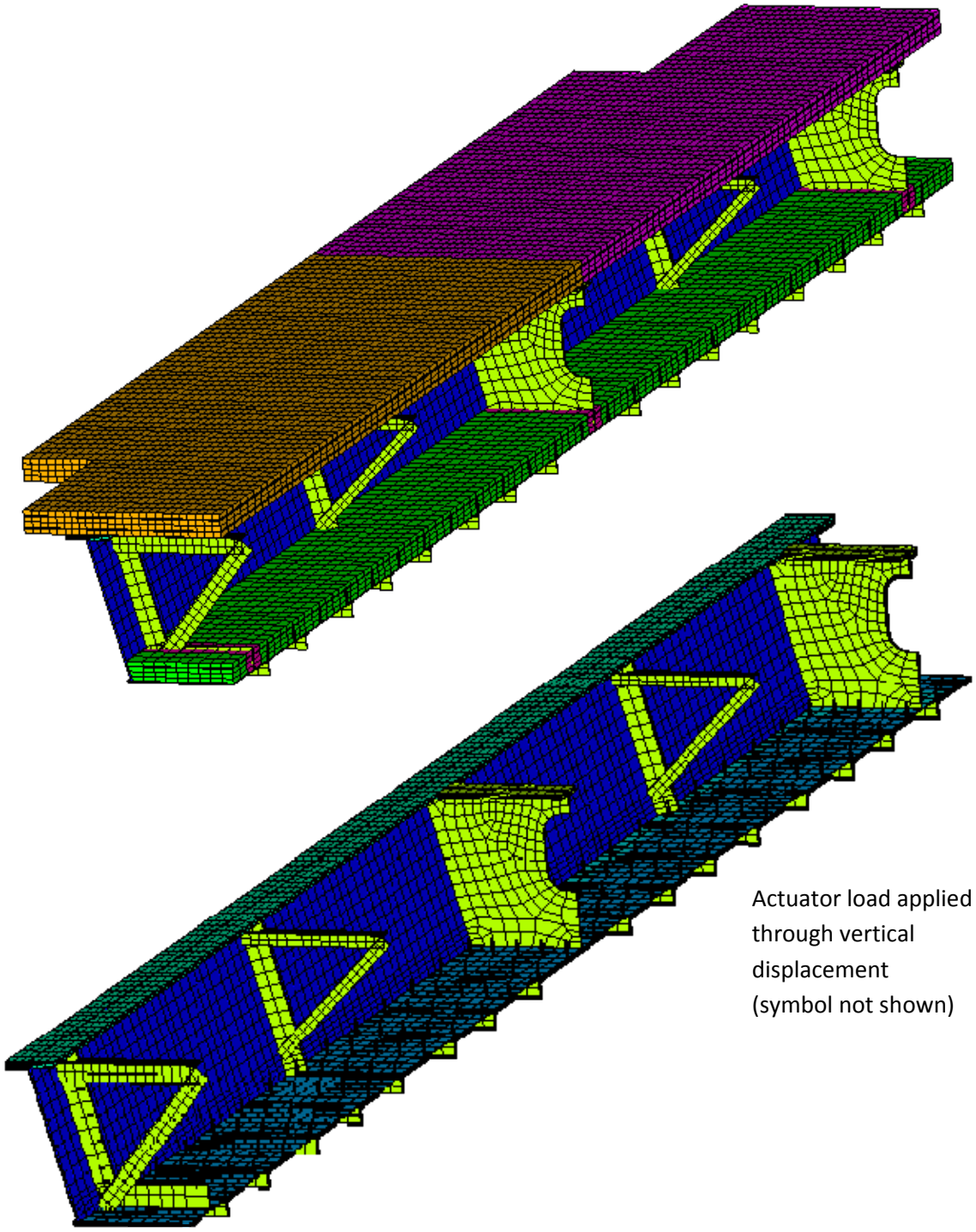


**Figure H.2** Finite element mesh – post-test.

Test results shown in Chapter 7 indicates that the bottom flange buckles (see Fig. 7.8) and therefore does not act compositely with the bottom slab, therefore the post-test model has independent set of nodes at the bottom slab and bottom flange interface. Since buckling of bottom flange is a function of its rotational stiffness, individual shear studs were explicitly modeled (see Figure H.2b) on the bottom flange using beam elements (BEAM188) with circular cross-section of 3/4" diameter. Contact elements (CONTAC174 and TARGET170) were used at the bottom flange to bottom slab interface to accurately model the non-composite interaction between the two parts. To simplify the analysis, friction between the interface was ignored since shear transfer is expected to occur primarily through shear studs. The top flange was assumed to act perfectly composite with top slab and their interface was modeled with common nodes.

Compared to the pre-test model, meshing of the final model was far more complex due to the need to explicitly model shear studs, temporary bracing at the bottom flange, the cross-frames, loading frame and diaphragms. Available computational resources limited the size of the model that was considered practical given the run-times and data storage requirements. The mesh density was selected based on studies performed on representative simpler model of the bottom flange to ensure it can accurate predict buckling based on closed form predictions available in textbooks such as Roark's Handbook [H.3]. The final post-test model comprised of 31K nodes, 46K elements, which is more than double the size of the pre-test mesh. The larger model size and additional complexities (such as contact elements) required use of a powerful computer to perform the analysis. The run time for the model was between 28-36 hrs on a Quad core Q9300 PC with Vista 64 & 6GB of RAM. Size of a typical set of result file generated from a single analysis ranged from between 30 GB to 120 GB. In combination with inherent complexity of non-linear analysis, the long run times and computational resources required for the final model made refinement and debugging process extremely time consuming.

### H.2.2 Material Properties

To accurately account for the observed behavior of the structure during testing, material models of the structural steel (HPS), reinforcing steel and concrete included non-linear portion of the stress-strain curve. Concrete material model in ANSYS [H.4] includes the ability to capture change in stiffness due to tensile cracking and compressive crushing. It can also include a non-linear stress-strain relation. Based on preliminary analysis, the crushing feature was disabled due to difficulty to obtain a converged solution at even at relatively low loads due to presence of localized regions with high compressive loads. Instead, the loss of stiffness due to crushing was modeled by using a stress-strain curve a very small slope at the crushing load based on a modified Hognestad model shown below [H.5] (see Figure H.3a).

$$\sigma = f''_c \frac{\varepsilon}{\varepsilon_0}\left(2 - \frac{\varepsilon}{\varepsilon_0}\right) \qquad \text{(H.1)}$$

$$\varepsilon_0 = \frac{2f''_c}{E_t} \qquad \text{(H.2)}$$

$$f''_c = r_c f'_c \qquad \text{(H.3)}$$

Here $\sigma$ is the stress at a specified strain $\varepsilon$, $\varepsilon_0$ is the strain corresponding to the maximum compressive stress, and $f'_c$ is the compressive strength of concrete. A value of $r_c$ of 0.85 is typically used for hand calculations (also see section 9.3.2), which corresponds to the factor used when the compression block at ultimate condition is approximated with a rectangular block with uniform compressive stress of $0.85f'_c$. However, since the finite element model can more accurately model the compression block at ultimate load (it doesn't have to be represented by a rectangle), a value of $r_c = 1$ is used to generate the stress strain curves used for the analysis, which was found to be a good approximation of typically measured stress-strain curves [H.6]. Although, based on the assumed model, the strain at maximum stress is 3500 με for the bottom slab (see Figure H.3a), based on typical test results [H.5] and limits found in ACI [H.7], ultimate strain of concrete was assumed to be 3000 με. Fig. 9.9 shows concrete stress-strain curve including parts of stress-strain curves beyond 3000 με, where the stiffness is negative. This part of the curve does not affect the capacity of the double composite section, and therefore was omitted to avoid numerical difficulties caused by negative stiffness.

Since the non-linear procedure used by ANSYS uses the tangent modulus to compute the stiffness matrix, the stress-strain curve data was input using a fine resolution of twenty equally spaced points between 0 strain and strain at maximum stress (eqn. H.2). Different concrete strengths were used for bottom slab, and two halves of the top slab as shown in Table H.1 (also see Appendix B). Poisson's ratio of concrete was assumed to be 0.2. For dead load computation, density of reinforced concrete was assumed to be 150 pcf. Concrete shrinkage strains for top and bottom slab were estimated based on CEP FIP 1990 [H.9]. Bottom slab shrinkage strain were estimated to be 140 με based on approximately 480 days of shrinkage and top slab strain to be approximately 98 με based on 300 days of shrinkage. These values are lower than typical values found in other sources [H.10-H.11]. Due to low sustained concrete stresses, concrete creep effects were ignored.

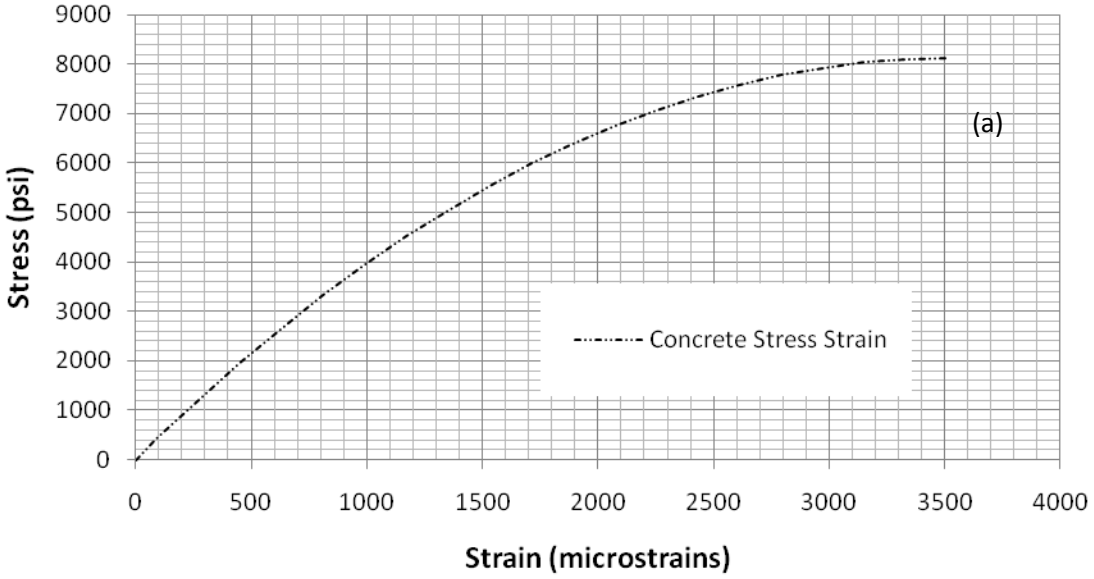


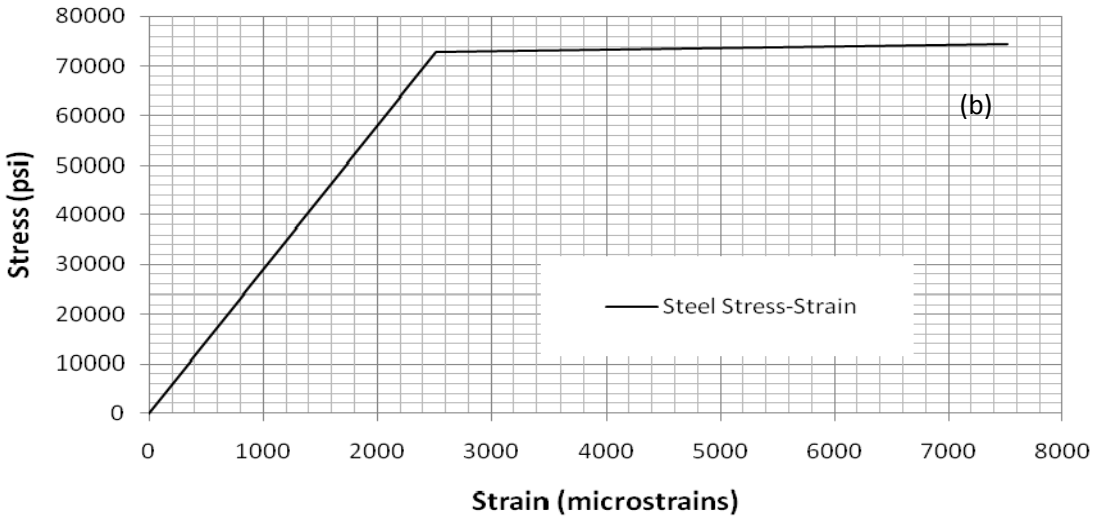


**Figure H.3** Typical stress-strain curve a) Concrete - Modified Hognestad model b) Steel - Bilinear.

**Table H.1** Material Properties

| Part | Modulus of Elasticity (ksi) | Stress-strain Model | Yield Stress (steel) or Compressive Strength (slab) (psi) |
|---|---|---|---|
| **Top Slab - Hold Down Side** | 4,487* | Modified Hognestad | 7,650 (5778**) |
| **Top Slab Actuator Side** | 5,162* | Modified Hognestad | 10,124 (7824**) |
| **Bottom Slab** | 4,622* | Modified Hognestad | 8,118 (6872**) |
| **Top Flange** | 28,400 | Bi-linear | 80,471 |
| **Web** | 31,690 | Bi-linear | 80,458 |
| **Bottom Flange** | 30,875 | Bi-linear | 80,875 |
| **Rebar** | 29,000 | Bi-linear | 73,000 |
| **Shear Stud** | 29,000 | Bi-linear | 73,000 |
| **Diaphragms, Cross frame, Loading Frame and Temporary Bracing** | 29,000 | Linear | N/A |

*Modulus modified by factor 0.9 to adjust for Florida limerock coarse aggregate [H.8]
**28 day compressive strength used for shrinkage computations

Based on test data reported in the Appendix, HPS steel was modeled with a bi-linear kinematic hardening model (see Figure H.3b). The slope of the curve past the yield point was set to an arbitrary small value of 1% of modulus of elasticity. Different yield strengths were used for the top flange, web and bottom flange. The yield strength and modulus of elasticity were set to the average value reported in the Appendix B (see Table H.2). Based on test data, reinforcing steel and shear stud was also modeled with bi-linear kinematic hardening model, with an average

yield strength of 73 ksi based on test results reported in the Appendix B. Poisson's ratio of steel was assumed to be 0.3. Density of structural steel was assumed to be 490 pcf for dead load computations.

### H.2.3 Boundary Conditions and Loading

The following DOF constraints were applied to the model

a. As stated in Section H.2.1.1, since only half the section was modeled due to symmetry and symmetry boundary conditions (constrained out of plane motion and rotations) were applied at the symmetry plane (see Figure H.4).

b. Actuator load was modeled by applying vertical displacement at appropriate node. This was done because non-linear solutions tend to be more stable when subjected to applied displacements rather than forces. The actuator load corresponding to an applied load was obtained from the computed reaction at the displaced node.

c. Nodes located at top slab at the hold-down location were constrained vertically to model the hold-down restraints.

d. Bottom flange nodes at the center support locations were constrained in the vertical and longitudinal directions.

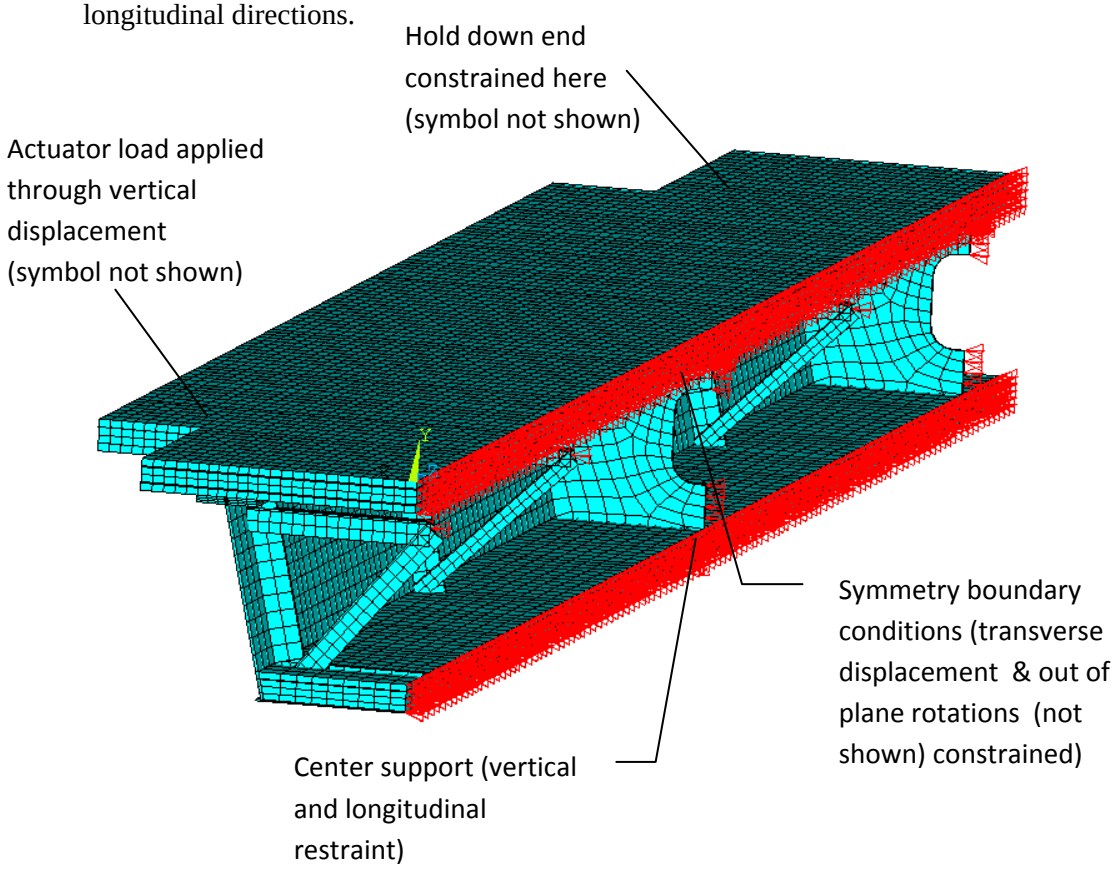


**Figure H.4** Primary boundary conditions.

Interfaces between various parts were modeled as follows.

a) Top slab (shell) to rebar (spar) - Based on assumption of strain compatibility all rebar modeled share nodes with the concrete slab elements.

b) Top-slab (solid) to top flange (solid)- As stated in Section H.2.1.2, based on assumption of composite action, common nodes were used at the interface between the top flange and the top slab. Shear studs were not explicitly modeled on the top flange.

c) Top flange (solid) to web (shell) - The web is embedded through the depth of the top flange (solid elements) to ensure proper transfer of moments between the shell element to the solid element.

d) Web (shell) to bottom flange (shell) - These members share common nodes at the interface.

e) Bottom flange (shell) to shear stud (beam) - These members share common node (lower most node of the shear stud is shared with the bottom flange).

f) Bottom flange (shell) to bottom slab (solid) - As stated in Section H.2.1, the interface between the bottom flange and bottom slab was modeled using contact elements without friction. The bottom flange steel deforms under self weight and dead weight of the concrete. For contact elements to work accurately, the bottom slab nodes had to be redefined to take the deformed profile of the bottom slab (while maintaining the 7" thickness).

g) Bottom slab (solid) to shear stud (beam) - Each shear stud is modeled with three elements with a total of four nodes per shear stud. As stated above, the bottom node is shared with the bottom flange element and results in a perfect bond between the shear stud and the bottom flange. The other three nodes are common nodes between the shear stud and the bottom slab, again resulting in a rigid interface. To model shear transfer between the bottom shear stud node and bottom slab, displacement DOF that occur in the plane of the bottom flange are coupled (i.e., in plane displacements will be compatible), however, out of plate displacement of bottom node is permitted (such as due to axial stretching of the shear stud).

h) Bottom flange to temporary bracing elements - Since each end of the bracing element is bolted on to the bottom flange, the outermost node (near the web) is coupled in all three displacement degrees of freedom. Contact between the bottom flange and the bracing element is modeled by coupling vertical displacement of the bracing element nodes and bottom flange node located at the same location. As stated in Section H.2.1.1, coupling of DOF results in the DOF are the coupled nodes having the same value (essentially enforcing compatibility of the specified DOF).

i) Web and flanges to diaphragms, cross frame and loading frame - All these members share common nodes at the interfaces.

j) Diaphragms to bottom slab – Vertical interface between diaphragm and bottom slab results in discontinuity of top fiber strain in the bottom slab. This is modeled by changing the bottom slab material on either side of the diaphragm to have zero tensile strength (i.e., concrete cracks at any non-zero load). Interaction between the diaphragm and the bottom slab due to compression is ignored and compressive loads are transferred directly to the adjacent concrete element (i.e., no common nodes are used between the diaphragm and bottom slab).

k) Web to bottom slab - Load transfer at this interface was ignored since it is expected to be small since the loads are primarily longitudinal. Due to omission of contacts at this interface, transverse loads from the web are transferred to the bottom slab through the shear studs.

The test specimen was loaded in the sequence shown in Table H.2 to account for the construction staging. In ANSYS elements that do not exist at a certain construction stage (example, concrete slabs in the initial condition) can be deactivated (or KILLed[H.1]). When KILLed, the stiffness of the elements is reduced to a small value and its dead load is set to zero. These elements can be activated by making them ALIVE [H.1]. When an element is made ALIVE, its initial strains are set to zero and full stiffness and dead load is restored.

## H.3 Results

Numerical results shown in Figs H.5 - H.40. Description of the comparisons can be found in Chapter 8.

**Table H.2** Load steps

| Load Step | Loading | Active elements (Live elements) | Inactive elements (Dead elements) | Comment |
|---|---|---|---|---|
| **1** | Self weight of the steel | Steel box + Temporary bracing | Top & Bottom Slab (including rebar) | Soffit constrained at center support and hold down end. |
| **2** | Previous load step + Wet concrete dead load | Steel box + Temporary bracing | Top & Bottom Slab (including rebar) | Pouring of bottom slab. |
| **3** | Previous load step | Steel box + Temporary bracing + bottom slab (including rebar) | Top slab(including rebar) | Bottom slab cured |
| **4** | Previous load step + shrinkage strain in bottom slab | Steel box + bottom slab (including rebar) | Top slab (including rebar) + Temporary bracing | Temporary bracing removed |
| **5** | Previous load step + top slab dead load | Steel box + bottom slab (including rebar) | Top slab (including rebar) + Temporary bracing | Top slab being poured. Soffit constrained at center support, hold down end and actuator end. |
| **6** | Previous load step + top slab shrinkage strain + bottom slab updated shrinkage strain | Steel box + bottom slab (including rebar) + top slab (including rebar) | Temporary bracing | Top slab cured. Top and bottom slab subjected to shrinkage between being cured and commencement of testing. |
| **7** | Previous load step + Actuator deflection of 15 inches | Steel box + bottom slab (including rebar) + top slab (including rebar) | Temporary bracing | The load is subdivided into 750 steps. Solution stops when the structure becomes unstable. Soffit constrained at center support, top slab constrained at hold down location. |

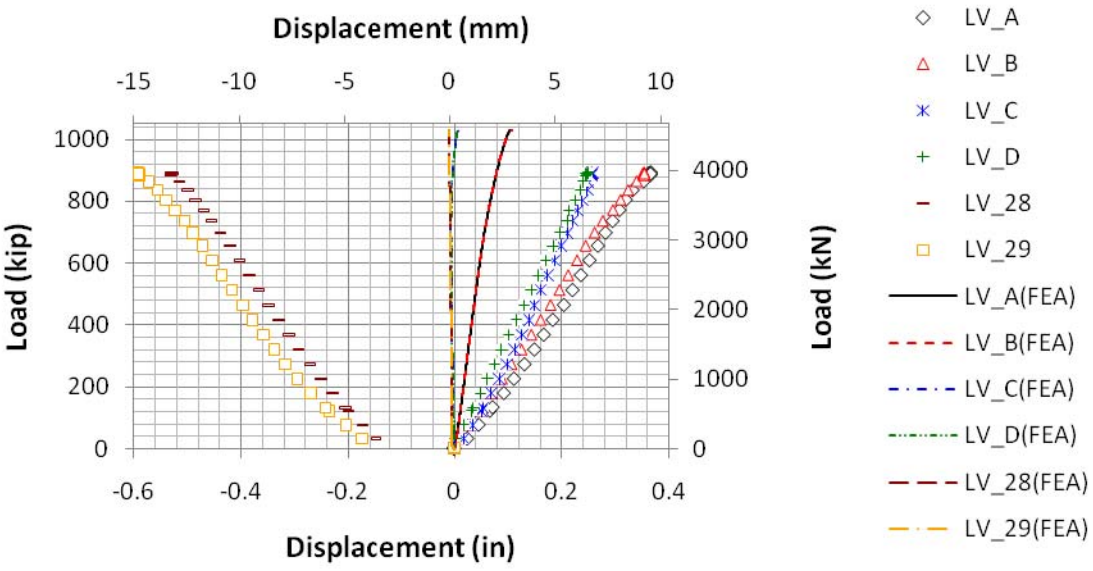


**Figure H.5 Deflections near center supports (LV A through LV D) and hold down end (LV 28 and 29).**

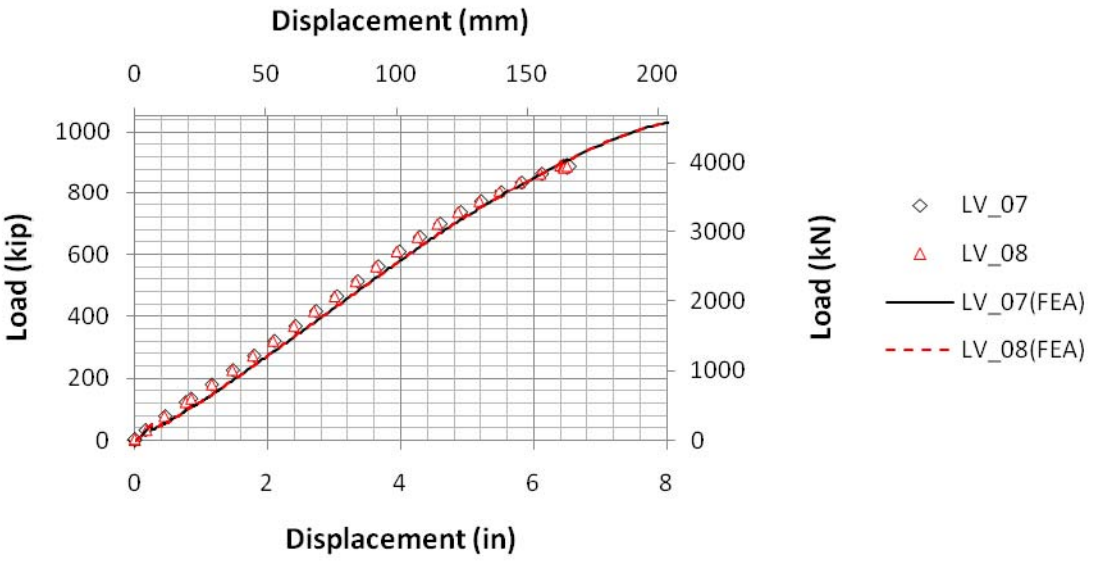


**Figure H.6 Adjusted actuator deflection.**

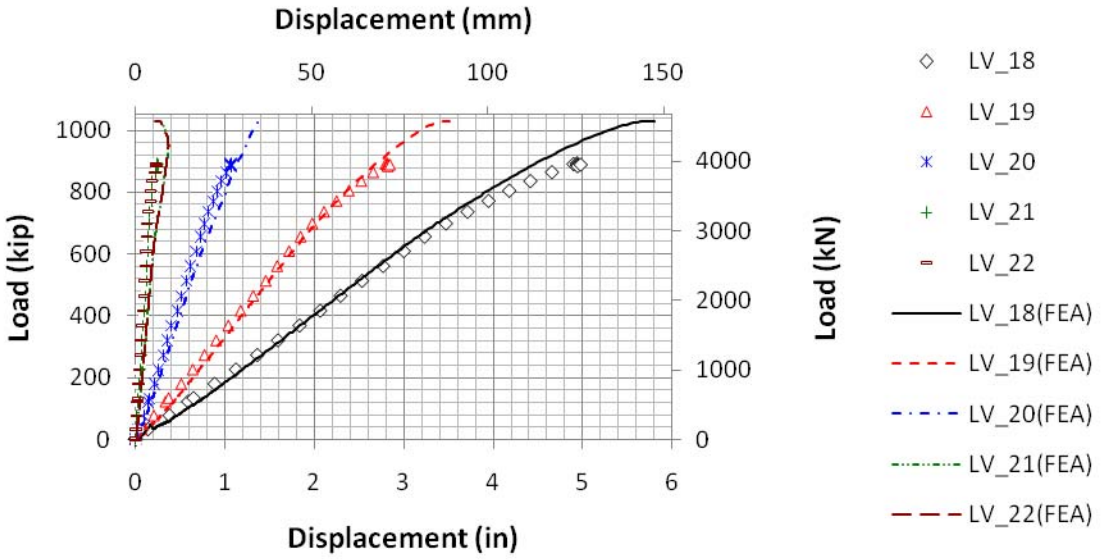


**Figure H.7 Adjusted bottom flange deflection on actuator side (LV 18 - 1H.75ft from center support at CL box, LV 19 - 12.5 ft from center support at CL box, LV 20 6.25 ft from center support at CL box, LV 21 - 2'-0 1/4" from center support 1.5 ft west from CL box, LV 22 - 2'0 1/4" from center support, 1.5 ft east from CL box).**

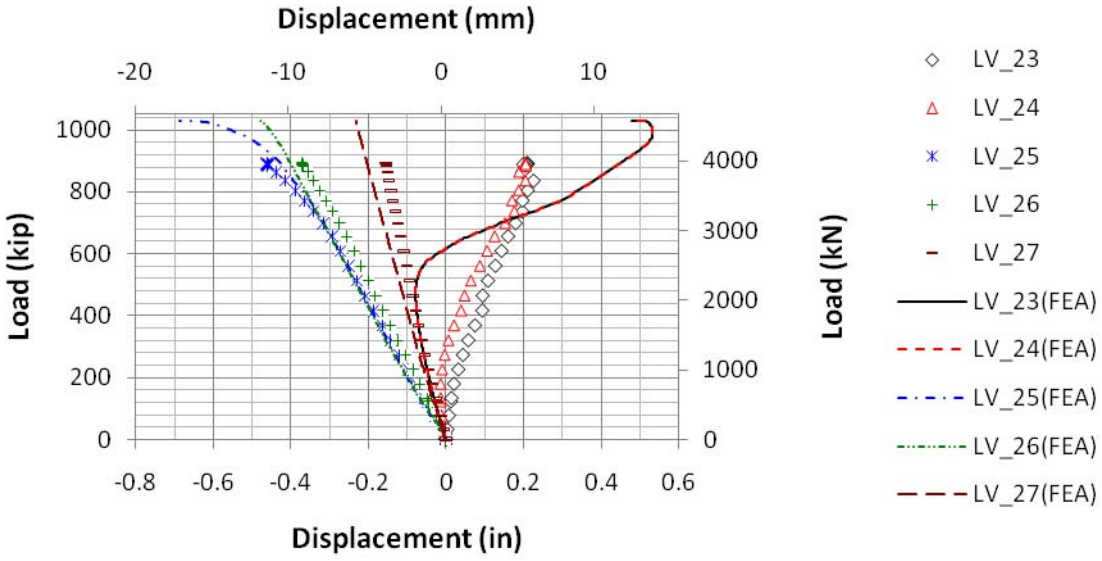


**Figure H.9 Adjusted bottom flange deflection on hold-down side.**

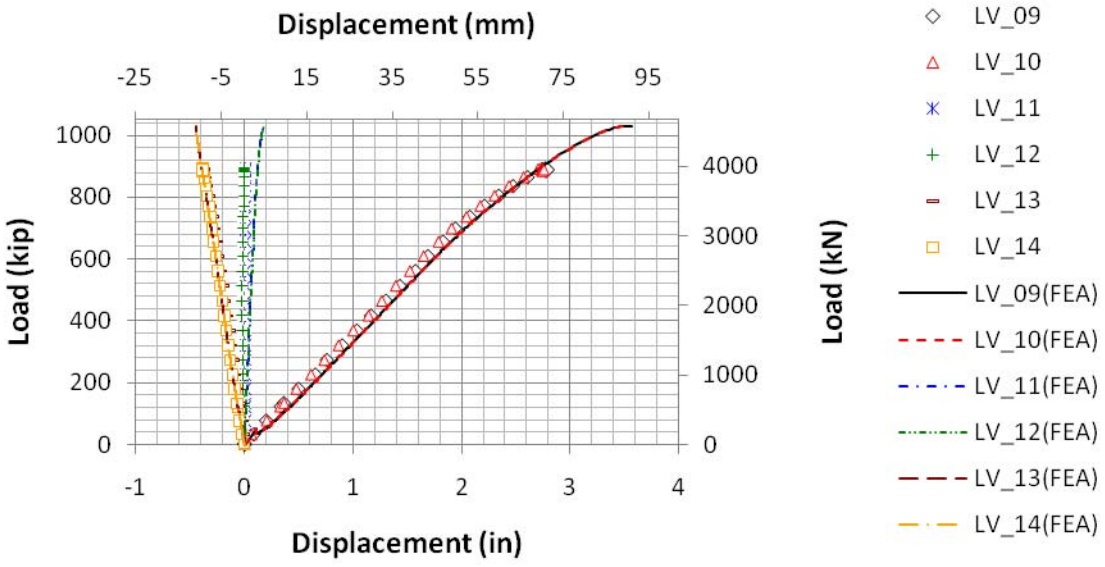


**Figure H.10 Adjusted top flange deflection.**

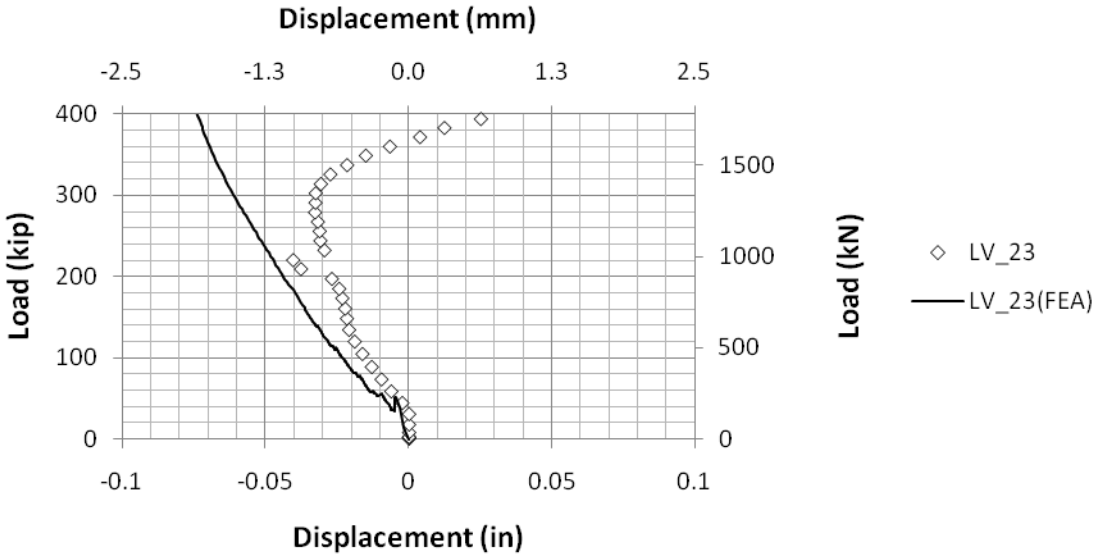


**Figure H.11 Adjusted bottom flange deflection Service I cycle 1.**

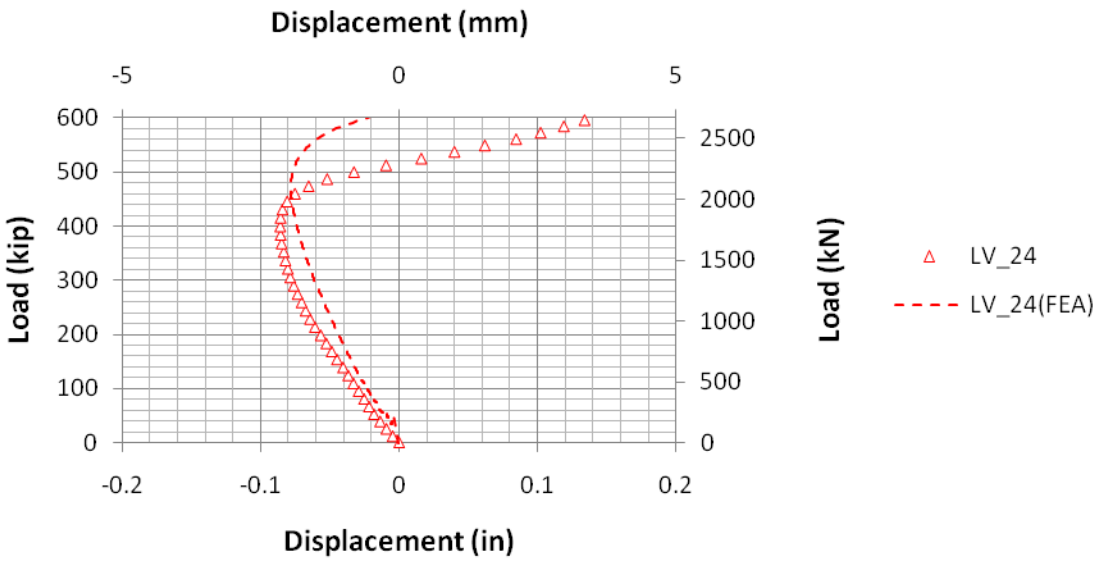


**Figure H.12 Adjusted bottom flange deflection Service II cycle 1.**

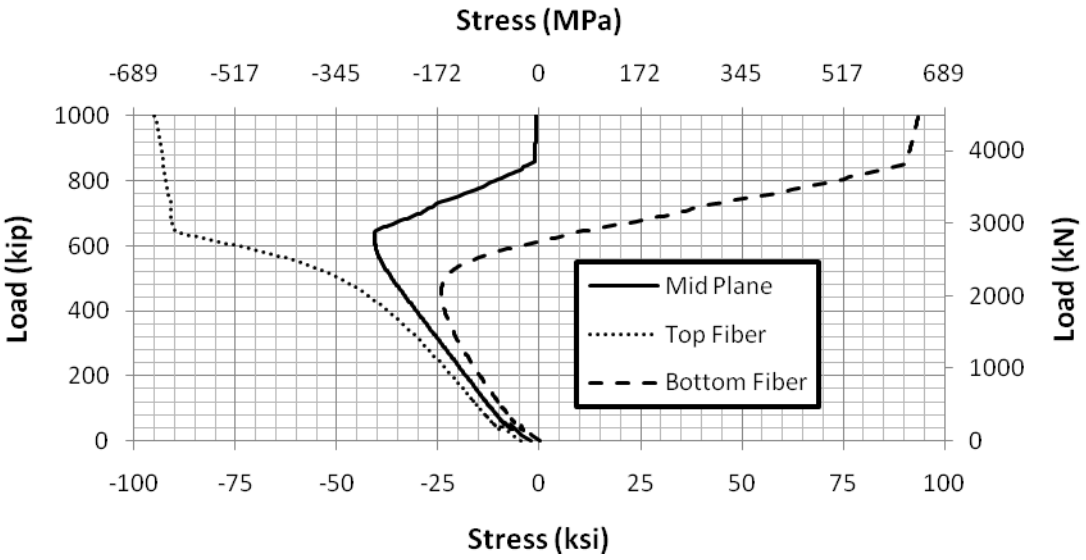


**Figure H.13 Longitudinal bottom flange stress in the buckled region.**

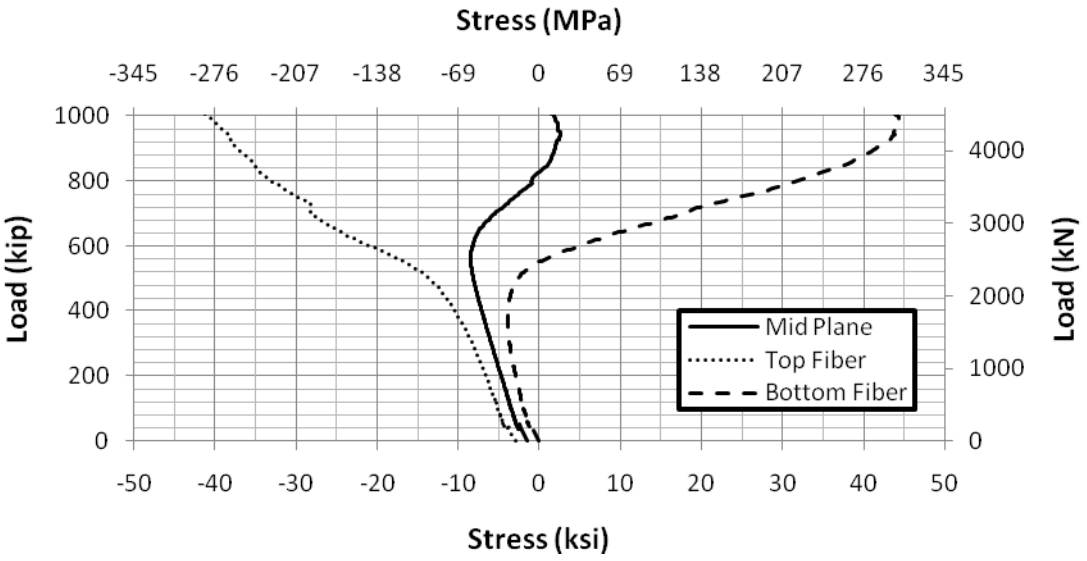


**Figure H.14 Transverse Bottom flange stress in the buckled region.**

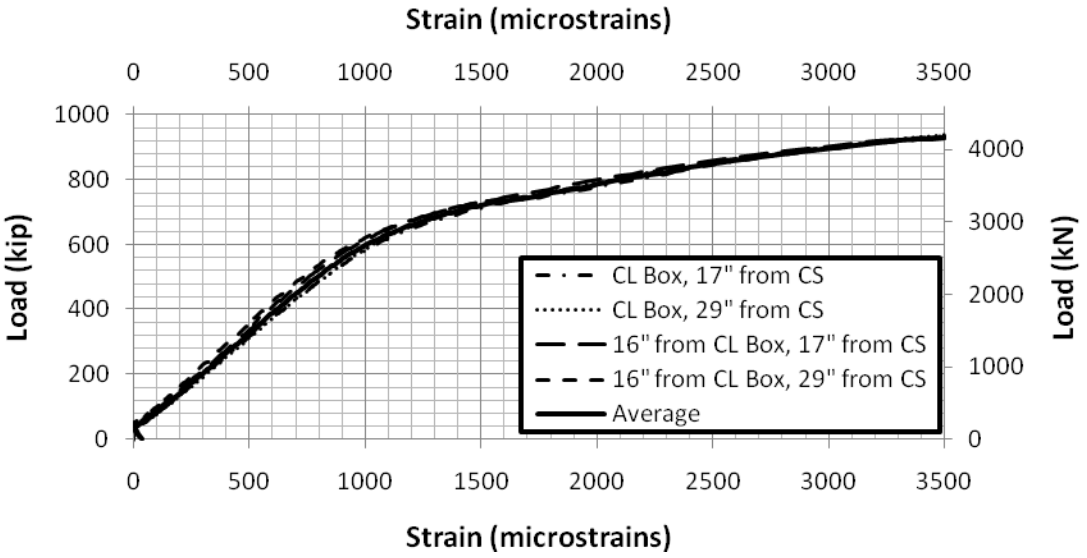


**Figure H.15 Bottom slab bottom fiber concrete strain at buckled region on hold down side (transverse variation in strain shown).**

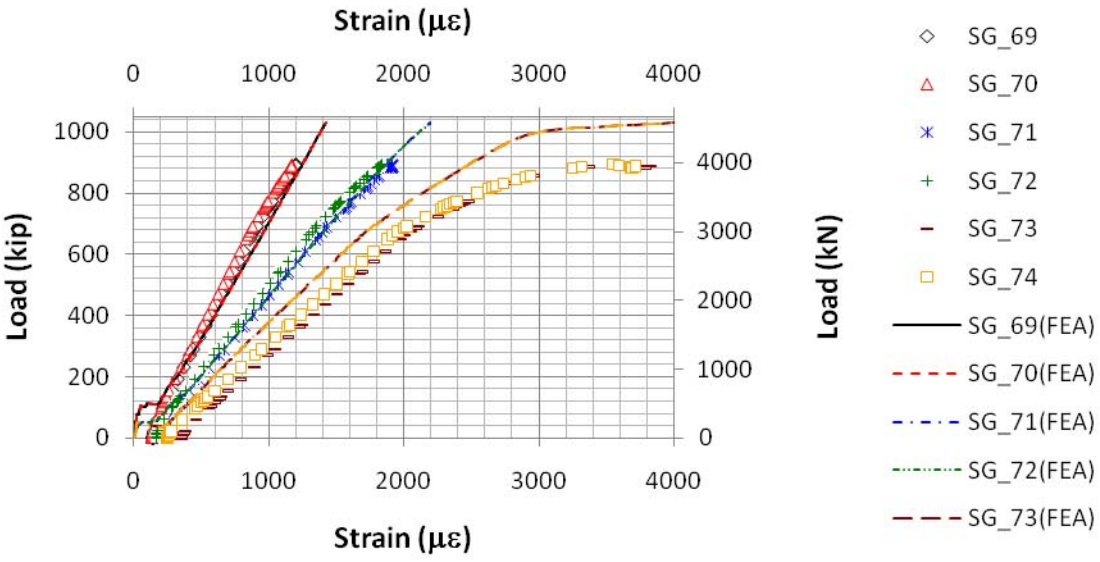


**Figure H.16 Top flange strains on the actuator side.**

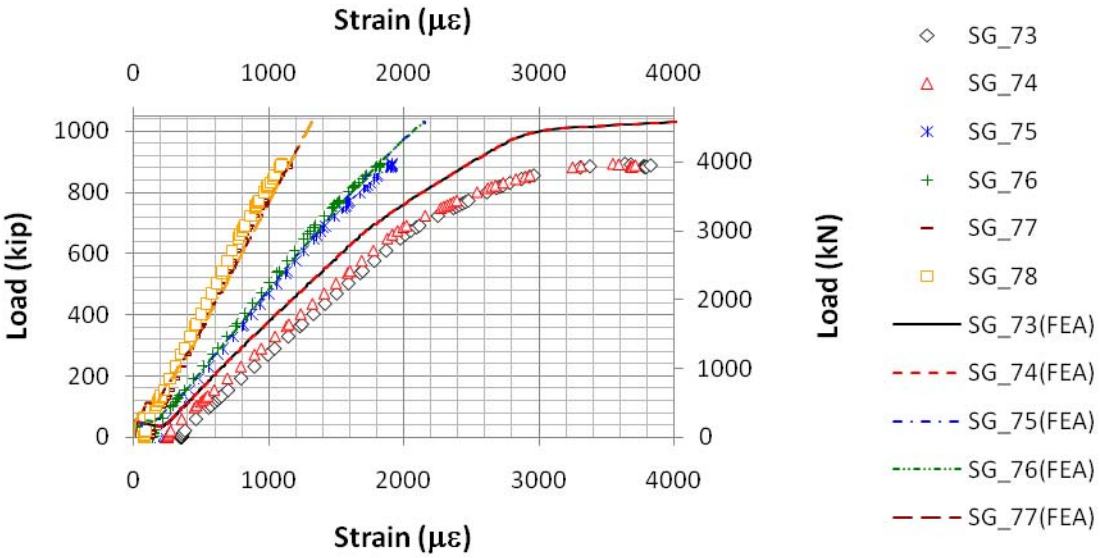


**Figure H.17 Top flange strains on the hold-down side.**

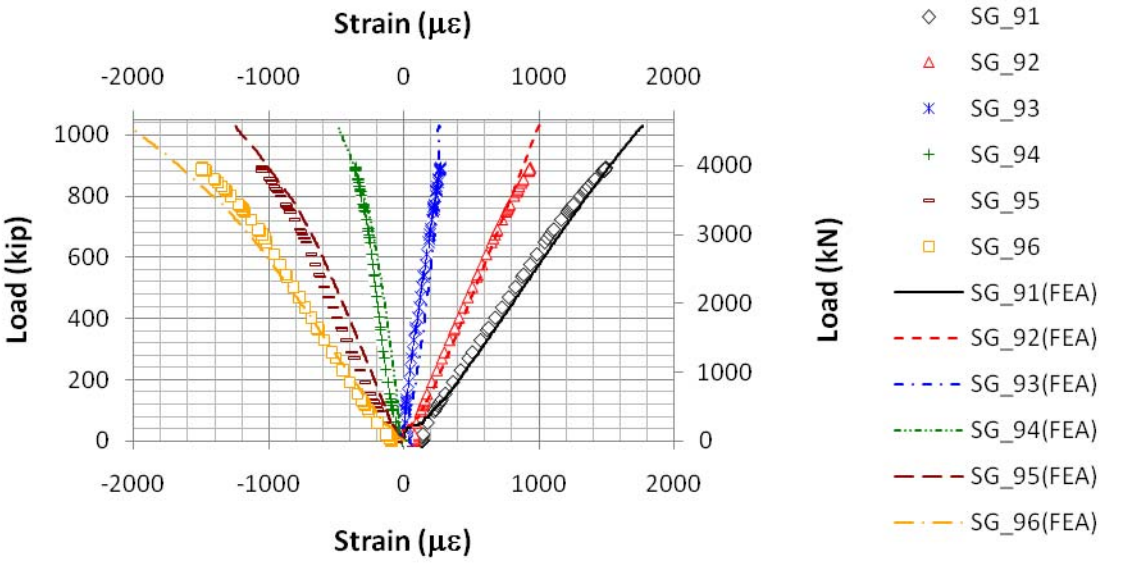


**Figure H.18 West Web exterior face strains 4'-10 1/8" from center support on the actuator side.**

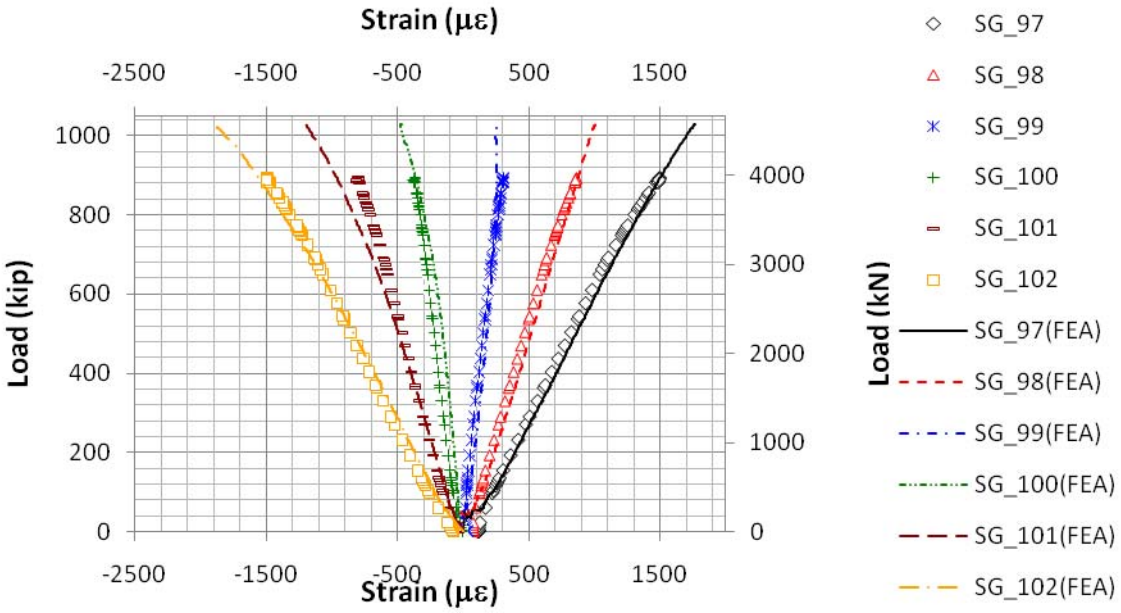


**Figure H.19 West Web exterior face strains 4'-10 1/8" from center support on the hold-down side.**

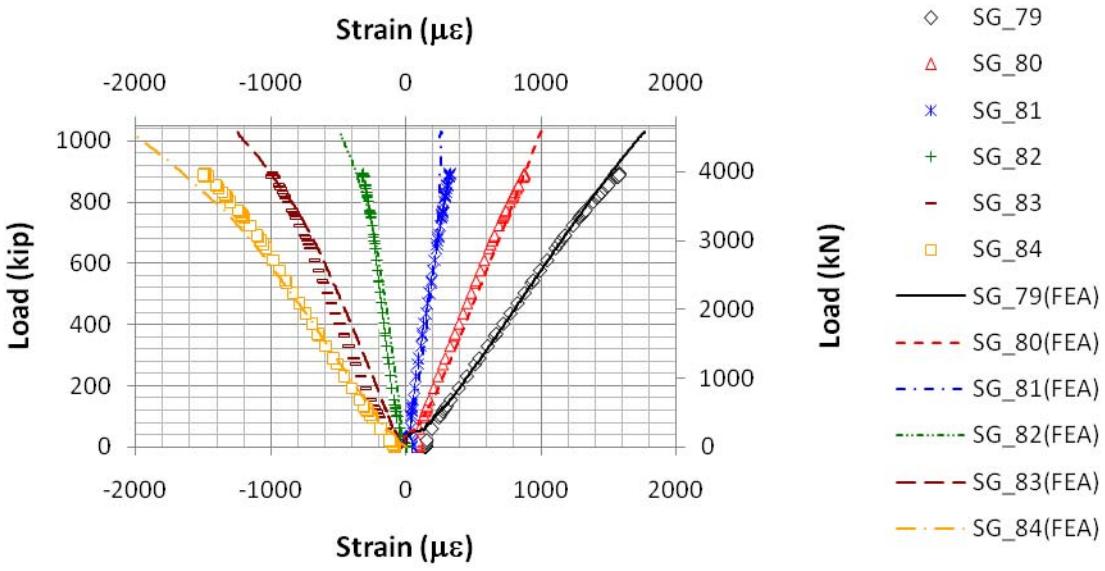


**Figure H.20 East Web exterior face strains 4'-10 1/8" from center support on the actuator side.**

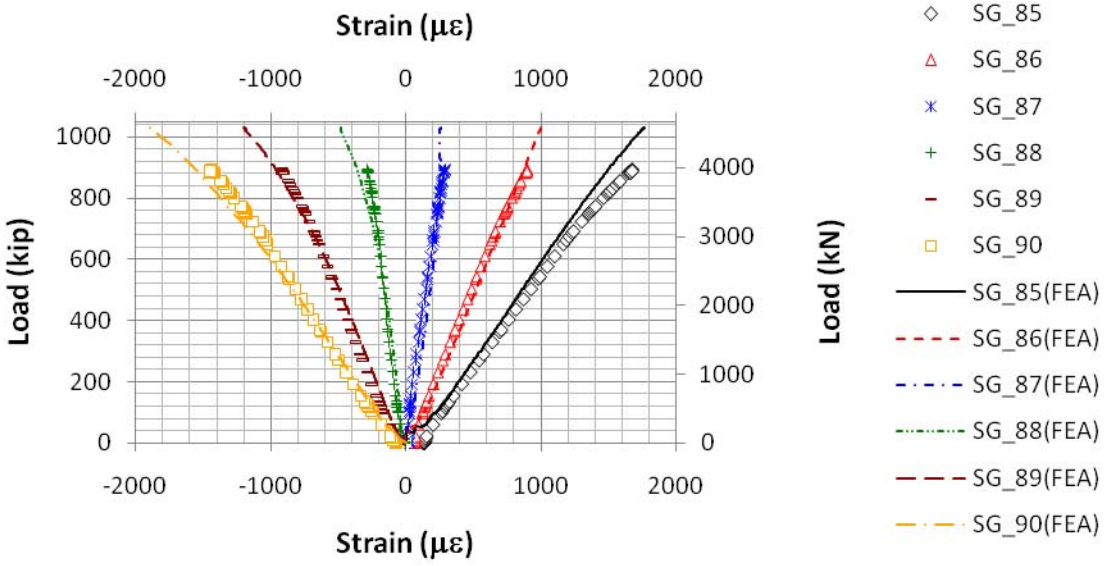


**Figure H.21 East Web exterior face strains 4'-10 1/8" from center support on the hold-down side.**

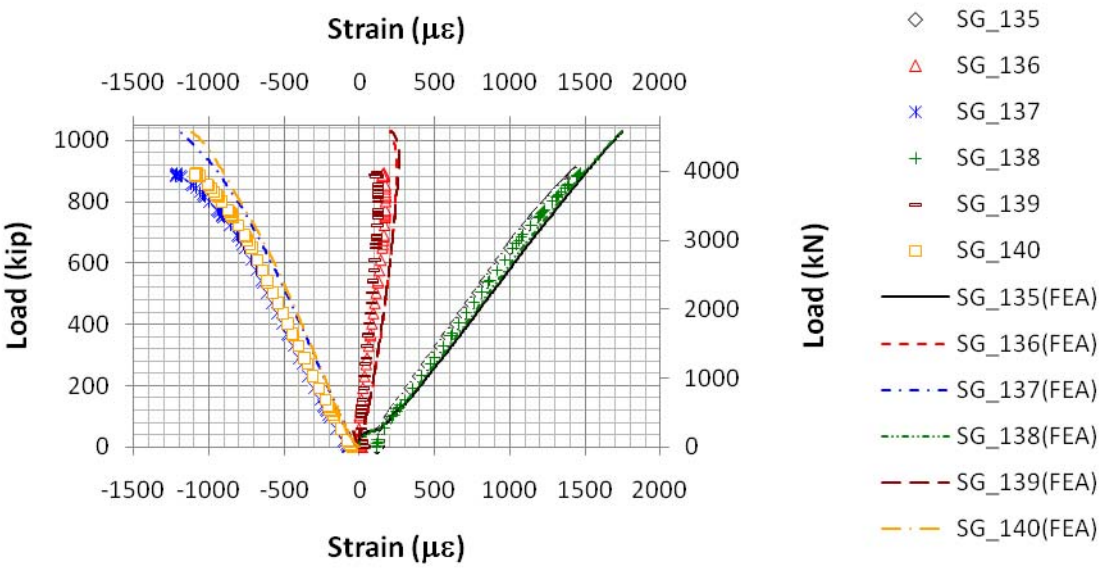


**Figure H.22 West Web interior face strains 4'-10 1/8" from center support on the actuator and hold-down side.**

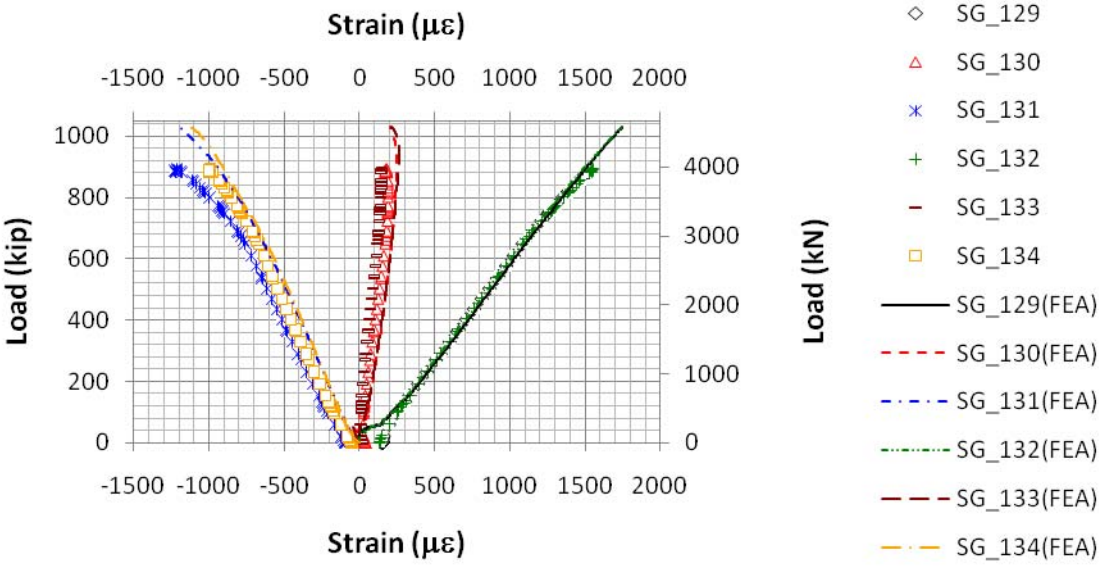


**Figure H.23 East Web interior face strains 4'-10 1/8" from center support on the actuator and hold-down side.**

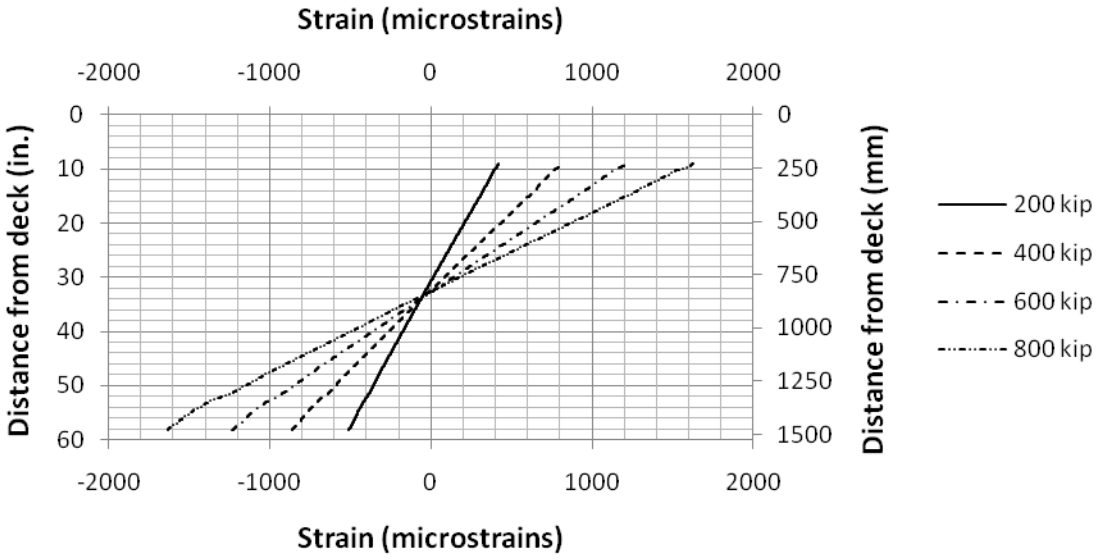


**Figure H.24 Neutral axis determination on 4'-10 1/8" from center support on hold-down side.**

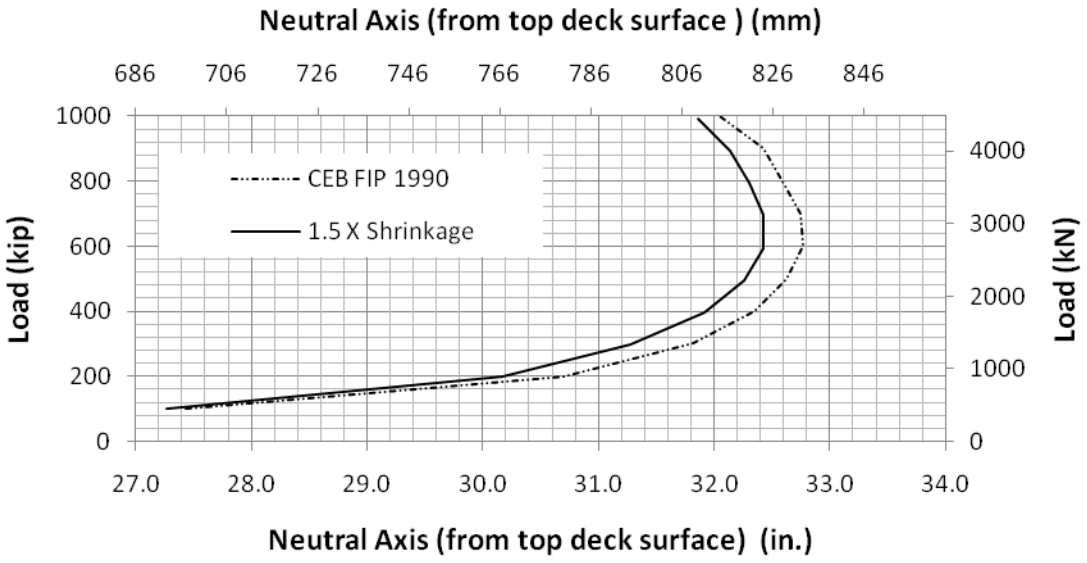


**Figure H.25 Neutral axis movement on 4'-10 1/8" from center support on hold-down side.**

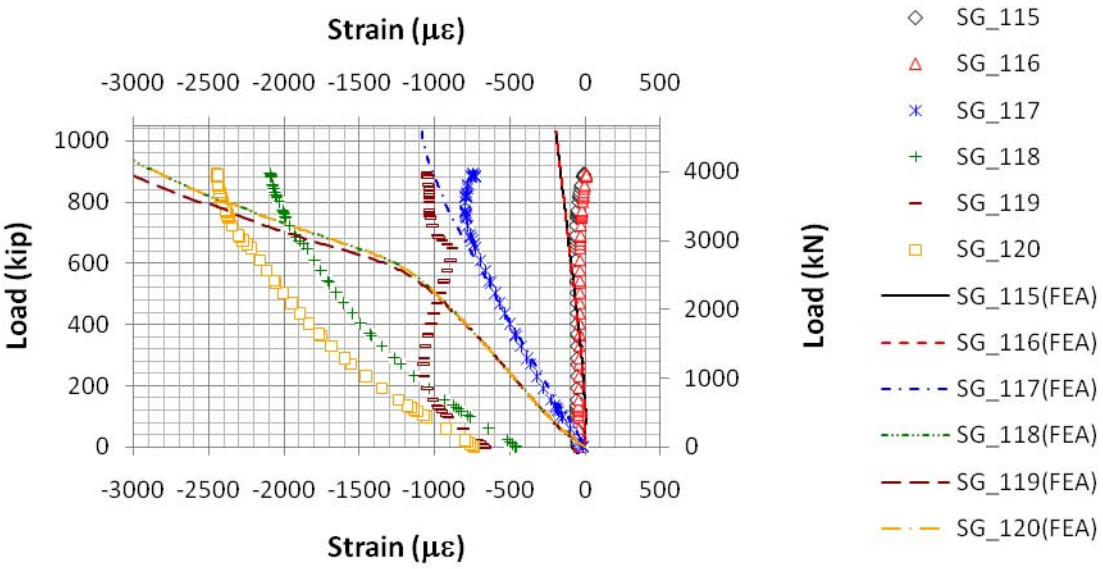


**Figure H.26 Bottom flange strain on the actuator side (Ultimate).**

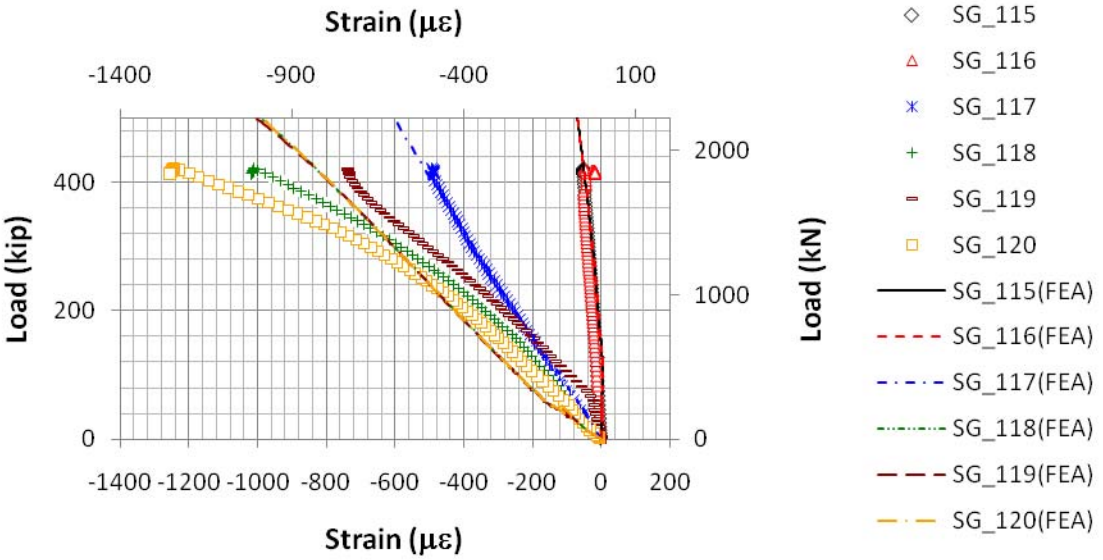


**Figure H.27 Bottom flange strain on the actuator side (Service I, Cycle 1).**

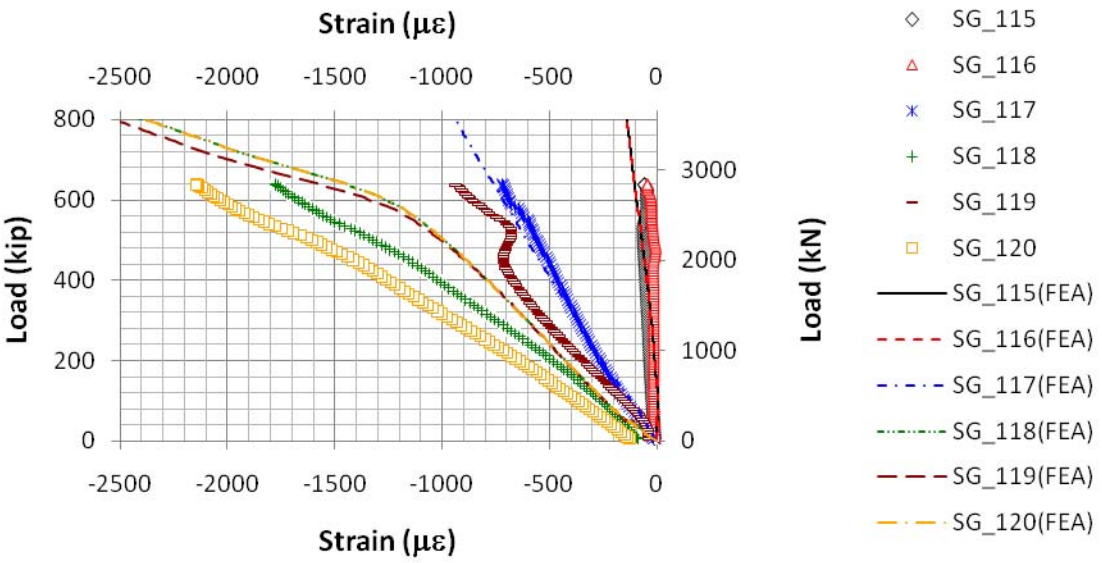


**Figure H.28 Bottom flange strain on the actuator side (Service II, Cycle 1).**

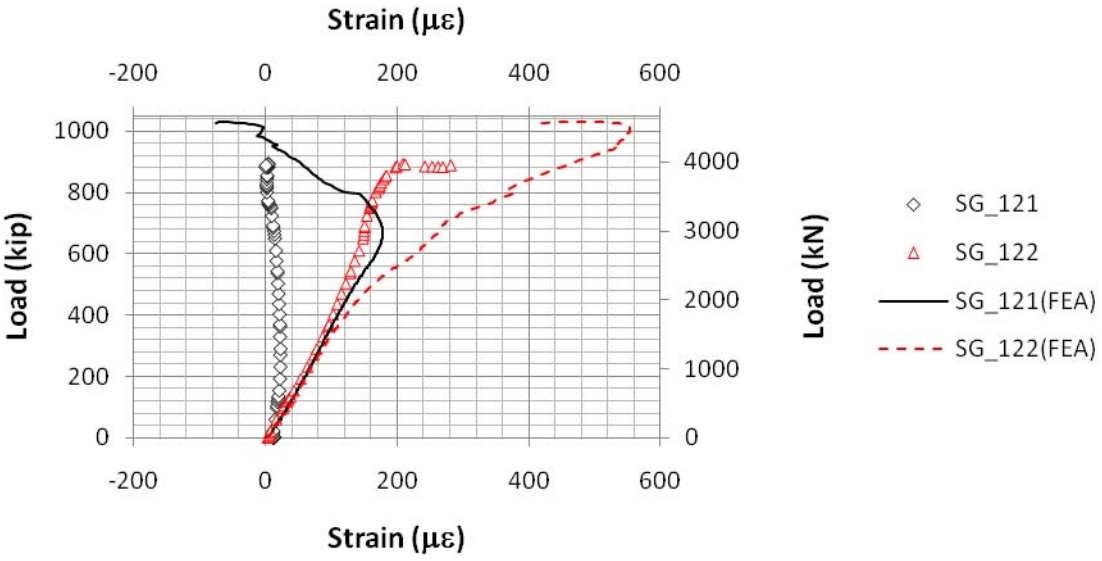


**Figure H.29 Bottom flange strain transverse strain.**

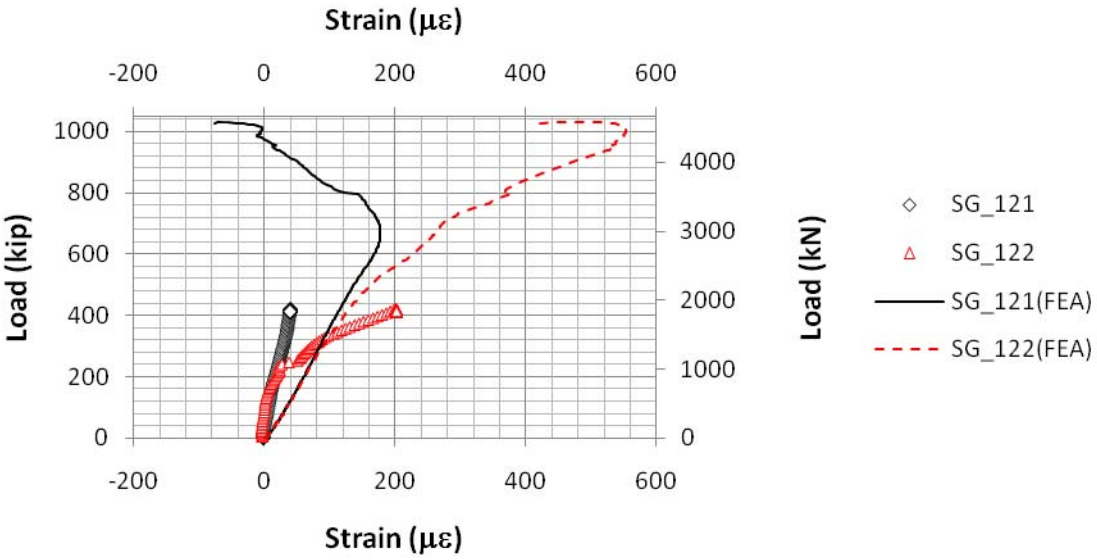


**Figure H.30 Bottom flange strain transverse strain (Service I, Cycle 1).**

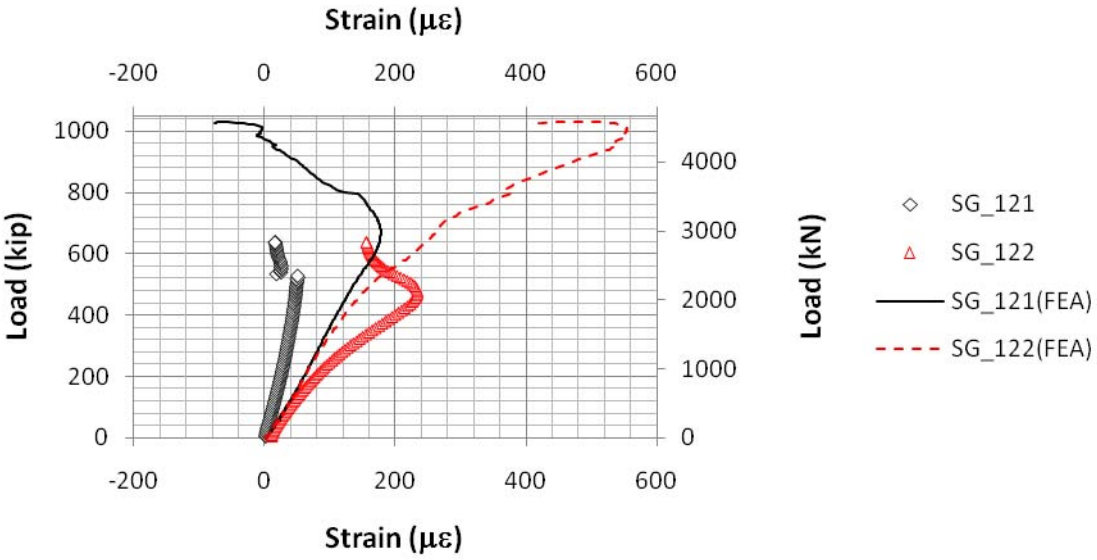


**Figure H.31 Bottom flange strain transverse strain (Service II, Cycle 1).**

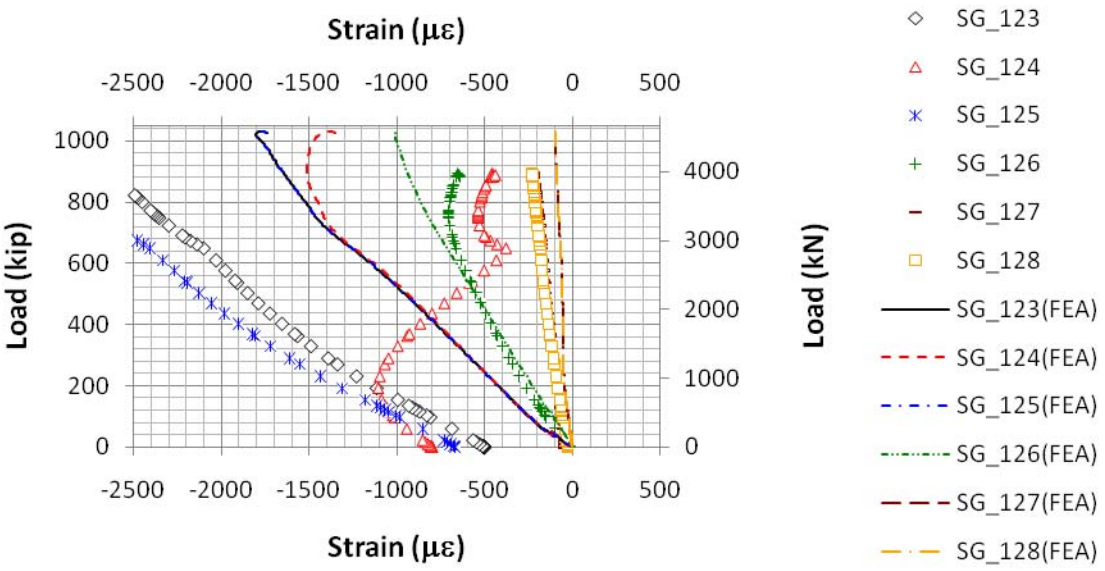


**Figure H.32 Bottom flange strain on the hold-down side (Ultimate).**

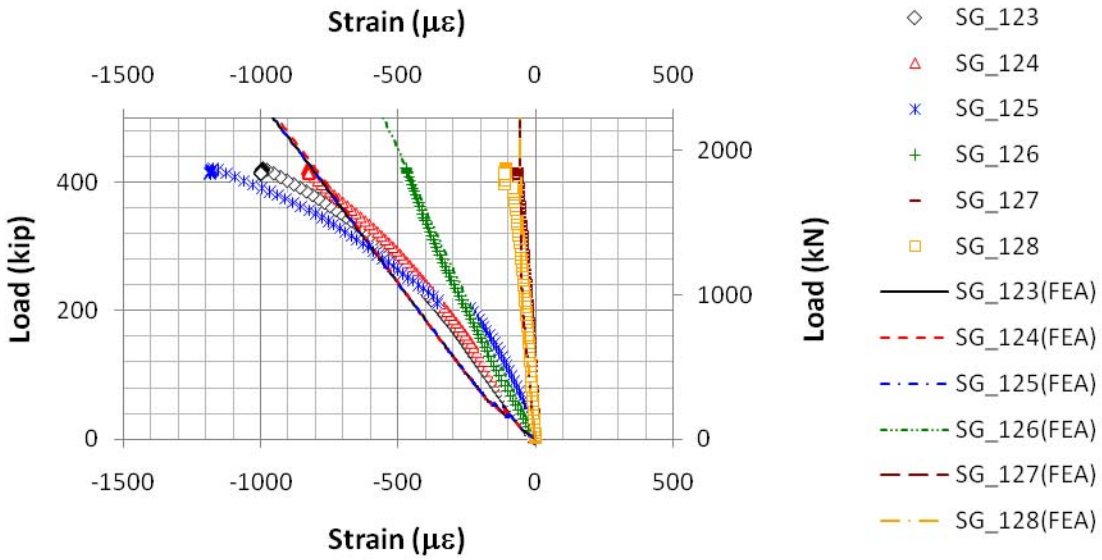


**Figure H.33 Bottom flange strain on the hold-down side (Service I, Cycle 1).**

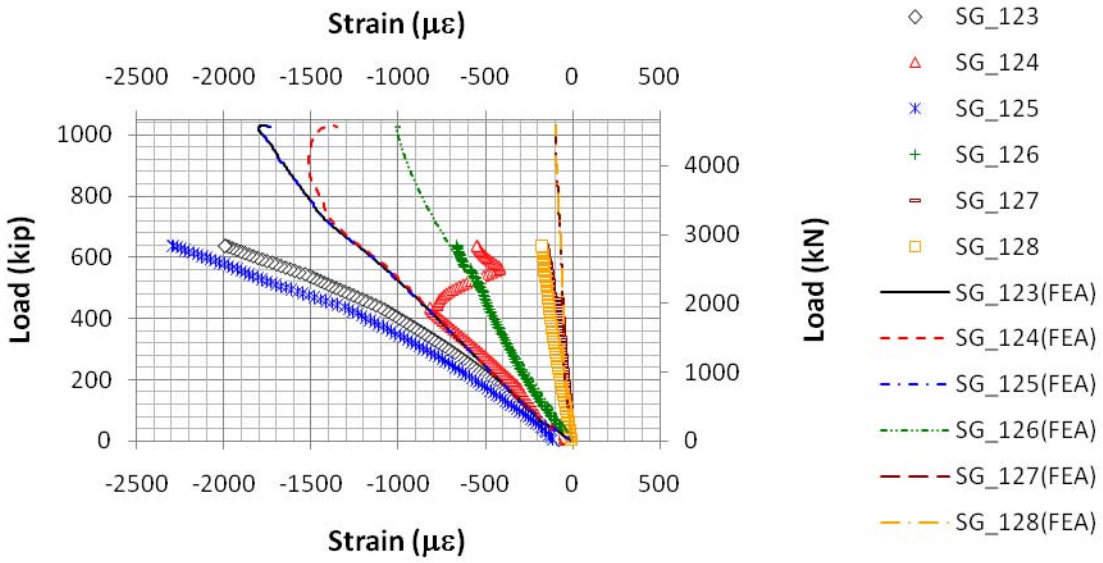


**Figure H.34 Bottom flange strain on the hold-down side (Service II, Cycle 1).**

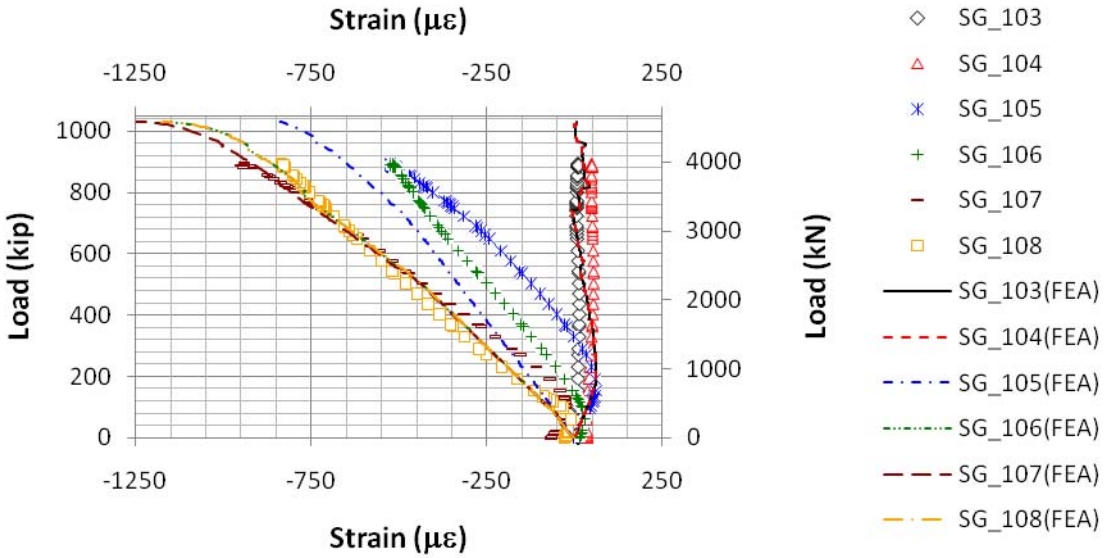


**Figure H.35 Bottom slab top fiber strain on the actuator side (Ultimate).**

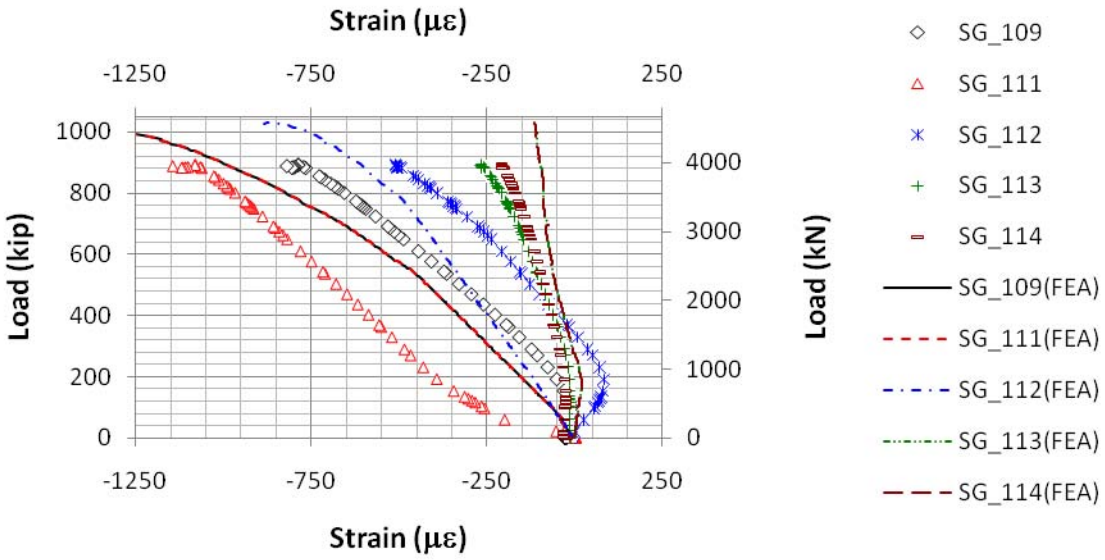


**Figure H.36 Bottom slab top fiber strain on the hold-down side (Ultimate).**

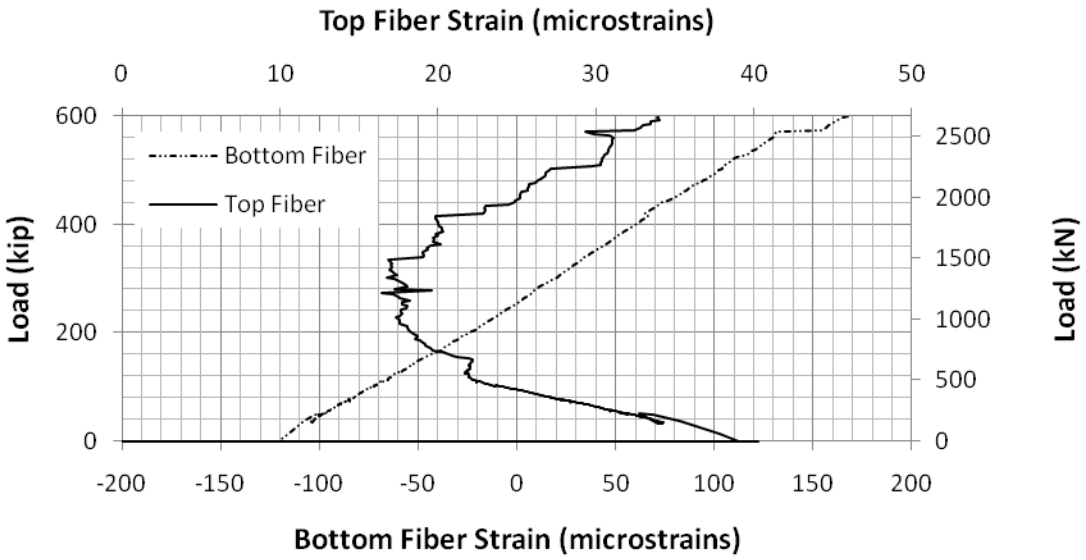


**Figure H.37 Computed bottom slab top and bottom strain at center line box, 1.5ft from the actuator towards the center support.**

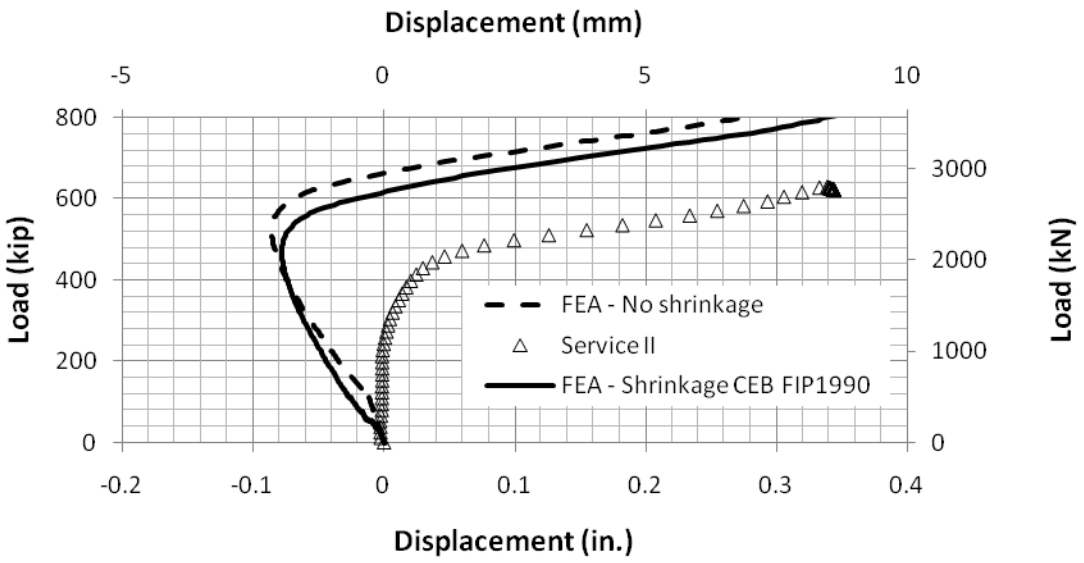


**Figure H.38 Impact of shrinkage on predicted deflection at LVDT 24.**

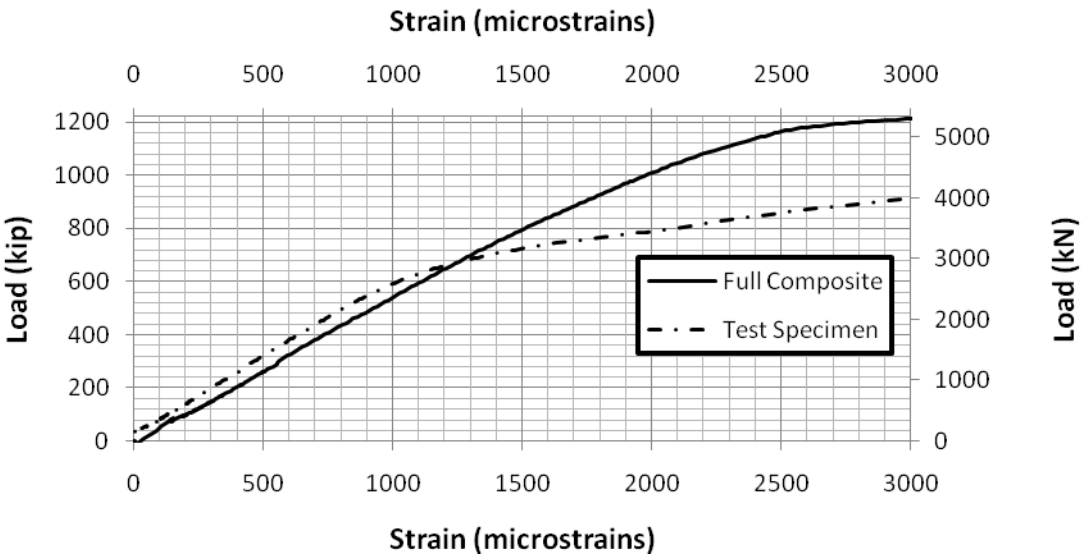


**Figure H.39 Computed concrete strain at buckled region with buckling (test specimen) and without buckling (full composite).**

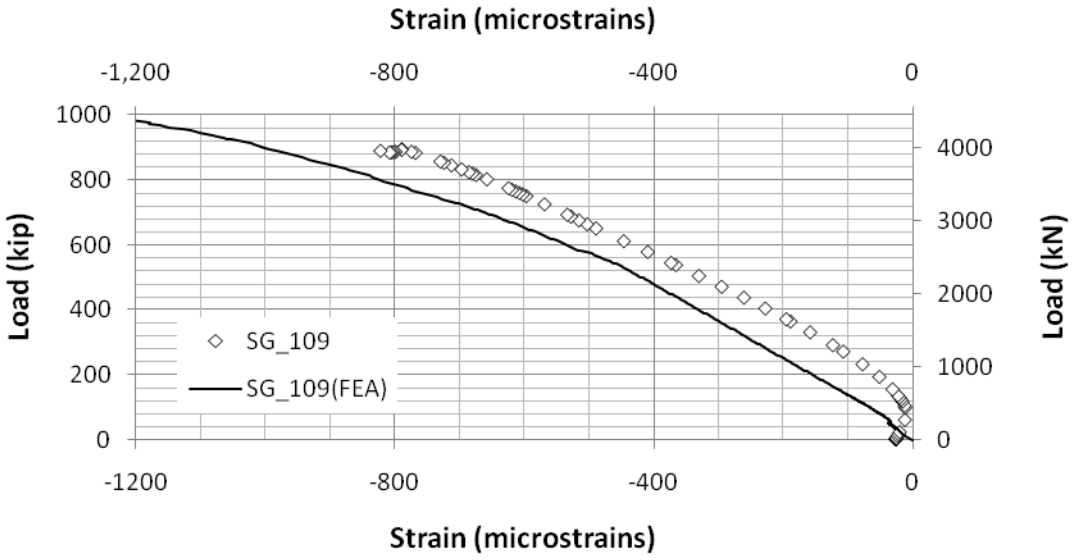


**Figure H.40 Ultimate test bottom slab top fiber strain on the 4'-10 1/8" from the hold-down side**

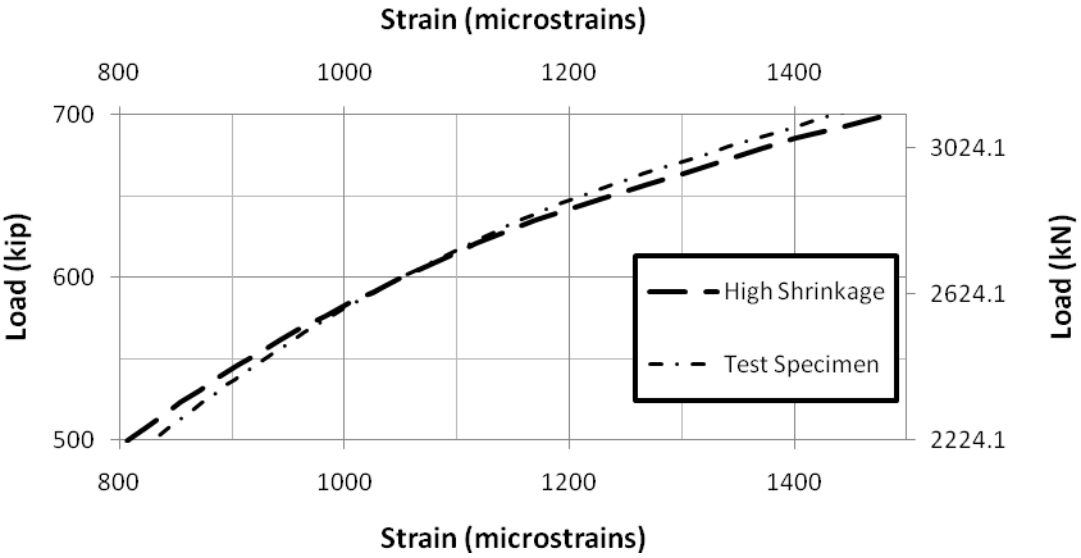


**Figure H.41 Concrete strain response with different amount of cracking.**

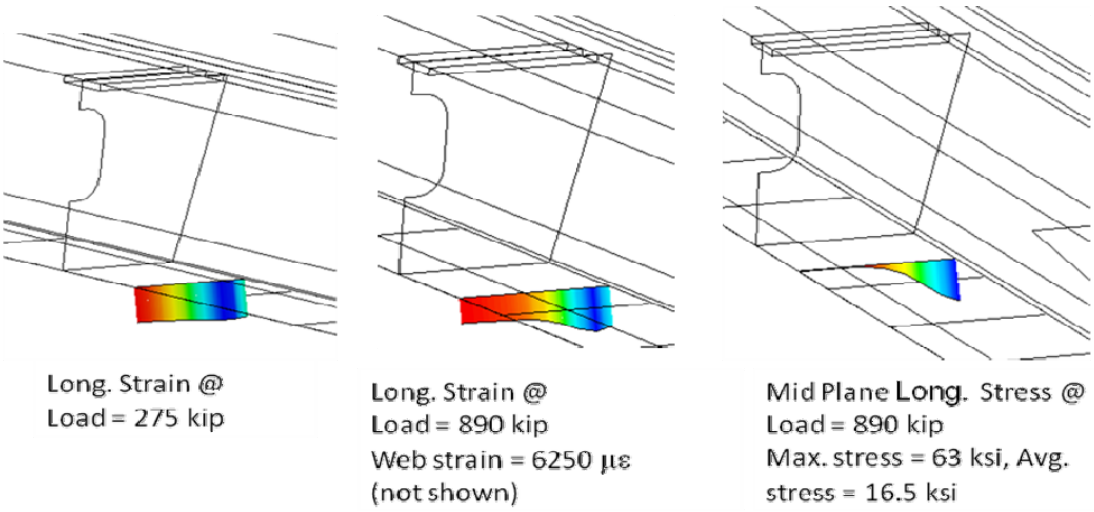


**Figure H.42** Bottom flange shear lag behavior.

## H.4 Discussion on Concrete Ultimate Strain Limit

The average failure strain from bottom slab cylinder tests was 2230 με (see Appendix I). The FDOT Structures Research Center has argued (see Appendix I) that this should be used as the ultimate strain limit. From Chapter 8, it should be apparent that the experimental data was complex and engineering judgment was necessary to explain many of the observations. Based on careful review of the test data, current industry practice and analysis results, the ultimate strain limit used in the finite element analysis was the AASHTO and ACI prescribed limit of 3000 με. Some key justifications for the use of the this limit are as follows:

a) A concrete cylinder test involves application of uniform compression and does not have a varying strain across the cross-section as in the double composite test specimen, Fig. H.43 shows longitudinal strain variation along the depth of the bottom slab at the failure zone and 4'-10" away from the center support on the hold down side. Clearly the strains are not uniform along the depth. In fact, there is a large variation in the strain from the top to bottom fiber, especially in the failure zone.

b) The ultimate strain limit could not be verified through direct test measurements due to lack of strain gage instrumentation at the failure zone. However, one can estimate the lower bound based bottom flange strain readings 4 ft 10 1/8 in from the center support. From ultimate test data for gages 123 and 125 (hold-down side), the strain range measured after correcting for non-zero initial strain due to residual strains are 2029 and 2278 με. As discussed in Chapter 8 (see Fig. H.44 and Fig. 8.10), due to superposition of tensile flexural stresses from local buckling, the maximum compressive strain does not occur at the bottom fiber of the bottom flange, but rather at the top fiber. This means that the compressive strain of the concrete fiber adjacent to the top fiber of the bottom flange can be higher than 2278 με (since there is significant flexural stress from buckling at the ultimate load, see Fig. 8.10). Given that the region adjacent to SG 123 and 125

did not crush, it follows that the ultimate strain limit must be higher than 2278 με. See Section 8.3.3.1 for discussion on comparison of experimental results with analytical predictions.

c) Due to inclined webs, the concrete in the failure region is in a bi-axial state of compression similar to the bottom flange (see Figs. H.45,.8.10 and 8.11), which increases the compressive capacity of the concrete [H.12] due to confinement effects and by slowing down propagation of micro-cracks.

d) The behavior of the test specimen was highly non-linear due to buckling of the bottom flange, non-linearity of concrete at high strain levels (see Fig. 9.9) and localized region of strain compatibility with the bottom flange (at shear stud locations). For example, Fig. H.46 plots results from the finite element model showing the variation in the bottom slab bottom fiber strain along the center line of the box (CL – in blue) and close to the web (in brown) as a function of distance from the actuator end. It may be seen that in areas where the plate buckled, the strain is significantly higher along the center-line because the bottom flange is ineffective and sheds its load to the bottom slab. However, at 4'-10 1/8" away from the center support, the predicted strain is moderate. Any hypothesis based on linear extrapolation of measured strains from 4'-10 1/8" to failure zone will give misleading results due to this highly non-linear response resulting from buckling. Note that these strains include dead load strain and shrinkage strain and are therefore not directly comparable to the experimentally measured values.

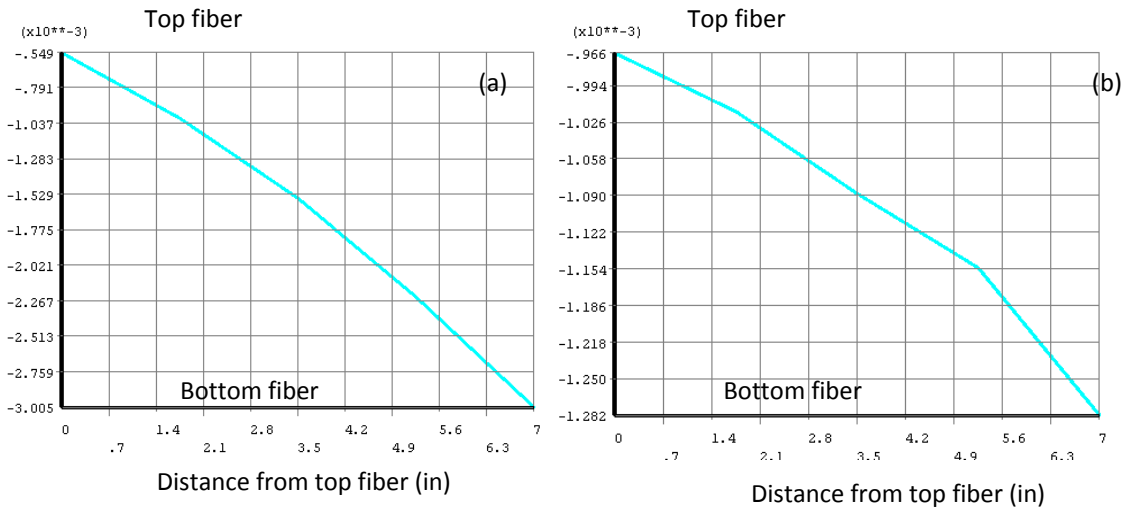


**Figure H.43** FE predicted longitudinal strain variation in bottom slab at (a) Failure zone (b) Approx 4'-10" from center support on hold down side.

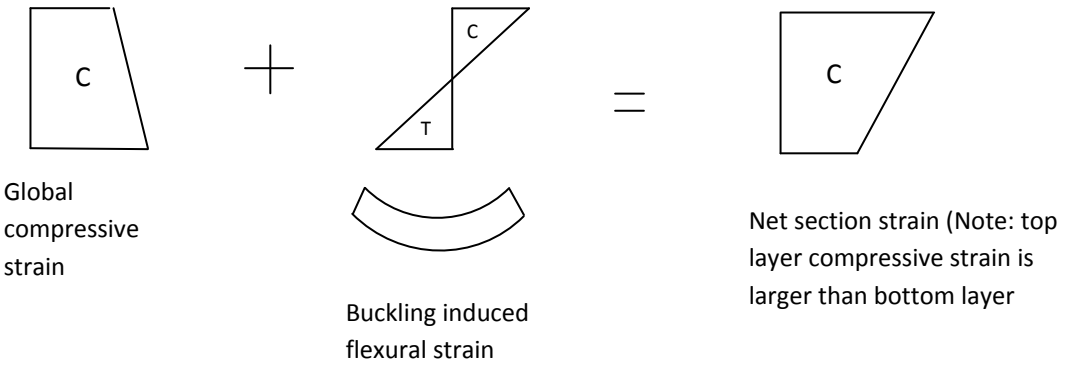


**Figure H.44** Simplified behavior of bottom steel flange due combined compression + flexure.

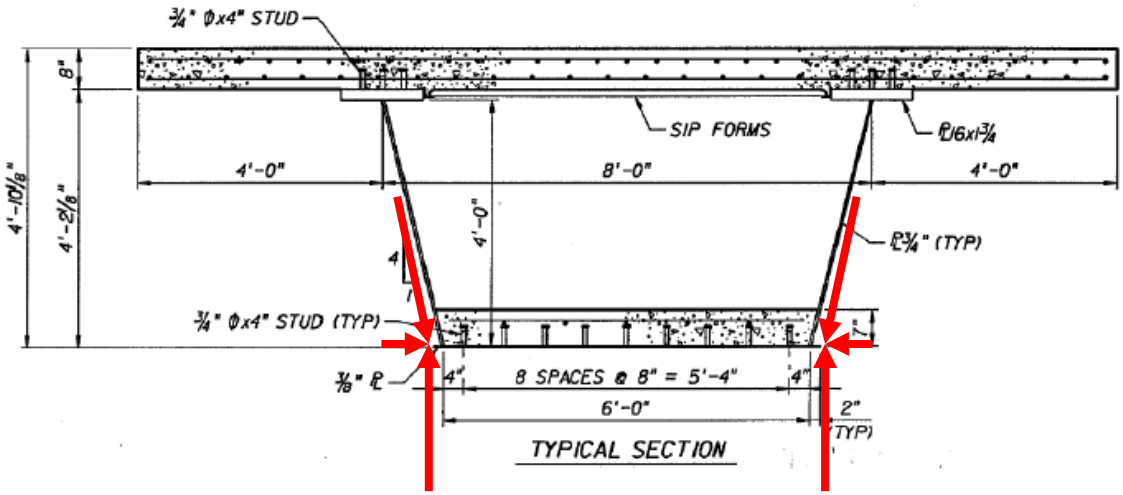


**Figure H.45** Load resolution at web to bottom flange interface at center support to illustrate cause of compression in bottom flange. (Note: compression also carried by diaphragm, which is not shown).

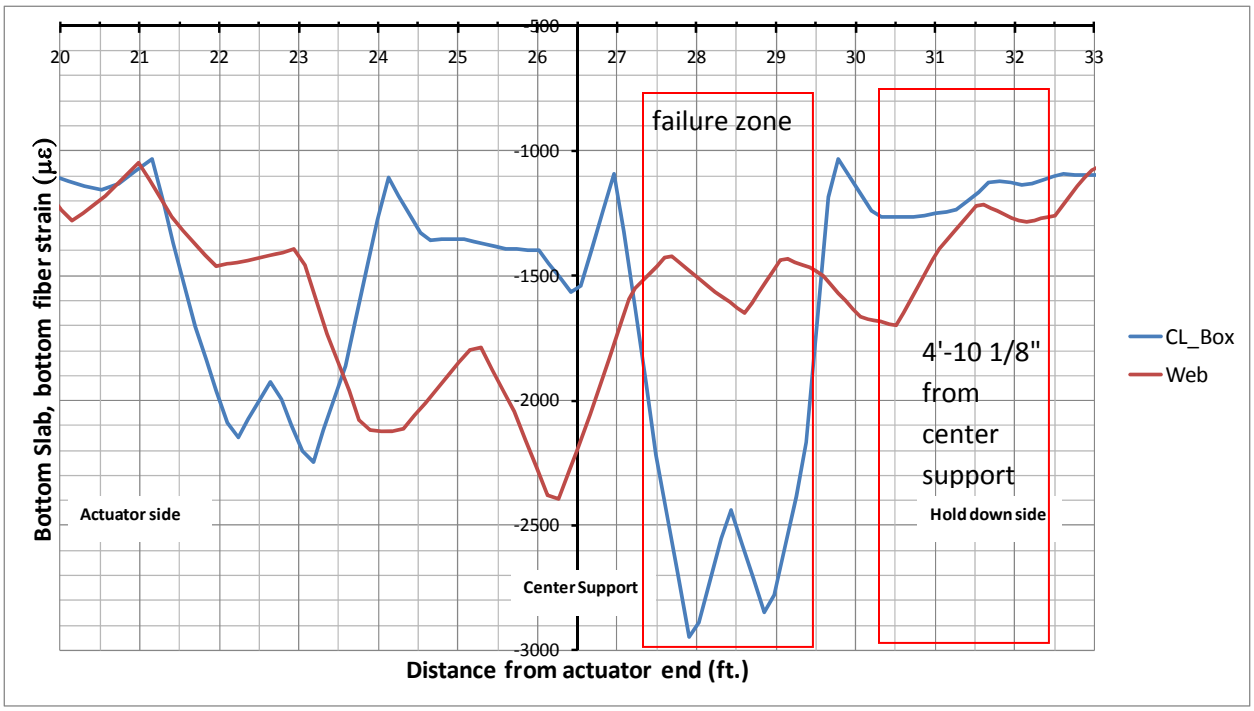


**Figure H.46** Concrete strain at bottom slab, bottom fiber from FE Model.

## REFERENCES


H.1 SAS IP Inc. (2007). "Release 11.0 Documentation for ANSYS", ANSYS, Inc., Canonsburg, PA.

H.2 Chung, W., and Sotelino, E.D.(2006). "Three-dimensional finite element modeling of composite girder bridges", Engineering Structures, Vol 28, pp. 63–71.

H.3 Young, W., and Budynas, R. (2001). "Roark's Formulas for Stress and Strain", McGraw-Hill Professional, New York.

H.4 Willam, K. J., and Warnke, E. D. (1975). "Constitutive Model for the Triaxial Behavior of Concrete", Proceedings, International Association for Bridge and Structural Engineering, Vol. 19, ISMES, Bergamo, Italy, p. 174.

H.5 Kang, Y,J (1977). "Nonlinear geometric, material and time dependent analysis of reinforced and prestressed concrete frames", Final Report, Div. of Structural Engineering and Structural Mechanics, California Univ., Berkeley, CA.

H.6 Oztekin, E., Pul, S., and Husem, M. (2003). "Determination of rectangular stress block parameters for high performance concrete", Engineering Structures, Vol 25, pp. 371-376.

H.7 ACI Committee 318 (2004). "Building Code Requirements for Structural Concrete (ACI 318-05) and Commentary (ACI 318R-05)", American Concrete Institute, Farmington Hill, Michigan..

H.8 Structures Design Office (2009). "Structures Manual", Florida Department of Transportation, Tallahassee, FL, pp. 16.

H.9 Comit E Euro-International Du B Eton (1993). "Ceb-Fip Model Code 1990", Telford, London.

H.10 Nawy, E. G. (2000). "Reinforced Concrete: A Fundamental Approach", 5th Edition, Prentice Hall, Upper Saddle River, New Jersey.

H.11 PCI Industry Handbook Committee (2004). "PCI Design Handbook", 6th Edition, Precast/Prestresed Concrete Institute, Chicago, Illinois.

H.12 Kupfer, H., Hilsdorf, H., and Rusch, H. (1969). “Behavior of Concrete Biaxial Stress”, ACI Journal, Vol 75, No 10, October 1978, pp. 533-542.

# APPENDIX I

Investigation of the Double-Composite Box Girder Failure Criteria

The following addendum provides alternative commentary on the failure mechanism of the Double Composite box girder as described in Chapter 8 and Appendix H.

# Investigation of the Double-Composite Box Girder Failure Criteria

**FDOT Structures Research Center**

Will Potter, E.I.

Marc Ansley, P.E.

January 13, 2010

**Overview**

The FDOT Structures Research Center performed testing to evaluate the concept of double composite action in steel bridges in October of 2008. The testing consisted of fatigue, service, and ultimate tests. The fatigue test was completed by loading the specimen to approximately 5.6 million cycles from 5 to 105 kips. No immediate distress to the specimen was detected after the fatigue test. The service test involved three load cases with the 1st and 2nd load case being repeated 5 times. The loads for the 1st and 2nd load case were 421.0 kips and 638.8 kips, respectively. The load was held each time for a brief period before retracting. The final load case for service, which became the ultimate load case, involved loading the specimen to 894.2 kips. It was intended during this load case to hold the load at 894.2 kips for several minutes, for examination of the specimen, and then continue until failure or 1200 kips, whichever came first. During the first minute the load was being held, due to the nature of the hydraulic system, a small percentage of the load, approximately 12 kips, was lost. While attempting to regain the 12 kips of load a sudden failure occurred in the specimen. Buckling of the bottom steel plate and concrete failure were observed near the support or maximum moment region. The specimen cross-section and elevation are given in Figures 1 and 2, respectively. An examination of the recorded load, strain, and displacement data was made by the Research Center to determine the cause of the failure.

**Failure Synopsis**

A visual examination of the failed specimen found that the bottom flange plate buckled between shear stud lines near the support, which were longitudinally spaced at 23 inches. Also, the concrete failure occurred at the general location of the first and second shear stud lines in the same general region of the buckled plate. A depiction of these locations is shown in Figure 3. It was noted that the bottom plate buckled at other locations along the beam also between stud lines; however, this location was the most severe.

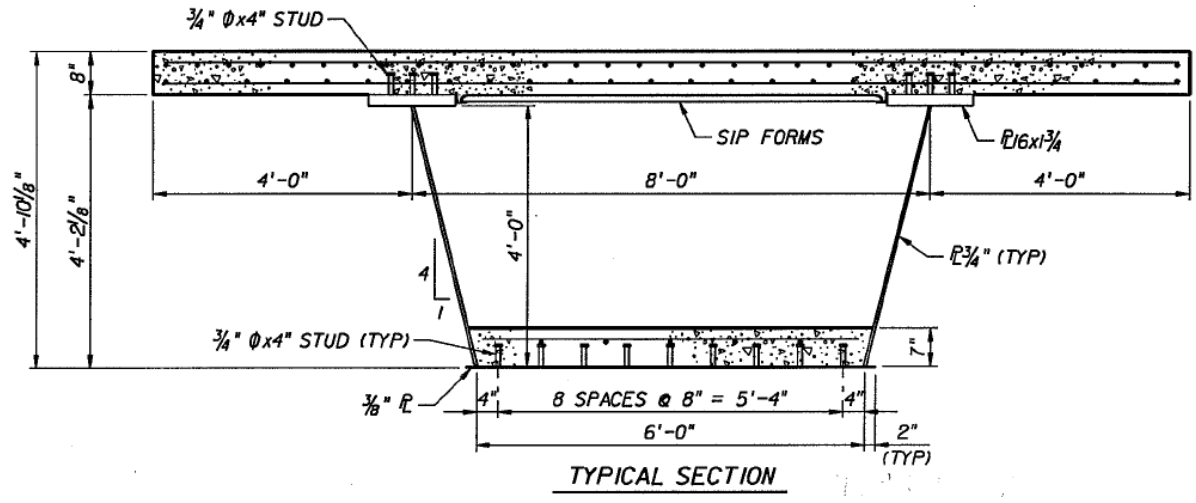


**Figure 1: Typical Cross-Section**

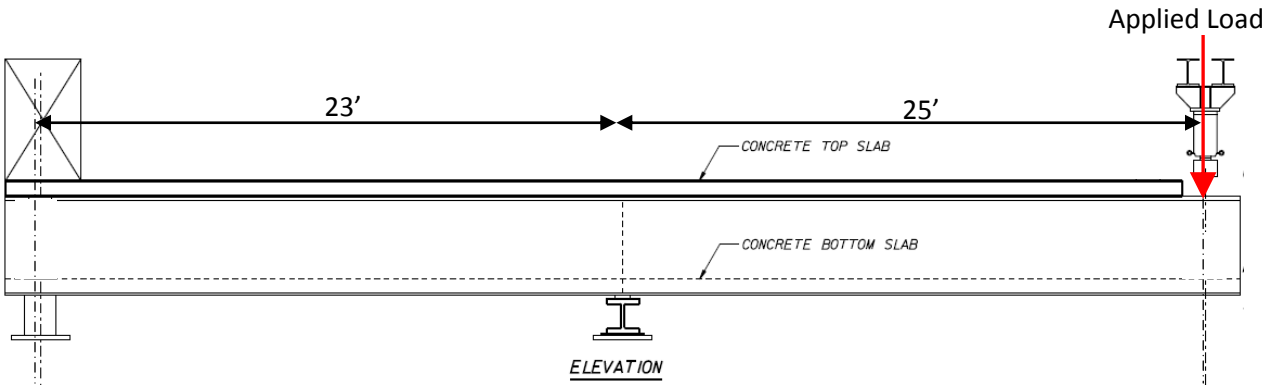


**Figure 2: Elevation**

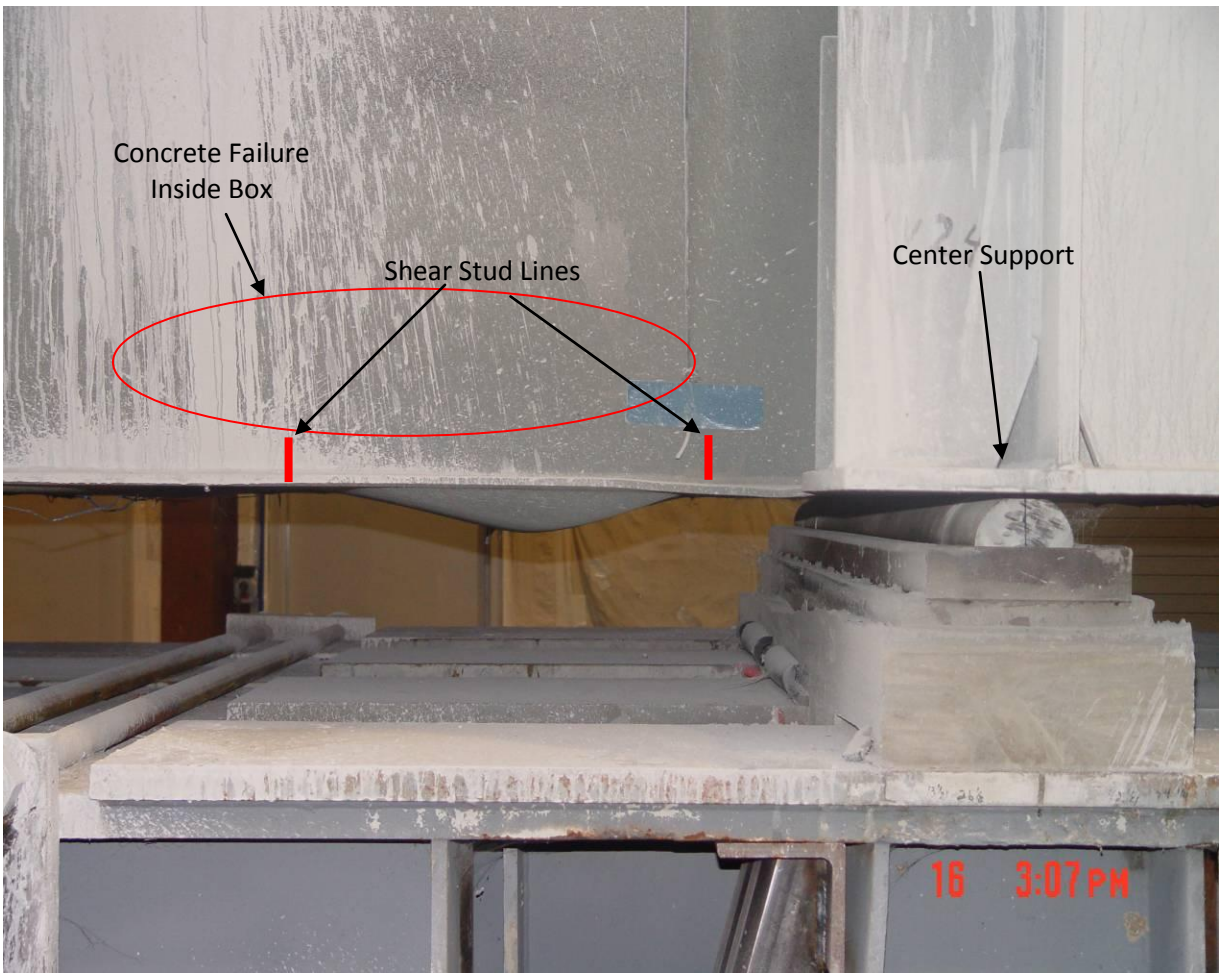


**Figure 3: Location of Failure**

After analyzing, the data indicates plate buckling occurred in the early stages of loading. A load versus deflection curve for the 1st and 2nd service load case, 1st cycle, is given in Figure 4 for two displacement gages, LV 23 and LV 24, that were located in the region where buckling occurred. This load-deflection curve should theoretically be linear with positive slope. However, there is a noticeable slope change at approximately 130 kips which is indicative of buckling. It is further magnified at gage LV23 above 300 kips on the 1st cycle then around 200 kips on subsequent cycles. A transverse strain gage at the location of failure also suggests that out of plane bending occurred at low loads. Figure 5 is a load versus micro-strain graph showing nonlinearity which is apparent around 150 kips.

Calculations based on *Roark's Formulas for Stress and Strain* were used to study the critical buckling stress in the bottom steel flange. The formula considers a rectangular plate under uniform compression on two opposite edges. It was assumed that all edges were simply supported. The values used in the equation are as follows: ⅜"plate thickness, 23" buckling length, and 72" width between webs. Based on the given setup and equation the critical stress for this location was 8.75 ksi. The calculations are given in the Appendix. The low critical stress level explains the early buckling of the bottom flange. The applied load needed to achieve this stress in the bottom flange at the critical location was 152 kips, based on a composite section. The value of the critical stress or load could vary a small amount due to the exactness of the boundary conditions and should be taken as the lower bound. This early buckling condition eliminated the added benefit of using high-performance steel in the bottom flange (HPS 70).

The behavior of the test specimen during the initial loading stage of this test was complex with the slab and bottom flange not acting completely integral. Due to shrinkage there are minute cracks and gaps at the diaphragms that prevent the concrete from being loaded immediately. This in turn can accentuate the amount of the initial loading resisted by the steel in the bottom flange. This would lower the required load, 152 kips, to produce the critical buckling stress. Once buckling of the bottom flange has occurred the bottom slab concrete would resist a majority of the additional load. Higher stresses would result in the concrete due to the lack of composite action.

At the time in the test when the load was being held, at 894 kips, the concrete capacity was exceeded, resulting in a sudden brittle failure. The concrete cylinder strength was 8700 psi at the time of testing. The concrete failure is visible in the top portion of the bottom slab, see Figures 6 and 7. This region has little confinement with the exposed face and shear studs only extending 4 inches into the 7 inch slab, at a spacing of 23 inches. Two strain gages, SG 109 and 111, located on the top of the bottom slab at 4'-10⅛" from the diaphragm on the hold down side revealed that the concrete in the bottom slab was under distress during the load hold. Figure 8 is a plot of load versus micro-strain, using the average of gages SG 109 and 111, and depicts increasing strain while the load was held constant at 894 kips. By averaging the strain gages along the depth of the box at 4'-10⅛" from the diaphragm on the hold down side and using linear extrapolation the approximate strain level at 11 inches from the diaphragm was 2148 micro-strain in the bottom fiber of the bottom slab and 1513 micro-strain in the top fiber of the bottom slab in compression. The average measured strain gradient along the depth of the box, at failure, is shown in Figure 9. This data includes the average for gages in the top flange, web and bottom

slab. The stress-strain curves for three cylinders of the bottom slab concrete are given in Figure 10. The average maximum failure strain for the three cylinders is 2230 micro-strain. The situation for the Double Composite is similar to a cylinder test in that due to the position of the neutral axis there is a small strain gradient across the depth of the bottom slab, however, the cylinders were tested at the ASTM prescribed load rate, as opposed to a held load in the double composite test. Concrete fails at lower stresses under sustained load.

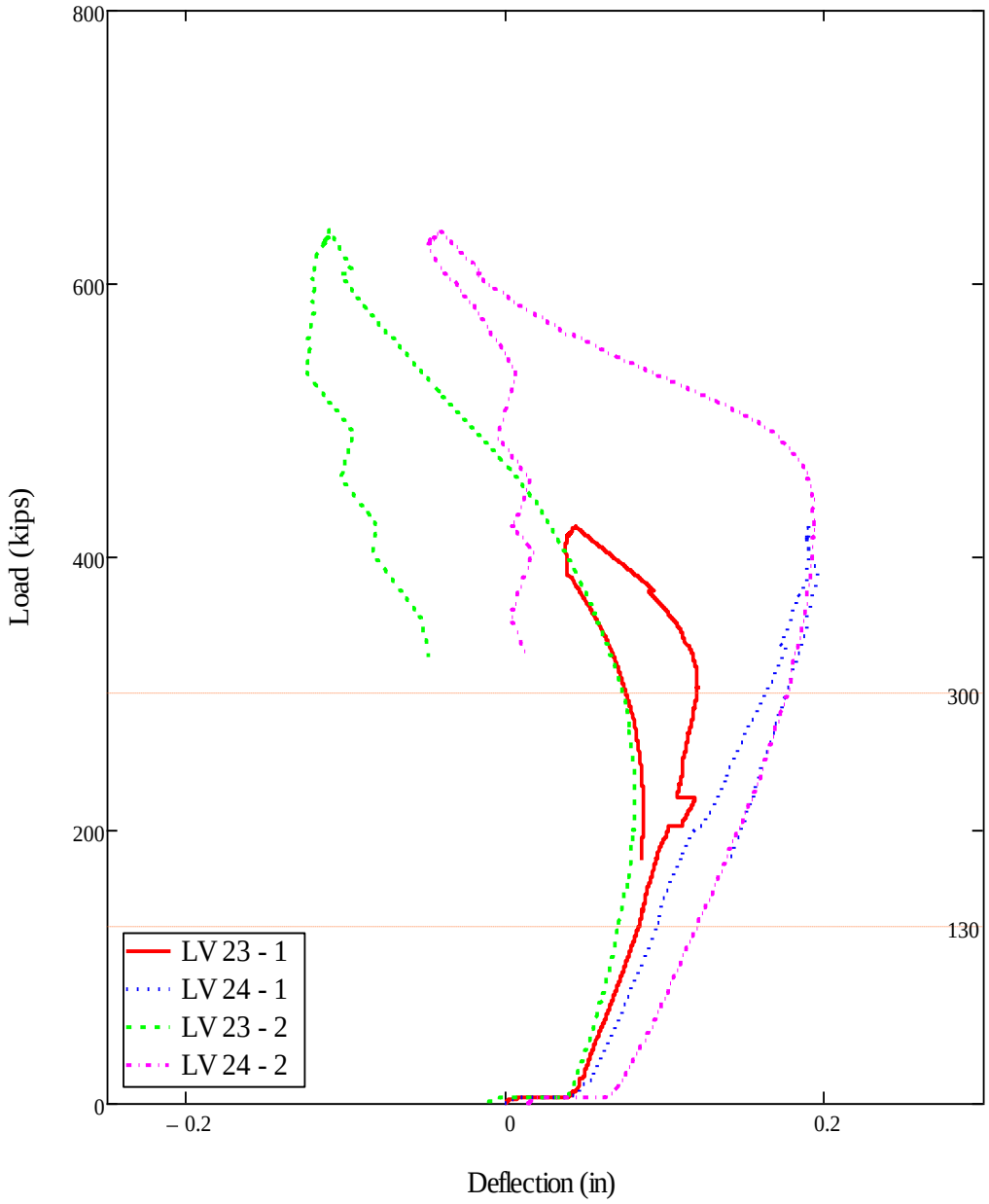


**Figure 4: Load versus Deflection (LV 23-24)**

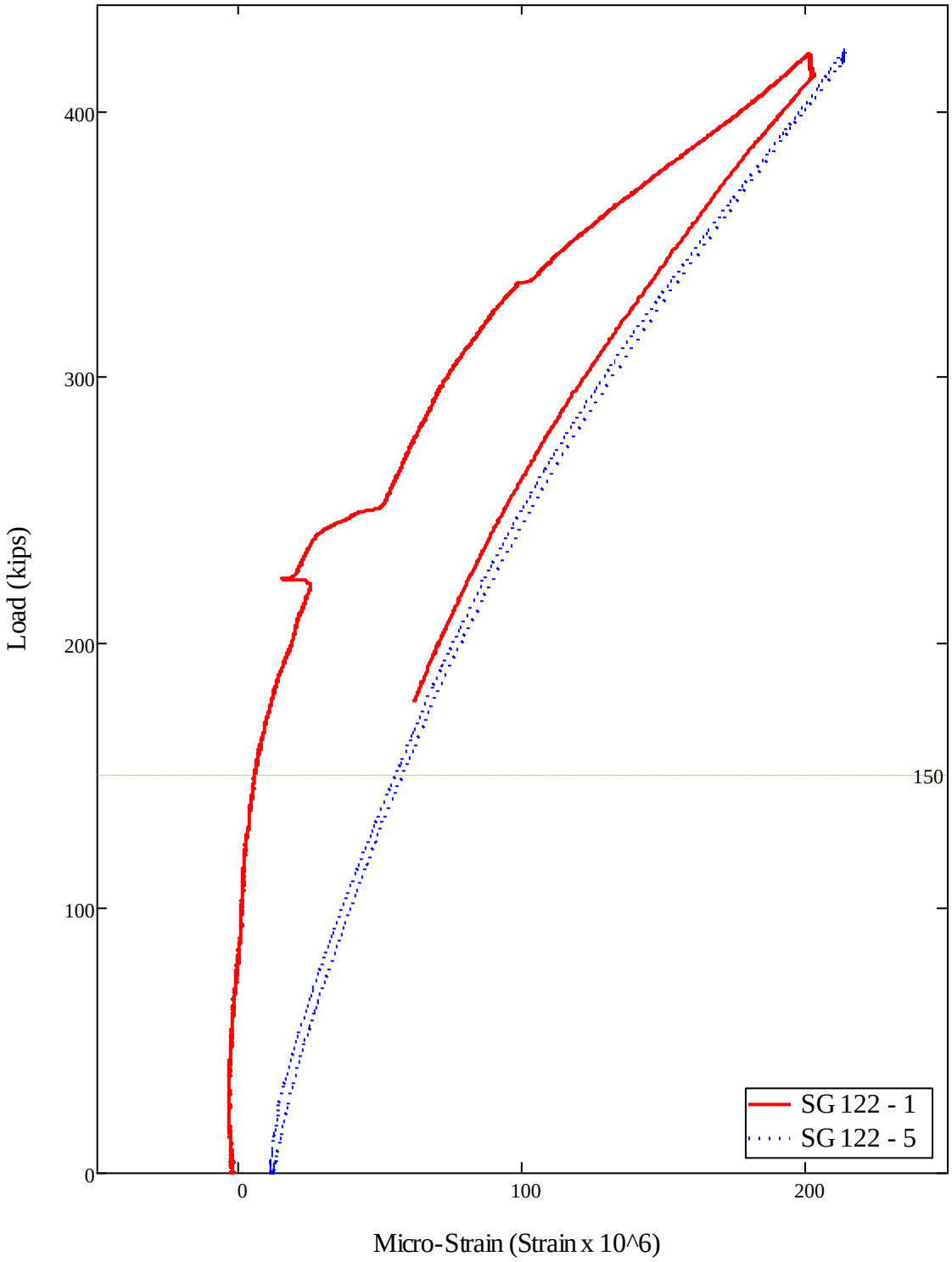


**Figure 5: Load versus Micro-strain (SG 122 – Transverse)**


**Figure 6: Concrete Failure**


**Figure 7: Concrete Failure (Removal of Loose Pieces)**

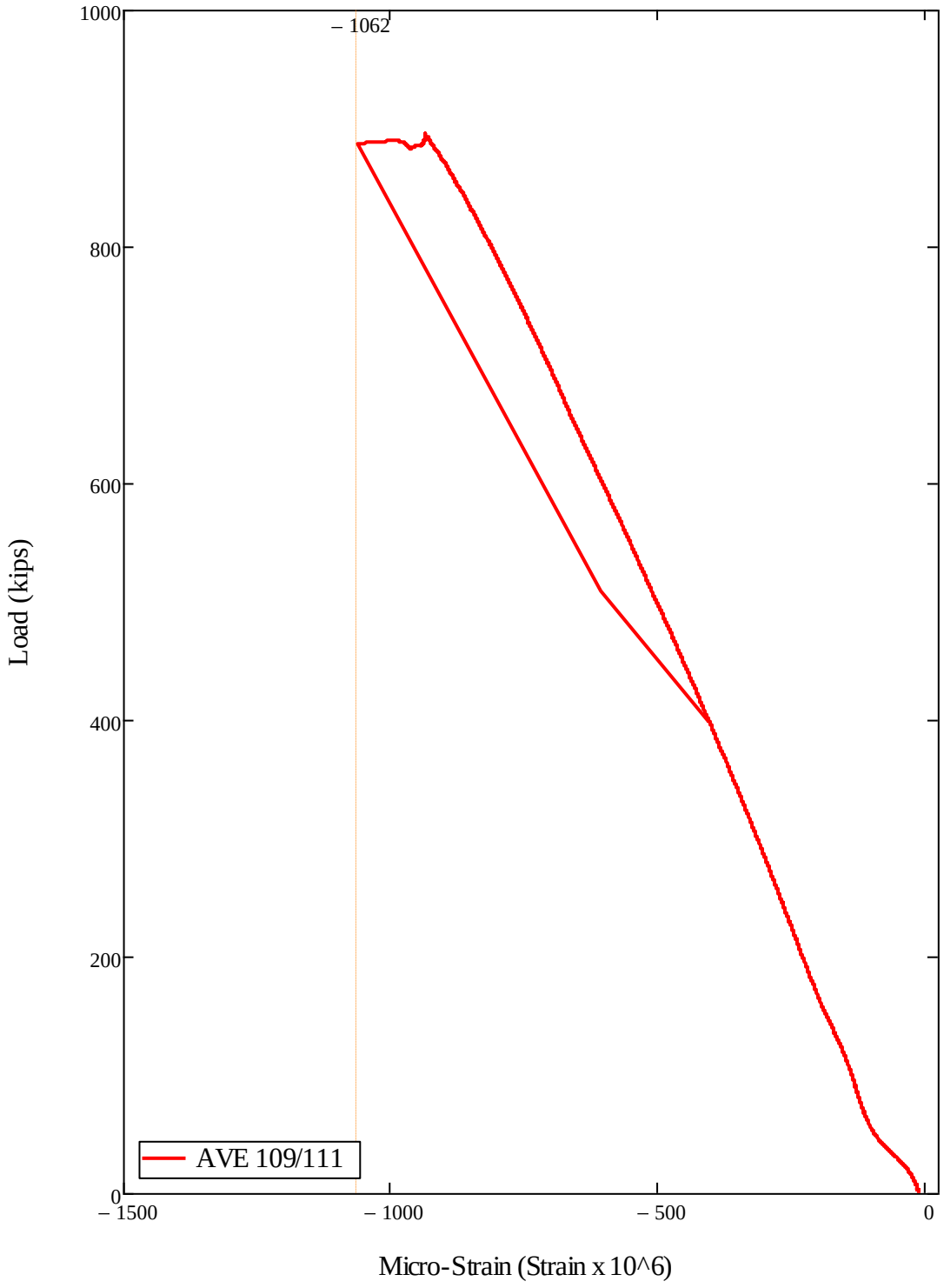


**Figure 8: Load versus Micro-Strain (Bottom Slab Strain)**

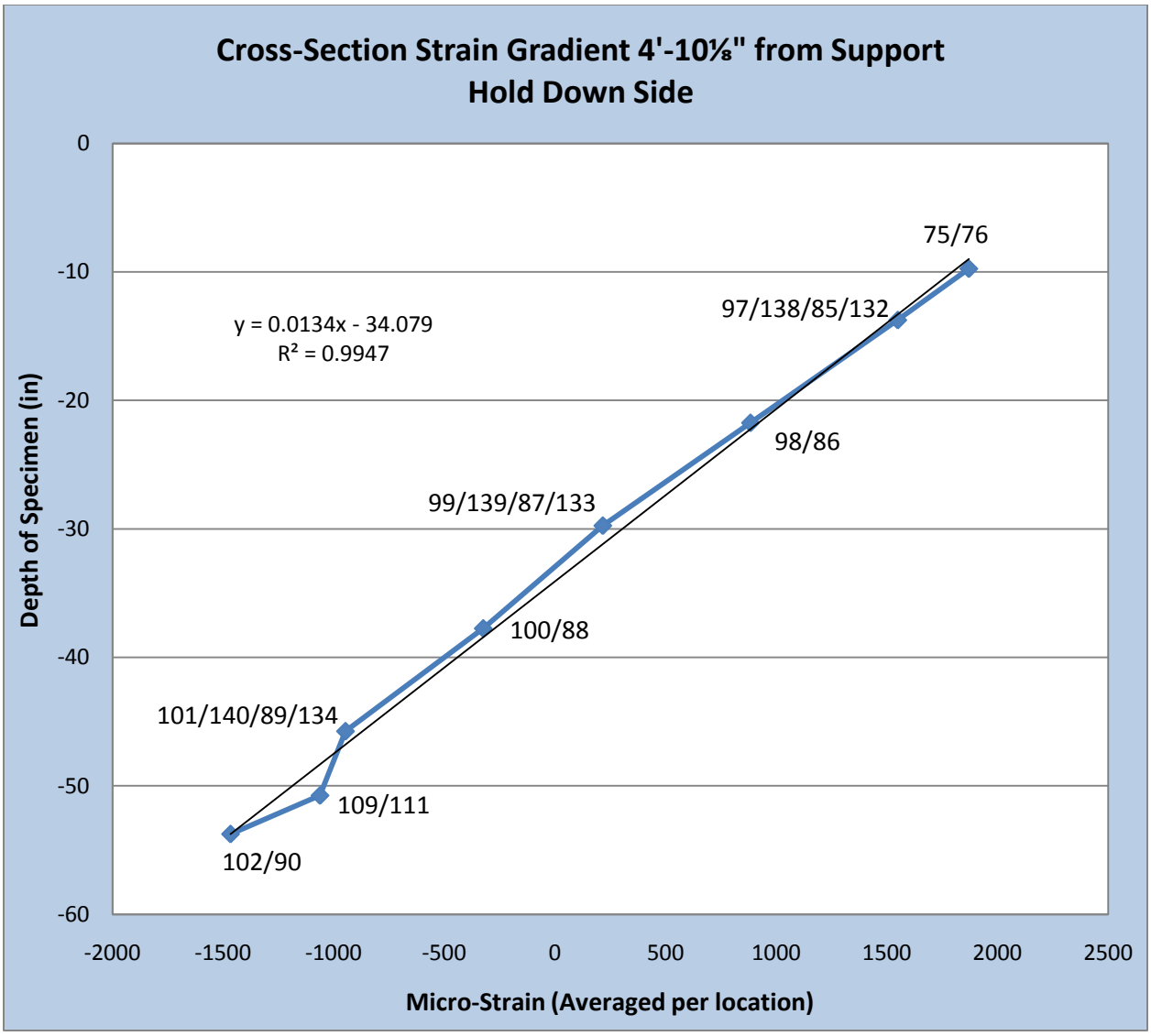


**Figure 9: Strain Gradient at 4'-10⅛" from Support – Hold Down Side**

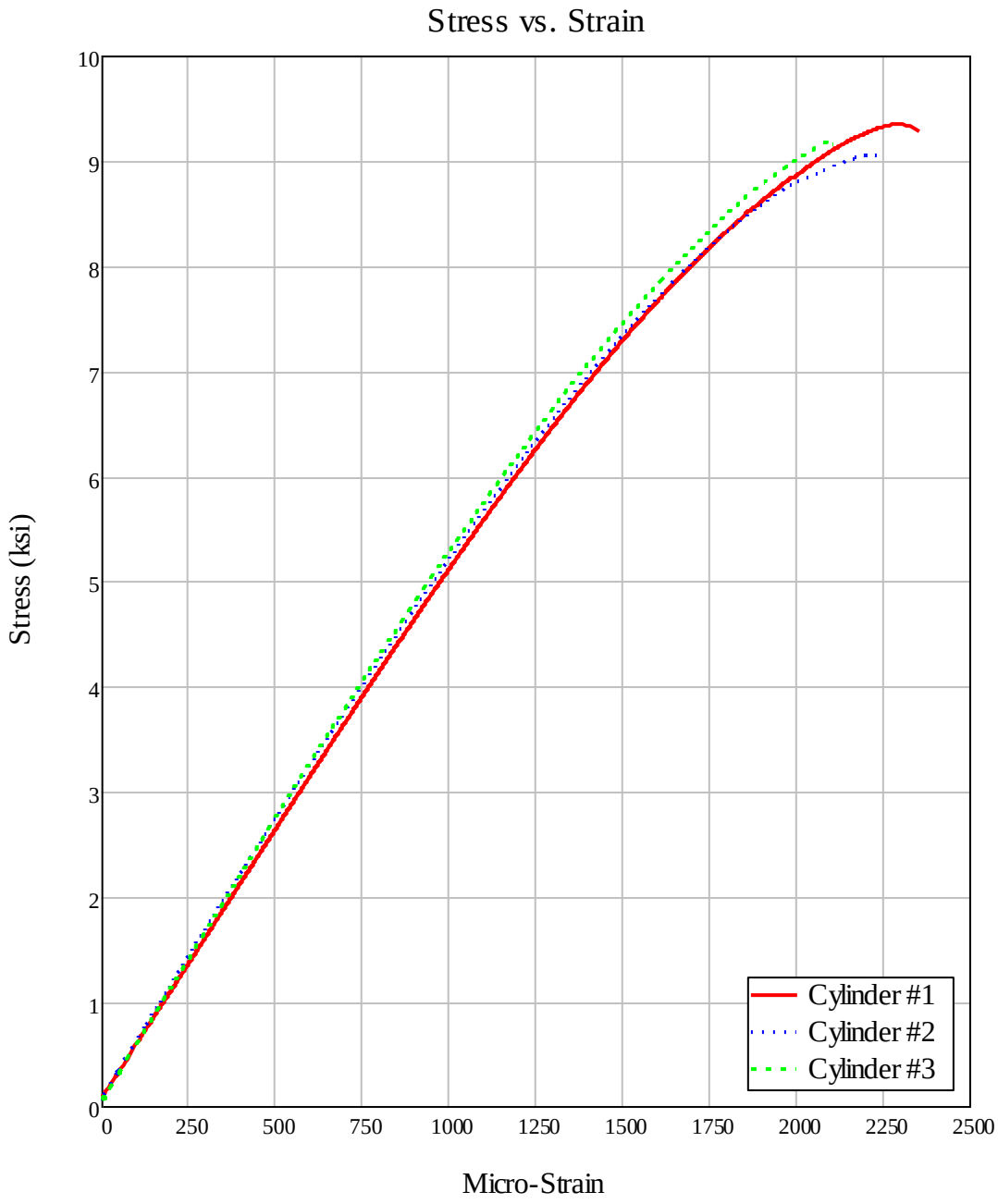


**Figure 10: Stress versus Strain from Bottom Slab Concrete Cylinders**

**Conclusion**

The failure mechanism for the given setup was a sudden brittle concrete failure that occurred after elastic buckling of the steel bottom flange at low load levels. The bottom flange buckling could potentially be resolved by using a tighter spacing of studs closer to the support which would reduce the buckling length. This also could provide additional confinement to the concrete. A higher capacity could be obtained; however, this would still entail a sudden concrete failure if the entire section is required to achieve plasticity. For designs of this type the bottom concrete slab and bottom steel flange are composite requiring that the strain levels in the materials match. The concept of achieving the full plastic moment capacity is not possible due to the concrete bottom slab's inability to withstand strains equal to the yield strain of the steel bottom flange. In this particular case, the bottom steel flange yielded at 2750 micro-strain. The concrete failed at approximately 2230 micro-strain in compression. The double-composite design should be limited in design, in negative moment regions, to achieving full plasticity in the top flange only.

# -Appendix-

***Roark Formulas*** *- Elastic Stability of Plates - Rectangular Plate under equal uniform compression on two opposite edges b. Assuming all edges simply supported. Table 15.2.1a (p. 703)*

$a := 23in$ $b := 72in$ $E_s := 29000ksi$ $\nu := 0.3$

$$ab := \begin{pmatrix} 0.2 \\ 0.3 \\ 0.4 \\ 0.6 \\ 0.8 \\ 1.0 \\ 1.2 \\ 1.4 \\ 1.6 \\ 1.8 \\ 2.0 \\ 2.2 \\ 2.4 \\ 2.7 \\ 3.0 \end{pmatrix} \qquad K := \begin{pmatrix} 22.2 \\ 10.9 \\ 6.92 \\ 4.23 \\ 3.45 \\ 3.29 \\ 3.40 \\ 3.68 \\ 3.45 \\ 3.32 \\ 3.29 \\ 3.32 \\ 3.40 \\ 3.32 \\ 3.29 \end{pmatrix}$$

$\frac{a}{b} = 0.319$

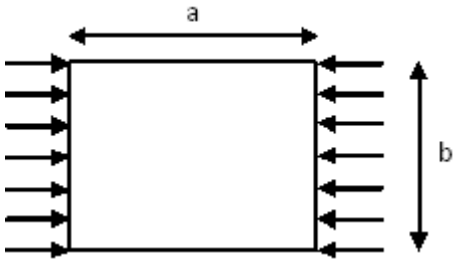


$K' := linterp\left(ab, K, \frac{a}{b}\right)$ $K' = 10.126$

$$\sigma' := K' \cdot \frac{E_s}{1 - \nu^2} \cdot \left(\frac{t}{b}\right)^2$$

$\sigma' = 8.754 \cdot ksi$

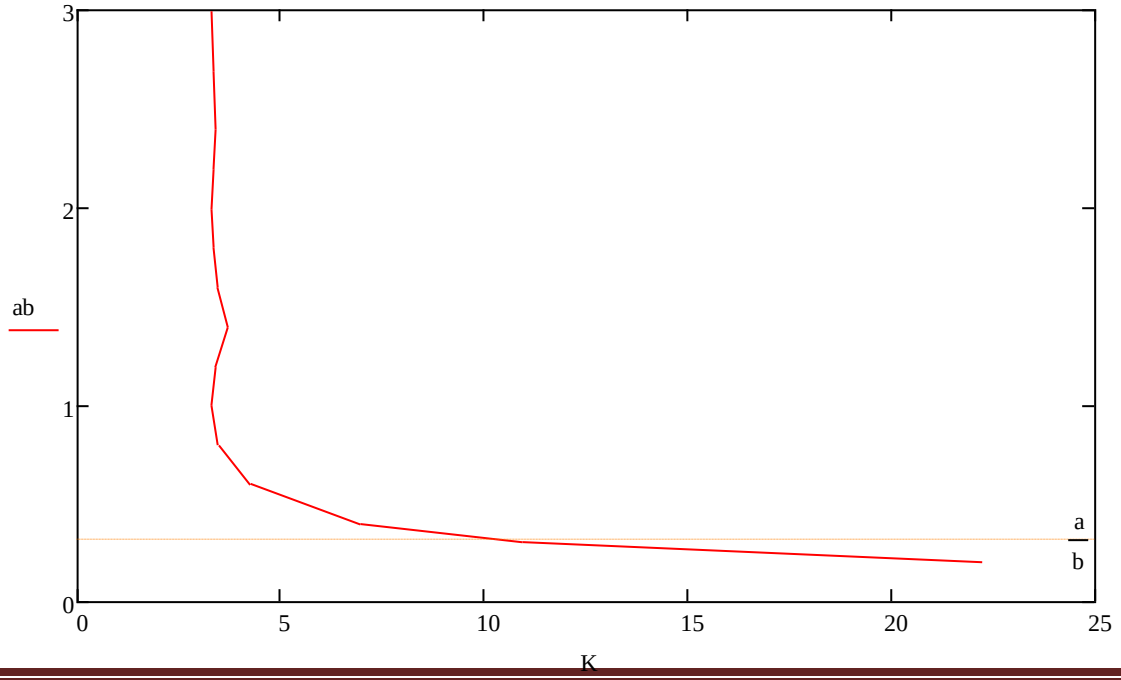

***Plate Analysis***

$f'_c := 8700\,psi$ $\quad E_c := (0.9)\cdot 57000\cdot\sqrt{\frac{f'_c}{psi}}\,psi$ $\quad E_c = 4784.945\,ksi$

$n := round\left(\frac{E_s}{E_c}, 1\right)$ $\quad n = 6.1$

*Effective Width* $\quad b := 72in$ $\quad \frac{b}{n} = 11.803\cdot in$

*Slab Thickness* $\quad t_{bs} := 7in$

*Section Properties - Total Properties*

$A_b := 254.126in^2$ $\quad I_b := 112671.273in^4$ $\quad y_t := 33.291in^3$ $\quad y_b := 22.521in$

$S_b := 5002.875in^3$ $\quad S_t := 3384.417in^3$ $\quad d := 55.813in$

*Moment at **11 inches** from support on "Hold Down" end, i.e. north end*

$M_{appl} = \left(\frac{25}{23}\right)(22.0833ft)\cdot P_{appl}$

*Back out moment/load needed to produce the critical stress found in Roark's Formulas*

$M_{back} := \sigma'\cdot S_b$ $\quad M_{back} = 3649.516kip\cdot ft$

$P_{back} := \frac{23}{25}\cdot\frac{M_{back}}{22.0833ft}$ $\quad P_{back} = 152.04kip$

***Theoretical** Computed Bottom Flange Steel Stresses with applied load, assuming elastic section throughout loading.*

$P_{appl} := \begin{pmatrix} 0 \\ 421 \\ 638 \\ 894 \\ 1441 \end{pmatrix} kip$ $\quad \sigma_{appl} := \frac{\left(\frac{25}{23}\right)\cdot(22.0833ft)\cdot P_{appl}}{S_b}$ $\quad \sigma_{appl} = \begin{pmatrix} 0 \\ 24.239 \\ 36.733 \\ 51.472 \\ 82.966 \end{pmatrix}\cdot ksi$